Frontiers in Sedimentary Geology

Frontiers in Sedimentary Geology

A.H. Bouma
Editor-in-Chief

Submarine Fans and Related Turbidite Systems
A.H. Bouma, W.R. Normark, and N.E. Barnes (editors)

New Perspectives in Basin Analysis
K.L. Kleinspehn and C. Paola (editors)

Microstructure of Fine-Grained Sediments: From Mud to Shale
R.H. Bennett, W.R. Bryant, and M.H. Hulbert (editors)

Seismic Facies and Sedimentary Processes of Submarine Fans and Turbidite Systems
P. Weimer and M.H. Link (editors)

Marine Clastic Reservoirs: Examples and Analogues
E.G. Rhodes and T.F. Moslow (editors)

E.G. Rhodes T.F. Moslow
Editors

Marine Clastic Reservoirs

Examples and Analogues

With 262 Illustrations in 306 Parts

Springer-Verlag
New York Berlin Heidelberg London Paris
Tokyo Hong Kong Barcelona Budapest

E.G. Rhodes
Landmark Graphics Corporation
16001 Park Ten Place
Houston, TX 77084
USA

T.F. Moslow
Department of Geology
University of Alberta
Edmonton, Alberta T6G 2E3
Canada

Series Editor
Arnold H. Bouma
School of Geoscience
Louisiana State University
Baton Rouge, LA 70803-4101 USA

Cover Illustration:

Royalite No. 4 well in the Turner Valley Field, Alberta, circa 1924. The Turner Valley Field was the first major hydrocarbon discovery in the Foothills of Western Canada, with estimated reserves of one billion barrels of oil and three trillion cubic feet of natural gas. The earliest wells were drilled in 1914 near gas seeps on a surface anticline and encountered oil and gas in marine clastic reservoirs of lower Cretaceous age.

The cover illustration was produced by Pam Lobo of Landmark Graphics, Houston and derived from an historical photograph. The original photograph (NA-246-1) was provided by the Glenbow Museum Photo Archives Division, Calgary, Alberta, Canada.

Dedication: To Anthea, Susan and Maxine

ISBN 978-1-4757-0162-3 ISBN 978-1-4757-0160-9 (eBook)
DOI 10.1007/978-1-4757-0160-9

Library of Congress Cataloging-in-Publication Data
Marine clastic reservoirs : examples and analogues / [edited by]
E.G. Rhodes, T.F. Moslow.
p. cm. — (Frontiers in sedimentary geology)
Includes bibliographical references and index.
ISBN 978-1-4757-0162-3
1. Reservoirs. 2. Sedimentation and deposition. 3. Marine sediments I. Rhodes, Eugene G. II. Moslow, Thomas F. III. Series.
TD396.M375 1992
551.3'53—dc20 92-2969
CIP

Printed on acid-free paper.

Production managed by Terry Kornak; manufacturing supervised by Jacqui Ashri.
Typeset by Asco Trade Typesetting, North Point, Hong Kong.

9 8 7 6 5 4 3 2 1

Series Preface

The *Frontiers in Sedimentary Geology* series has matured into a suite of volumes that provides information about current topics of interest. These topics are selected because they are not effectively summarized elsewhere in recently published abstracts or journal articles. The number of individual publications in numerous journals makes it very difficult, and often impossible, to keep up with a particular focus or specialization of current interest. The division of geoscience into topical areas is a natural process and, in some cases, a necessity that, however, can work against advancements regarding interdisciplinary approaches or multi-expert teams. For such reasons, a series like this one is unique as it contains integrated perspectives and contrasting views about a topic of current interest.

Each volume in the *Frontiers in Sedimentary Geology* series is initiated by one or more persons who select the particular topic and divide it into major themes that are integrated through the use of introductory chapters written by them as editors or other invited authors. Each introduction is followed by chapters that either highlight a specific aspect of that theme or provide a specific example. Although it is virtually impossible to compile a complete coverage of an entire topic, the compilation editors develop the outline of their volume in such a manner that maximum integration and discussion will be presented. Equally important is regular and constructive contact between the editors and the authors, thereby ensuring high-quality manuscripts that contribute directly to the theme of the volume.

The present volume, *Marine Clastic Reservoirs: Examples and Analogues*, edited by Eugene (Skip) Rhodes and Thomas Moslow, is a good example of how the series fulfills its role. The idea for this publication emerged during an SEPM core workshop. However, rather than having all core workshop contributors provide a manuscript, resulting in an eclectic collection of descriptive works, the editors used the strength of that workshop to redesign an integrated volume. Analog-oriented geoscience was combined with well-founded stratigraphic-sedimentologic descriptions to present a wide spectrum of shallow to deep marine sandstones as reservoir bodies. The result is a process-based analysis of sandstone facies that provides the reader with insight into the geometries of such units. A treatment like this is vital to the development or management of reservoirs that are highly irregular in shape and variable in character. The calculation and prediction of fluid flow behavior and the determination of

reserves through computer simulation requires the best information on reservoir geometry and heterogeneity.

The *Frontiers in Sedimentary Geology* series differs from the *Casebooks in Earth Sciences*, another Springer-Verlag series. Consequently, the present publication is different from, and complimentary to, the *Sandstone Petroleum Reservoirs* volume, edited by J.H. Barwis, J.G. McPherson, and J.R.J. Studlick recently released in the *Casebooks in Earth Sciences* series. The present volume offers a more genetic approach including sequence stratigraphy and the influence of relative sea level variations. Such a "basic" perspective places the sandstone bodies in a framework that can be broken down into building blocks or individual parasequence. The application of these concepts to the discussion of both modern and ancient sandstone bodies clearly suggests that modern examples resulting from Holocene depositional controls may not always be viable as models for the ancient analogs. However, a combination of modern and ancient examples can result in the construction of the best model for the particular sandstone reservoir.

Baton Rouge, Louisiana
August 1991

Arnold H. Bouma
Series Editor

Preface

About the volume

The idea for this volume was conceived with the collaboration of contributors and participants during a Society for Sedimentary Geology (SEPM) core workshop at Atlanta in 1986. The initial concept proceeded through a metamorphosis after discussions with the publisher and Arnold Bouma, the series editor. Further change occurred as the volume began to take shape during the past two years as contributors submitted their first drafts and a clearer picture of the volume emerged. As a consequence, the initial themes were reshaped and focussed. In addition, this volume has benefited from the wide spectrum of contributions and the diverse experience of the authors.

The volume is a forum in which the editors and the contributors advocate analog-oriented geoscience based on rigorous stratigraphic and sedimentologic description and interpretation. Analog-oriented analysis of reservoirs emphasizes the use of examples that reside on a spectrum of variability. Such analysis contrasts with model-oriented analysis by supporting a wider acceptance of variability and encourages a greater depth of description and quantification especially in terms that are useful to the other petroleum sciences that are downstream from exploration, such as development geophysics and reservoir engineering.

The description of reservoirs in a sequence stratigraphic context is pivotal to this volume although it is arguable that sequence stratigraphy remains a model-oriented methodology. Embracing the underlying concepts of sedimentary and stratigraphic response to relative sea level change necessitate the acceptance of process-response models that are both generalized and somewhat imprecise at the reservoir scale. However, the regional framework in which most marine clastic reservoirs reside is most effectively explained in terms of sequence stratigraphic principles. Furthermore, as the acceptance and utilization of sequence stratigraphy broadens, the inventory of marine-clastic analogs may soon match that of the model-oriented aspects of sequence stratigraphy. Consequently, we devoted the opening section of this volume to the analysis of marine clastics in terms of parasequences, parasequence sets, and the resulting sequence stratigraphic packages that characterize the ancient record.

An edited volume really reflects the summation of a loosely knit group of scientists who are the contributors. As the volume developed and the anticipated threads of

continuity emerged among the articles, we encouraged collaboration among contributors at both a formal and informal level. Each chapter was evaluated by reviewers from within the volume as well as by external reviewers. Although we encouraged individualistic writing styles, we attempted to mold the volume into a consistent collection of well-researched scientific writings that offers a spectrum of paradigms for the study and analysis of marine clastic reservoirs and the environments in which they are deposited (Fig. 1).

The volume is organized into three discrete but related sections that support analog-oriented characterization of reservoirs. Because the parasequence is defined as the primary building block of the individual reservoir, the first section consists of three articles that progress the reader from a general to a specific use of sequence stratigraphy to catalog, identify, and predict marine clastic reservoir facies. The second section contains two contributions on modern analogs that each present a unique perspective on the value of modern sedimentology and geomorphic description. The last section, containing seven contributions, is organized in a progression from deltaic environments to the deep-sea fan and offers a collection of ancient analogs that we believe represent improved concepts in geoscience description and analysis.

About the Authors and Editors

We encourage readers to contact contributors directly regarding additional discussions about individual chapters. A list of authors' addresses can be found at the end of this section. The diverse nature of the chapters presented suggests that readers might want to know about each author's individual perspectives. Consequently, we asked all contributors to prepare brief biographic sketchs of their previous experience and present interests. The following paragraphs summarize the authors' biographic profiles.

Eduardo Bagnoli currently works as chief supervisor of the geological laboratory of the Petrobras office in Natal, NE Brazil, where he specializes in the sedimentology of ancient and recent environments and the petrography/diagenesis of sedimentary rocks. Mr. Bagnoli holds a BS degree in geology from the University of Sao Paulo and a MS degree in reservoir geology from the University of Ouro Preto, Minas Gerais State, Brazil.

Jeremy M. Boak is a Physical Scientist with the U.S. Department of Energy's Office of Civilian Radioactive Waste Management and currently coordinates performance assessment activities for the Yucca Mountain Site Characterization Project in Las Vegas, Nevada. He formerly worked in exploration and development for ARCO Alaska and ARCO Oil and Gas Company. His publications include papers on mineralogy, metamorphic petrology, geochemistry, geochronology, and reservoir characterization.

Bruce E. Bowen received his BS and PhD degrees in geology from Iowa State University in 1967 and 1974, respectively. As a PhD candidate he spent most of his time in Africa, where he helped to develop the time-stratigraphic framework for early man sites in the East African Rift. He joined Texaco's Research Group in 1974 and later, in 1977, Gulf Oil Company, where he headed a taskforce assigned to determine petroleum potential of the Atlantic margin and to develop exploration models for deep-water plays in the Gulf of Mexico. Dr. Bowen left Gulf in 1984 to help found Everest GeoTech, and in 1989, joined Calibre Consulting Services, Inc.

Doug J. Cant is a sedimentologist/stratigrapher employed by the Geological Survey of Canada to study the petroleum-bearing clastic rocks of the Alberta foreland basin. In addition to pursuing detailed sequence stratigraphic work on the Mannville Group, he is attempting to understand the stratigraphy of the basin in terms of fore-

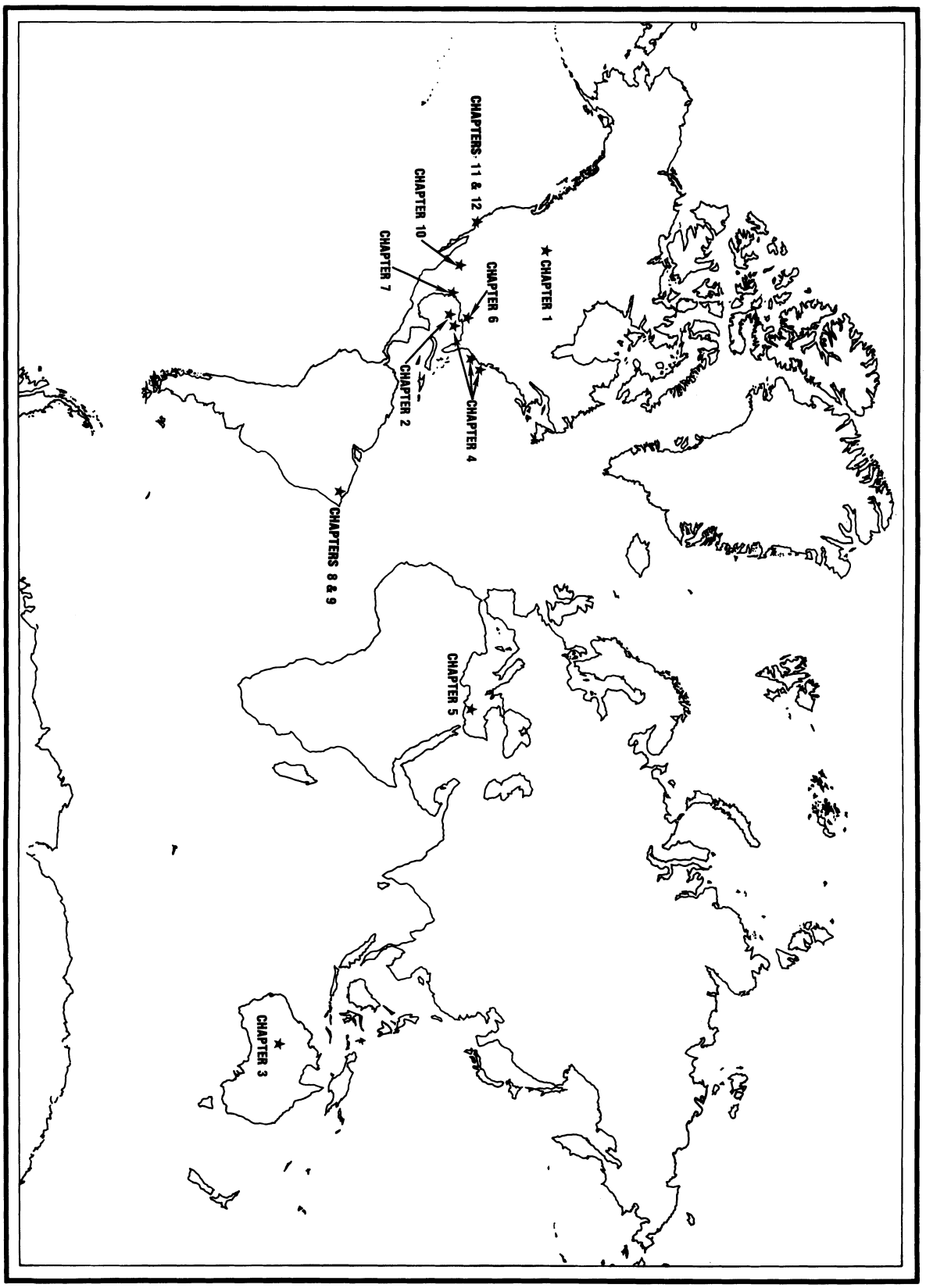

Figure 1. Generalized map of the world showing locations of study areas contained in each chapter.

land tectonics. He has worked in the petroleum industry in the United States and for the Alberta Research Council. His undergraduate degree is from University of Toronto, and graduate degrees are from McMaster University.

JOEL C. DE CASTRO worked for over twenty years at the Exploration Division of PETROBRAS Research Center (CENPES), Rio De Janeiro, Brazil. He holds a BS from the School of Mines of Ouro Preta and a PhD in Geology from the Paulista State University, Brazil, where he is currently a Professor in the Geosciences Institute. His specialty is physical stratigraphy and clastic reservoirs, and he has been working with facies and stratigraphic analysis of Brazilian marginal-marine and cratonic basins.

JUNE GIDMAN is a senior research geologist at Chevron Oil Field Research Company, La Habra, California. She is a sedimentologist who specializes in core handling and preservation, and correlation of core, petrophysical, and log properties. Previous experience includes exploration and development geology of the North Sea and Williston Basin areas. She received a BSc Honors degree in geology from Leicester University and a PhD in geology from Liverpool University.

JOHN D. GORTER is Chief Geologist of Petroz N.L. He worked in the oil industry for 20 years (Bureau of Mineral Resources, Esso, Pancontinental, AGIP, Sydney Oil, Command, Norcen) after graduating in 1971 from the Australian National University with honors. He recently completed a part time PhD from the University of New South Wales. Specific interests are sedimentology, biostratigraphy and source rocks.

CHRIS W. GRANT is a Senior Research Assistant at Chevron Oil Field Research Company. His specialies include petrography and sedimentology. He has worked primarily in EOR-related clastic projects and in researching permeability heterogeneity in carbonates. He received his BS in geology at California State University Fullerton in 1985 and is finalizing his MS in geology at California State University Long Beach, where he is studying depositional and organic geochemical characteristics of the recent anaerobic environment in Santa Barbara Basin, California.

STEVEN J. JOHANSEN has worked in the reservoir geology section of Texaco Exploration and Production Technology Division since 1987, where he applies sedimentologic and petrographic analysis to hydrocarbon exploration and production in clastic sequences. His studies in schools of the American southwest (BS, New Mexico Institute of Mining and Technology, 1976; MS, University of Arizona, 1981; PhD, University of Texas at Austin, 1986) were mixed with employment in environmental geology, uranium exploration, and related areas.

MARTIN B. LAGOE, Associate Professor, Department of Geological Sciences, University of Texas at Austin, previously worked for ARCO Oil and Gas Co. and ARCO Exploration Co. His research focuses on foraminiferal micropaleontology, quantitative stratigraphy, paleoceanography and basin analysis. He has a BS in geology from Rensselaer Polytechnic Institute, an MS in geology from the University of Wisconsin-Madison, and a PhD in geology from Stanford University.

JOHN F. LINDSAY is presently a Senior Principal Research Scientist with the Australian Bureau of Mineral Resources in Canberra, Australia. John is a sedimentologist and seismic interpreter with a broad interest in the larger-scale relationships between basin dynamics and sedimentation controls. Prior to joining the Bureau of Mineral Resources he worked for Exxon Production Research, the University of Texas and NASA's Johnson Space Center all in Houston, Texas. An Australian, he received his early education at the University of New England in Armidale, Australia, where he completed a bachelor's and master's degree before moving to Ohio State University in Columbus Ohio to complete a PhD.

JEFFREY A. MAY is a Senior Geologist with Marathon Oil Company at their Petroleum Technology Center in Littleton, Colorado. His work focuses on deltaic, shallow-marine, and deep-water clastic depositional systems. Jeff has been involved in corporate training, special projects, and technology development. He received his BA

from Earlham College in 1975, an MS in geology from Duke University in 1977, and a Ph.D. in geology from Rice University in 1982.

Yossi Mart is a senior scientist at the National Institute of Oceanography in Haifa, Israel and teaches marine geology at Haifa University. His research interests focus on the tectonic framework and seismic stratigraphy of the eastern Mediterranean and the northern Red Sea. He received his professional education at the Hebrew University in Jerusalem and at Texas A&M University in College Station, Texas.

Thomas F. Moslow is an Associate Professor at the University of Alberta. His field of expertise is in clastic sedimentology with much of his current research focusing on marine clastic sequences of Triassic and lower Cretaceous age in the Western Canada Basin, Gulf of Mexico, and Western Canadian Continental Margin. Dr. Moslow received his PhD in Geology in 1980 from the University of South Carolina. He worked as a research geologist at the Cities Service Technology Center and later held a joint appointment with the Basin Research Institute and Geological Survey at Louisiana State University.

Jory A. Pacht received his bachelor's degree in geology from Ohio University in 1973. He worked as a well-site geologist and later completed his MS degree in 1976 at the University of Wyoming. He received his PhD in geology in 1980 from Ohio State University. In 1980, he joined the staff of the Exploration Research Group of ARCO Oil and Gas Company, where he served as a Senior Research Geologist. Dr. Pacht left ARCO and joined RPI International in 1988 as a Senior Scientist where he worked on sequence stratigraphic projects. He joined Calibre Consulting Services, Inc. in 1990.

Sandra Phillips is currently a Senior Geologist in Geoscience Operations with ARCO Alaska Inc., in Anchorage, Alaska. Her previous position was in Exploration Research with ARCO Oil and Gas Company. Her primary focus is the sequence stratigraphy and sedimentology of clastic depositional systems, and their applications for stratigraphic exploration. She holds BS and MS degrees in geology from Texas A&M University, and a PhD in geology from Cornell University.

Bill R. Pottorf received a BS in Geophysics from Colorado School of Mines in 1965. Immediately after graduation he joined Exxon U.S.A. (then Humble Oil Co.) as a geophysical interpreter. He held a variety of positions in interpretation, processing and acquisition with Exxon. In 1977, Pottorf became Manager of Technical Services at Geoquest International, Inc. He left Geoquest in 1980 to become Vice President of Criterion Consulting, Inc., where he developed geophysical techniques for the delineation of petroleum reservoirs. In 1983 he became an independent consultant.

Alan A. Reed is a Senior Research Geologist at Chevron Oil Field Research Company, La Habra, California. He is a sedimentologist and petrographer currently specializing in reservoir characterization and reservoir modeling. Alan has also worked as an explorationist and development geologist for Chevron U.S.A. He earned his BSc and MS degrees in geology from the University of Massachusetts.

Eugene G. (Skip) Rhodes is presently a Senior Staff Geologist with Concurrent Solutions, the interpretive subsidiary of Landmark Graphics Corporation, Houston, Texas, where he provides development plans for mature producing trends and properties through the integration of reservoir engineering with reservoir geology. After completing Bs and MS degrees from the University of Massachusetts, and nearly six years with the U.S. Army Corps of Engineers, he gained a PhD at the Australian National University. He held positions with the Australian Institute of Marine Science, Comalco Aluminium, and Gulf Oil before becoming the Chief Geologist of RPI International during the period 1985–1990.

Robert W. Ruggiero is currently an exploration geologist with BP Exploration, Inc. in Houston, Texas. His focus is regional play analysis and new play synthesis,

working on offshore lease sales and developing prospects in shallow and deepwater paleoenvironments. He received his Master of Arts degree in Geology from the University of Texas at Austin.

BERNARD L. SHAFFER received his BS degree in Geology from Wichita State University in 1958, his MS degree from University of Missouri in 1962, and his PhD from Michigan State University in 1969. Dr. Shaffer then joined Gulf Oil where he worked as a research biostratigrapher for 16 years. In 1984 he became Director of Biostratigraphic Applications at Everest GeoTech. Dr. Shaffer worked as a consultant during 1989, the joined Calibre Consulting Services, Inc. in 1990.

W.J. (WILL) SCHWELLER currently is a senior research geologist with Chevron Oil Field Research Company in La Habra, California, specializing in analysis of turbidite systems and sequence stratigraphy in continental margin basins. His work experience includes seismic stratigraphic studies of deltaic margin sequences and active margins with Gulf Research and Development. His education includes degrees in geology from Pennsylvania State University and Cornell University and in geological oceanography from Oregon State University.

ROGER M. SLATT is Head of the Department of Geology and Geological Engineering at the Colorado School of Mines, Golden, Colorado. Prior to this, he was Manager of Formation Evaluation at ARCO International Oil & Gas Co. in Plano, Texas, and previously worked for ARCO Oil and Gas Co.'s research group, Cities Service Oil Co.'s research group and served on the faculties of Memorial University of Newfoundland and Arizona State University. He has published extensively on such topics as glacial geology, geochemical exploration, marine, reservoir, and Pleistocene/Quaternary geology, seismic stratigraphic and depositional systems. He holds a PhD degree in geology from the University of Alaska.

ROBERT S. (BO) TYE is presently a Senior Geologist with ARCO Alaska, Anchorage, and was a Senior Research Geologist in the Stratigraphic Analysis group at ARCO Research. Bo received a BS from the College of Charleston (1978), an MS from the University of South Carolina (1981), and a PhD from Louisiana State University (1986). His career began as a Reservoir Geologist with Cities Service Company (1981–1983) in Tulsa, Oklahoma, and since, has included Research Associate positions with the Louisiana Geological Survey and the Coastal Studies Institute at Louisiana State University and with the Bureau of Economic Geology, University of Texas at Austin (1987–1989).

Acknowledgments

We greatly appreciate the numerous friends and associates within the industry who provided ideas and encouragement for this project during its conception and growth. We are particularly indebted to Anthea Turner, Susan Welch and Maxine Moslow for their patience, encouragement and support during the preparation of the volume. We thank the employers of the contributors for publication approval and support of the authors' participation within this book. We also appreciate the administrative and graphic arts support provided by Landmark/Concurrent Solutions during the final phases of volume preparation. The review and refinement of the chapters that follow is the result of much hard work and commitment by a large group of reviewers. The structure of the volume required that contributions be reviewed by at least another author within the volume and an external reviewer outside of the volume. We thank the reviewers listed below in addition to those who wish to remain anonymous.

Doug Cant
Neal Barnes
Jim Deckleman
Brad Hayes
Mitch Harris
Don Keith
Barbara Luneau
Dan Nedland
Doug Nester
Sean O'Connell
Jory Pacht
Ray Rahmani
Bob Ruggiero
Mark Scheihing
Will Schweller
Roger Slatt
Chuck Siemers
Jerry Sinise
Dave Smith
Rod Tillman
Bo Tye
Darrell Wightman

Houston, Texas
Edmonton, Alberta
August, 1991

E.G. (Skip) Rhodes
Tom F. Moslow
Editors

Contents

Series Preface v
Arnold H. Bouma

Preface vii

Acknowledgments xiii

Contributors xvii

Section I Stratigraphic Analysis of Marine Clastic Reservoirs 1

1 The Stratigraphic and Paleogeographic Context of Shoreline—Shelf Reservoirs 3
Douglas J. Cant

2 Systems Tracts, Seismic Facies, and Attribute Analysis Within a Sequence-Stratigraphic Framework—Example from the Offshore Louisiana Gulf Coast 21
Jory A. Pacht, Bruce Bowen, Bernard L. Shaffer, and William R. Pottorf

3 Clastic Petroleum Reservoirs of the Late Proterozoic and Early Paleozoic Amadeus Basin, Central Australia 39
John F. Lindsay and John D. Gorter

Section II Perspectives from Modern Environments 75

4 Tidal Inlet Reservoirs: Insights from Modern Examples 77
Robert S. Tye and Thomas F. Moslow

5 The Sedimentologic and Geomorphologic Provinces of the Nile Fan 101
Yossi Mart

Section III Ancient Analogues 113

6 Depositional and Structural Controls on the Diagenesis of Lockhart Crossing Reservoir (Wilcox); Gulf Coast of Louisiana (U.S.A.) 117
Steven J. Johansen

7 Shelf Sandstones of the Deep Wilcox Trend, Central Texas Gulf Coast 135
Jeffrey A. May

8 Facies, Reservoirs and Stratigraphic Framework of the Mossoró Basin Member (Latest Cenomanian Earliest Turonian) in Potiguar Basin, NE Brazil: An Example of a Tide and Wave Dominated Delta 161
Joel Carneiro De Castro

9 The Mossoró Sandstone, Canto do Amaro Oil Field, Late Cretaceous of the Potiguar Basin, Brazil: An Example of a Tidal Inlet-Channel Reservoir 183
Eduardo Bagnoli

10 Depositional History and Performance of a Permian Bell Canyon Sandstone Reservoir, Ford-Geraldine Field, West Texas 201
Robert W. Ruggiero

11 Reservoir Character of Deep Marine Sandstones, Inglewood Field, Los Angeles Basin 231
June Gidman, Will J. Schweller, Chris W. Grant, and Alan A. Reed

12 Scales of Geologic Heterogeneity of a Deep-Water Sand Giant Oil Field, Long Beach Unit, Wilmington Field, California 263
Roger M. Slatt, Sandra Phillips, Jeremy M. Boak, and Martin B. Lagoe

Index 293

Contributors

EDUARDO BAGNOLI, PETROBRAS/DEBAR/DINTER, Av. Interventor Mario Camara, 2783 Nazare - Natal/RN, 59.070 - Brazil

JEREMY M. BOAK, Department of Energy, Yucca Mountain Project Office, Las Vegas, NV 89193-8518, USA

BRUCE BOWEN, Calibre Consulting Inc., Houston, TX 77002, USA

DOUGLAS J. CANT, Geological Survey of Canada, Calgary, Alberta T2L 2A7 Canada

JOEL CARNEIRO DE CASTRO, Universidade Estadual Paulista, Instito de Geociencias E Ciencias Exatas, Departmento Geologia Sedimentar, 13.500 Rio Claro, Brazil

JUNE GIDMAN, Chevron Oil Field Research Company, La Habra, CA 90631, USA

JOHN D. GORTER, Petroz, Perth, Western Australia 6000, Australia

CHRIS W. GRANT, Chevron Oil Field Research Company, La Habra, CA 90631, USA

STEVEN J. JOHANSEN, Exploration and Production Technology Division, Texaco U.S.A., Houston, TX 77042, USA

MARTIN B. LAGOE, Department of Geological Sciences, The University of Texas at Austin, Austin, TX 78713-7909, USA

JOHN F. LINDSAY, Bureau of Mineral Resources, Division of Continental Geology, Canberra, ACT 2601, Australia

YOSSI MART, Israel Oceanographic and Limnological Research Ltd., 31080 Haifa, Israel

JEFFREY A. MAY, Marathon Oil Company, Littleton, CO 80160, USA

THOMAS F. MOSLOW, Department of Geology, University of Alberta, Edmonton, Alberta T6G 2E3, Canada

Jory A. Pacht, Calibre Consulting Inc., Houston, TX 77002, USA

Sandra Phillips, ARCO Alaska, Inc. Anchorage, AK 99510-0360, USA

William R. Pottorf, Houston, TX 77077, USA

Alan A. Reed, Chevron Oil Field Research Company, La Habra, CA 90631, USA

Robert W. Ruggiero, BP Exploration Inc., Houston, TX 77210, USA

Will J. Schweller, Chevron Oil Field Research Company, La Habra, CA 90631, USA

Roger M. Slatt, Department of Geology and Geological Engineering, Colorado School of Mines, Golden, CO 80401, USA

Bernard L. Shaffer, Calibre Consulting Inc., Houston, TX 77702, USA

Robert S. Tye, ARCO Alaska Inc., Anchorage, AK 99510, USA

SECTION I

Stratigraphic Analysis of Marine Clastic Reservoirs

E.G. Rhodes and T.F. Moslow

At the exploration stage, the search for the hydrocarbon-charged reservoir emphasizes genetic units at varying scales. It is the association of certain types of stratal units with reservoir analogs that encourages the explorationist to focus his search within certain large-scale genetic packages. These large-scale packages, which are bounded by major unconformities or their correlative conformities, are the sequences of sequence stratigraphy (Mitchum, 1977). Within the sequences are parasequences and parasequence sets, which are bounded by a hierarchy of marine flooding surfaces (Van Wagoner et al., 1990). Conversely, once development of a reservoir commences, the genetic hierarchy, defined by parasequences and parasequence sets, is modified by concepts associated with flow unit description. Flow units are rock units that appear to behave in a similar fashion during the delivery of reservoir fluids into the well bore (Hearn et al., 1984; Tye et al., 1986; Slatt and others, this volume). Because flow units are empirically defined by petrophysical and engineering parameters, such units may cross-cut genetic units defined by parasequences. With this perspective on reservoir description in mind, we commence the volume with a discussion of reservoir occurrence as parasequences (this section). Although each of the authors applies the concepts of sequence stratigraphy to a varying degree within their contributions, the deposition and preservation of reservoir facies, as controlled by relative sea-level change, remains a central thread within the other two sections of the volume.

We asked Doug Cant to prepare the opening position paper on the stratigraphic framework of marine clastic reservoirs, in a context that helps geoscientists consider the positioning of these facies in terms of sequence stratigraphy. In his chapter, Cant clarifies the roles of relative sea level and sediment supply with regard to their control on systems tract location and geometry. By using terms such as "relative highstand" and "relative lowstand," as opposed to merely "highstand" and "lowstand," Cant disarms some of the contention surrounding terminology and proceeds to answer the question, "Where's the reservoir?"

By suggesting that a sequence generated by eustatic variation may not be reflected at every location, Cant demonstrates that relative sea-level change causes facies migration that is visible on well logs and seismic sections. Such observations, when combined with hypotheses surrounding sediment supply, such as autocyclic switching of depositional fairways, provides leads to reservoir locations.

According to Cant, rocks described at the parasequence level represent the individual reservoir. This building-block approach to reservoir architecture helps us understand the origin of the relatively small, subtle features that are shallow marine or shoreline reservoirs. Many of these, especially those deposited as "relative lowstand" deposits, have been extensively modified by transgressive processes. Cant provides the "rules" for predicting such subtle features once the relative sea-level history has been modeled.

In the second chapter, Jory Pacht and his co-authors propose an interpretive methodology that complements the paleogeographic framework presented by Cant. This chapter offers both an expansion of, and a differing perspective on, the concepts explained by Cant. Using examples drawn from Plio Pleistocene sequences within the Gulf of Mexico, these authors suggest a hierarchy of interpretation that leads to predictive strategies similar to Cant's. According to Pacht and his associates, iterative analysis of depositional sequences and systems tracts provides a finite suite of seismic facies for each systems tract. This suite of seismic facies

has distinct attributes that can be associated with depositional facies, especially reservoir units. When such methods are supported by analogy to historical production performance, they may directly indicate exploration targets.

Although the growth-faulted shelf margin reservoirs of the Gulf of Mexico exhibit geometries that differ markedly from some of Cant's shallow-water examples, Pacht and his co-authors demonstrate that a parallel methodology arrives at similar results. In addition to using comparable methods, these authors proceed farther along the interpretive pathway by constructing a link between the sequence stratigraphic framework at a regional scale and the interpretation of seismic attributes within specific systems tracts.

Pacht and his co-workers create a facies column that mixes both descriptive and genetic terminology. Some of these labels describe seismic character rather than rock lithology. Although unorthodox in the view of some workers, this practice illustrates an important template for the merger of geophysics and geology or, more broadly, any of the disparate petroleum science disciplines. Interdisciplinary interpretation may require relaxation of the more rigorous rules that are internal to individual disciplines. In this case, other workers might subdivide the systems tracts differently, but the interpretive template would remain analogous.

In the third chapter, John Lindsay and John Gorter apply sequence-stratigraphic concepts to an interior basin on the Australian craton. An exciting aspect of this basin analysis is the opportunity to take a fresh look at "frontier" onshore basins where previous studies have been encumbered with traditional dogma. There are strong similarities between intracratonic sedimentation on the North American continent, especially western Canadian sedimentary basins (see Cant, this volume) and some of the interior basins of Australia. Australian resource companies have long appreciated the contribution that the well-documented North American analogs have made to predictive exploration analogs for Australia.

In their chapter, Lindsay and Gorter have packaged the analysis of a central Australian basin for export. Their analysis advances two hypotheses: 1) at a regional scale, clastic reservoir units develop predictably during two specific stages of basin history and, 2) although large-scale basin dynamics control the positioning of prospective systems tracts, there are local factors at the parasequence and parasequence set levels that predetermine reservoir quality. Lindsay and Gorter's description of such large-scale and local controls on porosity and permeability within the Amadeus Basin further strengthens the explorationist's view that new oil fields are being found with the drill bit managed by sound interpretation.

References

Hearn, C.L., Ebanks, W.J., Jr., Tye, R.S., Ranganathan V., 1984, Geological Factors Influencing Reservoir Performance of the Hartzog Draw Field, Wyoming: Journal of Petroleum Technology, v. 36, p. 1335–1344.

Mitchum, R.M., 1977, Seismic stratigraphy and global changes of sea level, Part 1: Glossary of terms used in seismic stratigraphy, *in* Payton, C.E., ed., Seismic Stratigraphy—Applications to Hydrocarbon Exploration: American Association of Petroleum Geologists Memoir 26, p. 205–212.

Tye, R.S., Ranganathan, V., and Ebanks, W.J., Jr., 1986, Facies analysis and reservoir zonation of a Cretaceous shelf sand ridge: Hartzog Draw Field, Wyoming, *in* Moslow, T.F. and Rhodes, E.G., eds., Society of Economic Paleontologists and Mineralogists Core Workshop No. 9, Atlanta: SEPM, Tulsa, Oklahoma, p. 169–216.

Van Wagoner, J.C., Mitchum, R.M., Campion, K.M. and Rhamanian, V.D., 1990, Siliciclactic sequence stratigraphy in well logs, core, and outcrops: Concepts for high-resolution correlation of time and facies: American Association of Petroleum Geologists Methods in Exploration Series, No. 17, 55 p.

CHAPTER 1

The Stratigraphic and Paleogeographic Context of Shoreline—Shelf Reservoirs

Douglas J. Cant

Introduction

This chapter reviews the stratigraphic and paleogeographic setting of shallow marine reservoirs by discussing the sequences in which they occur, the fundamental variables that control them, their geometries, and common occurrences. Many of the concepts of sequence stratigraphy will be discussed as they apply to these kinds of deposits. The development of unconformities, truncation surfaces, diastems, or ravinement surfaces is of primary importance in exploration for, or development of, shoreline and shallow marine reservoirs.

Sequence stratigraphy is fundamentally only an elaboration of basic geological principles. However, it has revolutionized concepts of facies relationships on a large scale, primarily because it is linked to the idea of relative sea-level variation—a parameter of great importance in controlling the stratigraphy and sedimentology of sedimentary rocks. A change of depositional base level imposed upon a basin where active sedimentation is occurring has extreme effects on facies distributions, especially on shoreline and shallow marine deposits. The origins of relative sea-level changes are debatable, but eustatic sea-level variation appears to be a fundamental control, which is, at present, imperfectly understood. The concepts and models in this discussion apply whether a sea-level change is absolute or only relative.

Major External Variables

The major external variables affecting the deposition, erosion, preservation, and large-scale organization or architecture of all sediments are: subsidence (Sub), eustatic sea-level variation (E), and the thickness of sediment deposited (Sed). Climate, an extremely important variable, is reflected by the amount and type of sediment supplied or formed. The parameters are related to the change in depth of water (D) by the following equation (Cant, 1989):

$$(E + \text{Sub}) - \text{Sed} = D.$$

This equation shows that variations in any of the other three parameters can cause changes in D, the parameter that describes transgressions and regressions, or in Sed, which describes the amount of deposition or erosion. The architecture of shallow marine reservoirs is largely determined by the occurrence of transgressive-regressive sequences and erosional or nondepositional sequence boundaries. This chapter will discuss development of shallow marine reservoirs in terms of sequence-stratigraphic elements, as generated by external variables.

In recent years, many authors have attributed the formation of marine sequences of different scales to eustatic variations. However, as discussed by Burton et al. (1987), the actual cause of a stratigraphic effect is difficult to interpret. The areal extent of sequences is significant in this context, whether the sequence is local, basinal, or global, because eustasy—on the scale that markedly affects sedimentary deposits—is global, while the other variables are uniform only over individual basins or parts of basins. However, a global signal may be overwhelmed by a strong local effect, such as rapid sediment supply, so that sequences generated by eustatic variation may not be reflected in every location.

Variations in rates of sedimentation may occur because of variations in the rates of tectonic processes that generate

relief in the sediment source area, or due to climatic changes that affect transport capacities of sedimentary environments. On a smaller scale, sediment supply-rate variations also occur because of autocyclicity in sedimentary systems. Autocyclicity (Beerbower, 1964) is the shifting of locations of deposition because of factors intrinsic to the sedimentary system. The switching of active lobes in the Mississippi Delta in the last 8,000 years is the best-known example of this (Frazier, 1967). Autocyclic switching of sediment input points, and the resulting variations in local sedimentation rates, are major factors in the development and preservation of marine facies sequences. For example, transgressive barrier bars may migrate over nonmarine deposits on abandoned delta lobes, while active lobes are forming regressive sheet or distributary sands. Autocyclicity has been treated by geologists as a totally independent factor, but the rate of autocyclic switching is influenced by the other factors mentioned above. During periods of high sediment supply, rapid deltaic progradation occurs, and the basic cause of this autocyclicity (low slopes on lengthened distributaries) results in switching of the sediment input points at increased rates. Autocyclicity is therefore not entirely independent of the major external factors.

One possible criterion for interpretation of the origins of unconformity-bounded sequences is the rate and period of base-level change necessary to create them. A tectonic uplift of 50 m will accomplish the same stratigraphic effects as a 50 m sea-level drop. However, some eustatic fluctuations (Haq et al., 1987) seem to be shorter in period (<3 m.y.), with relatively high amplitudes (100–300 m), compared to episodes of tectonic subsidence as understood from geodynamic models. While many of the concepts of sequence stratigraphy were developed on the premise that eustatic variation is the parameter that most affects the stratigraphy and sedimentology of sedimentary sequences, the ideas and models are still valid when relative sea-level change is considered.

Two fundamentally different types of sequences occur in sediments of all kinds. Unconformity-bounded sequences require a relative base-level drop, a combination of eustatic fall and/or tectonic uplift of the area. These sequences must be differentiated from those that can be generated only by variations in the rate of sediment deposition with uniform or steadily rising base level. A period of reduced sediment supply with ongoing subsidence causes formation of a condensed section, commonly a well-cemented submarine hardground. In many cases, this hardground is overlain by clinoforms that baselap onto it, formed by increased sediment supply to the area during the following relative highstand. The angular relationship between the condensed section and the highstand clinoforms can be mistaken for a low-angle unconformity, particularly in subsurface work. Sequences that are defined by the presence of clinoforms are useful, in many cases, for subdividing rock units, but they have different implications for facies distribution patterns. An erosional sequence boundary requiring a base-level fall may imply incision and a lowstand shoreline deposit seaward on the unconformity. A sequence boundary that requires only variation in sediment supply rate has no such implication; in shoreline facies, it may be reflected only by a transgression and subsequent regression. For example, autocyclicity by itself does not develop unconformity-bounded sequences, only deposional facies sequences. Determination of the types of sequences and their boundaries is therefore extremely important in understanding facies distributions of shallow marine reservoirs.

Facies Architecture of Shallow Marine Sediments

The architecture or geometric organization of shallow marine facies depends on the geometries of the depositional systems and the lateral and vertical movements of the depositional systems that control the formation, preservation, and stacking of sedimentary sequences in the geologic record. Because exploration and development of shallow marine and shoreline reservoirs—generally small, subtle features—requires detailed understanding of their origins, some space will be devoted to development of sequences.

Generation of Sequences

Transgressions, regressions, aggradation, and degradation result from variations in amounts of sediment deposited or eroded and relative sea-level change. From Figure 1.1, the angle of facies migration can be expressed as follows:

$$\tan \theta_p = \Delta\text{RSL} \tan \theta_{nm} / \Delta D_1$$
$$\text{or } \tan \theta_p = \Delta\text{RSL} \tan \theta_{nm} / \Delta\text{Sed}_1 - \Delta\text{RSL}.$$

The angle of facies migration can be described geometrically by the thickness of sediment deposited or eroded, and the relative sea-level rise. The implications of different patterns of movement can be investigated diagrammatically using concepts developed in the 1960s for climbing bedforms (Jopling and Walker, 1968; Allen, 1970); these concepts were first applied to depositional sequences by Larue and Martinez (1989). During transgression or regression of a shoreline, the degree of preservation or erosion of nonmarine, shoreline, and shallow marine sediments depends on the angle of climb of the facies transitions compared to the slopes of the sediment surface in the different environments. The degree of preservation of each facies during migration in any direction can be demonstrated graphically by tracing the outline of the sediment surface and translating it radially outward in that direction. Zones of preserva-

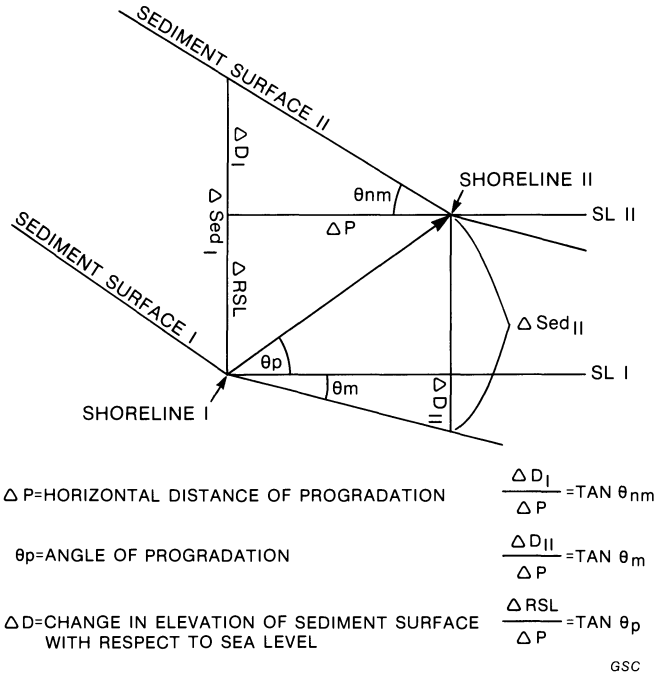

Figure 1.1. Sketch illustrating progradation from SHORELINE I to SHORELINE II. The angle of facies migration depends on the amount of sediment deposited or eroded and the relative sea-level change (eustatic change + subsidence).

tion and erosion can then be delineated, depending on whether the sediment surface moves up or down from the initial profile in the different facies. Because of the curving surfaces, complex patterns of erosion and deposition can occur at certain angles of translation. For this reason, a simplified case, with straight lines approximating the sediment surface (Fig. 1.2) in the marine and nonmarine areas, will be presented first. The complications caused by the concave surfaces will be discussed below.

Shoreline translation into sector A of Figure 1.2, either during regression (facies and slope break move seaward) or transgression (landward movement), causes deposition of both marine and nonmarine sediments. Regression at an angle above the horizontal may explain why ancient shoreline sandstones commonly range up to 30 m in thickness, while modern sandy shorefaces generally extend to less than 15 m depth (see McCubbin, 1982, for examples). A regression to sector B results in erosion of shoreline and shallow marine sediments, with nonmarine deposition above the erosion surface on the former shelf. A transgression or regression into sector C results in erosion of both marine and nonmarine sediments, i.e., formation of an unconformity. Transgression into sector D first causes erosion of nonmarine deposits, then marine deposition, i.e., cutting of a ravinement surface followed by transgressive sedimentation in shallow marine environments.

In a more realistic model of the sediment profile, marine and nonmarine depositional surfaces are concave upward. The upper profile of Figure 1.3 shows directions of four transgressions (A, B, C, D) at different angles compared to environmental slopes. The corresponding profiles below show the initial and final sediment profiles, initial (SL1) and final (SL2) sea levels, depositional facies, and areas of erosion. Because the shoreface is steeper than the lower nonmarine area, transgression at an angle shallower than the shoreface causes formation of a barrier island and a ravinement surface (profile C).

During regressive episodes, similarly complex patterns of erosion and deposition result (Fig. 1.4) because of the laterally varying slope of the sediment surface. This diagram (Fig. 1.4) is organized like Figure 1.3; the upper profile shows directions of shoreline migration compared to slopes on the different environments, and the corresponding sections below show patterns of erosion and deposition. Part C shows a regression with sea-level fall such that an isolated shoreline sandstone sitting on an erosion surface is formed.

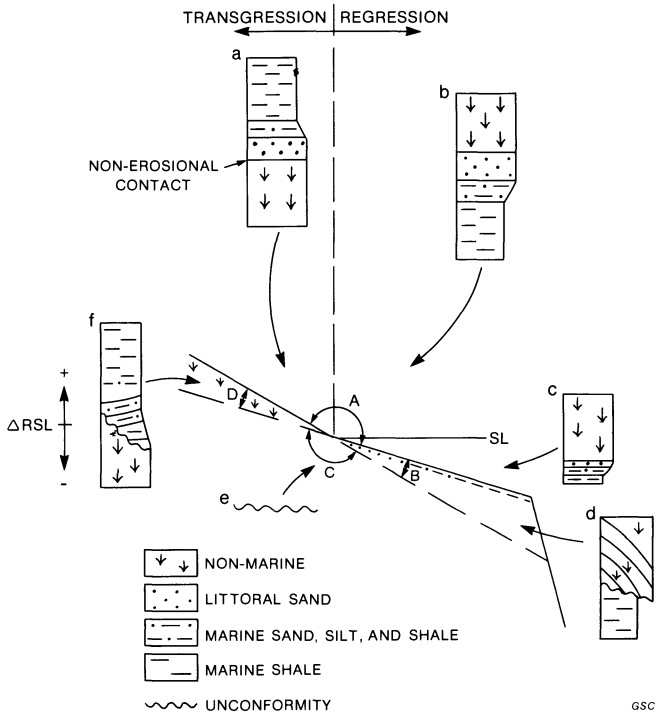

Figure 1.2. Simplified profile of the sediment surface with the nonmarine and marine areas shown as straight lines. Translation of the shoreline into the different sectors "A" through "D" occurs because of variations in sedimentation (Sed) and relative sea level (Sub + E), and results in formation and preservation of the sequences and unconformity shown in sequences a through f. The sequence generated by translation of the shoreline into any area can be determined by tracing an overlay of the profile and moving it into the desired area. The rise or fall of the surface in the different environments indicates preservation or erosion.

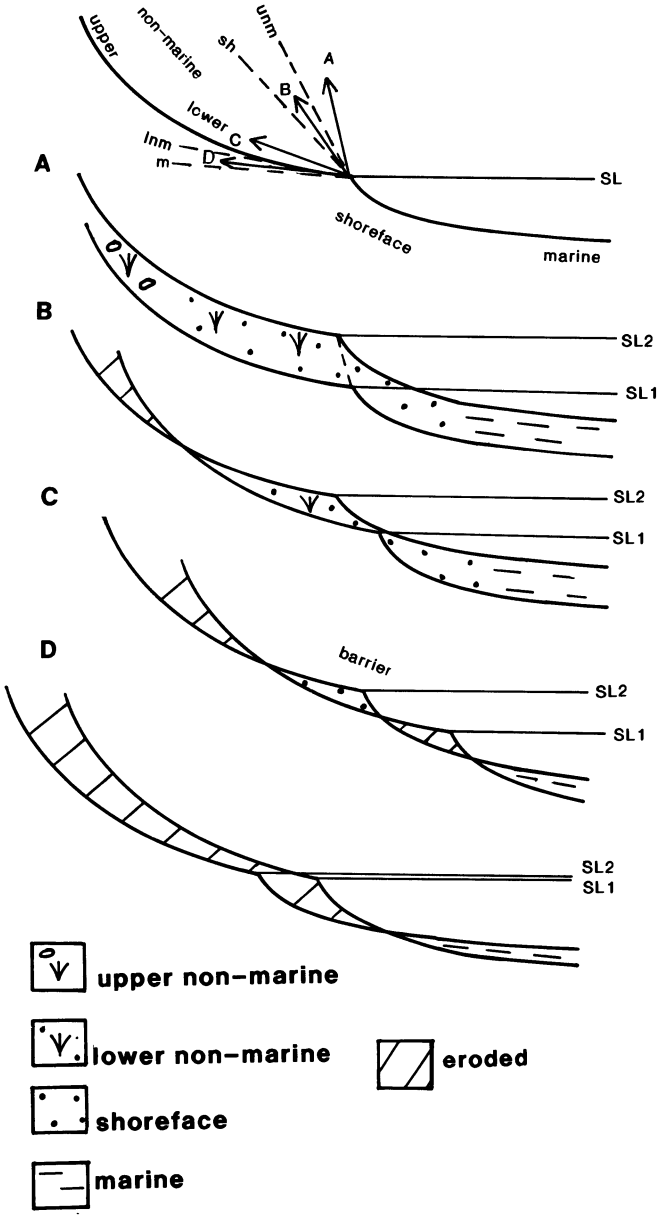

Figure 1.3. Models of transgression. The upper diagram shows transgressive paths (A to D) at different angles compared to the slopes of the sedimentary environments (unm = upper nonmarine; sh = shoreface; lnm = lower nonmarine; m = marine shelf). Initial and final sea levels are indicated. The lower four diagrams show the resulting patterns of erosion and deposition of the corresponding migration path.

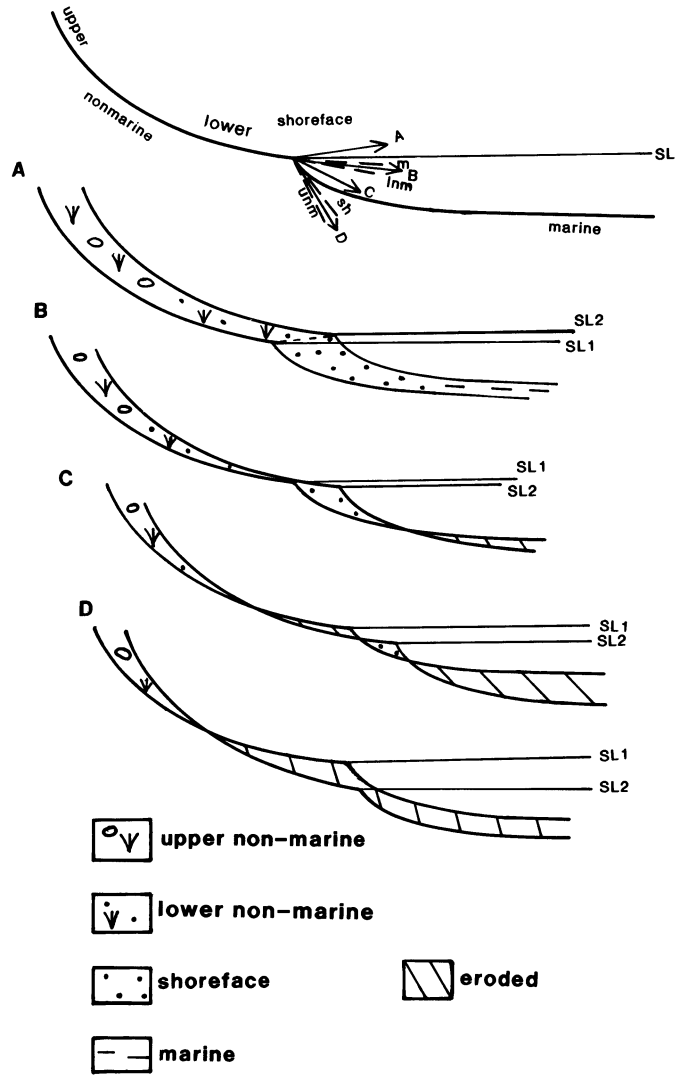

Figure 1.4. Models of regression. Organized similarly to Figure 3, this figure illustrates regression along different paths in the upper profile with the resulting patterns of deposition and erosion in the corresponding profiles below.

If this sand body is transgressed afterward, then it may be covered by marine muds, forming what has been termed an "offshore bar" in the past.

Transgression or regression with downcutting at an angle steeper than the sediment surface anywhere (sector C of Fig. 1.2) creates an unconformity, a Type 1 sequence boundary in the terminology of Mitchum et al. (1977).

Geometries of Shoreline—Shelf Reservoirs

Studies of modern sediments have shown that sands are not transported offshore in large quantities by waves or tides much below fair-weather wave base, which is commonly only a few tens of meters in most cases. Sands do occur on modern shelves at much greater depths, however, separated from the coastal zone by hundreds of kilometers of muddy sediments (e.g., Amos and Knoll, 1987). These sands were transported far onto the shelf during the Pleistocene sea-level lowstand, and are presently relict or being reworked by waves, tides, or marine currents (Amos and Knoll, 1987). In recent years, the role of sea-level fluctuations in formation of "offshore bars," or isolated shelf

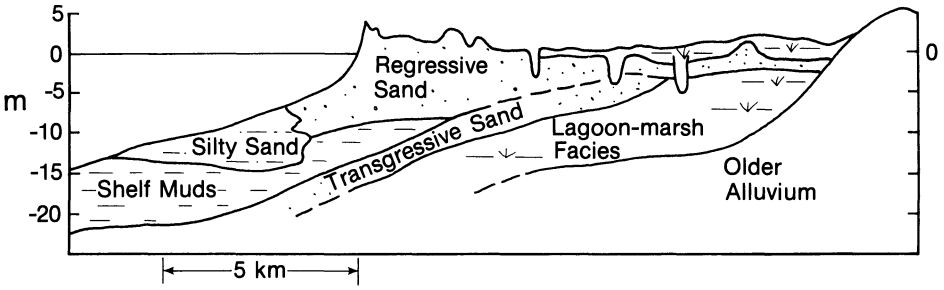

Figure 1.5. High sediment supply rates during the recent period of relatively stable sea level have allowed seaward progradation of this shoreline and initiation of sheet sand development. Modified from Curray et al. (1969).

sandstone bodies, has become appreciated (Weimer, 1984; Cant and Hein, 1986; Bergman and Walker, 1987; Plint and Walker, 1987; Plint, 1988). The quality, geometry, and stratigraphic relationships of shoreline and shallow marine reservoirs therefore depend on the depositional and diagenetic characteristics, sizes, and shapes of coastal sand bodies, their migration paths, and stacking patterns. The following discussion assumes a relatively straight shoreline, the kind that occurs most commonly in wave-dominated situations.

Sandstone thicknesses, distributions, and geometries are controlled by the angle of facies migration relative to depositional slopes as discussed above, as well as the third-dimensional extent of the facies. Modern shoreline sands in many cases extend tens of kilometers along depositional strike. Under stable or gradually rising relative sea level, progradation of this kind of environment generates a laterally extensive sheet sand. A well-documented example of this occurs on the Pacific coast of Mexico, where abundant sand supply to the wave-dominated shore zone has formed a sand body (Curray et al., 1969), which will eventually become an extensive sheet if depositional conditions persist for a long period (Fig. 1.5). Therefore, regression with rising relative sea level (migration path A of Figure 1.4) forms sheet-like, coarsening-upward sand bodies, which may be capped by shoreline facies. The thickness of the sandstone produced depends on the angle of climb of the facies. This type of sandstone body has been documented by many authors as occurring commonly in the ancient record (e.g., Young, 1957; Clifton, 1981; Cant, 1984). Regression at a very low angle (path B, Fig. 1.4) may generate a sharp-based shoreline sandstone sitting directly on marine shales (Fig. 1.6) because of very thin lower shoreface deposits. If the migration path were slightly shallower, along path C of Figure 1.4, its base would be slightly erosional.

With the same rising sea level but lower rates of sediment input, transgressive facies show a greater variety of geometries. As discussed above, the angle of shoreward translation compared to the slope of the shoreface controls the degree of preservation of shoreline facies. The resulting sand bodies may be thin (less than 5 m) sheets of sand (path B,

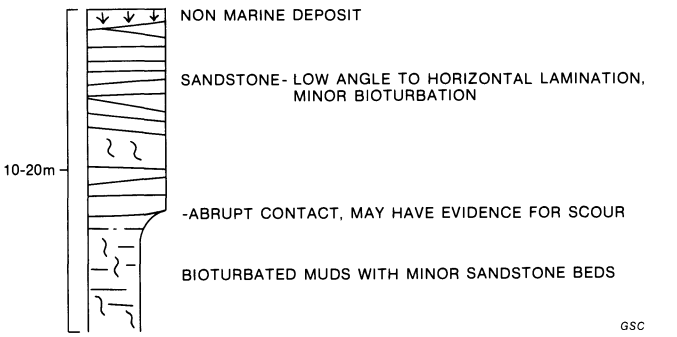

Figure 1.6. A profile of a sharp-based shoreline sand resulting from migration path B in Figure 1.4. If complete truncation of the lower nonmarine facies takes place, migration path C of Figure 1.4 is more appropriate.

Fig. 1.3), patchy remnants of sand, or isolated transgressive barrier deposits 10 to 15 m thick (path C, Fig. 1.3). In some cases, these transgressive barriers preserve the morphology of the original barrier island, as shown by many oil field reservoir studies (McCubbin, 1982). Considerable excellent documentation of the morphology, facies, and preserved record of a modern transgressing barrier has been given by Demarest and Kraft (1987).

A regression with falling sea level (paths B and C, Fig. 1.4), a "forced regression" in one terminology (Van Wagoner, et al., 1987), generates a sequence with a basal unconformity and a sharp-based sand sitting on it. Some modern sand accumulations on modern shelves show sequences of this kind (Amos and Knoll, 1987), but the documentation is sparse because of sampling problems. Ancient examples or what appear to be comparable deposits have been described by Plint (1988). These types of deposits in many cases consist of linear sand bodies deposited during the low sea-level stand as shoreface-to-beach sequences sitting on an erosional surface. These lowstand strandline deposits are commonly localized by a zone of slightly steeper slope on the older sea bottom, which is itself, in some cases, related to deeper structural control. Progradation of most lowstand shorelines appears to have been limited, resulting in relatively narrow (less than a few kilometers) sandstone bodies that may extend tens of kilometers along deposi-

tional strike. Transgression over this kind of deposit may truncate or rework its upper surface, resulting in removal of shoreface and beach facies and making interpretation of the sand body difficult (Plint, 1988). Blanketing with mud during the later transgression or highstand forms classic stratigraphic traps in many basins (McCubbin, 1982; Nielsen and Porter, 1984).

The sequences resulting from the simplified model above may provide a basis for understanding some situations, particularly those involving movements of a linear shoreline. In the real world, of course, the basic assumptions of the shoreline-translation model above (no variation of environmental slopes, no variation in type of sediment, two-dimensionality) may not hold. For example, relative sea-level fall (movement into sectors "B" or "C" of Figure 1.2) commonly results in incision of narrow valleys across shelves, which may be filled by later deposition. Swift (1973) has shown that the Hudson paleovalley, cut during the Pleistocene lowstand, extends across the Atlantic continental shelf. It is filled by estuarine and perhaps shallow marine sediments, because the deepest erosional scour occurred at the mouth of the estuary during the subsequent transgression. This scour translated shoreward at a lower angle than the slope of the low to falling-stage fluvial valley fill, thus largely removing it. The geometries of the estuarine sandstones, therefore, probably reflect the shape of the subaerial valley.

One other major factor that modifies the basic distribution of reservoir facies in shoreline and shallow marine deposits is the location and type of sediment supply. In many cases, coarser facies extend only a short distance from their input point around a deltaic distributary or fluvial channel. If the sediment is supplied by an incised channel cut during a base-level fall, then the marine reservoir facies may be even more laterally restricted. The degree to which marine processes rework and transport sands and gravels depends on the energy of the environment and the size of the sediment. The sediment supply factor can be assessed by integration of facies analysis and mapping of reservoir bodies.

Types of Sequences

The discussion above has considered only simple, unidirectional patterns of change of the major external variables through time. Repeated changes in the variables on different time scales generate more complex types of composite sequences, which have become the focus of modern developments in sequence stratigraphy. Sequences of different scales and ranks have been recognized in outcrops and cores, on well logs, and on multichannel seismic data (Fig. 1.7).

Parasequence: An individual depositional sequence resulting from an episode of migration of sedimentary environments, as discussed above, is termed a parasequence (Fig. 1.7) to distinguish clearly from any type of composite sequence. Individual reservoirs occur on the parasequence level.

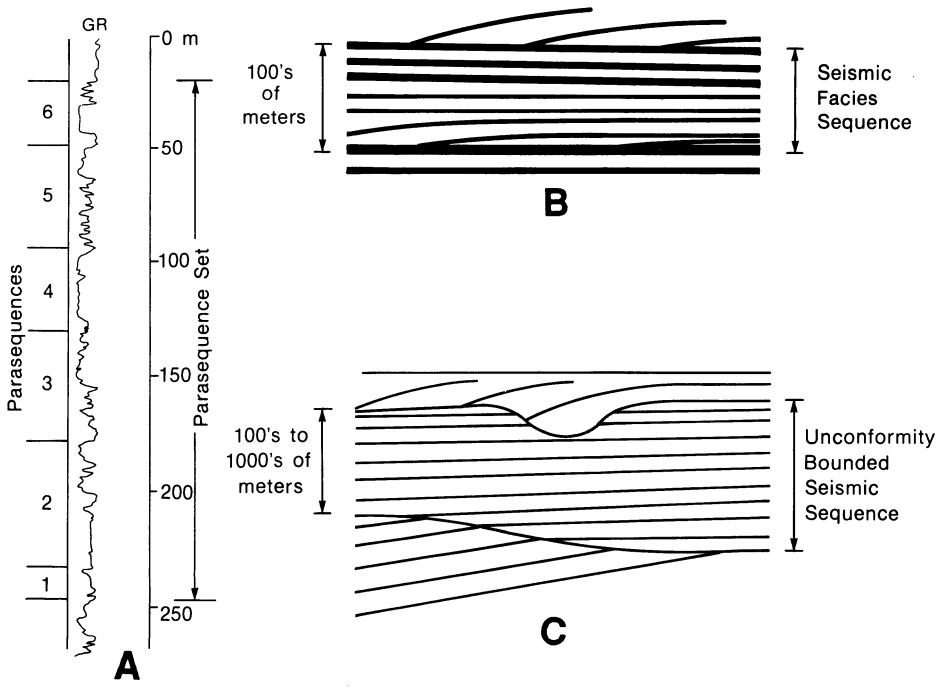

Figure 1.7. Different types of sequences recognized in marine sediments. Part A shows a gamma-ray log with individual coarsening-upward sequences or parasequences marked on the left and a parasequences set on the right. Parts B and C show different definitions of seismic sequences. The unconformity-bounded sequence will be used throughout this chapter.

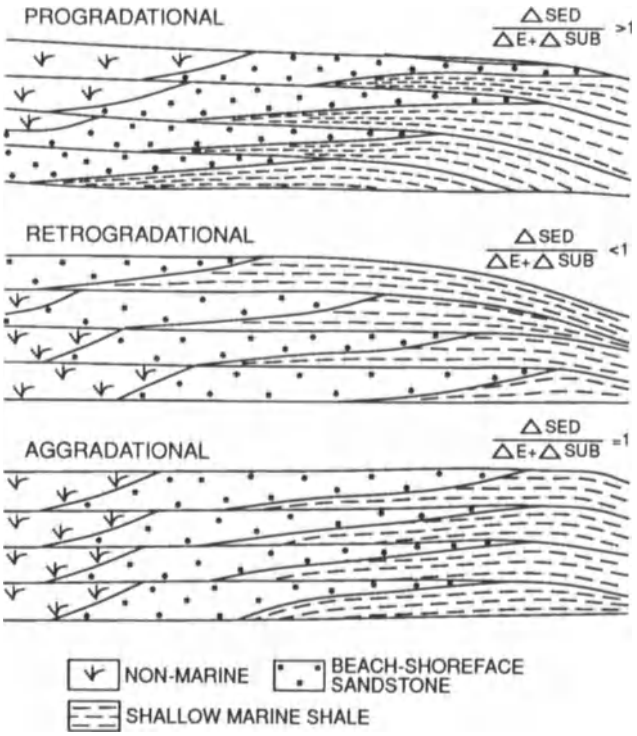

Figure 1.8. Three types of parasequence sets, defined in terms of the stacking patterns of the parasequences. As indicated, the different types are controlled by the ratio between the amount of sedimentation and the relative sea-level change. After Van Wagoner et al. (1987).

Parasequence set: A parasequence set is a succession of genetically related parasequences that have a distinctive stacking pattern (Figs. 1.7, 1.8). Recognized commonly on well logs, they usually either coarsen upward (progradational), show no change (aggradational), or fine upward (retrogradational). Note that this does not mean that the individual parasequences within a retrogradational parasequence set, for example, will necessarily be deposited in transgressive conditions. In most cases, parasequence sets are bounded by major flooding or transgressive surfaces (Van Wagoner et al., 1987), or unconformities.

Unconformity-bounded sequence: The largest-scale sequence is the unconformity-bounded composite sequence (Fig. 1.7) commonly defined on seismic lines, the fundamental unit of seismic sequence stratigraphy (Vail et al., 1977; Mitchum et al., 1977). Formation of an unconformity requires a relative fall in base level, unlike flooding or transgressive surfaces or condensed sections.

Depositional Systems Tracts

These large-scale composite units (Van Wagoner et al., 1987) form an important link between sequences that are controlled by base-level change, and the individual depositional facies sequences that control reservoir distribution. They can be defined and interpreted in the subsurface on the basis of their bounding surfaces (nature and relative extent of transgressions), the stacking pattern of parasequence sets on well logs, and their relationships to erosional sequence boundaries and clinoforms on seismic sections (Fig. 1.9). A correctly interpreted set of depositional systems tracts within unconformity-bounded sequences also allows delineation of the large-scale architecture of the basin fill. Depositional systems tracts have been genetically related to variations in sea level by Van Wagoner et al. (1987), but even if the eustatic origin is not correct in all cases, the generalized lithofacies distributions within them are still valid, and form a necessary link between composite seismic or well log sequences and the individual depositional facies. Highstand and lowstand systems tracts have been named assuming eustasy is the controlling factor (Van Wagoner et al., 1987), but here the nongenetic terms "relative highstand" and "relative lowstand" will be used.

Variations in Proportions of Systems Tracts

While the general pattern of depositional systems tracts shown in Figure 1.9 seems to occur in many different types

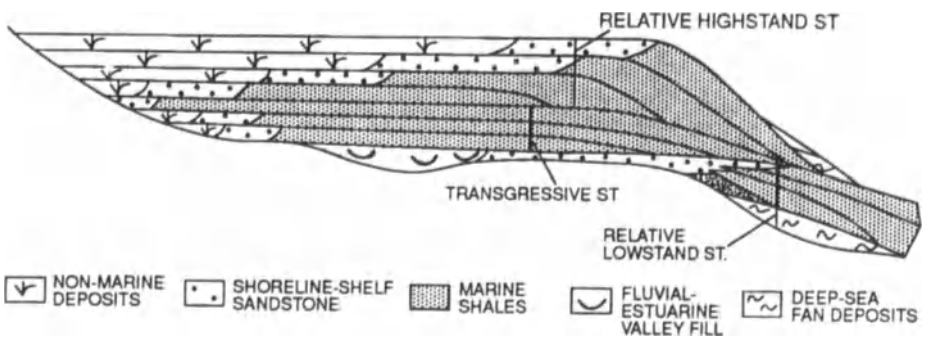

Figure 1.9. The three major types of systems tracts (ST) in the context of an unconformity-bounded sequence. Although developed for large-scale passive margins, this model seems to work well for a variety of different basin types. Differences arise in the proportions of the systems tracts in basins with different tectonic histories. Modified from Van Wagoner et al. (1987).

of basins, the proportion of each systems tract is highly variable. The pre-existing morphology of the basin, as controlled by its tectonic history, is important in the relative development of systems tracts. The general diagram of systems tracts (Fig. 1.9) was developed essentially for large-scale passive margins. Where slopes and deep-water facies are absent, the lowstand systems tract may be very thin and almost unrecognizable.

The distribution and thickness of systems tracts is perhaps most generally controlled by variations in the subsidence and sedimentation rates. For example, the transgressive systems tract (Fig. 1.9) was deposited because average rates of subsidence exceeded average rates of sedimentation after base level began to rise. If sedimentation occurs at very low rates, the transgressive systems tract may be quite thin, and deep-water conditions may develop. If rates are nearly balanced and slow, thick transgressive deposits may accumulate if the situation persists long enough. If rates are nearly balanced and high, a thick transgressive systems tract can develop in a short time interval. These variations are probably controlled by eustasy in some cases, but generally, the tectonic evolution of the basin controls the rates of subsidence and sedimentation (Beaumont, 1981), at least on a large scale.

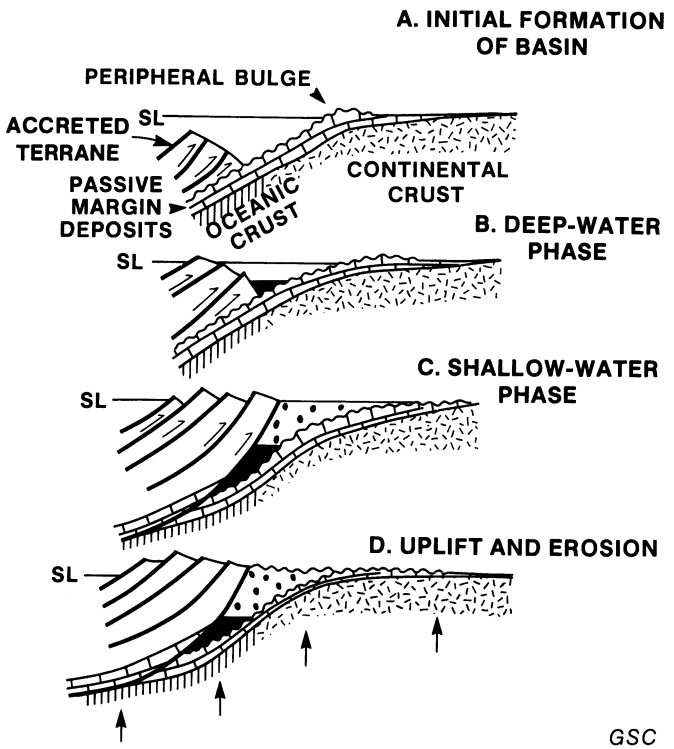

Figure 1.10. Development of an unconformity-bounded foreland basin sequence. A. Migration of a peripheral bulge in front of the basin uplifts shallow-water sediments cutting an unconformity. Little sediment is supplied because accretion initially takes place on the continental slope in deep water. B. Ongoing thrusting pushes part of the orogen above sea level, supplying sediment to the deep basin (flysch phase). C. Rapid sedimentation fills the basin to sea level and above (molasse phase). D. With the end of convergence, erosion lightens the load, the basin rebounds, and another unconformity is cut. From Cant and Stockmal (1989).

Foreland Basin Examples

In foreland basins, episodes of basin subsidence are caused by thrusting in the associated orogen, which loads the lithosphere and also creates the topography that supplies the sediment (Price, 1973; Beaumont, 1981). Cant and Stockmal (1989) analyzed the stratigraphy of foreland basins in terms of a theoretical sequence that results from a single episode of terrane accretion, lithospheric loading, foreland depression, and uplift of sediment sources (Fig. 1.10). Migration of a flexural bulge ahead of the depression causes uplift and erosion of the pre-existing shallow-water passive-margin sediments. Early in the process, accretion takes place on a continental slope, so little topographic relief is built above sea level and little sediment is shed into the subsiding foreland. Deep-water conditions develop in the basin initially, but as thrusting proceeds above sea level, great volumes of sediment are shed rapidly, first in deep water, then in shallow water, as the basin fills. This is the classic flysch-to-molasse sequence of Alpine foreland basins, also described from a Pleistocene foreland by Covey (1987) and a modern one by Crook (1989). After thrusting ceases, erosion removes some of the load from the lithosphere, and the basin is partly uplifted, resulting in erosion of the top of the fill. The resulting sequence is unconformity bounded above and below, shallows upward from deeper marine to shallow marine sediments, and is capped by nonmarine deposits. The fundamental control on the systems tract development is the time lag between the onset of relatively high rates of subsidence and high rates of sedimentation. This delay resulted in development of what are probably deep-water relative lowstand deposits in the flysch (Caron et al., 1989), succeeded by transgressive and relative highstand deposits in the molasse. Systems tracts in the molasse have been related to eustatic variation in some cases (Homewood et al., 1986).

Where multiple accretion events occur on a continental margin, the later sequences differ, because terrane accretion does not take place onto the continental slope. Later terranes push the earlier ones farther inboard, with sediment supply established almost as quickly as subsidence. Deeper marine deposits therefore may be absent from later clastic wedges. Some of the later clastic wedges show a much-reduced time lag effect, interpretable from the sys-

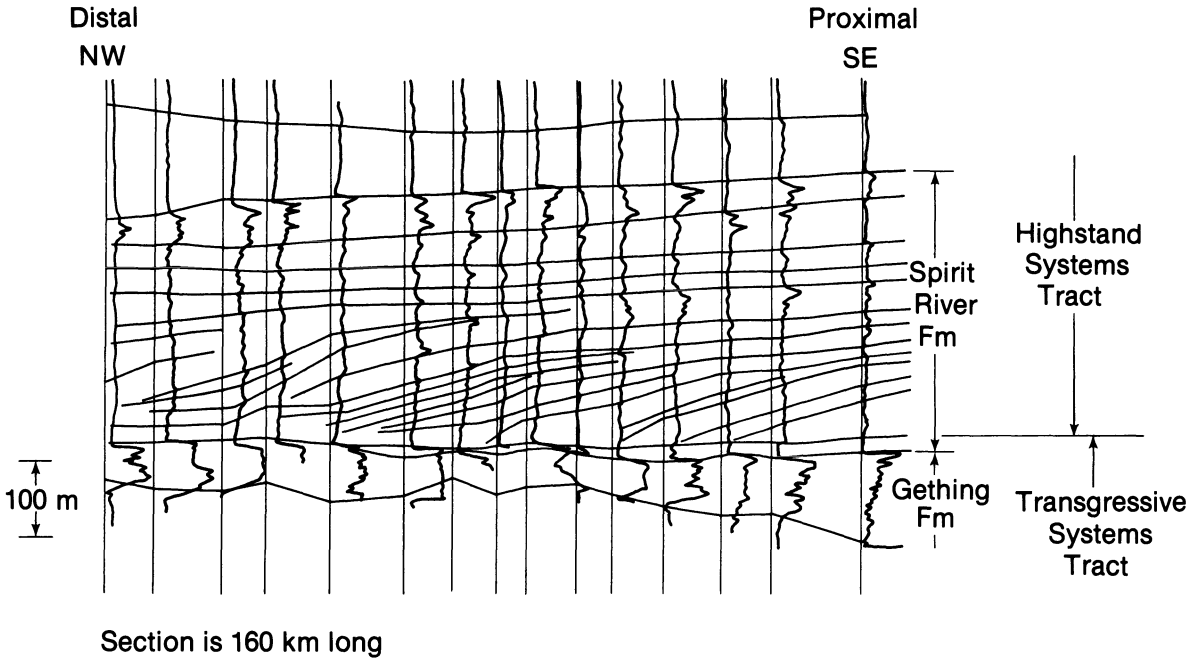

Figure 1.11. A well log cross-section of the Mannville clastic wedge showing transgressive and relative highstand systems tracts. Shoreline deposits backstepped toward the nonmarine area through the Gething Fm until the transgression abruptly swept several hundred kilometers southeastward. In the Spirit River Fm, small-scale depositional sequences baselap seaward onto the condensed section, a typical configuration for a relative-highstand systems tract. Modified from Mitchum et al. (1977).

tems tracts developed in them. The second major clastic wedge in the Alberta foreland basin sits on the sub-Cretaceous unconformity. The Lower and Middle Mannville (Fig. 1.11) make up a transgressive systems tract, comprising shallow marine, marginal marine, and non-marine facies. The shoreline deposits backstep southward, forming transgressive shorelines and estuaries, while the nonmarine Gething Fm was being deposited over much of the basin. The rate of transgression increased markedly as the shoreline moved abruptly southward at the peak of the transgression. When rates of sedimentation increased and began to exceed rates of subsidence, the relative highstand Upper Mannville (Spirit River Fm) formed a series of northward-prograding clinoforms. This clastic wedge resembles the foreland-basin sequence model proposed by Devlin et al. (1990) for the Wyoming foreland. The extent of time-lag effect between subsidence and sedimentation is believed to be the controlling factor in determining the types, thicknesses, and facies of the depositional systems tracts. The time lag itself is interpreted to result from the tectonic development of the basin. In other cases, eustatic variation can also markedly affect the distributions and thicknesses of depositional systems tracts. In the next section, examples from the Mannville clastic wedge will be used to describe the systems in more detail.

Examples of Shallow Marine Reservoirs

The remainder of the chapter consists of examples of shallow marine reservoirs discussed in the context of the systems tracts. Details of the stratigraphy and sedimentology will not be presented; rather, the distribution and geometry of lithologic units will be emphasized.

One complicating factor with the utilization of the systems tract concept should also be mentioned. Systems tracts are necessarily considered in a hierarchical arrangement, because each can commonly be subdivided further on a more detailed scale. Multichannel seismic data cannot resolve stratigraphic sequences on the same scale as well log cross-sections, which do not show stratigraphic details obtainable from some large outcrops. Higher-order, but thinner sequences with their own systems tracts may occur within a larger-scale sequence. The degree of stratigraphic subdivision or predictability of reservoir facies distribution achievable utilizing the systems tract concept does depend on the scale of observation.

Relative lowstand systems tracts: Lowstand systems tracts lap onto the slopes of passive continental margins when sea level drops below the shelf break. In these large-scale cases, the resulting deposits are commonly coarse deep-sea fans, sometimes with lowstand shoreline sandstones on the upper

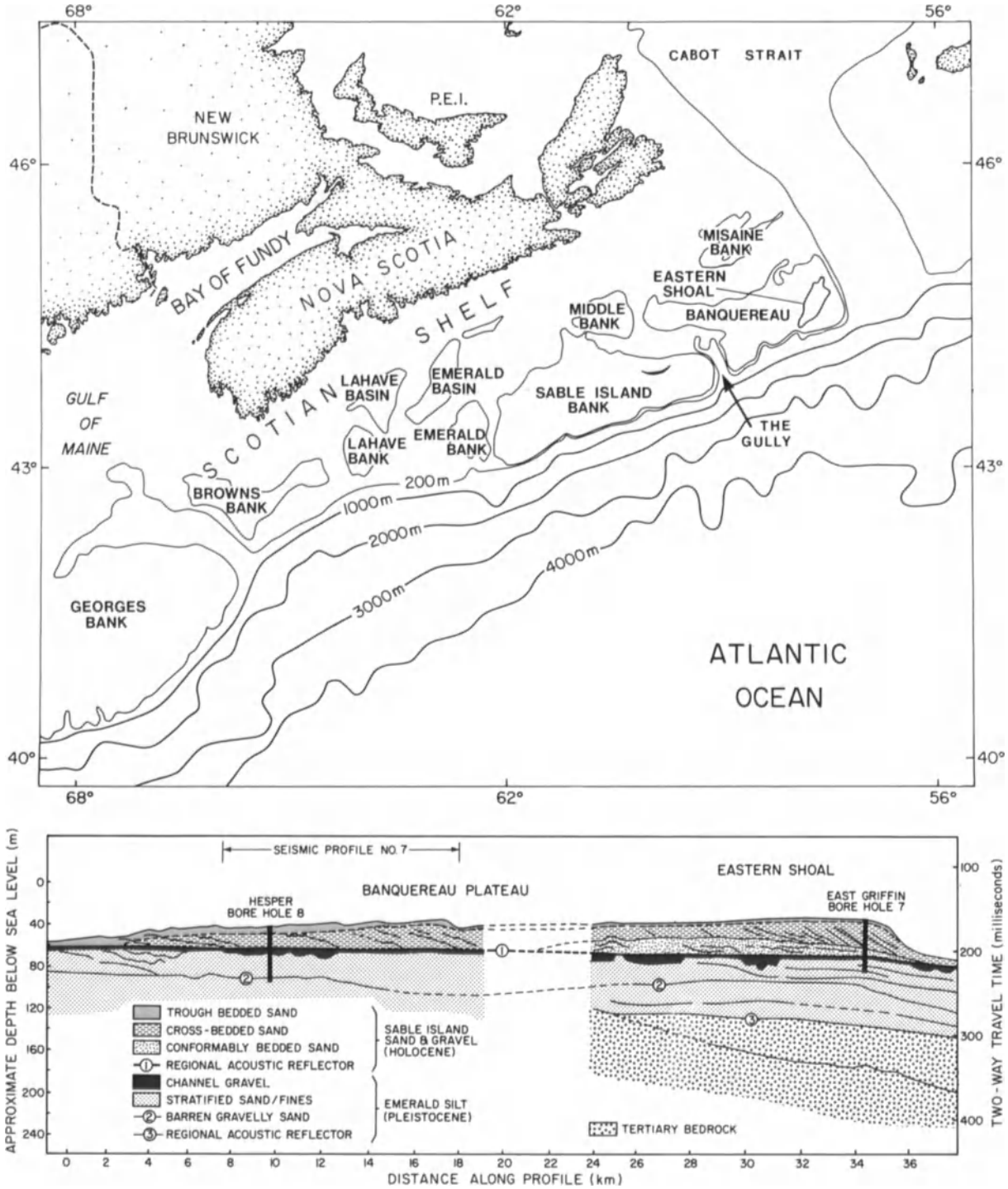

Figure 1.12. Outer-shelf sand bodies on the modern Scotian Shelf (Browns Bank, LaHave Bank, Emerald Bank, Banquereau Bank, Eastern Shoal, Misane Bank), with an interpreted high-resolution single-channel seismic line underneath. The sands were transported across the shelf during the Pleistocene lowstand when channels were cut, and are presently being reworked in the transgressive shelf environment. From *Geological Society of America Bulletin*, v. 98, Amos. C. L., and Knoll. R. G. (1987).

slope. In higher-order, thinner sequences, or in basins without continental-margin relief, the depositional slopes are low in amplitude, on the order of tens of meters. Lowstand wedges deposited upon these are not deep-water facies, but consist of shoreface to nonmarine deposits. In many cases, these sit on short-period unconformities cut into marine shales, forming "shelf" sand bodies. This process is similar to the erosion followed by shoreline deposition shown in path C of Figure 4. The deposition of lowstand shoreline sandstones is associated with incision of valleys into nonmarine and marginal marine areas (Weimer, 1984).

This general process of the formation of shelf sand bodies during a relative sea-level drop and subsequent rise can be illustrated from modern shelves. During the Pleistocene lowstand, coarse sediment was carried to the edge of the shelf by glacial and periglacial processes. During the subsequent sea-level rise, much of this material was reworked into isolated sand bodies on the outer shelves, separated from the shoreline by muddy basins. One of the best examples of this occurs on the Scotian Shelf of eastern Canada, where Sable Bank and Banquereau Bank form part of a line of shelf-edge sand bodies (Fig. 1.12). Most of the sediment of these banks was transported across the shelf during Pleistocene times (Amos and Knoll, 1987), when a maximum sea-level drop of about 110 m occurred. The surface resulting from the drop shows major channels filled by gravel (Fig. 1.12). An erosion surface was cut during the transgression at the beginning of the Holocene, upon which reworking of older material created the shelf sands that are being transported presently by waves and tides on the banks. Some disagreement exists between workers as to the identification of the transgressive unconformity, but most agree on the overall interpretation of a reworked glacial and periglacial deposit because of Pleistocene eustatic fluctuations.

These kinds of lowstand shoreline deposits on shelves generally form sharp-based sandstone or conglomeratic shoreline deposits (migration path C of Fig. 1.4, or Fig. 1.6), which may be capped by non-marine deposits. These kinds of facies sequences occur in a complex situation in the Cardium Fm of Alberta. As documented in many publications, up to seven erosion surfaces were cut, many of which have lowstand shoreline reservoir conglomerates deposited upon them. The complex stratigraphy is well documented by Bergman and Walker (1987) and Plint et al. (1987).

Marginal marine and nonmarine lowstand deposits may be modified during the subsequent transgression over them. In the Cardium and Viking Fms of Alberta, reworking of the tops of the sand bodies has superimposed tidal and other marine sedimentary structures and textures and obliterated all shoreline and nonmarine indicators. This, combined with their position in the shale basin, has resulted in these lowstand and transgressive deposits being termed

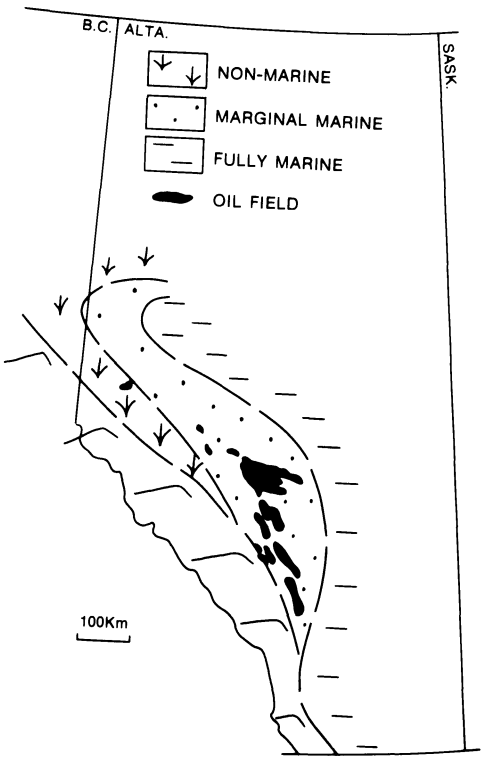

Figure 1.13. A map of Cardium oilfields in western Canada showing their different morphologies and gross depositional facies. Some of the large fields can be interpreted as low-stand deltas or transgressively reworked deltas. The very linear fields can be interpreted as low-stand barriers or transgressive tidal-current ridges. The eastward curve of the facies belt at its north end has been questioned recently.

"offshore bars" in the past, but a relative sea-level fall is now recognized as necessary for their formation. Some lowstand reservoirs seem to be totally reworked during the transgression, but others retain what could be interpreted as their lowstand morphologies (Fig. 1.13).

Transgressive systems tracts: When relative sea level rises, an ongoing supply of sediment causes deposition in transgressive systems. As discussed above, this does not necessarily mean that individual parasequences are necessarily transgressive. Seismic-scale examples are composite, made up of one or more retrogradational parasequence sets (Fig. 1.9) on top of the sequence boundary, or if present, on top of the lowstand systems tract. In outcrop or well-log-scale examples, transgressive systems tracts may consist of single parasequences.

The Mannville clastic wedge of the Alberta Basin shows well-developed transgressive systems in the Lower to Middle Mannville (Figs. 1.11, 1.14). On top of a long-period tectonic unconformity, the nonmarine Lower Mannville consists mostly of meandering-stream sandstones and shales, along with coals. These rocks grade northward into shallow-marine sediments; the transition shows retrograda-

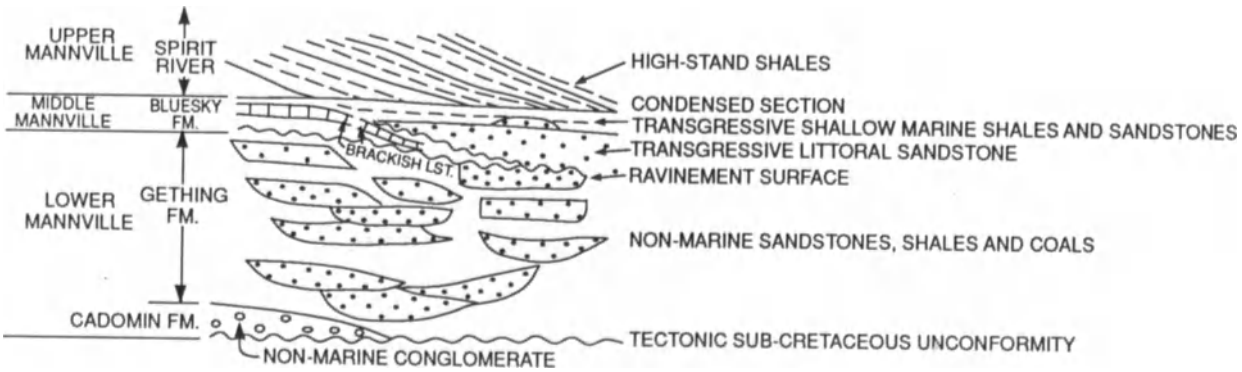

Figure 1.14. More detailed stratigraphy of part of the Mannville Group, showing the nonmarine Lower Mannville, the marginal marine Middle Mannville, and the deeper marine (but still shelf depth) Upper Mannville. The nonmarine Gething is interpreted as the basal part of the transgressive systems tract because of the retrogradation of the shoreline in this unit. The ravinement surface was cut as the shoreline transgressed. Ongoing sediment supply during the transgression generated the littoral Bluesky Sandstone, the restricted marine carbonates, and some shallow marine shale. Upper Mannville shales clinoform onto the top of this unit.

tion with increasing stratigraphic elevation. In many places, the nonmarine deposits can be traced into thick estuarine sandstones, characteristic of many transgressive shorelines. In Middle Mannville time, the distance of transgression increased markedly, reaching hundreds of kilometers south to the U.S. border. The shoreline-to-marginal marine Bluesky Fm overlays the nonmarine deposits, forming a thin, irregular sheet over much of the basin. These transgressive sands are deposits of beaches, barrier bars or islands, and tidally reworked sand ridges. Where the shoreline sands sit directly on top of the nonmarine deposits, they have a sharp base, probably reflecting a minor disconformity or ravinement surface (path C, Fig. 1.3). Later truncation and reworking of the shoreline sand during the transgression has resulted in areas in northern Alberta where "offshore bars" are preserved.

Overlying the shoreline deposits are marine shales that exhibit high radioactivity. Cross-sections of this interval

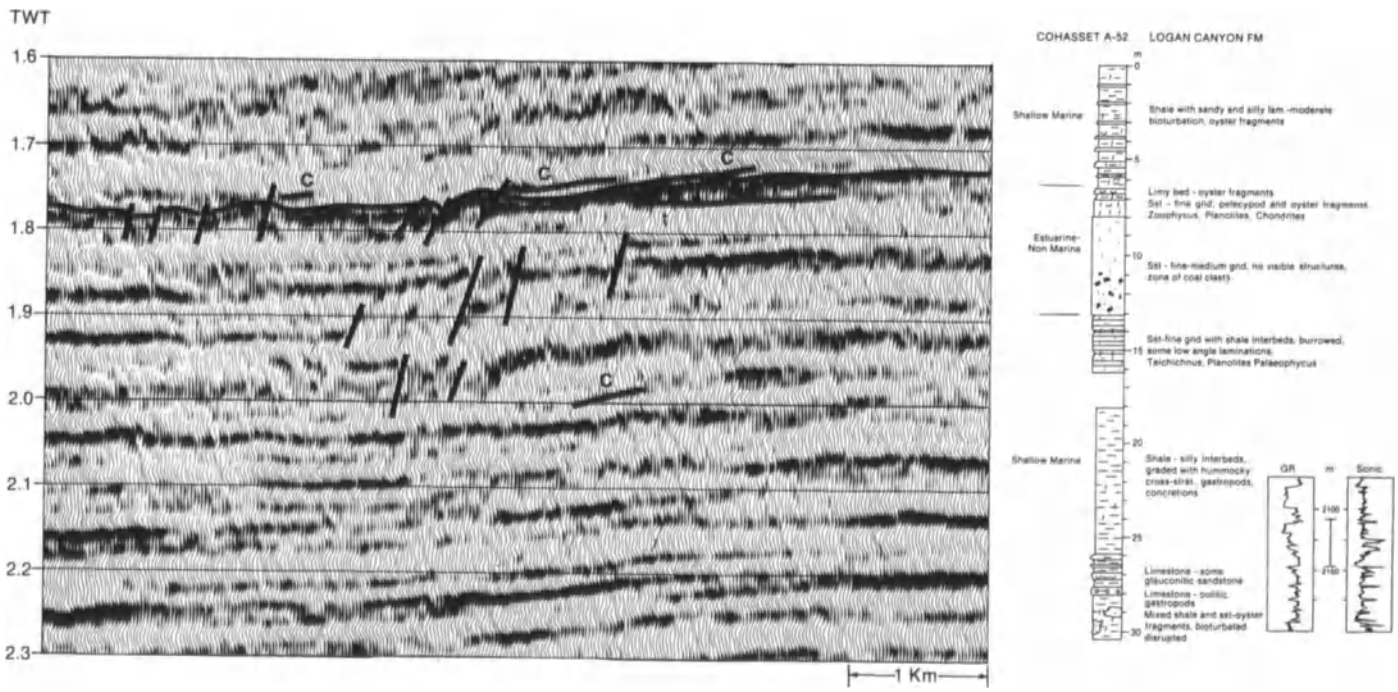

Figure 1.15. A core with gamma-ray log from the Logan Canyon Fm, and the seismic expression of the unit (1.8 to 2.2 sec). The sand body has a sharp base and top, and appears erosive in the core. The seismic line shows reflections with irregular amplitudes, depths, minor clinoforms, and faults. No amplitude or frequency sequences are developed. Cohasset A-52 occurs off this line, but in the same unit.

show that at least some of these shales occur in the same transgressive unit (Figs. 1.11, 1.14) as the shoreline deposits, as defined by clinoforms that baselap onto them (Mitchum et al., 1977). Recent work has shown that these shales contain shallow-water and nonmarine microfossils (D. Leckie, personal communication, 1988) and are therefore part of the transgressive systems tract.

In southern Alberta, the transgressive sandstones pinch out, probably onto a ravinement surface. The brackish-water transgressive shales are interbedded with marginal marine limestones of the Ostracod Zone and Calcareous Member (Fig. 14). These carbonates and the associated shales were probably deposited where sea water invaded estuaries, bays, and lagoons ahead of shoreline migration, a so-called brackish transgression.

On a larger scale, transgressive systems may be composite and much thicker than those just described. On the Scotian Shelf, the Albian to Cenomanain Logan Canyon Fm consists of very shaly, coarsening-upward parasequences, which are organized into retrogradational parasequence sets. The upper units are capped by chalks, deposited during times of almost complete lack of clastic input. The shales display small, laterally impersistent clinoforms, indicating minor relative highstands, and contain neritic microfaunas. Sharp-based interbedded sandstones display sharp, erosive bases in cores (Fig. 1.15), coal clasts, and bioturbation in their upper parts. They are interpretable as estuarine to shallow marine transgressive sands deposited during the relative sea-level rise. No sequences are apparent on seismic lines through the interval (Fig. 1.15). Some of the lateral irregularities along reflections in this figure are interpreted to result from irregular scouring at the bases of these sandstone beds. Plint (1988) has described complexly interbedded estuarine and shelf deposits from the Eocene Hampshire Basin in England (Fig. 1.16). In both the Logan Canyon and the Hampshire Basin examples, the sandstones sit on minor erosion or incision surfaces cut during the lowstands. It is not clear in all cases whether the erosional sur-

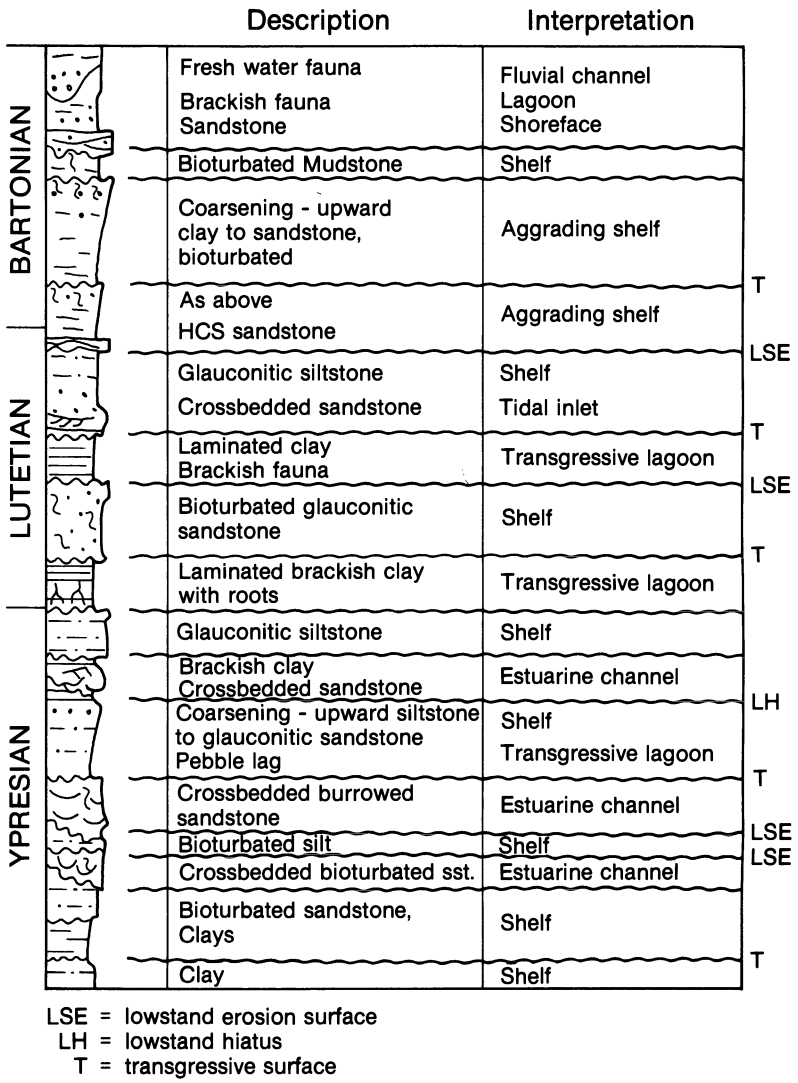

Figure 1.16. Toward the edge of a basin, sea-level fluctuations are represented by interbedded shelf, shoreline, and lagoon/estuary deposits (where preserved). Most of the deposits here can be regarded as part of the transgressive systems tract. Modified from Plint (1988).

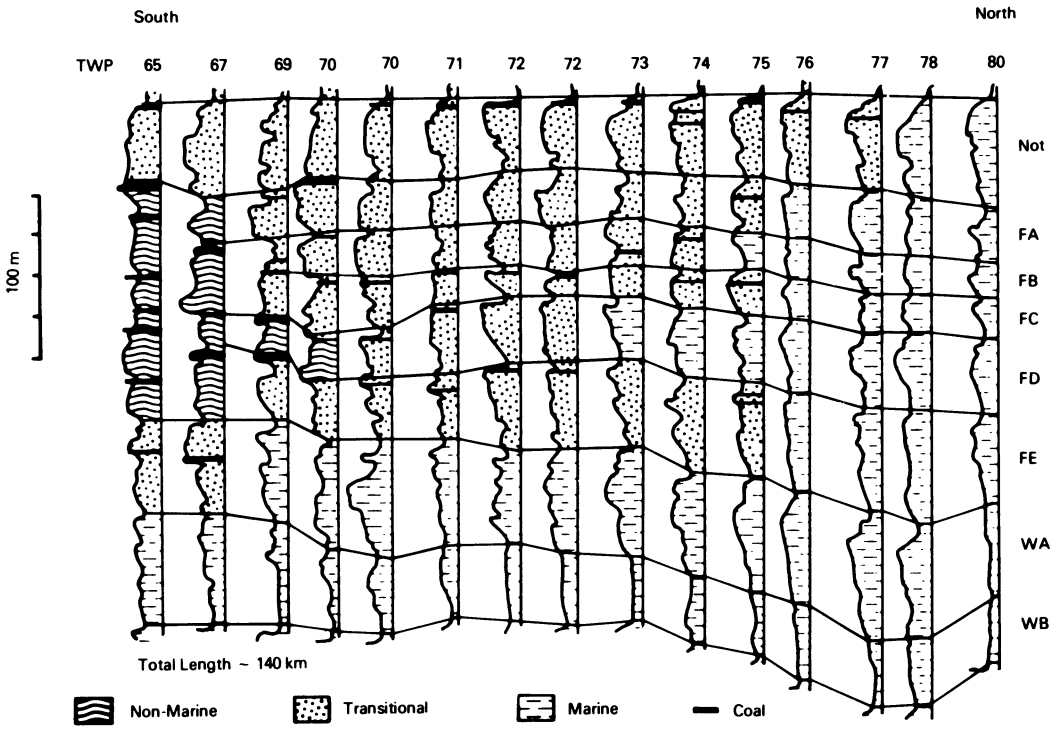

Figure 1.17. A gamma-ray log cross-section of the Upper Mannville (Spirit River Fm) with depositional environments indicated. The Upper Mannville is a parasequence set comprising 8 parasequences. Sediment transport was south to north. Farther south in the nonmarine area, or much farther north in the shaly equivalents, no parasequences can be detected in the unit. From Cant (1984).

face is flat or not, but the estuarine sands definitely sit in channels in the Hampshire case. Linear estuary fills up to 30 m deep cut into shoreline and nonmarine deposits are a common transgressive facies in many areas (e.g., Wood and Hopkins, 1989).

Other transgressive systems tracts differ from those described in that they completely lack parasequence sets, at least on the most common scale. The Cape Sebastian Sandstone of Oregon (Campanian-Maastrichtian) consists of 200 m of transgressive sandstone overlying an erosion surface (Bourgeois, 1980). The Gog Sandstone (Cambrian) is 800 m thick, overlies a minor unconformity, and is capped by a limestone (Hein, 1987; Cant and Hein, 1986). Both units appear to lack parasequences or regressive depositional sequences; however, in each case, if the units could be traced seaward far enough, parasequences might become apparent (D. James, personal communication, 1988).

Relative highstand systems tracts: These systems tracts occur in the upper parts of sequences (Fig. 1.9) when rates of sedimentation have outstripped subsidence. In western Alberta, the Upper Mannville unit is a relatively simple highstand tract (Figs. 1.11, 1.14), in that it consists of a single progradational parasequence set (the Spirit River Fm), which advanced longitudinally along the basin to the north. Each of the 8 widely correlatable parasequences coarsens upward from marine shales to marine or shoreline sandstones (Fig. 1.17). Because of variations in the rate of thrusting, the parasequences have been interpreted to result from variations in the sedimentation rate (Cant, 1984; Leckie, 1986). None of these parasequences have significant erosion associated with them; an appropriate model for preservation of the shoreline facies is migration path A of Figure 1.4. Over most of the basin, the basal pair of parasequences are largely marine and dominantly shaly (Leckie and Walker, 1982), while the upper parasequences contain shoreline and nonmarine deposits (Fig. 1.17). Because of the excellent well control in the unit, it can be shown that the sandstones are sheet-like and extensive in all directions. Individual parasequences show minor internal markers that downlap onto the basal transgressive surfaces (Cant, 1984), which are therefore condensed sections (Fig. 1.18). On a larger scale, farther north, the lower parasequences baselap onto transgressive shales and sandstones below (Mitchum et al., 1977), forming large clinoforms and a condensed section (Fig. 1.11) characteristic of the lowest parts of relative high-stand systems tracts (Van Wagoner et al., 1987).

The upper parasequences are much coarser, with shelf and shoreline sandstones deposited by wave and tidal processes (Leckie and Walker, 1982). The shelf sandstones are attached to the shoreline sands, forming continuous sheets that extend some 90 km beyond the maximum shoreline regression before they grade into shale. Some of the upper

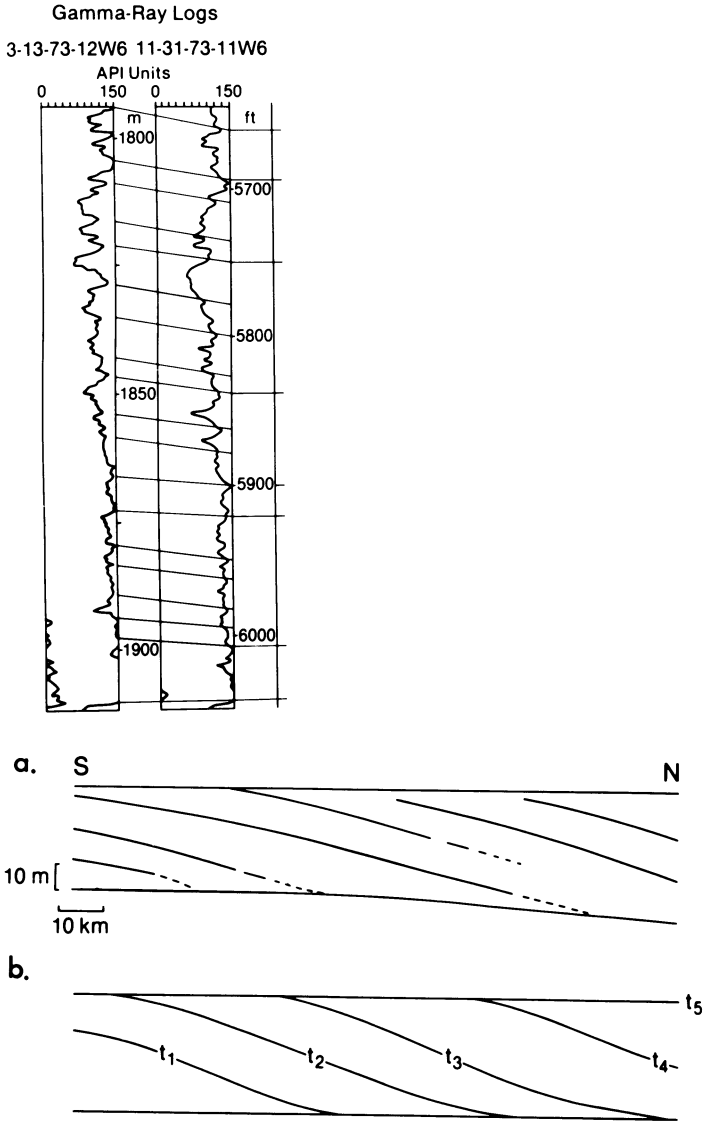

Figure 1.18. Gamma-ray logs from the two basal parasequences of the Spirit River Fm, showing correlations of minor sequences and markers. Below, a tracing of the baselapping correlation lines in one parasequence (a) and their interpretation as time lines (b). From Cant (1984).

parasequences contain chert-pebble conglomerates (Cant, 1984), formed on beaches and at river mouths discharging onto beaches (Cant, 1984; Rahmani, 1984). In places, the conglomerates pinch out abruptly into sandstones along the shoreline trend, indicating that granules and pebbles were not transported far by littoral processes. At the base of one parasequence, a thin (less than 5 m), irregular transgressive conglomerate and sandstone unit is preserved. Regionally, all conglomerates grade laterally into sandstones eastward away from the orogenic belt (Rahmani, 1984). These shoreline conglomerates are highly porous and permeable, forming the principal reservoir rocks of the giant Elmworth gas field (Masters, 1984).

The sequence labelled FC on Figure 1.17 thickens seaward at Township 73, and develops a sharp base. These anomalous features suggest that a minor sea-level drop affected this shoreline, creating a situation similar to migration path B on Figure 1.4, a forced regression. This illustrates that minor erosion surfaces reflecting smaller (higher order) base-level changes may occur within a highstand systems tract.

The Barremian to Aptian Upper Missisauga Fm of the Scotian Shelf of eastern Canada is similar, in that it is also composed of a series of transgressive-regressive sequences, organized into progradational parasequence sets (Fig. 1.7). Relative sea-level rise has caused stacking of tidal channel sands or lagoonal sands on top of the shoreline deposits, resulting in continuous sandstones up to 130 m thick (Fig. 1.19). The major flooding or transgressive surface on top of most parasequence sets is marked by an oolitic limestone sheet laid down during the transgression. In this case, the absence of clastics allowed carbonate deposition, forming the best seismic reflectors in this part of the basin fill (Fig. 1.20). As in the case of the Spirit River Fm, eustatic effects are difficult to recognize, probably because of high subsidence and deposition rates. The distributions of shallow marine and shoreline sandstones and conglomerates are similar in the Missisauga and Spirit River Fms. As shown in Figure 1.9, coarser facies are concentrated initially in proximal areas of the basin, but spread basinward because of large amounts of progradation.

When basins receive small quantities of coarse sediment, marine shales and carbonates make up most of the relative highstand deposits. On the Scotian Shelf, these are best shown by the Paleocene Banquereau Fm (Hardy, 1975), which has large clinoforms composed of silty mudstones (Fig. 1.21) that contain outer neritic microfossil assemblages. The clinoforms are up to about 80 m thick, and the basal set downlaps onto the Wyandot chalk, deposited at the maximum extent of the Logan Canyon transgression discussed above. In places, the clinoforms show rotational faults (Fig. 1.21), reflecting the kinds of gravitational failures that affect modern continental slopes (Coleman and Prior, 1982). Because of the low rates of coarse sediment input, no reservoir facies are developed in these deposits.

Conclusions

The setting of shallow marine reservoirs, both stratigraphically and paleogeographically, can best be understood in terms of depositional sequences of different scales and types, as well as bounding unconformities. In progradational parasequences, most sandstone reservoirs are laterally extensive and sheet-like in geometry, grading off seaward into marine shales. In the same situation, conglomerate reservoirs are much more restricted because of the limited trans-

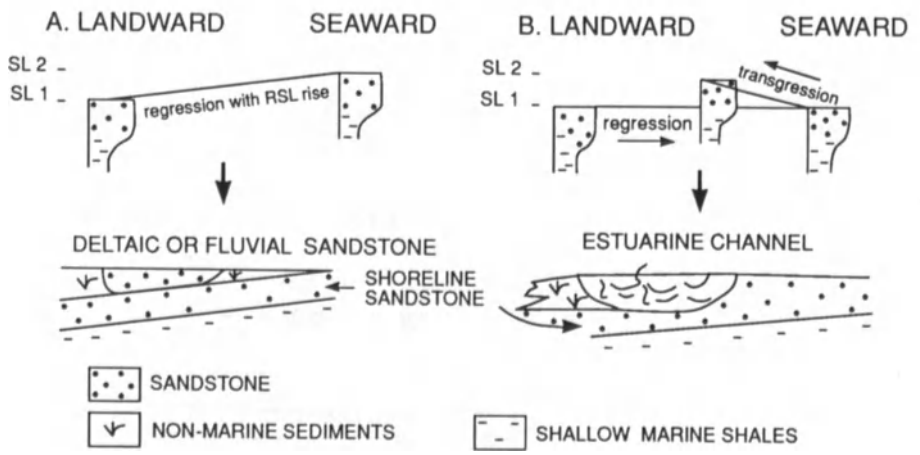

Figure 1.19. Two ways in which sandstones can be stacked up on shoreline deposits. Part A shows regression with major amounts of subsidence, resulting in deltaic or fluvial sandstones on top of the littoral sandstone. Part B shows a minor transgression, which promotes formation of estuaries, lagoons, barrier islands, and tidal channels. Sediment supply variations, therefore, cause great differences in the types of sand bodies preserved.

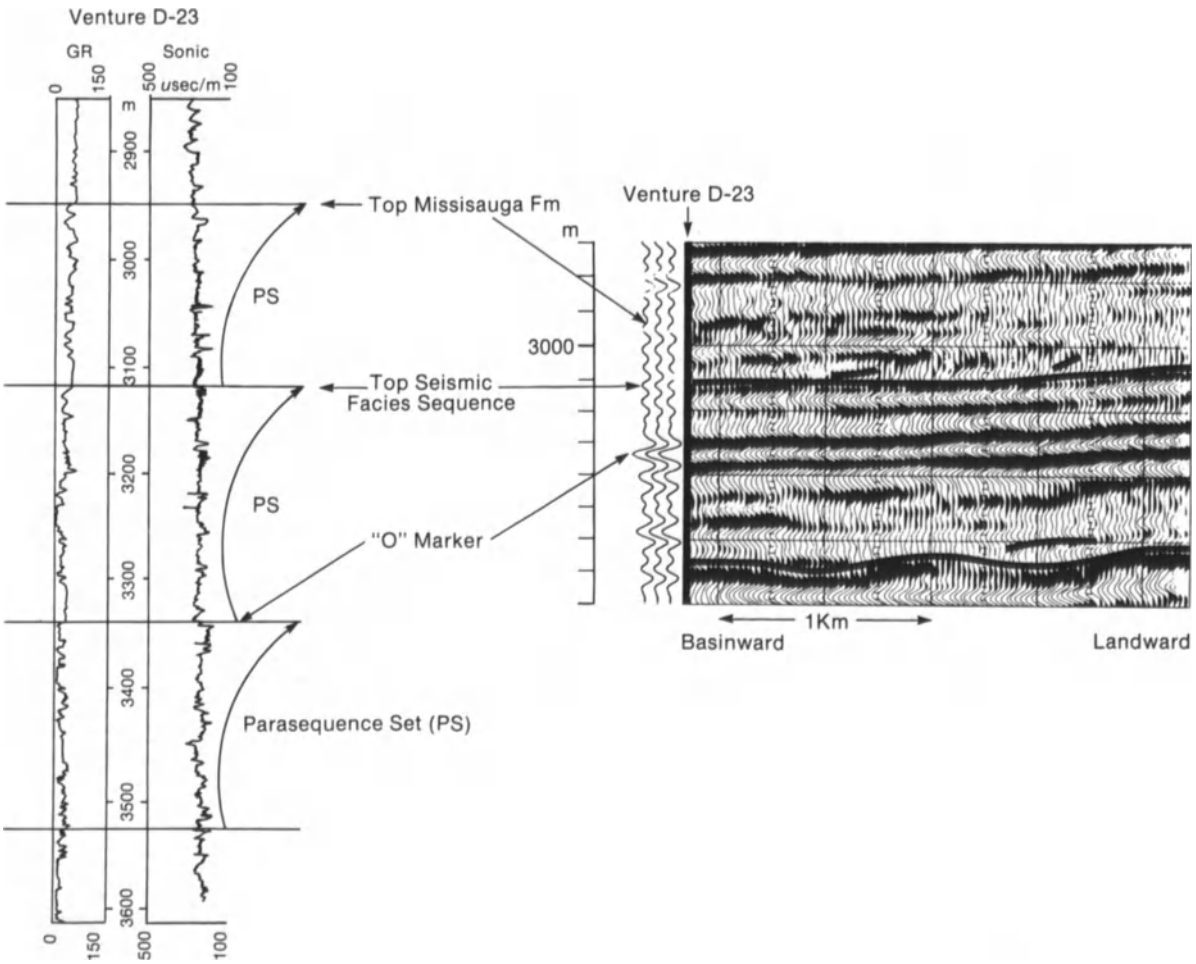

Figure 1.20. Coarsening-upward parasequence sets from the Upper Missisauga Fm of the Scotian Shelf, eastern Canada. They are capped by high-velocity carbonate beds, of which the "O" Marker is the most widespread seismic marker in the basin.

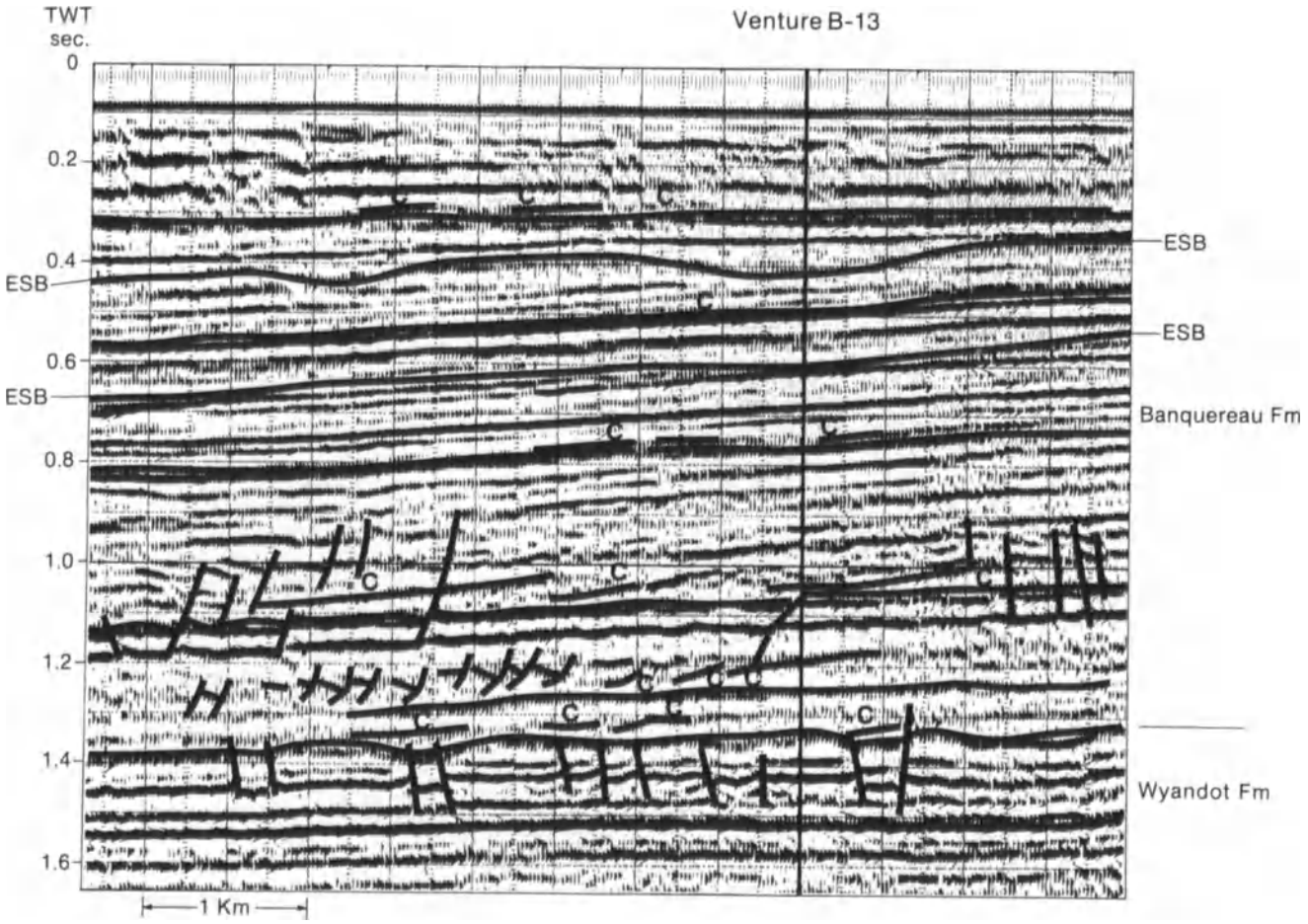

Figure 1.21. A seismic line from the Scotian Shelf illustrating relative-highstand deposits in the lower part of the Tertiary Banquereau Fm. Clinoforms (C) are indicated, which are developed in silty mudstone. Rotational faults are indicated between 1.0 and 1.3 sec, which have disrupted two sets of clinoforms. Near the top, erosional sequence boundaries (ESB) are indicated, which on other lines, show considerable downcutting.

port of gravels offshore, or even, in many cases, in shore-parallel directions. Most shoreline conglomerates form somewhat elongated lenses a few tens of kilometers in maximum dimension around the fluvial or deltaic input point.

Lowstand sandstone and conglomerate reservoirs may form isolated bodies surrounded by shales. These have the potential to form large, stratigraphically trapped fields—the Cardium Pembina Field of Alberta has recoverable reserves of 1.8 billion barrels or 0.25×10^9 m^3 (Nielson and Porter, 1984). Fields in the Cardium seem in some cases to have morphologies inherited from the relative low-stand depositional systems, but some may be totally reworked during the transgression, so that their morphologies more closely resemble the outer-shelf sand bodies on modern shelves.

On a larger scale, shallow marine reservoirs occur in each kind of depositional systems tract. Using seismic or regional well-log data, the general distributions of the different depositional systems tracts give reasonable predictions of the distributions of these facies. The general model of systems tract distribution is modified by the tectonic and eustatic setting of the sediments.

References

Allen, J.R.L., 1970, A quantitative model of climbing ripples and their cross-laminated deposits: Sedimentology, v. 14, p. 5–26.

Amos, C.L., and Knoll, R.G., 1987, The Quaternary sediments of Banquereau, Scotian Shelf: Geol. Soc. Am. Bull., v. 98, p. 244–260.

Beerbower, J.R., 1964, Cyclothems and cyclic depositional mechanisms in alluvial plain sedimentation, *in* Merriam, D.F., ed., Symposium on cyclic sedimentation: Kansas Geol. Surv. Bull. 169, v. 1, p. 31–42.

Beaumont, C., 1981, Foreland basins: Geophysical J. Roy. Astron. Soc., v. 55, p. 291–329.

Bergman, K.M. and Walker, R.G., 1987, The importance of sea-level fluctuations in the formation of linear conglomerate bodies; Carrot Creek Member of Cardium Formation, Cretaceous western interior seaway, Alberta, Canada: J. Sediment. Petrol., v. 57, p. 651–665.

Bourgeois, J., 1980, A transgressive shelf sequence exhibiting hummocky

stratification: The Cape Sebastian Sandstone (Upper Cretaceous), southwestern Oregon: J. Sediment. Petrol., v. 50, p. 691–702.

Burton, R., Kendall, C. G. St. C., and Lerche, I., 1987, Out of our depth: On the impossibility of fathoming eustacy from the stratigraphic record: Earth sci. Rev., v. 24, p. 237–277.

Cant, D.J., 1984, Development of shoreline-shelf sand bodies in a Cretaceous epeiric sea deposit: J. Sediment. Petrol., v. 54, p. 541–556.

Cant, D.J., 1989, Simple equations of sedimentation: Applications to sequence stratigraphy: Basin Research, v. 2, p. 73–81.

Cant, D.J., and Hein, F.J., 1986, Depositional sequences in ancient shelf sediments. Some contrasts in style, *in* Knight, R.J., and McLean, J.R., eds., Shelf sands and sandstones: Can. Soc. Petrol. Geol. Memoir 11, p. 302–311.

Cant, D.J., and Stockmal, G.S., 1989, Stratigraphy of the Alberta foreland basin: An interpretation in terms of Cordilleran tectonics: Can. J. Earth Sci., v. 26, p. 1964–1975.

Caron, C., Homewood, P., and Wildi, W., 1989, The original Swiss Flysch: A reappraisal of the type deposits in the Swiss Prealps: Earth Sci. Rev., v. 26, p. 1–45.

Clifton, H.E., 1981, Progradational sequences in Miocene shoreline deposits, southeastern Caliente Range, California: J. Sed. Petrol., v. 51, p. 165–184.

Coleman, J.M., and Prior, D.B., 1982, Deltaic environments, *in* Scholle, P.A., and Spearing, D.R., eds., Sandstone depositional environments: Am. Assoc. Petrol. Geol. Mem. 31, p. 139–178.

Covey, M., 1986, The evolution of foreland basins to steady state; evidence from the western Taiwan foreland basin, *in* Allen, P.A., and Homewood, P., eds., Foreland Basins: Internat. Assoc. of Sedimentol. Special Paper No. 8, p. 77–90.

Crook, K.A.W., 1989, Suturing history of an allochthonous terrane at a modern plate boundary traced by flysch-to-molasse facies transition: Sed. Geol., v. 61, p. 49–79.

Curray, J.R., Emmel, F.J., and Crampton, P.J.S., 1969, Holocene history of a strand-plain, lagoonal coast, Nayarit, Mexico, *in* Castanares, A.A., and Phleger, F.B., eds., Coastal lagoons—a symposium: Universidad Nacional Autonoma, Mexico, p. 63–100.

Demarest, J.M., and Kraft, J.C., 1987, Stratigraphic record of Quaternary sea levels; implications for more ancient strata, *in* Nummedal, D., Pilkey, O.H., and Howard, J.D., eds., Sea-level fluctuations and coastal evolution: Soc. Econ. Paleont. Mineral. Sp. Pub. 41, p. 223–240.

Devlin, W.J., Rudolph, K.W., Ehman, K.D., and Shaw, C.A., 1990, The effect of tectonic and eustatic cycles on accommodation and sequence stratigraphic framework in the southwestern Wyoming foreland basin: Abstracts of Papers, 13th Int. Sed. Congress, Nottingham, England, p. 131.

Frazier, D.E., 1967, Recent deltaic deposits of the Mississippi Delta: Their development and chronology: Trans. Gulf Cst. Assoc. Geol. Socs., v. 17, p. 287–315.

Hardy, I.A., 1975, Lithostratigraphy of the Banquereau Formation on the Scotian Shelf, *in* Offshore geology of eastern Canada: Geological Survey of Canada Paper 74–30, p. 163–174.

Haq, B.U., Hardenbol, J., and Vail, P.R., 1987, Chronology of fluctuating sea levels since the Triassic: Science, v. 235, p. 1156–1167.

Hein, F.J., 1987, Tidal/littoral offshore shelf deposits—Lower Cambrian Gog Group, southern Rocky Mountains, Canada: Sed. Geol., v. 52, p. 155–182.

Homewood, P., Allen, P.A., and Williams, G.D., 1986, Dynamics of the Molasse Basin of western Switzerland, *in* Allen, P.A., and Homewood, P., eds., Foreland Basins: Int. Assoc. Sediment. Spec. Pub. 8, p. 199–217.

Jopling, A.V., and Walker, R.G., 1968, Morphology and origin of cross-lamination, with examples from the Pleistocene of Massachusetts: J. Sed. Petrol., v. 38, p. 971–984.

Larue, D.K., and Martinez, P.A., 1989, Use of bedform climb models to analyse the geometry and preservation potential of clastic facies and unconformity surfaces: Am. Assoc. Petrol. Geol., v. 73, p. 40–53.

Leckie, D.A., and Walker, R.G., 1982, Storm and tide-dominated shorelines in Cretaceous Moosebar–Lower Gates interval—outcrop equivalents of Deep Basin gas trap in western Canada: Am. Assoc. Pet. Geol. Bull., v. 66, p. 138–157.

Leckie, D.A., 1986, Rates, controls, and sand-body geometries of transgressive-regressive cycles: Cretaceous Moosebar and Gates Formations, British Columbia: Am. Assoc. Pet. Geol. Bull., v. 70, p. 516–535.

Masters, J.A., 1984, Lower Cretaceous gas in western Canada, *in* Masters, J.A., ed., Elmworth—case study of a Deep Basin gas field: Am. Assoc. Petrol. Geol. Mem. 38, p. 1–34.

McCubbin, D.G., 1982, Barrier island and strandplain facies, *in* Scholle, P.A., and Spearing, D.R., eds., Sandstone depositional environments: Amer. Assoc. Petrol. Geol. Mem. 31, p. 247–280.

Mitchum, R.M. Jr., Vail, P.R., and Thompson, S. III, 1977, Seismic stratigraphy and global changes of sea level; Part 2—The depositional sequence as a basic unit for stratigraphic analysis, *in* Payton, C.E., ed., Seismic stratigraphy—applications to hydrocarbon exploration: Am. Assoc. Pet. Geol. Memoir 26, p. 53–62.

Nielsen, A.R., and Porter, J.W., 1984, Pembina oil field—in retrospect, *in* Stott, D.F., and Glass, D.J., eds., The Mesozoic of middle North America: Can. Soc. Pet. Geol. Memoir 9, p. 1–13.

Plint, A.G., 1988, Global eustacy and the Eocene sequence in the Hampshire Basin, England: Basin Research, v. 1, p. 11–22.

Plint, A.G., and Walker, R.G., 1987, Morphology and origin of an erosion surface cut into the Bad Heart Formation during major sea-level change, Santonian of west-central Alberta: J. Sed. Petrol., v. 57, p. 639–650.

Plint, A.G., Walker, R.G., and Bergman, K.M., 1987, Cardium Formation 6. Stratigraphic framework of the Cardium in subsurface: Bull. Can. Pet. Geol., v. 34, p. 213–225.

Price, R.A., 1973, Large-scale gravitational flow of supracrustal rocks, southern Canadian Rocky Mountains, *in* DeJong, K.A., and Scholten, R.A., eds., Gravity and Tectonics: Wiley Interscience, New York, p. 491–502.

Rahmani, R.A., 1984, Facies control of gas trapping, Lower Cretaceous Falher A cycle, Elmworth area, northwestern Alberta, *in* Masters, J.A., ed., Elmworth—case study of a deep basin gas field: Am. Assoc. Pet. Geol. Memoir 38, p. 141–152.

Swift, D.J.P., 1973, Delaware shelf valley: Estuary retreat path, not drowned river valley: Geol. Soc. Am. Bull., v. 84, p. 2743–2748.

Vail, P.R., Mitchum, R.M. Jr., and Thompson, S., 1977, Seismic stratigraphy and global changes of sea level; Part 4, Global cycles of relative changes of sea level, *in* Payton, C.E., ed., Seismic stratigraphy—applications to hydrocarbon exploration; Am. Assoc. Pet. Geol. Mem. 26, p. 83–97.

Van Wagoner, J.C., Mitchum, R.M. Jr., Posamentier, H.W., and Vail, P.R., 1987, Key definitions of seismic stratigraphy, *in* Bally, A.W., ed., Atlas of seismic stratigraphy: Am. Assoc. Petrol. Geol. Studies in Geology No. 27, p. 11–14.

Weimer, R.J., 1984, Relation of unconformities, tectonics, and sea-level changes, Cretaceous of western interior, U.S.A., *in* Schlee, J.S., ed., Interregional unconformities and hydrocarbon accumulation: Am. Assoc. Pet. Geol. Mem. 26, p. 7–36.

Wood, J.M., and Hopkins, J.C., 1989, Reservoir sandstone bodies in estuarine valley fill: Lower Cretaceous Glauconite Member, Little Bow Field, Alberta, Canada: Am. Assoc. Petrol. Geol. Bull., v. 73, p. 1361–1382.

Young, R.G., 1957, Late Cretaceous cyclic deposits, Book Cliffs, eastern Utah: Am. Assoc. Petrol. Geol. Bull., v. 41, p. 1760–1774.

CHAPTER 2

Systems Tracts, Seismic Facies, and Attribute Analysis Within a Sequence-Stratigraphic Framework—Example from the Offshore Louisiana Gulf Coast

Jory A. Pacht, Bruce Bowen, Bernard L. Shaffer, and William R. Pottorf

Introduction

Seismic stratigraphy has developed almost as three separate disciplines. The first, pioneered by Vail and others (1977), is seismic sequence analysis. Sequence analysis is the study of recognizing and correlating regional stratal surfaces to define genetically related rock units that represent discrete chronostratigraphic intervals (Van Wagoner et al., 1988). Seismic data are used extensively in sequence stratigraphy, as primary seismic reflections are generated by time-correlative bedding surfaces, and surfaces that separate sets of contemporaneous depositional systems (systems tracts) (Van Wagoner et al., 1988).

The second discipline is commonly called seismic facies analysis. It is defined as the description and geological interpretation of packages of seismic reflections. Parameters within these packages include configuration, continuity, amplitude, phase, frequency, and interval velocity (Vail et al., 1977).

The third discipline is seismic attribute analysis. Subtle changes in properties of particular reflections are examined to determine rock properties, including fluid content (Sengbush, 1962; Harms and Tackenburg, 1972; Domenico, 1974; Ensley, 1980; Balch et al., 1981 Slatt et al., 1987; and others).

Our approach to exploration integrates these three disciplines. We propose that seismic interpretation should be conducted in three iterative stages: (1) Delineate depositional sequences and systems tracts. (2) Delineate and map seismic facies within each systems tract. (3) Evaluate attributes within specific seismic facies. Well-log and biostratigraphic data must be integrated at all phases of this interpretation effort.

This paper describes techniques used in a regional study of Plio-Pleistocene strata in the south additions of the West Cameron through Grand Isle areas, offshore Louisiana (Fig. 2.1). These techniques have direct application to petroleum exploration and development within the study area and to analogous play types.

We examined over 20,000 line-miles of migrated seismic data and 300 well-log suites. Detailed analyses of nannofossils and planktonic foraminifera were conducted in 48 of these wells. Depositional sequences were delineated and then subdivided into systems tracts. Each systems tract was further subdivided into seismic facies. Seismic facies were mapped in each systems tract in each sequence, along with total isochron thickness of the systems tract itself. These maps and sections allow seismic attributes to be evaluated relative to their location within specific facies.

Sequence Stratigraphic Analysis

Plio-Pleistocene strata in offshore Louisiana were divided into depositional sequences. Each depositional sequence was then divided into systems tracts. Finally, seismic facies were delineated within each systems tract. Systems tracts are sets of contemporaneous depositional systems (Brown and Fisher, 1977) that develop when sea level is at a certain position relative to the shelf edge, and is rising or falling at a certain rate (Van Wagoner and others, 1988; Posamentier et al., 1988) (Fig. 2.2). Although the lowstand basin-floor fan, slope fan, and prograding wedge systems tracts are named after specific depositional environments that are parts of these systems tracts, they include all environments within it. Thus, the lowstand slope-fan systems tract in-

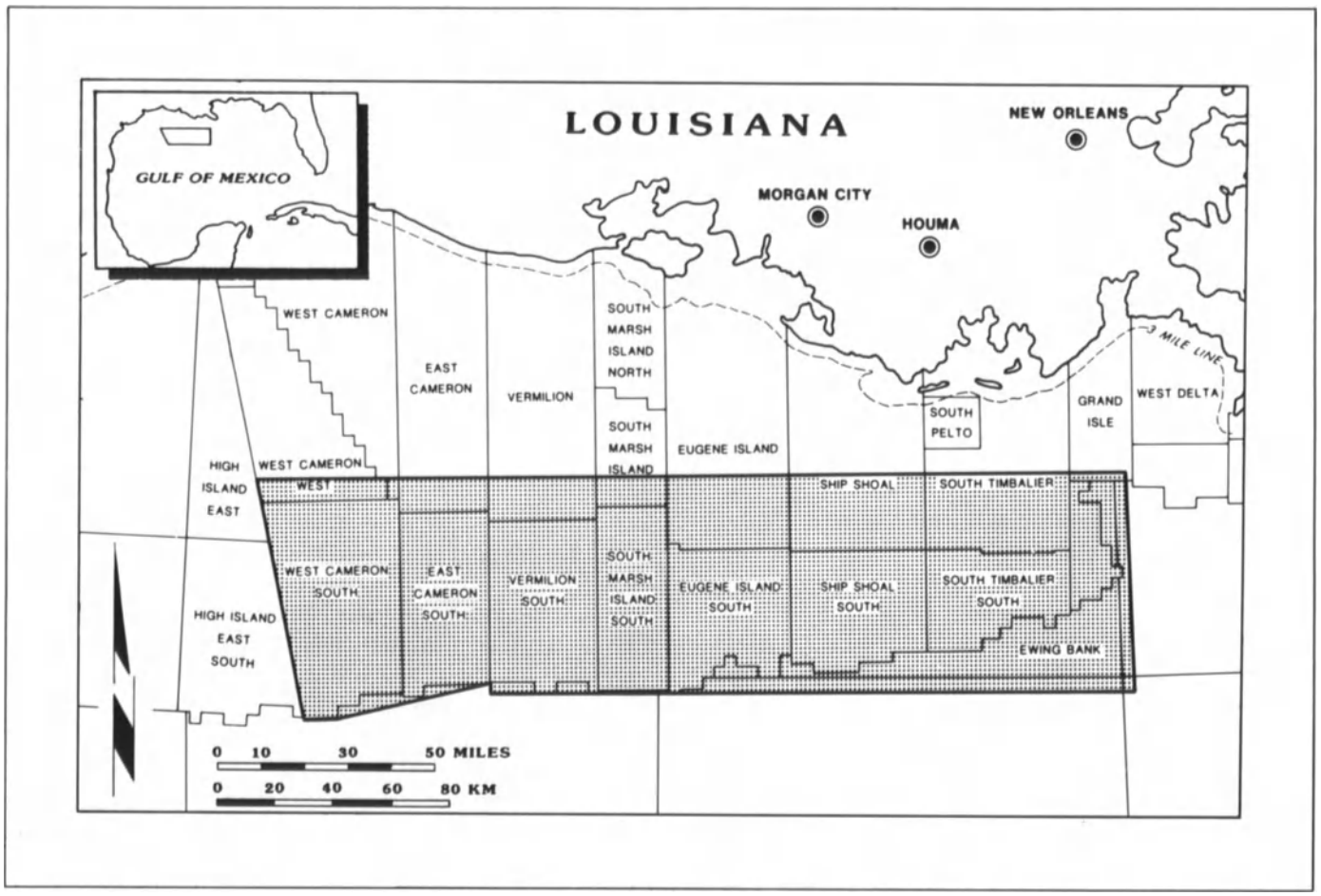

Figure 2.1. Index map of the offshore Louisiana Gulf Coast, showing the study area.

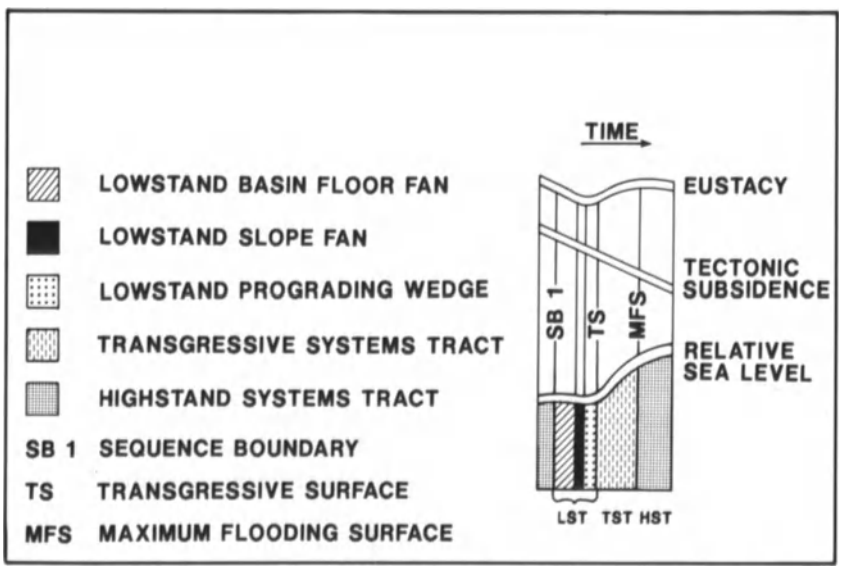

Figure 2.2. Diagram illustrating the relation between eustatic sea-level fluctuations (hingeline subsidence along an passive margin), and relative sea-level fluctuations (From Vail, 1987, reprinted by permission).

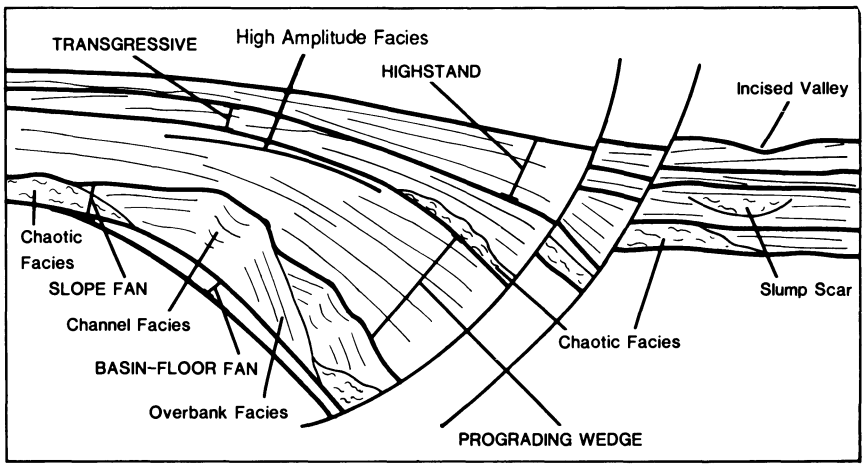

Figure 2.3. Sequence, systems tract, and seismic facies geometry developed along unstable progradational, passive continental margins.

cludes not only slope-fan facies but contemporaneous updip and downdip deposits as well.

The characteristics of depositional sequences and associated systems tracts along stable progradational, passive margins have been studied in detail by many researchers (Vail et al., 1977; Vail 1987; Haq et al., 1987; Jervey, 1988; Posamentier et al., 1988; Posamentier and Vail, 1988). The Plio-Pleistocene Gulf Coast of offshore Louisiana, however, is an unstable progradational continental margin (Winker, 1982; Winker and Edwards, 1983). As a result, systems tracts exhibit different geometries and different geologic characteristics (Vail, 1987; Mitchum et al., 1990; Pacht et al., 1989; 1990a; 1990b) (Fig. 2.3). An approach that integrates seismic, well-log, and biostratigraphic data is needed to delineate systems tracts and associated seismic facies with the highest degree of accuracy possible.

Biostratigraphic Criteria for Identification of Systems Tracts

Calcareous nannofossils and planktonic foraminifera exhibit abundance peaks at maximum flooding surfaces (the boundary between the transgressive and highstand systems tracts) (Shaffer, 1987, 1990; Armentrout, 1987, 1990; Bowen et al., 1989; Pacht et al., 1990a; 1990b; Wornardt and Vail, 1990). In several sequences, a second abundance peak occurs at the top of the slope-fan systems tract (Shaffer, 1990; Bowen et al., 1989; Pacht et al., 1990) (Fig. 2.4). These abundance peaks are named for highest occurrence datums of specific nannofossils and/or planktonic foraminifera that occur at or near the peak (Shaffer, 1987).

Abundance peaks at the maximum flooding surface developed when relative sea level was at its highest (Haq et al., 1987; Vail, 1987; Posamentier et al., 1988) (Fig. 2.2). At this time, the rate of terrigenous sedimentation was relatively low. Therefore, planktonic microfossils were preserved in greater concentrations relative to clastic debris. High sea level in the Plio-Pleistocene is associated with interglacial intervals. A more temperate world climate existed than during glacial intervals, and isotopic data (Williams, 1984; Williams et al., 1988, Trainor and Williams, 1990) suggest that sea-water temperature was higher. Warmer sea water resulted in higher overall faunal abundance and diversity (Beard et al., 1969, 1982; Shaffer, 1987, 1990; Bowen et al., 1989).

The abundance peak at the top of the slope-fan systems tract developed as a result of a shift in sedimentary systems. Sea level was below the shelf edge during development of the slope-fan systems tract (Posamentier and others, 1988). Sediment delivered through incised valleys was transported long distances on the slope and abyssal plain in channel-levee complexes (Bouma et al., 1986). In contrast, the lowstand prograding wedge developed when sea level was at or near the shelf edge. Sediment was deposited in marine-dominated deltas and moved along the shoreline by longshore currents. Therefore, significant time may have passed before sediment of the lowstand prograding wedge was deposited over much of the slope-fan systems tract. Slow, hemipelagic sedimentation occurred on top of the slope fan during this time interval, and abundance peaks developed as a function of the high ratio of planktonic microfossils to terrigenous debris (Bowen et al., 1989; Shaffer, 1990).

Seismic and Well-log Criteria for Identification of Systems Tracts

Systems tracts in Plio-Pleistocene strata of offshore Louisiana cannot be identified solely by the surfaces that bound them. They commonly exhibit a concordant relation with one another. Downlap, toplap, and onlap are often poorly expressed. Therefore, individual systems tracts were

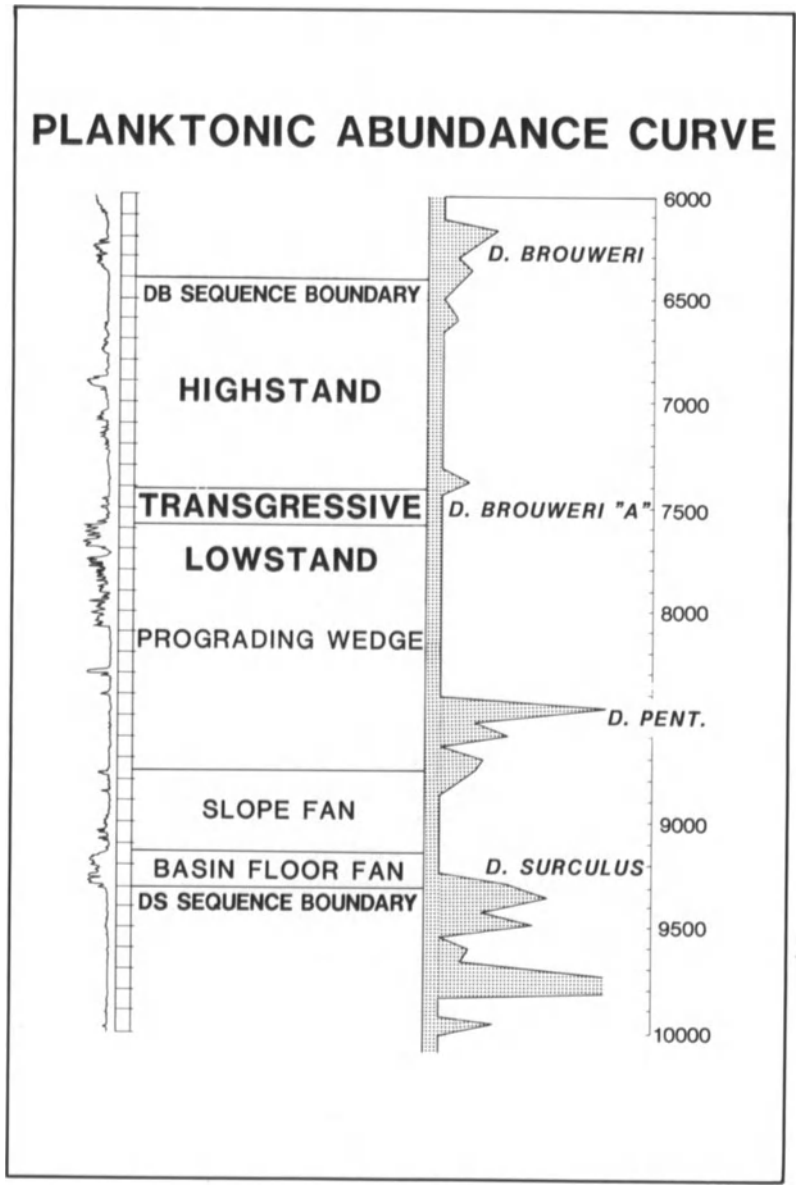

Figure 2.4. Diagram illustrating the relation between systems tracts, well-log profiles, and abundance peaks.

identified by examining both the bounding surfaces and the seismic facies contained within them. Systems tracts in Plio-Pleistocene strata of offshore Louisiana also exhibit specific upward-coarsening, upward-fining, and aggradational patterns on spontaneous potential and deep induction well-logs. Specific criteria used in delineating systems tracts and associated facies on seismic and well-log data in these strata are discussed below.

Lowstand Basin-Floor-Fan Systems Tracts

Lowstand basin-floor fans are the basal systems tracts within the depositional sequences. They developed during relative sea-level fall, which occurred when the rate of eustatic sea-level fall was greater than the rate of rise associated with subsidence (Jervey, 1988; Posamentier et al., 1988; Vail, 1987) (Fig. 2.2). Sandy sediment was prograded farther out onto the shelf during sea-level fall. At some point, perhaps near the shelf-edge, oversteepening occurred, and sediment was transported downdip into nearby intraslope basins by sediment gravity flows (Pacht et al., 1990b) (Fig. 2.5). Much of the shelf was greatly eroded during this time interval.

Basin-floor fans in the study area are characterized by a continuous reflection that either downlaps or onlaps against the underlying sequence boundary (Fig. 2.6). Alternatively, it may abut against the downthrown side of a growth

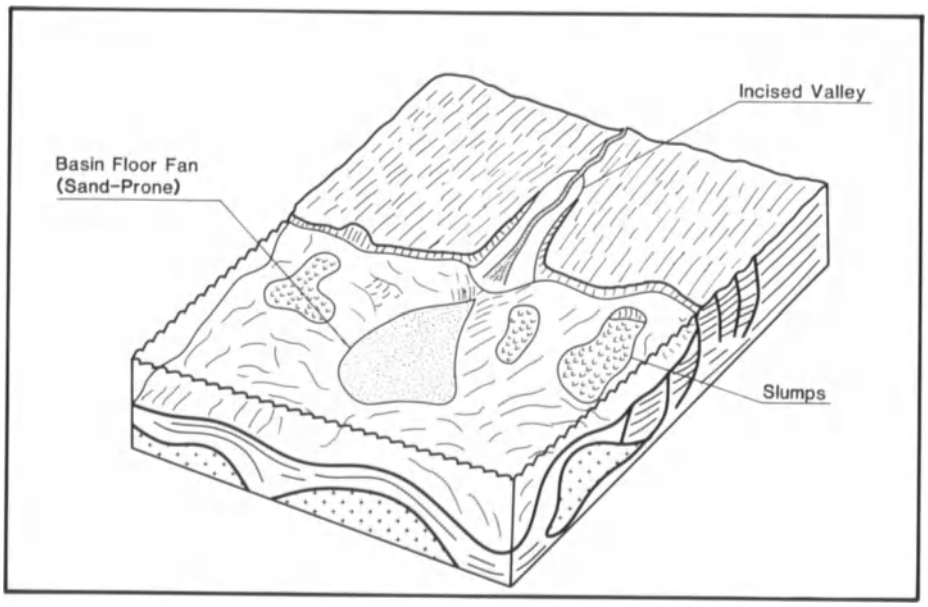

Figure 2.5. Block diagram illustrating lowstand basin-floor fan systems tract as developed in offshore Louisiana.

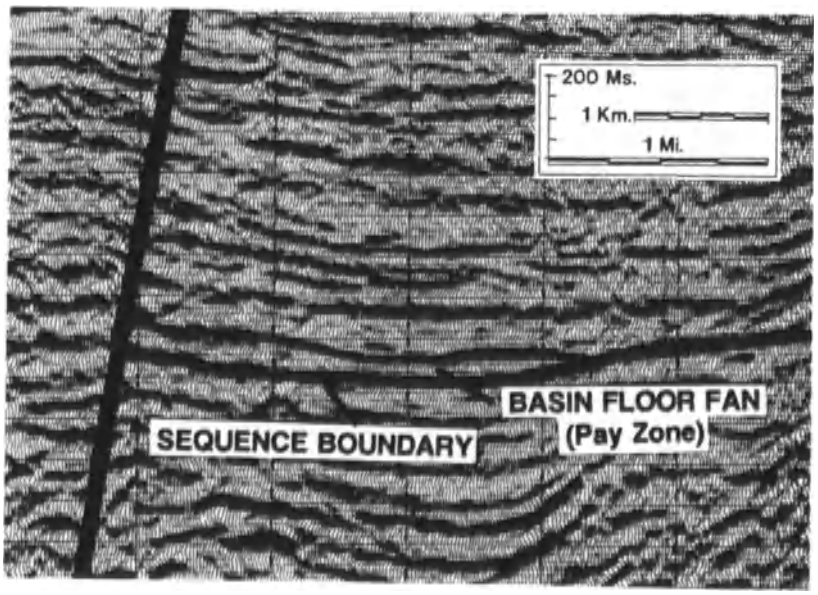

Figure 2.6. Seismic section showing a basin-floor fan. A gas field is developed within this basin-floor fan. Nearly 100 bcf has been produced from this field in only three years on-stream.

fault (Table 2.1). Where this upper boundary is not a good reflection, it can be defined by a series of downlapping reflections in the overlying slope fan. Basin-floor fans are commonly less than 300 feet (91.5 m) thick. Where they are thick enough to exhibit internal reflections, these reflections are poorly defined, or the fan is characterized by a transparent zone. Basin-floor fans in offshore Louisiana occur in local topographic lows and are commonly characterized by thick sandstones (Fig. 2.4).

Lowstand Slope-Fan Systems Tracts

Slope-fan systems tracts developed during the first stages of relative sea-level rise (Vail, 1987; Posamentier et al., 1988; Jervey, 1988; Pearlmutter, 1985) (Fig. 2.2). Sediment stored in glaciers was released and flowed downslope through topographic lows on the shelf directly onto the slope. In contrast to deposits on stable progradational continental margins (as described by Vail, 1987), contempor-

Table 2.1 Seismic, well-log, and lithologic characteristics of seismic facies in Gulf Coast systems tracts.

Sys. Tract	Facies	Seismic Characteristics	Lithology and Well-log Characteristics
Basin-floor Fan	Basin-floor Fan	Well-developed reflection or discontinuity surface, which forms upper boundary. Surface downlaps against the sequence boundary or abuts against the downthrown side of a growth fault.	Well-logs exhibit thick, well-sorted sands.
Lowstand Slope Fan	Channel-levee Facies	Channels exhibit concave-upward reflections. Levees exhibit discontinuous to semi-continuous reflections that downlap away from them.	Channels commonly exhibit aggradational or fining-upward sequences of blocky sands. Some channels may be shale-filled, however. Levees exhibit variable lithologies.
	Chaotic Facies	Random discontinuous seismic reflections.	Chaotic facies are commonly sand-rich where they were formed by small channel-levee complexes. They exhibit variable lithology where they were formed by mass wasting.
	Overbank Facies	Discontinuous to semi-continuous seismic reflections that are subparallel to the sequence boundary.	This facies is generally mud-rich. Thick muds are separated by spiky aggradational sands.
	Hemipelagic Facies	Parallel semi-continuous to continuous reflections. These reflections may exhibit moderate to high amplitudes.	Thick clays and muds. These muds are carbonate rich in some cases.
	Updip Parallel Facies	Parallel semi-continuous to continuous reflections.	Variable lithology. The facies exhibits aggradational, coarsening-upward, or fining-upward sequences of sand, silt, and mud. Strata commonly correlatable over several miles.
Lowstand Prograding Wedge	Semicontinuous to Continuous Facies	Semi-continuous to discontinuous reflections that are either concordant or diverge toward the downthrown sides of growth faults.	Generally sand rich but may be mud rich in some areas. Well logs generally exhibit coarsening-upward sequences where they represent delta-front sedimentation. Finding-upward sequences are developed in associated delta plain and fluvial deposits, and aggradational deposits are commonly formed by sediment gravity flows.
	High-amplitude Facies	Reflection or set of reflections that exhibit high to very high amplitude.	This facies commonly forms at impedance contrast between clean sandstones at the top of a coarsening-upward sequence and muds at the base of the sequence that overlies it. The facies also may occur where thick muds are deposited on top of the slope fan.
	Chaotic Facies	Random discontinuous seismic reflections.	Lithology is highly variable; however, most deposits are mud rich.
Transgressive	Semicontinuous to Discontinuous Facies	Semi-continuous to discontinuous reflections that are concordant. Rare divergence toward the downthrown sides of growth faults. Interval is usually thin and commonly below seismic resolution.	This facies is usually composed of thick muds. Poorly developed fining-upward sequences are sometimes present.
	Chaotic Facies	Random discontinuous seismic reflections.	Facies is mud rich.
Highstand	Semicontinuous to Discontinuous Facies	Semi-continuous to discontinuous reflections that are concordant or diverge toward the downthrown sides of growth faults.	Facies exhibits thick muds and silts or poorly developed, mud-rich coarsening-upward sequences.
	Chaotic Facies	Random discontinuous seismic reflections.	Facies is mud- and silt-rich.

aneous fluvial-deltaic facies were preserved updip of slope-fan depositional systems (Fig. 2.3). Sediment was transported through these depositional systems downdip into intraslope basins by sediment gravity flows (Fig. 2.7).

The lowstand slope fan is commonly the most distinctive systems tract in Gulf Coast strata. Slope-fan strata directly overlie sequence boundaries or, where present, basin-floor fans.

The underlying sequence boundary is commonly defined by downlap of slope-fan strata. Alternatively, it may be de-

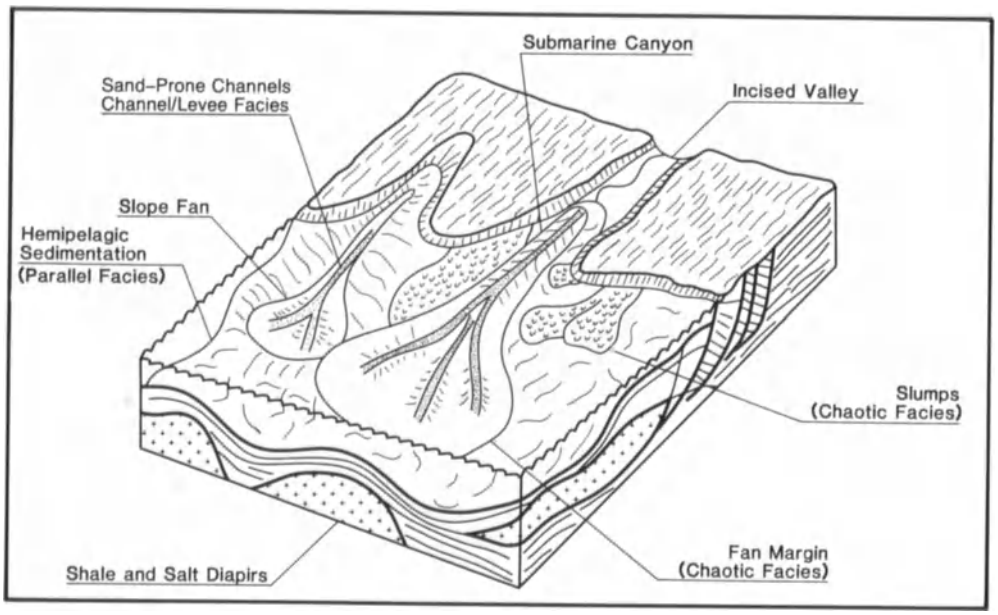

Figure 2.7. Block diagram illustrating a lowstand slope-fan systems tract, as developed in offshore Louisiana.

lineated by the change in reflection style from the more continuous reflections of the underlying highstand or basin-floor fan systems tracts. The sequence boundary commonly does not exhibit a well-developed reflection.

The slope fan systems tract is characterized by several facies, each of which exhibits specific reflection geometries (Weimer, 1989, 1990; Feeley et al., 1990; McHargue and Webb, 1986). These reflection geometries include channel, levee, overbank, chaotic, hemipelagic, and updip parallel deposits (Pacht and others, 1990a, 1990b) (Table 2.1). Facies that represent individual depositional features or processes were named for those features and processes. Facies that may develop by several depositional processes were given descriptive names.

Channel facies in the slope-fan systems tract are defined by curved, concave-upward reflections that vary in size from 2 miles (3.23 km) in width to less than seismic resolution. Associated levee reflections are cut by channel reflections, and downlap away from them (Fig. 2.8). These channels and levees commonly occur in stacked complexes. The overbank facies exhibits semi-continuous to discontinuous reflections that are subparallel to the sequence boundary.

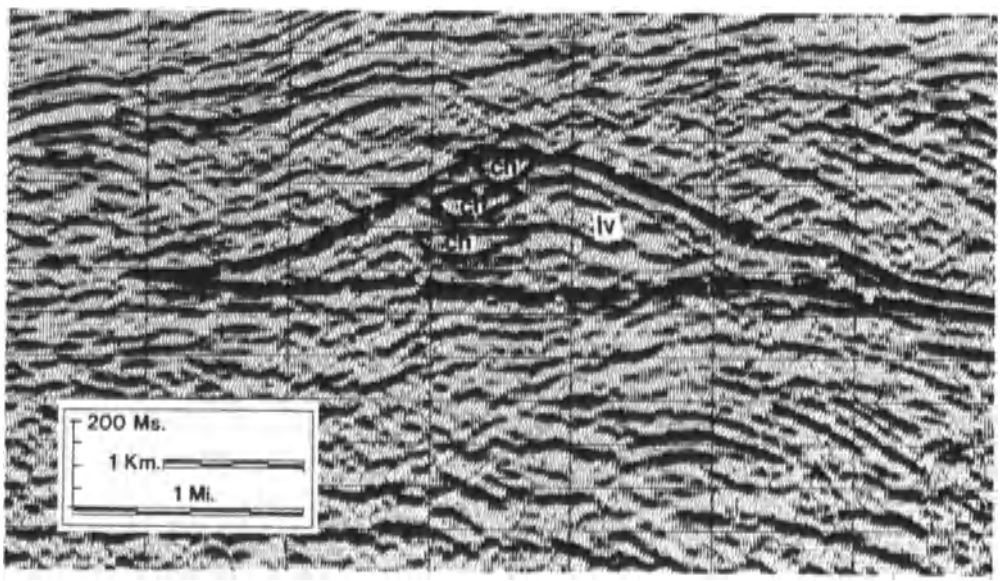

Figure 2.8. Channel and levee facies in a lowstand slope-fan systems tract (ch = channel; lv = levee).

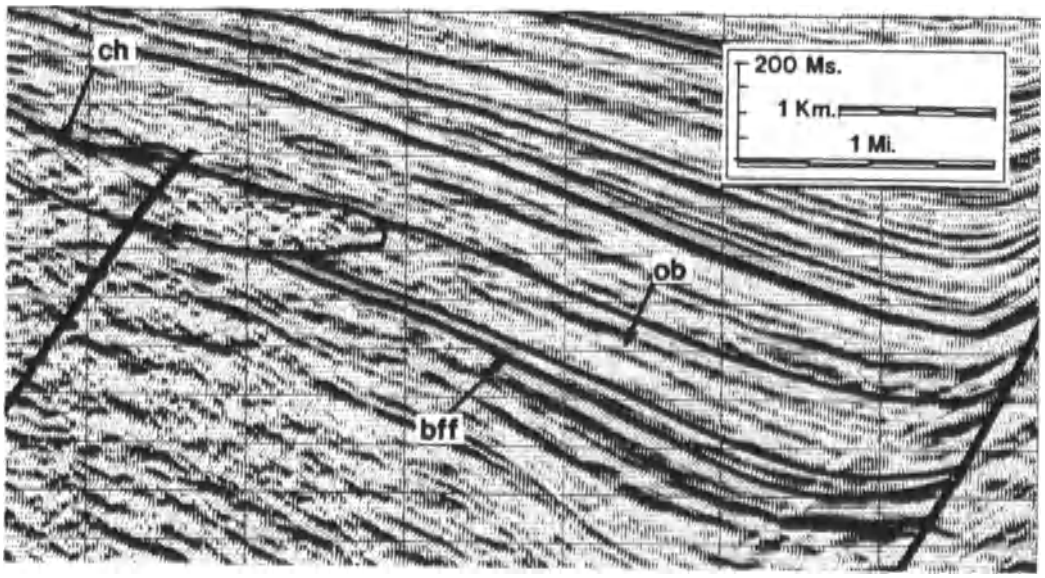

Figure 2.9. Overbank and chaotic facies in a slope-fan systems tract. Diagram also shows a basin-floor fan (bff = basin-floor fan facies; ob = overbank facies; ch = chaotic facies).

This facies develops alongside channel-levee complexes (Fig. 2.9).

Channels commonly exhibit thick, well-sorted sandstones or sand/shale fining-upward sequences. Levees associated with large channels may exhibit thick, well-sorted sandstones as well, although their lithology is highly variable. Overbank facies, however, are commonly mud-rich (Fig. 2.4). Sandstone percentage decreases greatly away from channel-levee complexes.

Chaotic facies exhibit random, discontinuous reflections (Fig. 2.9). Well-logs through this facies suggest that it contains less than 10% to greater than 70% sandstone. Chaotic facies may be formed by mass wasting and gravity sliding of both sand and mud-rich masses. In addition, a series of nested channel complexes at or near seismic resolution will also exhibit a chaotic pattern. Chaotic facies that represent stacked channel-levee complexes generally exhibit greater than 50% sand.

Hemipelagic facies exhibit continuous to semi-continuous reflections, which in some cases, are high in amplitude (Fig. 2.10). This facies consists largely of carbonate-, mud-, and clay-rich shales, probably deposited largely by

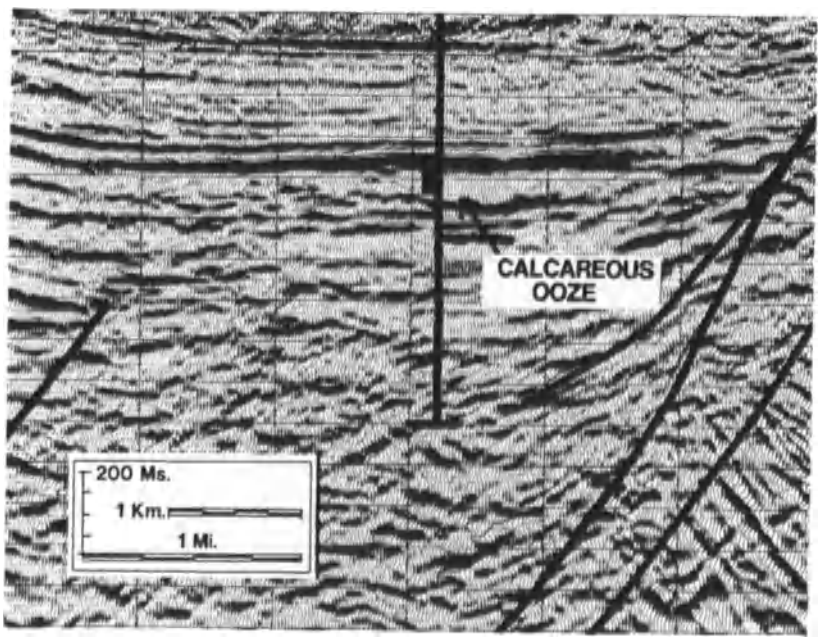

Figure 2.10. Hemipelagic facies of the slope-fan systems tract. This amplitude anomaly was formed by carbonate-rich ooze. No sand or hydrocarbons were observed.

hemipelagic processes (Pacht et al., 1990a). It also may also include deposits of other systems tracts that are highly condensed and are below seismic resolution.

Reflection characteristics in the updip parallel facies are similar to those developed in the hemipelagic facies; however, the updip parallel facies may contain thick sands. The updip parallel facies is characterized by aggradational and coarsening-upward sand/shale sequences. This facies probably represents shallow-water, fluvial-deltaic strata (Pacht et al., 1990a).

Although lithologies of the hemipelagic and updip parallel facies are very different, both facies exhibit analogous seismic signatures, probably because the geometry of depositional units within them is quite similar. Clastic units of the updip parallel facies can be correlated over several miles and exhibit little thickness variation relative to the resolution of seismic data. Hemipelagic units are characterized by thin turbidites interspersed between accumulations of pelagic debris. These units also exhibit uniform lithology and thicknesses over large areas.

Lowstand Prograding Wedge Systems Tract

Lowstand prograding wedges developed when sea level was at or near the shelf edge and was rising at a rate slow enough for sedimentation to keep pace (Vail, 1987; Posamentier et al., 1988) (Fig. 2.2). Deltas developed at or near the shelf margin (Pacht and others, 1990a) (Fig. 2.11). Since wave energy was not dissipated by movement across a broad, shallow shelf, it remained relatively high, and these deltas were commonly marine-dominated (term from Galloway, 1975). The deltas deposited well-sorted reservoir sands that extend several miles along strike.

The morphology of this systems tract in the study area, however, is quite different from lowstand prograding wedge deposits developed along stable progradational margins (as defined by Haq et al., 1987; Vail, 1987; and Posamentier et al., 1988). Progradation is not observed in seismic sections. Instead, reflections diverge toward the downthrown sides of growth faults (Fig. 2.12).

These reflections are commonly semi-continuous to continuous and exhibit low to moderate amplitudes. Chaotic facies and continuous high-amplitude reflections are also present (Table 2.1). The lower boundary of this systems tract is commonly defined by onlap and/or downlap onto the slope-fan systems tract. Strata of the lowstand prograding wedge also may exhibit greater reflection continuity and less variation in reflection amplitude than the underlying slope-fan deposits (Fig. 2.12).

The lowstand prograding wedge is commonly sand-rich, although it is characterized in many areas by thick shales. Well logs exhibit coarsening-upward patterns (Fig. 2.4) throughout much of the study area. High-amplitude reflections (as opposed to "bright spots," which are discussed later in this chapter) in this systems tract commonly are formed by the acoustic impedance contrast between sands at the top of one of these coarsening-upward sequences and shales at the base of the succeeding one. Alternatively, high-amplitude reflections in this systems tract may also be formed by thick shales deposited immediately above the lowstand slope fan.

Fining-upward sequences are observed in proximal units of this systems tract, near the northern boundary of the

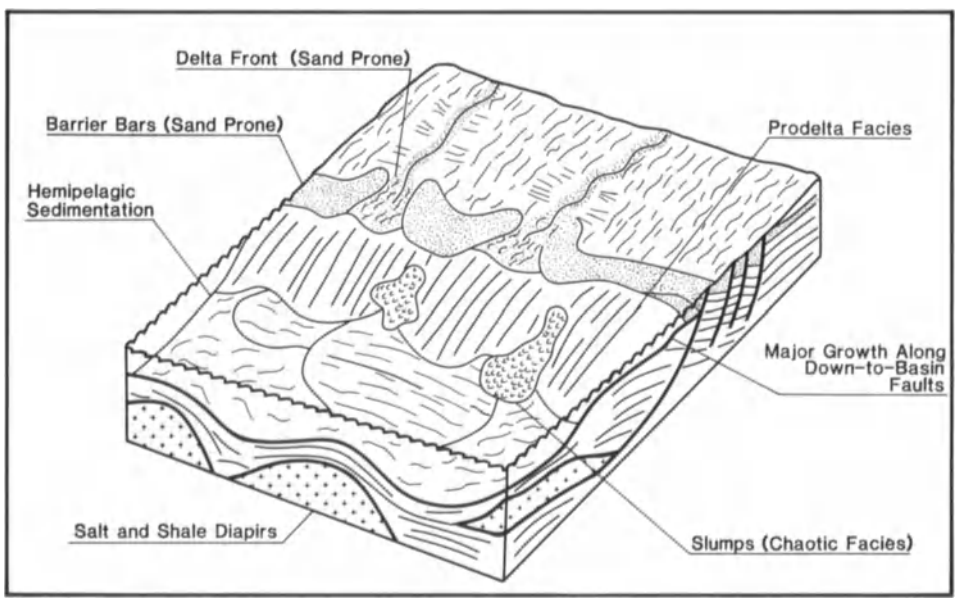

Figure 2.11. Block diagram illustrating the lowstand prograding-wedge systems tract, as developed in offshore Louisiana.

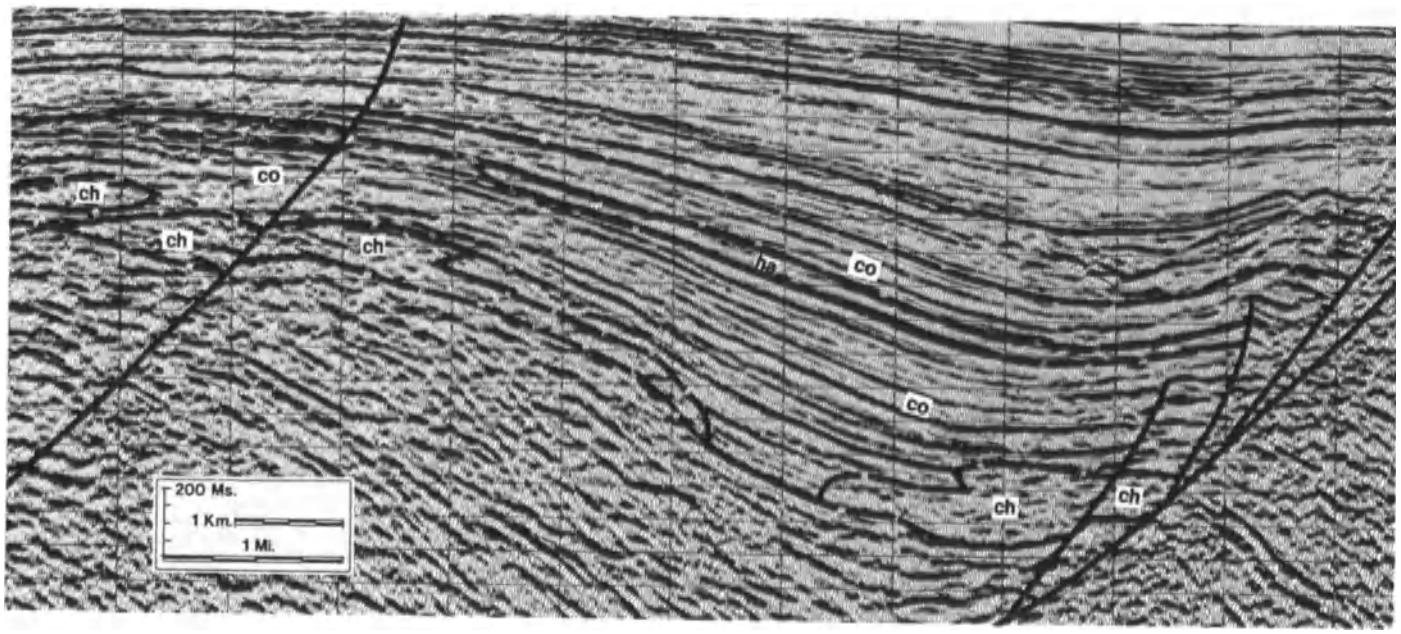

Figure 2.12. Seismic section of the lowstand prograding wedge systems tract (co = continuous to semi-continuous facies; ch = chaotic facies; ha = high-amplitude facies).

study area. In contrast, downdip equivalents of the lowstand prograding wedge may exhibit aggradational sequences and thick, well-sorted sands.

Coarsening-upward sequences were probably formed largely by delta-front sedimentation. Updip fining-upward sequences may have formed in the associated delta-plain and fluvial deposits, whereas downdip aggradational deposits probably formed as a result of transport by sediment gravity flows. Slump scars characterized by chaotic fill are sometimes observed updip of these aggradational units. The lithology of the chaotic fill varies considerably; however, it commonly contains a greater amount of mud than deposits characterized by more continuous reflections in this systems tract.

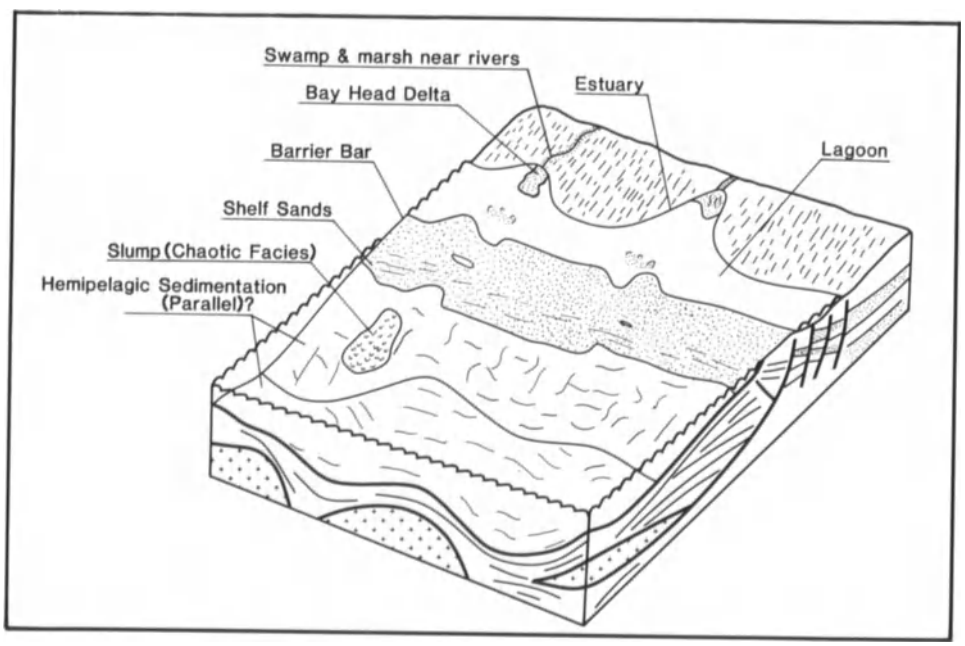

Figure 2.13. Block diagram illustrating transgressive systems tract as developed in offshore Louisiana.

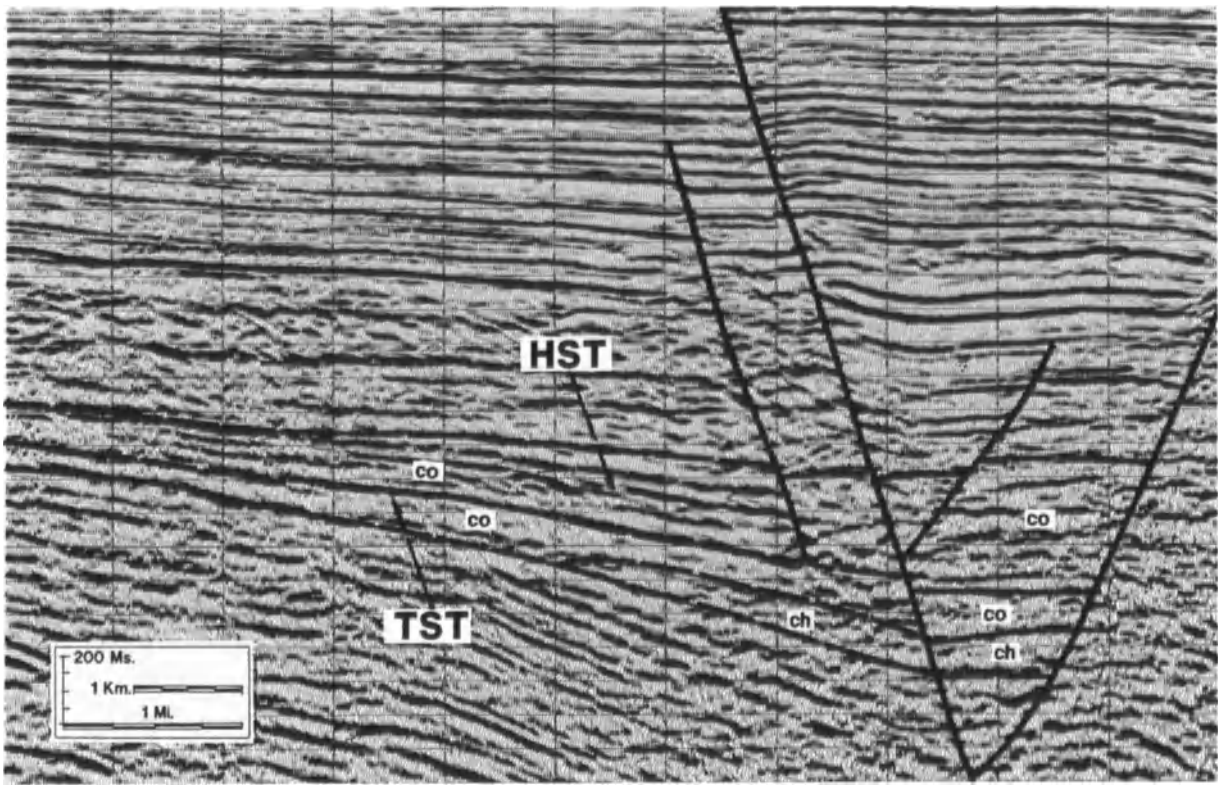

Figure 2.14. Seismic section of the transgressive and highstand systems tracts. This figure shows one of the thickest examples of the transgressive systems tract in the study area (HST = highstand systems tract; TST = transgressive systems tract; co = continuous to discontinuous facies; ch = chaotic facies).

Transgressive Systems Tract

The transgressive systems tract developed when the rate of sea-level rise increased to the rate at which sedimentation could no longer keep pace (Fig. 2.2), and the shelf was flooded. Deltaic progradation ceased, and most sand was trapped in updip estuaries (Posamentier et al., 1988; Vail, 1987) (Fig. 2.13).

The transgressive systems tract is very thin over much of the study area and is commonly below seismic resolution. Where it is thick enough to be interpreted, it is generally characterized by discontinuous to semicontinuous, concordant reflections (Fig. 2.14, Table 2.1). Some chaotic bedding is also present. Little to no thickening is observed along the downthrown sides of growth faults in this unit. The transgressive systems tract is separated from deposits of the lowstand prograding wedge by the transgressive surface (Haq et al., 1987; Vail, 1987; Van Wagoner et al., 1988). This surface is commonly defined by a reflection exhibiting moderate to high amplitude. Most classic structure maps in this area were made on transgressive surfaces. Well-log data suggest that the transgressive systems tract is dominantly composed of mud and clay. Poorly developed, fining-upward sequences are sometimes observed at the base of the unit; however, sandstones are relatively rare (Fig. 2.4).

P.R. Vail (personal communication, 1988) and Pacht et al. (1989) observed that the base of the transgressive systems tract may be characterized by a very well-sorted sand. This sand was probably deposited during development of the lowstand wedge and reworked by shelf currents during development of the transgressive systems tract. However, without core data, the reworked sand layer is hard to differentiate from clean sands deposited during formation of the lowstand prograding wedge. In this chapter, therefore, the reworked sand layer is considered to be part of the lowstand prograding wedge.

Highstand Systems Tract

Highstand systems tracts developed when the rate of relative sea-level rise slowed to the rate at which sedimentation was able to keep pace again (Vail, 1987; Posamentier et al., 1988). Sediment prograded seaward in large deltaic complexes. These deltas however, were fluvial dominated, as opposed to the marine-dominated deltas observed in the lowstand prograding wedge (Pacht et al., 1990a) (Fig.

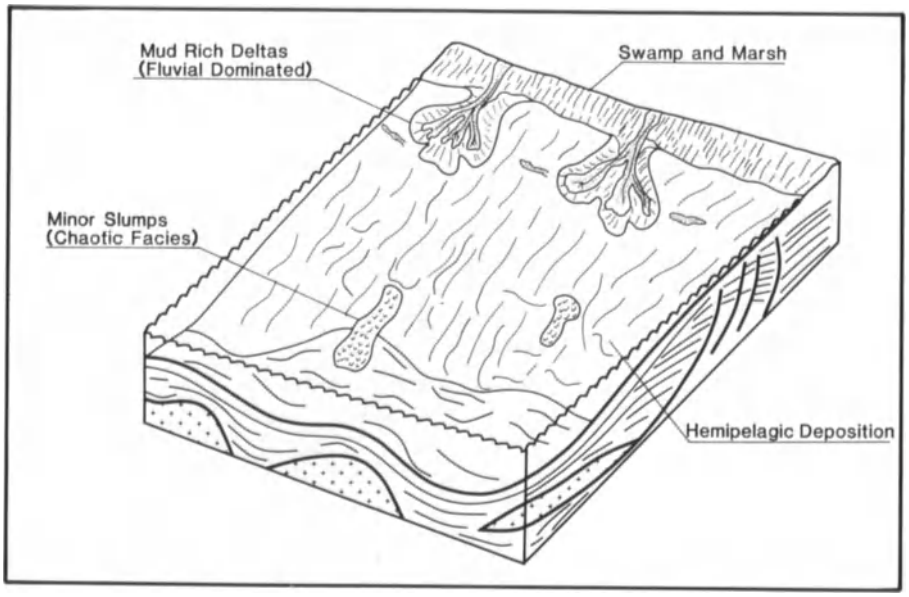

Figure 2.15. Block diagram illustrating highstand systems tract facies as developed in offshore Louisiana.

2.15). The deltas are developed well updip of the shelf margin, and wave energy is attenuated by movement across the shelf.

Highstand strata in offshore Louisiana are defined by semi-continuous to discontinuous reflections on seismic data. Progradational sequences are rare. Instead, reflections are either concordant or diverge slightly toward the downthrown sides of growth faults (Fig. 2.14). Some chaotic facies are present. The highstand systems tract is separated from underlying deposits of the transgressive systems tract by the maximum flooding surface (term from Haq et al., 1987; Vail, 1987) (Fig. 2.2). Since this surface is commonly *not* characterized by downlap of the overlying highstand systems tract (as is the case along stable progradational margins; Haq et al., 1987), it is commonly difficult to identify without well-log and biostratigraphic data.

Well-logs in the highstand systems tract exhibit either silt- and mud-rich coarsening-upward sequences or thick shales (Fig. 2.4). The highstand systems tracts in the study area are usually less than 300 feet (91.5 m) thick. However, local highstand depocenters are present in which these strata are over 2,000 feet (609.8 m) thick. These depocenters trend along dip.

Systems Tract Mapping

Sequence, systems tract, and facies boundaries, as well as all structural features (faults, salt diapirs, etc.), were tied throughout the data grid, and maps were constructed for each systems tract. The maps show isochron thickness and seismic facies for individual systems tracts as well as structural attributes.

An example of a map within a slope-fan systems tract can be shown to illustrate the techniques involved in their construction (Fig. 2.16). Similar techniques were used in constructing maps from each systems tract.

Multiple seismic facies may occur within a given thickness of strata at any particular point. Therefore, certain rules were set up for mapping each systems tract. For example, channel, overbank, and chaotic facies occur in the slope-fan systems tract shown in Fig. 2.16). Since both overbank and chaotic facies are common in this systems tract, if the systems tract exhibited greater than 50% chaotic facies, it was mapped as such. If it exhibited greater than 50% overbank facies, this was plotted on the map.

Channels, however, were plotted regardless of the relative percentage of this facies in the overall systems tract. Channels were noted on maps wherever they occurred within the specific systems tract. Therefore, channel facies shown on the map may not correspond to individual channels that developed contemporaneously. Instead, they may represent channel complexes developed within the systems tract throughout its depositional history. Chaotic facies proximal to growth faults probably developed by mass wasting, whereas chaotic facies developed near and along the periphery of the major channel complexes may represent a series of smaller channel complexes.

Exploration Strategy

Once seismic facies within each systems tract were defined and mapped, specific exploration strategies were devised to locate reservoir sands in these units and to properly evaluate amplitude anomalies within them.

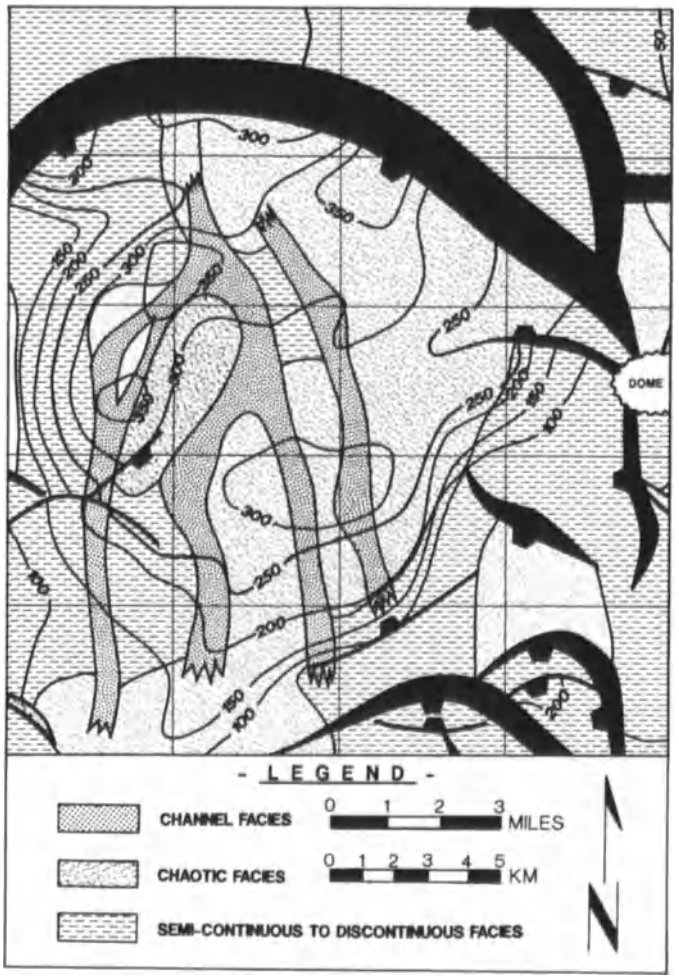

Figure 2.16. Facies and isochron thickness map of part of a lowstand slope-fan systems tract in the south additions of offshore Louisiana. Thicknesses are in milliseconds.

Seismic attributes (amplitude, phase, and frequency of specific wavelets) are widely studied in the Gulf Coast due to their value as direct hydrocarbon indicators. Plio-Pleistocene gas sands in the offshore Louisiana Gulf Coast are normally unconsolidated and undercompacted. They exhibit lower impedance than encasing shales and water-wet sands (Rutherford and Williams, 1989; Domenico, 1974). As water saturation is reduced, sand velocity decreases as a function of increasing fluid compressibility (Gassman, 1951; Domenico 1974). A large impedance contrast develops, and an amplitude anomaly is commonly observed on stacked seismic sections (Fig. 2.17).

Unfortunately, many other geologic variables can result in large impedance contrasts in these sections. For example, carbonate-rich shales exhibiting high sonic velocities, overlain by lower-velocity silt- and mud-rich shales may also exhibit a well-defined amplitude anomaly (Domenico, 1980) (Fig. 2.10). Domenico (1980) and R.M. Slatt (personal communication, 1981) observed that shales in the Gulf Coast may exhibit velocities that are much faster or much slower than the sands they surround. Small variations in shale composition can create large variations in both velocity and density. Finally, Gardner et al. (1974) noted that amplitude anomalies decrease in intensity with depth.

Alternatively, reservoirs characterized by multiple, thin pay zones, or those overlain by shales with similar impedance, may not show amplitude anomalies (Rutherford and Williams, 1989; Anstey, 1980) or may show anomalies that are very small relative to reserve size. Therefore, attribute analysis must be done within a sequence-stratigraphic framework.

Basin-floor Fan

The basin-floor fan systems tract is the most productive in the Gulf Coast per unit volume of sediment (Fig. 2.18). Basin-floor fans are relatively local, however, and developed in topographic lows. Where present, hydrocarbons are trapped along updip pinchouts (Figs. 2.6, 2.19). These fans are generally not present along the tops of large structures.

Amplitude anomalies may not be associated with hydrocarbon accumulations in this systems tract. Basin-floor fans are commonly overlain by shales of the overlying, distal slope fan. These shales are commonly organic rich, and

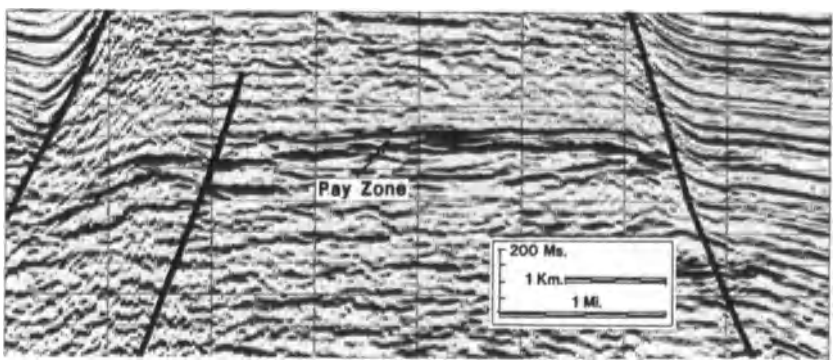

Figure 2.17. Amplitude anomaly developed in the upper portion of the lowstand prograding wedge. This anomaly delineates gas sands in a field with 735 bcf proven reserves.

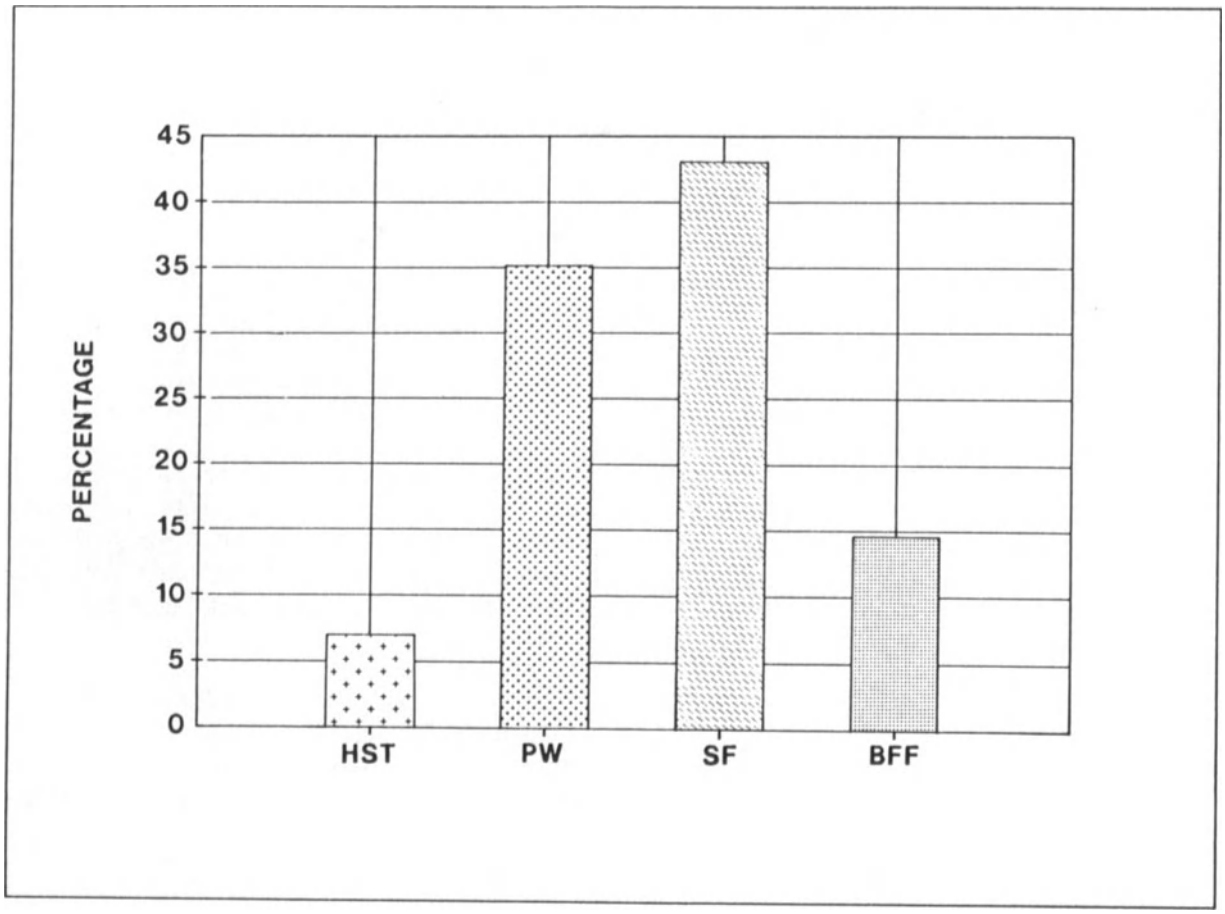

Figure 2.18. Histogram illustrating relative amounts of production per systems tract in gas and oil fields within the study area. HST = Highstand systems tract; PW = Prograding wedge; SF = Slope fan; BFF = Basin floor fan.

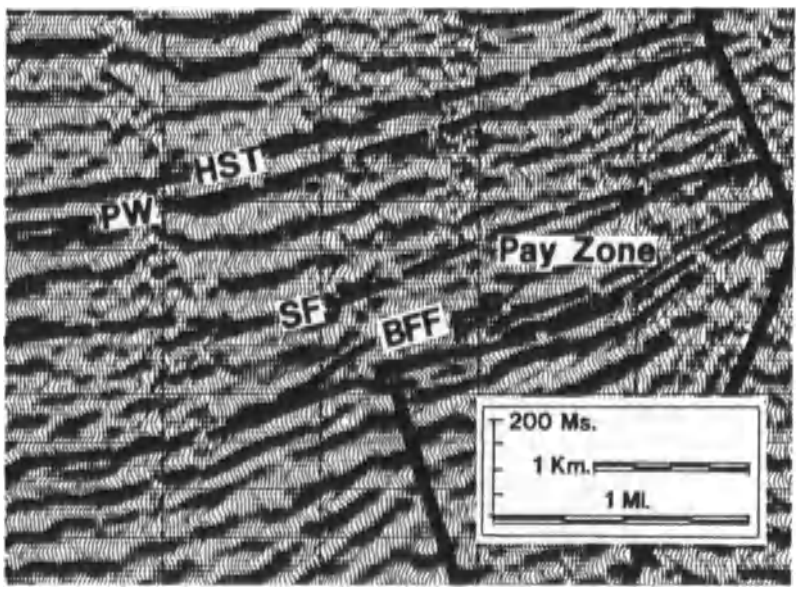

Figure 2.19. Seismic section across the same basin-floor fan as shown in Figure 6. This section shows a trap developed along an updip pinchout.

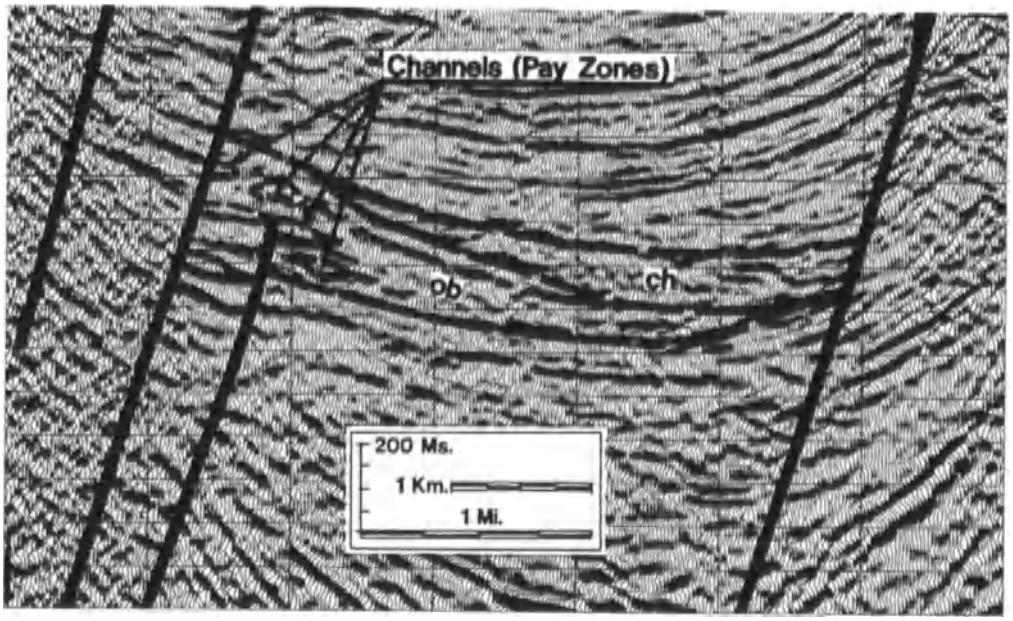

Figure 2.20. Oil and gas field within a slope-fan systems tract. This field is characterized by small amplitude anomalies, which exhibit concave-upward patterns characteristic of channels in this systems tract.

may be characterized by relatively low velocity and density. Therefore, the impedance contrast between gas-saturated sands in the basin-floor fan and overlying shales may be relatively low.

Alternatively, basin-floor fans may also exhibit "false anomalies" (high amplitudes not associated with hydrocarbons). The impedance contrast between well-sorted sands in the basin-floor fan and the muds that overlie it and underlie it may be sufficient to produce high amplitudes.

Basin-floor fans may be the most underexplored reservoirs in the Gulf Coast, because they occur well away from the crests of large structures. There are many examples of undrilled basin-floor fans throughout offshore Louisiana (Fig. 2.9).

Slope-fan Systems Tract

The slope-fan systems tract is the most productive systems tract in the study area (Fig. 2.18) (Pacht et al., 1990b). Much of this production occurs in channels and levee deposits near channels. Sandstone percentage is commonly much lower in overbank facies.

Large, continuous amplitude anomalies (such as Fig. 2.17) are usually not present in slope-fan gas fields. If present at all, amplitude anomalies may be small and follow the concave-upward pattern associated with channel deposits (Fig. 2.20). However, small anomalies in the slope-fan systems tract may be characteristic of much larger reserves than similar-size anomalies in other systems tracts. Slope-fan fields commonly produce from many reservoir sand bodies. Although these sand bodies may be interconnected, each one exhibits limited areal extent.

Lowstand Prograding Wedge

The lowstand prograding wedge is the most sand rich and second-most productive systems tract in the Gulf Coast (Fig. 2.18). It also has been the most explored. Large, thick sands that trend along strike are frequently present, and most classic hydrocarbon anomalies occur in this systems tract (Fig. 2.17). Reserve size can be more accurately related to the geographic extent of specific hydrocarbon anomalies than in the slope-fan or basin-floor fan systems tracts.

Stratigraphic traps are commonly not developed in this systems tract due to its sand-rich nature. Most hydrocarbons occur in classic structural traps. The critical element in plays in this systems tract is not reservoir, but rather the presence of seal facies, in either the lowstand prograding wedge or overlying transgressive systems tract. Fields are generally characterized by fewer, larger, and more continuous pay zones than are observed in the slope-fan systems tract.

Deep-water reservoirs are also developed in this systems tract in downdip turbidite equivalents of the shelf-edge delta facies. Since these sands were already extensively winnowed by shallow-water marine processes, they are often very well sorted and can exhibit excellent porosity.

Highstand and Transgressive Systems Tracts

Hydrocarbons are relatively rare in both the transgressive and highstand systems tracts within our study area. The transgressive systems tract contains few reservoir sandstones. Most sands were deposited north of the study area, along more proximal portions of the shelf, during development of transgressive systems tracts.

Minor hydrocarbon production occurs in the highstand systems tract. Fields in this systems tract are commonly small, although they may exhibit well-defined hydrocarbon anomalies. Production often occurs in delta-front sands. "False bright spots" (amplitude anomalies not associated with production), however, are also quite common. Well-log data suggest that some of these form as a result of impedance contrasts developed between shales of different compositions.

Conclusions

Seismic attribute analyses of one sort or another have often been presented as "black-box solutions" to the problems of petroleum explorationists. Case studies are published that illustrate successful use of a particular technique, and the technique is then used by other scientists in different areas. Initial enthusiasm, however, is rapidly followed by disillusionment. Attempts to use wavelet properties to interpret fluid or rock properties yield non-unique solutions. Seismic attributes are dependent on a complex interaction of many variables. A specific seismic signature that suggests gas-saturated sands in one area may indicate silt-rich mudstone in another.

Sequence-stratigraphic and seismic-facies analysis can provide important geologic information concerning a particular area, and help to limit variables that control reflection characteristics. This is particularly true in offshore Louisiana, where exploration has focused largely on delineation of hydrocarbon anomalies. Most well-defined anomalies have already been leased, and expensive "false bright spots" have been drilled in many areas.

Future exploration in this area will require an integrated approach. When hydrocarbon indicators are evaluated within a sequence-stratigraphic framework, predictions of reserve size can be made with greater accuracy. Plays can be delineated in which anomalies are not present, or the anomalies are very small in relation to reserve size. The probability that an amplitude anomaly does not represent a hydrocarbon accumulation can also be assessed. For example, in this study area, an amplitude anomaly developed within a lowstand prograding-wedge systems tract is clearly much more attractive than one formed on top of the transgressive systems tract. The amplitude anomaly within the lowstand prograding wedge is likely to be a gas-saturated sand developed at the top of a coarsening-upward sequence. In contrast, the one formed at the top of the transgressive systems tract may simply represent the impedance contrast between carbonate-rich shales in a condensed section (Loutit et al., 1988; Shaffer, 1990) and the mud-rich shales that surround it.

Acknowledgments

We would like to thank Calibre Consulting Inc., TGS Offshore Geophysical, and GECO Geophysical Company for permission to publish this paper. Robert O. Brooks, Robert Lawrence, and David Worthington, of TGS Offshore Geophysical, have been especially helpful. The paper is a small part of a larger project that has involved numerous people, including John Beard, Matthew Bognar, Abu Chowdhury, Gloria Cummins, Jeffry Crisp, Larry Dunn, James Lamb, Dave Risch, Sue Rostrom, Lee Smith, Kenneth Thies, and Gordon Weisser. Peter R. Vail, Arnold H. Bouma, and John Sangree served on an advisory council set up for this project and helped us greatly. Last, but certainly not least, we would like to thank our clients for their encouragement and support.

References

Anstey, N.A., 1980, Seismic exploration for sandstone reservoirs: (International Human Resources Development Corporation), Boston, 138 p.

Armentrout, J.M., 1987, Testing a benthic foraminiferal biofacies model—Plio Pleistocene, Gulf of Mexico, integration of biostratigraphy and seismic stratigraphy: Society of Economic Paleontologists and Mineralogists Eighth Annual Research Conference, Proceedings, p. 6–14.

Armentrout, J.M., 1990, Integrated stratigraphic analysis: Society of Economic Paleontologists and Mineralogists Short Course Notes, Course #1, American Association of Petroleum Geologists Annual Meeting.

Balch, A.H., Lee, M.W., Miller, J.J., and Ryder, R.T., 1981, Seismic amplitude anomalies associated with the First Leo sandstone lenses, eastern Powder River Basin, Wyoming: Geophysics, v. 46, p. 1519–1527.

Beard J.H., 1969, Pleistocene paleotemperature record based on planktonic foraminifers, Gulf of Mexico: Gulf Coast Association of Geologic Societies, Transactions, v. 19, p. 535–553.

Beard, J.H., Sangree, J.B., and Smith, L.A., 1982, Quaternary chronology, paleoclimate, depositional sequences and eustatic cycles: American Association of Petroleum Geologists Bulletin, v. 66, p. 158–169.

Bouma A.H., Coleman, J.M., and Meyer, A.H., 1986, Introduction, objectives and principal results of Deep Sea Drilling Project Leg 96, *in* Bouma, A.H., Coleman, J.M., Meyer, A.H., and others, Initial Reports of the Deep Sea Drilling Project, v. 96: U.S. Government Printing Office, Washington D.C., p. 533–540.

Bowen, B.E., Shaffer, B.L., and Pacht, J.A., 1989, Seismic identification and the use of condensed sections in the Plio-Pleistocene Gulf of Mexico: Society of Exploration Geophysicists, Expanded Abstracts, 1989 Technical Program, v. 2, p. 801–802.

Brown, L.F., and Fisher, W.L., 1977, Seismic stratigraphic interpretation and petroleum exploration: American Association of Petroleum Geologists Continuing Education Course Note Series, No. 16, 56 p.

Domenico, S.N., 1974, Effect of water saturation on seismic reflectivity of sand reservoirs encased in shale: Geophysics, v. 39, p. 759–769.

Domenico, S.N., 1980, Velocity and lithology, *in* Stratigraphic interpretation of seismic data school, course notes: American Association of Petroleum Geologists/Society of Exploration Geophysicists, p. 1–62.

Ensley, M.B., 1980, Interpretation of stratigraphy and lithofacies from seislogs, *in* Stratigraphic interpretation of seismic data school, course notes: American Association of Petroleum Geologists/Society of Exploration Geophysicists, p. 5.1–5.16.

Feeley, M.H., Moore, T.C., Loutit, T.S., and Bryant, W.R., 1990, Sequence stratigraphy of the Mississippi Fan related to oxygen isotope index: American Association of Petroleum Geologists Bulletin, v. 74, p. 407–424.

Galloway, W.E., 1975, Process framework for describing the morphologic and stratigraphic evolution of deltaic depositional systems, *in* Broussard, M.L., ed., Deltas: Models for exploration: Houston Geologic Society, Houston, Texas, p. 87–98.

Gardner, G.H.F., Gardner, L.W., and Gregory, A.R., 1974, Formation velocity and density—the diagnostic basis for stratigraphic traps: Geophysics, v. 39, p. 770–780.

Gassman, F., 1951, Elastic waves through a packing of spheres: Geophysics, v. 15, p. 673–685.

Haq, B.U., Hardenbol, J., and Vail, P.R., 1987, Chronology of fluctuating sea-levels since the Triassic (250 million years to the present): Science, v. 235, p. 1156–1167.

Harms, J.C., and Tackenburg, P., 1972, Seismic signatures and sedimentation models: Geophysics, v. 37, p. 45–58.

Jervey, M.T., 1988, Quantitative geological modeling of siliciclastic rock sequences and their seismic expression, *in* Wilgus, C.K., and others, eds., Sea-level changes: An integrated approach: Society of Economic Paleontologists and Mineralogists Special Publication No. 42, p. 47–70.

Loutit, T.S., Hardenbol, J., Vail, P.R., and Baum, G.R., 1988, Condensed sections: The key to age dating and correlation of continental margin sequences, *in* Wilgus, C.K., and others, eds., Sea-level changes: An integrated approach: Society of Economic Paleontologists and Mineralogists Special Publication No. 42, p. 183–213.

McHargue, T.R., and Webb, J.E., 1986, Internal geometry, seismic facies and petroleum potential of canyons and inner fan channels of the Indus Submarine Fan: American Association of Petroleum Geologists Bulletin, v. 70, p. 161–180.

Mitchum, R.M., Sangree, J.B., Vail, P.R., and Wornardt, W.W., 1990, Sequence stratigraphy in the Late Cenozoic expanded sections, Gulf of Mexico, *in* Sequence Stratigraphy as an Exploration Tool: Concepts and Practices in the Gulf Coast, Eleventh Annual Research Conference: Gulf Coast Section, Society of Economic Paleontologists and Mineralogists, p. 237–256.

Pacht, J.A., Beard, J.H., Weisser, G., Bouma, A.H., Bowen, B.E., and Vail, P.R., 1989, Seismic-stratigraphic analysis of Plio-Pleistocene depositional facies, East and West Cameron, offshore Louisiana: Society of Exploration Geophysicists, Expanded Abstracts, 1989 Technical Program, v. 2, p. 801–802.

Pacht, J.A., Bowen, B.E., Beard, J.H., and Shaffer. B.L., 1990a, Sequence stratigraphy of Plio-Pleistocene depositional facies in the offshore Louisiana South Additions, Gulf Coast Association of Geologic Societies, v. 40, p. 643–660.

Pacht, J.A., Bowen, B.E., and Pottorf, W.R., 1990b, Sequence stratigraphy in the offshore Louisiana Gulf Coast—Applications to hydrocarbon exploration, *in* Sequence stratigraphy as an exploration tool: Concepts and Practices in the Gulf Coast: Gulf Coast Society of Economic Paleontologists and Mineralogists, Eleventh Annual Research Conference, Proceedings, p. 269–285.

Pearlmutter, M.A., 1985, Deep-water clastic reservoirs in the Gulf of Mexico: A depositional model: Geo-Marine Letters, v. 5, 105–112.

Posamentier, H.W., Jervey, M.T., and Vail, P.R., 1988, Eustatic controls on clastic deposition, I—Conceptual framework, *in* Wilgus, C.K., and others, eds., Sea-level changes: An integrated approach: Society of Economic Paleontologists and Mineralogists Special Publication No. 42, p. 109–125.

Posamentier, H.W. and Vail, P.R., 1988, Eustatic controls on clastic deposition II—sequence and systems tracts models, *in* Wilgus, C.K. and others, eds., Sea-level changes: An integrated approach: Society of Economic Paleontologists and Mineralogists Special Publication No. 42, p. 125–154.

Rutherford, S.R., and Williams, R.H., 1989, Amplitude with offset variation in gas sands: Geophysics, v. 54, p. 680–688.

Sengbush, R.L., 1962, Stratigraphic trap study in Cottonwood Creek Field, Big Horn Basin: Geophysics, v. 27, p. 427–444.

Shaffer, B.L., 1987, The potential of calcareous nannofossils for recognizing Plio-Pleistocene climatic cycles and sequence boundaries on the shelf: Society of Economic Paleontologists and Mineralogists Eighth Annual Research Conference Proceedings, p. 142–145.

Shaffer, B.L., 1990, The nature and significance of condensed sections in Gulf Coast late Neogene stratigraphy: Gulf Coast Association of Geologic Societies, v. 40, p. 767–776.

Slatt, R.M., Robinson, J.C., Lighty, K.A., and Moore, G.F., 1987, Seismic reflection character analysis of stratigraphic traps in Cretaceous Cardium Formation, Alberta Canada: American Association of Petroleum Geologists Bulletin, v. 71, p. 298–307.

Trainor, D.W., and Williams, D.F., 1990, Quantitative analysis and correlation of oxygen isotope record from planktonic and benthonic foraminifera and well log records from OCS well G-1267 No. A-1 South Timbalier, Block 198, northcentral Gulf of Mexico, *in* Sequence stratigraphy as an exploration tool: Concepts and practices in the Gulf Coast: Eleventh Annual Research Conference, Gulf Coast Section Society of Economic Paleontologists and Mineralogists, p. 237–256.

Vail, P.R., 1987, Seismic stratigraphy interpretation procedure, *in* Bally, A.W., ed., Atlas of seismic stratigraphy, Volume I: American Association of Petroleum Geologists, Studies in Geology No. 27, p. 1–10.

Vail, P.R., Mitchum, R.M., Todd, R.G., Widmier, J.M., Thompson, S., Sangree, J.B., Bubb, J.N., and Hatelid, W.G., 1977, Seismic stratigraphy and global changes in sea-level, *in* Payton, C.E., ed., Seismic stratigraphy—Application to hydrocarbon exploration: American Association of Petroleum Geologists Memoir 26, p. 49–212.

Van Wagoner, J.C., Posamentier, H.W., Mitchum, R.M., Vail, P.R., Sarg, J.F., Loutit, T.S., and Hardenbol, J., 1988, An overview of sequence stratigraphy and key definitions, *in* Wilgus, C.K., and others, eds., Sea-level changes: An integrated approach: Society of Economic Paleontologists and Mineralogists Special Publication No. 42, p. 39–48.

Weimer, P., 1989, Sequence stratigraphy of the Mississippi Fan (Plio-Pleistocene), Gulf of Mexico: Geo-Marine Letters, v. 9, p. 185–272.

Weimer, P., 1990, Sequence stratigraphy, facies geometry, and depositional history of the Mississippi Fan: American Association of Petroleum Geologists Bulletin, v. 74, p. 425–453.

Williams, D.G., 1984, Correlation of Pleistocene marine sediments of the Gulf of Mexico and other basins using oxygen isotope stratigraphy, *in* Healy-Williams, N., ed., Principles of Pleistocene stratigraphy applied to the Gulf of Mexico: (International Human Resources Development Corporation), Boston, Massachusetts, p. 65–118.

Williams, D.F., Thunell, R.C., Tappa, E., Rio, D., and Raffi, I., 1988, Chronology of the Pleistocene oxygen isotope record: 0–1.88 m.y.B.P.: Palaeogeography, Palaeoclimatology, Palaeoecology, v. 64, p. 221–240.

Winker, C.D., 1982, Cenozoic shelf margins, northwestern Gulf of Mexico Basin: Gulf Coast Association of Geologic Societies Transactions,

v. 32, p. 427–448.

Winker, C.D., and Edwards, M.B., 1983, Unstable progradational continental clastic shelf margins, *in* Stanley, D.J., and Moore, G.T., eds., The Shelfbreak, Critical Interface on Continental Margins: Society of Economic Paleontologists and Mineralogists Special Publication No. 33, p. 121–137.

Wornardt, W.W., and Vail, P.R., 1990, Revision of the Plio-Pleistocene cycles and their application to sequence stratigraphy of shelf and slope sediments in the Gulf of Mexico, *in* Sequence Stratigraphy as an Exploration Tool: Concepts and Practices in the Gulf Coast: Eleventh Annual Research Conference, Gulf Coast Section, Society of Economic Paleontologists and Mineralogists, p. 237–256.

CHAPTER 3

Clastic Petroleum Reservoirs of the Late Proterozoic and Early Paleozoic Amadeus Basin, Central Australia

John F. Lindsay and John D. Gorter

Introduction

The Amadeus basin is a broad intracratonic depression that formed the setting for the deposition of as much as 14 km of predominantly shallow-marine sediments during the Late Proterozoic and Early Paleozoic (Figs. 3.1, 3.2). The basin, which covers approximately 155,000 km^2, lies at the center of the Australian craton to the south of Alice Springs. From east to west, along its longest axis, it extends for 800 km. It is one of a number of similar shallow intracratonic depressions that were initiated across the Australian craton in the Late Proterozoic. They are the product of two separate and distinct periods of crustal extension that appears to relate to the breakup of the Proterozoic supercontinent (Lindsay et al., 1987). All these basins contain shallow-marine to nonmarine successions, and all appear to have been interconnected through much of their history.

The Amadeus basin has become increasingly important over the last three decades, with the discovery of significant reserves of oil and gas within the Late Proterozoic/Cambro-Ordovician succession (Schroder and Gorter, 1984) (Fig. 3.3). Most of the area is desert, however, and sparsely populated. The remoteness affects the viability of some prospects, and the basin is only now beginning to reach its full development potential, following the completion of oil and gas pipelines to Alice Springs and Darwin from the major fields.

Basin Morphology and Evolution

The Amadeus basin consists of three major sub-basins connected by shallow troughs along the northern margin (Fig. 3.1). To the south and west, the sub-basins are separated from a much larger platform area by a tectonic ridge, which at times, acted as a barrier to sedimentation. The basin evolved in three stages. Crustal extension of Stage 1 began at about 900 Ma and was followed by an extended period of thermally induced subsidence. A second crustal extension (Stage 2), less intense but major nevertheless, occurred toward the end of the Late Proterozoic at about 600 Ma. Stage 2 was followed by a major compressional event (Stage 3) in which major, southward-directed thrust sheets caused progressive downward flexing of the northern margin of the basin, and sediment was shed from the thrust sheets into the downwarps.

The two major stages of crustal extension are clearly complex episodes involving major initial extensional events followed by longer term, low-intensity extension, perhaps in the form of small steps. Unfortunately, details of the extensional process cannot be resolved due to limited time control on the stratigraphy. These extensional stages and their associated thermal recovery produced large-scale relative sea-level effects, upon which eustatic sea-level cycles were superimposed. Relative sea-level rose with the initiation of each extensional stage, and then gradually declined as sedimentation commenced and the peripheral bulge began to rise due to sediment loading. Following the demise of the peripheral bulge, relative sea level again appeared to rise as thermal subsidence became the dominant controlling mechanism. The style of sedimentation and major sequence boundaries were controlled, to a large degree, by basin dynamics. As a consequence, a predictable depositional pattern occurred during each extensional stage, thus allowing the prediction of potential source and reservoir rocks (Lindsay and Korsch, 1989, 1991).

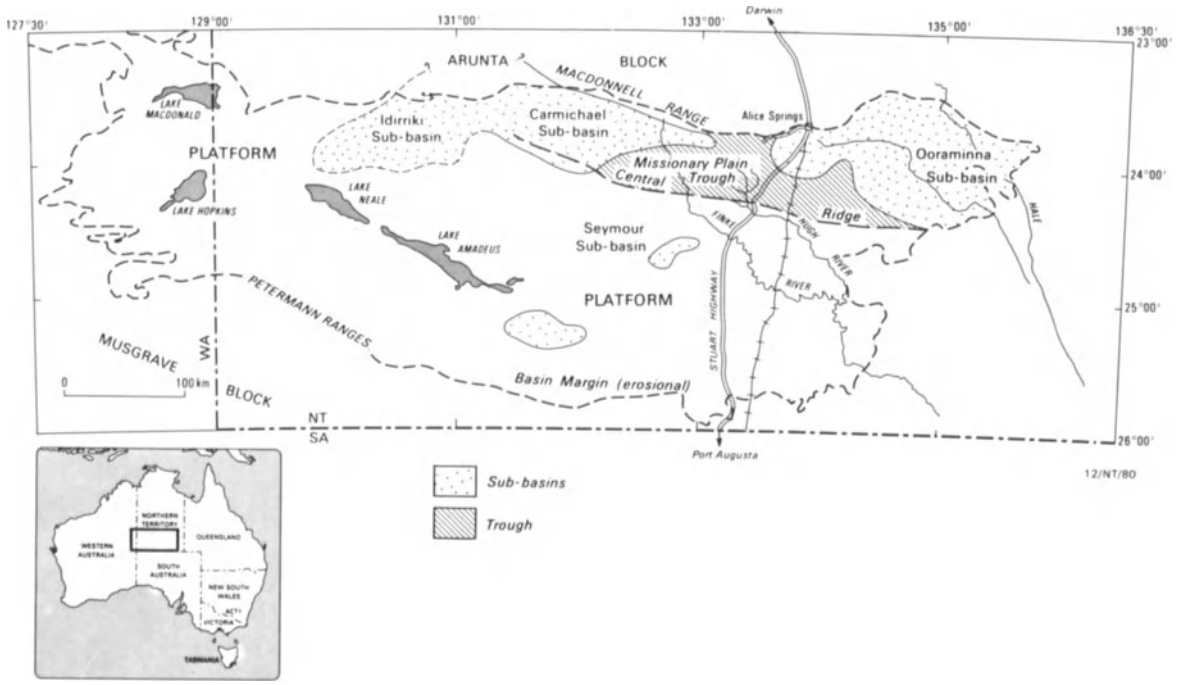

Figure 3.1. Map showing location of the Amadeus basin and the main morphologic features discussed in the text (sub-basins, trough, platforms, and ridges). The Petermann Ranges, which form part of the Musgrave Block, were an active source of clastic sediment during deposition of the Arumbera Sandstone.

Using a combination of (1) subsidence due to rifting followed by thermally induced subsidence, (2) the growth and demise of the Central Ridge (peripheral bulge?), (3) relative sea level derived from both of the above, and (4) the sedimentary facies observed in the Amadeus basin, it is possible to construct an idealized sedimentary succession for a single stage of basin development due to crustal extension (Fig. 3.4).

Assuming latitudinal stability during the period of basin formation, the predictable nature of the main features of the depositional succession can be related to the onset of thermal subsidence and the initiation and ultimate decay of the peripheral bulge. Following extension, the basin was open to the ocean, and clastic sediments derived from an unrestricted hinterland were deposited in a shallow-marine setting. As sedimentation and thermal subsidence proceeded, crustal loading resulted in flexure and the development of a peripheral bulge. The basin was shallow, so that the bulge, even though of small amplitude, restricted the sources of clastic sediments. This resulted in a shift from clastics to evaporites and carbonates. As the amplitude of the bulge grew and peaked, sediments onlapped it at first, and ultimately were transported over it, producing a long-term rise and then a fall in relative sea level, which ended in an erosional sequence boundary. As the peripheral bulge decayed and sediments filled the existing basin, a broader hinterland once again became available to provide a source for clastic sediments. Relief of the source area was reduced by this time; thermal subsidence was also slowing, and as a consequence, the sediments were progressively reworked. Superimposed upon the general depositional pattern are the effects of eustatic sea-level change (Lindsay and Korsch, 1989, 1992).

The Basin Fill

Basin stratigraphy is complex, and its nomenclature is still evolving (Fig. 3.2). Sedimentation began in the Late Proterozoic and continued until Late Devonian (Fig. 3.2).

Stage 1

The Late Proterozoic sedimentary rocks deposited in Stage 1 (the first extensional episode) of the Amadeus basin consist of a well-preserved succession of shallow-marine to nonmarine sedimentary rocks, which rests unconformably upon the much older Arunta and Musgrave Complexes (Fig. 3.2).

Recently, Lindsay and Korsch (1989) have suggested that successions of fluvial sediments with associated extrusives

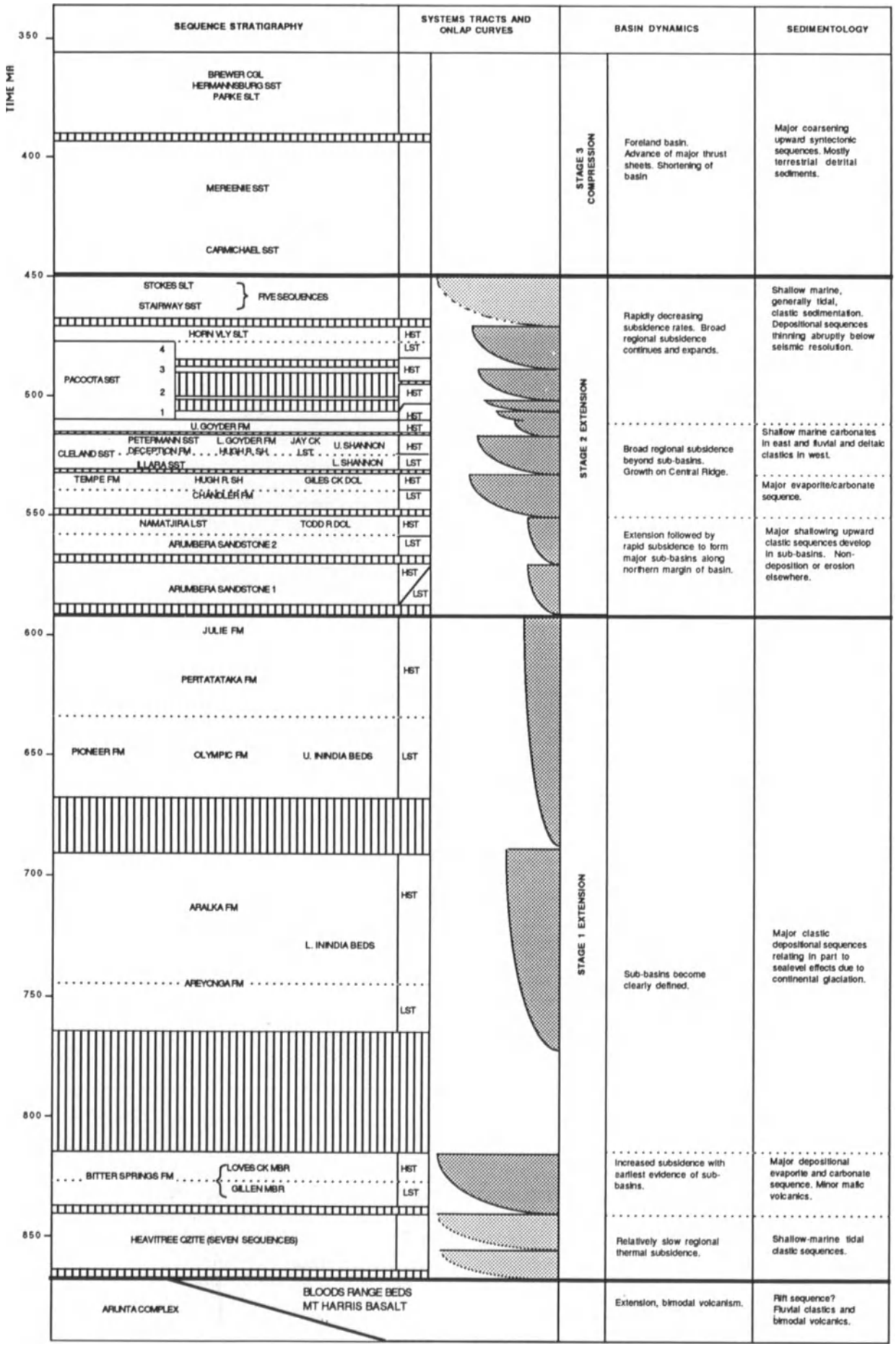

Figure 3.2. Simplified sequence-stratigraphic chart and onlap curves for the Late Proterozoic to Devonian sequences in the Amadeus basin (after Lindsay and Korsch, 1991). Onlap curves are based on onlap of the southern margin of the basin.

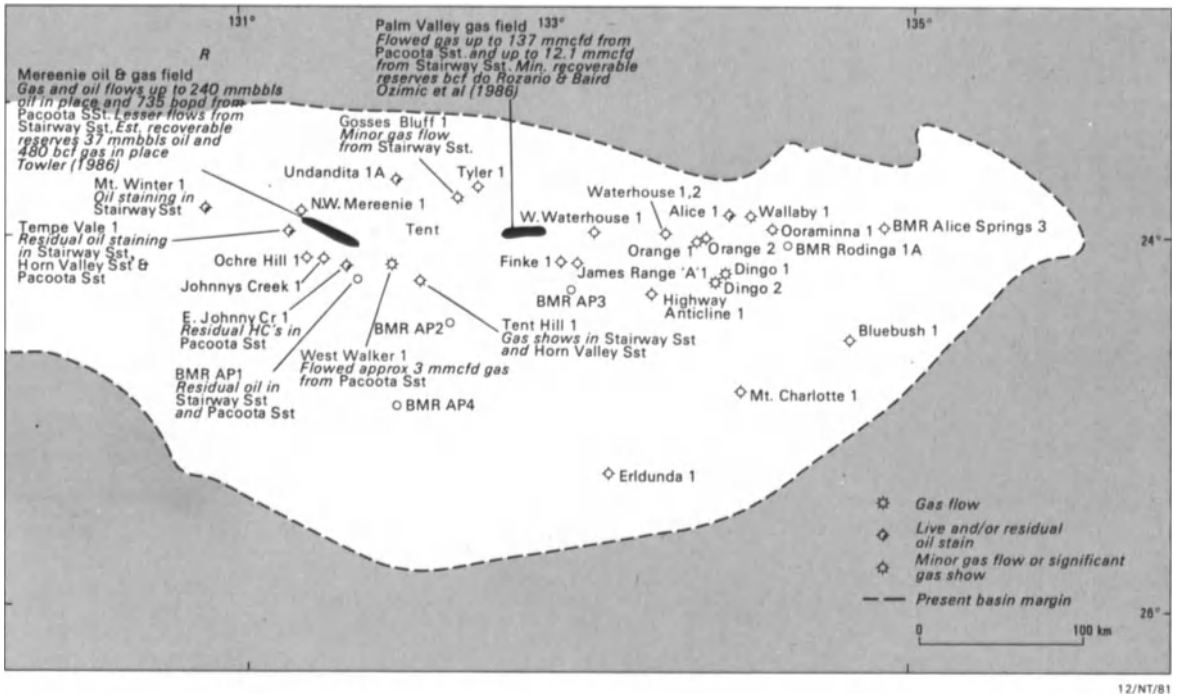

Figure 3.3. Hydrocarbon occurrences within the Larapinta Group (modified from Jackson et al., 1984).

may have formed a rift sequence locally prior to thermal recovery, which commenced with the deposition of the Heavitree Quartzite. There is, however, considerable uncertainty about the timing of the deposition of these rocks, and they may relate to earlier events.

The widespread deposition of the Heavitree Quartzite (and correlative Dean Quartzite) and the carbonates and evaporites of the Bitter Springs Fm suggest a marked change in depositional patterns as thermal subsidence became the dominant tectonic mechanism. These two units are among the most widespread units in the basin and are mostly shallow marine (often tidal).

The Bitter Springs Fm is terminated by an erosional sequence boundary, upon which the fluvial and glacigene sedimentary rocks of the Areyonga Fm and its equivalents were deposited. The Pertatataka and Julie Fms, at the top of the Stage 1 succession, form a single, shallowing-upward depositional sequence that begins with somewhat deeper-water pelagic and turbidite units and terminates abruptly with oolitic carbonates deposited in a platform setting. These sediments appear to have been deposited in a post-thermal subsidence setting, and their deposition may relate to local tectonism and sea-level change.

Exclusive of the rift sequence, the total thickness of the Proterozoic succession deposited during Stage 1 averages about 2,000 m, although in the northeast, it may be as thick as 3,000 m. Where observed, the sedimentary rocks of the rift sequence are highly variable in thickness and may locally exceed 2,000 m in thickness. The mean thickness of the Gillen Member evaporites is 810 m, but locally, beneath major structures, it may exceed 2,000 m (Lindsay, 1987b).

Stage 2

Depositional patterns within the Amadeus basin change abruptly at the sequence boundary between the Julie Fm and the Arumbera Sandstone, with the initiation of the Stage 2 extensional event (Fig. 3.2). Above the sequence boundary, sedimentation was largely restricted to the major sub-basins and the troughs in the north. The southern platform area became an area of sediment bypass or nondeposition. Sedimentation within the sub-basins was relatively continuous, but there are significant time breaks in the successions in the Missionary Plain Trough and the platform areas. In the west, the Early Paleozoic section is dominated by fluvial units, while to the east, shallow-marine units, of both clastic and carbonate sediments, dominate. The deposition of carbonates in the northeast occurred when the Central Ridge began to develop along the southern margin of the sub-basins, which precluded deposition of clastic sediment. The growth of this ridge appears to have been triggered by flexure as a response to sediment loading in the sub-basins and the flow of Proterozoic salt into the growing structure (Lindsay and Korsch, 1989, 1991).

Sedimentation began in the latest Proterozoic with the

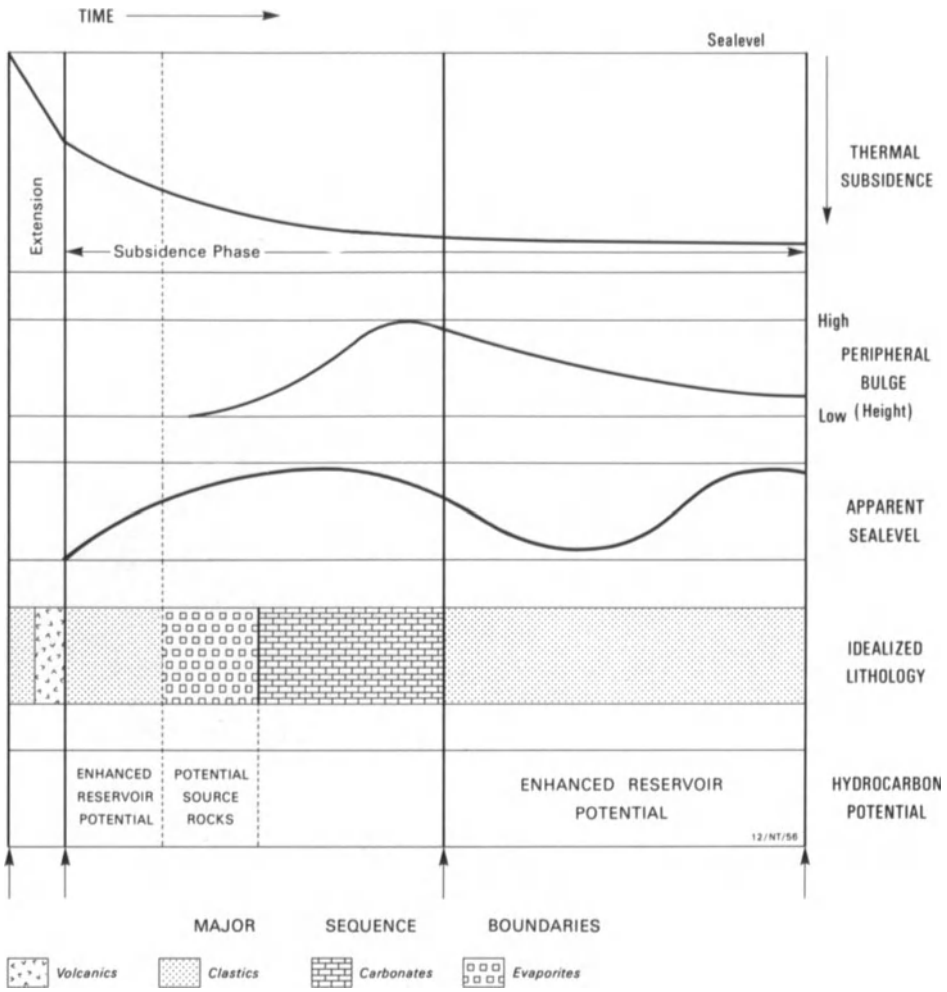

Figure 3.4. An idealized sedimentary succession for a single stage of rifting and thermal subsidence, showing the relation between lithology, relative sea level, depositional sequences, and basin mechanics in a situation where the continents maintain latitudinal stability. Relative sea level is controlled, to a large degree, by basin dynamics (i.e., extension, thermal subsidence, and the growth of the peripheral bulge due to sediment loading). (After Lindsay and Korsch, 1989.)

deposition of the Arumbera Sandstone—a major potential reservoir, and one of the major units to be discussed in the following sections (Fig. 3.2) (Lindsay, 1987a). In general, Cambrian sedimentation was restricted to the sub-basins and their interconnecting troughs (Fig. 3.1 and and 3.5). However, successive formations onlapped to the south onto the margin of the sub-basins as subsidence progressed. The most dramatic change in depositional patterns occurred in the Middle Ordovician, when the area of deposition expanded rapidly (Lindsay and Korsch, 1989, 1991).

A major sequence boundary within the Late Cambrian Goyder Fm (Fig. 3.2) marks a significant time gap (Shergold, 1986) and a major change in depositional style, and represents the time at which the Central Ridge ceased to be a major barrier to clastic sediments (Lindsay and Korsch, 1989, 1991). Consequently, Ordovician sediments onlapped the southern margin of the basin such that by the Early Ordovician (Arenig), shallow-marine conditions extended over much of the Amadeus basin, and clastic sedimentation was dominant. During this time, sediment supply was, for the most part, in step with available depositional space, so that, with some exceptions, water depth remained shallow and commonly within the tidal range. Water depth appears to have increased abruptly for a short period due to a eustatic sea-level rise, which resulted in deposition of the Horn Valley Siltstone, the basin's main potential source rock. The basin's major petroleum reservoir, the Pacoota Sandstone, was also deposited during this time interval.

The depocenters were more complex during Ordovician time than they were in the Cambrian, due in part to a general eastward shift of sedimentation into the Missionary Plain Trough and the appearance of a secondary depocen-

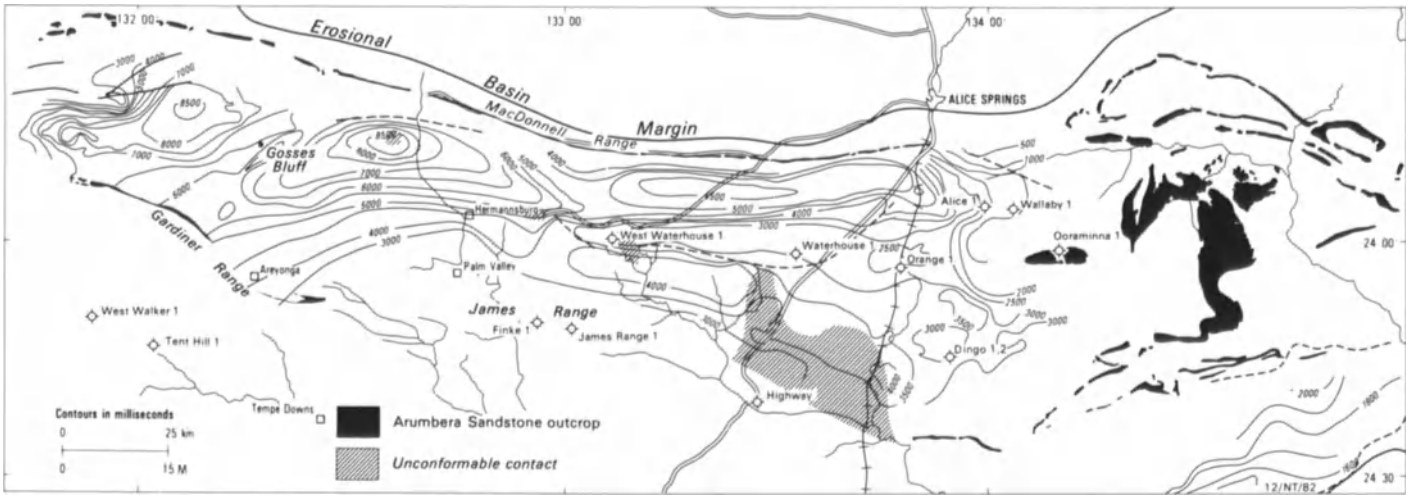

Figure 3.5. Two-way time to the base of the Arumbera Sandstone. Contour interval is 250 m. (After Lindsay, 1987a).

ter in that area. Although the sub-basins were subsiding faster than other areas of the basin, they were not nearly as sharply defined as in the Cambrian.

Stage 3

The final depositional episode in the Amadeus basin began in the Devonian, as major, southward-directed thrust sheets caused progressive downward flexing of the northern margin of the basin, and sediment was shed from the thrust sheets into the downwarps (Fig. 3.2) (Wells et al., 1967; Jones, 1972; Shaw et al., 1984; Korsch and Lindsay, 1989; Lindsay and Korsch, 1989, 1991). This event shortened the basin by 50 to 100 km and effectively concluded sedimentation (Korsch and Lindsay, 1989). Events relating to this stage of basin development are responsible for most of the obvious structural patterns (anticlines, domes, and thrust faults) visible in the surface geology today.

The mid-Paleozoic sedimentary rocks of Stage 3 are best described as molasse. They are widely distributed in the Amadeus basin, but when viewed in their entirety, are much thicker in the Carmichael sub-basin than elsewhere. Locally in that sub-basin, they are more than 5,000 m thick, but they average 4,200 m thick.

Structural History

Significant discoveries in the Amadeus basin all have been in structural traps in the crests of major domes or anticlines, all of which are cored by salt derived from the Late Proterozoic evaporites of the Gillen Member of the Bitter Springs

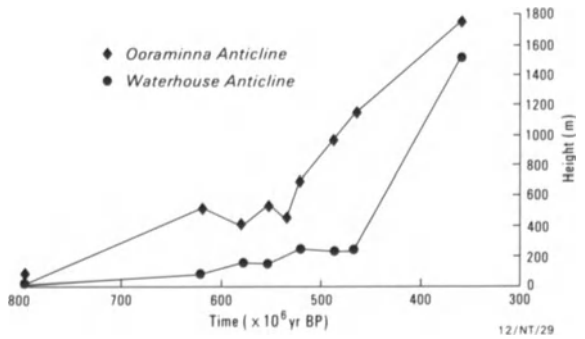

Figure 3.6. Amplitude of the evaporite high beneath the Ooraminna and Waterhouse anticlines as a function of time. Note that salt appears to have moved out of, or been dissolved from, the structures on occasion, and that the growth rate increases through time. Amplitudes were derived by using each mapped seismic surface as a datum, on the assumption that since the sediments were deposited in shallow water, original depositional surfaces were essentially horizontal. (After Lindsay, 1987b).

Fm (McNaughton et al., 1968; Lindsay, 1987b). Thinning over the salt structures suggests that, in some cases, they were initiated as early as the middle of the Late Proterozoic, but that most structural growth occurred over an extended period in the later Paleozoic during the Alice Springs Orogeny (Lindsay, 1987b) (Fig. 3.6). Salt tectonics contributed significantly to depositional patterns as well as structural style in the basin.

At least two generations of thrust faulting are present in the Amadeus basin, with thrusting from both north and southwest. Schroder and Gorter (1984) suggested that wrench faulting may have played a part in the development of the en echelon anticlinal trends in the western part of the basin. The initial thrusting or wrenching events probably

took place during the Petermann Ranges Orogeny, and were rejuvenated to some degree during the Alice Springs Orogeny.

The Amadeus basin has been stable since the Alice Springs Orogeny, although general uplift and erosion have continued, with the removal of 2 to 3 km of sediment by erosion, probably since the Carboniferous. Superimposed drainage and relict high-level gravels attest to prior erosive episodes, some of which may date back as far as the Late Mesozoic or Early Tertiary. As a consequence, the present basin margins are erosional rather than depositional.

Hydrocarbon Resources

Hydrocarbons are produced at present from two fields within the Amadeus basin—Mereenie Field and Palm Valley Field—while a third, Dingo Field, remains undeveloped (Fig. 3.3). Fourteen other uneconomic hydrocarbon accumulations also have been discovered in the Amadeus basin since the first hydrocarbon discovery was made in 1963 (Ozimic et al., 1986). All are present in structural traps in the Carmichael and Ooraminna sub-basins and the Missionary Plain trough. Estimates suggest that the basin's petroleum resources consist of 5.74×10^6 m^3 of oil, 1.53×10^6 m^3 of natural gas liquids, and 14.93×10^9 m^3 of sales gas (Ozimic et al., 1986). Oil and gas from Mereenie Field are carried by pipeline 146 km to Alice Springs, while gas from the Palm Valley Field is carried 1,537 km by pipeline to Darwin on the continent's northern coast.

Hydrocarbon Potential

Depositional models, based on an understanding of basin dynamics, suggest that source and reservoir rocks are more likely to be deposited during particular stages of basin evolution, depending on subsidence rates and supply of clastic or nonclastic sediments (Lindsay and Korsch, 1989, 1991) (Fig. 3.4). However, such models are idealized, and other effects, particularly major eustatic sea-level changes and latitudinal migration of the plates, may modify this general pattern.

Potential source rocks are most likely to develop in restricted marine settings, which are very sensitive to both basin dynamics and eustatic sea-level effects. The effects of eustatic sea-level changes vary depending on the timing of their interaction with basin dynamics. Source rocks are most likely to be deposited when water depths are increasing rapidly and bottom conditions become anoxic. In the Amadeus basin, this occurred shortly after crustal extension, when thermal subsidence was at its maximum (Fig. 3.4). If sea level falls rapidly at the same time, the inflow of seawater is limited at a time when the basin is deepening rapidly, which results in a deep restricted basinal setting. At the same time, crustal flexure due to sediment loading may restrict the movement of clastic sediments into the sub-basins. The results is deposition of evaporites and carbonates under anoxic conditions, with concurrent preservation of organic materials. Two major units with source-rock potential were deposited following both extensional stages in the Amadeus basin: the Late Proterozoic evaporites of the Gillen Member of the Bitter Springs Fm, and the Early Cambrian evaporites of the Chandler Fm. Both have exhibited source-rock potential, although the Gillen Member is overmature over much of its northern extent (Jackson et al., 1984).

The model suggests that clastic reservoir units are likely to be deposited during two stages of basin development (Fig. 3.4):

(1) In the early stages of basin development, either concurrent with or immediately following extension and the onset of thermal subsidence.
(2) Late in basin development as subsidence declines and sedimentation rates are reduced, allowing considerable reworking of the detrital materials.

Reservoirs associated with the first setting are likely to be fluvial or deltaic in origin, while those from the second setting are more likely to be shallow marine or tidal in origin.

Coincidentally, the two major reservoir units in the Amadeus basin, the Arumbera Sandstone and the Pacoota Sandstone, come, one each, from these two settings (Fig. 3.2). The Late Proterozoic to Early Cambrian Arumbera Sandstone was deposited shortly after the second extensional event in the Amadeus basin and is coastal plain or deltaic in origin; the Ordovician Pacoota Sandstone was deposited late in the thermal-subsidence phase of basin development and is largely tidal or shallow marine in origin. This allows an interesting comparison to be made between the two depositional settings.

Most of the hydrocarbons discovered to date in the Amadeus basin were sourced from the Ordovician Horn Valley Siltstone (Schroder and Gorter, 1984; Jackson et al., 1984), an organic-rich black shale sequence deposited, during a sea-level high stand, deposited between relatively clean sandstones towards the end of Stage 2. The reservoir for the hydrocarbons is usually the Pacoota Sandstone, which lies stratigraphically immediately below the Horn Valley Siltstone (Fig. 3.2). Source rock–reservoir rock associations, such as the Horn Valley Siltstone and the Pacoota Sandstone, result from the interaction between eustatic sea-level rises and the predictable pattern of basin dynamics.

Petroleum exploration in the basin has focused on the reservoir potential of the Arumbera and Pacoota Sand-

stones, with source and seal provided by the Tempe Fm, Hugh River Shale and Chandler Limestone, and the Horn Valley Siltstone. Results from recent exploration and Bureau of Mineral Resources research indicate that significant potential may exist for additional accumulations in less well-explored parts of the succession, especially in the Late Proterozoic units.

Arumbera Sandstone

Basinal Setting

Age and Stratigraphy

The Arumbera Sandstone lies at the base of the Cambro-Ordovician succession straddling the Proterozoic–Cambrian boundary (Taylor, 1959; Preiss et al., 1978; Burek et al., 1979; Lindsay, 1987a; Walter et al., 1989) (Fig. 3.2). In the more southerly areas of the basin, coarser lensoidal units—the Quandong Conglomerate and the Mount Currie Conglomerate, including the arkoses at Ayres Rock—are thought to be equivalent to the Arumbera Sandstone (Forman, 1966, Ranford et al., 1966). Early stratigraphic work involving the Arumbera Sandstone is discussed by Wells et al. (1965, 1970).

Regional Distribution

The greatest development of the Arumbera Sandstone occurs north of the Central Ridge in a broad synclinal complex between the MacDonnell and Idirriki Ranges in the north, and the James and Gardiner Ranges in the south and southwest (Fig. 3.7). The sediments accumulated in three sub-basins: the Idirriki in the west, the Carmichael in the center, and the Ooraminna to the east (Lindsay, 1987a) (Fig. 3.1). All three features and their connecting troughs lose definition rapidly to the south as they approach the Central Ridge.

The thickest development of the Arumbera Sandstone occurs in the Carmichael sub-basin, where it approaches 2,000 m (Fig. 3.7). To the south and southwest, the Arumbera Sandstone thins rapidly as it approaches the Gardiner Range (Fig. 3.8). Foreshortening occurs across the Gardiner Range thrust where thinner sediments from several kilometers farther south have been thrust over thicker sediments closer to the center of the Carmichael sub-basin. Few data have been produced to the south of the range, other than some isolated well-control data, which suggest that the formation pinches out rapidly to the south of the Gardiner Range. From the Carmichael sub-basin into the Missionary Plain trough, the formation thins rapidly. Average thicknesses of 600 to 700 m in the Carmichael sub-basin are reduced to about 300 m in the Missionary Plain trough. Southward, toward the James Range, the formation thins and pinches out against the Central Ridge. From the longitude of Alice Springs eastward, the formation again thickens rapidly into the Ooraminna sub-basin (Fig. 3.7). The Ooraminna sub-basin is a broader, more open feature than the Carmichael sub-basin, and the maximum formation thickness exceeds 1,100 m. The formation gradually thins to the south onto the extension of the Central Ridge (Fig. 3.8).

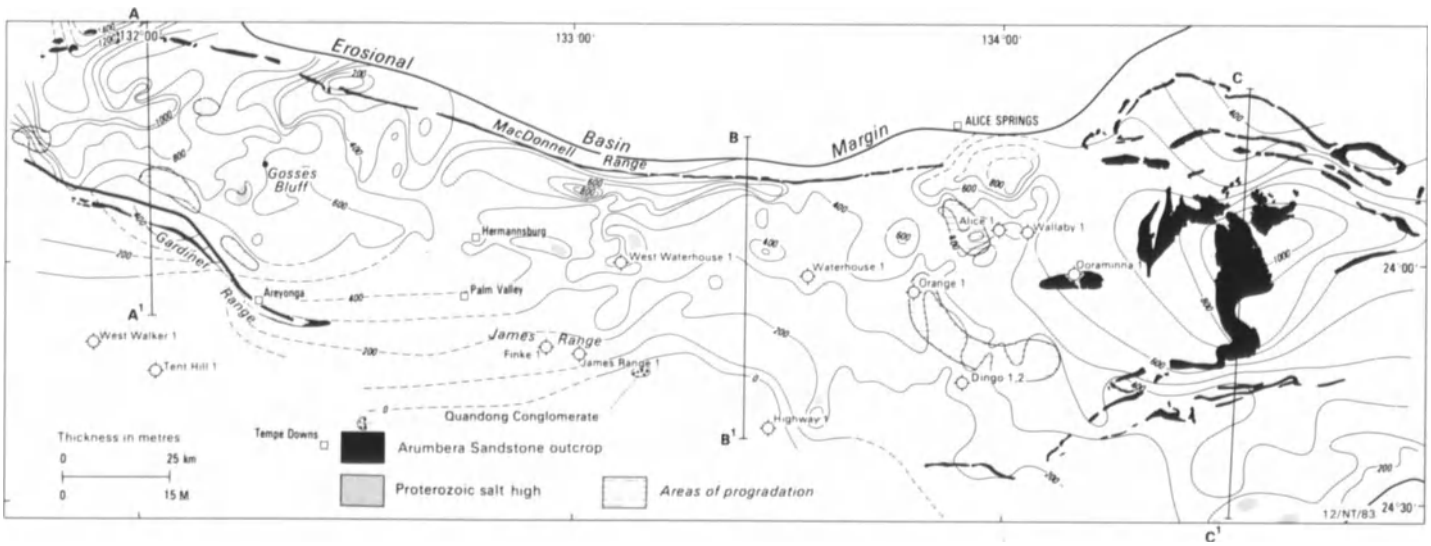

Figure 3.7. Isopach map of the Arumbera Sandstone showing areas of progradation and onlap and the location of Bitter Springs Fm salt highs. Contour interval is 100 m. (Adapted from Lindsay, 1987a.)

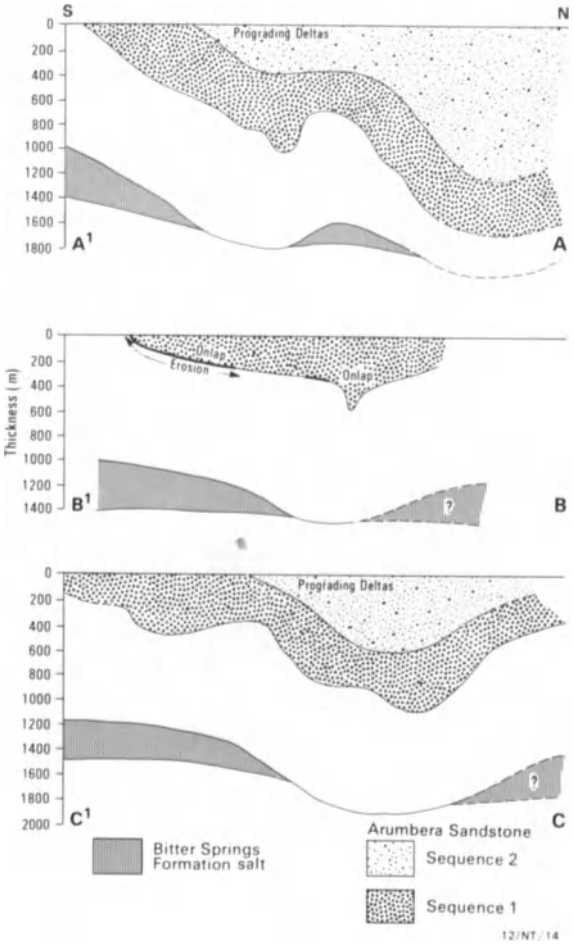

Figure 3.8. Idealized north-south cross sections through (a) the Carmichael sub-basin, (b) the Missionary Plain trough and (c) the Ooraminna sub-basin, showing the relation between the two depositional sequences within the Arumbera Sandstone and the relation of the formation to the underlying Bitter Springs Fm. The top of the Arumbera Sandstone forms the datum for these sections.

South of the Central Ridge, the Arumbera Sandstone is not well known due to a lack of seismic data and poor outcrop. Where the formation or its equivalent can be seen, it is very thin, suggesting that the area to the south and southwest of the Central Ridge was, for the most part, an area of sediment bypass during Arumbera deposition.

Facies Analysis

The Arumbera Sandstone and the associated Todd River Dolomite form two depositional sequences that begin abruptly above the platform carbonates of the Julie Fm (Figs. 3.9, 3.10, 3.11) (Lindsay, 1987a). In lithologic terms, each sequence forms a large-scale, coarsening-upward cycle. In general terms, the two sequences are similar lithologically, but there are significant differences. The lowermost sequence, sequence 1, begins abruptly above the carbonates of the Julie Fm as fine-grained, red, highly fissile, silty shales (Fig. 3.9). Higher in the section, thin, irregularly spaced, fine-grained sandstone beds begin to appear with increasing frequency. The sandstone beds, which are mostly 2 to 3 cm thick, all have sharp bases and gradational upper contacts. Internally, most are finely laminated, and some contain climbing ripples. The sandstone beds all appear to be "distal" turbidites deposited into a somewhat deeper-water pelagic environment. The sediments of this part of the sequence are perhaps best described as pelagic or basinal. The thin turbidite units appear to have been generated upslope during extreme storm or flood events and are probably similar to those discussed by Woodrow (1985) and Lundegard et al. (1985) from the Catskill Delta.

Higher in the sequence, the thin sandstones cease abruptly and are replaced by much thicker sandstone beds, which like their predecessors, have sharp lower contacts and gradational tops (Fig. 3.9). Initially, these beds are relatively infrequent and have a maximum thickness of 1 m. Higher in the section, they become more frequent and have maximum thicknesses of 2 to 3 m. Ultimately, the sandstones become the dominant lithology and then begin to oscillate back and forth through more shaley and then more sandy intervals. The lower contacts of these thicker sandstones are not only sharp but bear both flute and load casts. Internally, they are poorly laminated, and many units have poorly developed hummocky cross stratification. As the sandstones thicken higher in the sequence, they tend to become more massive and featureless. Approximately 10% of these sandstone units are highly deformed as a result of soft-sediment failure. Generally, the deformed units are less than 50 cm thick. These sandstone units all appear to have been generated by storm or flood events in a slope environment.

The uppermost part of sequence 1 is considerably more variable than the lower part of the sequence. In the Ooraminna sub-basin, the sandstones that form the uppermost part of the sequence are thick, massive, and largely featureless, with rare indications that they are, in part, large-scale channels. In the Missionary Plain trough and the Carmichael sub-basin, the upper unit is not as monolithic and consists of stacked, shallowing-upward cycles that are predominantly massive sandstone.

Of these small cycles, the lower or earlier ones begin in silty shales or poorly sorted silty sandstones that are generally featureless. Better sorted and more regularly bedded sandstones appear above them. Internally, the sandstones are well laminated (varve-like, according to Schumm, 1968), and toward the top, they are highly contorted due to both soft-sediment folding and water-escape structures. The intensity of soft-sediment deformation increases up-

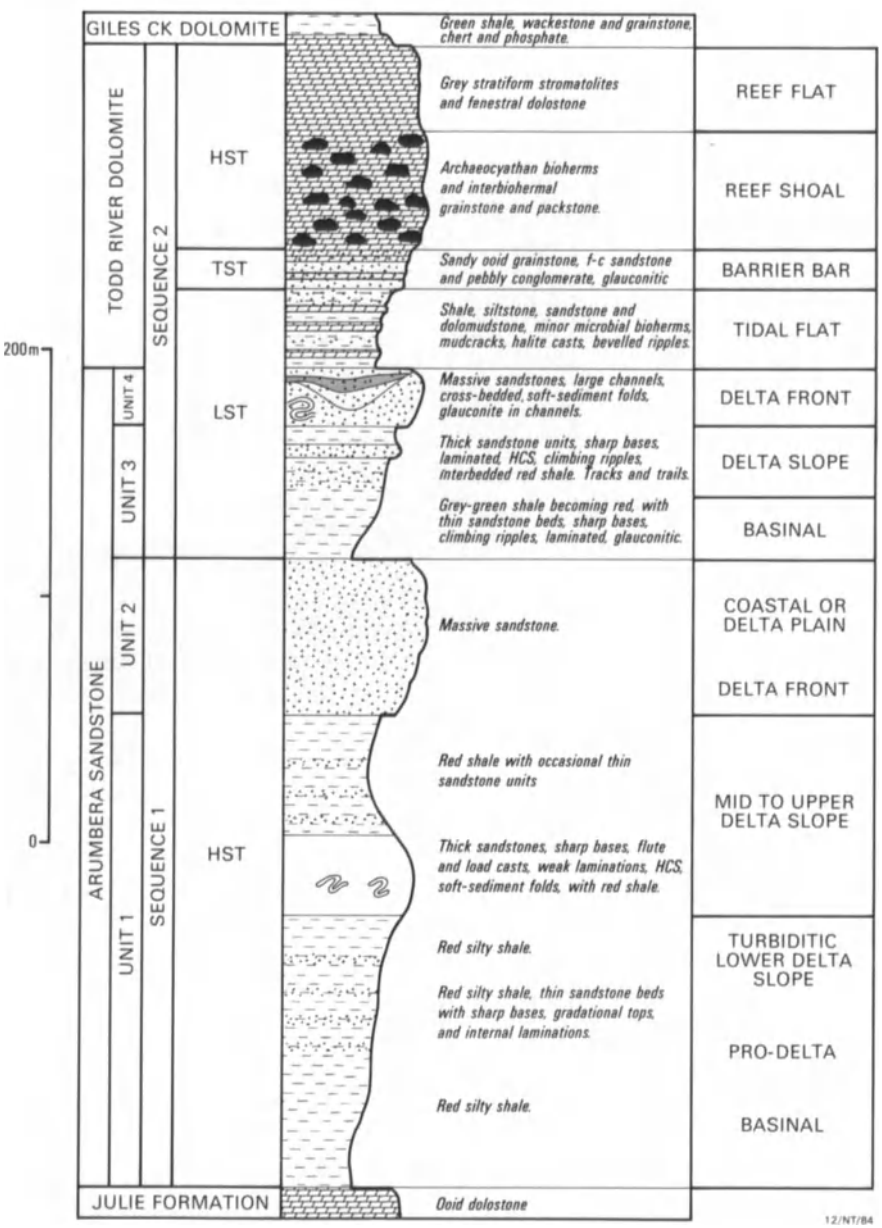

Figure 3.9. A detailed section through the Arumbera Sandstone in the Ooraminna sub-basin (134°29′E, 23°36′S) showing the two depositional sequences and the interpreted facies associations. At this locality, the clastic sediments of sequence 2 are relatively thin compared with its development closer to the center of the sub-basin (After Lindsay, 1987a, and Kennard and Lindsay, 1991) HST = highstand systems tract, TST = transgressive systems tract; and LST = lowstand systems tract.

ward until more massive cross-bedded sandstones, which are locally intersected by large channels, begin to dominate. Slump folds and mud-chip breccias are common features of the channel sandstones. Soft-sediment deformation is more common in the Gardiner Range area on the southern margin of the Carmichael sub-basin than elsewhere, perhaps in response to a locally steeper paleoslope. The massive, well-sorted sandstones near the tops of the cycle form prominent strike ridges. In the west, the upper unit is entirely fluvial sandstone. These varve-like and channelled sandstones are interpreted as part of a coastal or delta plain association.

To the south, where the formation onlaps the Central Ridge (Fig. 3.7, 3.8), major cycles within sequence 1 terminate locally in as much as 2 m of poorly sorted conglomerate. The conglomerates are interpreted as braided-stream deposits. Locally, at the eastern end of the Gardiner Range, the Arumbera Sandstone appears to interfinger

Figure 3.10. Areal photograph, taken from approximately 500 m above the ground, showing (1) the Julie Formation, (2) sequence 1, and (3) sequence 2 of the Arumbera Sandstone in the Ooraminna sub-basin 50 km to the east of Alice Springs. (After Lindsay, 1987a.)

laterally with marine stromatolitic carbonates that were deposited in a shallow interdistributary embayment where terriginous sedimentation was precluded.

Sequence 2, like sequence 1, begins in fissile, featureless siltstones. However, the siltstones are grey-green in the lower part of the section, and only become red about halfway up the section; they do not include the thin turbidite units present in sequence 1. Instead, the shales contain thin (1 to 7 cm thick) better sorted sandstone units, which are often internally laminated or contain climbing ripples. Their upper and lower contacts are sharp. Some of the thicker sandstone units are much coarser and highly glauconitic.

As in sequence 1, thick sandstone units with sharp bases begin to appear about halfway through the section. Internally, these units contain climbing ripples and well-developed hummocky cross stratification. Ultimately, thick, featureless sandstone units begin to dominate, and invertebrate tracks and trails and evidence of bioturbation appear. Within a small stratigraphic interval, sandstone predominates, and large channels appear. The channels are 2 to 4 m thick and contain relatively well-sorted, medium-grained sandstones with some glauconite. The sandstones are often cross bedded, and large-scale soft-sediment folds appear in the base of the channels, apparently as a response to sediment loading. Mud-chip breccias likewise are a common feature. Locally, traces of copper mineralization appear near the base of these channelized sandstones in an association similar to that described by Smith and Rose (1985) in the Catskill Delta. As in sequence 1, the lower part of sequence 2 appears to pass upward from a basinal or pelagic facies through the shoreface environment to a coastal plain and deltaic depositional system.

In contrast to sequence 1, the more massive channel sandstones are missing at the top of sequence 2 in the Ooraminna sub-basin, such that it passes abruptly upward into laminated shales, silts, and carbonates, interbedded with 60- to 90-cm-thick sandstone units (Fig. 3.9). Festoon cross bedding and mud-chip breccias are a common feature of the thicker sandstone units, which are laterally quite variable in thickness. Toward the top of the sequence, the thicker sandstone units disappear, and thinly bedded shales and carbonates dominate (Fig. 3.9). Herringbone cross stratification is present but poorly developed in the thinner units. Occasional halite casts suggest hypersaline conditions in the final phase of deposition. All of these features strongly suggest a tidal flat depositional system. These tidal deposits, while temporally part of the Arumbera sequence, are mapped lithologically as part of the Todd River Dolomite. Intraclastic conglomerates associated with the surface of transgression within the Todd River Dolomite form the upper boundary of sequence 2.

In general, the above patterns within the major cycles can be observed throughout much of the basin. In detail,

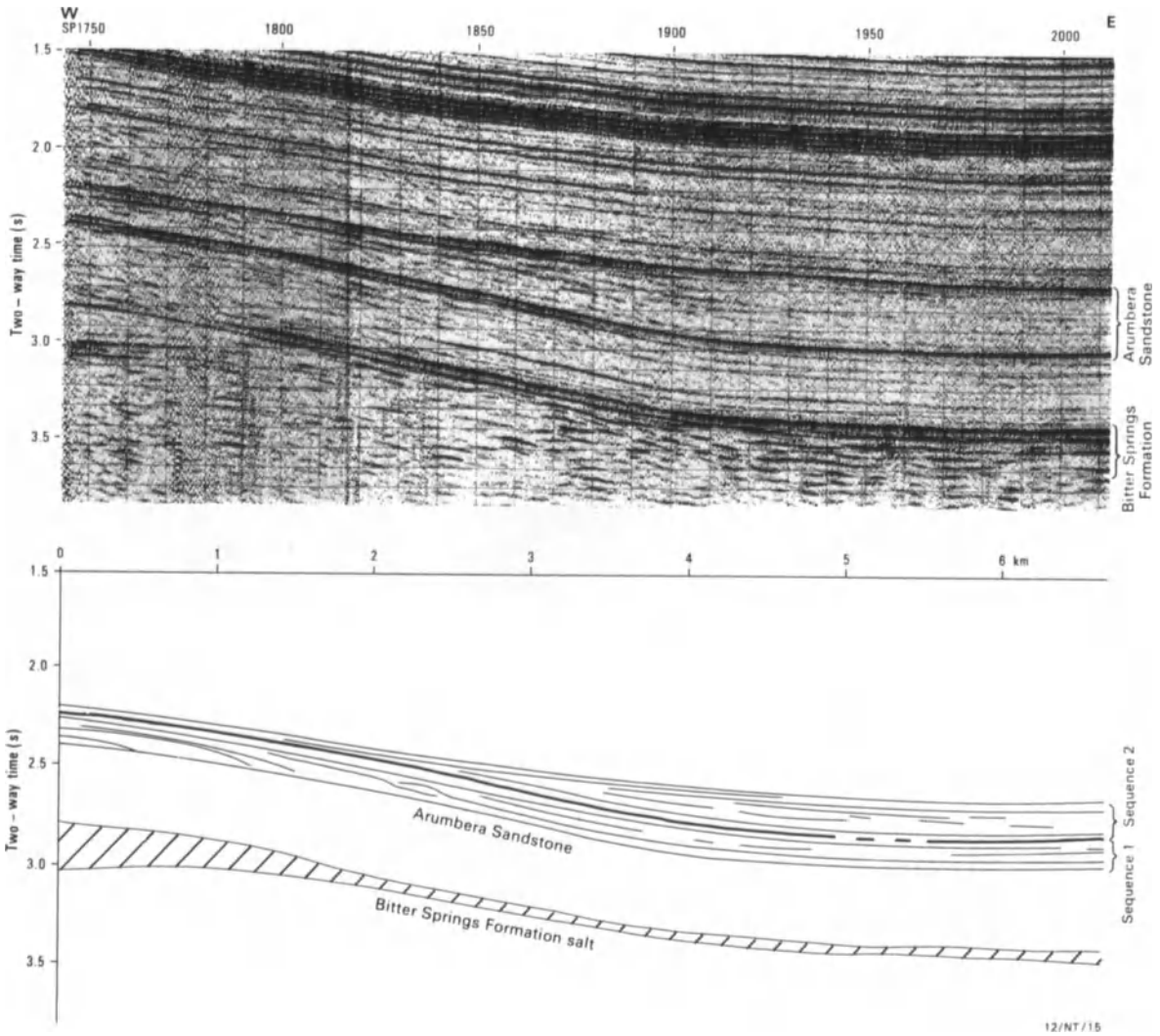

Figure 3.11. A seismic line across the western margin of the Carmichael sub-basin showing the two sequences within the Arumbera Sandstone. The boundary between the two sequences appears to be the Proterozoic-Cambrian boundary. (After Lindsay, 1987a.)

however, they are much more complex, in that they consist of numerous small-scale, coarsening-upward parasequences (van Wagoner et al., 1987), similar to coal-measure cyclothems but modified in that vascular plants had not evolved at the time the Arumbera Sandstone was being deposited. The parasequences vary in composition and completeness according to their position in the depositional sequence. Where the dominant environment was in the deeper water basinal facies, parasequences are, at best, difficult to define. However, as the overall depositional environment shallowed, parasequences became better developed, because small changes in water depth had a significant effect on the sedimentary structures preserved. Thus, as discussed previously, toward the top of the sequence, the parasequences are much more prominent as they progress from variably bioturbated, poorly sorted sandstones to more massive, well-sorted sandstones of a coastal plain/deltaic depositional system.

Depositional Setting

The depositional space into which the Arumbera Sandstone was deposited was created in large part by the initiation of the second extensional episode of basin formation at about 600 Ma, which led to the development of the major sub-basins along the basin's northern margin (Lindsay, 1987a, b; Lindsay et al., 1987; Lindsay and Korsch, 1989, 1991). The Petermann Ranges Orogeny modified the southwestern margin of the basin at approximately the same time (Forman, 1966) and further accelerated the development of growth structures and, in particular, the Central Ridge

(Lindsay, 1987b). Sediments derived from upthrust blocks developed during the Petermann Ranges Orogeny to the south and southwest provided the primary clastic source for the formation. Thus, by the time Arumbera sedimentation began at the end of the Proterozoic, a shallow, rapidly subsiding, east-west-trending depositional basin had developed along the basin's northern margin. A broad growth structure, the Central Ridge (McNaughton and Huckaba, 1978; Lindsay 1987a), formed concurrently to the south of the main depocenters, which were being fed by an active source of sediment to the southwest.

The Arumbera Sandstone was deposited during two major eustatic sea-level cycles, one on either side of the Proterozoic-Cambrian boundary. Sea-level rose rapidly following deposition of the platform carbonates of the Julie Fm at the end of the previous sea-level cycle. This rapid rise, combined with the rapidly subsiding sub-basins, resulted in development of a single large-scale, coarsening-upward highstand systems tract in all three sub-basins and their connecting troughs. Locally, a relatively thin transgressive systems tract developed on the margins of the sub-basins; this is the unit that forms the major reservoir interval in the Dingo Field (a significant point discussed in more detail in the following section). As a consequence of the rapid changes in relative sea level, lowstand deposits are of minimal importance in sequence 1. They are seen neither in outcrop nor well logs, but are indicated on seismic sections in the center of the Carmichael sub-basin as poorly defined mounded units—presumably a lowstand fan (Lindsay, 1987a).

Sedimentation occurred in a shallow-marine and deltaic or coastal plain environment in a setting similar to that of the Devonian Catskill Delta of North America. The facies transition from the shallow-water oolitic platform carbonates at the top of the Julie Fm to the deeper-water pelagic shales and turbidites of the basal Arumbera Sandstone is abrupt, suggesting that, for a brief period, the combined effects of rising eustatic sea level and rapid basin subsidence resulted in available depositional space outpacing sediment supply. Sediment was supplied from the southwest by braided streams. The sediments were probably deposited in a coastal plain setting, for the most part, with small-scale deltas prograding across the carbonate platform sediments of the Julie Fm (Figs. 3.11 and 3.7).

During accumulation of the second sequence, sea level at first fell rapidly, exposing large areas of sediment deposited during the first cycle and restricting sedimentation to the steep-sided, rapidly subsiding sub-basins. Deposition continued in the sub-basins as a series of major deltaic complexes prograded into the sub-basins from their southern and southwestern margins (Fig. 3.11). Deposition was thus, in large part, progradational. Between the major delta complexes, a depositional environment similar to sequence 1 predominated. The two sub-basins remained in communication by way of the deep channel along the northern margin of the Missionary Plain trough. Thus, the lowstand systems tract produced a large-scale, coarsening-upward succession lithologically similar to the highstand systems tract of sequence 1 but with many smaller differences, as discussed previously.

As sea level began to rise again, the depositional setting changed abruptly. The supply of clastic sediment was dramatically reduced, so that the transgressive and highstand systems tracts are dominated by carbonates deposited in a shallow, often tidal or reefal, setting. The transgressive and highstand systems tracts consist of the Todd River Dolomite and the Namatjira Fm, which have been mapped separately from the Arumbera Sandstone as lithologically distinct entities. The controls on sedimentation leading to this abrupt lithologic change are complex and not completely understood. In large part, the change results from the growth of the Central Ridge, which may have been triggered by flexure in response to sediment loading. Certainly, there is evidence that clastic sediments were being blocked by the Central Ridge and redirected around its western end into the Idirriki sub-basin. The change from clastics to carbonates along the east-west axis of the sub-basins in post-Arumbera time is gradational and well documented. The slowing of basin subsidence and the broadening of regional subsidence are probably also important, because an extensive shallow platform began to develop south of the Central Ridge between the sub-basins and their source of clastic sediment, thus reducing movement of clastics. The abundance of clastic sediments in the post-Arumbera Cleland Sandstone and other units in the Idirriki sub-basin suggests that the availability of clastics in the source area had not been reduced but that transport of clastics into the two eastern sub-basins was restricted.

Reservoir Characterization

Texture and Mineralogy

Texture and mineralogy of the sedimentary rocks of the Arumbera Sandstone are largely determined by facies associations and the general depositional setting. In general, the two depositional sequences preserved in the Arumbera Sandstone are coarsening-upward sequences with fine-grained, clay-rich pelagic sediments at their bases, grading upward to the quartz-rich, better-sorted sandstones of a coastal plain/deltaic depositional system. Potentially the best reservoir units might be expected to occur at the tops of the major coarsening-upward cycles in sandstones deposited in a coastal plain/deltaic setting (Lindsay, 1987a). In reality, the more quartzose, better sorted sandstones at the

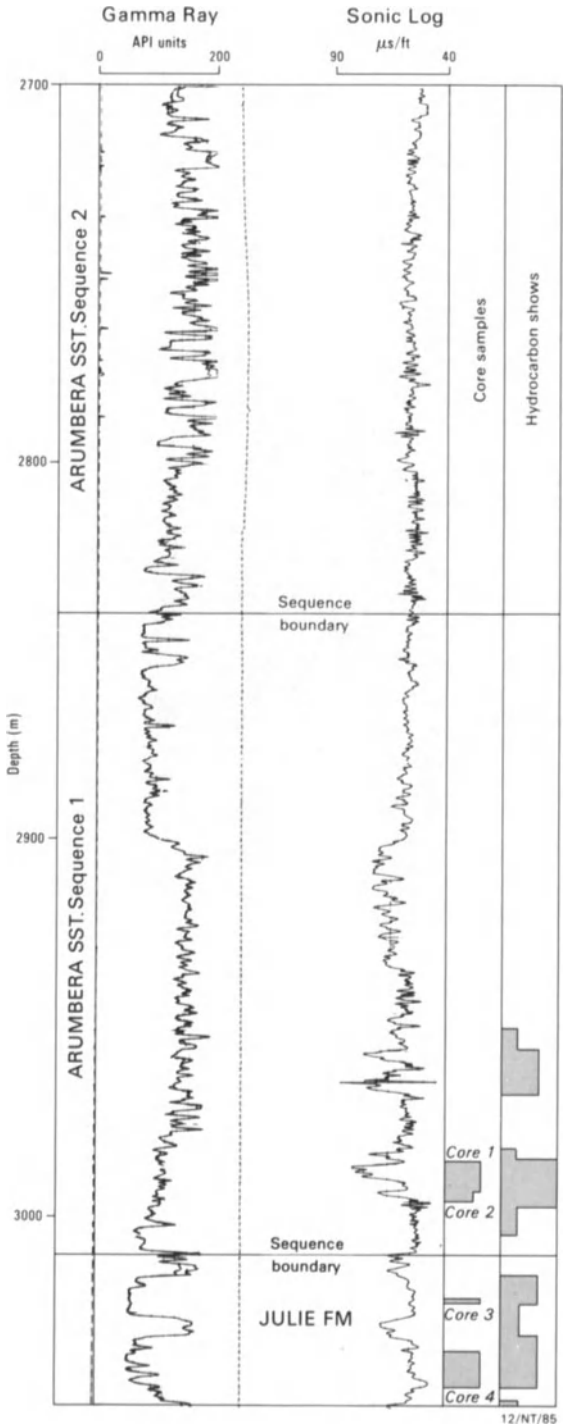

Figure 3.12. Gamma-ray and sonic logs of the Arumbera Sandstone in the Dingo #2 well. This sequence includes small depositional cycles that contain thin reservoir sandstones at their tops. A high feldspar content confuses the gamma-ray logs, so the reservoir sandstones cannot be seen. However, the sonic log clearly shows the higher porosities in the units.

tops of the major cycles are heavily cemented and are often poor reservoirs. In the Dingo Gas Field, however, the reservoir occurs in a thin, basal transgressive sandstone that is more feldspathic than the sandstones at the top of the major cycles. Similarly, reservoir potential is greater in sandstones at the tops of small-scale, shallowing-upward cycles within sequence 1. These sandstones are generally thinly laminated or varve-like and appear to be sheet-flood deposits associated with a coastal-plain setting. As discussed later, much of the porosity is secondary, due either to dissolution of feldspar or anhydrite. These lower, small-scale cycles are more feldspathic than the sandstones at the tops of the major cycles.

Because of the arkosic nature of many of the sandstones, the log response of the Arumbera Sandstone is complex and in need of some explanation (Fig. 3.12). In a simpler situation, the gamma-ray log might be expected to respond directly to grain size and sorting: as clay content decreases, the gamma-ray count would decrease in sympathy. In sequence 1 of the Arumbera Sandstone in the Dingo Gas Field, the lower, shalier portion of the sequence, in general, has a higher gamma-ray count, while the massive sandstones of the coastal plain environment at the top of the sequence have lower values. However, the gamma-ray values do not decrease consistently upward as might be expected in a shallowing-upward sequence, but instead increase upward at first and then decrease abruptly below the massive sandstones at the top of the sequence. Nor does the gamma-ray log respond to the small-scale, shallowing-upward cycles present lower in the sequence. There is, in fact, no indication of the most promising reservoir sandstones. This apparent anomaly relates directly to K-feldspar content of the sandstones. In the case of the thin reservoir sandstones, the K-feldspar content is high and thus gives a strong log response, while the massive sandstones at the top of the cycle, which were more intensely reworked, are more mature. In contrast, the sonic log shows the small, porous reservoir sandstones clearly, while offering little indication of the presence of the well-cemented massive sandstones at the top of the sequence (Fig. 3.12). Correlation of porosity values calculated from sonic-log data between wells shows that the reservoir sandstones at the tops of the small cycles in sequence 1 are very continuous, because the same porous intervals can be identified in the Dingo #1 and Dingo #2 wells, which are 2.5 km apart (Fig. 3.13). Very similar log patterns can be identified in sequence 1 of the Arumbera Sandstone in the James Range #A1. Orange #2, and Wallaby #1 wells, and to a lesser extent, in the Waterhouse #2 well (Fig. 3.3). Outcrop studies of sequence 1 in the MacDonnell Range between Alice Springs and Ellery Creek 90 km to the west show that these small depositional cycles are persistent and can be followed in continuity for at least 30 km. It would thus appear that reservoirs within the Arumbera, while thin, are very continuous.

The reservoir sandstones are fine grained (0.24 to 0.25 mm), with an average grain size of 0.25 mm. Sorting is vari-

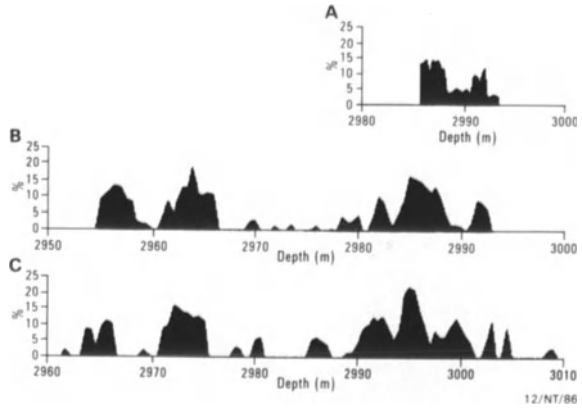

Figure 3.13. Porosity logs for the reservoir interval in the Dingo Gas Field. A and B are calculated porosities derived from sonic logs for the Dingo #1 and #2 wells; C shows core porosities for one reservoir unit in the Dingo #2 well. Note the similarities between the two wells, suggesting that the small cycles, including the reservoir sandstones, are laterally continuous.

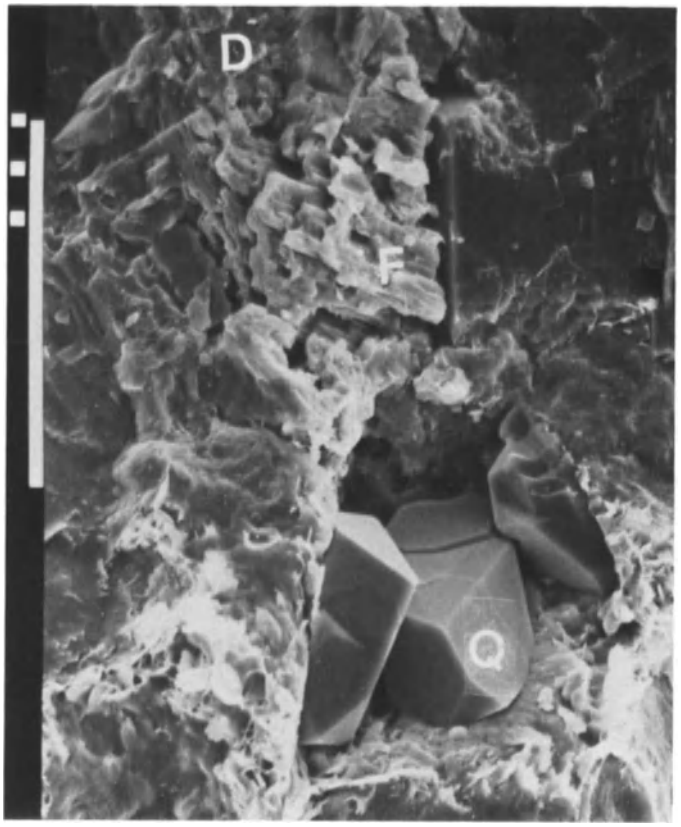

Figure 3.14. Dolomite (D) and microquartz crystals (Q) are common pore-filling materials in the reservoir interval of the Arumbera Sandstone. Some secondary porosity has been generated by partial dissolution of feldspar (F). Scale bar = 1.0 mm.

able, depending on the abundance of detrital clays, and ranges from well sorted to poorly sorted. In general terms, the reservoir sandstones are arkoses or subarkoses. Quartz, feldspar, and to a lesser extent, clay minerals, chert, and lithic rock fragments are the predominant clastic components. Well-rounded quartz grains form the bulk of the detrital fraction of these sandstones (56 to 67%). Most are monocrystalline grains (48 to 63%), although polycrystalline grains are also present (4 to 12%). The feldspars, mostly orthoclase form 9 to 23% of the detrital fraction. Some grains exhibit dissolution features; others appear fresh (Fig. 3.14). The feldspars are discussed in more detail in a following section on reservoir quality. Apart from polycrystalline quartz, chert (trace to 2%) and metamorphic rock fragments (2 to 3%) are the most important lithic fragments (Davies and Associates, 1980, 1982).

Clays of both detrital and authigenic origin form from 1 to 12% of the reservoir sandstones. Illite and hematite coatings on detrital grains (0 to 12%), have been interpreted as pedogenic (soil) clay rims (Davies and Associates, 1980). Clay matrix is volumetrically more important toward the top of the sequence and is generally lacking from the base of the reservoir interval. This observation is consistent with the facies interpretation: the lower sandstones were deposited in a shallow-marine setting, while the upper sandstones were deposited in a coastal-plain setting where intermittent soil formation would be expected (Lindsay, 1987a).

A wide range of authigenic minerals have been encountered in the sandstones of the Arumbera Sandstone, including silica, feldspar, compact and fibrous illite, chlorite, kaolinite, iron oxides, pyrite, dolomite and anhydrite. Silica occurs as quartz overgrowths (1 to 12% of the rock), as euhedral terminations on detrital quartz grains, and as micro-quartz crystals (Figs. 3.14 and 3.15). Authigenic feldspar occurs in minor quantities as pore lining and as overgrowths on detrital feldspar grains. Ankerite and dolomite are the dominant carbonate minerals in the reservoir interval. Dolomite (0 to 2%) and anhydrite (2 to 10%) occur as large poikilotopic patches that occlude primary porosity. Among the clay minerals, fibrous illite (18 to 72% of the clays) (Figs. 3.16, 3.17) occurs in all samples examined, whereas chlorite (0 to 11%) and kaolinite (0 to 23%) are only sporadically recorded.

Reservoir Quality

Porosity determined from cores within the reservoir interval varies from as low as 3% to a maximum of 14.5% (Fig. 3.18). Over the same interval, permeability ranges from 0.1 to 11.9 md (Fig. 3.18). As might be expected, there is a general overall linear relation between the two variables, such that permeability increases with porosity. The relation

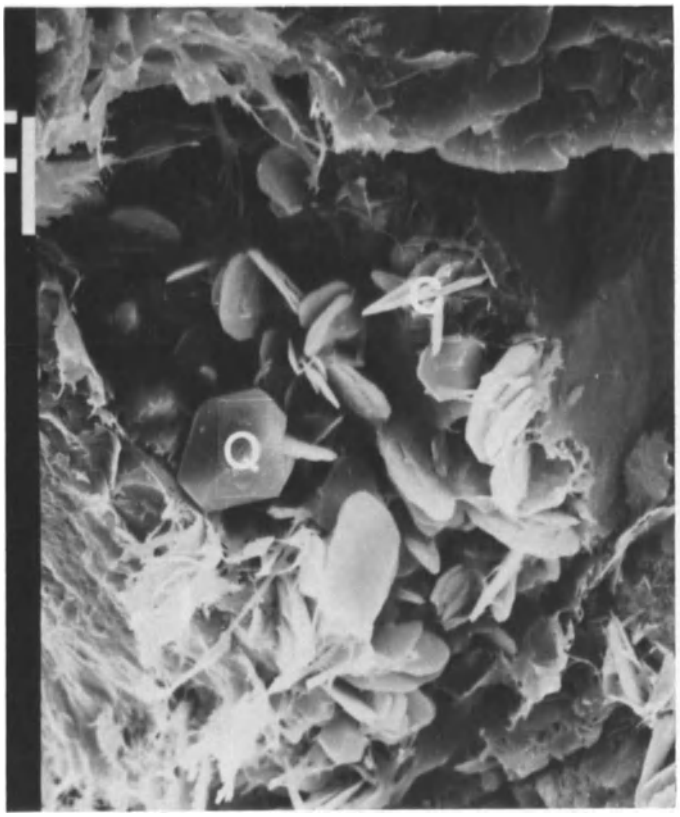

Figure 3.15. In addition to chlorite (C) and illite, microquartz crystals (Q) occlude pore space. Scale bar = 0.1 mm.

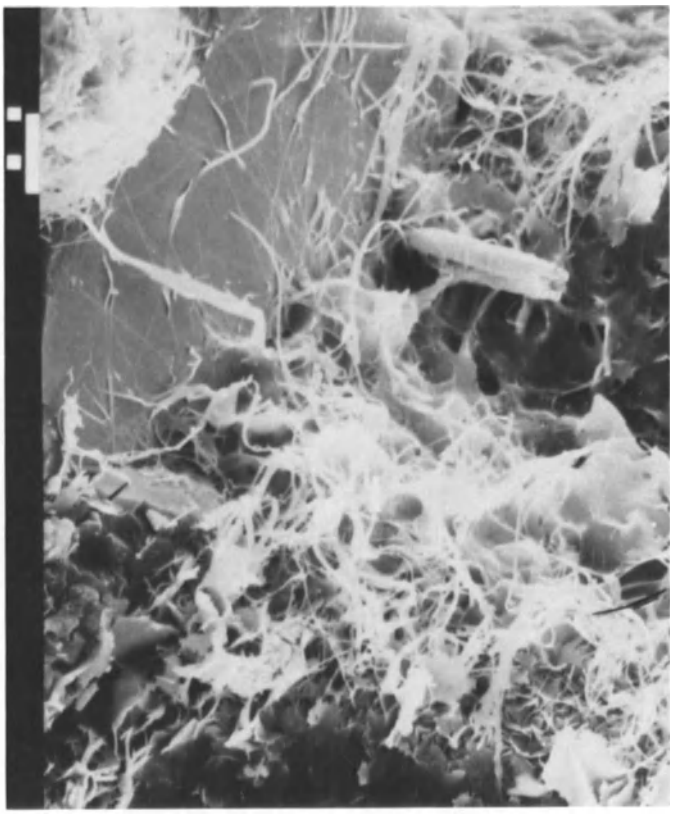

Figure 3.16. Fibrous illite occludes porosity. Scale bar = 1.0 mm.

is weak, however, and in some cases, porous units have very low permeabilities (Fig. 3.18).

Primary porosity is determined in large part by facies. Better reservoir parameters occur toward the top of the small, shallowing-upward cycles in the better sorted but sub-arkosic sandstones of sequence 1. However, as discussed above, reservoir quality declines at the very top of the reservoir interval due to the appearance of pedogenic clays in sandstones from the coastal-plain depositional system.

Diagenesis

All sandstones from the reservoir show some indication of reduced reservoir quality due to diagenesis. Diagenesis has resulted in both a decrease in primary porosity and permeability and an enhancement of porosity through generation of secondary porosity. The order of these events has been inferred from textural relations of cements as follows (Davies and Associates, 1980).

Early Diagenesis

1. Development of pedogenic clay rims on detrital grains.
2. Precipitation of anhydrite cement in some portions of the sand.
3. Shallow burial and grain rotation, resulting in tighter packing.
4. Early development of syntaxial quartz overgrowths on detrital quartz grains. Silica cement largely filled pores not occluded by anhydrite (Fig. 3.15).
5. Dolomite cementation (Fig. 3.14).

Late Diagenesis

6. Development of secondary porosity. Primary pore network partially exhumed through dissolution of anhydrite pore fillings.
7. Leaching and partial dissolution of some feldspar grains (Fig. 3.14).
8. Development of feldspar overgrowths on some detrital feldspar grains.
9. Precipitation of authigenic clays.

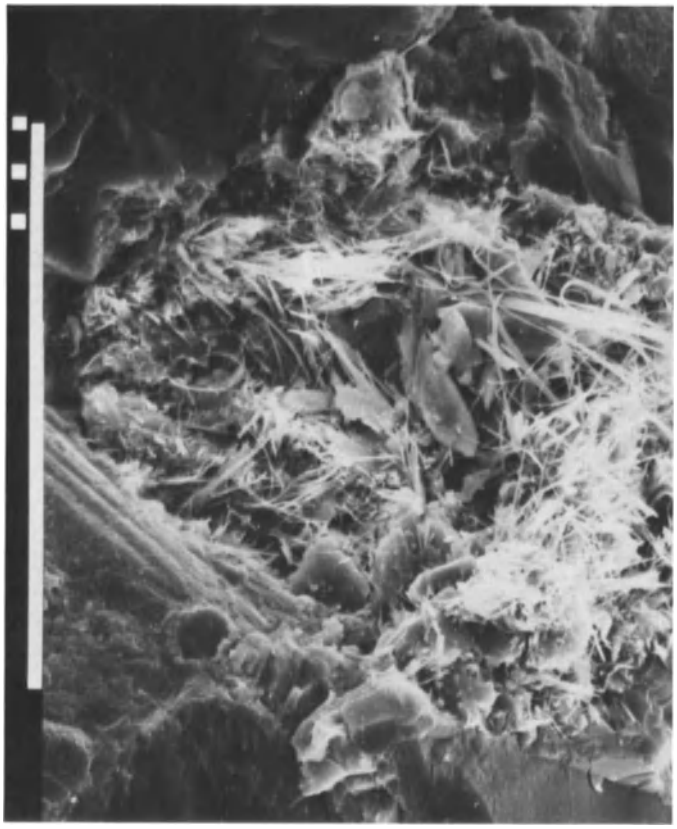

Figure 3.17. Fibrous illite in Arumbera Sandstone Reservoir interval. Scale bar = 0.1 mm.

A number of primary authigenic mineral phases are responsible for the reduction of porosity in the reservoir sandstones; however, fibrous illite, silica overgrowths on quartz grains, pedogenic clay coating on detrital grains, and anhydrite are the most important (Fig. 3.14, 3.16, 3.17). In particular, dolomite and fibrous illite (Fig. 3.16) occur throughout the pore system. Dolomite is abundant and frequently fills pore spaces completely. Many of the primary pores visible in thin section are partially occluded by anhydrite cement and silica overgrowths. Open primary porosity appears to have formed through dissolution of anhydrite. This anhydrite cement, precipitated prior to silica cementation of the sandstones, precluded development of silica overgrowths in the pores. Later, dissolution of anhydrite resulted in exhumation of some original primary porosity. Similarly, dissolution of feldspar has increased porosity (Fig. 3.14). Because of the suite of mineral phases present in the pore system, the formation is susceptible to formation damage, particularly if migration of fibrous illite takes place.

A further reduction in primary porosity occurred as a result of compaction of the sandstones during early diagenesis. Burial compaction has resulted in a loss of approximately 10% of the original sandstone pore volume through a rearrangement of grain packing.

Hydrocarbon Potential

Gas has been discovered in the Arumbera Sandstone at a number of localities. The Wallaby structure, which was located seismically in 1980 about 28 km southeast of Alice Springs, was the first structure in which a direct attempt was made to exploit the Arumbera Sandstone (Fig. 3.3). Gas was encountered in a thin transgressive sandstone at the base of sequence 1 of the formation, but drill-stem tests failed to produce gas at the surface in spite of the presence of porosity (Schroder and Gorter, 1984). The Dingo structure, a broad anticline or dome trending slightly west of north about 75 km south of Alice Springs (Figs. 3.19 and 3.20), which was drilled in 1982, is the only structure so far to show economic potential (Fig. 3.3). The areal closure of the structure is 68.9 km^2, with a vertical closure of 160 m.

The best potential source rocks within the Late Proterozoic section are contained in the Pertatataka and Areyonga Fms and the Gillen Member of the Bitter Springs Fm (Jackson et al., 1984). While the Gillen Member is by far the most widespread of the units, it is unlikely to have been the source for the gas at the Dingo Field. The most probable source lies within the Pertatataka Formation, which directly underlies the Arumbera reservoir (Schroder and Gorter, 1984). In general, the Proterozoic source rocks are overmature beneath the Missionary Plain (Fig. 3.1), and maturation levels decrease to the south, concomitant with decreasing depth of burial. Farther south, within the oil fairway, the Arumbera thins rapidly. The divide between the oil and gas fairways coincides with the Central Ridge and appears to be connected with basin mechanics. North of the Central Ridge, sub-basins developed during the second extensional stage of basin evolution and accumulated a considerable thickness of sediment, including the Arumbera Sandstone. Maturation is highest in those areas where the sub-basins developed and the sediment pile is greatest.

Pacoota Sandstone

The Pacoota Sandstone is the most important hydrocarbon reservoir of the Amadeus Basin. It is widely distributed, extending over 700 km across the northern half of the basin (Fig. 3.3). The formation is dominantly quartzose sandstone and forms the base of the Larapinta Group (Fig. 3.2).

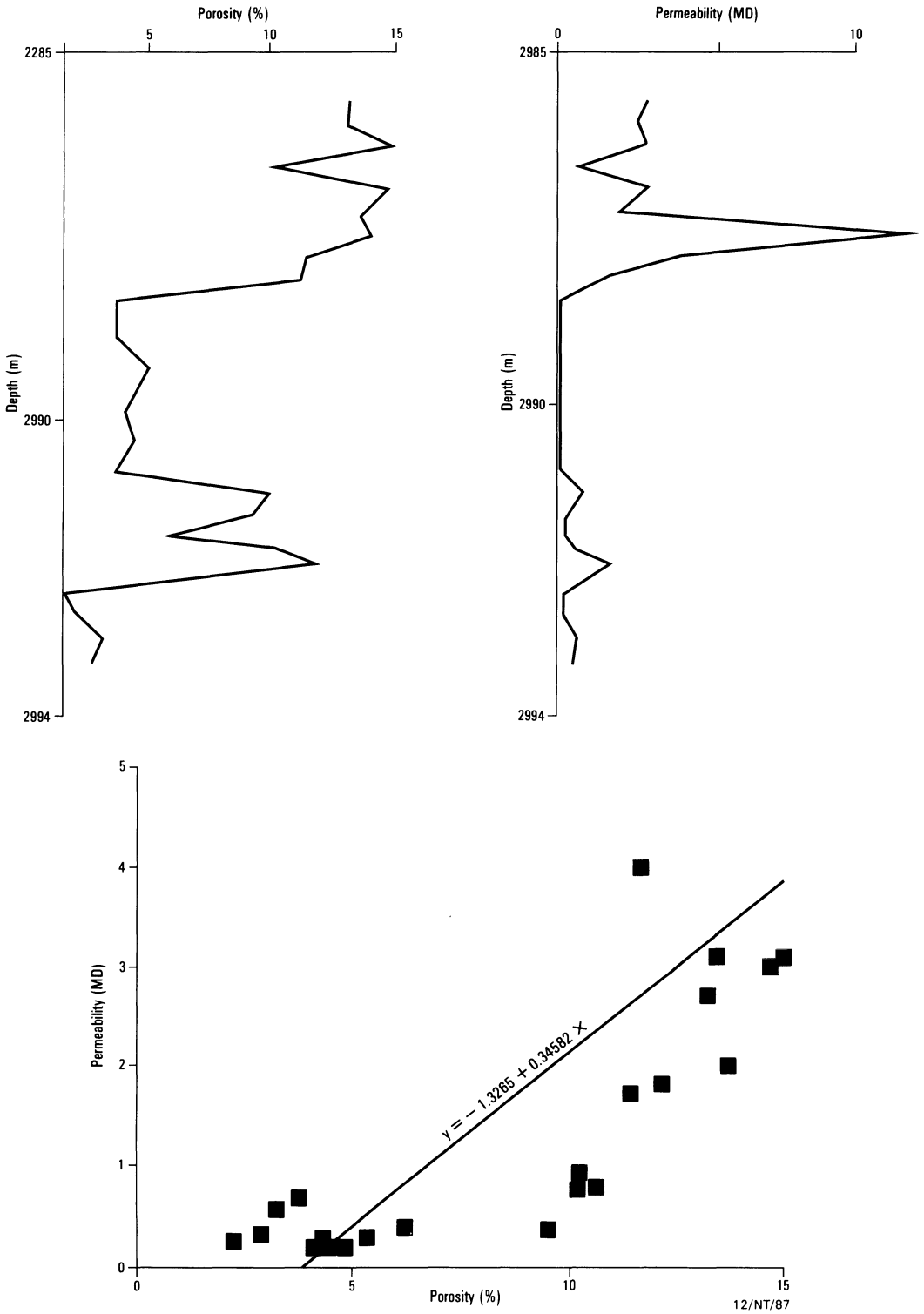

Figure 3.18. Arumbera Sandstone reservoir quality. Upper plots show porosity and permeability across the main reservoir interval in Dingo #2. Lower plot shows porosity vs. permeability for the same interval. Note that the linear correlation is poor.

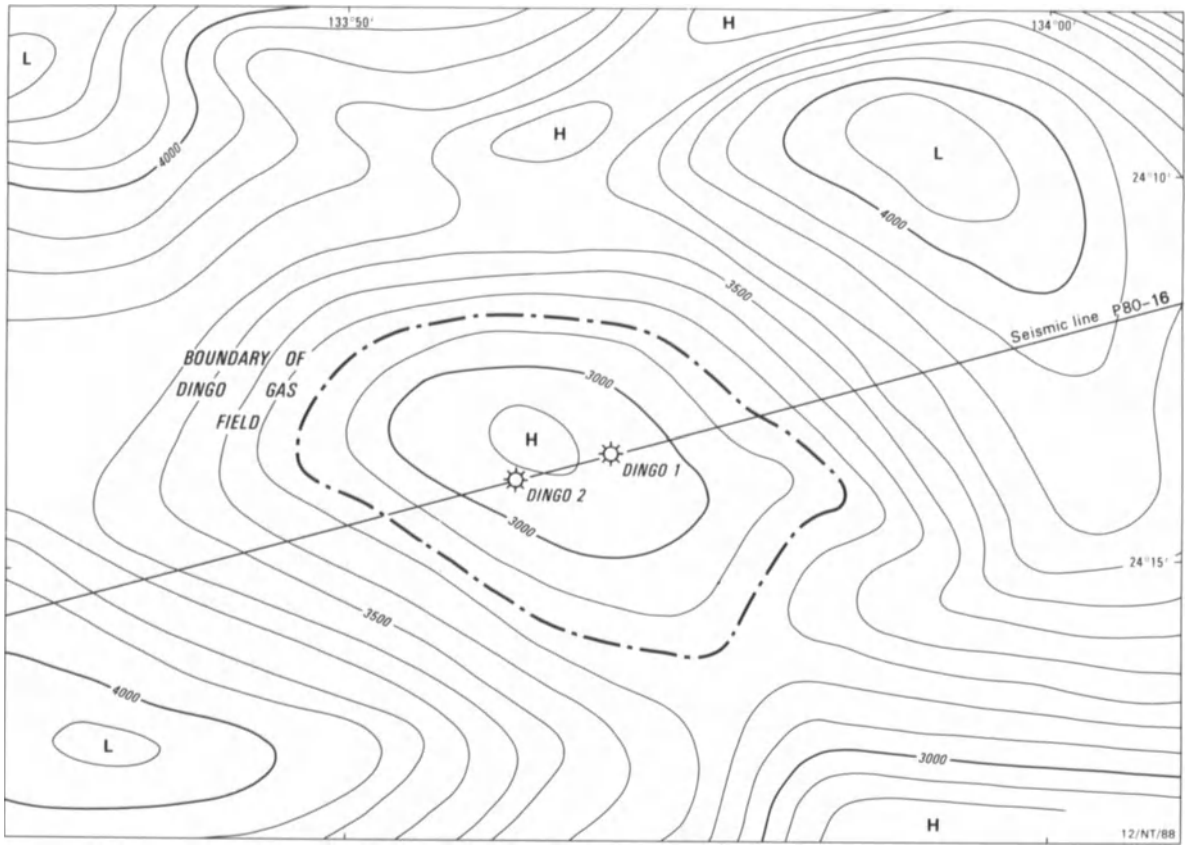

Figure 3.19. Structure contour map of the top of the first gas pay in the Dingo Field.

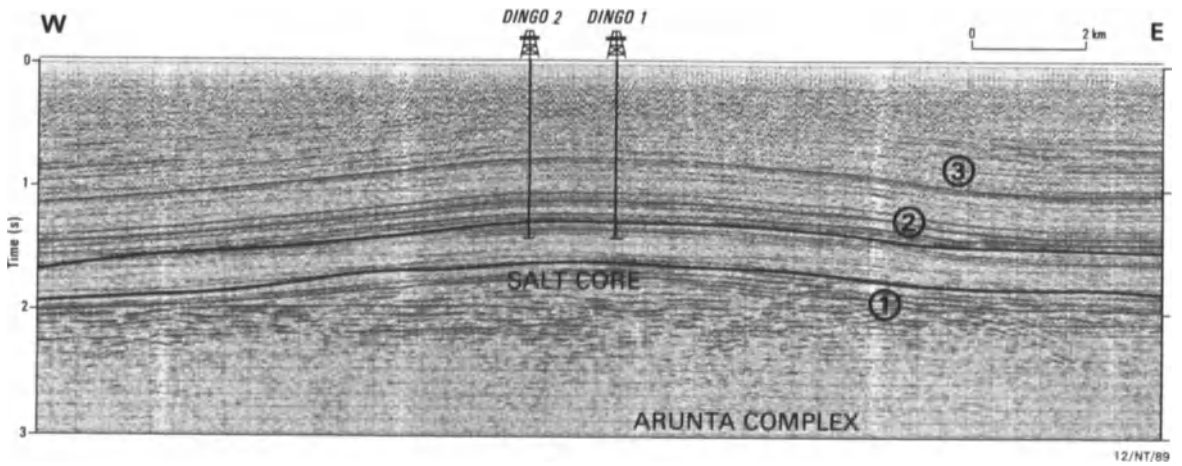

Figure 3.20. Seismic section (P80-11) across the Dingo Field, showing well locations and the reservoir interval. Note the massive salt core formed from the Gillen Member of the Bitter Springs Fm.

Benbow (1968) noted that the whole Pacoota section at Mereenie Field is generally abrasive, with porosity and permeability developed in lenses within the major sandstone horizons. He stated that porosities and permeabilities within those sandstone bodies are extremely variable, and that both are better developed on the crest of the anticline. Williams et al. (1965) earlier noted this phenomenon at Mereenie Field, and attributed it to better sorting of sands

on the crest of a structure that grew during deposition of the Pacoota Sandstone.

During the early 1970s, the Australian Bureau of Mineral Resources undertook studies of the reservoir characteristics of the Pacoota Sandstone in the Mereenie Field and the Palm Valley Field. A summary of the Bureau of Mineral Resources findings, published in 1976 (Kurylowicz et al., 1976), remains the standard reference to date, and was the first to recognize the importance of diagenesis in the destruction and development of porosity in the Pacoota Sandstone. Further drilling in the Amadeus basin since 1980 (Schroder and Gorter, 1984), and a reappraisal of previously drilled wells, have also contributed to the understanding of the porosity development and distribution in the Pacoota Sandstone.

Despite the recognized need for more detailed analysis of the porosity distribution in the various members of the Pacoota Sandstone, all the published studies have treated the complex depositional and diagenetic history of the Pacoota as a whole. In this paper, subunits of the Pacoota Sandstone are discussed in detail.

Subdivision of the Pacoota Sandstone

An informal subdivision of the Pacoota Sandstone was developed from the Mereenie Field by Williams et al. (1965), and was extended basinwide by Kurylowicz et al. (1976). These subdivisions, called P1 to P4 in descending order, were differentiated on the basis of gross lithology and log characteristics (Fig. 3.21). Kurylowicz et al. (1976) applied the P1 to P4 units to the Pacoota Sandstone at Palm Valley Field, but later drilling on the field showed that some of the correlations were incorrect. Do Rozario and Baird (1987) also applied the P1 to P4 terminology to the Palm Valley Field (Fig. 3.21), but some of the subdivisions cannot be substantiated (Gorter, 1992). It is therefore not possible to directly correlate statements made by the various authors about the reservoir properties of the subunits of the Pacoota Sandstone. Furthermore, most correlations east of Palm Valley are now known to be incorrect.

To provide a more meaningful depositional framework from which to discuss reservoirs within the Pacoota, and to avoid the confusion generated by the application of at least two partly exclusive informal field subdivisions using the same nomenclature, Gorter (1992) applied depositional sequence concepts to further the understanding of both depositional environments and reservoir distribution within the Pacoota Sandstone. A number of the parasequence sets are correlated basinwide, and are numbered from the base upward with the prefix PS (i.e., PS1, PS2, etc.) on Figures 3.25 to 3.28. The correlation of the parasequence sets with previous nomenclature is shown in Figures 3.21 and 3.22. A correlation of the sequences and parasequence sets recognized and the terminology used at Mereenie Field (Towler, 1986) are shown in Figure 3.22. The following discussions of reservoir development and properties will use the sequences and parasequences as defined by Gorter (1992), but reference will be made to informal field units where these have been previously applied. In the stratigraphic table (Fig. 3.23), the sequences defined by Gorter (1992) are correlated with nomenclature published by Benbow (1968) and Towler (1986). Also shown are the major interpreted sequence stratigraphic events that are considered important in the depositional history of the Pacoota Sandstone.

Age and Stratigraphy

The biostratigraphy of the Pacoota Sandstone is based primarily on trilobites (Shergold, 1986), although molluscs and brachiopods are also stratigraphically important in some horizons, and conodonts—which are confined to specific horizons—may prove useful in subdividing the upper Pacoota (Fig. 3.23). Three faunal assemblages have been described. The first, which occurs in parasequence set 3 and is widespread in the Amadeus basin, has been assigned to the local Australian late Payntonian to early Datsonian stage (Shergold et al., 1991) and is broadly equivalent with the latest Cambrian and earliest Ordovician. The second assemblage, which has a much wider distribution, occurs in the middle Pacoota in parasequence sets 8 to 11, and belongs to the late Warendian stage (Shergold et al., 1991), which is broadly equivalent to the terminal Tremadoc. There are few fossils known from parasequence sets 4, 5, 6, and 7, although trace fossils are abundant.

Taxonomic documentation of the faunas of the upper Pacoota parasequence sets 12 to 13 are as yet incomplete, but conodont faunas are provisionally assigned to the early Arenig.

Reservoir Characterization

That the bulk of the Pacoota Sandstone is of marine origin is unquestioned, because of the contained marine faunas and trace fossils, authigenic marine minerals such as glauconite, and characteristic associations of sedimentary structures. Fluvial facies are also present in places. We have interpreted the sedimentary environments of the Pacoota Sandstone in light of what is known of shallow-marine deposits, processes, and biota and placed the various units defined within the systems-tract scheme of Vail (1987) and van Wagoner et al. (1987).

The systems-tract methodology allows predictions to be

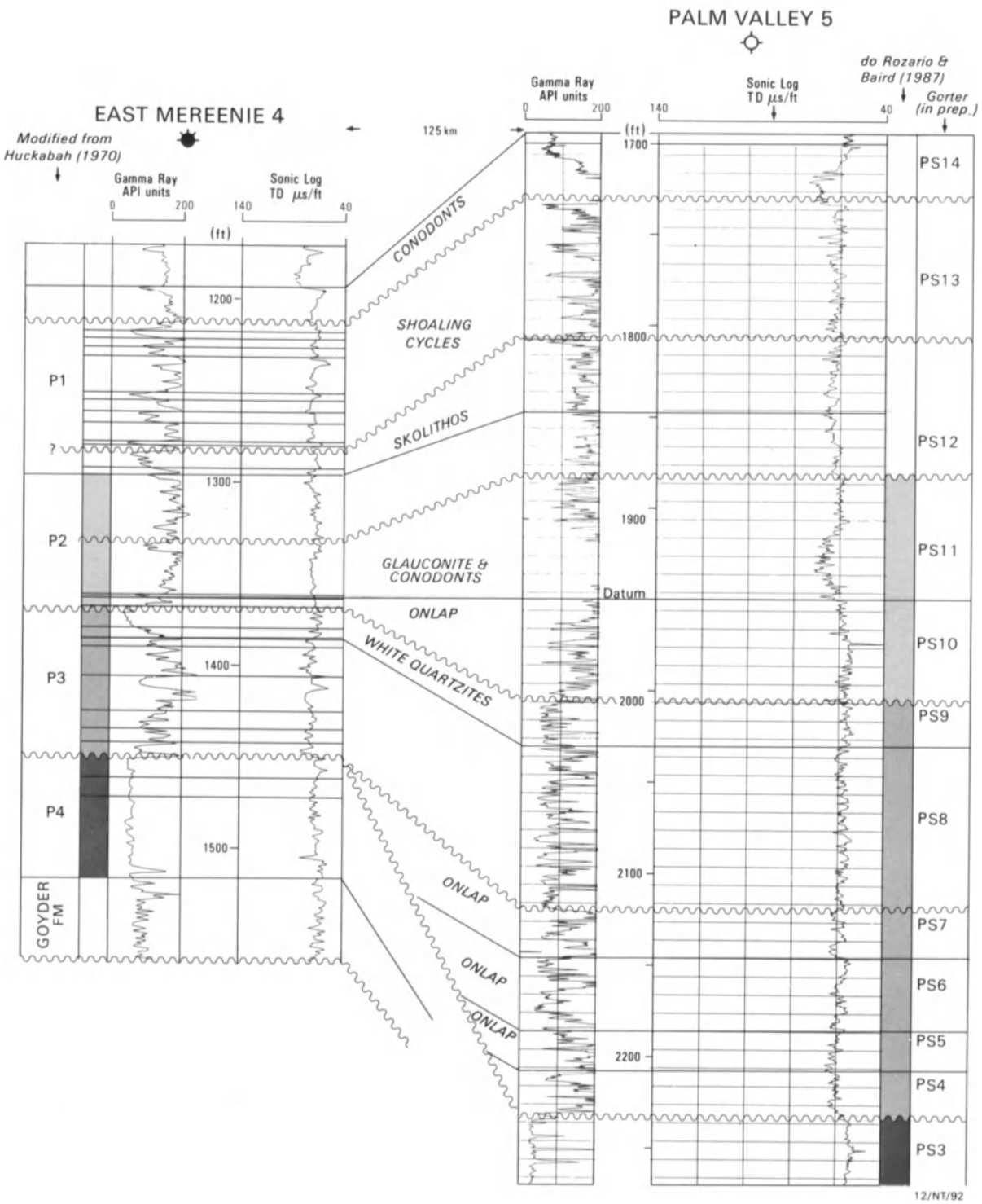

Figure 3.21. Correlation of Pacoota Sandstone Units defined from Palm Valley Field and Mereenie Field to illustrate unconformities, pinchout, and onlap relations. (From Gorter, 1992.)

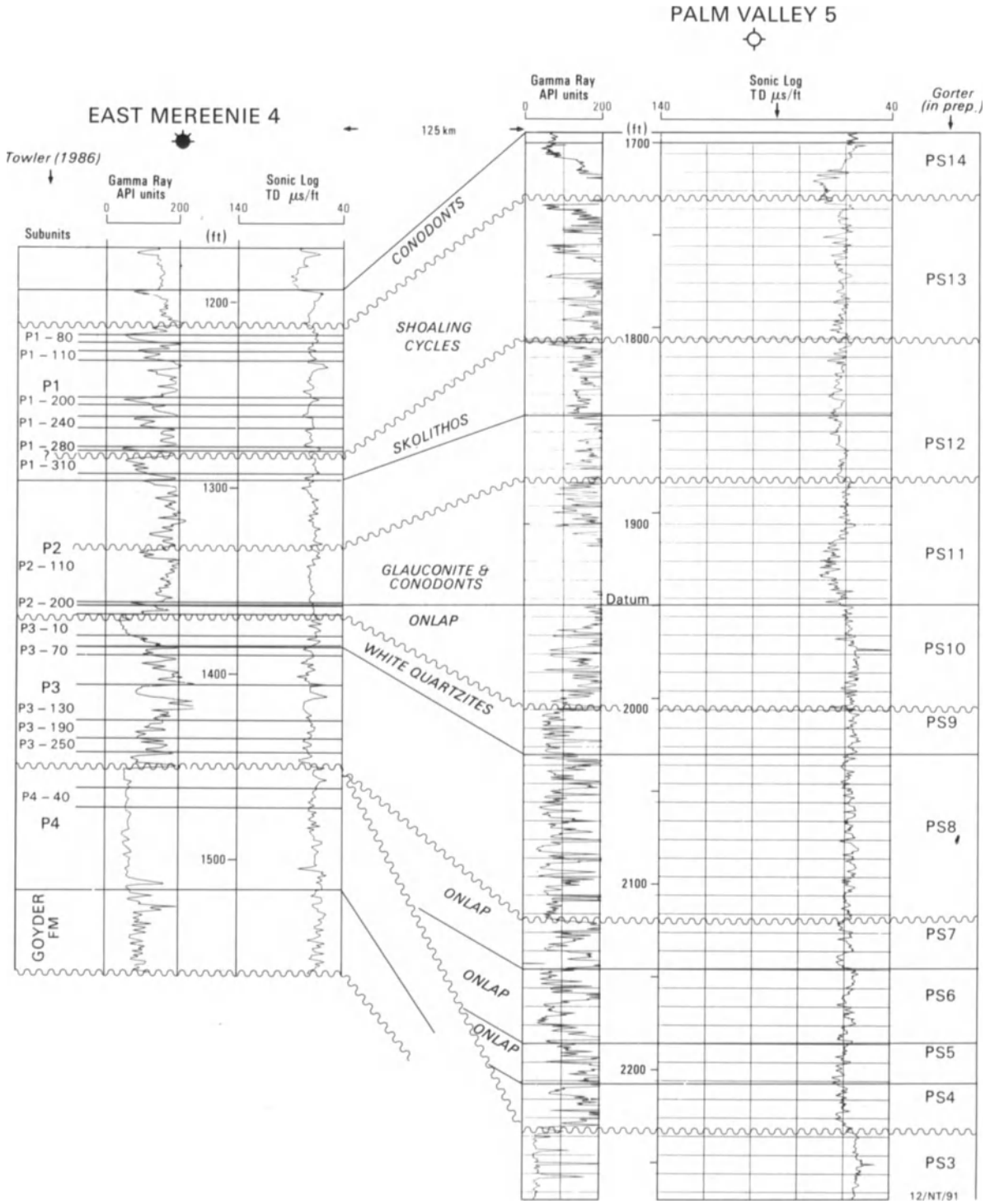

Figure 3.22. Correlation of Pacoota Sandstone units defined from Palm Valley Field to Mereenie Field to illustrate the major sand nomenclature at Mereenie Field. (After Towler, 1986.)

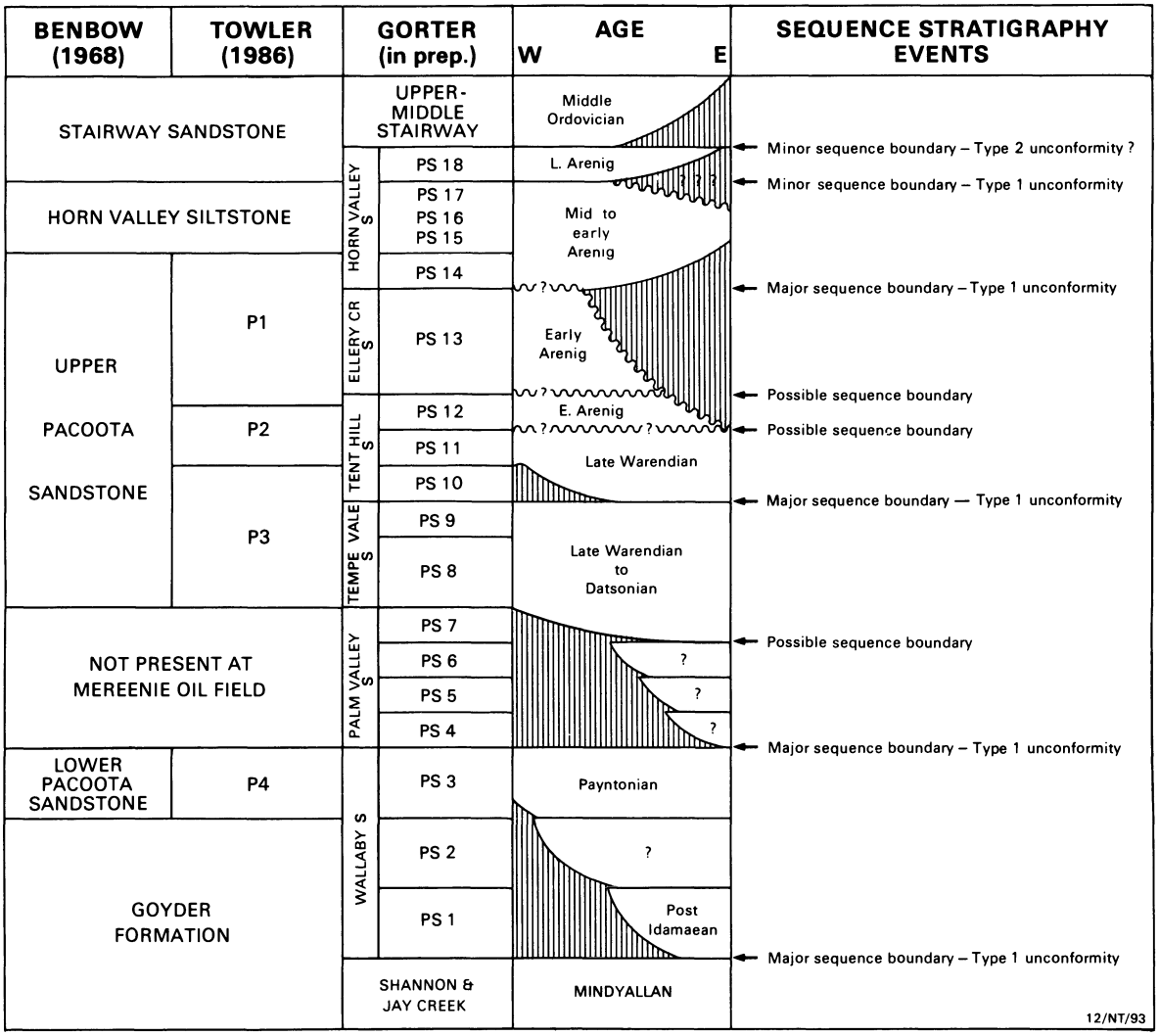

Figure 3.23. Comparison of stratigraphic subdivisions of the Pacoota Sandstone based on published Mereenie Field usage (Benbow, 1968; Towler, 1986) and that developed by Gorter (in prep.). Ages from Shergold et al. (in press).

made about the type of hydrocarbon reservoir developed in the different systems tracts, and the source, seal, and trap configuration required to produce a viable hydrocarbon accumulation (Vail, 1987). In the lowstand systems tract in a ramp basin, reservoir sands are typically developed in incised valley fills by braided streams (as in the west part of the Amadeus basin), and in lowstand prograding wedges as tidal sands, beach, and storm deposits (Vail, 1987). The latter are generally better developed in basins with a more pronounced shelf edge. While the Central Ridge still existed during Pacoota deposition, its influence was much less marked than in earlier times, and basin morphology was more ramp-like.

In the transgressive systems-tract, reservoir sands are best developed in beach and shoreface sands (Vail, 1987), where permeability and porosity are generally excellent due to winnowing of the sediments by waves. Offshore shelf sands may also form good reservoirs in this scenario, due to constant reworking by currents. In the highstand systems tract, reservoirs are generally best formed by fluvial sands or deltaic processes, with minor shoreface and development (Vail, 1987).

Destruction or enhancement of reservoir properties in sandstones is not purely a product of the depositional process; diagenesis of the sandstone is also an important factor. The type and sequence of diagenesis are dependent on the original composition of the sand (i.e., the composition of the framework grains), the grain size and sorting (e.g., original porosity), and the initial cementation. Diagenesis begins immediately after sedimentation, generally by the introduction of a primary cement, and continues in response to increasing overburden and temperature. Diagenesis in

sandstone generally leads to a loss of porosity and a reduction in permeability, although destruction of labile grains, such as feldspar and metamorphic rock fragments, may lead to secondary porosity.

Kurylowicz et al. (1976) used the acoustic velocity (sonic) log, calibrated by core porosity data, to determine the porosity distribution in the P units of the Pacoota Sandstone at Mereenie Field. They noted that porosity appeared to be less for the whole Pacoota Sandstone interval over the crest of the structure (cf., Williams et al., 1965) and increased down flank and along the plunging noses of the anticline. This conclusion was based on analyses of six wells available at the time.

Tectonic stress caused by faulting and flexure of impermeable formations may also form fracture porosity systems. Palm Valley Field is a prime example of a fracture porosity reservoir in the Pacoota Sandstone (do Rozario and Baird, 1987), and the West Walker #1 gas discovery may prove to be another.

Parasequence Set 3

Parasequence set 3 is characterized by the blocky shape of the gamma-ray curve (Fig. 3.21) and can be readily correlated across the basin (Fig. 3.24a). In outcrop in the northwest part of the basin at Watsons Range, parasequence set 8 is unconformable upon parasequence set 3, and this is also the case at Mereenie Oil Field (Fig. 3.21), located on the Central Ridge. However, in the Missionary Plain trough to the northeast, parasequence sets 4 to 7 intervene between parasequence sets 8 and 3 (e.g., Palm Valley Field, Fig. 3.21).

In general, the unit thickens slightly to the south and west, and thins to the north and east of Mereenie. The maximum thickness is about 75 m at Mereenie Field. The unit is 58 m thick at Tempe Vale #1, and 54 m at Wallaby #1.

Sedimentary structures in parasequence set 3 include both herringbone cross-bedding and unimodal cross-strata, often associated with reactivation surfaces. Megaripples are sometimes abundant, as are symmetrical and asymmetrical current ripples showing several different current vectors on the same bedding plane. Occasional mudcracked horizons are also noted. Other features are overturned cross-lamination, scour and fill, mud clasts, climbing ripples, and other ripple forms. Trace fossils, including *Skolithos* and U-shaped burrows, and a marine fauna are sometimes abundant. Parasequence set 3 is interpreted as a tidally influenced shelf sandstone deposit. From the distribution and generally uniform thickness of parasequence set 3, it is considered that the Central Ridge had no influence on sedimentation patterns in latest Cambrian time.

The reservoir characteristics of parasequence set 3 are best known in the Mereenie Field in the southwestern part of the basin, where several cores were taken in the interval, and in the fully cored Tempe Vale #1 well.

At Tempe Vale #1, parasequence set 3 is composed of fine- to medium-grained, occasionally coarse, poorly to generally moderately well-sorted and occasionally well-sorted siliceous sandstone. The sandstone often has a reddish color due to iron oxide rims on the original detrital grains and in part to a ferruginous cement. Porosity in parasequence set 3 is mostly occluded by silica and ferruginous cements. These ferruginous cements are a breakdown product of the sometimes abundant arkosic sandstones in the southwestern area, and perhaps parallel an increasing fluvial component of the sediments in this direction. The best permeability is related to abundant, though patchy, zones of sub-horizontal fracturing. Minor porosity is present (5.3%) in bioturbated zones (*Skolithos*) near the base of the section.

Parasequence set 3 forms a generally poor reservoir for hydrocarbons in the Mereenie Field because of the reduction of porosity by carbonate cement and burial diagenesis. However, reservoir sandstones do occur in parasequence set 3 at Mereenie (e.g., P4-40 sand; Towler, 1986) and owe their reservoir character to weathering at the pre-parasequence set 3 unconformity. A range of 6 to 10% porosity is calculated in the parasequence set at Mereenie Field, where parasequence set 3 consists of fine- to medium-grained and occasionally coarse sandstones. The sandstones are generally well sorted, although sorting becomes poorer with increasing depth. At East Mereenie #2, the sandstones consist of 75% monocrystalline quartz, with 8% polycrystalline quartz grains, 15% silica cement, and 2% dolomitic cement, with only trace amounts of feldspar and anhydrite. Visual porosity is poor, except in coarser lenses, and stylolites are present, indicating that pressure solution has taken place. Pore space was reduced initially by fibrous illite and later by quartz or chlorite deposition.

In the Missionary Plain trough, parasequence set 3 was intersected by several wells. In the Palm Valley Field (Fig. 3.25), the clean sandstones are impermeable due to dolomite cementation and later burial-induced quartz overgrowth. Dolomite cement was probably introduced contemporaneous with deposition of these shallow subtidal to tidal sands, or soon after. As there is no evidence for exposure of these rocks prior to deposition of the overlying sediments, there was little chance for dedolomitization to have taken place. At Orange #2, sonic logs also suggest that the parasequence set is nonporous (Fig. 3.25), and at Alice #1, in the fine-grained, generally nonporous sandstones, limonite coated the original grains prior to the deposition of dolomitic cements and the final quartz overgrowth phase.

In parasequence set 3, porosity generally is occluded by dolomitic cement in the northeast and by silica overgrowths

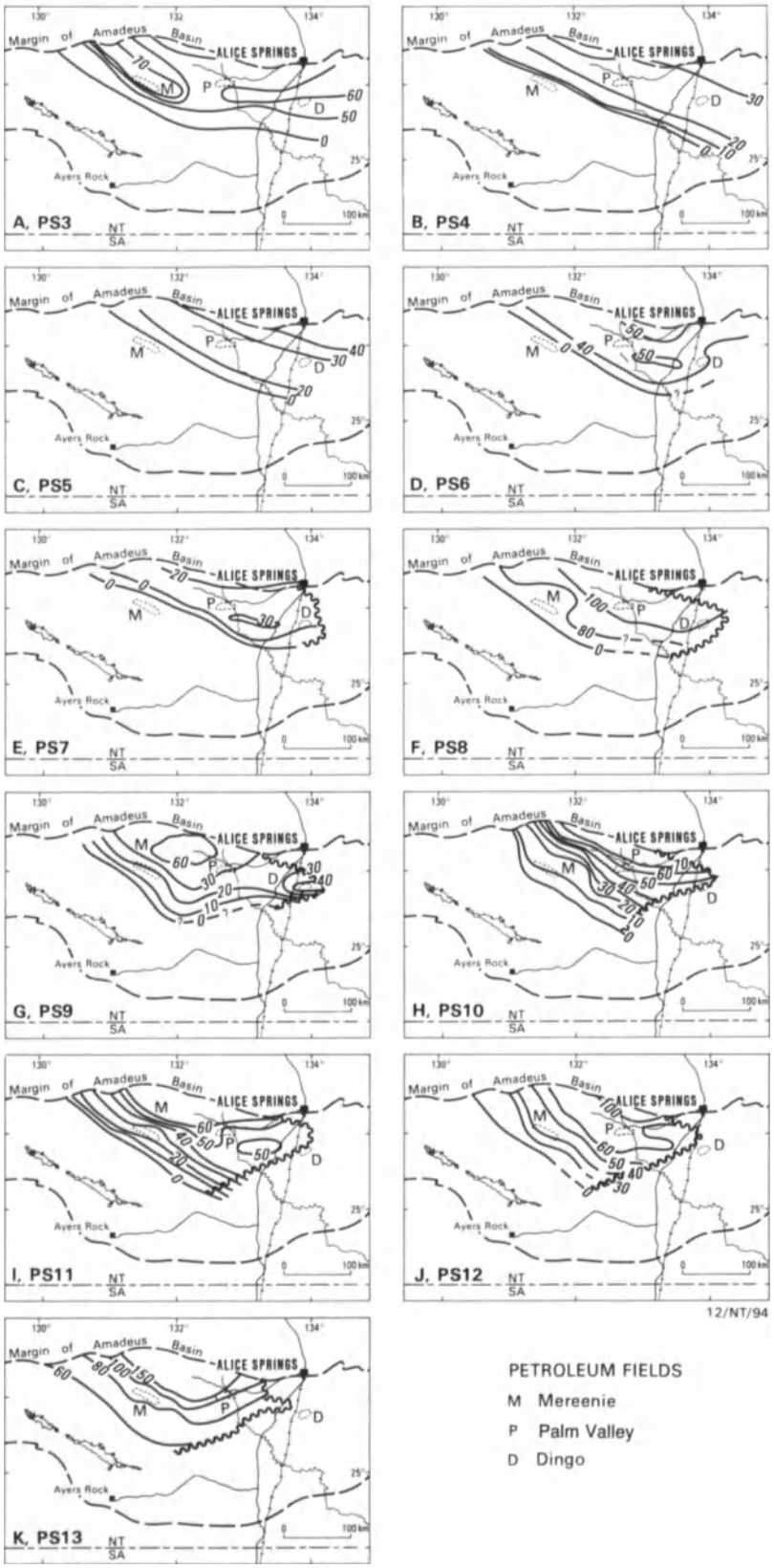

Figure 3.24a–k. Distribution and isopachs of parasequence sets 3 to 13. Contour intervals in meters.

in the west. The clean nature of the predominantly quartzose sandstone suggests that the more labile grains, such as feldspar, were either not supplied from the sediment provenance area, or were removed during mechanical abrasion prior to deposition. Primary dolomitic cement was introduced soon after burial and before compaction, as shown by the floating contacts between many grains. Interlocking grain boundaries and stylolitization show that later pressure solution caused a further porosity reduction upon deep burial, probably during the Late Devonian molasse deposition (stage 3).

Secondary porosity is present in some samples, especially in the southwest, suggesting leaching of the dolomitic cement. Leaching may have taken place under conditions of deep weathering, during the hiatus preceding the deposition of parasequence set 8 in the Mereenie area, and is shown by the characteristic reddish, spotted appearance of many sandstones in the Mereenie Oil Field and at Tempe Vale #1. Such evidence of weathering is lacking in the core at Alice #1, suggesting that the time available for deep weathering in this area prior to deposition of parasequence set 4 was much less than on the Central Ridge.

Parasequence Sets 4 and 5

Parasequence sets 4 and 5 (Fig. 3.24b, c) occur in the eastern part of the basin and are not present at Mereenie Field (Fig. 3.21). At Palm Valley Field, they have been previously included within the P3 unit of do Rozario and Baird (1987) (Fig. 3.21).

On gamma-ray logs, parasequence set 4 is clearly a coarsening-upward cycle, i.e., a progradational parasequence set (Fig. 3.25). The unit passes downward from medium-grained, well-sorted sandstones to finer-grained sandstones and interbedded siltstone and shale. Mica is often abundant, and minor glauconite is present. The upper beds are cross-bedded and contain *Skolithos*; below the uppermost sandstone, inarticulate brachiopod fragments, trough cross-beds, ripple marks, scour and fill, and rip-up clasts are present. Parasequence set 5 is also a generally coarsening-upward cycle on gamma-ray logs, but is composed of several smaller coarsening upward cycles (Fig. 3.21). A similar succession is present.

The evidence suggests that parasequence sets 4 and 5 are transgressive marine in origin: both coarsen upward from siltstones and shales, with sporadic glauconite through thin-bedded sandstones, into trough cross-bedded sandstones containing the intertidal trace fossil community.

Parasequence set 4 is not present at Mereenie Field (Fig. 3.21), and was not cored in any of the Palm Valley wells or in many wells in the northeast part of the basin (Fig. 3.25). Consequently, there are few quantitative data available on the reservoir properties of the sequence.

An average sonic-derived porosity of 12% was calculated in the upper sandstones of the shoaling cycle (Fig. 3.25) at

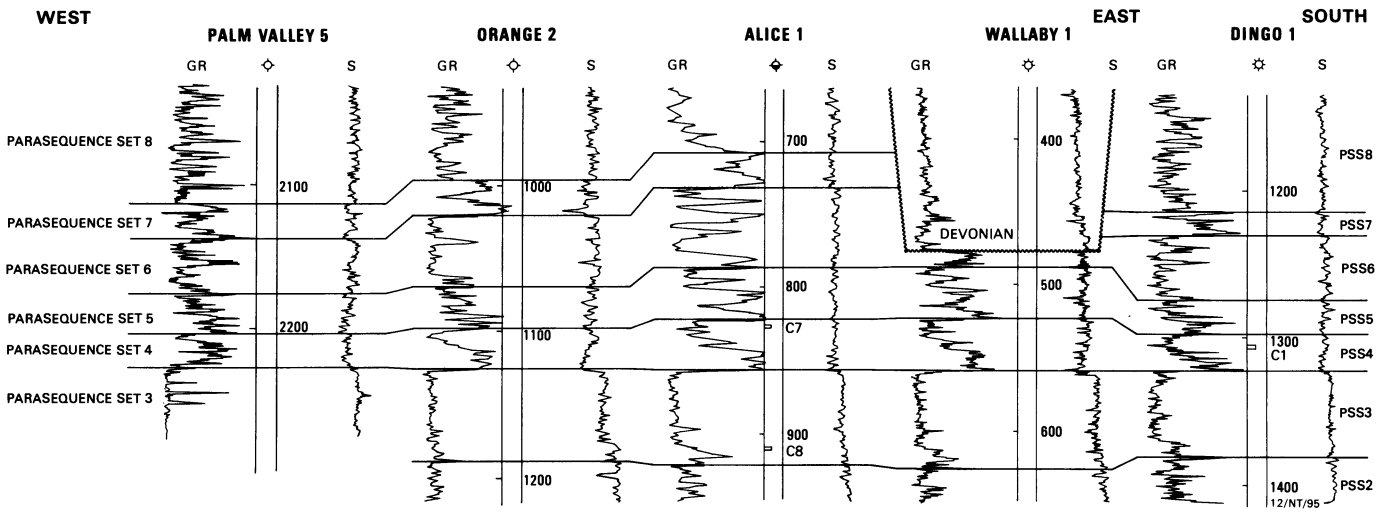

Figure 3.25. Sonic log-gamma-ray log curves of parasequence sets 3 to 7 eastward from Palm Valley #5 to Wallaby #1, and south to Dingo #1. Note the Rodingan erosion on Wallaby #1. The generally impermeable lithology of parasequence set 3, due probably to primary dolomitic cements and lesser burial-induced silicification, is well illustrated by the higher transit times on the sonic logs. The clean sandstones at the top of the shoaling cycles of parasequence sets 3 and 5 are invariably impermeable due to burial-induced quartz overgrowths, and lesser authigenic illite and later dolomite cementation. Porosity in parasequence set 6 is generally reduced due to burial diagenesis and quartz cementation in the cleaner sandstones and because of remobilization of carbonate cements in more arkosic sandstones. Note that decalcification of the sandstones at Alice #1 and Wallaby #1 is thought to be a result of weathering accompanying the Devonian erosion cycle and subsequent relatively shallow burial, compared to wells in the Palm Valley area. The central sandstone in parasequence set 7 is generally clean and cemented by quartz.

Alice #1. A single core plug porosity of 35% was measured from the base of core #7 in a sample taken from near the top of the cycle in the cleanest sandstone, as indicated by gamma-ray interpretation. This porosity is remarkably high for the Pacoota Sandstone, and may reflect the presence of fracturing in the core, although this is not mentioned in the original core descriptions. The upper part of the core is composed of generally clean, very fine- to medium-grained sandstone with coarse streaks. Some quartz recrystallization is reported, and the rock is fairly well cemented with silty argillaceous material, except where it is slightly arkosic and friable. There is also minor patchy development of calcareous cement.

The correlative section at Orange #1 has a reduced porosity of 9.5% over the upper sandy interval (Fig. 3.25), and Kurylowicz (1975) thought the difference in porosity compared to Alice #1 was due to a greater depth of burial at Orange #1. However, a calculated sonic-log porosity of 5% from the same interval at Wallaby #1 (Fig. 3.25), where the unit is less deeply buried than at Alice #1, indicates that depth of burial is not the only reason for the reduction of porosity in this area. The porosity at Wallaby #1 was described from cuttings as intergranular, and there is little calcareous cement; the main mechanism of porosity occlusion is quartz overgrowth.

At Dingo #1, Core #1 was cut in the middle of parasequence set 4 below the main sandstone horizon of the shoaling cycle. Visible porosity in the upper sandier part of the core was poor, and no reservoir analysis was attempted. Furthermore, log interpretation suggested that the overlying main sandstone horizon of the shoaling cycle has minor porosity development, and permeability also appeared to be poor from the dual caliper-log response. Thin-section petrographic analyses, fine-fraction x-ray diffraction (XRD) analyses, and scanning electron microscope (SEM) examinations were carried out. All samples were well-sorted, fine-grained quartzose sandstones consisting of 54 to 77% monocrystalline quartz, and trace to 2% polycrystalline quartz. Potassium feldspar content was highest in the lowermost sample, but plagioclase feldspar in all four samples was a uniform 1% of the grain composition. Accessories were generally in trace amounts and included chert, clay balls, and shell fragments. Only a trace of detrital clay matrix was present. The most variable character of the rock is the cement composition; no two samples exhibit the same proportion of the various cements. Porosity is generally poor and has been generated by the dissolution of unstable grains (i.e., feldspar). All other detrital grains are cemented by silica. Many of the detrital quartz grains were coated with iron oxide and chlorite before minor secondary silica overgrowth. Authigenic clays and dolomite form the primary cements, particularly in the two samples with the lower monocrystalline quartz content. Illite was the only clay mineral detected by fine-fraction XRD analyses (17 to 75%), but it does not seem to be confined to any particular rock composition. This fibrous illite is sometimes a major pore-fill mineral in this part of the Pacoota and occludes the intergranular pore space, although quartz cements and minor dolomite usually are the occluding minerals. Pyrite occurs in trace amounts and is a late-stage precipitate. The diagenetic sequence appears to have been quartz overgrowth, authigenic illite precipitation, dissolution of labile feldspar grains, late-stage pyrite introduction, and finally, dolomite crystallization in the remaining pore throats.

Little is known about porosity distribution of parasequence set 5 due to a complete lack of cores. Porosities of 13 to 13.5% were calculated at Alice #1, 11% at Orange #1 (Fig. 3.25), and an average of 9% from Wallaby #1. There are some inconclusive indications of permeability from the dual caliper logs at Dingo #1. Because of the similarity in depositional environment between parasequence sets 4 and 5, it would be expected that the diagenetic destruction of porosity followed the same pathways.

Parasequence Set 6

Like parasequence sets 4 and 5, parasequence set 6 is not present in the Mereenie Field (Fig. 3.24d). Parasequence set 6 is clearly defined on electric logs at the Dingo, Orange, and Palm Valley wells (Fig. 3.21). A consistent feature is very high gamma-ray values in the center of this essentially sandstone-dominated unit (Fig. 3.25), reflecting the presence of a highly micaceous greenish siltstone unit. Parasequence set 6, composed of fine to occasionally coarse and pebbly cross-bedded sandstone, is quite clearly of marine origin and was deposited at the culmination of a major transgressive event. It contains shallow intertidal indicators such as the trace fossil assemblage. The lithology, trace fossil suite, and sedimentary structures indicate a tidally influenced depositional environment.

Sonic log–derived porosity values of 3.5 to 7% were calculated in parasequence set 6 at Orange #1, and higher values of 11.5 to 12% occur at Alice #1 (Fig. 3.25). A sonic log–derived porosity of 50% was calculated from immediately below the Rodingan unconformity at Wallaby #1. This exceedingly high porosity is thought to represent decalcification of the sandstones during weathering in the later Paleozoic, and the subsequent shallow depth of burial (present depth is 441 m). At Dingo #1, porosity of only 3% and a lack of significant permeability at present depths of 1320 to 1360 m are noted.

At Palm Valley #3, the sequence is composed of relatively pure quartz-rich sandstones, in which quartz makes up over 95% of the framework grains, with minor tourmaline and chert. In all samples, the sand grains are well rounded

and well sorted, but quartz overgrowths have occluded all porosity. Some grain boundaries are sutured, and rare indented boundaries are also present. Illite does not occur on grain boundaries in the clean rocks, in comparison to the more arkosic sediments, suggesting a primary depositional control. Calcite cement is generally rare to absent in these quartz-rich rocks, indicating that in more arkosic sandstones, the calcite cements have been derived from the dissolution of feldspars under burial diagenesis.

Parasequence Set 7

On electric logs, parasequence set 7 is represented by the sequence of high-low-high gamma values (Fig. 3.25), reflecting the change from shales gradationally upward to coarser sandstones in the center part, and then a return to finer clastics. In outcrop, the sandstones are fine to medium grained and are coarsest in the middle part of the unit. The sandstones are mostly trough cross-bedded and contain *Skolithos*, but the coarser-grained sandstones may be planar cross-laminated. Trilobite traces are present in the trough-cross-stratified beds. Minor glauconite is present in the sequence at Dingo Field and at Orange #2 in both the siltstones and the finer sandstones. Glauconite and hummocky cross-stratification are present in outcrop at Ellery Creek (Gorter, 1992).

Parasequence set 7 records a major transgressive event. The presence of fine-grained clastics, hummocky cross-stratification, and glauconite suggests deeper-water marine deposition. The top is eroded below the Type 1 sequence boundary at the base of parasequence set 8.

Parasequence Set 8 and Parasequence 9

By early parasequence-set-8 time, the Central Ridge was flooded, and sediments of this unit form the primary reservoirs at Mereenie Field (Fig. 3.21). The top of the unit is truncated by later erosion east of Dingo Field and in the eastern James Ranges (Fig. 3.24f).

As shown by the gamma-ray logs at Palm Valley Field and Mereenie Oil Field (Fig. 3.26), parasequence set 8 is dominantly sandstone, but contains intervals of siltstone and shale. Sedimentary structures include trough and planar cross-beds, herringbone cross-lamination, ripple marks, megaripples, and fining-upward cycles beginning with pebbly sandstones, especially in the west part of the Mereenie Field and at Tempe Vale #1 well. A fluvial depositional environment, probably in braided rivers, is thought likely for the coarse-grained, unfossiliferous sediments.

The lower beds of parasequence set 8 in the northeast contain ample evidence of deposition in intertidal to subtidal environments. Trace fossils of the *Skolithos* assemblage are locally common.

Parasequence 9 is a widespread clean quartzitic unit (Fig. 3.26) that is present in both the Palm Valley and Mereenie fields and as far southwest as Tempe Vale #1 (Fig. 3.24g). The initial sediments are siltstones and shales, sometimes glauconitic, and the unit coarsens upward to sandstones. The presence of a *Cruziana* trace fossil suite in these sandstones suggests an upward shift to a more marine depositional environment. The large-scale ripple features and the clean nature of the sandstones, coupled with the characteristically fragmentary shelly fossils, infer a turbulent energy regime with strong current activity. The dominance of east and west current indicators suggests that deposition may have taken place in a tidally influenced seaway.

Parasequence set 8 is more arkosic to the south and west, and the gamma-ray logs reflect the lithology by a characteristic "hot" gamma-ray signature (Fig. 3.26). To the east and northeast, the sandstones are more quartzose, reflecting the increased distance from the provenance area.

Investigations of reservoir conditions at Mereenie Field by the Bureau of Mineral Resources were summarized by Kurylowicz et al. (1976). Towler (1986) carried out a computer reservoir simulation of the field to evaluate the recovery of oil from wells situated on the northern and southern flanks of the Mereenie anticline. All authorities are agreed that the major reservoir at Mereenie occurs in the P3 unit, which is broadly correlatable with parasequence set 8 and 9. Within parasequence set 8 at Mereenie, the P3-120/130 sandstones (Fig. 3.22) are consistently permeable in all parts of the field, and form the major producing sandstone (Towler, 1986).

At East Mereenie #2, core-derived porosity ranges from 2.3 to 14.4% in parasequence set 8, but the porosity occurs in discrete zones. Core #20, from the top of the clean quartzite at the top of parasequence set 9, has porosities ranging between 3.5 and 8.7% and permeabilities between 0.1 and 2.6 md, whereas Core #21 (1447.2 to 1456 m), in the lower part of the P3-130 sand (parasequence set 8), has porosities ranging from 10.3 to 14.4% and permeabilities between 0.1 and 129 md. These two cores have very different gamma-ray-log characters; the higher gamma-ray values from the P3-130 sand reflect the arkosic content of the rocks.

In Core #20 from the top of parasequence 9 (1419.8 m), feldspar made up only 3% of the detrital grains. The rock is generally well cemented with silica, but the coarser sandstones retain some well-developed porosity. These pores are partially infilled by silica overgrowths and quartz druse, and lined by patches of fibrous illite and illite-smectite. Core porosity of 8.5% was measured at this depth.

In Core #22, from fine sandstone near the base of para-

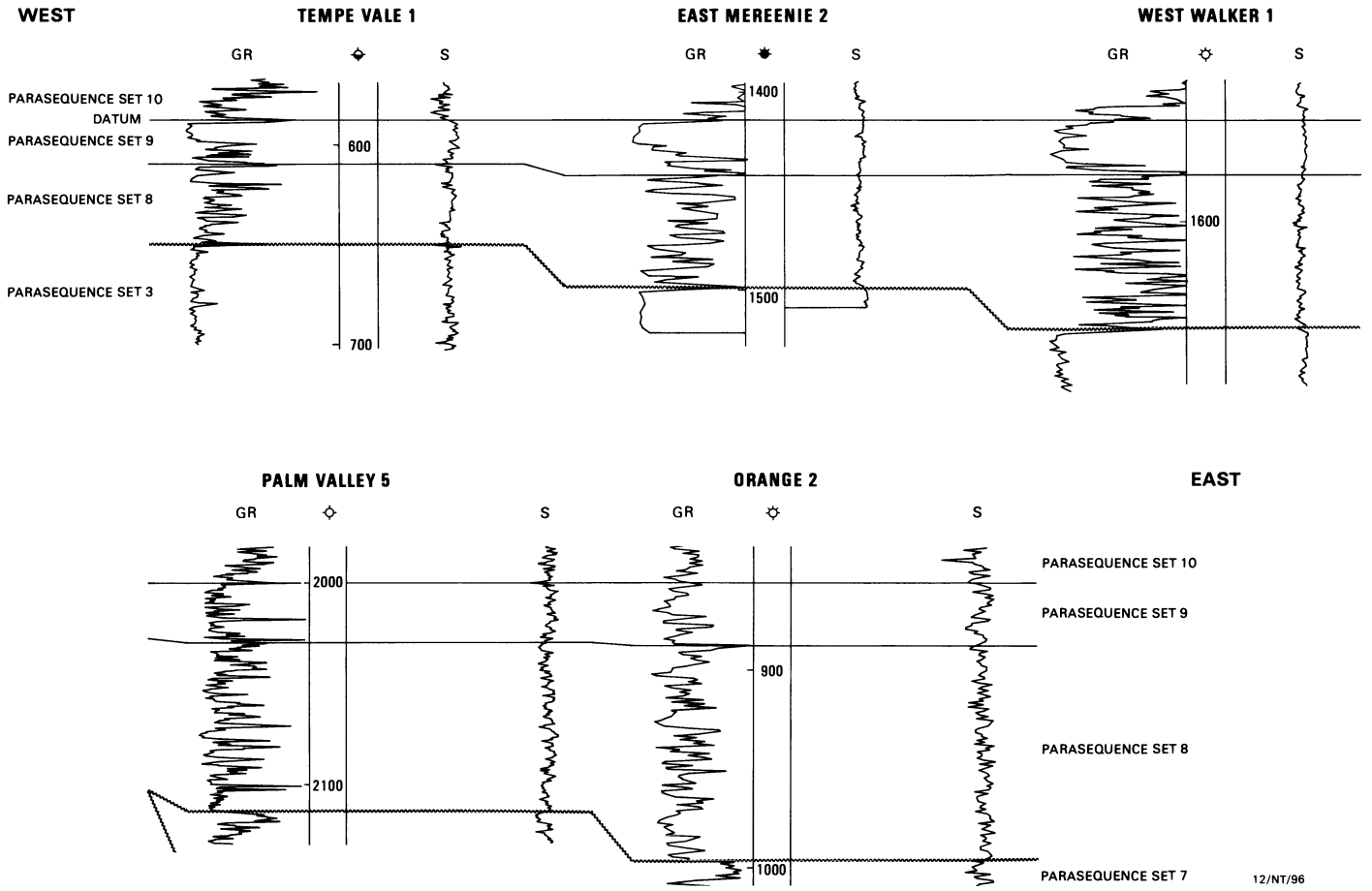

Figure 3.26. Sonic log–gamma ray log correlation of parasequence sets 8 to 9 eastward from Tempe Vale #1 to East Mereenie #2, West Walker #1, Palm Valley #5, and Orange #2. The cleaner sandstones at the top of the shoaling parasequence set 9 are impermeable because of early dolomite cementation and later silica overgrowths formed under burial diagenesis, especially in the wells to the west. Parasequence set 8 becomes more arkosic to the southwest, with a characteristic "hot" gamma-ray character and a progressive westward change from shoaling marine cycles, as at West Walker #1, to fining- upward cycles in the lower beds at East Mereenie #2 and Tempe Vale #1 (i.e., there is a facies change from barrier bar to fluvially influenced deposition westward onto the Central Ridge). The cleaner, wave-reworked sandstones are now silica cemented; however, the best porosity is developed above the base parasequence set 8 sequence boundary on the Central Ridge, where the arkosic, more nonmarine sandstones have secondary porosity due to dissolution of labile grains, and to preservation of original porosity not infilled by marine carbonate cements. Depth of burial was less at Mereenie than at Palm Valley, and consequently, the amount of silica overgrowths is reduced.

sequence set 8, feldspar increased to 7% of the detrital grains, and core porosities of 8 to 10% were recorded from the same depth (1465 m). The pores in this rock are partially occluded by silica cement and authigenic clays, including fibrous illite in large secondary pores.

We conclude, on the basis of these two samples, that the original sorting of the sandstones appears to be an important control on the reservoir quality of this part of the Pacoota Sandstone. The more poorly sorted sandstones, characterized by the greatest content of detrital clay matrix, are the poorest quality reservoirs. However, no rocks with secondary porosity development were specifically studied from the producing sandstones.

Routine core analyses were carried out on cores from parasequence sets 8 and 9 in Tempe Vale #1 well. Porosities from the upper clean sandstone of parasequence set 9 (589 to 613 m) range from a low of 3.3% to a high of 13.7%, although the latter values may be in part the result of fractures seen in the core. Permeability ranges from 10.3 to 106 md. The lower, non-fractured part of the unit (619 to 649 m) has poor to occasionally fair visible porosity. Porosity was measured at 5.5% and the permeability was only 1.64 md. Secondary chlorite occludes the pore space in this sample, but most of the section has silica and, in part, ferruginous cements.

A more detailed analysis was carried out on two samples from clean sandstones of parasequence sets 8 and 9 in Tempe Vale #1. These sandstones have porosities ranging

from 8.5% (581.85 m, top of parasequence set 9) to 13.7% (611.4 m, top of parasequence set 8), and permeabilities between 70 and 72 md, respectively. Sorting ranges from moderate in the upper sample, with bimodal grain size, to well sorted in the lower, unimodal sandstone, but does not appear to have influenced porosity or permeability, in contrast to the findings at Mereenie. There is also no clear relation between these parameters and grain size.

The upper sample is composed dominantly of quartz with minor clay, whereas the lower specimen has 7.7% potassium feldspar, minor mica, and 7.3% clay. The feldspar has been altered to clay, and many grains are partly dissolved to form secondary pores. The clays are dominantly authigenic kaolinite, with minor illite occurring as an isolated pore filling.

The main porosity reducing process has been quartz cementation, with overgrowths often completely filling the original intergranular porosity. However, quartz overgrowths in parasequence set 8 have, to some extent, been inhibited by the presence of clays in the pore spaces or by the presence of feldspars. Partial dissolution of unstable framework grains to form secondary pores is common in the sample from 611.4 m, in which large pores were formed. These secondary pores tend to be randomly distributed and not always interconnected; thus, permeability may be low. It is suggested that the diagenetic sequence in parasequence set 8 sandstones was dissolution of some feldspars and formation of authigenic kaolinite, followed by quartz overgrowth cementation and later microstylolitization, probably due to burial.

No cores were cut in parasequence set 8 in West Walker #1, but log evaluation of the upper, cleaner sandstones of parasequence 9 (1550 to 1573 m) suggests that porosity is less then 4%. Cuttings and samples from the junk sub show that the section is extremely well cemented with silica, and that dolomitic cements are rare. Parasequence set 8 in the well is composed of more arkosic sandstone beds, several of which show porosity development on the density and sonic logs. These more porous sandstones generally are of the coarser grain size but are often silty and poorly sorted. A drillstem test (DST #4) that covered this interval recovered salty formation water, indicating some permeability in the lower part.

At Tent Hill #1, three core samples analyzed from parasequence set 8 showed porosity ranging from 56 to 7.4% with permeabilities varying between 16.1 and 25 md. However, a permeability of only 4.7 md was calculated for this sandstone from a drillstem test.

Although gas is produced from the Pacoota Sandstone at Palm Valley Field, it is from fracture porosity (do Rozario and Baird, 1987). Most sandstones in parasequence sets 8 and 9 are impermeable, with very low calculated porosities (e.g. average 1%, maximum 4%, from parasequence 9 in Palm Valley #3; Kurylowicz, 1975). Samples from parasequence 9 are quartz-rich sandstones in which quartz makes up over 85% of the framework grains, the others being tourmaline and chert. In both samples, the sand grains are well rounded and well sorted, but quartz overgrowths have occluded all porosity. Some grain boundaries are sutured, and rare indented boundaries are also present. Illite is rare to absent.

Below 2374 m in parasequence set 8, sorting is poorer commensurate with an increase in other mineral grains, principally potassium feldspar and illite. The uppermost sample contains 88% well-rounded and well-sorted quartz grains, and 2% calcite in the pore space. Sorting deteriorates with increasing feldspar content and depth (4 to 10%), and grains are less well rounded. Microstylolites, formed from illite are present along grain boundaries, and there are some sutured boundaries. All the original pore space is now occluded with the growth of authigenic minerals including calcite.

Detailed analyses of the reservoir rock characteristics at Palm Valley #1 well were carried out. One core sample of a clean quartzitic sandstone was analyzed from the upper part of parasequence set 8 (2029.4 m), and shown to have about 1% feldspar and 8% dolomite cement. XRD analysis of the <5-μm fraction demonstrated the dominant clay type to be illite (25%), with 5% chlorite and only a slight trace of kaolinite. Sorting was poor, reflecting the high clay content (39%) of the sample. The sandstones exhibit poor porosity, with occlusion of primary pores by detrital clay during deposition and later dolomite cementing. The dolomitic cementation appears to have occurred early in the diagenesis of the sandstone prior to compaction, for the detrital quartz grains either float in the dolomite cement or display point contacts with one another.

At Orange #1, Core #4 was cut in parasequence 9, and Core #5 in parasequence set 8. Quartz content varies from 70 to 90%, with orthoclase varying inversely from 30 to 5%. An increase of visual porosity to 15% is commensurate with kaolinized feldspar in the feldspar-rich specimen. Core-derived porosity ranges from 8 to 13% and permeability from 0 to 73 md, better in the horizontal plane. Core #5 has embayed quartz and secondary overgrowths in samples with 90% quartz and some kaolinized feldspar. Porosity is occluded by ferruginous and argillaceous interstitial material and minor calcareous cement, but reaches 12% with 3 to 31 md permeability. Kurylowicz (1975) calculated sonic log–derived porosities ranging from 3.5 to as high as 18% in Orange #1. However, the sonic-log response is unreliable in this well, and he questioned many of the higher values.

We conclude that parasequence 9 is a clean, quartz-rich sandstone, with pore spaces occluded by secondary quartz overgrowths, most likely by the mobilization of silica in solution, under pressure induced by burial diagenesis. The

clean nature of the sandstones resulted from the winnowing action of waves, which removed the more labile detrital grains such as feldspar, and did not allow the deposition of primary clays such as illite, both of which may have contributed to the later development of secondary porosity in parasequence set 8.

Parasequence Sets 10 and 11

Parasequence set 10 is a transgressive unit (retrogradational parasequence set) that is thickest in the northeast and thins to the southwest, where it onlaps the Central Ridge (Fig. 3.24h). It is present at Mereenie Field (Fig. 3.21) but is not present at Tempe Vale #1. The gamma-ray logs (Fig. 3.27) reflect the increasing content of glauconite in the sediments as the sequence grades upward into the largely glauconitic sediments of parasequence set 11. The basal beds are often pebbly but contain marine fossils including trilobites. Thin limestones are present in the more glauconitic sediments of parasequence set 11. The parasequence set is present over a large area (Fig. 3.24i) and overlaps the Central Ridge. The parasequence set thins to the southwest toward the Mereenie Field, where it is usually less than 10 m thick, while further west at Tempe Vale #1, it is absent.

The basal beds of parasequence set 10 are nearly everywhere coarse and pebbly, usually trough cross-bedded, and have a wedge-shaped geometry that thickens to the north. The presence of basal conglomerates in the south indicates that, in these areas, parasequence set 10 is unconformable upon parasequence set 3. Combined with seismic evidence for channels at the base of the parasequence set in the central Missionary Plain trough, indicative of a Type 1 sequence boundary in the terminology of van Wagoner et al. (1987), these sediments belong either to the lowstand systems tract or the transgressive systems tract. The presence of marine indicators, (herringbone cross-lamination, etc.) in the basal beds indicates that the transgressive systems tract is the most appropriate model. In parasequence set 10, the deepest-water deposition occurs immediately above the last parasequence seen on logs and is marked by a condensed sequence (high gamma-ray values). This is particularly well displayed at Palm Valley Field (Fig. 3.27).

The lower part of parasequence set 11 is characterized by abundant glauconite and phosphatic sandstone consisting of finely comminuted inarticulated brachiopods and other fauna. Sporadic interbedded *Skolithos*-bearing sandstones and associated sedimentary structures (e.g., herringbone cross-stratification) indicate that environments remain, in part, extremely shallow in the southwest toward the depositional margin. A northward increase in the *Cruziana* trace-fossil suite and the dominance of finer-grained sediments at Ellery Creek suggest deepening water to the north.

Glaucogenesis occurred in response to relatively slow sedimentation rates in cool, agitated water, within a depth range of 20 to 800 m. Such criteria suggest sedimentation in deeper water than that of the majority of the Pacoota sandstones. However, the ubiquitous cross-bedding of the glauconitic sandstones is evidence for strong current activity and argues against a deep depositional environment. The phosphatic sandstones also indicate an active depositional regime, since they are largely composed of comminuted infauna. The decrease in the abundance of glauconite up sequence suggests shallowing of the sea from the maximum depth attained during the phase of glaucogenesis. Further evidence for shallowing is the appearance of herringbone cross-stratification near the top of parasequence set 11. The diverse fauna of several genera of gastropods, bivalves, nautiloids, trilobites, conodonts, and brachiopods is consistent with an offshore, open-marine environment.

The top of parasequence set 11 is marked by a rapid change to clean, non-glauconitic sandstone, readily identified in wells and many outcrop sections (Fig. 3.27). The sandstone is generally medium to coarse grained, with low-angle trough cross-beds, is often ripple-marked, and contains scolithids, *Diplocraterion*, shell fragments, and phosphatic nodules.

In the transgressive systems tract model (Vail, 1987), the best reservoirs are developed in the beach-to-shoreface, zone due to the reworking of sediment by the transgressing sea. In the case of parasequence set 10, such reservoirs could be expected to lie in the lower beds, but none is known to be present in this part of the section to date.

This parasequence set is best developed at Palm Valley Field and in West Waterhouse #1. Two cores cut in the top of parasequence set 10 at West Waterhouse #1 (Fig. 3.27) show that the section has no intergranular porosity preserved. The original pore space was destroyed by secondary silicification and the introduction of dolomitic and calcareous cements. Similar reservoir characteristics are seen at Palm Valley Field. A core from the upper part of the section at Palm Valley #1 consists of well-sorted sandstone, with 69% quartz, 2% glauconite, 3% pyrite, and 2% heavy minerals. The major cementing agent is dolomite (18%) with minor silica (1%). Feldspars make up about 1% of the rock fragments, and illite forms the dominant clay in the <5-μm fraction, with up to 37% dolomite present occluding the porosity. In outcrop, this parasequence set has a very heterogeneous grain size and often contains pebbles. The presence of a soluble cement (i.e., dolomite) is indicated, because the unit is often friable and, consequently, poorly exposed.

Parasequence set 11 forms the main glauconitic horizon at both Palm Valley and Mereenie Fields (Fig. 3.27). At Mereenie (P2 unit of Towler, 1986), porosity ranges from 0 to 7% in core analyses (Kurylowicz et al., 1976). Similar-

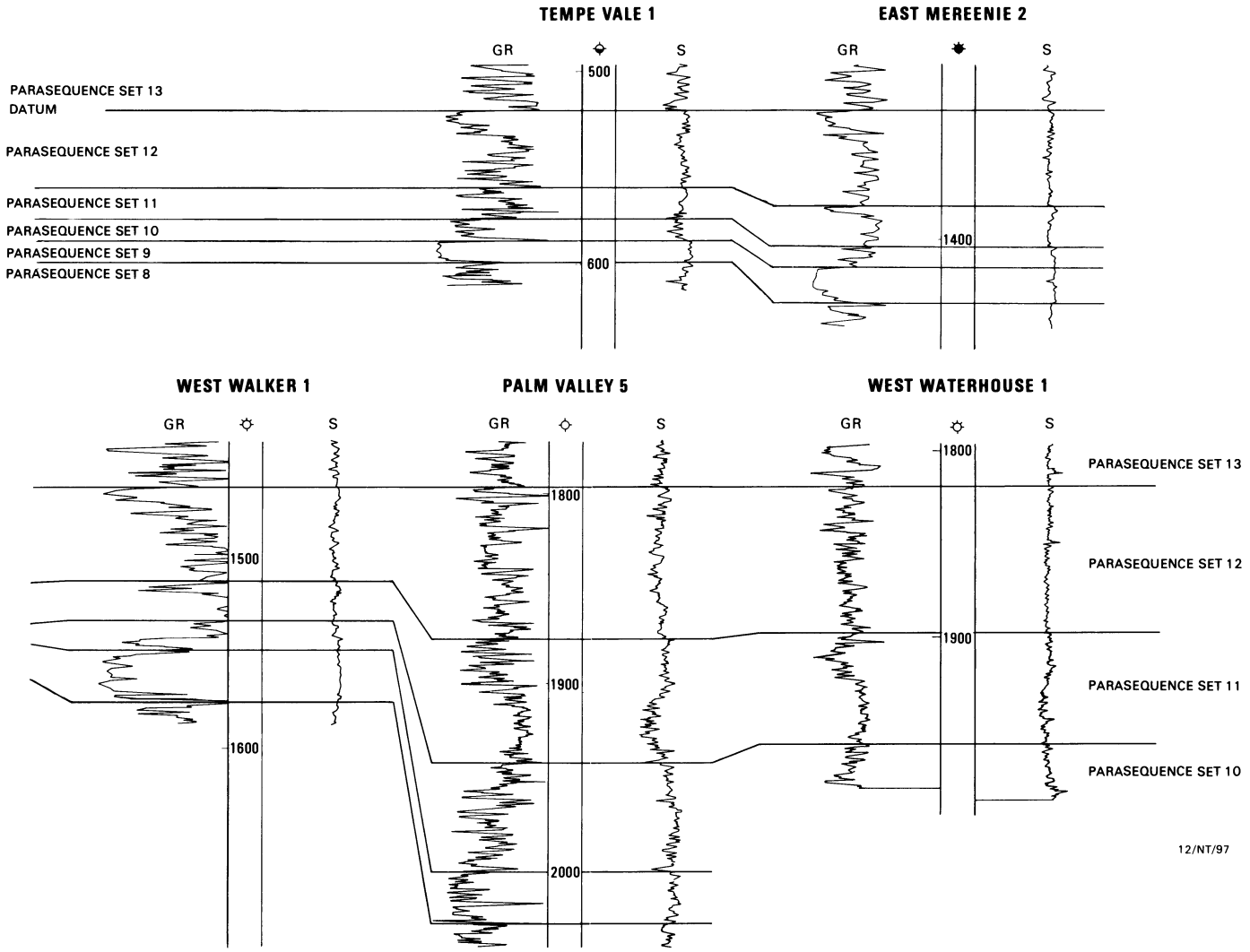

Figure 3.27. East-to-west gamma-ray and sonic-log cross section from Tempe Vale #1 to West Waterhouse #1, to illustrate development of parasequence sets 10 to 12. Note that the transgressive systems tract sediments (parasequence set 10) are thickest in the centrally located wells such as Palm Valley #5, and thinner in wells on the Central Ridge. The generally low porosity of parasequence set 10 is shown by the sonic logs and is due to dolomitic cement, probably introduced soon after deposition. On the Central Ridge, the sandstones are poorly developed, and porosity is occluded by dolomitic or silica cements, although in the more arkosic sandstones ("hot" gamma-ray character) at Tempe Vale #1, some porosity is evident from the logs, probably due to dissolution of feldspar. The glauconitic sandstones in the lower part of parasequence set 11 are invariably impermeable due to carbonate cementation. Interbedded cleaner sandstones have low porosity due to silica overgrowths. The clean sandstones at the top of the shoaling cycle are impermeable due to burial-induced quartz overgrowth although some vertical permeability is present where the sandstones are riddled with burrows. Minor primary porosity has been preserved where anhydrite cement is present in the Mereenie wells. Sandstones in parasequence set 12 are generally of low porosity due to silicification and minor calcite cement.

ly, the unit is impermeable at Palm Valley Field, with a maximum of 4.9% porosity (Kurylowicz et al., 1976). Authigenic quartz fills most of the pore space in the interbedded, non-glauconitic sandstones, leaving little primary porosity.

The upper part of parasequence set 11 was deposited in tidally influenced, shallow-water environments. In the highstand systems-tract model, the best reservoirs are developed within discontinuous fluvial and deltaic facies and minor shoreface facies. Fluvial and deltaic facies have not been recognized at the top of parasequence set 11, although they may have been developed along the shoreline and have subsequently been reworked or eroded by the ensuing transgressive events. These upper beds are clean, quartzitic sandstones that contain shallow water trace fossils, and are known at Mereenie Field as the P2-110 sand (Towler, 1986). Porosity is generally poor due to burial-induced silicification and quartz overgrowths, although some vertical

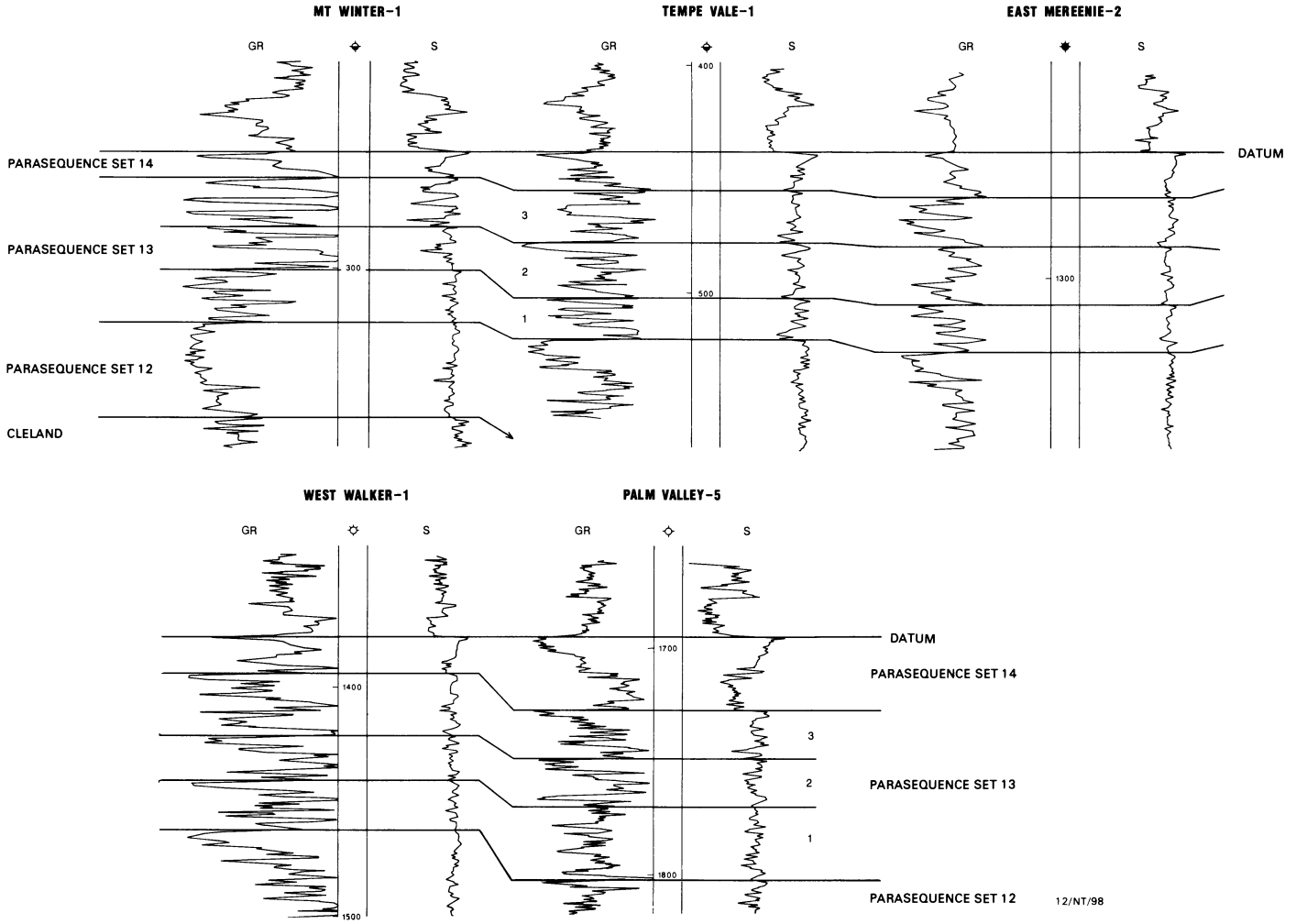

Figure 3.28. East-to-west cross section from Tempe Vale #1 to Palm Valley #5, showing parasequences within parasequence set 13. The upper sandstones in these shoaling cycles are generally clean, but porosity is usually occluded by silicification. When arkosic, however, as at Tempe Vale #1, the contained feldspar has partially inhibited formation of quartz overgrowths. Sandstones in the Palm Valley Field are impermeable due to dolomitic cements and silicification.

porosity is present where the sandstone is riddled with burrows. Log interpretation suggests that the upper sandstone (P2-110 sandstone of Towler, 1986) (Figs. 3.22 and 3.28) is generally impermeable.

At East Mereenie #2, siliceous and dolomitic cement is present in the well sorted sandstones. However, moderate primary porosity occurs where anhydrite cement is present, and poor porosity was noted in the same well with anhydrite, dolomite, or detrital clay occluding pore space. There are no available petrological studies of the upper sandstones in other wells, but the low gamma-ray values and lack of porosity evident on sonic and density logs suggest that silicification in the beds is ubiquitous. Dolomite and calcite cements are also suggested by the density-log response in several wells.

Parasequence Set 12

Parasequence set 12, a progradational parasequence set (Fig. 3.27), has been included previously in the P2 at Mereenie Oil Field and the P1 at Palm Valley Gas Field (Fig. 3.21). It is distributed across the northern part of the basin from Orange Gas Field to Mount Winter #1 and overlaps the Central Ridge (Fig. 3.24i). The lower beds are interbedded, heavily bioturbated sandstone and shale. Basal contacts of the sandstone beds higher in the section are often sharp, and beds are usually less than 1 m thick, generally 10 cm, and the frequency of scoured basal contacts increases up section. Shale clasts and phosphatic pellets are scattered throughout the unit, but sometimes occur in concentrated lag deposits. Up section, the shales become

darker, more finely laminated, and less bioturbated. The sandstone also becomes less bioturbated and thinner bedded, and lenticular bedded sandstone is often present in the shales immediately below the uppermost pipe rock. These uppermost beds are low-angle to flat-bedded sandstones that are riddled with burrows, some of which are escape burrows, suggesting rapid and episodic sedimentation in a shelf environment *Skolithos*, *Ophiomorpha?*, *Monocraterion*, *Diplocraterion*, and *Phycodes* are the most common trace fossils. Shelly fossils, including inarticulate brachiopods and other bivalves, are often present.

At Mereenie Field (Fig. 3.27), the upper clean, quartzose sandstones of parasequence set 12 are known as the P1-310 sand (Towler, 1986). Porosity is generally poor and restricted to burrowed horizons. Silicification has generally destroyed original porosity due to remobilization and precipitation under burial diagenesis.

At Palm Valley #3, the sandstones contain up to 10% potassium feldspar and variable amounts of illite (0 to 20%), which fills primary void spaces. However, most porosity destruction has taken place by pressure solution and reprecipitation of quartz. Minor calcite infill is also sometimes present.

Parasequence Set 13

Parasequence set 13 is the most widespread of the Pacoota Sandstone subunits: it is recorded as far west as Sausage Hill, and as far south as the Oval Syncline and Maloneys Creek. In the northeast, it has been progressively deeply eroded from the western Waterhouse Range and the area to the east. It ranges in thickness from 30 m in wells to the south to over 120 m at Ellery Creek in the MacDonnell Range to the north (Kurylowicz et al., 1976). It is about 75 m thick at Palm Valley Field.

This unit is the most heterolithic of the Pacoota Sandstone units (Fig. 3.28). Much of the parasequence set is siltstone and shale, and as a result, is not often exposed. In the subsurface, the gamma-ray logs reflect the presence of multiple coarsening-upward cycles (parasequences) (Fig. 3.28). The top of each cycle is terminated abruptly, and a new cycle is established with another shale. A typical cycle consists of a basal black shale overlain by bioturbated siltstone, followed by a thicker interval of thin-bedded, sharp-based, rippled sandstone interbedded with siltstone. The cycles are capped by low-angle, cross-bedded and bioturbated sandstone. The uppermost sandstone often contains vertical burrows, U-shaped burrows, arthropod traces such as *Phycodes*, and other trace fossils.

The uppermost cycles usually do not contain *Skolithos* tubes, although they are ubiquitous in lower cycles. The lack of these shallow-water indicators in the uppermost beds suggests deepening water in the later stages of deposition of the parasequence set. Deepening water is also suggested by the appearance of conodonts upward in the succession at Ellery creek, a greater proportion of the *Cruziana* ichnofauna in the trace fossil communities, and the general increase in finer-grained clastics to the north. Hummocky cross-bedding is also present in the upper beds, indicating deposition at depths near storm wave base. This supports deposition in a transgressive sea with episodic, small-scale regressive cycles superimposed upon the overall transgression. The unit conforms to the definition of an aggradational to weakly progradational parasequence set (van Wagoner et al., 1987).

Reservoir rocks are present at the top of some of the shoaling cycles at Mereenie Oil Field, but whereas the continuity of the reservoir interval "appears reasonable" (Towler, 1986) over the field, the permeability is sporadic. The upper sandstones in these cycles are generally clean, as shown by core and the gamma-ray log (Fig. 3.28), and porosity is usually occluded by silicification. However, the best reservoir sandstone in Tempe Vale #1 well (equivalent to the P1-80 sandstone of Towler, 1986) contains up to 21.7% feldspar. Feldspar in this sandstone has partially inhibited formation of quartz overgrowths. Sandstones in the Palm Valley Field are invariably impermeable due to dolomitic cementation or silicification induced by burial. It is suggested that the better reservoirs in parasequence set 13 will be developed along the Central Ridge, where arkosic sandstones are more likely to be present because of proximity to fluvial sources, and the sandstones have not been buried so deeply.

Conclusion

The best reservoir rocks in the Pacoota Sandstone are concentrated above the major sequence boundary between parasequence sets 3 and 8 in the southwest, where feldspar in the sandstones affects reservoir development and preservation. Diagenesis resulted in partial dissolution of some of the labile grains and development of secondary porosity.

These conclusions are predicated on studies showing that, at Tempe Vale #1, a high percentage of the feldspars have undergone dissolution to form large secondary pores, and the moderate porosity from the sequence at East Mereenie #2 is dominantly secondary, although some primary porosity remains. However, the evidence is not conclusive, due to the small number of samples analyzed. The best indicator of reservoir potential at Mereenie is possibly the gamma-ray log: the cleaner the sandstone (i.e., lower the radioactivity), the poorer the reservoir.

To the northeast at Palm Valley Field, the sediments are more marine and have been subjected to greater winnowing and destruction of labile grains such as feldspar. Subsequent deep burial in this area led to compaction and diagenesis with silicification, resulting in generally impermeable rocks. However, dolomitic cementation appears to have occurred in the diagenesis of the parasequence set 8 sandstones prior to compaction.

At Orange #1, porosity development is commensurate with a high component of kaolinized feldspar, but is occluded by ferruginous and argillaceous material and minor calcareous cement. However, where pre-Devonian erosion has allowed access of meteoric water to remobilize calcareous material, and subsequent burial-induced diagenesis and quartz overgrowth are not excessive, as at Alice #1, good porosity is present.

Discussion

When viewed from the larger perspective of basin dynamics, the two major reservoir units of the Amadeus basin—the Arumbera and Pacoota Sandstones—at first might appear to be dissimilar, because the two units were deposited at very different-times in basin evolution. The Arumbera was deposited soon after extension of stage 2, when basin subsidence was close to its maximum, so that the margins of the sub-basin were well defined, and the paleoslope large. In contrast, the Pacoota was deposited in a ramp setting late in stage 2, when subsidence was much reduced.

In spite of these larger-scale differences, the units have many features in common both texturally and mineralogically, and in terms of reservoir quality. Both units were deposited in shallow-marine settings, the Arumbera in a coastal-plain or deltaic depositional system, and the Pacoota as part of a shallow-marine to tidal depositional system with occasional significant fluvial input. The reservoir sandstones of both units are moderately sorted and arkosic. Both are, in part, heavily cemented with silica or dolomite, and both have a reduced reservoir quality due to clay minerals. Both have secondary porosity generated by the dissolution of feldspar.

The main reservoir of the Arumbera Sandstone lies close to the base of the formation directly overlying the major sequence boundary and was probably deposited as part of the transgressive systems tract. Similarly, the main Pacoota Sandstone reservoir (parasequence set 8) occurs in arkosic sandstones immediately above the major sequence boundary at Mereenie Field. The similar depositional setting of these basal reservoir sandstones, their arkosic nature, and development of at least some secondary porosity by feldspar dissolution, suggest a common depositional control. That is, local factors involving facies ultimately control reservoir quality, rather than the larger-scale factors controlling basin dynamics, although clearly, both must be involved.

Sandstones at the top of the transgressive cycles in both the Arumbera and Pacoota Sandstones have been cleaned of labile grains by wave and tidal reworking. These sandstones, while possessing a relatively high original porosity, have been extensively dolomitized and later silicified by introduction of quartz under deep burial diagenesis. Consequently, these clean sandstones are now poor reservoirs (e.g., parasequence 9 of the Pacoota and the top of Arumbera sequence 2.).

In both formations, the key to the survival and creation of porosity has been a balance between mechanical sorting of the detrital materials and later diagenetic alteration. Where sands were well sorted at the tops of the major cycles, feldspar was removed and the sands became quartz rich. This resulted in massive quartz cementation. In less well-sorted sands, primary porosity was poor and was reduced even further by clay minerals. In the reservoir units at the tops of shallowing-upward cycles, lower in both formations, the sands are well sorted and provide primary porosity without the extremes of either quartz cementation or clay minerals, while feldspars were abundant enough to allow the development of significant secondary porosity. However, even arkosic sandstones may be impermeable due to dolomite cementation.

Acknowledgments

We wish to thank Magellan Petroleum Australia Limited for providing access to data and facilities during the course of this study. We further wish to thank the Amadeus Basin Joint Venture Parties for permission to use their data.

References Cited

Benbow, D.D., 1968, Case history—Mereenie Field: Australian Petroleum Exploration Assoc. Journal, v. 8, p. 114–119.

Burek, P.J., Walter, M.R., and Wells, A.T., 1979, Magnetostratigraphic tests of lithostratigraphic correlation between latest Proterozoic sequences in the Ngalia, Georgina and Amadeus basins, central Australia: Bureau of Mineral Resources Journal of Australian Geology and Geophysics, v. 34, p. 47–55.

Davies and Associates, 1980, Formation evaluation study—Arumbera Sandstone, Pancontinental Wallaby No. 1 well, Amadeus basin, Northern Territory. Report for Pancontinental Petroleum Ltd., Sydney, Australia, 24 p. (unpublished).

Davies and Associates, 1982, Fluid sensitivity analysis and reservoir quality of the Pacoota, Arumbera and Julie Formations, Dingo No. 1 well,

Amadeus basin, central Australia: Report for Pancontinental Petroleum Ltd., Sydney Australia.

do Rozario, R.F., and Baird, B.W., 1987, The detection and significance of fracture in the Palm Valley Gas Field. Australian Petroleum Exploration Assoc. Journal, v. 27, p. 264–280.

Forman, D.J., 1966, Regional geology of the south-west margin, Amadeus basin, central Australia: Australian Bureau of Mineral Resources (Australia), Geology and Geophysics, Report 87.

Gorter, J.D., 1992, Late Precambrian to Early Ordovician sedimentation in the Amadeus basin, central Australia [Ph.D. thesis]: University of New South Wales, Sydney, Australia.

Jackson, K.S., McKirdy, D.M., and Deckelman, J.A., 1984, Hydrocarbon generation in the Amadeus basin, central Australia: Australian Petroleum Exploration Assoc. Journal, v. 24, p. 42–65.

Jones, B.G., 1972, Upper Devonian to Lower Carboniferous stratigraphy of the Pertnjara Group, Amadeus basin, central Australia: Journal of the Geological Society of Australia, v. 19, p. 229–249.

Kennard, J.M., and Lindsay, J.F., 1991, Sequence stratigraphy of the Latest Proterozoic-Cambrian Pertaoorrta Group, northern Amadeus basin, central Australia: Australian Bureau of Mineral Resources (Australia), Geology and Geophysics, Bulletin 236, p. 171–194.

Korsch, R.J., and Lindsay, J.F., 1989, Relationships between deformation and basin evolution in the Amadeus basin, central Australia. Tectonophysics, v. 158, p. 5–22.

Kurylowicz, L.E., 1975, Basin analysis and petroleum prospects of the Larapinta Group, Amadeus basin, with particular reference to porosity evaluation [Ph.D. thesis]: Australian National University, Canberra.

Kurylowicz, L.E., Ozimic, S., McKirdy, D.M., Kantsler, A.J., and Cook, A.C., 1976, Reservoir and source rock potential of the Larapinta Group, Amadeus basin, central Australia: Australian Petroleum Exploration Assoc. Journal, v. 16, p. 49–65.

Lindsay, J.F., 1987a, Sequence stratigraphy and depositional controls in Late Proterozoic–Early Cambrian sediments of Amadeus basin, central Australia: American Association of Petroleum Geologists Bulletin, v. 71, p. 1387–1403.

Lindsay, J.F., 1987b, Late Proterozoic evaporites in the Amadeus basin, central Australia and their Role in basin tectonics. Geological Society of America Bulletin, v. 99, p. 852–865.

Lindsay, J.F., and Korsch, R.J., 1989, Interplay of tectonics and sea-level changes in basin evolution: An example from the intracratonic Amadeus basin, central Australia: Basin Research, v. 2, p. 3–25.

Lindsay, J.F., and Korsch, R.J., 1991, The evolution of the Amadeus basin, central Australia: Australian Bureau of Mineral Resources, Geology and Geophysics, Bulletin 236, p. 7–32.

Lindsay, J.F., Korsch, R.J., and Wilford, J.R., 1987, Timing the breakup of a Proterozoic supercontinent: Evidence from Australian intracratonic basins: Geology, v. 15, p. 1061–1064.

Lundegard, P.D., Samuels, N.D., and Pryor, W.A., 1985, Upper Devonian turbidite sequence, central and southern Appalachian basin: Contrasts with submarine fan deposits, *in* Woodrow, D.L., and Sevon, W.D., eds., The Catskill Delta. Geological Society of America Special Paper 201, p. 107–121.

McNaughton, D.A., and Huckaba, W.A., 1978, Reservoir rock characteristics of Arumbera Sandstone and Late Proterozoic sediments: Technical Introduction Sheet O, Report for the Magellan Petroleum Company.

McNaughton, D.A., Quinlan, R.M., Hopkins, R.M., and Wells, A.T., 1968, Evolution of salt anticlines and salt domes in the Amadeus basin, central Australia: Geological Society of America Special Paper 88, p. 229–247.

Ozimic, S., Passmore, V.L., Pain, L., and Lavering, I.H., 1986, Australian Petroleum Resources Report 1, Amadeus basin, central Australia: Canberra, Australian Bureau of Mineral Resources (Australia), 64 p.

Preiss, W.V., Walter, M.R., Coats, R.P., and Wells A.T., 1978, Lithological correlations of Adelaidean glaciogenic rocks in parts of the Amadeus, Ngalia, and Georgina basins. Bureau of Mineral Resources Journal of Australian Geology and Geophysics, v. 3, p. 45–53.

Ranford, L.C., Cook, P.J., and Wells, A.T., 1966, Geology of the central part of the Amadeus basin, Northern Territory: Australian Bureau of Mineral Resources (Australia), Geology and Geophysics, Report No. 86, 74 p.

Schroder, R.J., and Gorter, J.D., 1984, A review of the recent exploration and hydrocarbon potential of the Amadeus basin, Northern Territory: Australian Petroleum Exploration Assoc. Journal, v. 24, pt. 1, p. 19–41.

Schumm, S.A., 1968, Speculation concerning paleohydrologic controls of terrestrial sedimentation. Geological Society of America Bulletin, v. 79, p. 1573–1588.

Shaw, R.D., Stewart, A.J., and Black, L.P., 1984, The Arunta Inlier: A complex ensialic mobile belt in central Australia; Part 2: Tectonic history: Australian Journal of Earth Sciences, v. 31, p. 457–484.

Shergold, J.H., 1986, Review of Cambrian and Ordovician paleontology of the Amadeus basin, central Australia: Australian Bureau of Mineral Resources (Australia), Geology and Geophysics, Report 276, 21 p.

Shergold, J.H., Gorter, J.D., Nicoll, R.S., and Haines, P.W., 1991, Stratigraphy of the Pacoota Sandstone (Cambrian-Ordovician), Amadeus basin, N.T.: Bureau of Mineral Resources (Australia), Geology and Geophysics, Bulletin 237, p. 1–14.

Smith, A.T., and Rose A.W., 1985, Relation of red-bed copper-uranium occurrences to the regional sedimentology of the Catskill Formation in Pennsylvania, *in* Woodrow, D.L., and Sevon, W.D., The Catskill Delta: Geol. Society of America Special Paper 201, p. 183–197.

Taylor, D.J., 1959, Palaeontological report on the southern Amadeus region, Northern Territory: Report for the Frome–Broken Hill Co. Pty. Ltd., Report No. 4300-G-27.

Towler, B.F., 1986, Reservoir simulation in the Mereenie Field: Australian Petroleum Exploration Assoc. Journal, v. 26, p. 428–446.

Vail, P.R., 1987, Seismic stratigraphy interpretation using sequence stratigraphy. Part 1: Seismic stratigraphy interpretation procedure, *in* Bally, A.W., ed., Atlas of Seismic Stratigraphy: American Assoc. of Petroleum Geologists Studies in Geology, No. 27, v. 1, p. 1–10.

van Wagoner, J.C., Mitchum, R.M., Posamentier, H.W., and Vail, P.R., 1987, Seismic stratigraphy interpretation using sequence stratigraphy. Part 2: Key definitions of sequence stratigraphy, *in* Bally, A.W., ed., Atlas of Seismic Stratigraphy: American Assoc. of Petroleum Geologists Studies in Geology No. 27, v. 1, p. 11–14.

Walter, M.R., Elphinstone, R., and Hey, G.R., 1989, Proterozoic and Early Cambrian trace fossils from the Amadeus and Georgina basins, central Australia: Alcheringa, v. 13, p. 209–256.

Wells, A.T., Forman, D.J., and Ranford, L.C., 1965, Geological reconnaissance of the north-western part of the Amadeus basin, Northern Territory: Bureau of Mineral Resources (Australia), Geology and Geophysics, Report No. 85, 45 p.

Wells, A.T., Forman, D.J., Ranford, L.C., and Cook, P.J., 1970, Geology of the Amadeus basin: Australian Bureau of Mineral Resources, Geology and Geophysics, Bulletin No. 100, 222 p.

Wells, A.T., Ranford, L.C., Stewart, A.J., Cook, P.J., and Shaw, R.D., 1967, The geology of the north-eastern part of the Amadeus basin, Northern Territory: Bureau of Mineral Resources (Australia), Geology and Geophysics, Report No. 113, 97 p.

Williams, G.K., Hopkins, R.M., and McNaughton, D.A., 1965, Pacoota reservoir rocks, Amadeus basin, N.T., Australia: Australian Petroleum Exploration Assoc. Journal, v. 5, p. 159–167.

Woodrow, D.L., 1985, Paleogeography, paleoclimate, and sedimentary processes of the Late Devonian Catskill Delta, *in* Woodrow, D.L., and Sevon, W.D., The Catskill Delta: Geological Society of America Special Paper 201, p. 51–63.

SECTION II

Perspectives from Modern Environments

E.G. Rhodes and T.F. Moslow

This section demonstrates how and why surficial and subsurface analyses of modern sedimentary environments can be used in predicting reservoir behavior and performance in marine clastic parasequences. In this volume, the application of geological information gained from the study of modern environments proceeds beyond the more common—and much simpler—utilization of modern environments for the somewhat circular process of constructing a facies model.

For many years, modern environments of deposition were used almost solely for the purpose of providing an analog to an ancient reconstruction. Conversely, most reconstructions are predominantly rooted in the summation of sedimentological observations. Therefore, *precise* or *specific* modern analogs are inappropriately utilized to defend an interpretation of the ancient. Such application of modern analogs has led to their misconception as static, rigid templates, into which all sedimentological observations of ancient sequences are incorporated, or force-fitted if necessary. This perspective of "putting the cart before the horse" has compromised some trust and value for the role of the modern analog.

Modern environments of deposition, especially when they include a three-dimensional framework obtained through coring, provide insight toward the understanding and prediction of facies relations, sand body continuity and geometry, and process-sedimentologic controls on facies reservoir quality. Such insights have immediate application to predicting reservoir heterogeneities, as demonstrated in the chapter by Tye and Moslow. On a broader scale, as in the chapter by Mart, surficial studies of modern depositional systems can be used readily to predict the spatial and temporal distribution of reservoir-quality facies on a basinal level. While still useful as an analog to an ancient reconstruction, the study of modern environments provides insights and predictive capabilities to the reservoir geologist, especially regarding reservoir quality and geometry within marine clastic parasequences.

Bo Tye and Tom Moslow demonstate a paradigm for analysis of modern examples that helps bond the application of such examples to the interpretation of the ancient. The authors selected tidal inlet facies to demonstrate this perspective, although almost any Holocene parasequence or parasequence set could have been utilized.

Petroleum geologists often ignore the likely and probable mode of preservation when determining the environment of deposition for reservoir facies. Of course, such interpretation is essential when predicting reservoir occurrence, extent, and volumetrics at either the exploration or development level. However, many modern environments of deposition and their resulting facies have a low potential for preservation, especially under transgressive sea-level conditions. Tye and Moslow demonstrate that even within the Holocene, inlet-fill facies have a greater likelihood of preservation than their conterminous strandline deposits. Consequently, modern analogs should always be considered within the context of reasonable preservation potential rather than merely matching facies characteristics by sedimentary structures. It is this aspect of analogy-oriented interpretation that requires modern sedimentologists to be more quantitative about facies geometries.

Facies geometry as a significant parameter within reservoir analysis is a central theme within Tye and Moslow's chapter. The authors show that thickness-to-width ratios of preserved inlet facies cluster within the range of 1:125 to 1:500. Such ratios not only indicate the amount of material that is rework-

ed or modified during the drowning of prograded coasts during relative sea-level rise, but they also hint at the number of subtle but important sea-level oscillations that must have accompanied the development of stacked reservoir facies within such formations as the Eocene- and Oligocene-aged sands of the Texas Gulf Coast, especially the Yegua and Frio barrier/strandplain systems (Galloway et al., 1982, 1983; Galloway, 1986; Tyler and Ambrose, 1986).

Sedimentologists and stratigraphers frequently regard the discipline of geomorphology as that part of the earth sciences that deals strictly with surficial processes. The association of geomorphology with geographic sciences within many universities further distances the petroleum industry professional from geomorphic analysis. Ironically, it is the geomorphologist's validation of many process-response interpretations that offers the development geologist a predictive analog for the distribution of reservoir-quality rock.

With this premise in mind, we asked Yossi Mart to present a geomorphic viewpoint on the parameters that control sediment distribution within a deep-sea-fan complex, specifically, the Nile Fan. Mart describes the geomorphic asymmetry between the western and eastern provinces of the Nile Fan. The consequential reservoir facies distribution and heterogeneity of this asymmetry bear a striking resemblance to the hypotheses tested regularly by explorationists in the Gulf of Mexico. In reading Mart's chapter, the geoscientist familiar with the Gulf of Mexico province will see analogs between the disruption of sediment supply by faulted escarpments and salt ridges within the eastern Nile Escarpment and the diversion of sediment fairways by growth faults and salt tectonics in the Gulf of Mexico.

In Chapters 1 and 2 of Section One, Cant and Pacht and his co-authors presented interpretive strategies to identify facies-tract positions. In this chapter, Mart offers a geomorphological explanation for sediment distribution within a deep marine complex that has not been extensively described in the literature.

References

Galloway, W.E., 1986, Reservoir facies architecture of microtidal barrier systems: American Association of Petroleum Geologists Bulletin, v. 70, p. 787–809.

Galloway, W.E., Hobday, D.K., and Magara, K., 1982, Frio Formation of the Texas Gulf Coast basin–depositional systems, structural framework, and hydrocarbon origin, migration, distribution, and exploration potential: University of Texas Bureau of Economic Geology Report of Investigations 122, 78 p.

Galloway, W.E., Ewing, T.E., Garrett, C.M., Tyler, N., and Bebout, D.G., 1983, Atlas of major Texas oil reservoirs: University of Texas Bureau of Economic Geology Special Publication, 139 p.

Tyler N., and Ambrose, W.A., 1986, Facies architecture and production characteristics of strand-plain reservoirs in North Markham–North Bay City field, Frio Formation, Texas: American Association of Petroleum Geologists Bulletin, v. 70, p. 809–829.

CHAPTER 4

Tidal Inlet Reservoirs: Insights from Modern Examples

Robert S. Tye and Thomas F. Moslow

Introduction

The coasts of North Carolina, South Carolina, and Louisiana are excellent examples of the range of sand-body types deposited along a terrigenous-clastic barrier island shoreline (Fig. 4.1). Submergence during the Holocene and the presence of reworked Holocene and Pleistocene sediment sources resulted in the formation of barrier-island, tidal-inlet, flood- and ebb-tidal delta, estuarine, and complex backbarrier environments. Hayes (1975), Nummedal et al. (1977), and Davis and Hayes (1984) determined that the geomorphic variability of barrier islands and tidal inlets along the southeast U.S. coast is controlled by regional changes in wave regime, tidal range, and tidal prism. In addition, Nummedal et al. (1977) and Hubbard et al. (1979) noted the geomorphic differences among wave-dominated, transitional, and tide-dominated tidal inlets.

Kumar and Sanders (1974), Heron et al. (1984), and Moslow and Tye (1985) cored barriers on Long Island, New York, and North Carolina and South Carolina, and determined that tidal-inlet-deposited sediment composes 5 to 25% of these barrier islands. Given the significant percentage of inlet-fill material deposited within barrier islands and the high preservation potential of the inlet sequence, it is imperative that the geometry, occurrence, distribution, and sedimentary characteristics of tidal inlets be understood. Only with this knowledge can ancient barrier-island reservoir facies be evaluated properly.

Using high-resolution seismic profiles, historical maps and charts, and aerial photographs, the following objectives were addressed: (1) the physical factors that control tidal-inlet stratigraphy; (2) the variability and distribution of tidal-inlet sand bodies; (3) the subsurface geometry of inlet-fill sequences and their relations to adjacent barrier islands; and (4) the preservation potential of tidal-inlet deposits in modern shoreline settings. The first three objectives were achieved by comparing tidal inlets along the North Carolina and South Carolina coastlines of the southeastern United States (Fig. 4.2). The fourth objective, determining the preservation potential of inlet deposits, was achieved through an examination of cores and seismic data from the shoreface and inner continental shelf of the Louisiana coastline, northern Gulf of Mexico (Fig. 4.1). These data are rare along modern coastlines (Rampino and Sanders, 1980), including the wave- and/or tide-dominated barrier shorelines of North and South Carolina (Hine and Snyder, 1985).

Physical and Depositional Setting

Patterns of morphology, sedimentation, and stratigraphy of tidal inlets were examined along the sharply contrasting shorelines of North Carolina, South Carolina, and Louisiana. The Carolina shoreline arc forms the northern and central portion of the Georgia embayment (Fig. 4.2). Coastal geomorphology varies widely within this embayment because of differences in the hydrographic regime (wave energy and tidal range), inner-shelf slope, and tidal prism (Nummedal et al., 1977; Hayes, 1979).

The arcuate shape of the embayment and the increasing width of the continental shelf toward the center of the arc have opposing effects on wave height and tidal range (Nummedal et al., 1977; Hayes, 1979). The flanks of this arc (North Carolina and Florida) have a narrow continental shelf, resulting in high wave energy and a low tidal range. Conversely, the widening shelf amplifies the tidal range at

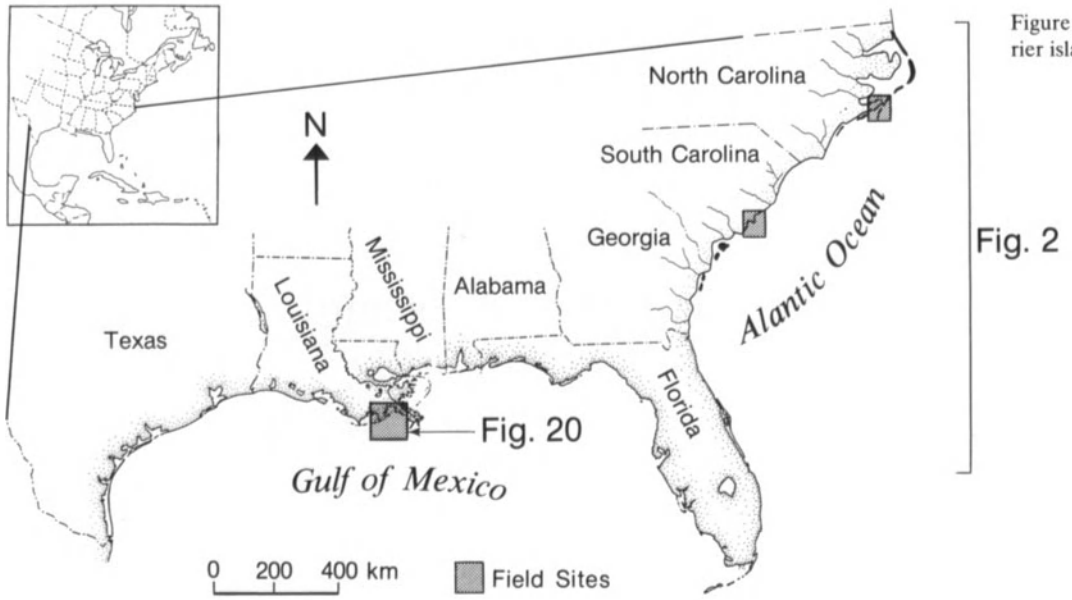

Figure 4.1. Regional map of the three barrier island shorelines examined.

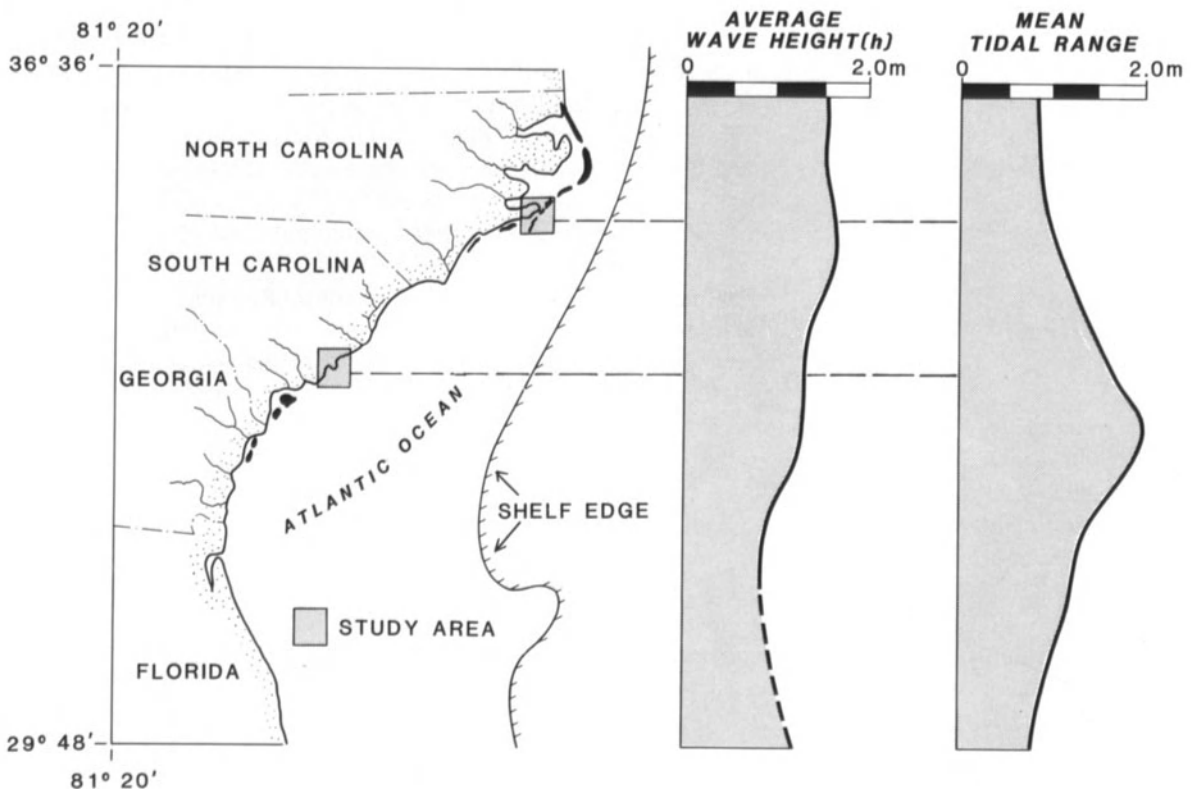

Figure 4.2. Comparison of average wave heights and mean tidal range for the mid-Atlantic and southeastern coastlines of the United States. (Modified from Nummedal et al., 1977.)

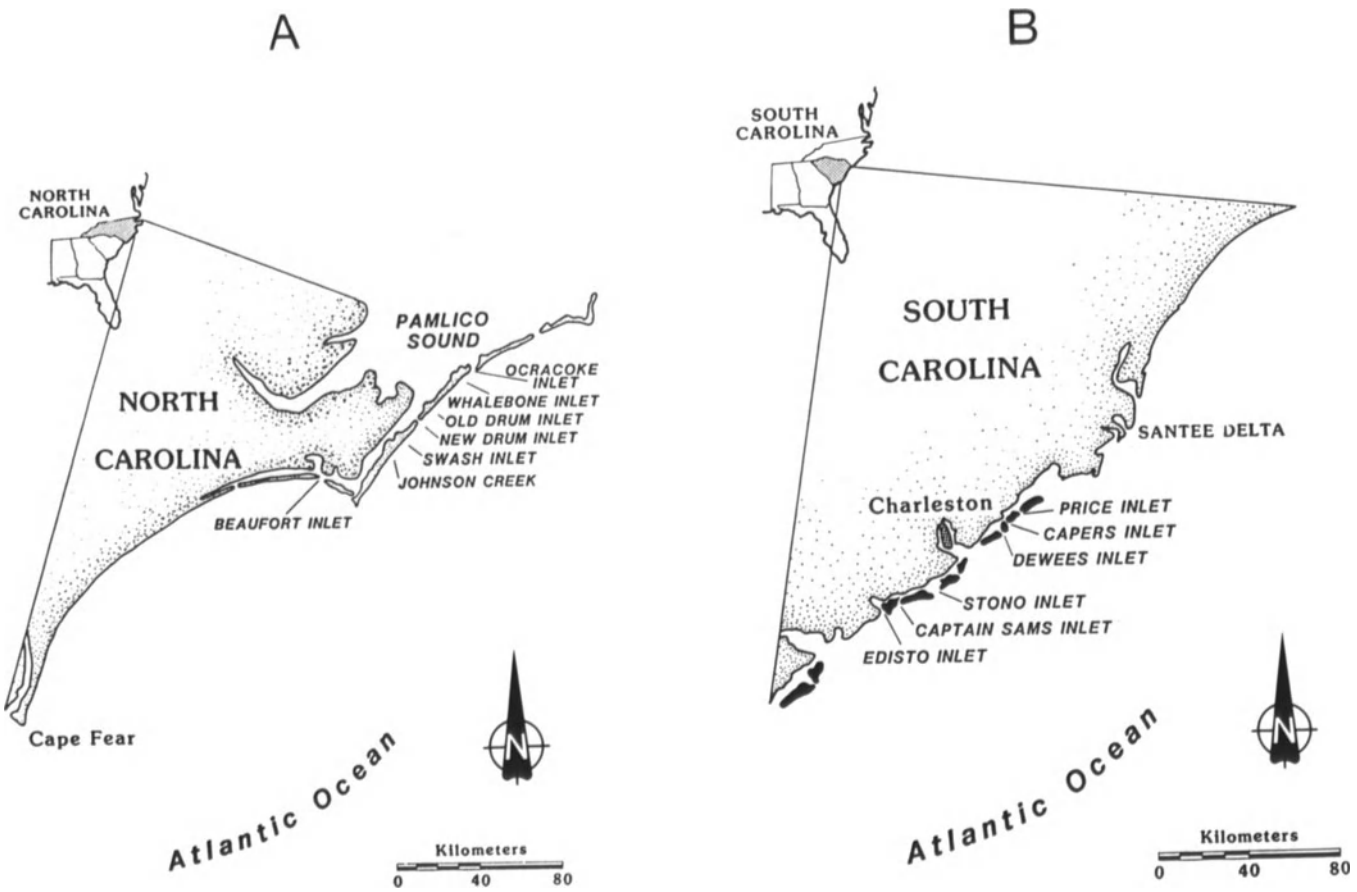

Figure 4.3. (A) Location of active and relict (i.e., abandoned), wave-dominated tidal inlets examined along the barrier islands forming the Cape Lookout cuspate foreland in North Carolina. (B) Location of tide-dominated central South Carolina coastline illustrating the general location of tidal inlets discussed. All tidal inlets studied are active at present.

the apex (South Carolina and Georgia) while attenuating the wave energy. Funnelling of the tidal wave into the apex further enhances the tidal range to a maximum of approximately 2.5 m. This change in shelf bathymetry produces microtidal (tidal range, or T.R., ≤2 m; Davies, 1964), wave-dominated shorelines on the flanks of the embayment, and a mesotidal (T.R. 2–4 m; Davies, 1964), mixed-energy (both tides and waves are important) shoreline in the center of the Georgia embayment (Hayes, 1979). A dominant northeasterly wave approach into the Georgia embayment results in a net southward longshore transport of sediment.

The Cape Lookout cuspate foreland in North Carolina (Fig. 4.3A) exhibits many characteristics of a wave-dominated coast: (1) long, linear, narrow barriers; (2) broad, open lagoons; (3) widely spaced tidal inlets; and (4) large flood-tidal deltas. Average wave heights in this area are 1.7 m, whereas the tidal range is extremely low (<1.0 m; Nummedal et al., 1977). In contrast, the more tidally influenced, mixed-energy central South Carolina coast (Fig. 4.3B) experiences average wave heights of 60 cm (Hayes, 1979; Kana, 1979). The mean tidal range is 1.6 m, increasing to 2.1 m during spring tides (U.S. Department of Commerce, 1982). This mesotidal coastline consists of: (1) short, stubby barrier islands; (2) extensive backbarrier salt marsh; (3) numerous tidal inlets; and (4) prominent ebb-tidal deltas (Hayes and Kana, 1976). Within this hydrographic and geomorphic context, tidal inlets on the North Carolina coast are referred to as wave-dominated inlets. Conversely, the majority of tidal inlets studied in South Carolina are referred to as tide dominated.

Inlet Morphology and Processes

Numerous studies have dealt with tidal-inlet formation, morphology, and occurrence (Hoyt and Henry, 1967; Hayes, 1967; Bruun and Gerritsen, 1959; Pierce, 1970; Kumar and Sanders, 1974; FitzGerald et al., 1978; Hubbard et al., 1979; and Hayes, 1980). Morton and Donaldson

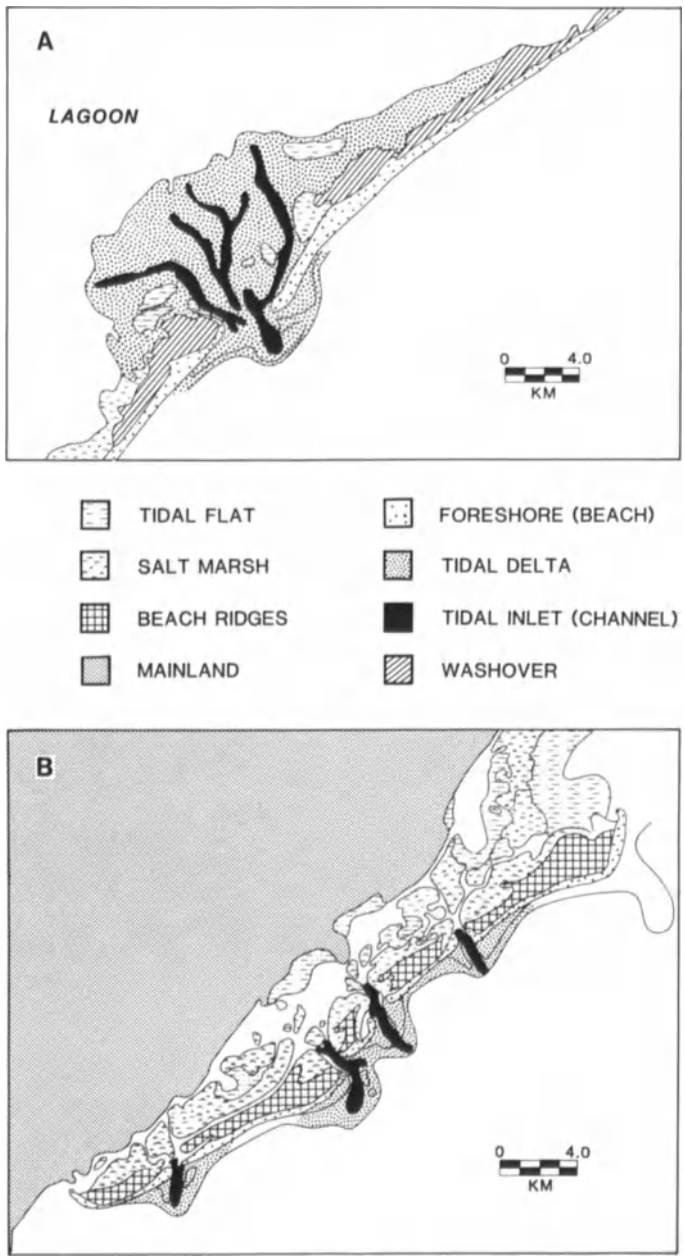

Figure 4.4. Schematic diagram illustrating (A) wave-dominated, and (B) tide-dominated inlet geomorphology and associated depositional environments. (Modified from Moslow and Tye, 1985.)

(1973), Halsey (1979), Price and Parker (1979), and Tye (1984) allude to paleotopographic control in the development of tidal inlets and suggest that many tidal inlets are confined to Pleistocene fluvial valleys and estuaries. Hayes (1967) and Pierce (1970) documented the formation of shallow, narrow inlets by the seaward return flow of storm surge. The relation between high wave energy and the occurrence of tidal inlets was established by Goldsmith et al. (1974) and may be an important factor in inlet formation. Hayes (1980) presents a concise review of the morphology and sediment distribution patterns on flood and ebb-tidal deltas.

In microtidal settings, long, narrow, wave-dominated barriers extend for tens of kilometers and are separated by ephemeral, rapidly migrating tidal inlets (Fig. 4.4A). The associated flood-tidal deltas, deposited by waves and tidal currents, form large, lobate sand bodies in the lagoon. Wave energy and flood-tidal currents exert more influence on sedimentation than ebb currents; therefore, ebb-tidal delta development is poor. Wave-dominated inlets migrate laterally along the shoreline in a downdrift direction for many kilometers and at relatively rapid rates. As the hydraulic efficiency of the inlet decreases, wave-reworked ebb-tidal delta sands accumulate in the inlet mouth, resulting in closure of the inlet channel and abandonment of the flood-tidal delta (Fig. 4.5A). Fine-grained sediment accumulates on the relict flood-tidal delta, which is ultimately vegetated by salt marsh (Fig. 4.5A). Fisher (1962) identified positions of former tidal inlets in the Cape Lookout area of North Carolina by locating vegetated relict flood-tidal deltas attached to the landward side of the barriers.

Unlike wave-dominated coasts, tidally influenced mesotidal barrier islands often assume a stunted, drumstick-shaped configuration (Hayes, 1975) (Fig. 4.4B). These barriers are wider, extend for several kilometers, and are separated by numerous, more stable tidal inlets. The back-barrier lagoon and flood-tidal delta of the wave-dominated shoreline are replaced by salt marsh and tidal creeks. Tidal current dominance over wave energy helps to confine these inlets, restricting downdrift migration distance to less than 2 km. Tidally influenced inlet channels are deflected downdrift by preferential addition of sand to the updrift lobe of the ebb-tidal delta. These inlet channels lose hydraulic efficiency and breach the barrier to form a shorter updrift channel. Large sediment lobes are reworked from the former ebb-tidal delta and eventually weld onto the barrier, closing the earlier inlet channel (Fig. 4.6A) (FitzGerald et al., 1978; Tye, 1984). This process of inlet channel migration and ultimate closure by wave-reworked, ebb-tidal delta sand is called bar bypassing (Bruun and Gerritsen, 1959). Landward, out of the influence of wave transport, silt and clay accumulate in the former channel due to the absence of strong tidal currents.

Bar bypassing is the major process of channel abandonment at tide-dominated inlets. Migration occurs through downdrift overextension of the main-ebb channel and subsequent breaching of a shorter, updrift channel. Bar bypassing occurs rapidly at small inlets (Bruun and Gerritsen, 1959; Sexton and Hayes, 1982), but one cycle of inlet-channel migration and abandonment took more than 100

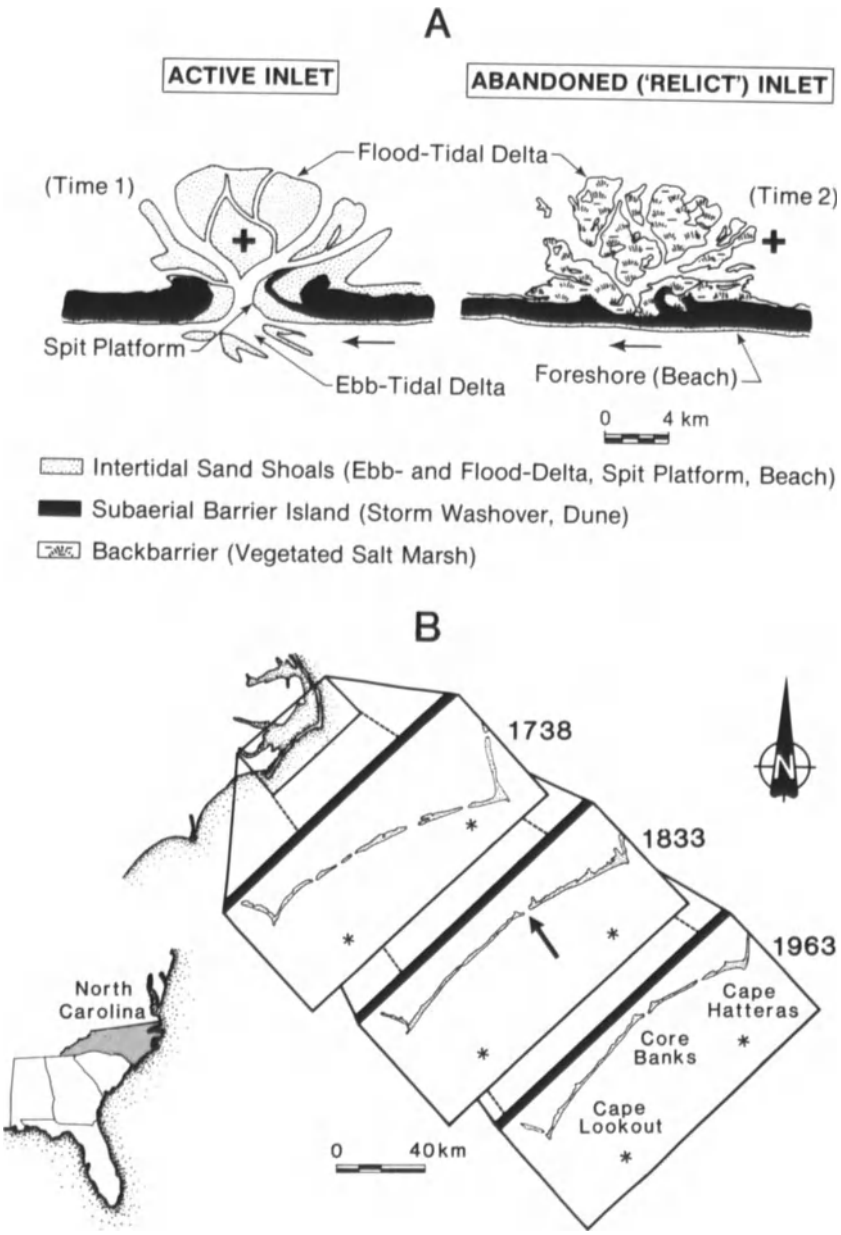

Figure 4.5. (A) Mechanism of wave-dominated inlet channel closure resulting primarily from longshore sediment transport. (Modified from Fisher, 1962.) Cross provides reference point to illustrate migration of inlet and flood-tidal delta: (B) Historic evolution of the central North Carolina coast. Note that during historic time (since A.D. 1650), only Ocracoke Inlet (arrow) has remained stable.

years at Capers, Price, and Stono Inlets (Fig. 4.6B) (FitzGerald et al., 1978; Tye, 1984).

Controls on Tidal Inlet Stratigraphy

The inverse relation between wave height and tidal range along the North and South Carolina coasts results in distinct tide- versus wave-dominated tidal inlets. In addition to the hydrologic regime (waves, tides, storms), sediment supply (quantity and lithology) and the pre-Holocene substrate (topographic relief and lithology) modify the distribution, geometries, and sequences of tidal inlets.

Hydrographic Regime

Wave-dominated inlets migrate rapidly downdrift and are constantly forming new flood-tidal deltas, due to: (1) high rates of longshore sediment transport associated with a wave-dominated environment, (2) the fact that predominantly sandy substrates commonly underlie tidal inlets, and (3) the narrowness of the barrier islands. Downdrift extension of the inlet channel results in hydraulic inefficiency and induces channel abandonment. Landward sand transport by waves closes the former channel mouth.

Extratropical storms and hurricanes can lead to the development of tidal inlets (Hayes, 1967; Pierce, 1970),

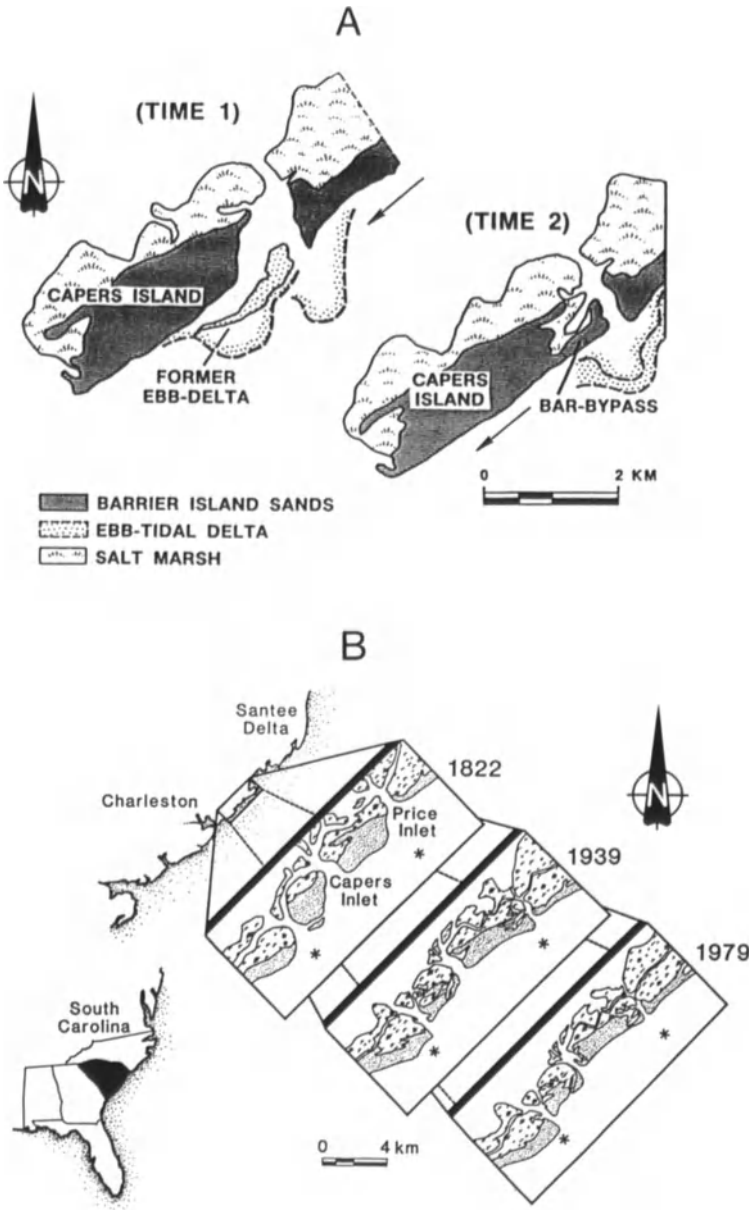

Figure 4.6. (A) Illustration of the bar-bypass mechanism of inlet channel abandonment; and (B) historic examples from Price and Capers Inlets, South Carolina. Note that these tide-dominated inlet channels and ebb-tidal deltas do not migrate extensively alongshore.

because storms cut numerous channels through narrow barrier islands. Post-storm conditions heal most of these breaches, but the more efficient channels are tidally maintained and form new tidal inlets. A historical analysis of the Cape Lookout area (Fig. 4.5B) illustrates the ephemeral nature and variable distribution of wave-dominated tidal inlets. The location and number of tidal inlets in North Carolina have varied significantly through time. For example, between 1738 and 1833, four of these inlets were closed, leaving only one inlet channel. Between 1833 and 1963, a second tidal inlet opened just south of Cape Hatteras. Fisher (1962) documented that Ocracoke Inlet has been the only stable tidal inlet throughout historic time (since 1650).

Tide-dominated inlets are more stable, and because of the short, stubby morphology of mesotidal barriers, they occur more frequently than wave-dominated inlets. In addition, owing to strong ebb currents along this portion of the shoreline, the inlets exhibit well-developed ebb-tidal deltas (Hayes, 1975). Because tide-dominated barrier islands are relatively wide, and because the inlet channel cuts into an underlying cohesive substrate, the inlet throat tends to be stabilized (FitzGerald et al., 1978), and is inhibited from extensive lateral migration. The seaward extension of the main-ebb channel migrates downdrift, but is abandoned by bar bypassing at the inlet mouth.

Hurricanes breach fewer inlets through wide mesotidal barriers, but they can initiate or accelerate abandonment through bar bypassing (Sexton and Hayes, 1982). Bar

bypassing can result in the preservation of abandoned-inlet channel-fill deposits (Fig. 4.6A).

Sediment Supply

The textural differences apparent between wave- and tide-dominated inlet sequences (Moslow and Tye, 1985) are a function of the mode of channel abandonment. Waves transport large volumes of sand alongshore and into wave-dominated inlet mouths. Inlet channels choked by the ebb-tidal delta and an updrift recurved spit are ultimately abandoned and filled with sand.

Hydraulically inefficient tide-dominated channels are closed by landward-migrating swash bars. The sandy swash bar fills only the depositional downdip (most seaward) portion of the abandoned channel, thereby creating a low-energy, shallow-water body (similar to an oxbow lake) landward of the swash bar (Fig. 4.6). The newly formed main-ebb channel inhibits alongshore spit migration, and the ebb-tidal delta acts as a sediment sink for sediment transport alongshore. Thus, a sand deficiency exists in the former inlet channel, and it fills with fine-grained sediment.

Pre-Holocene Substrate

In the central and southern part of the Georgia Bight (South Carolina and Georgia), the onset of the Holocene transgression initiated the alluviation of Pleistocene drainage systems. In response to this transgression, a primary barrier island chain formed roughly 6,000 yr B.P. (Moslow and Colquhoun, 1981). Topographically high interstream divides provided a focal point for barrier genesis, whereas tidal channels occupied the positions of former fluvial channels (Morton and Donaldson, 1973; Halsey, 1979; Price and Parker, 1979; Tye, 1984).

Geomorphic and subsurface evidence from North Carolina suggests that the antecedent topography was subordinate to marine processes in influencing shoreline evolution and tidal-inlet positioning (Fisher, 1962; Hoyt, 1967; Hoyt and Henry, 1967; Swift, 1968; Moslow and Heron, 1978). Thus, inlet formation and distribution are mostly functions of storm surge and hurricane impact.

Paleotopography is a factor independent of hydrologic regime and sediment supply controlling tidal-inlet stratigraphy. Examples of inlet channels confined or influenced by Pleistocene topography are evident on the U.S. Atlantic and Gulf coasts (Morton and Donaldson, 1973; Herbert, 1978; Price and Parker, 1979). Distances of channel migration or stabilization of the inlet throat are functions of paleotopographic lows and substrate lithology. Constraints imposed by the Pleistocene surface are evident only at the deeper inlets.

Tidal-Inlet Fill Geometries

Wave-dominated

Cross sections of abandoned wave-dominated inlet channels are lenticular to wedge shaped when viewed along depositional strike (Fig. 4.7). Active and relict channels display obvious erosional and accretional margins, revealing

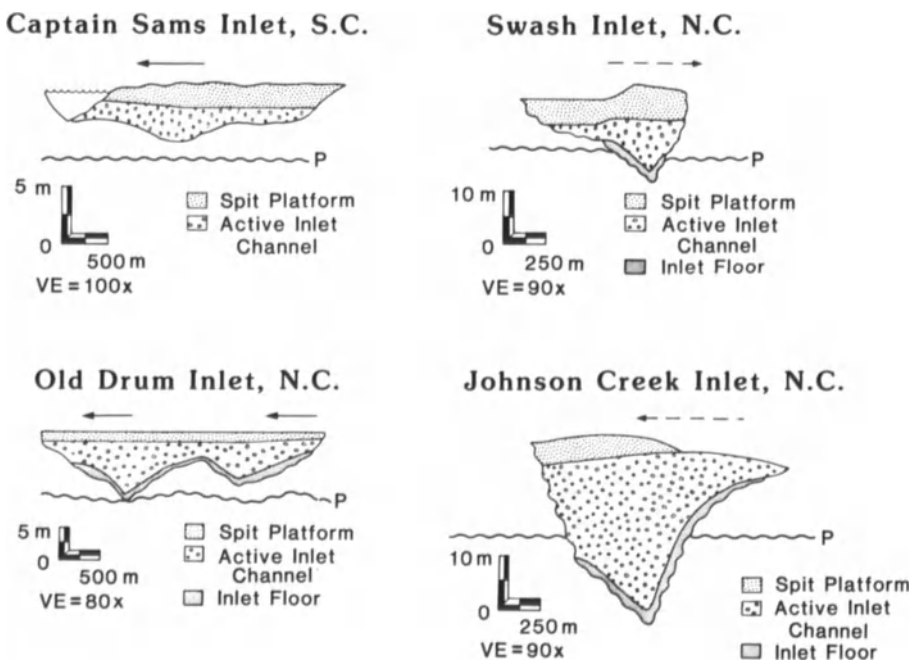

Figure 4.7. Representative examples of tidal-inlet fills showing the geometries and facies relations of wave-dominated inlet sand bodies. The unconformity shown in each diagram is the top of the Pleistocene (P).

Table 4.1. Linear Dimensions of Tidal Inlet-Fill Sequences in North and South Carolina

Inlet	Maximum Thickness (m)	Maximum Width (km)	Thickness-to-Width Ratio (Th/W)	Cross-Sectional Area (m^2)
		Wave-Dominated		
Captain Sams, SC[1]	5.5	2.7	1/490	9,200
Cedar Inlet, NC[2]	3.0	0.74	1/247	1,750
South Swash Inlet, NC[2]	9.0	1.4	1/127	6,300
Johnson Creek, NC[2]	16.8	2.1	1/125	17,640
South Zack Creek, NC[2]	7.7	1.9	1/246	12,350
North Zack Creek, NC[2]	3.4	0.88	1/259	2,640
1700's Drum Inlet, NC[1]	9.8	2.5	1/255	12,250
1933 Drum Inlet, NC[3]	7.3	1.95	1/267	7,117
Sand Island Inlet, NC[3]	5.8	2.4	1/414	12,000
Pilontary Inlet, NC[3]	5.2	2.5	1/481	11,750
North Swash Inlet, NC[3]	3.4	0.9	1/265	2,700
Whalebone Inlet, NC[3]	25.3	3.1	1/122	39,215
Whalebone Inlet, NC[3]	8.5	1.9	1/250	11.2
Mean	3.0–25.3	0.74–3.1	1/125–1/500	1,750–39,215
Range				
		Tide-Dominated		
Capers Inlet, SC[4]	7.0	1.0	1/142	7,000
Price Inlet, SC[4]	8.0	1.2	1/150	9,600
Doboy Inlet, GA[5]	15.0	3.75	1/132	24,000
Mean	10	2.0	1/150	13,500
Range	7.0–15.0	1.0–3.75	1/132–1/150	7,000–24,000

[1]From Moslow (1984); [2]From Moslow and Heron (1978); [3]From Herbert (1978); [4]From Tye (1984); [5]From Hayt and Henry (1967).

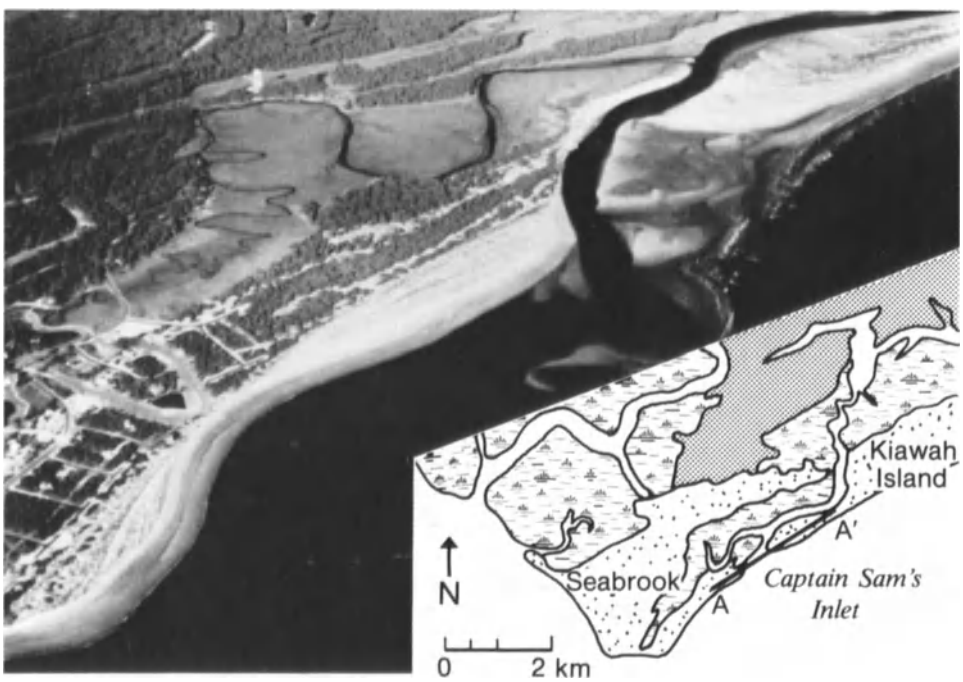

Figure 4.8. Oblique aerial photograph of Captain Sam's Inlet, South Carolina. Location of cross section in Figure 4.10 is shown by line A-A′ in the inset map. (Photo by M.O. Hayes.)

the direction of migration. A recurved spit constitutes the accreting margin and fills the inlet channel as it migrates. Once abandoned, the channel fill deposited in shallow, wave-dominated inlets is lenticular to tabular in cross section. Rapid channel migration and high sediment supply result in thin, laterally continuous sequences of tidal-inlet deposits. Deeper tidal inlets, entrenched in indurated or cohesive Pleistocene clays, are generally less laterally extensive and display wedge-shaped, strike-oriented geometries (Fig. 4.7). Thickness-to-width ratios, reflecting maximum scour depth and lateral migration, range from 1:250 for deep channels to 1:500 for shallower channels (Table 4.1). The high width-to-thickness ratio for shallow tidal inlets is due to the absence of paleotopographic control and rapid downdrift migration. Measurements of cross-sectional profiles from 12 wave-dominated relict tidal-inlet sand bodies in the study area consistently cluster at thickness-to-width ratios of 1:125, 1:250, and 1:500 (Table 4.1).

Captain Sam's Inlet is a shallow, rapidly-migrating inlet at the southern terminus of Kiawah Island, South Carolina (Fig. 4.8). It illustrates the way in which the balance between waves and tides influences inlet geometry. Although it is located on a mixed-energy, tide-dominated shoreline, the combination of a very small tidal prism ($4.0–6.0 \times 10^6$ m^3; Sexton and Hayes, 1982), constant wave energy, and intermittent storm processes produces a wave-dominated inlet fill. A characteristic sedimentary sequence is approximately 3.5 m thick, fines upward, and consists of cross-bedded active inlet-channel, spit platform, and eolian dune sands (Fig. 4.9). Because the inlet channel is migrating along a progradational barrier island, the inlet-fill sequence is eroded into lower shoreface sediments. As a result of rapid channel migration and recurved spit growth, a lenticular inlet-fill sand body is produced that extends 3.0 km along the shoreline (Fig. 4.10).

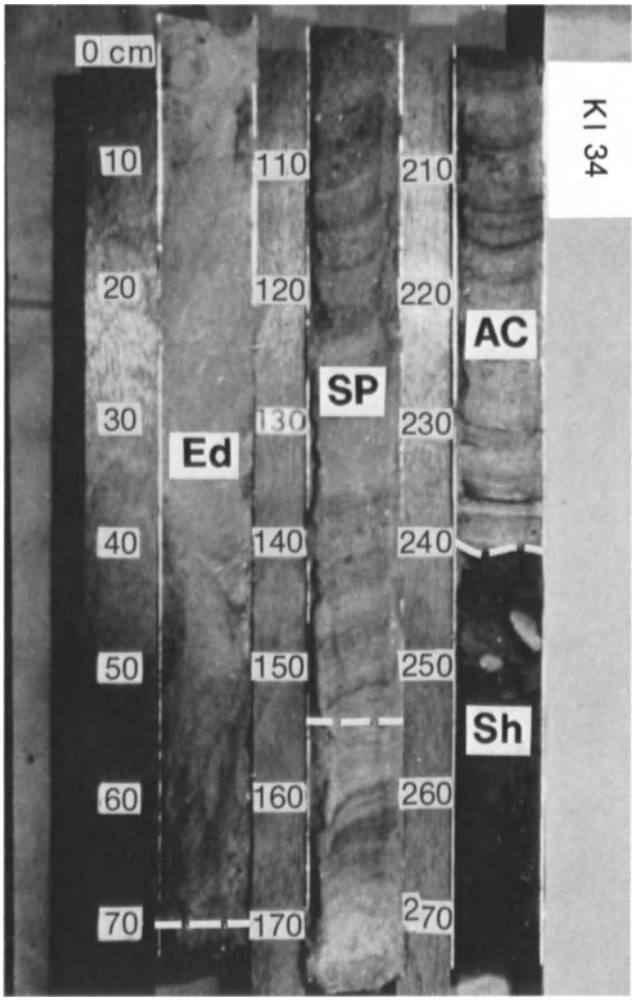

Figure 4.9. Photograph of cored wave-dominated inlet-fill sequence from Captain Sam's Inlet, South Carolina. Sedimentary facies are: lower shore face (LS), active channel (AC), spit platform (SP), and eolian dune (Ed). Core diameter is 7.5 cm.

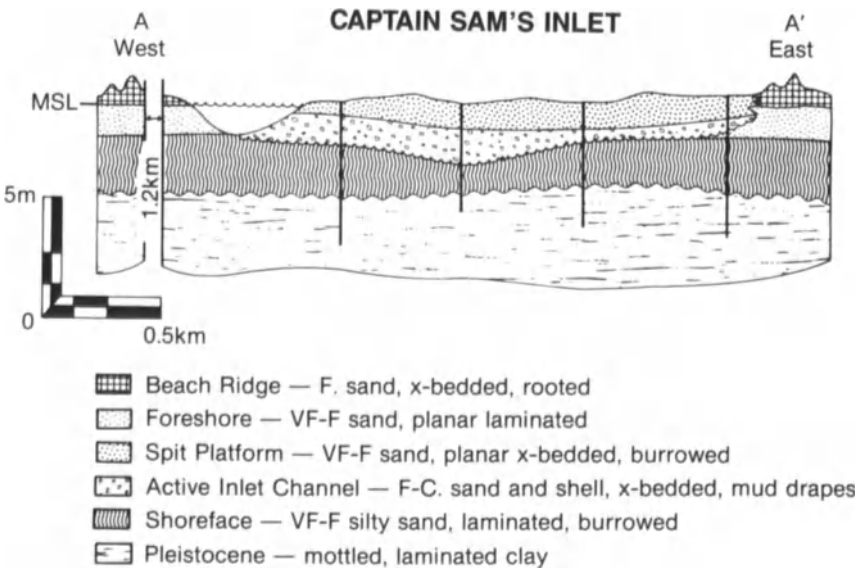

Figure 4.10. Strike-oriented cross section for wave-dominated Captain Sam's Inlet, South Carolina. Location given in Figure 4.8.

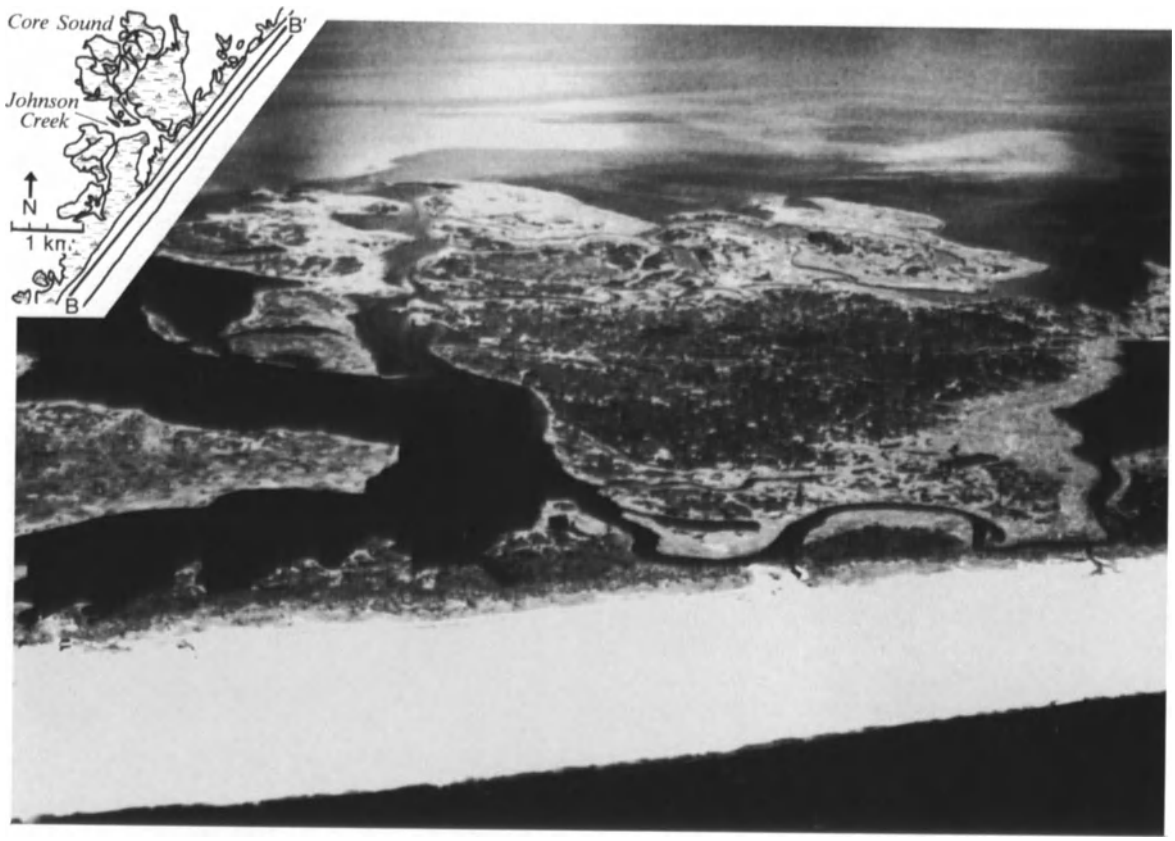

Figure 4.11. Oblique aerial photograph of abandoned flood-tidal delta at Johnson Creek, Core Banks, North Carolina. Line B-B′ in map inset gives location of cross-section in Figure 4.12.

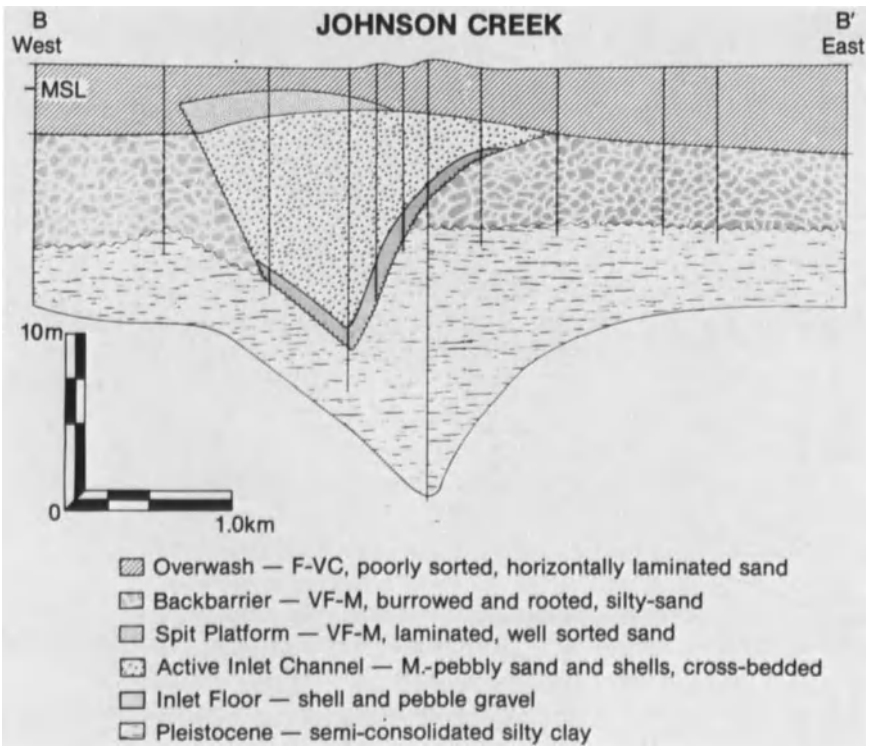

Figure 4.12. Strike-oriented cross section for Johnson Creek, North Carolina. Location given in Figure 4.11.

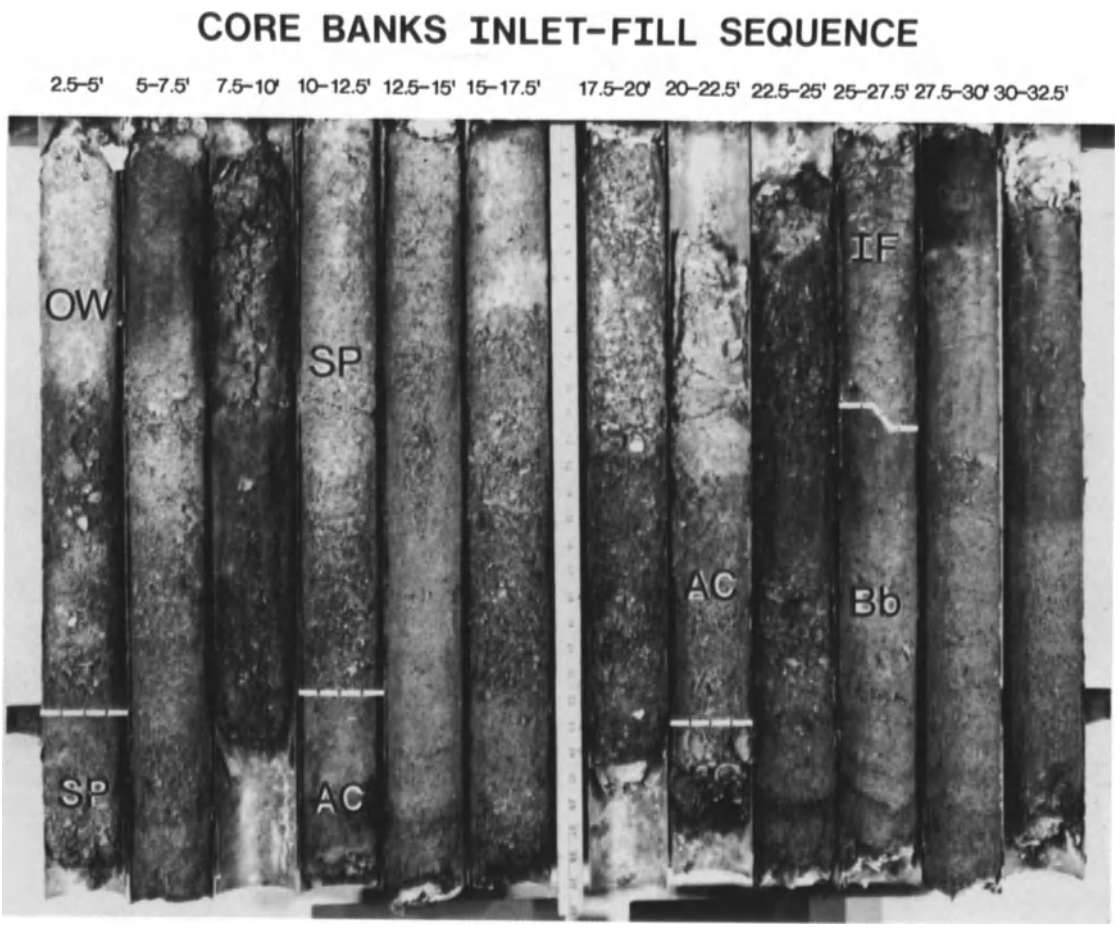

Figure 4.13. Core photograph of wave-dominated inlet-fill sequence from Core Banks, North Carolina. The inlet-fill sequence is approximately 8.0 m (25.75 ft) thick, and comprises inlet-floor (IF), active-channel (AC), and spit-platform (SP) facies. The sequence fines upward, consists of an approximately even mixture of fine-grained to coarse-grained sand and fragmented shell material, is eroded into underlying backbarrier (Bb) silts and Pleistocene clays, and is overlain by horizontally laminated overwash (OW) sands.

Channel scour into Pleistocene clays confined inlet-channel migration at Johnson Creek, North Carolina (Fig. 4.11) and produced a wedge-shaped inlet-fill deposit (Fig. 4.12). Channel confinement by Pleistocene sediments resulted in a single 9.5-m-thick, fining-upward sequence preserved within Core Banks. The inlet-fill sequence is fine- to very coarse-grained sand and fragmented shell material, and consists of inlet-floor, active-channel, and spit-platform facies (Fig. 4.13). Bioclastic channel fills within the Triassic Halfway Fm of Alberta and British Columbia are remarkably similar to the sequence found at the Johnson Creek tidal inlet (Munroe and Moslow, 1990), and are an important hydrocarbon reservoir facies in the Western Canada sedimentary basin.

Herbert (1978) described an inlet sequence of similar geometry at Whalebone Inlet, North Carolina (Fig. 4.3A). However, he observed four separate fining-upward cycles of inlet deposition. Inlet sequences may be stacked or vertically aggraded by sea-level rise, barrier-island subsidence, or successive filling of the thalweg of an old fluvial channel (Herbert, 1978; Price and Parker, 1979). The preservation of four stacked sequences indicates that sea-level rise or land subsidence was rapid enough to displace the previously deposited sediment and prevent it from being reworked. The stability of the inlet channel may account for only one channel sequence at Johnson Creek, but it is more likely that earlier deposits were reworked by successive episodes of tidal-inlet migration.

Tide-dominated

Tide-dominated inlet channels along the South Carolina coast exhibit symmetrical U-shaped, strike-oriented geometries (Fig. 4.14). Inlet throat stability and bar bypassing at the channel mouth inhibit extensive lateral migration; thus, tidal-inlet deposits accumulate in the updrift portion

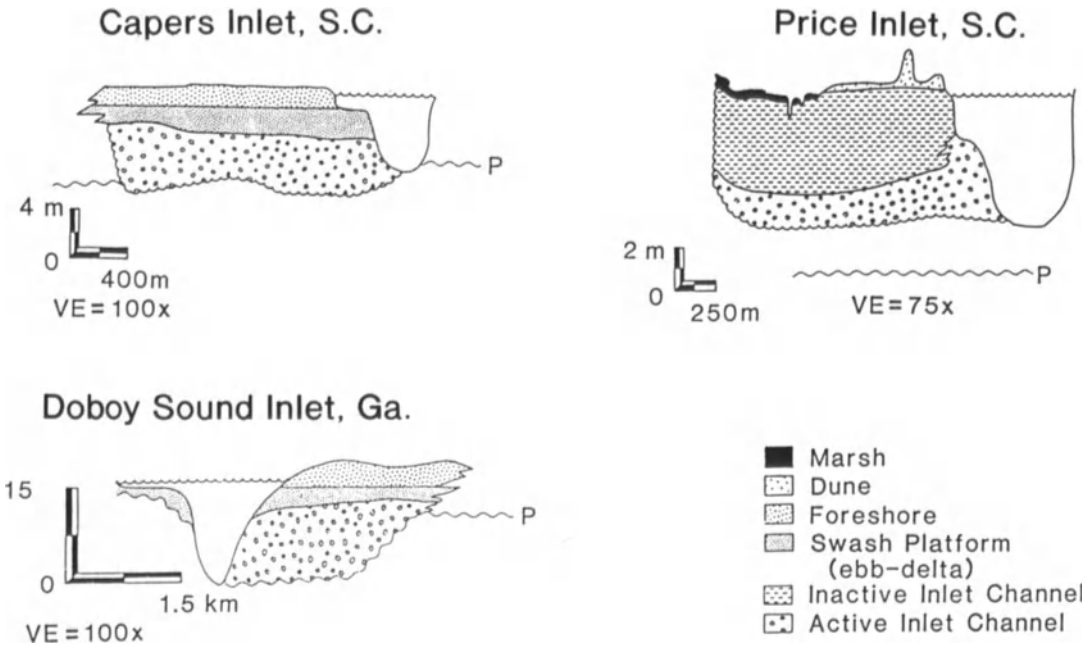

Figure 4.14. Representative examples of tidal-inlet fills showing the geometries and facies relationships of tide-dominated inlet sand bodies. The unconformity shown in each diagram is the top of the Pleistocene (P).

of adjacent barrier islands. The strike-oriented cross section at Price Inlet (Capers Island, Fig. 4.15A) illustrates the U-shaped inlet-fill geometry and the preservation of a concave-upward wedge of inlet-channel sand overlain by fine-grained abandoned-channel deposits (Fig. 4.16A). Compared to wave-dominated inlets, more time is required to completely close and fill an abandoned tide-dominated inlet channel. Inlet closure by a landward-migrating swash bar restricts current energy in the former channel and initiates deposition of a fine-grained abandoned channel-fill plug (Fig. 4.17). Inlet deposits thin toward the former channel margins and are separated from the barrier island by scour contacts. Similar inlet-channel geometries and lithologic associations were formed by the migration of Capers Inlet (Figs. 4.15B, 4.16B).

When viewed along depositional dip, tide-dominated inlet deposits thin landward and seaward of the inlet throat (Fig. 4.18). Foreshore sands reworked from the abandoned ebb-tidal delta interfinger with active- and abandoned-inlet deposits. Landward, inlet sediments interfinger with tidal-creek and salt-marsh silts and clays. Two episodes of inlet-channel migration and abandonment at Price Inlet are evident in the subsurface of northern Capers Island (Figs. 4.17, 4.18). Because tide-dominated inlets tend to pivot about the inlet throat during migration, each successive migration cycle obliterates the previous channel sediments, unless relative sea level rises.

Discussion

Subsurface Variability and Facies Relations

The variability of tidal-inlet sequences and geometries and their distribution along the North and South Carolina coasts are functions of paleotopography, hydrographic regime, and sediment supply. The combined relative influence of these geologic factors affects tidal-inlet migration rates, sedimentation patterns, and stratigraphy. This interaction of dynamic physical processes results in the formation of distinct inlet types and stratigraphic sequences on wave-dominated, versus tide-dominated, mixed-energy coasts. Stable inlets, freely migrating inlets, and inlets confined to a migration zone (Heward, 1981) are distributed systematically within the Georgia embayment as a result of these varying physical processes.

Wave-dominated tidal-inlet deposits typically thin toward channel margins and are scoured into barrier-island sands (Fig. 4.19). Along depositional dip, sandy wave-dominated inlets interfinger seaward with poorly developed ebb-tidal deltas and fine-grained, lower-shoreface to shelf deposits. Landward, the inlet deposits interfinger with flood-tidal delta and lagoonal sediments (Berelson and Heron, 1985). The sequence produced by lateral accretion, rapid infilling with clean quartzose sand, and rapid closure

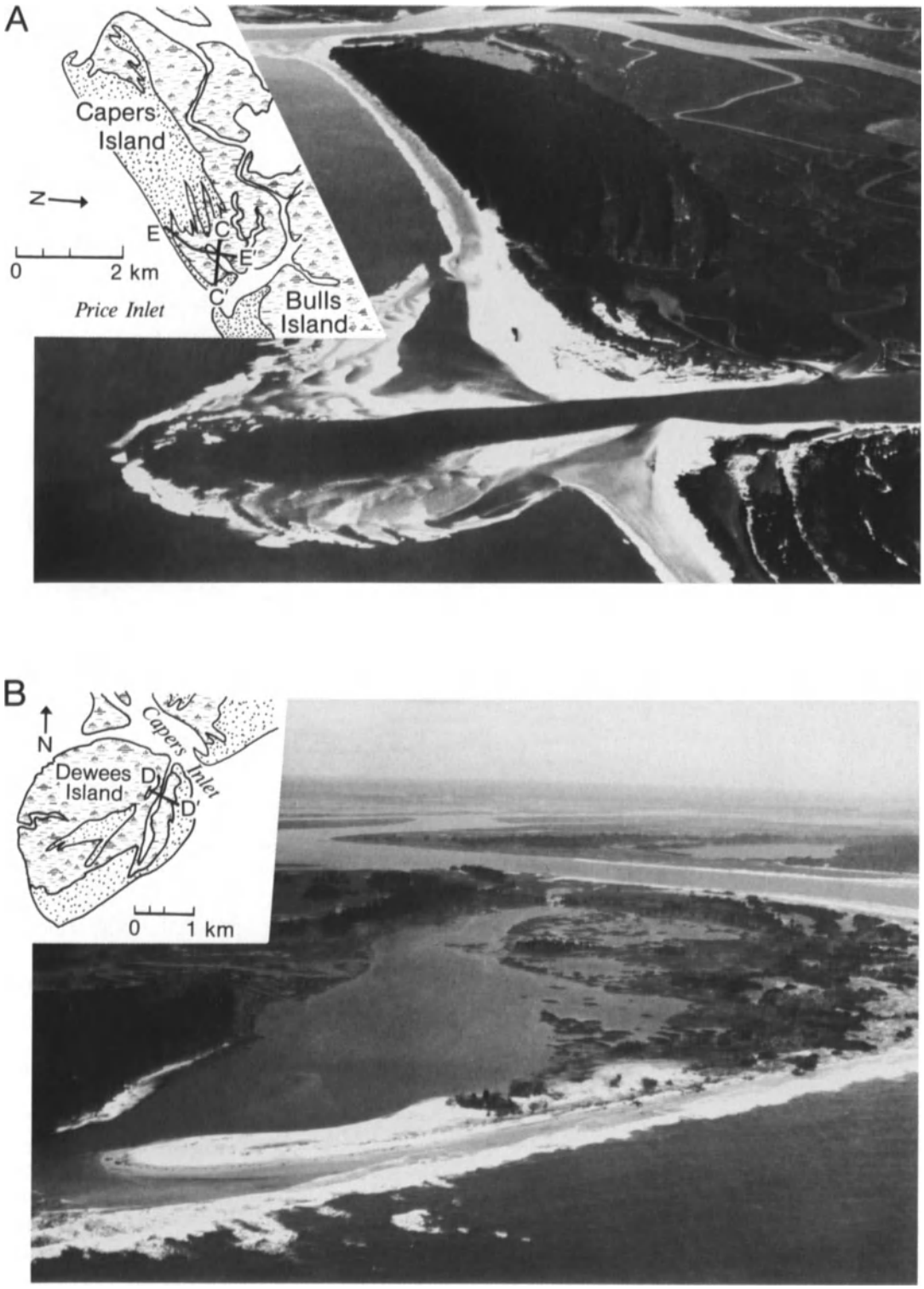

Figure 4.15. (A) Capers Island and Price Inlet, South Carolina. Map inset gives location of cross sections (photo by M.O. Hayes). (B) Photograph of the abandoned tidal inlet-channel on Dewees Island, South Carolina. The present channel of Capers Inlet is seen at the top. Location of cross section D-D′ is shown.

Table 4.2. Estimated Percentages of Holocene Tidal-Inlet Fill and Active-Tidal Inlets for Wave and Tide Dominated Barrier Island Shorelines.

Barrier Island	Percentage of Holocene as Inlet Fill
Wave-Dominated Barrier-Island Shoreline	
Core Banks, NC[1]	20
Portsmouth Banks, NC[2]	15
Bouge Banks, NC[2]	15
Shackleford Banks, NC[2]	80
Average Percentage of Inlet-Fill Sediment Per Barrier Island	35
Percentage of Shoreline Presently Represented by Active Tidal Inlets	5
Total	40
Tide-Dominated Barrier-Island Shoreline	
Kiawah Island, SC[3]	5
Seabrook Island, SC[3]	5
Capers Island, SC[4]	25
Dewees Island, SC[4]	25
Average Percentage of Inlet-Fill Sediment Per Barrier Island	15
Percentage of Shoreline Represented by Active Tidal Inlets	20
Total	35

[1]From Moslow and Heron (1978).
[2]From Heron and others (1984).
[3]From Moslow (1984).
[4]From Tye (1984).

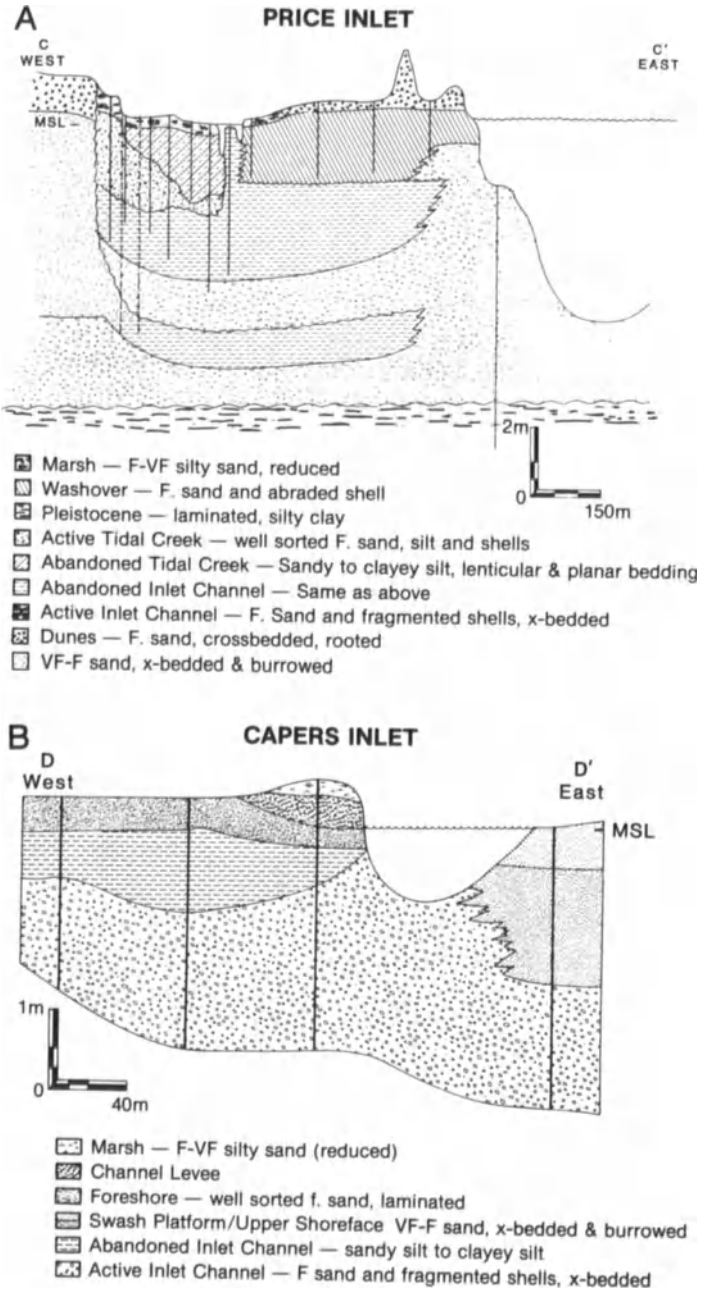

Figure 4.16. Strike-oriented vibracore transects across the abandoned inlet channels at (A) Price Inlet (C-C'), and (B) Capers Inlet (D-D'). Coarse-grained inlet sediments are in erosional contact with the barrier-island sands and are overlain by an abandoned channel plug. Stacked channel sequences are present at Price Inlet. Cross-section locations are shown in Figures 4.15A and B.

of these inlet channels is reflected in the blocky appearance of the hypothetical electric log (Fig. 4.19).

Mud- and sand-filled, tide-dominated inlet channels interfinger seaward with foreshore and ebb-tidal delta sands. The active inlet-fill grades landward into tidal-creek deposits, whereas abandoned inlet fill interfingers with salt marsh. Clay plugs in these abandoned channels separate barrier-island sands along strike and create localized impermeable boundaries among ebb-tidal delta, barrier island, and backbarrier tidal-creek facies. The gamma-ray log response through this inlet sequence would reveal stacked cycles of sand grading upward into mud (Fig. 4.19).

The extent of barrier-island reworking and the distribution of tidal-inlet deposits within the barriers varies widely in North and South Carolina. Excluding basement-controlled tidal inlets, wave-dominated inlets historically have been breached randomly through the narrow micro-tidal barriers. Downdrift migration and ultimate closure results in a sporadic distribution of inlet deposits along the coast. Distribution of tide-dominated inlet deposits is not random on the South Carolina coast.

Inlet migration and abandonment along wave- and tide-dominated coasts replaces coarsening-upward barrier-island sequences with fining-upward inlet-channel fills. Active tidal inlets account for 5% of the present longshore length on the wave-dominated North Carolina coast, and 20% on the tide-dominated South Carolina coast. In the subsurface, North Carolina barriers contain an average of 40% inlet fill, whereas South Carolina barriers average 15% inlet fill (Table 4.2). These percentages vary with each barrier island, but it can be concluded that the shorter barrier islands in each hydrographic setting commonly contain

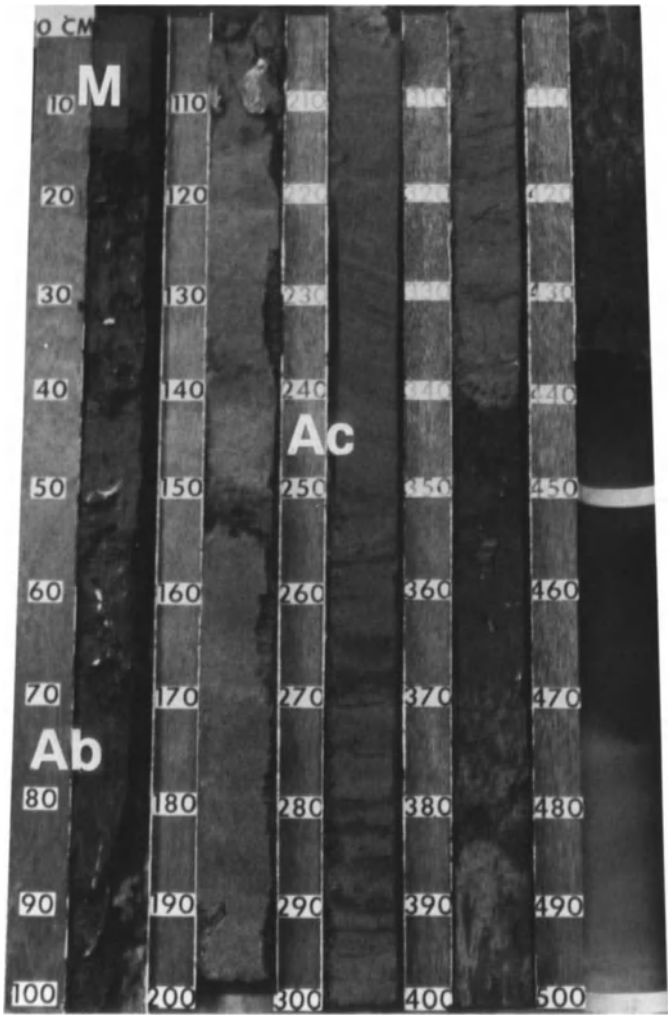

Figure 4.17. Photograph of core from tide-dominated inlet-fill sequence at Price Inlet, South Carolina. Sedimentary facies are active-inlet channel (Ac), abandoned-inlet channel (Ab), and salt marsh (M).

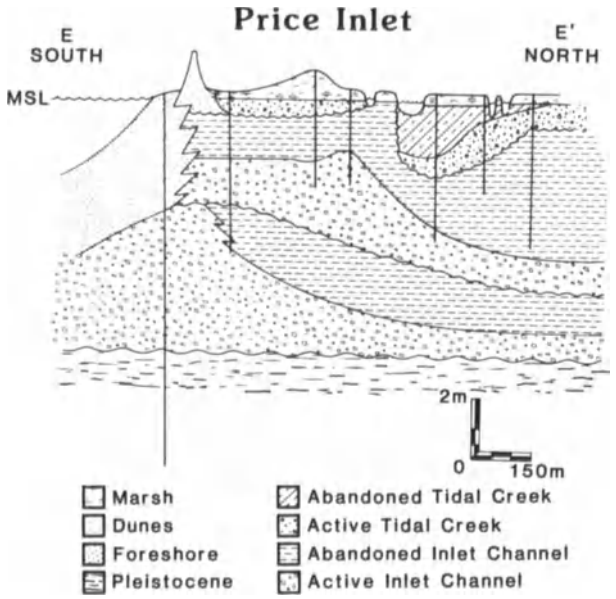

Figure 4.18. Cross section from Price Inlet. Dip-oriented transect E-E′ parallels the abandoned-inlet channel on Capers Island. Note the landward (northward) thickening of abandoned-inlet fill and its seaward pinchout. Location is given in Figure 4.15A.

more inlet-deposited material than longer barriers. For example, Shackleford Banks, North Carolina contains, 80% inlet fill; Capers and Dewees Islands, South Carolina, contain 25%; Core Banks, North Carolina, contains 14%, and Kiawah Island, South Carolina contains 5% (Table 4.2). Adding the volume of sediment required to fill the active tidal inlets on this shoreline to the average volume of inlet fill per barrier island reveals that wave- and tide-dominated mixed-energy coasts contain approximately equal proportions of inlet deposits (40% for North Carolina; 35% for South Carolina).

Preservation Style

The manner in which transgressed barrier islands are preserved is not clearly understood. However, it is certain that the major factors responsible for coastal lithosome preservation (rate of sea-level rise, basin subsidence, inner-shelf slope, sedimentation rate, and hydrographic regime) vary in importance and intensity along different shoreline settings. Therefore, under certain conditions, shallow-marine depositional systems are preserved in the rock record.

Several models of Holocene barrier transgression and reworking have been proposed by Swift (1968), Kraft and John (1979), Rampino and Sanders (1980), Swift and Moslow (1982), Demarest and Kraft (1987), and Nummedal and Swift (1987). Vertical sequences could vary from complete shoreface erosion and deposition of a ravinement surface (Swift, 1968), to nearly complete shoreline preservation by the vertical and landward displacement of the surf zone during a rapid rise in sea level (Rampino and Sanders, 1980). The rate of relative sea-level rise and the inner-shelf slope ultimately determine the sequence of preserved shoreline deposits (Fischer, 1961).

Although the Holocene sequences cored may not be truly indicative of what will be preserved in the rock record, these volumetric data can improve predictions. Because of the inlet's stratigraphic position and the common occurrence of overlying and underlying fine-grained sediments, tidal inlets are the most preservable portion of the barrier lithosome (Hoyt and Henry, 1967).

During transgression, the uppermost foreshore and shoreface sediments are reworked. Under present sea-level conditions, the preservation of Holocene shoreline sedi-

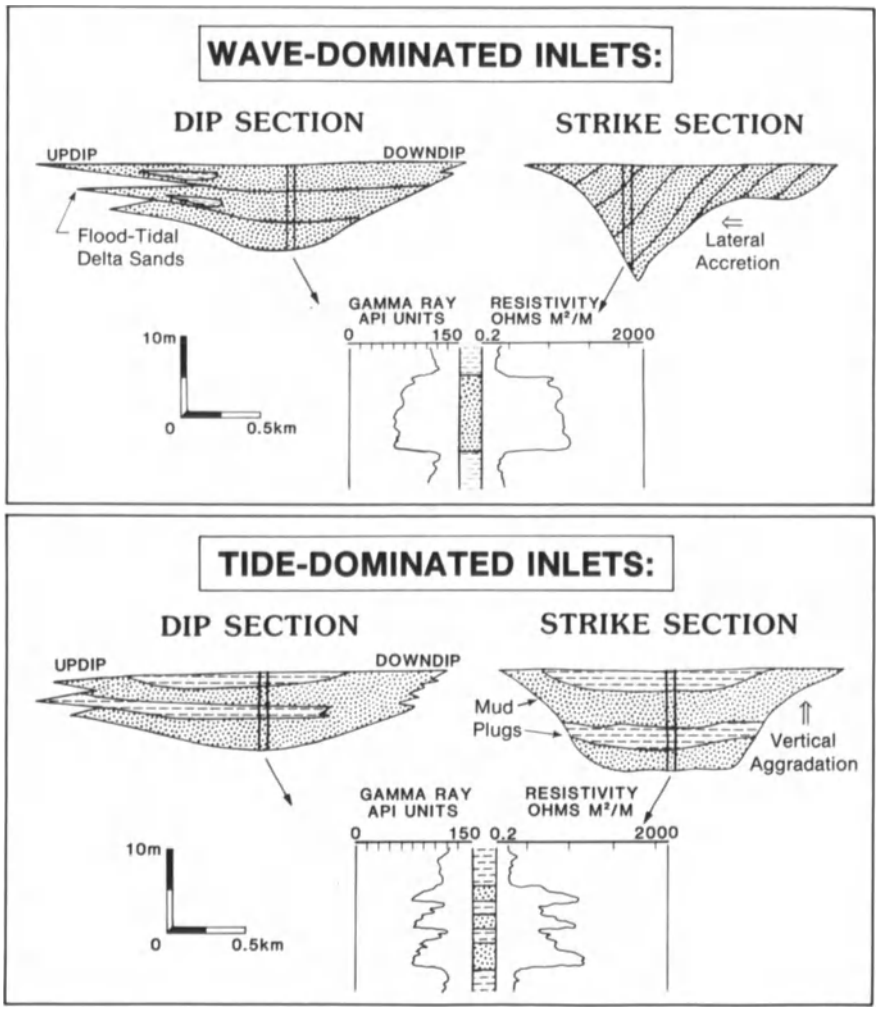

Figure 4.19. Schematic diagrams of composite strike- and dip-oriented channel geometries for wave- and tide-dominated inlets. Hypothetical gamma ray and resistivity logs illustrate the clean, blocky character of wave-dominated inlet deposits in contrast with the serrated pattern produced by fine-grained beds incorporated into the tide-dominated inlet sequences.

ments on the continental shelf is patchy off the coast of Delaware (Belknap and Kraft, 1985; Demarest and Kraft, 1987) and almost nonexistent along Bogue Banks, North Carolina (Hine and Snyder, 1985). Areas of remnant Holocene deposits on the U.S. Atlantic Shelf were deposited and preserved in topographically negative features on the Quaternary or Tertiary surface. Most of the preserved accumulations are tidal-inlet related. Hine and Snyder (1985) determined that the present ravinement surface, which is the result of sea-level rise, extends to a depth of approximately 12 m. The maximum depth of preserved inlet fills on Bogue Banks, North Carolina is 10 m (Heron et al., 1984); 15 m on Core Banks, North Carolina; and 15 to 18 m in central South Carolina (D.M. FitzGerald and D. Nummedal, personal communication, 1987). Therefore, during one sea-level rise event, if the upper 6 to 8 m in South Carolina, and 10 to 12 m in North Carolina, is eroded, only a thin, discontinuous sequence of shoreface deposits will be preserved to separate laterally abundant, 3- to 4-m-thick tidal-inlet fills.

Preservation Potential: Example from the Louisiana Continental Shelf

On the Louisiana shelf seaward of Barataria Bight (Fig. 4.20), a high-resolution (ORE Boomer) seismic-profile grid and vibracores were collected landward of the 10-m bathymetric contour. Owing to rapid relative sea-level rise (Ramsey and Moslow, 1987), these barrier islands have migrated landward several kilometers within the past few thousand years. Thus, the post-transgressive barrier-island sedimentary record is in the process of being preserved. The low wave energy (1.0 m average wave height), microtidal (36 cm mean tidal range) hydrographic setting for this area is characteristic for barrier-island shorelines throughout the northern Gulf of Mexico (Mossa, 1984). Using the criteria presented in this manuscript and elsewhere (Moslow and Tye, 1985) for the relative distribution of wave and tidal energy, most barrier-island coastlines in the northern Gulf of Mexico are wave dominated, as they are similar in morphology, depositional environments, and facies rela-

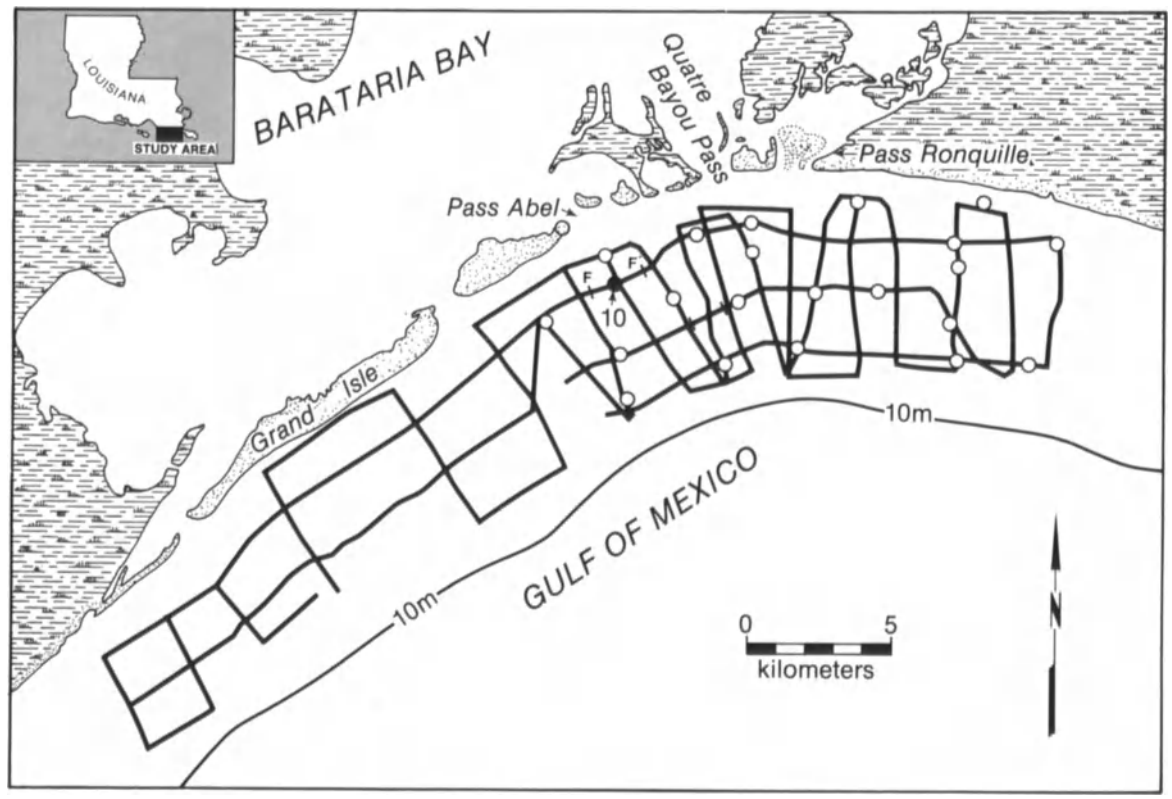

Figure 4.20. Location map of tidal inlets along the barrier-island shoreline fronting Barataria Bay, Louisiana. Solid black lines denote high-resolution seismic track lines; open circles are vibracore hole locations.

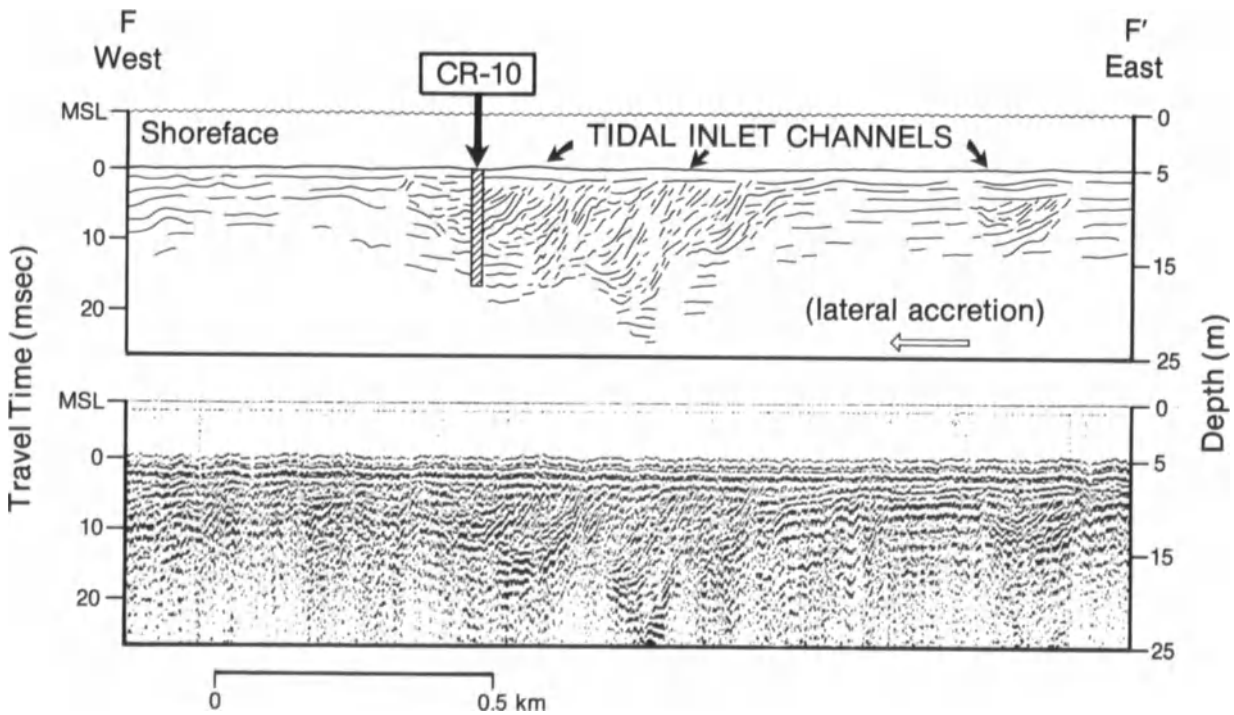

Figure 4.21. High-resolution seismic profile line F-F′ (below) and interpreted section (above) showing preservation of a tidal-inlet fill. Profile location is oriented parallel to the shoreline and shown in Figure 4.20. Vertical exaggeration is 15:1.

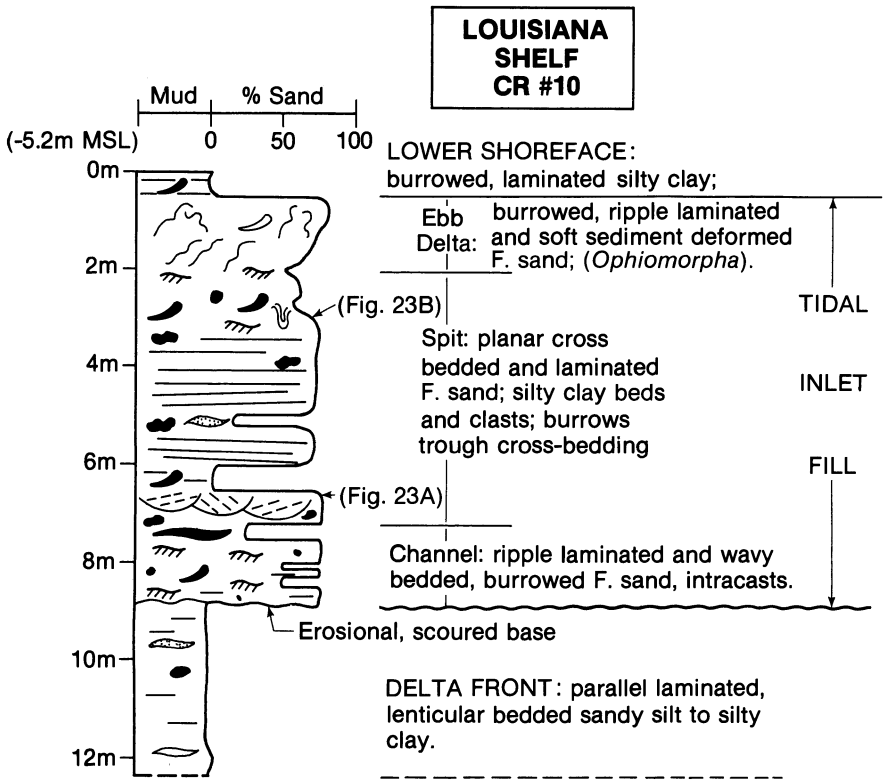

Figure 4.22. Graphic log of tidal-inlet and delta-front deposits in core CR#10 on seismic line F-F′. Location of core is shown in Figures 4.20 and 4.21.

tionships to those of North Carolina (Fig. 4.4A). Presently, five tidal inlets are active along the Barataria Bight shoreline (Fig. 4.20), two of which, Barataria Pass and Quatre Bayou Pass, are former distributary channels that have evolved into tidal inlets during shoreline transgression (Moslow and Levin, 1985). The remaining three inlets, including Pass Abel and Pass Ronquille, formed from storm breaching of the barrier islands. These inlets possess the well-developed flood-tidal deltas characteristic of wave-dominated inlets. Their net lateral migration is westward.

The post-transgressive stratigraphic record of Pass Abel is preserved within the adjacent lower shoreface. Seismic line F-F′ is oriented shore-parallel and located in approximately 5.0 m depth of water, 2.0 km from the mouth of Pass Abel (Fig. 4.20). A series of steeply dipping reflectors in this section outlines a tidal-inlet channel fill 0.75 km in shore-parallel (east-west) extent (Fig. 4.21). The internal reflectors have a unimodal direction of dip to the west, documenting the lateral accretionary nature of the inlet fill and the westerly migration of the inlet channel. The asymmetric, wedge-shaped to lenticular geometry of the inlet-channel fill in a shore-parallel direction is characteristic of wave-dominated inlets (Fig. 4.19). The inlet-fill has a maximum thickness of 12.5 m and is incised into delta-front silts and clays. These fine-grained deposits are represented by the flat-lying seismic reflectors in F-F′ (Fig. 4.21). An aggradational phase of inlet-channel deposition is indicated by a series of slightly concave to flat-lying discontinuous reflectors at the westernmost extent of the channel-fill. This aggradation coincides with the westernmost extent of inlet migration and likely represents a period of partial channel abandonment. Vibracore CR-10 is located in this portion of the inlet fill (Fig. 4.21) and is a fine-grained, sand-dominated sedimentary sequence with a sharp erosional base (Fig. 4.22). The tidal-inlet fill sequence contains channel, spit-platform, and ebb-delta sedimentary facies. The lower half of the sequence is a cross-bedded to cross-ripple-laminated, fine-grained sand with thin interbeds of burrowed to wavy-bedded silty sand to silty clay. The interbedding is a product of combined lateral accretion and vertical aggradation within this portion of the inlet-channel fill. Planar-tangential, cross-bedded sands within this part of the inlet sequence display mud drapes, mud couplets, and an increasing thickness in mud laminae upward (Fig. 4.23A). These bedding characteristics are interpreted as tidal bundles, and provide the best sedimentologic evidence of tidal-current processes. Rapid rates of sand deposition are inferred within the uppermost portion of the spit-platform facies by the multiple sets of cross-ripple laminations, ripple drift, and a 7.5-cm escape burrow trace (Fig. 4.23B). The tidal-inlet fill sequence is capped by a thin (1.0 m) *Ophiomorpha* burrowed and ripple-laminated ebb-

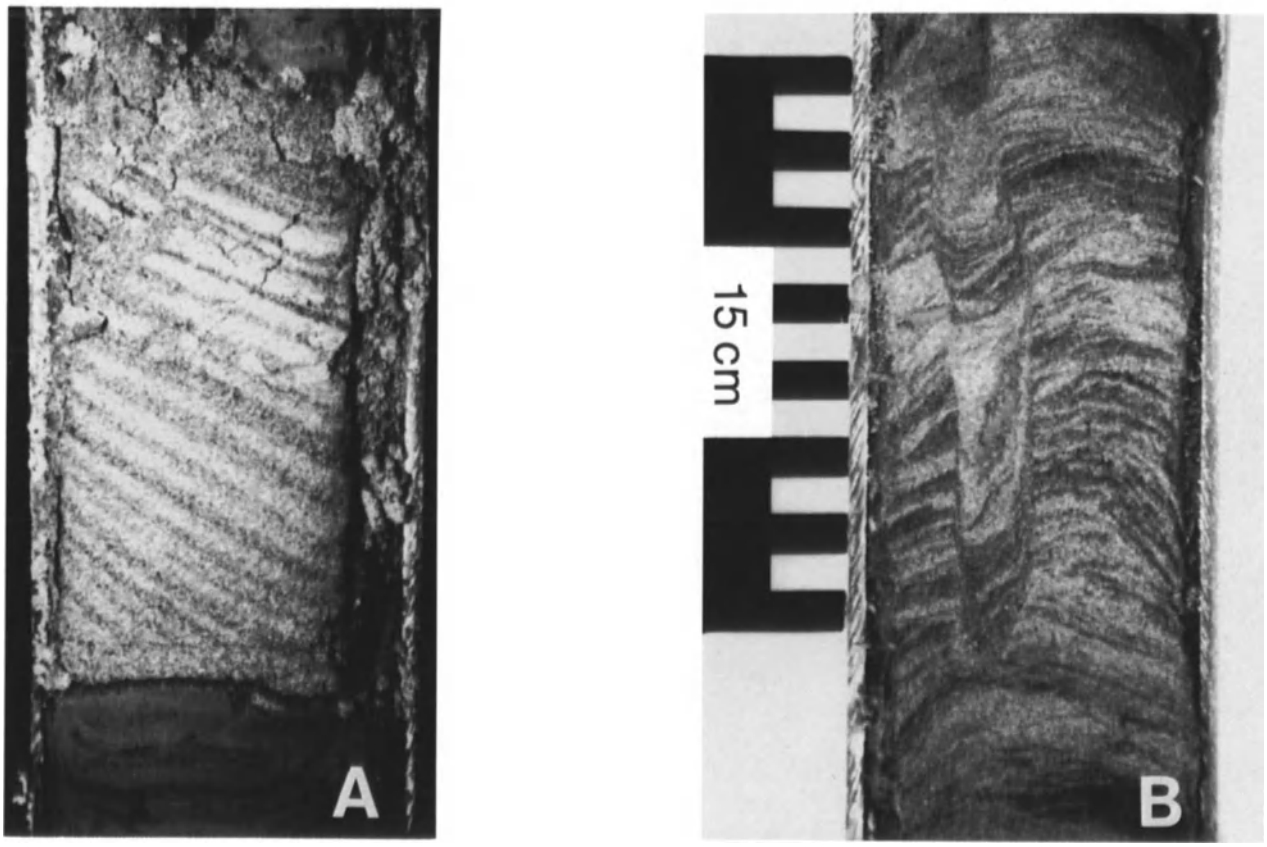

Figure 4.23. Close-up photographs of tidal-inlet fill deposits from vibracore CR-10 showing: (A) high- to moderate-angle, planar-tangential, cross-bedded, fine- to medium-grained sands with mud drapes, interpreted as tidal bundles; and (B) an escape burrow trace within cross-ripple-laminated fine-grained sands. Location of core photographs is shown in Figure 4.22. Cores are 7.5 cm in width.

tidal delta facies, and is encased in lower-shoreface (above) and delta-front (below) silty clays (Fig. 4.22).

Ancient Analogs

Regardless of the exact preservation mechanism, Ryer (1977), Leckie (1986A), and Donselaar (1989) have interpreted major transgressive sedimentary cycles in shoreline deposits of the Cretaceous Western Interior Seaway that are composed of thin progradational shoreline sequences and are separated by discontinuities. Further evidence for the preservation of barrier islands and inlet facies, plus their ability to perform as hydrocarbon reservoirs, can be inferred from interpretation of the Muddy Sandstone (McGregor and Biggs, 1968), the Cliffhouse Sandstone (Palmer and Scott, 1984), and the Menefee Formation (Donselaar, 1984), United States; the Halfway Formation (Campbell and Horne, 1986; Munroe and Moslow, 1990) and Milk River Formation, Alberta (Leckie, 1986B; Cheel and Leckie, 1990); and the Roda Sandstone, Spain (Yang and Nio, 1989).

Perhaps the best-described example of barrier-island/tidal-inlet reservoirs is in the Frio Formation of Texas (Galloway and Cheng, 1985). This detailed core and electric-log study defines the depositional facies of multiple microtidal barrier-island shoreline systems, and relates the facies stratigraphy to reservoir quality. Sandstone isopachs reveal dip-oriented inlet fills cutting the barrier core.

Galloway and Cheng (1985) describe the inlet-fill bodies as having differing geometries and vertical sedimentary sequences. The 41-A reservoir consists of two inlet-fill sequences of different sizes. Both have sharp bases, and at their downdip extent, the sandy inlet fill is capped by spit-platform sediments. The updip portion is filled by a mud plug. The 41-A reservoir is similar to the present setting at Kiawah Island, South Carolina. A large inlet (Stono Inlet) is accreting a thick, sandy inlet fill onto the northern terminus of Kiawah Island, and a much smaller inlet (Captain Sam's Inlet) at the southern end of the barrier is depositing a sandy-inlet/spit-platform wedge. At its depositional downdip extent, Captain Sam's Inlet is filling with sand, but the backbarrier portion of the inlet channel will fill with mud upon abandonment (Moslow, 1980; Moslow and Tye, 1985).

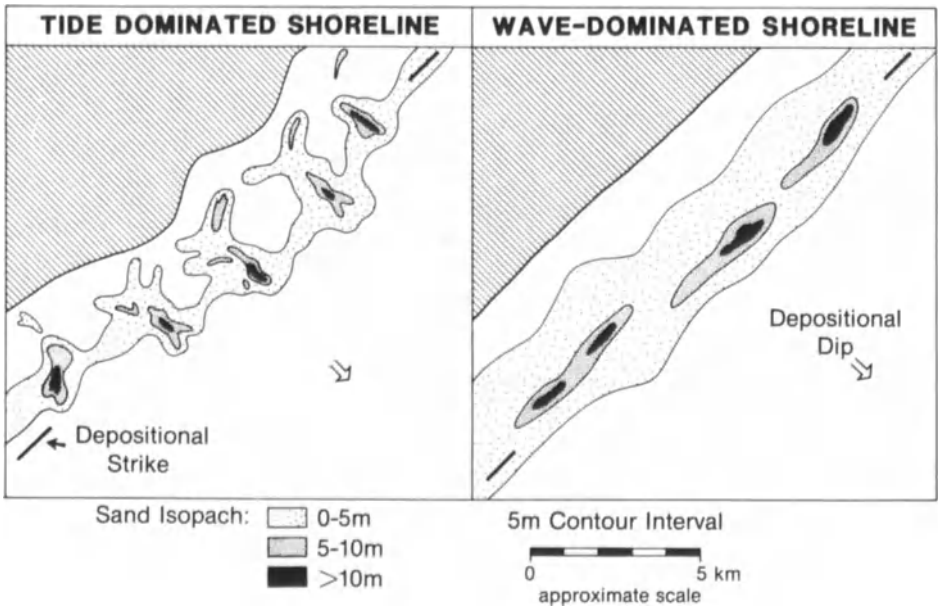

Figure 4.24. Hypothetical sediment isopach maps for one depositional episode on tide- and wave-dominated shorelines. Note the difference in orientation and geometry of the inlet-fill sand bodies.

Sandstone Distribution and Reservoir Potential

Isopach maps of preserved nearshore-marine sandstones deposited within an embayed shoreline can reveal a dominance of tidal-inlet and inlet-related deposits. These sequences will vary in thickness and lateral extent, but will grade from a shore-parallel orientation at the extremities of the embayment (wave-dominated) to a more shore-normal position near the apex (tide-dominated) (Fig. 4.24). Channel sequences will be thickest in the inlet throat, and are sometimes vertically stacked.

Homogeneous wave-dominated tidal-inlet and barrier-island sands could be preserved to form porous and highly permeable reservoirs. Inlet processes could actually enhance reservoir quality by reworking backbarrier and lagoonal sediments into channel, large flood-tidal delta, and smaller ebb-tidal delta deposits. Sand continuity is maintained in a shore-parallel direction, and the sequence thickens along dip due to the presence of deltaic facies (Fig. 4.24). In contrast, tide-dominated inlet-channel sequences are mud rich, thus disrupting the shoreline sand continuity. These deposits form regularly spaced (3–5 km apart along depositional strike), impermeable zones separating barrier-island, backbarrier, and ebb-tidal delta sand bodies. The barrier-island sequences are isolated and segmented into multiple, shore-parallel sand lobes (Fig. 4.24).

Summary and Conclusions

An inverse relation between wave regime and tidal range results in the deposition of variable yet distinct tidal-inlet sequences and channel geometries. Two additional factors controlling tidal-inlet stratigraphy are antecedent topography and sediment supply (i.e., lithology and quantity).

Inlet migration and abandonment produce subtle and dramatic variations in shore-parallel and shore-perpendicular sedimentary sequences. Wave-dominated inlet channels range in strike-oriented geometries from shallow (3 to 5 m), laterally continuous lenticular wedges to deep (15–18 m), V-shaped deposits. Tide-dominated inlets continuously migrate within a restricted zone and form U-shaped (along strike) and crescentic, concave-upward (along dip) channel geometries.

Active tidal inlets constitute 5% of North Carolina's wave-dominated coast and 20% of the tide-dominated South Carolina coast; however, subsurface data show that 40% of the Holocene shoreline deposits are tidal-inlet related. Contrasting lithologies and geometries of tide- and wave-dominated inlet fill can strongly affect the formation and quality of terrigeneous clastic shoreline reservoirs.

Tidal-inlet-deposited sediments in a wave-dominated setting are composed almost entirely of moderately well-sorted to poorly sorted, cross-bedded quartzose sand and shell, yielding very high primary porosities and permeabilities. Silt and clay generally account for less than 5 to 10% of the deposit. Therefore, wave-dominated inlet sequences would likely have relatively good reservoir potential with excellent vertical continuity (Fig. 4.25A). Grain size, percent sand, and percent shell material decrease upward, concurrent with an improvement in sorting (Moslow and Heron, 1978; Moslow and Tye, 1985). Wave-dominated inlets deposit porous, laterally continuous (1–10 km), wedge-shaped channel-sand bodies. Preserved channel fills are

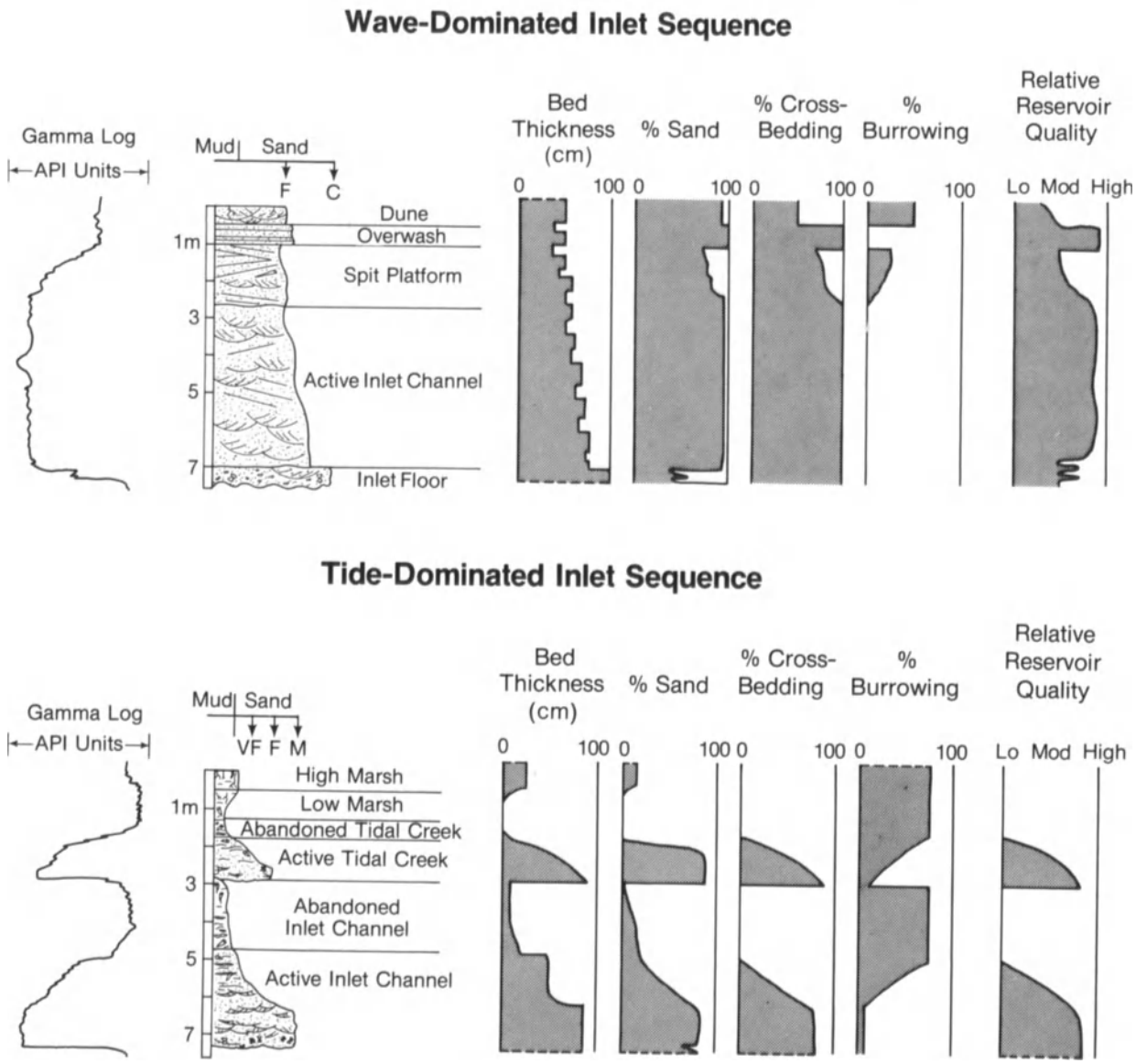

Figure 4.25. Summary diagram illustrating potential reservoir quality and gamma-log signatures for (A) wave-dominated; and (B) tide-dominated inlet sequences.

oriented shore-parallel to slightly oblique, depending on the degree of migration and the size of the associated flood- and ebb-tidal deltas, and exhibit consistent thickness-to-width ratios of 1:125, 1:250, or 1:500.

Tide-dominated inlet sequences are characteristically composed of fine-grained, clean, well-sorted quartzose sand, interbedded with layers of silt and clay up to 2.0 m thick. The individual sand layers have relatively good primary porosity, whereas the finer-grained intervals are relatively impermeable (Fig. 4.25B). These channel deposits are oriented shore-normal to oblique, and have thickness-to-width ratios of 1:150.

The association of barrier islands with fine-grained back-barrier and marine sediments creates excellent conditions for the formation of stratigraphic traps. An awareness of the intricate differences between wave- and tide-dominated inlet deposits is a valuable tool for predicting shoreline sand geometry, facies association, and controls on fluid migration and entrapment.

Acknowledgments

This study is based on research conducted by the authors at the University of South Carolina, Duke University, Louisiana Geological Survey, ARCO Oil and Gas Com-

pany, and the University of Alberta. The authors would especially like to thank Miles O. Hayes, RPI; S. Duncan Heron, Jr., Duke University; and colleagues at all institutions for providing insight and guidance toward an understanding of coastal-depositional systems and the application of this knowledge to characterizing marine-clastic reservoirs.

An earlier version of the text was reviewed by Dag Nummedal and Ellen N. Tye. Word processing and editorial assistance were provided by Jacquelyn Monday and Jennifer Kowal. The final version of this paper was reviewed by M.H. Scheihing, K.B. Loomis, and J. Sinise.

References

Belknap, D.F., and Kraft, J.C., 1985, Influence of antecedent geology on stratigraphic preservation potential and evolution of Delaware's barrier systems: Marine Geology, v. 63, p. 235–262.

Berelson, W.M., and Heron, S.D., Jr., 1985, Correlations between Holocene flood-tidal delta and barrier island inlet-fill sequences: Back Sound–Shackleford Banks, North Carolina: Sedimentology, v. 32, p. 215–222.

Bruun, P., and Gerritsen, F., 1959, Natural bypassing of sand at coastal inlets: American Society of Civil Engineers, v. 85 (WW4), p. 75–107.

Campbell, C.V., and Horne, J.C., 1986, Depositional facies of the Middle Triassic Halfway Formation, Western Canada Basin, *in* Moslow, T.F., and Rhodes, E.G., eds., Modern and ancient shelf clastics: Society of Economic Paleontologists and Mineralogists, Core Workshop no. 9, p. 413–459.

Cheel, R.J., and Leckie, D.A., 1990, A tidal-inlet complex in the Cretaceous epiric sea of North America. Virgelle Member, Milk River Formation, southern Alberta, Canada: Sedimentology, v. 37, p. 67–81.

Davies, J.L., 1964, A morphogenic approach to world shorelines: Zeit fur Geomorph, v. 8, p. 27–42.

Davis, R.A., Jr., and Hayes, M.O., 1984, What is a wave-dominated coast?: Marine Geology, v. 60, p. 313–329.

Demarest, J.M. II, and Kraft, J.C., 1987, Stratigraphic record of Quaternary sea levels: Implications for more ancient strata, *in* Nummedal, D., Pilkey, O.H., and Howard, J. D., eds., Sea-level fluctuation and coastal evolution: Society of Economic Paleontologists and Mineralogists Special Publication No. 41, p. 223–239.

Donselaar, M.E., 1984, Flood tidal delta sedimentation in the late Cretaceous Menefee Formation (Mesaverde Group), San Juan Basin, northwest New Mexico: Geologie en Mijnbouw, v. 63, no. 3, p. 323–331.

Donselaar, M.E., 1989, The Cliff House Sandstone, San Juan Basin, New Mexico: Model for the stacking of 'transgressive' barrier complexes: Journal of Sedimentary Petrology, v. 59, p. 13–27.

Fischer, A.G., 1961, Stratigraphic record of transgressing seas in the light of sedimentation on the Atlantic coast of New Jersey: American Association of Petroleum Geologists Bulletin, v. 45, p. 1656–1666.

Fisher, J.J., 1962, Geomorphic expression of former inlets along the Outer Banks of North Carolina [Thesis]: Durham, University of North Carolina, 120 p.

FitzGerald, D.M., Hubbard, D.K., and Nummedal, D., 1978, Shoreline changes associated with tidal inlets along the South Carolina coast: Proceedings Coastal Zone '78: American Society of Civil Engineers, v. 3, p. 1973–1994.

Galloway, W.E., and Cheng, E.S.-S., 1985, Reservoir facies architecture in a microtidal barrier system—Frio Formation, Texas Gulf Coast: Austin, Texas, Bureau of Economic Geology, Report of Investigations No. 144, 36 p.

Goldsmith, V., Morris, W.D., Byrne, R.J., and Whitlock, C.H., 1974, Wave climate model of the mid-Atlantic shelf and shoreline (Virginian Sea): Washington, D.C., National Aeronautics and Space Administration, NASA SP-358, 146 p.

Halsey, S.D., 1979, Nexus: New model of barrier development, *in* Leatherman, S.P., ed., Barrier islands: New York, Academic Press, p. 185–210.

Hayes, M.O., 1967, Hurricanes as geological agents, south Texas coast: American Association of Petroleum Geologists Bulletin, v. 51, p. 937–942.

Hayes, M.O., 1975, Morphology of sand accumulation in estuaries: An introduction to the symposium, *in* Cronin, L.E., ed., Estuarine Research, v. 2: New York, Academic Press, p. 3–22.

Hayes, M.O., 1979, Barrier island morphology as a function of tidal and wave regime, *in* Leatherman, S.P., ed., Barrier islands from the Gulf of St. Lawrence to the Gulf of Mexico: New York, Academic Press, p. 1–27.

Hayes, M.O., 1980, General morphology and sediment patterns in tidal inlets: Sedimentary Geology, v. 26, p. 139–156.

Hayes, M.O., and Kana, T.W., eds., 1976, Terrigenous clastic depositional environments: Columbia, University of South Carolina, Department of Geology, Coastal Research Division, Technical Report No. 11-CRD, p. 1-81–1-93.

Herbert, J.R., 1978, Post-Miocene stratigraphy and evolution of northern Core Banks, North Carolina [M.S. thesis]: Durham, NC, Duke University, 166 p.

Heron, S.D., Jr., Moslow, T.F., Berelson, W.M., Herbert, J.R., Steele, G.A. III, and Susman, K.R., 1984, Holocene sedimentation of a wave-dominated barrier-island shoreline: Cape Lookout, North Carolina: Marine Geology, v. 60, p. 413–434.

Heward, A.P., 1981, A review of wave-dominated clastic shoreline deposits: Earth Science Review, v. 17, p. 223–276.

Hine, A.C., and Synder, S.W., 1985, Coastal lithosome preservation: Evidence from the shoreface and inner continental shelf off Bogue Banks, North Carolina: Marine Geology, v. 63, p. 307–330.

Hoyt, J.H., 1967, Barrier island formation: Geological Society of America Bulletin, v. 78, p. 1125–1136.

Hoyt, J.H., and Henry, V.J., 1967, Influence of island migration on barrier island sedimentation: Geological Society of America Bulletin, v. 78, p. 77–86.

Hubbard, D.K., Oertel, G.F., and Nummedal, D., 1979, The role of waves and tidal currents in the development of tidal-inlet sedimentary structures and sand body geometry: Examples from North Carolina, South Carolina, and Georgia: Journal of Sedimentary Petrology, v. 49, p. 1073–1092.

Kana, T.W., 1979, Suspended sediment in breaking waves: Columbia, University of South Carolina, Department of Geology, Coastal Research Division, Technical Report 18-CRD, 153 p.

Kraft, J.C., and John, C.J., 1979, Lateral and vertical facies relations of transgressive barrier: American Association of Petroleum Geologists Bulletin, v. 63, p. 2145–2163.

Kumar, R., and Sanders, J.E., 1974, Inlet sequences: A vertical succession of sedimentary structures and textures created by the lateral migration of tidal inlets: Sedimentology, v. 21, p. 291–323.

Leckie, D., 1986A, Rates, controls, and sand-body geometries of transgressive-regressive cycles: Cretaceous Moosbar and Gates formations, British Columbia: American Association of Petroleum Geologists Bulletin, v. 70, p. 516–535.

Leckie, D., 1986B, Tidal channel facies of the Virgelle Member (Cre-

taceous Milk River Formation), southern Alberta, Canada: 12th International Sedimentological Congress, Canberra, Australia, p. 177.

McGregor, A.A., and Biggs, C.A., 1968, Bell Creek Field, Montana: A rich stratigraphic trap: American Association of Petroleum Geologists Bulletin, v. 52, p. 1869–1887.

Morton, R.A., and Donaldson, A.C., 1973, Sediment distribution and evolution of tidal deltas along a tide-dominated shoreline, Wachapreague, Virginia: Sedimentary Geology, v. 10, p. 285–299.

Moslow, T.F., 1980, Mesotidal barrier island stratigraphy [Ph.D. dissertation]: Columbia, University of South Carolina, 247 p.

Moslow, T.F., 1984, Depositional models of shelf and shoreline sandstones: American Association of Petroleum Geologists, Continuing Education Course Notes Series 27, Tulsa, Oklahoma, 102p.

Moslow, T.F., and Colquhoun, D.J., 1981, Influence of sea level change on barrier island evolution: Oceanis, v. 7, p. 439–454.

Moslow, T.F., and Heron, S.D., Jr., 1978, Relict inlets: Preservation and occurrence in the Holocene stratigraphy of southern Core Banks, North Carolina: Journal of Sedimentary Petrology, v. 48, p. 1275–1286.

Moslow, T.F., and Levin, D.R., 1985, Tidal inlet processes and deposits along a low energy coastline: Eastern Barataria Bight, Louisiana [abs.]: Geological Society of America Abstracts with Programs, v. 17, no. 7, p. 670.

Moslow, T.F., and Tye, R.S., 1985, Recognition and characteristics of Holocene tidal inlet sequences: Marine Geology, v. 63, p. 129–151.

Mossa, J., 1984, Wave climate studies in the northern Gulf of Mexico: Comparisons of visual surf, SSMO, hindcast, and gage data: Oceans '84, v. 2, p. 717–724.

Munroe, H.D., and Moslow, T.F., 1990, Reservoir quality and architecture of tidal inlet sandstones, Halfway Formation, northeastern British Columbia: Canadian Society of Petroleum Geologists Convention, Program and Abstracts, p. 103.

Nummedal, D., Oertel, G.F., Hubbard, D.K., and Hine, A.C., 1977, Tidal inlet variability—Cape Hatteras to Cape Canaveral: Proceedings, Coastal Sediments '77, American Society of Civil Engineers, p. 543–562.

Nummedal, D., and Swift, D.J.P., 1987, Transgressive stratigraphy at sequence-bounding unconformities: Some principles derived from Holocene and Cretaceous examples, *in* Nummedal, D., Pilkey, O.H., and Howard, J.D., eds., Sea-level fluctuation and coastal evolution: Society of Economic Paleontologists and Mineralogists Special Publication No. 41, p. 241–260.

Palmer, J.J., and Scott, A.J., 1984, Stacked shoreline and shelf sandstone of La Ventana Tongue (Campanian), northwestern New Mexico: American Association of Petroleum Geologists Bulletin, v. 68, p. 74–91.

Pierce, J.W., 1970, Tidal inlets and washover fans: Journal of Geology, v. 78, p. 230–234.

Price, A.W., and Parker, R.H., 1979, Origins of permanent inlets separating barrier islands and influence of drowned valleys on tidal records along the Gulf Coast of Texas: Gulf Coast Association of Geological Societies Transactions, v. 29, p. 371–385.

Rampino, M.R., and Sanders, J.E., 1980, Holocene transgression in south-central Long Island, New York: Journal of Sedimentary Petrology, v. 50, p. 1063–1080.

Ramsey, K.E., and Moslow, T.F., 1987, A numerical analysis of subsidence and sea level in Louisiana, *in* Kraus N.C., ed., Coastal Sediments '87, Volume II: American Society of Civil Engineers, p. 1673–1688.

Ryer, T.A., 1977, Patterns of Cretaceous shallow-marine sedimentation, Coalville and Rockport areas, Utah: Geological Society of America Bulletin, v. 88, p. 177–188.

Sexton, W.J., and Hayes, M.O., 1982, Natural by-passing of sand at a tidal inlet, *in* Eighteenth Coastal Engineering Conference Proceedings: American Society of Civil Engineers, v. 2, p. 1479–1495.

Swift, D.J.P., 1968, Coastal erosion and transgressive stratigraphy: Journal of Geology, v. 76, p. 444–456.

Swift, D.J.P., and Moslow, T.F., 1982, Holocene transgression in south-central Long Island, New York—Discussion: Journal of Sedimentary Petrology, v. 52, p. 1014–1017.

Tye, R.S., 1984, Geomorphic evolution and stratigraphy of Price and Capers Inlets, South Carolina: Sedimentology, v. 31, p. 655–674.

U.S. Department of Commerce, 1982, Tide tables, East coast of North and South America: Rockville, Maryland, National Oceanic and Atmospheric Administration, National Ocean Survey, 293 p.

Yang, C.-S., and Nio, S.-D., 1989, An ebb-tide delta depositional model—a comparison between the modern Eastern Scheldt tidal basin (southwest Netherlands) and the lower Eocene Roda Sandstone in the southern Pyrenees (Spain): Sedimentary Geology, v. 64, p. 175–196.

CHAPTER 5

The Sedimentologic and Geomorphologic Provinces of the Nile Fan

Yossi Mart

Introduction

The Nile Fan in the southeastern Mediterranean is a large, deep-sea sedimentary fan deposit that started to accumulate in the early Pliocene receiving its material from one primary source—the Nile River. The Nile River is 6,800 km long; it drains a basin of 3 million km^2, and has an average annual water discharge of 86 billion m^3 (Said, 1981). Prior to construction of the Aswan High Dam in 1964, the Nile discharged approximately 120 million m^3 of sediment annually to the southeastern Mediterranean basin (Said, 1981). Due to the Aswan High Dam and the intensive irrigation system in the Nile Delta area, the present rate of sedimentary discharge is negligible (A. Golik, personal communication, 1990). The Nile has constructed a large alluvial plain, covering an area of 22,000 km^2. Herodotus, in the fifth century B.C., was the first to apply the term "delta" to this plain of triangular shape.

The Nile Fan is a cone-shaped slope-and-rise depositional system covering an area of more than 70,000 km^2. It is composed of late Tertiary and Quaternary sediments extending from the present delta of the Nile River seaward toward the Mediterranean Ridge to the northwest, toward the Eratosthenes Seamount to the north, and toward the Levant Basin to the northeast (Fig. 5.1). The sedimentary accumulation of the Nile Fan has occurred since the early Pliocene, forming a structure with an estimated sediment volume of 400,000 km^3, an average thickness of 2 km, and a rate of sedimentation that exceeded 40 cm per 1000 yr in places (Ross and Uchupi, 1977).

The fan is divided into two distinct physiographic provinces. The western province (Fig. 5.2), also known as the Rosetta Fan (Emery et al., 1966) or the Nile Cone (Ross and Uchupi, 1977), is a gently undulating, seaward-dipping terrane that displays minor effects of faults and diapirs, except near the Mediterranean Ridge, where intensely folded sediments abound (Fig. 5.3). Cut-and-fill structures in the upper fan, and sinuous channels in the central and lower fans, are common in the western province. The eastern province (Fig. 5.2), also known as the Damietta Fan (Emery et al., 1966) or the Levant Platform (Ross and Uchupi, 1977), is intensively affected by faulted escarpments and elongated salt ridges (Ben-Avraham and Mart, 1981); it trends WNW–ESE and forms a series of abrupt changes in bathymetry, ranging from 100 to 400 m (Fig. 5.4). A long-range sonar survey in the eastern province of the fan encountered series of northwest-trending faulted escarpments and grabens, with some conjugate structures in places (Kenyon et al., 1975).

Another difference between the two provinces of the Nile Fan is the reduced thickness of the sedimentary sequence in the eastern province (Fig. 5.4). Both provinces rely on a unified source of sedimentary supply, and both are affected by the Mediterranean geostrophic current that flows eastward. The finding that the sedimentary sequence in the western province is considerably thicker than the contemporaneous sequence in the east is probably the result of interference by the faults and diapirs in the eastern province with the sedimentary distribution.

The Nile Fan and Its Geological Setting

Sea Level and Climate

The Nile is a young river that drains the East African and Ethiopian plateaus into the southeastern Mediterranean Sea. The present Nile was preceded by five earlier rivers

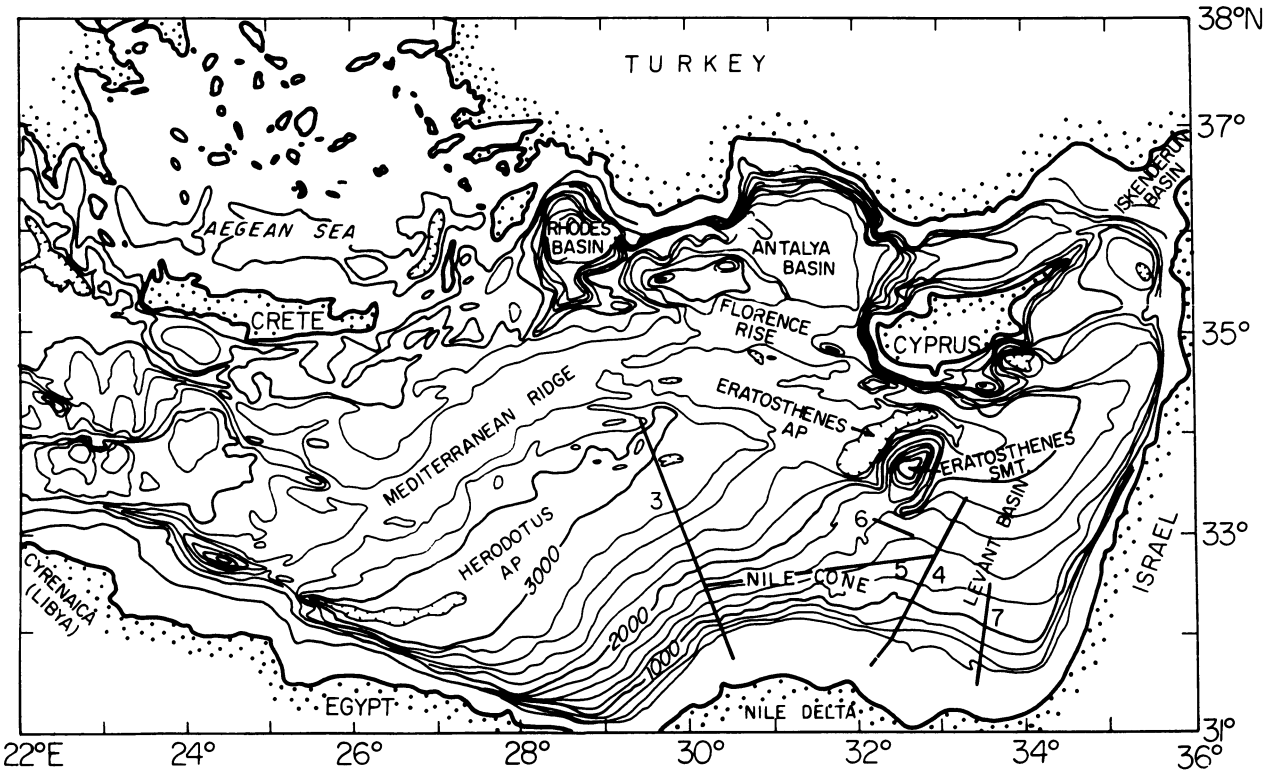

Figure 5.1. Generalized bathymetric map of the eastern Mediterranean. The Nile Fan is bounded by the Herodotus Abyssal Plain, by the eastern section of the Mediterranean Ridge and by the Eratosthenes Seamount and Abyssal Plain. Location of seismic profiles is indicated by figure numbers.

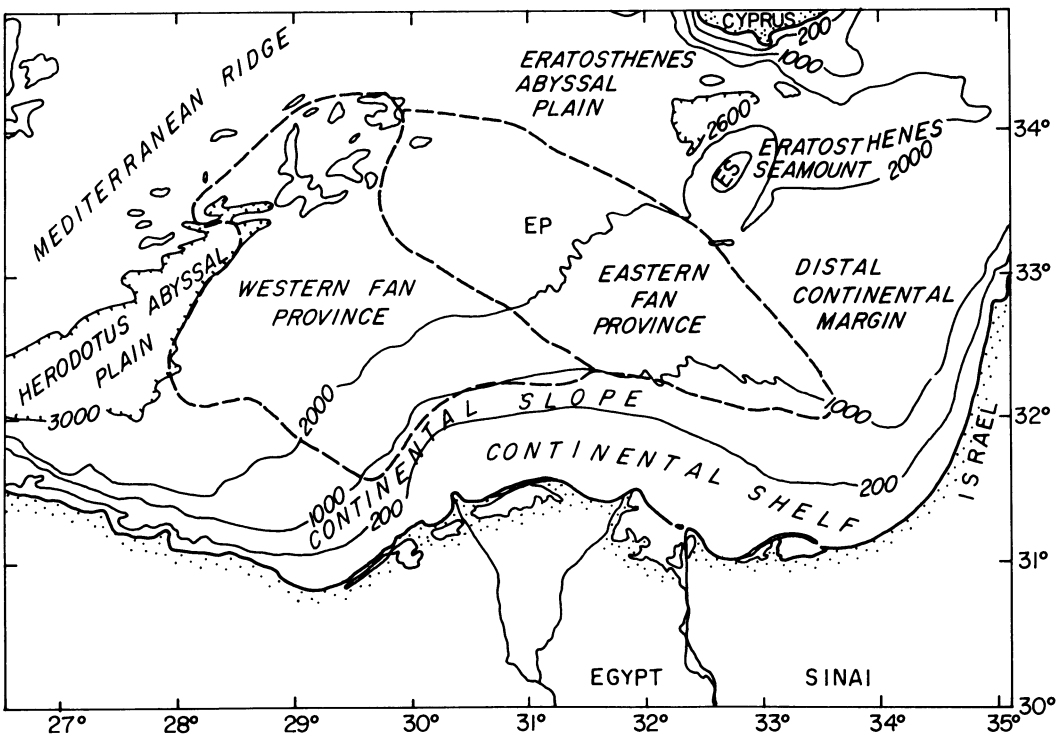

Figure 5.2. A generalized chart of the Nile Fan and adjacent areas, showing the main physiographic regions. Modified after Maldonado and Stanley (1979).

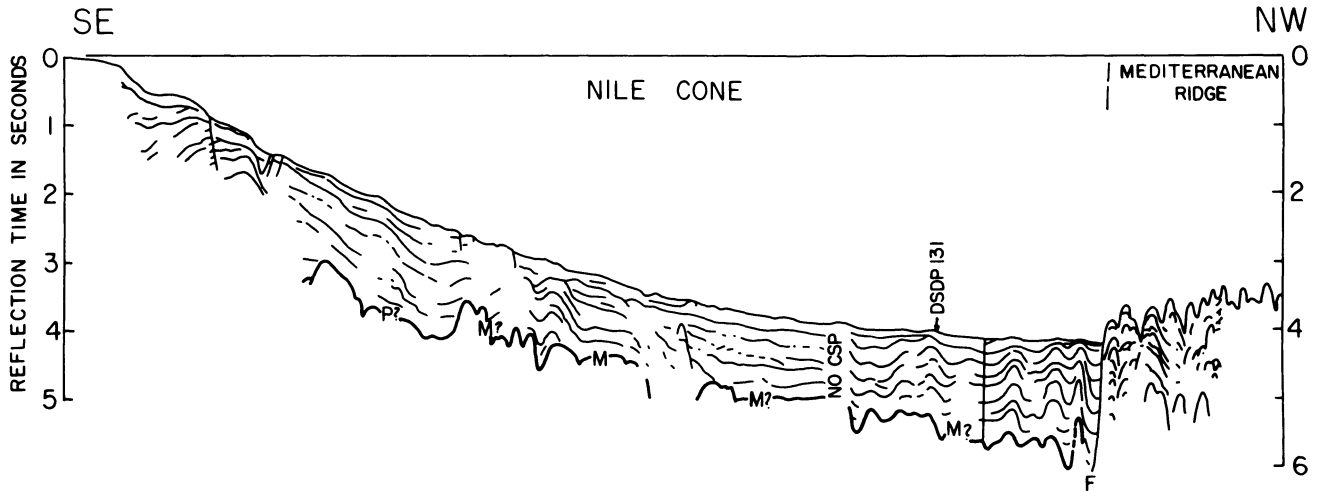

Figure 5.3. Cartoon of a seismic reflection profile along the western province of the Nile Fan, showing the smooth to slightly undulating seismic reflectors and a few shallow faults. The continuity of reflectors P and M is easily discernible, as is the abrupt change in seismic characteristics in the Mediterranean Ridge. See Figure 5.1 for location. After Ross and Uchupi (1977), reprinted by permission.

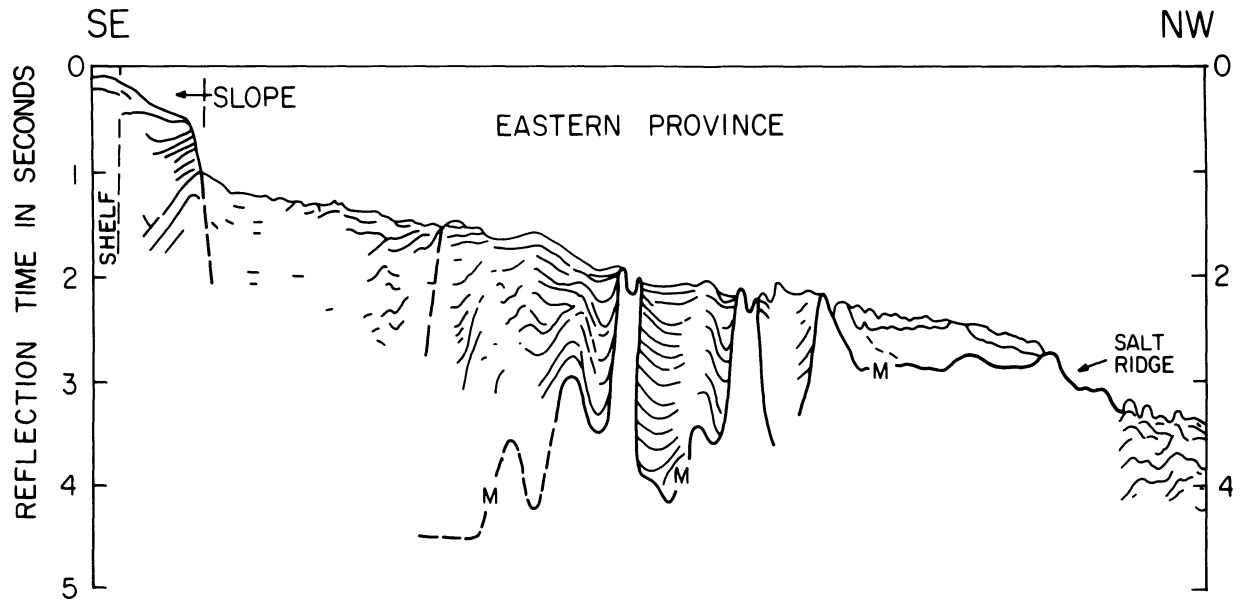

Figure 5.4. Cartoon of a seismic reflection profile along the eastern province of the Nile Fan, showing a faulted terrain with diapirs intruding in places. Note that the thickness of the sedimentary sequence of the fan seaward of the diapirs is considerably reduced, compared to the thickness along the shelf and the upper slope. See Figure 5.1 for location. After Ross and Uchupi (1977), reprinted by permission.

that flowed through nearly the same river bed, which was incised into the bedrock during the Messinian. The fluviatile system started to develop in the late Miocene as the Eonile, when the lowered sea level in the Mediterranean caused the entrenchment of a deep canyon that extended across the Egyptian plateau from the Mediterranean coast to at least as far south as Aswan (Said, 1981). The early Pliocene marine transgression brought the sea as far inland as Aswan forming a 1,100-km-long, 30-km-wide seaway. Subsequently, in the middle Pliocene marine regression, the river bed of the Eonile was occupied by the Paleonile, which started to build its delta and then its fan as well. The Paleonile dried out during the Pliocene–Pleistocene transition, a climatologically dry period in the Levant, characterized in the Egyptian stratigraphic sequence by deposits of eolian sand. The river that occupied

the river bed in the early Pleistocene was the Protonile, which was succeeded in the middle Pleistocene by the Prenile. Then, in the late Pleistocene, the river bed was occupied by the Neonile, and finally, in the Holocene, by the modern Nile River (Said, 1981).

The geomorphologic configuration of the Nile Delta is very dynamic, and is known to have changed drastically, even in historic times. The early Greek geographers—Herodotus in the fifth century B.C., and Strabo in the first century B.C.—reported seven distributaries in the delta; today there are only the Rosetta and the Damietta. Modern records show that the delta prograded seaward during the present century at an average rate of 10 m per year, but since the construction of the Aswan High Dam in 1964, the delta has been affected by severe coastal erosion (Goldsmith and Golik, 1980). and coastline retreat of more than 100 m can be discerned in places (V. Goldsmith, personal communication, 1986).

Controls on Sedimentation

The sediments of deep-sea fans are basically redeposited sediments that consist mainly of sand, silt, and mud, with biogenic debris and evaporitic and volcanic fragments as minor constituents. The origin of the sediment is terrigenous, biogenic, volcanogenic, or evaporitic. The sediment is transported by the river to the continental shelf, making it available for redeposition across the continental slope into the deep-sea fan. The quantity and type of sediments in the deep-sea fan depend mainly on the local shallow-marine conditions and the gradients of the continental slope. Resedimentation of the clastic deposits in the deep-sea fan is controlled mostly by turbidity currents and gravity mass flows, whereas transport of suspended load is of secondary importance (Stow et al., 1984). These sediment transport processes led to the development of the cone configuration of the Nile Fan, but tectonics, halokinetics, and other nonsedimentary depositional constraints led to the geomorphologic asymmetry between the western and the eastern provinces of the Nile Fan (Fig. 5.2). It should be noted that the redepositional processes that control transportation and the distribution of marine-fan sediments tend to mix the down-flowing sediments. Formerly deposited sands, silts, and clays, which were sorted by the wave regimes in both active and extinct near-shore and deltaic environments, are resedimented to form a heterogeneous sedimentary deposit.

Earlier studies suggested that the Nile River has built two distinct fans, western and eastern (e.g., Emery et al., 1966), each of which was ascribed to one of the Nile distributaries, the Rosetta or the Damietta. However, considering that only 2,000 years ago the Nile had seven distributaries (Said, 1981), this correlation seems unlikely. It is suggested in the present study that the differentiation of the Nile Fan into two provinces sharing a unified sedimentary source probably resulted from the effects of tectonics and halokinetics. Evidence was encountered that the eastern province is intersected by northwest-trending faults, which built a series of tilted blocks along the continental slope. Elongated diapirs ascended along these faults, forming salt walls in places. The orientation of the tilted blocks, as well as the elongated diapirs, probably interfered with the downslope turbiditic flow of the sediments, leading to thinner sedimentary accumulation in the eastern Nile Fan. The boundary between the western and the eastern provinces transects the Nile Cone; it trends northwestward and is structurally controlled by the northwest-trending faults (Ross and Uchupi, 1977; Mart, 1984).

Tectonics

The Nile Fan is deposited on a thick sedimentary sequence of passive continental margin that formed the boundary of the southwestern Tethys Ocean, and subsequently of the southeastern Mediterranean Sea, where the continental margin of the southeastern Mediterranean is located on top of the ancient margin of the southwestern Tethys. The geographic consistency of this transition zone between land and sea during more than 200 m.y. suggests a conspicuous tectonophysical constraint, such as variations in crustal composition, at the foundation of the southeastern Mediterranean margin region (Mart, 1987).

The Plio-Quaternary sedimentary prism of the Nile Fan was deposited on a thick sequence of strata of Mesozoic and early Cenozoic age (Ginzburg et al., 1979; Makris et al., 1983). Seismic reflection surveys indicated that the sedimentary sequences of the Nile deposits overlie two seismic reflectors attributed to the late Miocene erosional surfaces and the Messinian evaporites termed "P" (Ross and Uchupi, 1977) and "M" (Ryan et al., 1970). Most of the Nile sequence along the continental shelf and the upper continental slope is underlain by reflector P, and the sequence along the continental rise and lower slope is underlain by reflector M. Commonly, the lateral transition from one reflector to the other is marked only by a gradual increase in amplitude of the seismic signal, but in some places, these two reflectors are in faulted contact (Fig. 5.5). Considering data from exploration wells and seismic refraction profiles, it seems that reflector P is the top of an erosional surface carved in pre-Messinian marls and limestones (Chumakov, 1967; Mulder et al., 1975; Ross and Uchupi, 1977), and reflector M indicates the top of the late Miocene evaporite sequence (Ryan et al., 1973). Whereas reflector P is relatively smooth (Ross et al., 1978), reflector M com-

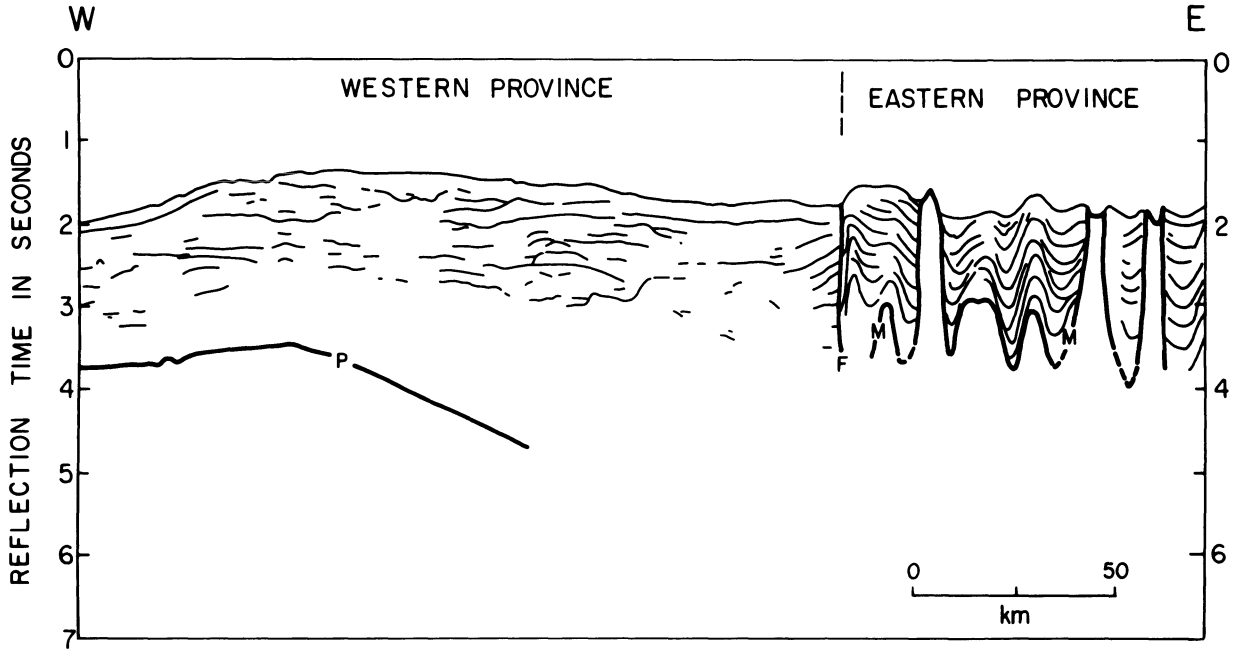

Figure 5.5. Cartoon of a seismic profile showing the contrasting structural patterns between the eastern and the western provinces of the Nile Fan. See Figure 5.1 for location. Modified after Ross and Uchupi (1977), reprinted by permission.

monly shows considerable relief in the fan region, probably due to the plastic flow and diapirism of the underlying evaporites.

The surface delineated by reflectors P and M slopes seaward from nearly sea level at Cairo to a depth of 3 km near the Egyptian coast. and to about 4.5 km under the deeper sectors of the fan (Fig. 5.4). The sediment cover is thickest underneath the outer shelf north of the delta, where it reaches thicknesses of approximately 3.5 km (Ross et al., 1978). The western province of the fan is characteristically well bedded, except for minor faults that offset the upper sedimentary sequence (Fig. 5.3). A structural dome was encountered beneath the upper slope, affecting the Messinian unconformity surface. The dome was attributed either to a basement uplift or to differential compaction above a pre-Messinian structure (Ross and Uchupi, 1977). Deformational folding of the lower fan strata becomes progressively intensive seaward, and at the Mediterranean Ridge, it is so intense that the details of the bathymetry and the seismic reflectors' structural parameters are obscured. The deformations of the outer fan and the Mediterranean Ridge are correlated with the evaporitic sequence below the M seismic reflector, and it is presumed that deformation was caused by a combination of halokinesis and tectonics (Woodside, 1977).

Intensive deformation of the sediment stratification, although less drastic than that of the Mediterranean Ridge, can be seen in the seismic profiles from the eastern province of the Nile Fan. The rough topography of this region is closely associated with diapirism and faulting (Emery et al., 1966; Kenyon et al., 1975). Additional topographic relief stems from collapse features, probably caused by the solution of salt at the crests of some diapiric structures (Fig. 5.6). Evidence was encountered for the occurrence of elongated salt ridges, trending west-northwest and ascending along a series of normal faults of similar trend (Ross and Uchupi, 1977; Ben-Avraham and Mart, 1981).

The northwestern faulting trend is a regional phenomenon in the Levant (Shalem, 1954), and was encountered in many places along the continental margin of Israel and North Sinai. Faulting probably originated during the middle Miocene and was reactivated in the Pleistocene (Mart, 1984). The faulting and the piercing of diapirs into the Plio-Pleistocene sedimentary sequence of the eastern province of the Nile Fan formed large undulations at the sea floor in some places, and horst-like structures in others (Fig. 5.7). The undulations and the uplifted blocks probably interfered with the turbiditic sediment flow from the shelf edge seaward, and also seem to be effective in reducing the amount of sediment transported eastward by the Mediterranean geostrophic current. Thus, the processes that enhance the thick deposition in the western province of the Nile fan are not very efficient in the eastern province. However, the large quantities and thicknesses of Nile-derived sediments that were encountered in the Levant and Cyprus basins suggest that the sedimentologic effects of the

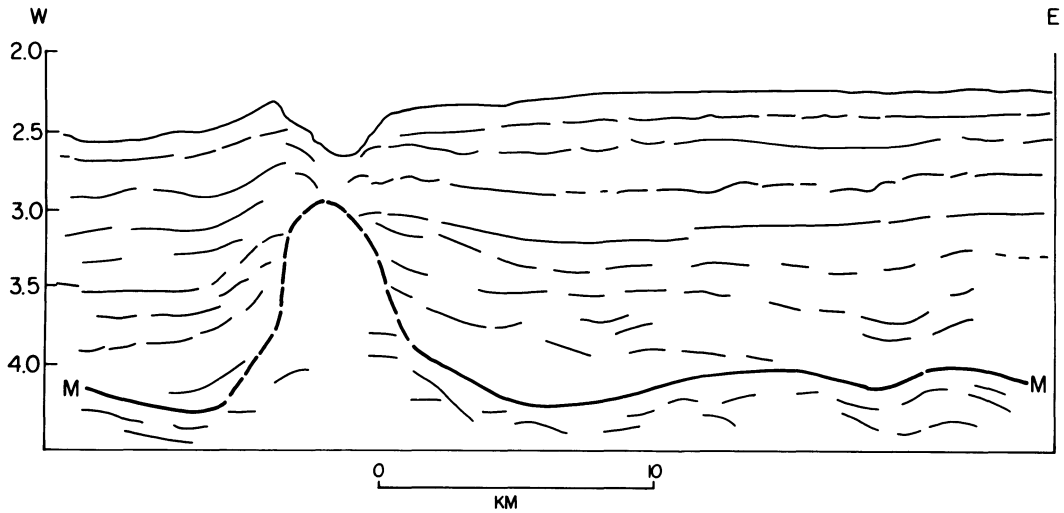

Figure 5.6. Cartoon of a seismic reflection profile showing a collapse structure in the eastern fan province. The structure is due to dissolution of the upper section of an outcropping salt diapir that stems from the Messinian evaporites. See Figure 5.1 for location. After Ross and Uchupi (1977), reprinted by permission.

structures off northern Sinai are relatively recent. The eastern province of the Nile fan probably covered larger areas in the Pliocene and was reduced to its present dimensions due to faulting, diapirism, and reduced rate of deposition. Furthermore, the occurrence of Nile-derived sediments on the Mediterranean Ridge suggested that the western province of the fan also covered wider areas than at present, and was reduced to its recognized size due to uplift and folding of the Mediterranean Ridge (Ryan et al., 1973).

Geomorphology

The western province of the Nile Fan is bounded on its seaward side by the Herodotus Abyssal Plain, the Mediterranean Ridge, and the Eratosthenes Abyssal Plain. The eastern province is bounded by the Eratosthenes Seamount and the Levant Basin (Fig. 5.1). The Herodotus and Eratosthenes Abyssal Plains, as well as the Levant Basin, are filled with turbiditic sediments that originated from the Nile, and Nile-derived sediments were also encountered on the Mediterranean Ridge (Maldonado and Stanley, 1978). Seismic activity associated with faulting could have been the trigger for turbiditic flows, and the rate of recurrence of earthquakes may thus affect the frequency and volume of sedimentary gravity flows feeding a submarine fan. The passive margin of the southeastern Mediterranean experiences infrequent earthquakes (Poirier et al., 1980; Mart, 1984, 1987; Armijo et al., 1986), the cumulative effects of which could significantly affect the sediment supply, because the prolonged intermittent periods could have led to a large buildup of sediment along the shelf break, which could flow downslope following an earth tremor.

Although the Nile Fan was deposited along an extinct Tethyan passive continental margin, a very old passive continental margin that should have been a tectonically stable region, the effects of geologic structures on the geomorphology of the fan were significant. The thick evaporitic sequences that were deposited in the Mediterranean basins gave the overlying sedimentary series an unstable foundation, and the tectonic activity associated with the opening of the northern Red Sea initiated and rejuvenated faulting systems along the southern continental margin of the Levant (Mart, 1987). The post-Miocene tectonic activity in he southeastern Mediterranean consisted of regional and local displacement phenomena, which included crustal subsidence at the delta area under the load of accumulated sediments (Ross and Uchupi, 1977), and the regional tectonic subsidence of the Mediterranean basins since the early Pliocene (Stanley, 1977). Furthermore, the dispersion patterns of the fan sediments were affected by the uplift of the Mediterranean Ridge and the Eratosthenes Seamount, by the topographic gradients of the continental slope, by halokinetic activity, and by the configurations of the receiving basins. In general, it seems that the tectonic vertical subsidence of the Mediterranean basins since the early Pliocene, combined with the local crustal subsidence caused by sedimentary loading, led to a "starved basin" depositional regime in the Nile Fan, where subsidence was more effective than the sediment supply. Tectonic events associated with the northern Red Sea initiated halokinetic activity in the southeastern Mediterranean area, which produced pro-

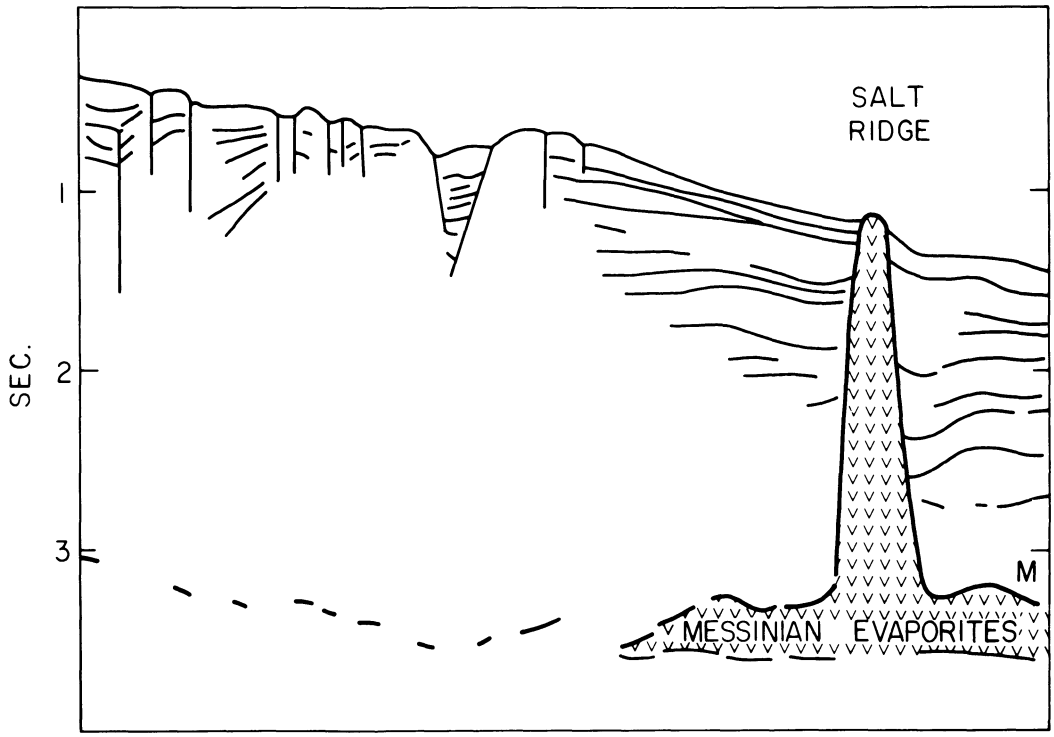

Figure 5.7. Cartoon of a seismic reflection profile running along the eastern province of the Nile Fan off Sinai. Note the series of horsts and grabens in the shallower sector and the diapiric salt ridge at the deeper sector of the profile. See Figure 5.1 for location. After Ben-Avraham and Mart (1981), reprinted by permission.

found effects on the sedimentary regime and the geomorphologic configuration of the Nile Fan.

Sedimentologic Patterns

Sedimentary Distribution

The Nile sediments are the principal constituent of a stratigraphic sequence that affected the morphology and sedimentology of the southeastern Mediterranean region from the early Pliocene to the present. Attaining its maximum thickness of more than 3 km along the upper continental slope off the delta, the Nile-derived sediments are predominant in the Plio-Pleistocene stratigraphic sequence of the eastern Mediterranean region, from the Mediterranean Ridge to the coasts of the Levant. To the east, the sand that accumulates along the Israeli coast consists mostly of Nile-derived quartz sand (Goldsmith and Golik, 1980). The Plio-Pleistocene sedimentary sequence that underlies the coastal plain and the continental margin of the southern Levant is also built predominantly of Nile-derived clay, silt, and sand (Gvirtzman, 1970; Mart, 1984). To the west, the Herodotus Abyssal Plain is filled with sediments transported by the Nile (Maldonado and Stanley, 1979, 1981), and similar provenance, mineralogy, and grain size were determined in samples from the Mediterranean Ridge as well. However, the major accumulation of the Nile sediments is in its deep-sea fan (Ross and Uchupi, 1977). The sediments were first deposited in the delta and adjacent continental shelf, and were transported again down the continental slope by turbidity currents, slumps, and submarine sediment slides, to be redeposited in the deep-sea fan on the upper continental rise.

Prior to construction of the Aswan High dam, the sediment discharge system of the Nile River transported to the continental shelf an average annual sediment supply of 120 million m^3, mostly silt and clay, causing a seaward delta progradation of up to 10 m/year. The sediment transport was enhanced by the flow regime of the Nile, which averaged around 12 million m^3 of sediment per month, but peaked at 75 million m^3 during the August–September flood season (Said, 1981). The sediments were distributed from the delta across the 60-km-wide continental shelf to the continental slope, to form a sediment apron with channel transport and erosion and interchannel deposition.

Unlike other prominent marine fans, the Nile Fan does not have a well-developed canyon and deep channel system. However, the marine transportation and redeposition of Nile sediments along the continental shelf and slope were

affected not only by the morphologic gradients, but also by the currents prevailing in the southeastern Mediterranean region. The coarser sediments on the shallow shelf were affected by the longshore sediment transport, whereas the finer sediments that reached the continental slope were affected by the geostrophic counterclockwise Mediterranean current. Both currents flow eastward (Rohrlich and Goldsmith, 1984), but whereas the coastal sediment accumulations show significant evidence for eastward drift, this trend was not observed in the continental slope and in the distribution of the deep-sea fan sediments.

Climatic Oscillations and Sedimentological Variations

The sedimentary record of the deep-sea fan indicates that the Nile depositional system was strongly affected by Quaternary climatic and sea-level oscillations, which not only modified the fresh-water flow of the Nile, but also resulted in geomorphologic changes of the delta and continental shelf, and variations in the patterns of sediment accumulation and discharge (Maldonado and Stanley, 1978, 1979). Sea-level changes strongly affected the circulation pattern of the Mediterranean water, and consequently, the type of sediments that accumulated in the eastern Mediterranean. At present, the well-known circulation pattern between the Atlantic Ocean and the Mediterranean Sea is such that the less dense water of Atlantic origin flows through the Straits of Gibraltar and eastward, above a westward flow of more saline and dense Levantine water, with salinities of approximately 38 ppt due to evaporation. However, during the glacial low-sea-level periods, such as the late Pleistocene marine regression, a contrasting exchange flow trend existed (Huang and Stanley, 1972). During these cold climate periods, decreased evaporation in the eastern Mediterranean basin and increased precipitation and fluvial output in the adjacent catchment areas caused the less dense Levantine water to become surface water and to flow westward above eastward-flowing, denser Atlantic water (Maldonado and Stanley, 1979). This current reversal at the Straits of Gibraltar led to stratification of the water mass in the eastern Mediterranean, with no water exchange occurring between the surface and the deep, resulting in development of anaerobic and euxenic deep water in the region (Fig. 5.8).

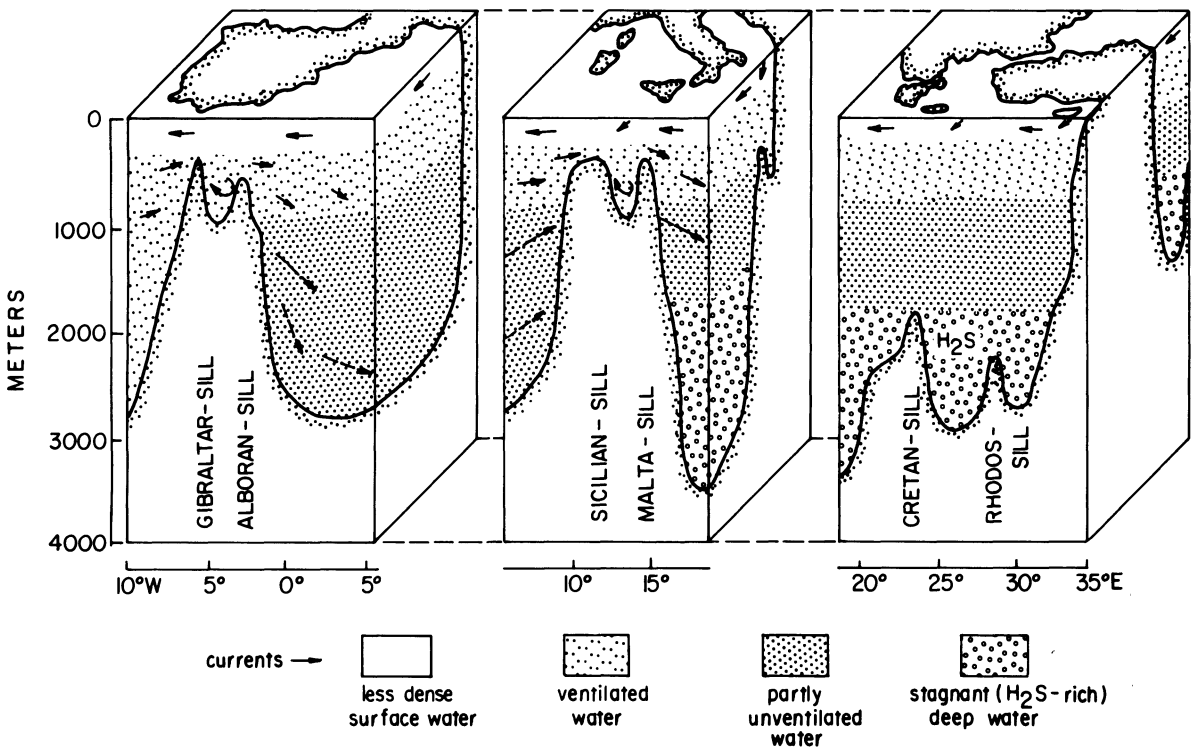

Figure 5.8. Schematic configuration of the oceanographic conditions that led to deposition of sapropelic and oxygenated sedimentation in the eastern Mediterranean region during glacial ages. (After Maldonado and Stanley, 1979.) The cold Atlantic water enters the Mediterranean at the lower part of the water column at the Straits of Gibraltar. This dense water mass does not come into contact with the atmosphere, but is depleted of its oxygen content as it flows eastward. This deoxygenated water mass forms a reducing and stagnant environment in the eastern Mediterranean Basin. At present (not shown) evaporation leads to increased density of the resident water mass, so that oxygenated warm and saline surface water descends, and the colder Atlantic water crosses the Gibraltar at the surface.

The sediments encountered in the Nile fan, and in other parts of the eastern Mediterranean, reflect these oceanographic oscillations by the cyclic sedimentation, leading to the alternating occurrence of sapropelic and well-oxygenated sediment layers.

Furthermore, fluctuations of sea level, either eustatic or regional (Vail et al., 1977; Pitman, 1979), strongly affected the offshore depositional patterns of river sediments. The periods of high sea level increased the area of the shallow seas and thus enhanced sediment accumulation on the contemporaneous continental shelves. Low sea-level stands led to intensive erosion of the emerging coastal plains, which were the continental shelves during the high sea-level stands, and gave the contemporaneous regions of coastal sedimentation an easier and shorter access to the continental slope. Therefore, it is presumed that low sea-level stands were associated with increased sediment supply to deep-sea fans (Stow et al., 1984). Sediment accumulation in the Nile Fan was further enhanced during low sea-level stands, when rainfall increased considerably in the Nile catchment area, unlike other major rivers whose water supplies were partially frozen during these time spans (Said, 1981).

Facies Distribution

The sedimentary sequence of the Nile deep-sea fan consists of clays and silts, as well as sandy, carbonaceous, sapropelic deposits. Differentiating between sediments on the basis of grain size depends on the mode of transport. Sediment was transported from the continental shelf to the fan as suspended load, (suspensites) gravitites, and turbidites (Maldonado and Stanley, 1981). Suspensites are sorted clays and silts transported in suspension, without being in contact with the bed of the slope. The gravitites are determined in beds of unsorted clastic sediments that display random particle arrangement and no internal bedding (Natland, 1976). Graded bedding, moderate sorting, and primary internal structures identity the turbidites. Medium- to coarse-grained quartz sand, feldspar rich in places, is probably a fan channel deposit (Bouma, 1962). Well-graded quartz sand, silt, and mud were deposited by turbidity currents, and hemipelagic mud, sapropel, and organic ooze are products of suspended transport. The channel depositional sequence includes layers of coarse- to medium-grained sand, up to 1 m thick, with common cut-and-fill structures. These sand deposits were affected by gravity mass flow and by bottom traction, and both features are commonplace in the middle and lower sections of the western province of the Nile Fan (Maldonado and Stanley, 1979). The turbiditic sequences include high ratios of pelitic and fine silt in most places, reflecting the basic type of sediment discharge of the Nile. The hemipelagic mud is commonly associated with minor amounts of biogenic sand and calcareous ooze, progressively grading to calcareous ooze and foraminiferal sand, with an increase in biogenic matter. Sapropel sequences indicate water mass stratification and anaerobic conditions on the sea floor due to climatic changes and eustatic sea-level variations (Vergnaud-Grazzini et al., 1988). When the sapropel is topped by organic ooze and oxidized sediment layers, there is an indication that the deep-sea water was becoming better oxygenated. In the upper continental slope, down to a depth of 450 m, a prodeltaic sedimentary sequence prevails (Figs. 5.9 a, b).

The facies distribution of Nile Fan sediments is highlighted by a broad tongue of gravity mass flow deposits in the western province, extending seaward from the Rosetta distributary down to the Herodotus Abyssal Plain There is evidence for downslope transport of prodeltaic sediments, and sorted coarse sand occurs at the lower section of the fan. There is a general increase with depth in the ratio of gravitites to suspensites reaching 4:1 in the Herodotus Abyssal Plain (Maldonado and Stanley, 1979). In general, sectors showing a high sedimentation rate correlate well with zones containing large proportions of gravitite deposits.

The eastern province of the Nile Fan is characterized by an irregular sedimentary lobe, with approximately 15% turbidite content, extending northward and northeastward from the Damietta distributary. Furthermore, in spite of the effects of the eastward-flowing Mediterranean geostrophic current, the quantity of recent Nile sediments in the eastern province is characteristically insignificant (Maldonado and Stanley, 1979). The symmetry of the off-delta sedimentation, and the eastward longshore sediment transport (Coleman et al., 1981, Murray et al., 1981), should have caused the eastern fan province to have a thicker sedimentary sequence. Therefore, the thin sedimentary sequence suggests a probable obstruction to the sediment transport. The obstacles that interfered with the downslope sediment flow are most probably the elongated salt ridges and WNW–trending horsts that were encountered in the continental slope off northern Sinai (Ben-Avraham and Mart, 1981). These structures probably affected the fan sediment transport processes, and the mineralogic composition of the sediments of the eastern province as well.

Turbid flows, an important mode of sediment transport to deep-sea fans, originate commonly from landslides and slumps on the upper continental slope, where metastable sediment accumulation is triggered to downslope motion (Bouma, 1962; Mart et al., 1979). However, the interference of the uplifted structures with the turbid flows in the eastern province, as indicated by the common occurrence of ponded sediments (Fig. 5.7), led to a thinner sedimentary sequence there. The upper slope off the Mississippi, for example, is a region where fine-grained prodel-

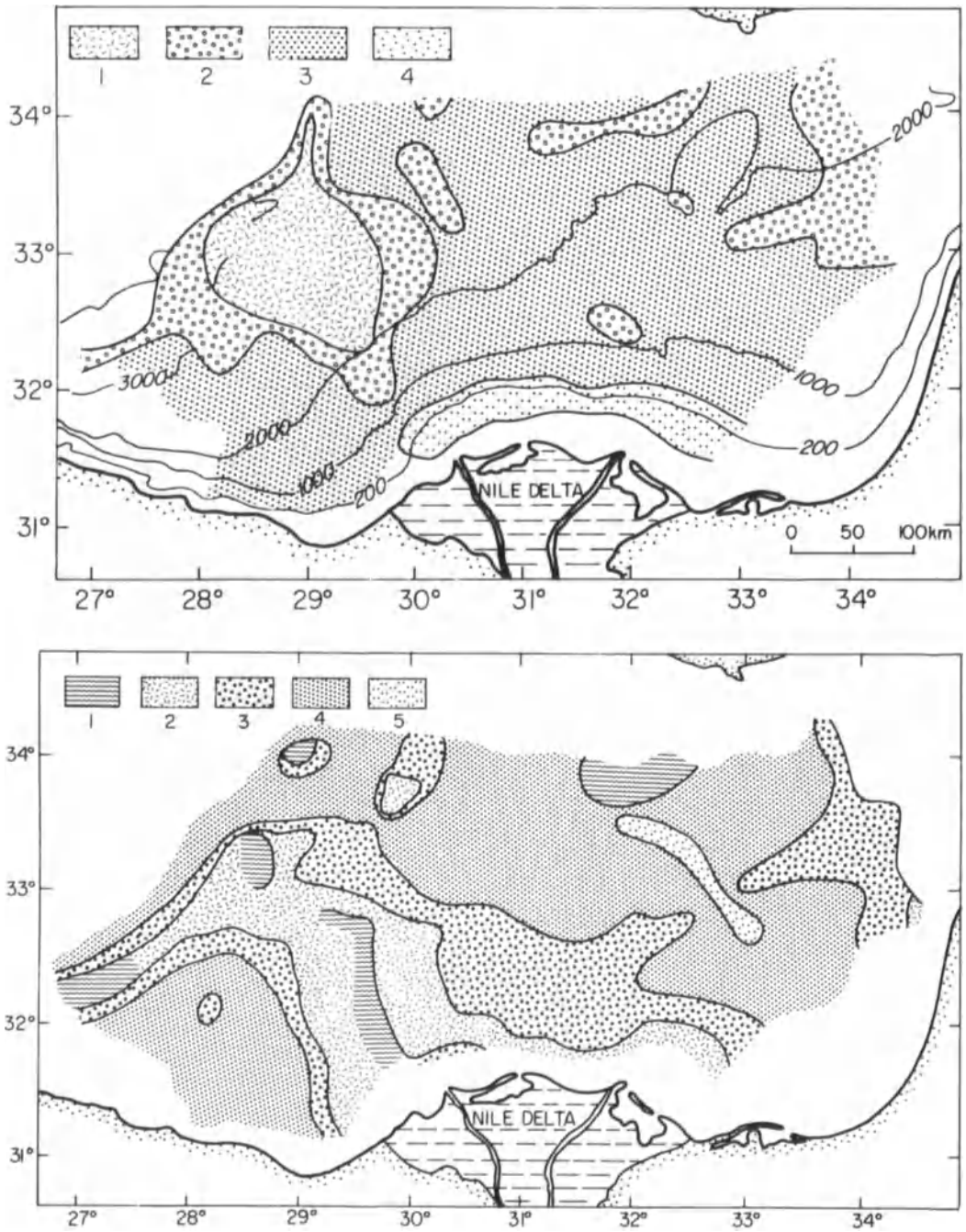

Figure 5.9. Lithofacies charts of the Nile Fan showing (a) average sedimentation rate during the past 60,000 years. The sedimentation rates are in centimeters per 1,000 years; (b) Distribution of major facies assemblages of late Pleistocene–Holocene sediments, showing lithology of turbiditic sequences. Note the distinct differences of the sedimentary facies between the eastern and western provinces of the fan. After Maldonado and Stanley (1979).

taic sediments accumulated rapidly during low sea-level stands (Walker and Massingill, 1970). Considering similarities between the sedimentologic regimes of the Mississippi and the Nile, as well as the marine basins into which they flow, the reduced rate of turbidites in the eastern province, which is structurally controlled, could be the reason for a high ratio of medium-grained to fine grained sediments in that province (Fig. 5.9b). During the period of the highest sedimentation rate of the Nile fan, that was recorded between 28,000 and 17,000 yr B.P., gravitites accumulated at

a rate exceeding 40 cm/1000 yr in places in the lower western fan province (Fig 5.9a), a record unmatched in the eastern province (Ryan et al., 1973; Maldonado and Stanley, 1979).

The trigger for downslope sediment flow off the Nile Delta could be attributed to earthquakes, to wider coastal plains and intensive erosion during low sea-level stands, or to down-flowing circulation of water masses in the eastern Mediterranean during periods of fluvial maxima. None of these processes could have caused the asymmetrical sediment distribution between the two provinces of the Nile Fan. Therefore, considering the differences between the high sedimentation rates in the western province and the restricted deposition in the eastern province, it is suggested that the structural interference with the downslope sediment flow in the eastern province was the principal cause for the different depositional regime of the two provinces, irrespective of the mechanism that triggered that downslope sediment transport. It is further suggested that the sediment deposited on the eastern portion of the continental shelf off the delta could not have moved down the slope due to the structural obstacles, but was transported eastward by the longshore current and subsequently distributed along the Levant shelf, slope, and basin. The considerable thickness of the Plio-Pleistocene sequence away from the Nile Fan, along the continental margin of the Levant, and in the Levant Basin (Mart, 1984), along with the predominance of Nile-derived near-surface sediments there (Venkatarathnam et al., 1972; Nir, 1984; Mart, 1989), could account for the masses of missing sediment from the eastern province of the Nile Fan.

Conclusions

Analysis of the sedimentology and structure of the Nile Fan reveals a huge sedimentary accumulation that originated in east and northeast Africa, and was transported to the southeastern Mediterranean since the late Miocene by the Nile fluviatile system. The Nile and its predecessor rivers built a delta with a distributary deltaic system that has been symmetric between its eastern and western sectors. The deep-sea fan associated with the same fluviatile system, on the other hand, displays remarkable differences between its eastern and western provinces. The eastern province is strongly affected by faulting and diapirism, and its sedimentary fan accumulation seems thinner than that of the western province, where the relatively regular sedimentation regime of a deep-sea fan has prevailed. Furthermore, the occurrence of a ubiquitous, Nile-derived sedimentary sequence, of Pliocene and early Pleistocene age, in the continental margin of the southern Levant suggests that the distribution patterns of the Nile sediments during the Pliocene were different from the present patterns. Since both provinces of the deep-sea fan overlie continental crust covered by a thick sedimentary sequence of early Mesozoic to mid-Tertiary age (Woodside, 1977; Makris et al., 1983), the differences between the provinces of the fan did not stem from crustal variability, and the radial symmetry of the delta rules out postulated effects of biased shelf sediment distribution.

It is suggested that the differences between the fan provinces resulted from the activity of a local faulting system, which affected only the eastern sector. Therefore, the Nile river developed two contemporaneous depositional systems that came from the same single sedimentary source and deposited upon the same type of passive continental margin. These two depositional systems show considerably different structural and sedimentologic patterns, because the faults and the diapirs in the eastern province interfered with the turbiditic flow of the sediment. Thus, the geomorphology and sedimentology of the Nile fan are unique in their asymmetric structure and sedimentation processes.

References

Armijo, R., DeSchamps, A., and Poirier, J.P., 1986, Carte seismotectonique de l'Europe et du bassin Mediterranean: Institut de Physique du Globe, Paris, 61 p., map.

Ben-Avraham, Z., and Mart, Y., 1981, Late Tertiary structure and stratigraphy of the North Sinai continental margin: Am. Assoc. Petrol. Geol. Bull., v. 65, p. 1135–1145.

Bouma, A.H., 1962, Sedimentology of some flysch deposits: Amsterdam, Elsevier, 168 p.

Chumakov, I.S., 1967, Pliocene and Pleistocene deposits of the Nile Valley in Nubia and Upper Egypt: Moscow, Acad. Sci. U.S.S.R., Geol. Inst. Trans., v. 170, p. 5 (in Russian).

Coleman, J.M., Roberts, H.H., Murray, S.P., and Salama, M., 1981, Morphology and dynamic sedimentology of the eastern Nile shelf: Mar. Geol., v. 42, p. 301–326.

Emery, K.O., Heezen, B.C., and Allan, T.D., 1966, Bathymetry of the eastern Mediterranean Sea: Deep-Sea Res., v. 13, p. 173–192.

Ginzburg, A., Makris, J., Fuchs, K., Frodehl, C., Kaminski, W., and Amitai, U., 1979, A seismic study of the crust and upper mantle of the Jordan–Dead Sea rift and their transition toward the Mediterranean Sea: J. Geophys. Res., v. 84, p. 1569–1582.

Goldsmith, V. and Golik, A., 1980, Sediment transport model of the southeastern Mediterranean coast: Mar. Geol., v 37, p. 147–175.

Gvirtzman, G., 1970, The Saqiye Group (late Eocene to early Pleistocene) in the Coastal Plain and HaShephela regions, Israel: Geol. Surv. Israel Bull., 52, p. 1–180.

Huang, T.C., and Stanley, D.J., 1972, Western Alboran Sea: Sediment dispersal, ponding and reversal of currents, *in* Stanley, D.J., ed., The Mediterranean Sea: A natural sedimentary laboratory: Stroudsburg, PA, Dowden, Hutchinson and Ross, p. 512–559.

Kenyon, N.H., Stride, A.H., and Belderson, R.H., 1975, Plan view of active faults and other features on the lower Nile Cone: Geol. Soc. Am. Bull., v.86,p. 1733–1739.

Makris, J., Ben-Avraham, Z., Behle, A., Ginzburg, A., Giese, P., Steinmetz, L., Whitmarsh, R.B., and Eleftherion, S., 1983, Seismic refrac-

tion profiles between Cyprus and Israel and their interpretation: Geophys. J. Roy. Astr. Soc., v. 75, p. 575–591.

Maldonado, A., and Stanley, D.J., 1978, Nile cone depositional processes and patterns in the late Quaternary, *in* Stanley, D.J., and Kelling, G., eds., Canyons, fans and trenches; Stroudsburg, PA, Dowden, Hutchinson and Ross, p. 239–257.

Maldonado, A., and Stanley, D.J., 1979, Depositional patterns and late Quaternary evolution of two Mediterranean submarine fans: A comparison: Mar. Geol., v. 31, p. 215–250.

Maldonado, A., and Stanley, D.J., 1981, Clay mineral distribution patterns as influenced by depositional processes in the southeastern Levantine Sea: Sedimentology, v. 28, p. 21–32.

Mart, Y., 1984, The tectonic regime of the southeastern Mediterranean continental margin: Mar. Geol., v. 55, p. 365–386.

Mart, Y., 1987, Superpositional tectonic patterns along the continental margin of the southeastern Mediterranean: A review: Tectonophysics, v. 140, p. 213–232.

Mart, Y., 1989, Sediment distribution in Akhziv Canyon off Northern Israel: Geo-Mar. Let., v. 9, p. 77–83.

Mart, Y., Auffret, G.A., Auzende, J.M., and Pastouret, L., 1979, Geological observations from a submersible dive on the western continental slope of the Armorican Massif: Mar. Geol., v. 31, p. M61–M68.

Mulder, C.J., Lehrner, P., and Allen, D.C.K., 1975, Structural evolution of the Neogene salt basins in the eastern Mediterranean and the Red Sea: Geol. en Mijnb., v. 54, p. 208–221.

Murray, S.P., Coleman, J.M., Roberts, H.H., and Salama, M., 1981, Accelerated currents and sediment transport off the Damietta Nile promontory: Nature, v. 293, p. 51–54.

Natland, M.L., 1976, Classification of clastic sediments; Am. Assoc. Petrol. Geol. Bull., v. 60, p. 702.

Nir, Y., 1984, Recent sediments of the Israel Mediterranean continental shelf and slope [Ph. D. dissertation]: Univ. Gothenburg, Sweden. 149 p.

Pitman, W.C., 1979, The effect of eustatic sea level changes on stratigraphic sequences at Atlantic margins, *in* Watkins, J.S., Montadert, L., and Dickerson, P.W., eds., Geological and geophysical investigations of continental margins: Am. Assoc. Petrol. Geol. Mem. 29, p. 453–460.

Poirier, J.P., Romanowicz, B., and Taher, M.A., 1980, Historical seismicity in the Near and Middle East, North Africa, and Spain from Arabic documents (VIIth–XIIIth century): Bull. Seismol. Soc. Am., v. 70, p. 2185–2201.

Rohrlich, V., and Goldsmith, V., 1984, Sediment transport along the Southeast Mediterranean: A geological perspective: Geo-Mar. Let., v. 4, p. 99–103.

Ross, D.A., and Uchupi, E., 1977, The structure and sedimentary history of the southeastern Mediterranean Sea–Nile Cone area: Am. Assoc. Petrol. Geol. Bull., v. 61, p. 872–902.

Ross, D.A., Uchupi, E., Summerhayes, C.P., Koelsch, D.E., and El Shazli, E.M., 1978, Sedimentation and structure of the Nile Cone and the Levant Platform, *in* Stanley, D.J., and Kelling, G., eds., Sedimentation in submarine canyons, fans and trenches: Stroudsburg, PA, Dowden, Hutchinson and Ross, p. 261–275.

Ryan, W.B.F., Stanley, D.J., Hersey, J.B., Fahlquist, D.A., and Allan, T.D., 1970, The tectonics of the Mediterranean Sea, *in* Maxwell, A.E., ed., The Sea: New York, Wiley, v. 4-II, p. 387–491.

Ryan, W.B.F., Hsu, K.J., and others, 1973, Initial Reports of the Deep Sea Drilling Program; Vol 13: Washington, D.C., U.S. Government Printing Office, 1447 p.

Said, R., 1981, The Geological evolution of the River Nile: New York, Springer Verlag, 151 p.

Shalem, N., 1954, The Red Sea and the Erythrean disturbances: Int. Geol. Cong. XIX, v. 15, p. 223–231.

Stanley, D.J., 1977, Post-Miocene depositional patterns and structural displacement in the Mediterranean, *in* Nairn, A.E.M., Kanes, W.H., and Stehli, F.G., eds., The ocean basins and margins: New York, Plenum Press, v. 4-A, p. 77–149.

Stow, D.A.V., Howell, D.G., and Nelson, C.H., 1984, Sedimentary, tectonic and sea level controls on submarine fan and slope-apron turbidite systems: Geo-Mar. Let., v. 3, p. 57–63.

Vail, P.R., Mitchum, R.M., and others, 1977, Seisrnic stratigraphy and global changes of sea level, *in* Payton, C.E., ed., Seismic stratigraphy—Applications to hydrocarbon exploration: Am. Assoc. Petrol. Geol. Mem. 26, p. 49–212.

Venkatarathnam, K., Biscaye, P.E., and Ryan, W.B.F., 1972, Origin and dispersal of Holocene sediments in the eastern Mediterranean Sea; *in* Stanley, D.J., ed., The Mediterranean Sea: Stroudsbourg, PA, Dowden, Hutchinson and Ross, p. 455–469.

Vergnaud-Grazzini, C., Borsetti, A.M., Cati, F., Colantoni, P., D'Onofrio, S., Saliege, J.F., Sartori, R., and Tampieri, R., 1988, Paleoceanographic record of the last deglaciation in the Strait of Sicily: Mar. Micropal., v. 13, p. 1–21.

Walker, J.R., and Massingill, J.V., 1970, Slump features on the Mississippi fan, northeastern Gulf of Mexico: Geol. Soc. Arn. Bull., v. 81, p. 3101–3108.

Woodside, J.M., 1977, Tectonic elements and crust of the eastern Mediterranean Sea: Mar. Geophys. Res., v. 3, p. 317–354.

SECTION III

Ancient Analogues

E.G. Rhodes and T.F. Moslow

Analog-oriented interpretation implies familiarity with a broad spectrum of examples that express the range of variability found within any specific depositional environment. Equally important to such interpretations are reliable, robust methods that guide the geoscientist in description and analysis. This third section of the volume continues to emphasize the thread of continuity associated with parasequence and facies description supported within the previous section.

We encouraged authors to present material that related the parameters of primary facies character, diagenetic modification, reservoir geometry, and production or test performance as fully as their data sets permitted. Because of the focus on sedimentary and diagenetic facies description, we asked authors to report their core or outcrop data as fully as possible. A significant emphasis was placed on reservoir description supported by core acquisition and analysis.

The seven chapters contained within this section represent a modest suite of reservoir facies examples that range in water depth from tidal inlets to deep-water fan complexes. Although demonstrative of some of the variability within these environments of deposition, this collection of examples offers a greater strength as a collection of templates and methodologies that encourage analog-oriented interpretation.

The Wilcox rocks that Steve Johansen describes in Chapter 6 are among the several clastic progradational wedges that dominate the Tertiary sediments of the northern margin of the Gulf of Mexico. Deposited at or near the continental shelf edge, sedimentary units such as Johansen describes are the subject of a recent prolific exploration trend along the Gulf Coast. These lower Eocene rocks are, at most locations, complex in terms of sedimentary facies distribution, partly due to the relative sea-level factors discussed in previous chapters.

Johansen demonstrates that understanding the original controls on primary facies distribution is a highly effective pathway to analyzing the distribution of diagenetic changes. Although Johansen points out that his diagenetic interpretation is not all-encompassing—even with the excellent data set available for Lockhart Crossing Field—his chapter establishes a template by which others may analyze the distribution of diagenetically induced reservoir heterogeneity.

As the gap between development geology and reservoir engineering closes, facies-oriented field studies that consider both the distribution of primary sedimentary facies and diagenetic overprint on these units will carry a greater mandate, especially prior to tertiary development phases. Johansen admits that he is unable to demonstrate complete omniscience concerning the distribution of primary and secondary lithofacies. However, he clearly identifies the primary factors affecting diagenesis as depositional architecture and tectonic structure. His chapter shows how the geoscientist must determine the position of primary reservoir facies and merge those data with a knowledge of the geometry of faults and folds. Johansen's contribution demonstrates that it is distribution of primary facies, modified by a structural overprint, that is the ultimate arbitrator of reservoir performance.

Jeff May tackles a highly contentious subject in Chapter 7—the paleoenvironmental interpretation of sediments within another of the progradational clastic wedges of the Gulf of Mexico. As Cant effectively illustrated in Chapter 1, relative sea level, rather than large-scale eustatic control, is most important to the placement of shallow-marine para-

sequences. May discusses a core-intensive study of two Deep Wilcox wells that contain strong evidence for shallow-water deposition within a framework that has been presumed to be dominated by submarine fan facies. The presence of shallow water parasequences at the mouth of a canyon thought to be entirely dominated by deep-marine sedimentation can impose a major revision on exploration or development strategy.

May's findings are valuable beyond the group of geoscientists concerned about exploration strategies for the Deep Wilcox. May demonstrates a template for facies analysis that quite objectively accepts rock-oriented data, even when such data are contrary to an almost overwhelming amount of previous interpretation. May's work contradicts previous interpretations through application of process sedimentology. The paradigm presented here is common within other chapters of this volume: core-based observation is a critical arbitrator for paleoenvironmental interpretation, especially in marine clastic reservoirs.

In Chapter 8, Joel de Castro embarks on the ambitious task of describing a progradational parasequence contained within a larger retrogradational sequence. The progradational sediments host four stratigraphically defined oil fields. Assisted by a wealth of core and outcrop data, de Castro has been able to precisely identify facies on the basis of primary sedimentary structures. A rare opportunity for oil-industry geoscientists, the author has made the most of this data set by interpreting the reservoir and seal rocks in the context of a single, closely constrained depositional system.

Many of the facies descriptions within Chapter 8 rely heavily on primary sedimentary structures and lithofacies texture, as indicated by core and log data. De Castro is thorough in his subdivision of the oil-field reservoirs based on rock character. He observes that the highly productive estuarine environment contains fining-upward aggradational facies units that provide internal seals—an issue that many development geoscientists notice during water-flood operations in such reservoirs. Similarly, de Castro's detailed description of the occurrence of fine-grained facies associated with higher water saturations is familiar to reservoir geologists who are concerned with capillarity and excessive water production within heterogeneous clastic reservoirs that contain low-permeability facies.

This chapter and its companion, written by de Castro's former co-worker, Eduardo Bagnoli, are exceptional because of their attention to sedimentologic detail and the relation between such detail and the reservoir character of these deltaic/marine oil fields. The data set, and the extent to which de Castro has interpreted this information, provide another example of the application of reservoir sedimentology to delineating the architecture of facies-controlled reservoirs.

In Chapter 9, Eduardo Bagnoli further analyzes the sedimentary architecture and facies distribution within the Canto do Amaro field, which is the largest of the four fields described by de Castro in Chapter 8 (over 100 million barrels of oil in place). Located in a downdip trend from the other fields, the Canto do Amaro oil field produces from sandstones that were deposited in tidal channels within a tide-dominated inlet system.

Bagnoli's analysis is unique because he is able to extend de Castro's regional framework down to the individual reservoir and facies level. Previously, de Castro showed that diagenetic alteration did not appear to significantly affect reservoir quality among the four fields. Bagnoli is able to further illustrate this with petrographic and petrophysical comparisons, showing that primary sedimentary facies remain the significant parameter in reservoir quality. Although diagenetic alteration has altered the Mossoro Sandstone by mechanical and chemical compaction and created secondary porosity along with authigenic cements, Bagnoli shows that primary facies distribution related to tidal-channel energy remains the significant controlling parameter in reservoir quality. Elsewhere, in Chapter 4, Tye and Moslow suggested a similar predictive basis for reservoir quality associated with their study of modern examples. Thus, reservoir-quality prediction is directly linked to paleoenvironmental interpretation, demonstrating the extent to which a new field can be analyzed with sufficient core control.

Chapter 10, by Bob Ruggiero, revisits an extremely mature basin and describes the process-response model that created the reservoir complex within a deep-marine environment of the Permian Basin. Not only has Ruggiero wrestled with the contentious issues surrounding the mode of deposition for these deep-water sediments, but he has effectively explained the controls on reservoir geometries within such environments.

By design, Ruggiero has avoided becoming immersed in discussion of the sequence-stratigraphic framework of these sediments. Though important to the overall understanding of the history of deep-water epicontinental basins such as the Delaware Basin, the management of fields such as Geraldine Field, in preparation for secondary and tertiary recovery, imposes a particular focus. Such a focus usually requires that an overall regional model be accepted to the degree that it explains emplacement of the reservoir units and their seals. As Ruggiero describes here, the challenge is to identify the sedimentary and diagenetic parameters that influence hydrocarbon recovery on a well spacing of 20 acres or less.

With more than 40 years of hindsight, Ruggiero's evaluation of the reservoir geometry imposed by subtle facies changes provides a unique example of reservoir sedimentology used to improve tertiary recovery. By the time a field

evolves from secondary to tertiary recovery, most of the evidence is in hand to devise an optimal management plan; it merely needs to be ordered and analyzed. Ruggiero's method of comparing sedimentological description against fluid production and injection histories is a powerful analog by which to study other fields prior to tertiary recovery.

The last two chapters deal with the sedimentology and stratigraphic architecture of deep-marine clastics within the Los Angeles basin. These deposits, on an active continental margin, host considerable hydrocarbon reserves in structurally and stratigraphically complex reservoirs that require extensive coring prior to secondary and tertiary recovery operations.

In Chapter 11, June Gidman and her associates describe a cored well within a mature field in considerable detail, providing a discussion of the lithofacies, depositional model, and reservoir quality within such sands. In the Inglewood Field, the authors show that facies associations clearly indicate gradual migration of a depositional lobe across the basin floor. Such interpretations exemplify the broader applications of reservoir studies beyond the confines of a field.

A highlight of this chapter is the discussion of permeability prediction. One of the principal goals of reservoir characterization is to provide quantitative description in support of reservoir simulation models. A significant input to such models is the determination of permeability and the variation of this parameter throughout the volume of the reservoir to be modelled. Gidman and her co-authors provide a rigorous and easy-to-follow comparison of two types of transformations from log-derived porosity to predicted permeability.

In Chapter 12, Roger Slatt and his co-authors illustrate a parallel observation to that of Lindsay and Gorter in Chapter 3. In Chapter 3, Lindsay and Gorter wrestled with the issue of reservoir quality prediction during the process of basin analysis. They found that large-scale trends could be identified within certain portions of the sedimentary architecture of a basin. However, they concluded that reservoir quality at the field scale could be quantified only by observation and sampling on a local grid that accounted for facies variability. Based on an extensively studied reservoir within the Wilmington Oil Field of the Los Angeles basin, Slatt and his associates arrive at a similar conclusion.

Similar to a theme presented in Chapter 11, by Gidman and her co-workers, an important aspect of Chapter 12 is the quantification of reservoir quality in terms of permeability, the parameter that is essential to most reservoir engineering endeavors. Combining permeability with lithofacies and porosity, Slatt and his associates delineate three numerically significant flow units. In this case, these units are facies defined, simplifying the reservoir description in favor of the authors, but strengthening their points concerning scales of heterogeneity. In brief, Slatt and his associates use a nearly unparalleded data set to illustrate the limitations of scaling reservoir observations outward into a multi-well domain. The findings presented here provide a standard by which to plan and evaluate the study of inter-well variability of production performance. Furthermore, comparison of Figures 14 and 18 in this chapter, and a review of interpretations that support these figures, strengthen the caveats that Pacht and his co-authors placed on prospecting at the facies-tract level (see Chapter 2).

Finally, the analysis of "fit" that Slatt and his associates apply to three current models of deep-marine sedimentation make this chapter valuable as a contribution in sedimentology and stratigraphy. The testing of three contrasting depositional models against a rigorously complete field-scale data set further illustrates the uncertainty of managing either development or exploration programs strictly on a model-based theme.

CHAPTER 6

Depositional and Structural Controls on the Diagenesis of Lockhart Crossing Reservoir (Wilcox); Gulf Coast of Louisiana (U.S.A)

Steven J. Johansen

Introduction

The diagenetic processes that control the distributions of cements and porosity within reservoirs are poorly known. However, two lines of reasoning suggest that cement and porosity distributions should reflect both the geometry of the depositional units and the geometry of faults and folds. First, diagenetic processes are stabilization processes. That is, the reactive components in the sediments interact with the subsurface environment to form more stable compounds. Because the original distribution of reactive components was controlled by the depositional systems, some spatial relation between the depositional architecture and the diagenetic products might be expected. Second, many of the processes that precipitate cement or modify porosity involve dissolution, transport, and re-precipitation by subsurface waters. Hydrology is strongly controlled by depositional architecture and tectonic structure, so the distribution of dissolution and precipitation products must also be controlled by these factors.

This chapter relates the three-dimensional diagenetic fabric of one reservoir to its depositional systems and tectonic structure. The described reservoir is Lockhart Crossing Field, in the uppermost Wilcox Group (Eocene) of southeastern Louisiana (Fig. 6.1). A detailed study of the diagenetic fabric of this reservoir was undertaken for several reasons. A major factor was the high density of geological information that was available; 22 cores and more than 50 electric logs from an area of about 9 mi^2 (about 25 km^2) were used in this study. It was hoped that results would aid in understanding the diagenesis of other Louisiana Wilcox reservoirs and similar reservoirs worldwide. Carbonate cements are present within Lockhart Crossing Reservoir, and electric-log correlations suggest they are laterally continuous in thin horizons that compartmentalize portions of the reservoir. Similar, though more extensive, carbonate cements totally occlude porosity in other Wilcox sandstones in the Lockhart Crossing area. Lockhart Crossing Reservoir curiously lacks the abundant acid-sensitive ferroan clays such as those that hinder development of stratigraphically similar reservoirs several tens of miles (20 to 40 km) away.

This study was funded by the Basin Research Institute and was possible because Amoco Production Company and Callon Petroleum Company generously granted Basin Research Institute access to cores, electric logs, porosity/permeability data, and water analyses. Previous studies of the reservoir include an overview of the geology presented by Self et al. (1986). Lowry (1987) reviewed the regional depositional systems of the Wilcox Group in central Louisiana and presented an interpretation of Lockhart Crossing Field that differs from the interpretations of Self et al. (1986) and this study. Detailed studies of the clay diagenesis of Lockhart Crossing were conducted by Strickler (1988; see also Strickler and Ferrell, 1990, 1992), and detailed studies of carbonate cement diagenesis will be presented in a later paper by Johansen, Strickler, and Ferrell (in preparation).

General Geology

Setting

Lockhart Crossing Field is typical of many Gulf Coast Tertiary oil fields. The reservoir sandstone, which is the up-

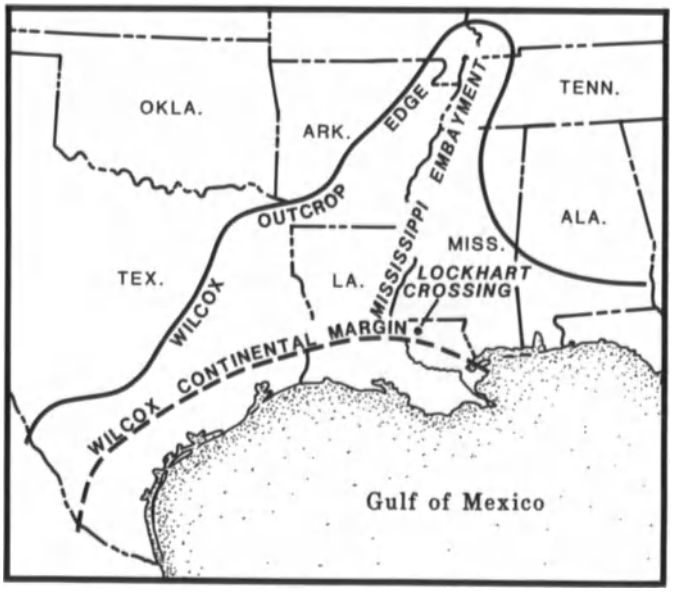

Figure 6.1. Location of Lockhart Crossing field and approximate position of the continental margin during Wilcox deposition. Margin position modified from Winker (1982).

permost sandstone in the Wilcox Group (Paleocene–lower Eocene) in this part of southeast Louisiana, is an amalgamation of marine, shoreline, and lower coastal plain depositional units. The field is a structural trap formed by a roll-over anticline that is down-dip from a large growth fault, and is modified by synthetic and antithetic growth faults (Figs. 6.2 and 6.3). Self et al. (1986) estimate 46 MMBO in place, and predict that 21 MMBO will be recovered by a water-flood program now in progress.

The present continental margin lies 150 miles (240 km) to the south, but the Lockhart Crossing area was in a shelf setting quite close to the continental margin at the time of upper Wilcox deposition (Fig. 6.1). Lockhart Crossing is east of the Mississippi embayment in a region where the rates of sedimentation and margin progradation were slow during Wilcox time (Lowry, 1987). This setting is distinct from areas west of the Mississippi embayment, where the continental margin prograded rapidly oceanward during Wilcox time, as huge volumes of sediment were delivered to the coast (Winker, 1982). As in most progradational continental margin settings, syndepositional growth faulting strongly influenced the depositional systems and hydrologic regimes of Lockhart Crossing.

The upper 500 ft (150 m) of the Wilcox Group at Lockhart Crossing consists of two distinct intervals (Fig. 6.2). The lower 200-ft (60 m) interval consists of upward-coarsening, progradational deltaic coastline and marine sequences. These are overlain by the upper 300-ft (90 m) interval of aggradational strandplain and nearshore marine sequences, consisting mostly of silty mudstones and subordinate amounts of sandstones. The Wilcox Group is overlain by the Reklaw Formation of the Claiborne Group, the base of which at Lockhart Crossing is a condensed horizon of calcareous and glauconitic, fossiliferous, rip-up clast–bearing, conglomeratic sandstone and calcareous mudstone. It is typical of transgressive lags developed in siliciclastic shelf and coastalplain sequences (cf., Stenzel, 1940). It is overlain by low-resistivity clayshales deposited in offshore marine settings.

Provenance

Most sandstones in the reservoir are very fine to fine grained, siliceous, texturally mature, lithic arkoses and feldspathic phyllarenites, using the nomenclature of Folk (1974) (Fig. 6.4). Their provenance was the southern Appalachians and uppermost Gulf Coastal plains. Lateritic, bauxitic, and kaolinitic paleosols distributed throughout the Cretaceous and Lower Tertiary intervals of the American southeast suggest a warm, humid climate for these source areas (Pryor and Glass, 1961; Dury, 1971; Sigleo and Reinhardt, 1988). Many geologists argue that the Appalachians were topographically subdued and experiencing low erosion rates in Lower Tertiary time (Judson, 1975), while an alternative view is that the Appalachians experienced a tectonic rejuvenation during Wilcox time (Todd and Folk, 1957). The petrology of Lockhart Crossing sandstones offers contradictory evidence. Their feldspathic nature suggests that weathering processes were not too intense, but some quartz grains have corrosion textures suggesting intense chemical weathering. Possibly the best interpretation is that sediment came from both moderate-relief uplands and low-relief coastal-plain source areas, both subjected to a warm, moist climate.

Sediment delivered to the coastal depositional systems was relatively stable, compared to the large amounts of immature detritus that the Laramide orogen was shedding into the western Gulf. The feldspars in the original Lockhart Crossing detritus contained many low- to intermediate-temperature forms from meta-sedimentary, meta-volcanic, and plutonic sources. Much alumino-silicate would have arrived as partially degraded chloritic and illitic clays, derived from Appalachian sedimentary and metamorphic rocks, and as kaolinite (Strickler and Ferrell, 1992). Iron probably was transported as limonite.

Depositional Systems

Figures 6.2 and 6.5 are cross sections across the depositional strike and dip of the reservoir. Underlying the reservoir are bioturbated, sparsely shelly, moderately to very dark

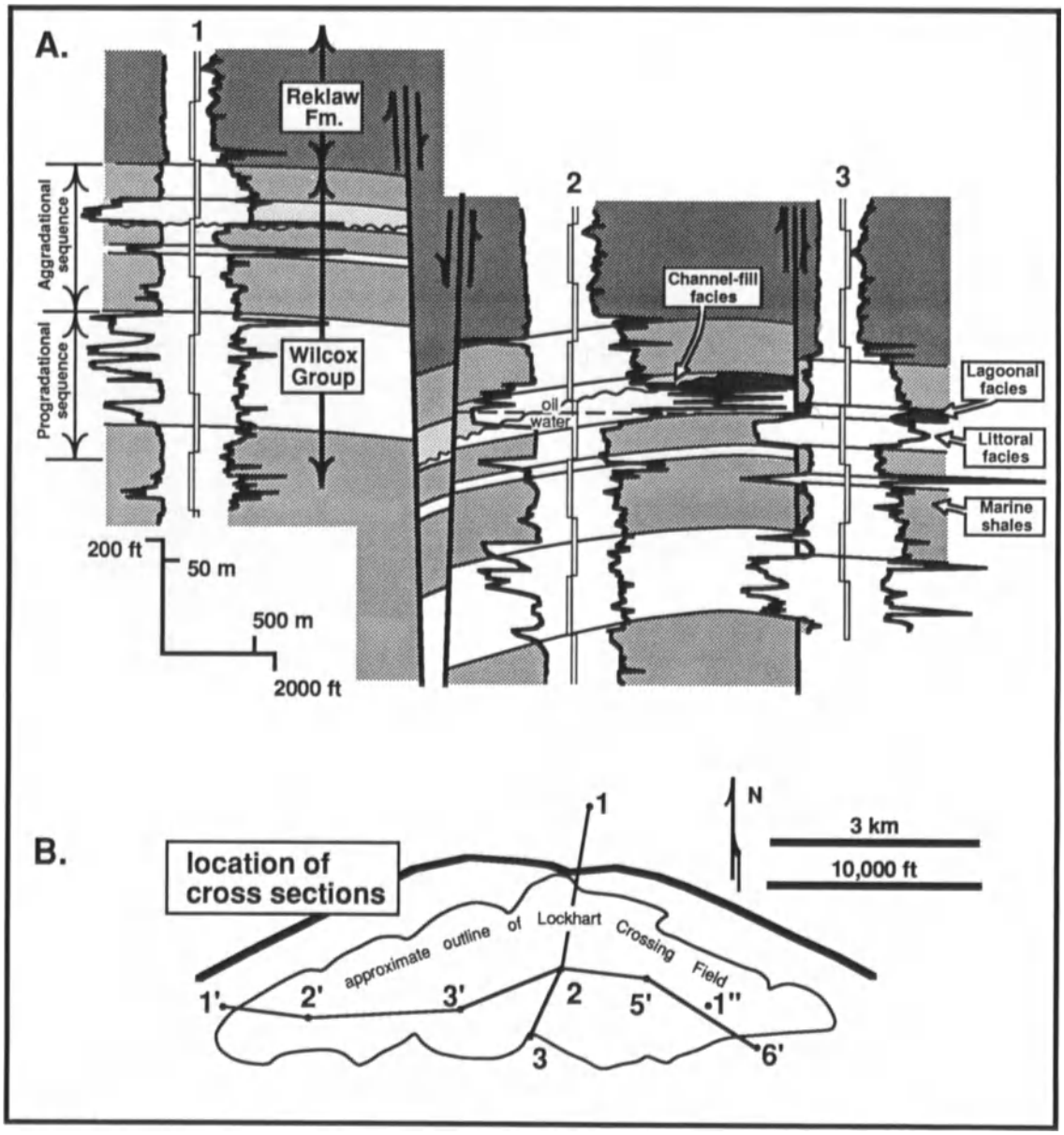

Figure 6.2. A. Dip-oriented cross-section across Lockhart Crossing field. B. Location map shows the line of this cross-section and the cross-section of Fig. 6.5. Location 1″ is the well illustrated in Fig. 6.6.

gray, slightly sandy mudstones of normal marine deposition. Several thin (1 to 3 ft, or 1/3 m to 1 m) beds of very pale blue, calcareous or bentonitic sandstone are present within 15 ft (5 m) of the base of the reservoir, but the sequence does not display a noticeable upward increase in sand content. Sparse calcareous fossils are present throughout the marine mudstones, but many calcareous fossils have been partially or totally dissolved, leaving only impressions in the encasing mudstone. The upper 6 inches (15 cm) of the mudstone sequence contains burrows about an inch (2.5 cm) in diameter filled with highly glauconitic sandstone.

Most of the reservoir consists of a 40- to 50-ft-thick (12 m to 15 m), upward-coarsening sequence of texturally mature, very fine to fine sandstone (Fig. 6.6). This is the *littoral facies*. Close examination leads to a differentiation of two subunits within this facies. The subtle boundary between the two subunits had profound effects on later hydrologic regimes and diagenesis. The lower subunit, which is 10 to 15 ft thick (3 m to 5 m), was deposited in a sandy offshore marine environment over an extended period of time. It consists of very fine-grained, siliceous cemented, slightly silty and clayey, glauconitic and shelly, feldspathic phyllare-

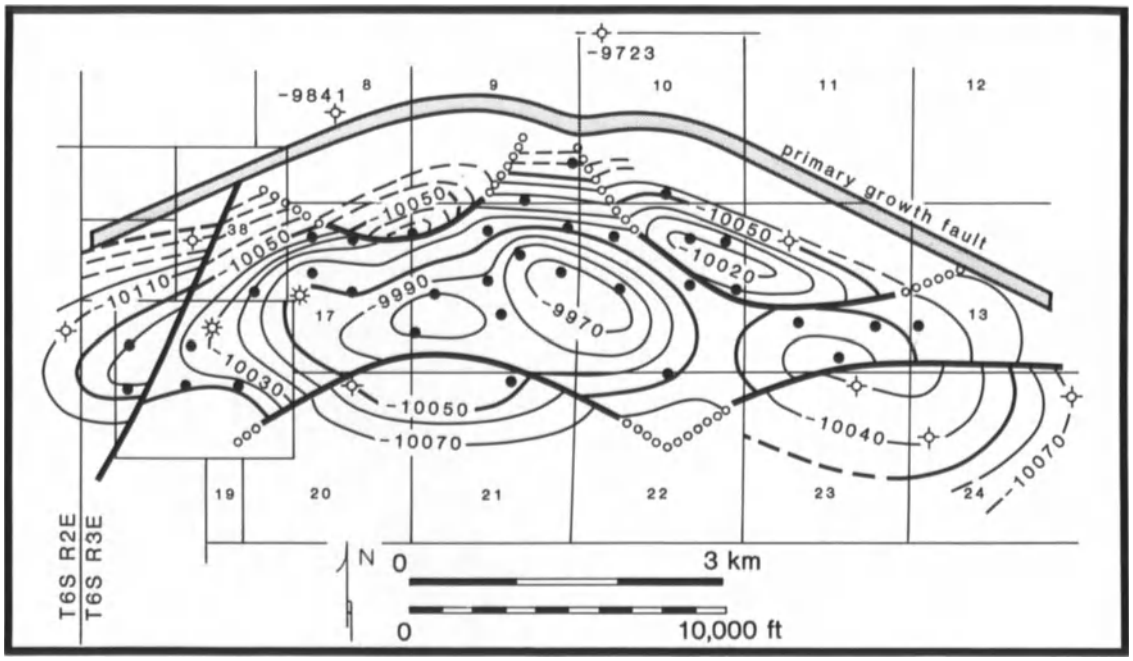

Figure 6.3. Structure contour map (feet below sea level) of the top of the Wilcox Formation, Lockhart Crossing field. The trend of the primary growth fault is generalized from Self et al. (1986).

nite sandstone. Glauconite and rip-up clay clasts are especially abundant in the lower 1 ft (1/3 m) (Fig. 6.7). No other systematic changes in grain size or physical sedimentary structures are recognized in this subunit due to destruction of original structures by intense bioturbation. The upper subunit within the littoral facies is a regressive shoreface sequence. It commonly coarsens upward and contains less glauconite, fewer clay rip-up clasts, less detrital matrix, and fewer bioturbation structures than the underlying offshore marine sandstone subunit. Low-angle cross laminations with disarticulated bivalves and reworked agglutinated burrow walls are rarely preserved in the uppermost portion of the sequence (Fig. 6.8). The subaerial portions of the regressive shoreface system are not preserved.

The littoral sandstone sequence is overlain throughout much of the field by 20 ft (6 m) of moderate to very dark gray, carbonaceous, pyritic and sideritic shales, which were deposited in a brackish-water lagoon or bay environment. This *lagoonal facies* contains abundant woody plant impressions, while bivalve impressions and glauconite are absent or very rare. Bedding is undisturbed except for very sparse, poorly-defined rootlet(?) or bioturbation(?) traces. Self and others (1986) collected from this unit a limited foraminiferal population of agglutinated forms, which they interpreted as a brackish-water assemblage.

The lagoonal facies is missing updip of the major growth fault north of the field, due to syndepositional faulting and resultant erosion or nondeposition. It is also partially or totally missing in about a quarter of the wells drilled downdip from the growth fault, because several channels were incised into the top of the lagoonal facies (Figs. 6.5 and 6.9). A large channel that incised the north flank of the field eroded through the total lagoonal facies, into the littoral sandstone facies. The *channel-fill facies* consists of interbedded sandy mudstones, clean sandstones, and sandy mudstone-clast conglomerates (Fig. 6.10). Mudstones are moderate dark gray to pale dark gray, the gray value reflecting the ratio of plant detritus versus sand content. Some display delicate, repetitive laminations. Sandstones are ripple-laminated and trough cross-bedded, and bioturbation is rare or absent. Grain size is variable, but many channel sandstones are upper fine grained to medium grained, and are distinctly coarser than any of the underlying littoral sandstones. Clasts in the mudstone-clast conglomerates were locally derived; they resemble mudstone lithologies that occur elsewhere in the channel-fill sequence.

The origins of the channels and channel-fill sequences are controversial. Possibly, the channels are paleovalleys that incised into the lower coastal plain during a minor sea-level fall, and these paleovalleys later filled with bayhead delta and/or estuarine sediments as base level rose during an ensuing transgression. The channel dimensions (Fig. 6.9) are similar to those of small stream valleys that incised the modern Gulf Coast lower coastal plain during the last glacial lowstand. The larger incised channel is located in

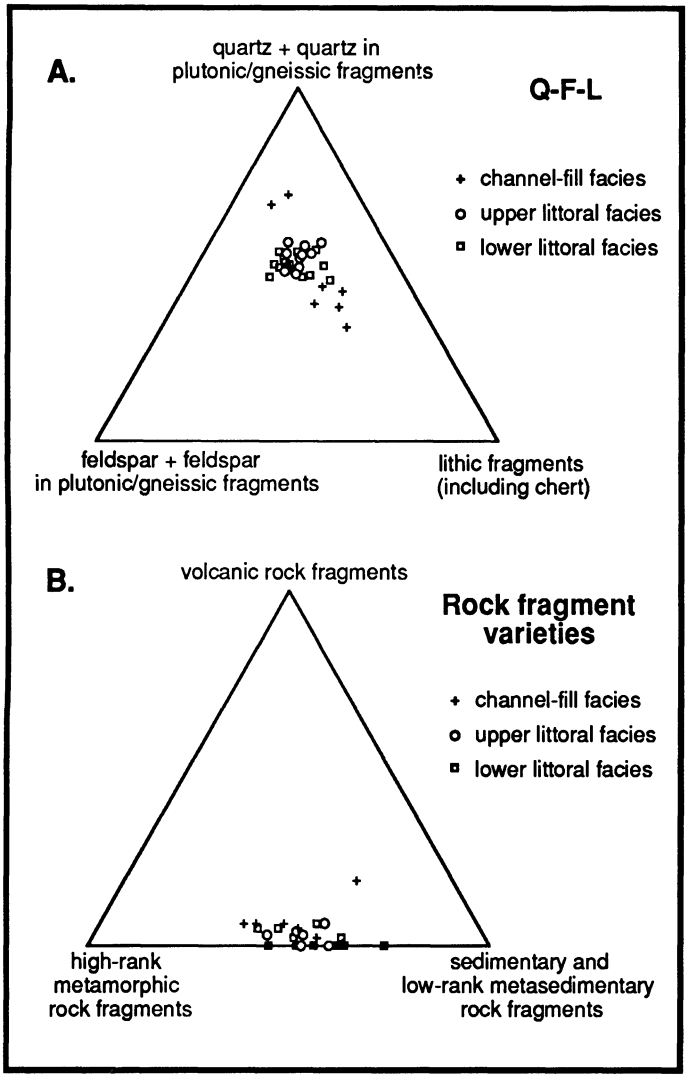

Figure 6.4. A. Q-F-L plot of framework grains for 46 samples from the Lockhart Crossing Reservoir. Based on 300 points per thin section, with sections stained for potash and plagioclase feldspars. Only grains with apparent diameters >30 μm were counted as framework grains, and if the counted point fell upon a crystal of >30 μm diameter within a polymineralic grain, it was counted as an individual mineral species, not a rock fragment. B. V-M-S plot for the same samples. Data are presented in Johansen (1987).

the zone of maximum subsidence of a contemporaneous growth fault (see structure discussion below), which is a reasonable incision course for a lower coastal-plain fluvial system.

An alternative interpretation is that the channel-fill facies represents the infill of fluvial estuary/tidal inlet systems developed landward of the regressive shoreface system, similar to those of the present Georgia coast described by Moslow (1984). These modem fluvial/tidal estuaries are oriented parallel to the shoreline, similar to the channel facies at Lockhart Crossing, and the modern fluvial-tidal estuaries are orthogonal tributaries to larger tidal inlet/fluvial estuarine systems that separate individual barrier islands. A larger tidal inlet or estuarine system might terminate the first Wilcox sandstone at Livingston Field, several miles (3 to 8 km) east of Lockhart Crossing field (P. A. Thayer, personal communication, 1985).

Abruptly overlying the lagoonal sequence and the channel-fill sequence (where present) are nearshore normal marine mudstones. The base of these marine mudstones contains, in some wells, an unsorted transgressive lag deposit of re-sedimented carbonate concretions, oyster shells, and glauconitic sandstone. In other wells the contact is an abrupt disconformity between the mudstones of the lagoonal facies and the overlying marine mudstones. In these wells, the sparsely glauconitic, shelly, and bioturbated marine mudstones can be separated from the lagoonal mudstones only by careful inspection.

Structure

Abrupt changes in the thickness of stratigraphic units reflect syndepositional movement of growth faults in the Lockhart Crossing area. Figure 6.3 is a structure contour map on the Reklaw/Wilcox contact; the basal Reklaw transgressive lag was a relatively flat surface across the field area at the time of its deposition. Figure 6.11 is an isopach map between the top of the Wilcox and the base of the second Wilcox sand (labelled in Fig. 6.5). This map represents a "paleostructure" map of the second Wilcox sand at the time of Reklaw deposition, if the effects of later shale compaction are ignored. Correction for compaction would accentuate the variations in thickness. Comparison of Figures 6.3 and 6.11 reveals that growth of the rollover anticline influenced the thickness of depositional units. Updip of the major growth-fault system, the interval is much thinner, and the lagoonal facies is missing (Fig. 6.5).

A fault trending N30°E cuts across the grain of the structure in the western portion of the field; it must be a post-Wilcox structure, for it has no expression in the isopachs. This fault dropped the western end of the field, which at the end of Wilcox deposition was a bit higher on the rollover anticline than the eastern end.

As mentioned above, the channel incision trends east-west, parallel to the ancient shoreline trend, following a zone of rapid subsidence along the major growth fault. In the northeastern portion of the field, the channel incised into the littoral sequence. This geometry (Figs. 6.9 and 6.12) exerted strong controls on the hydrologic history of the reservoir.

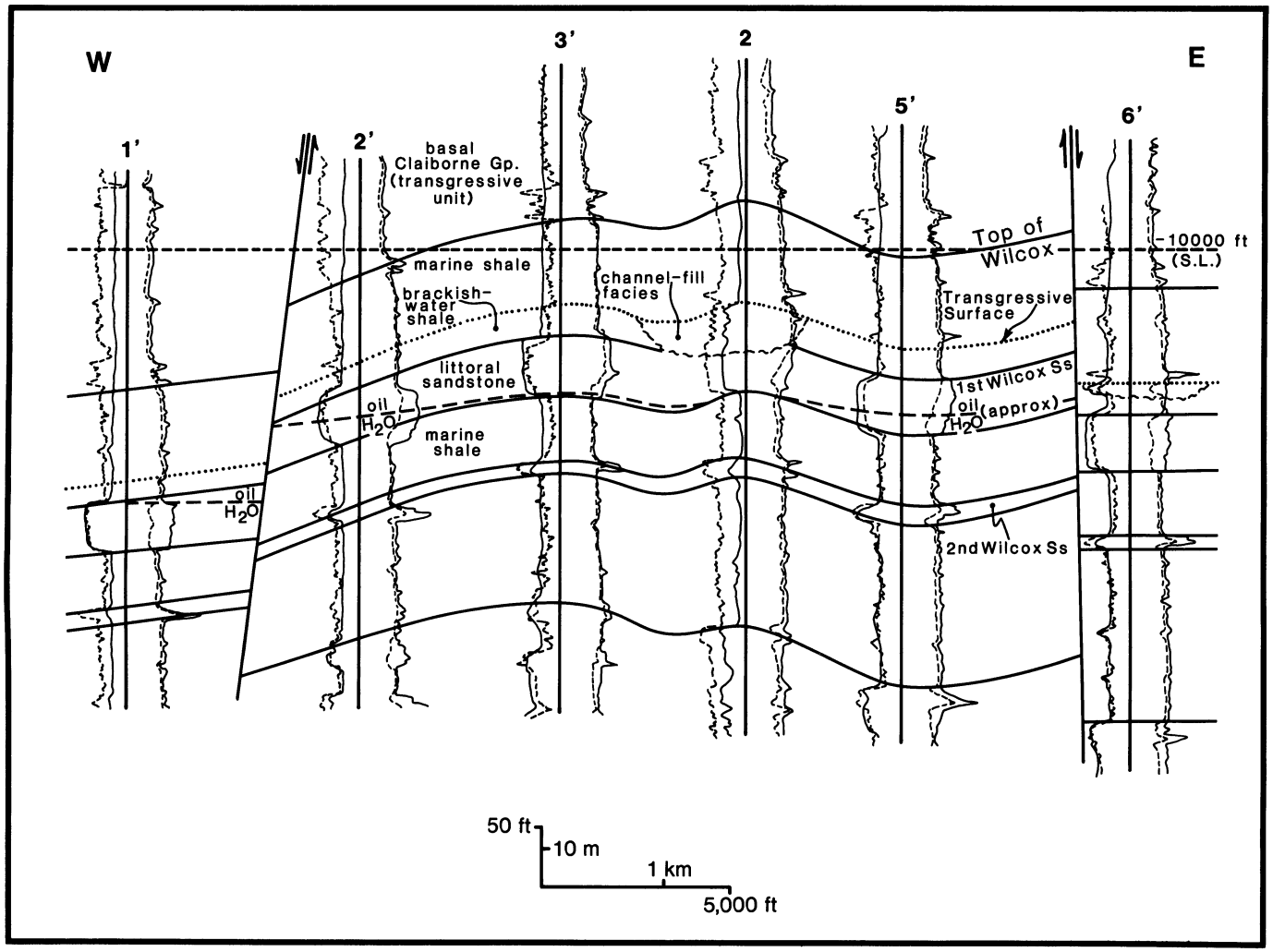

Figure 6.5. Strike cross section of Lockhart Crossing field. Location map is Fig. 6.1B. The channel-fill facies is present in two separate areas (wells 2 and 6'), but the channel did not incise totally through the brackish-water shales in well 6'. Oil-water contact is only approximated.

Porosity and Permeability Distribution—General Statement

The distribution of permeability and porosity in this field mostly reflects the original sediment texture. The channel-fill sequence on the northeast side of the reservoir has heterogeneous porosity and permeability trends, reflecting the intercalated sandstones, mudstones, and mudstone conglomerates of the channel fill. Permeabilites as high as 2 or 3 d are present in trough cross-stratified, medium-grained sandstones; these are intimately interbedded with more shaly or clay-clast-rich layers with permeabilites of 10 md or less. The bulk of the reservoir consists of the littoral sequence, which generally has a more equitable distribution of porosity and permeability (Fig. 6.6). The glauconitic and slightly clayey, very fine sandstones of the lower subunit, or offshore sandstone subfacies, have measured porosities of 15 to 20% and permeabilities of 1 to 10 md. The cleaner, upward-coarsening, very fine and fine sandstones of the overlying shoreface subfacies have generally upward-improving porosity and permeability trends, with permeabilities generally between 20 and 100 md and porosities of 20 to 24%.

Self et al. (1986) explained how the surface tension at the oil/water contact, in conjunction with the very small pores in the offshore marine facies, combined to give the oil water contact in this reservoir a concave-downward geometry. The very small pores in the offshore marine subfacies suck up water by capillary forces. Because the reservoir is a doubly-plunging anticline, the oil/water contact rises on the center of the structure in response to this capillary action.

These simple relations between depositional environments, permeability, and porosity do not hold at the contacts between different facies. Porosity and permeability

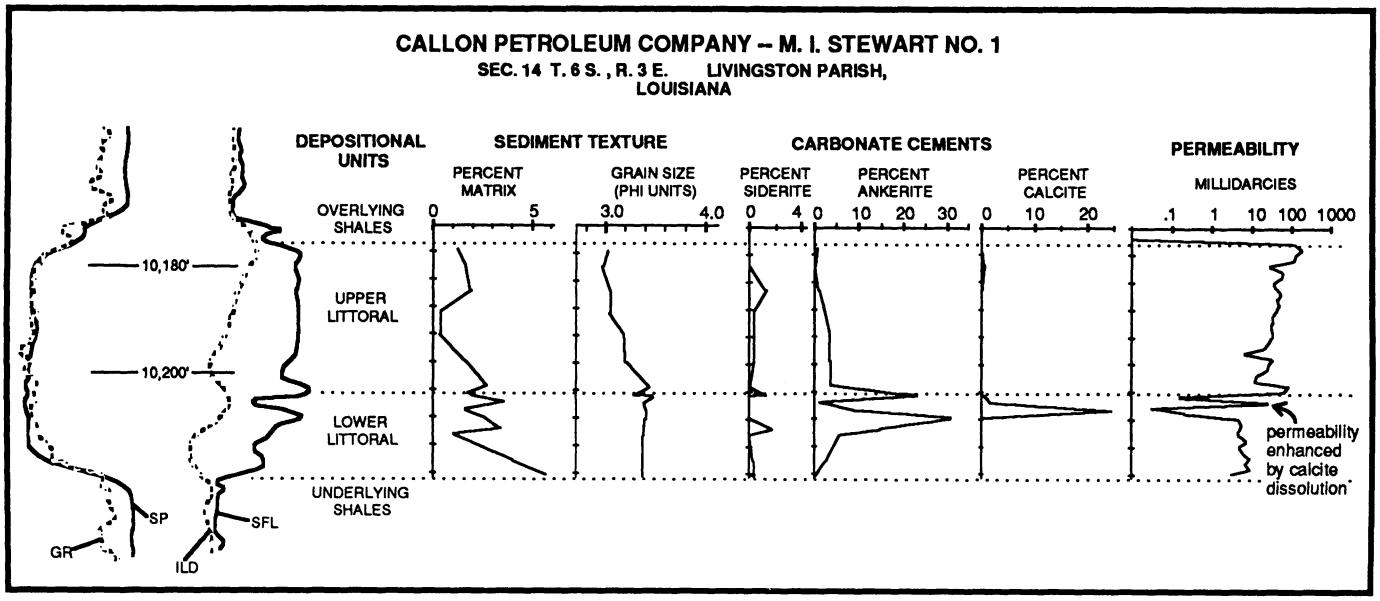

Figure 6.6. Sediment texture, carbonate cement, porosity and permeability trends through the littoral facies interval. Textural and cement data based on point counts of 16 standard thin sections (data in Johansen, 1987). Porosity and permeability data based on conventional core analysis on 1-ft intervals. Electric logs, porosity, and permeability data made available by Amoco Production Company. Location of well is shown as point 1″ in Fig. 6.1B.

are erratic at the contact between the offshore marine subfacies and the shoreface subfacies. In many wells, this contact is carbonate cemented, while in others, it is exceptionally porous and permeable. Complicated alternations of high and low porosity are present in some wells, with zones of low permeabilty correlating to zones of carbonate cement (Fig. 6.6). Carbonate cements are also common at contacts of the channel-fill sequence with other facies. When the channel fill is incised deep into the littoral sequence, carbonate cements are common near the contact. Carbonate cements are also common at the top of the channel-fill sequence or in the overlying conglomeratic transgressive lag deposits that are locally present. Examination of the neutron-activation porosity logs for the field (Fig. 6.13) reveals the extent of the carbonate cement. The carbonate-cemented zones are more common on the crest and updip limb of the anticline, and near faults. These zones of carbonate cementation could compartmentalize the reservoir into three facies-controlled flow units. Self et al. (1986) report no problems of this nature with the water-flood program now in progress. However, laterally continuous, thin zones of carbonate do compartmentalize other reservoirs (Kantorowicz, et al., 1987), and well-developed carbonate cements are a common destroyer of reservoir quality in siliciclastic sandstones.

The remainder of this paper investigates the interrelations between the paleohydrology and diagenesis of this field. The effects of diagenetic processes on reservoir quality are discussed, and a model is presented that links the hydrologic history of the reservoir to the present distribution of carbonate cements. This illustrates some general principles that control reservoir quality in this and in other reservoirs.

Hydrologic and Diagenetic History of Lockhart Crossing Reservoir

Hydrologic Regimes and the Present Reservoir Setting

Galloway (1984) divided the sedimentary fill of the Gulf Coastal Plain basin into three hydrologic regimes, and stressed that different diagenetic processes are common to each. The shallowest is the meteoric regime, in which the loosely compacted sediment is flushed with meteoric water. Galloway and Kaiser (1980) documented modern meteoric water penetration to about 5000 ft deep in the Frio interval of Texas. Recent computer modelling suggests that meteoric waters can circulate to great depths in coastal-plain sequences, well beyond the shoreline into submerged shelf sequences (Bethke et al., 1987). The second hydrologic regime is the compactional regime, in which the general fluid flow is upward, out of the sediment pile as the sediments compact and expulse waters. The third hydrologic regime is the thermobaric regime, which consists of sediments below the top of geopressure, typically at

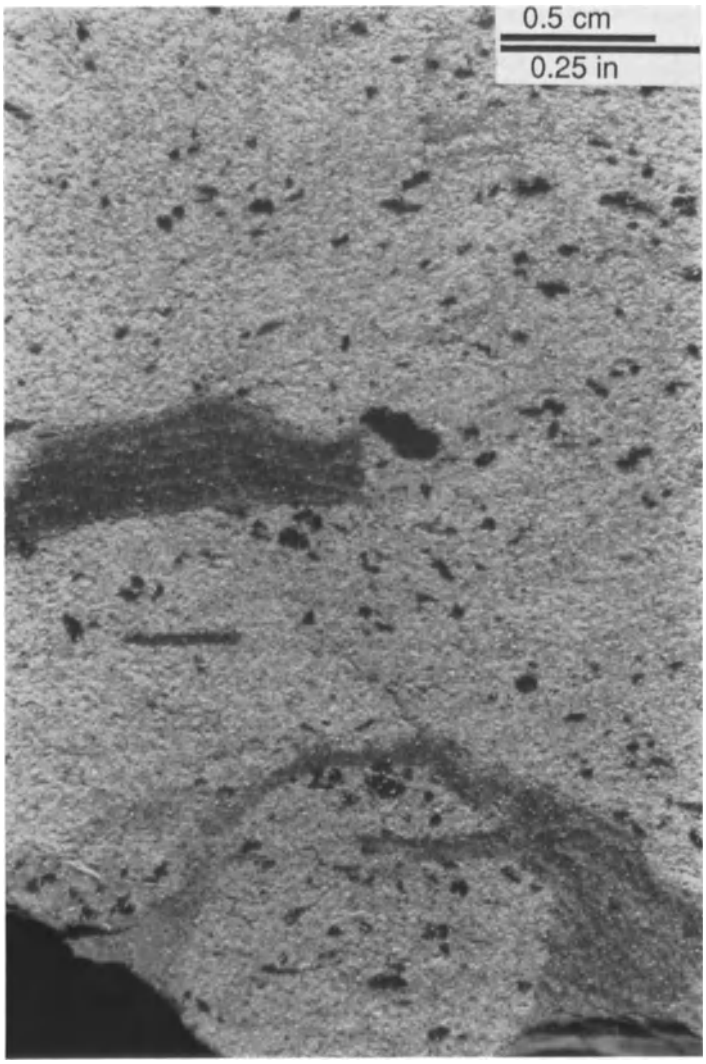

Figure 6.7. Glauconitic, clay-clast-bearing, extensively bioturbated very fine sandstone from the base of the littoral facies. 10,243-ft core depth, Amoco No. 3 J.A. Thom, Section 41, T6S, R3E, Livingston Parish, Louisiana.

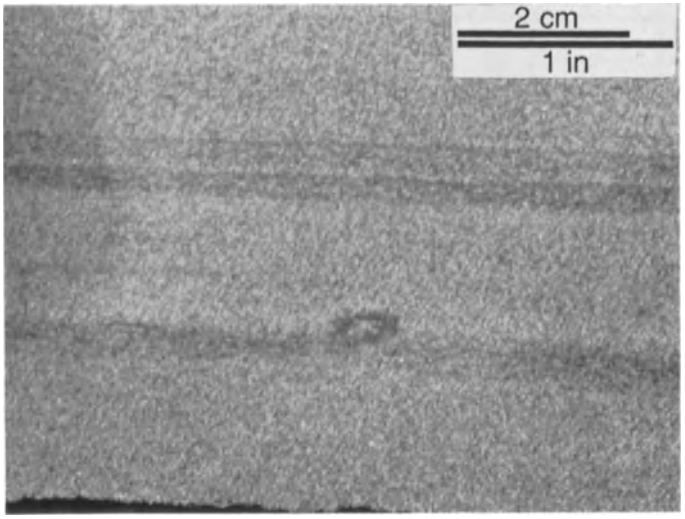

Figure 6.8. Low-angle to horizontally laminated, clean fine sandstone from the top of the littoral facies. Shell debris and reworked agglutinated burrows are present in some laminations. 10,204-ft core depth, same well as in Fig. 6.7.

6,000-ft (1800 m) to 12,000-ft (3700 m) depths. Exchange of fluids between the thermobaric regime and the overlying regimes is significantly retarded, and intense heat and pressure produce profound diagenesis verging on metamorphism.

At present, Lockhart Crossing Reservoir lies at a depth of about 10,200 ft (3100 m) (Fig. 6.5), which is 5,000 ft (1500 m) above the local top of geopressure, as determined from plotting mud weights. Formation temperatures prior to water-flooding were about 100°C (as estimated from bottom-hole temperatures using the method of Kehle, 1971). Salinity is about 50,000 ppm (personal communication with Amoco production geologists, 1986). Alkalinities reported to Amoco from commercial labs commonly estimate bicarbonate concentrations between 900 and 1100 mg/l (personal communication from Amoco production geologists, 1986); but these numbers probably represent total alkalinity titrations, and so may reflect the presence of weak organic acids (cf., Morton and Land, 1987; Surdam et al., 1984). Updip (north) from Lockhart Crossing and at shallower depths, water salinities are greater, possibly reflecting the dissolution of salt diapirs by circulating formation fluids (Hanor et al., 1986).

Sediment Modification in the Depositional Environment and Meteoric Regime

The most unstable components in this sediment at deposition had two fundamentally different origins. One source of unstable components was the original sediment provenance and the updip fluvial depositional systems that transported the sediment to the coastline. This source delivered muds rich in organic matter, limonite, and cation-poor clays. The second source for unstable material was the final depositional site. Because the final sedimentation site consisted of non-deltaic littoral and related coastal plain settings on a slowly prograding shelf, there was abundant time for carbonate allochems and detrital organic matter to get mixed into the sediment.

The distribution of these unstable components was determined by the depositional systems. The lower, offshore marine subunit of the littoral sequence contained large amounts of calcareous fossils and syndepositional rip-up

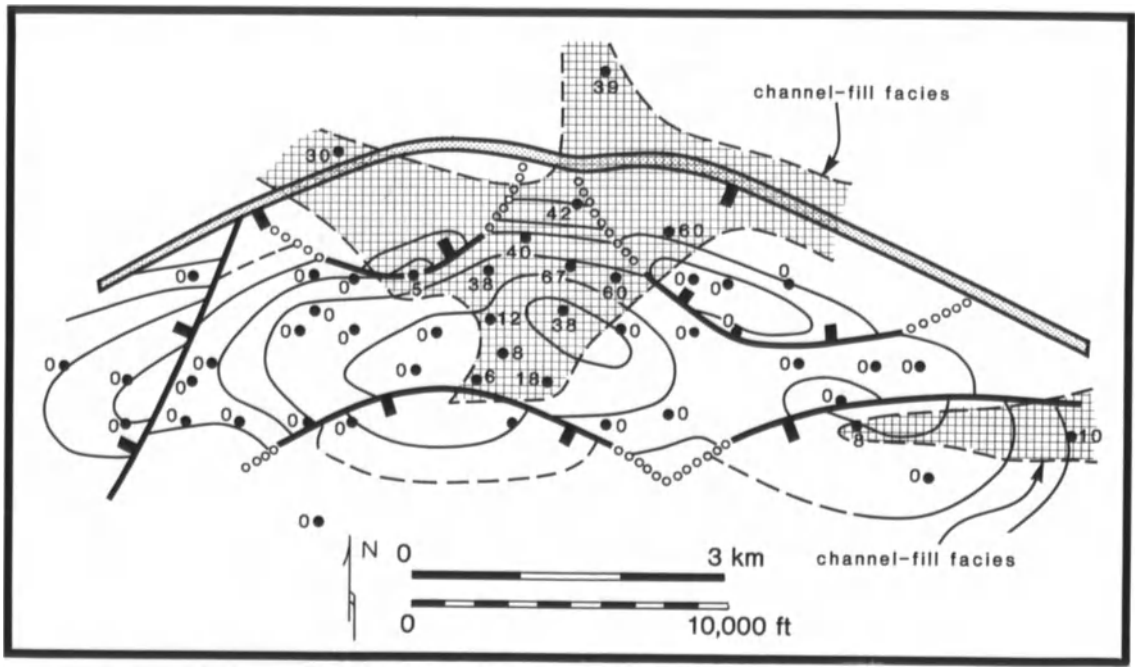

Figure 6.9. Distribution and thickness of the channel-fill facies superimposed upon a structure contour map of the Wilcox Formation top (Fig. 6.3). The channel-fill facies does not cut across the trend of the structural anticline, but seems to be oriented parallel to the bounding down-faulted blocks. This relation suggests that channel incision was partially controlled by contemporaneous structure. See also Fig. 6.11.

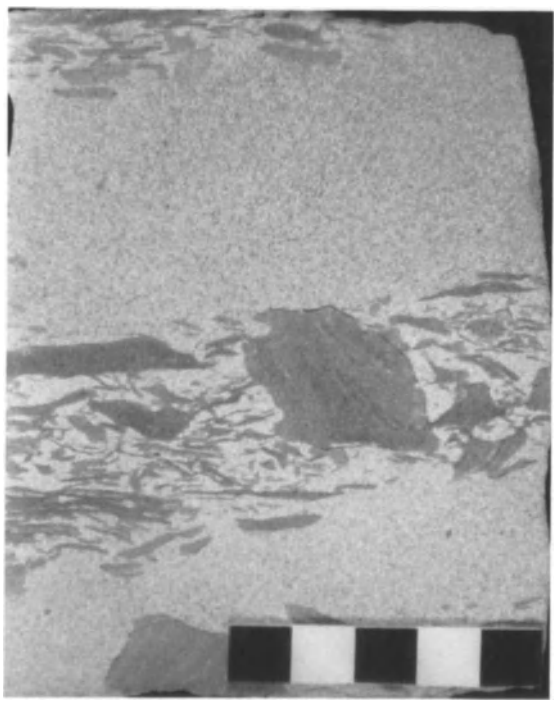

Figure 6.10. Interbedded fine and medium sandstones, shale-clast conglomerates, and laminated siltstones and shales (not shown here) are typical of the channel-fill facies. Note the lighter color of the matrix around the shale clasts, reflecting the abundant kaolinite that clogs pores adjacent to the shale clasts. Scale bar is 5 cm (about 2 in) long. From 10,208 ft core depth, Callon Pet. No. 1 O.M. Barnett, Sec. 16, T6S, R3E.

clasts and grain coatings of dolomite, calcite, and possibly aragonite (Fig. 6.14). These carbonate clasts and grain coats probably precipitated on the offshore marine sea floor, as similar carbonates form today in the North Sea marine floor (Hovland et al., 1987) or in shoreface settings of Modern Louisiana beaches (Kocurko, 1986). Calcareous fossils were also present in the underlying marine mudstones. Amorphous iron would not have remained for long in the marine sediments; they contained bacteria that converted sulfate (SO^{4+}) to sulfide, which in turn combined with the reactive limonite to form pyrite (Berner, 1980).

In contrast, the overlying lagoonal mudstones and incised channel-fill sequence contained abundant detrital limonite, little detrital carbonate, and fresh to brackish pore waters with little available sulfate for pyrite fixation of iron. Carbonate ions were generated in part by the bacterial oxidation of organic matter and sulfate reduction (Curtis and Coleman, 1986), and these combined with the iron to form stringers of siderite immediately above the littoral sequence, and scattered siderite rhombs throughout the littoral sequence.

Localized concretions of intergrown calcite, ferroan dolomite, ankerite, siderite, and pyrite are distributed throughout the littoral sequence and channel-fill sandstones. These also represent the stabilization of iron and dissolution/reprecipitation of carbonate from allochems as

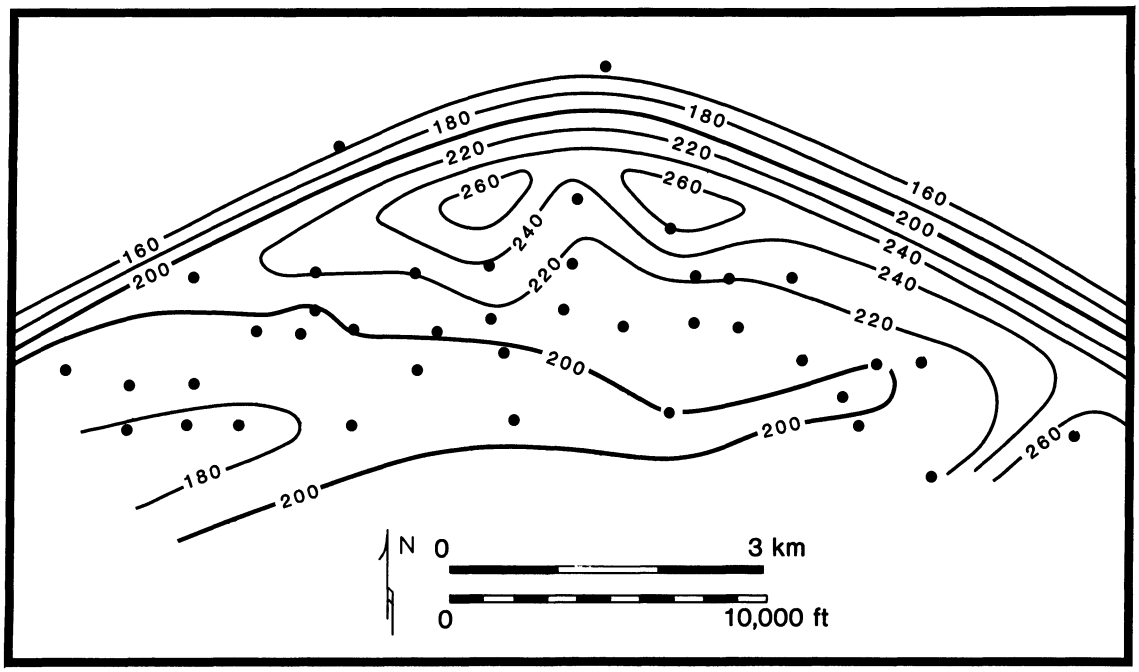

Figure 6.11. Isopach map of the interval between the top of the Wilcox Formation and the base of the second Wilcox sandstone. Compare to the structure contour map (Fig. 6.3) and the distribution of the channel-fill facies (Fig. 6.9). Subsidence was strongly controlled by contemporaneous growth faulting, but the northeast-trending fault that downdrops the western edge of the reservoir did not affect deposition; it formed after Wilcox deposition.

bacteria oxidized the unstable organic matter, and detrital iron compounds were reduced. The chemistry of the waters in which this occurred was complex. Coastal-plain sediments commonly are flooded with fresh, meteoric water to considerable depths. However, at Lockhart Crossing, the syndepositional development of growth faults with displacements in excess of 40 ft (12 m) served to isolate the littoral sandstone from its updip equivalents (Figs. 6.11 and 6.12). This isolation was not complete; where the channel-fill sandstone was partially incised into the littoral sandstone packet, the total sand thickness was as great as 80 ft (24 m), which allowed for a limited conduit across the growth fault. A record of this early paleohydrologic regime is recorded in the distribution of bacterially precipitated concretions. Concretions on the margins of the field are rich in pyrite (Fig. 6.15), which records the presence of sulfate-bearing, marine waters on the margins of the present field, and also records the influx of ferrous iron from the surrounding mudstones. Concretions close to the incision of the channel-fill facies and on the crest of the rollover anticline contain little or no pyrite, probably reflecting both the intrusion of fresh meteoric waters from updip, via the channel-fill facies, and the removal of the overlying, ferrous lagoonal mudstones by the channel incision.

Early Compactional Regime

Major burial diagenetic events in the sandstones are summarized in Figure 6.16. Isotope and petrographic studies constrain the timing and types of fluids involved (Johansen and Strickler, 1987; Johansen, 1987, 1988). The ankerite concretions continued to grow, probably in meteoric-derived waters, until temperatures of about 40°C were reached. Some scattered rhombs of ankerite may also have formed at this time, and some very early siderite was replaced by later ankerite. Potassium feldspar overgrowths formed in this early regime, before smectite soaked up all available potassium for the smectite to illite transformation. Significant mechanical compaction of the sandstones and adjacent shales also must have occurred at this time. Sandstone compaction decreased porosity in all sandstones, but was a significantly more important process in sandstones contain high amounts of glauconite, rip-up shale clasts, and detrital matrix (Fig. 6.17), because these ductile grains deform and flow into available pore space during compaction. Since the greatest concentration of ductile grains and matrix is in the offshore marine subfacies, this subfacies suffered the most serious losses of porosity/permeability due to compaction.

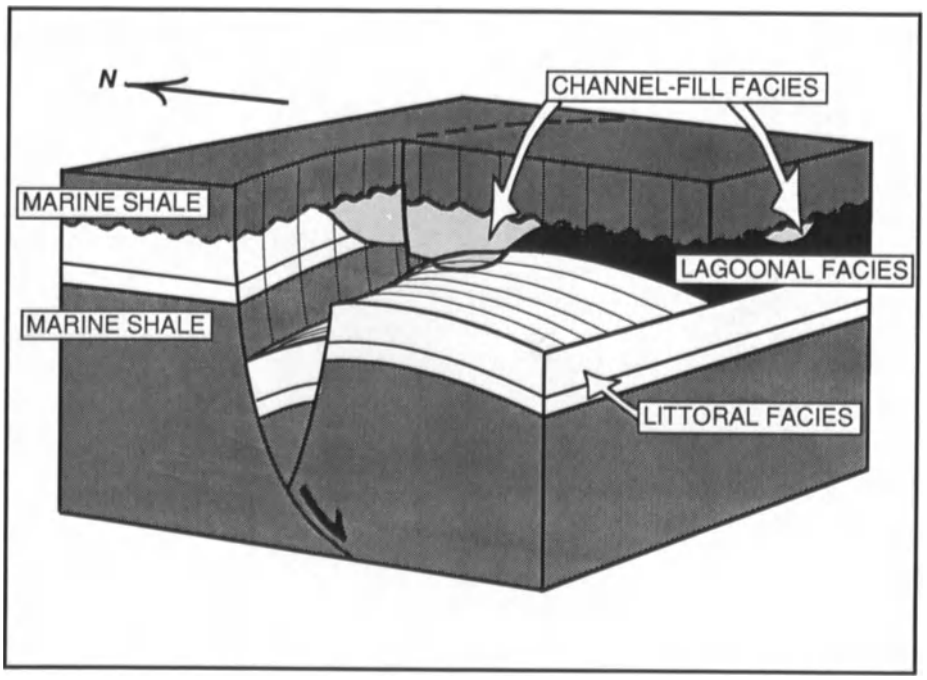

Figure 6.12. Sketch (not to scale) illustrating how contemporaneous growth faulting would have isolated much of the reservoir sandstone from its updip equivalents after several hundred feet of burial or less. This diagram neglects the preferential compaction effects of the shale sequences, and the expanded mudstone sequences at deposition would have further isolated the displacement across the faults. The stacking of the channel-fill facies upon the littoral sequence would have locally expanded the sandstone section, thus allowing fluid flow across the fault zone where the channel-fill sequence is present.

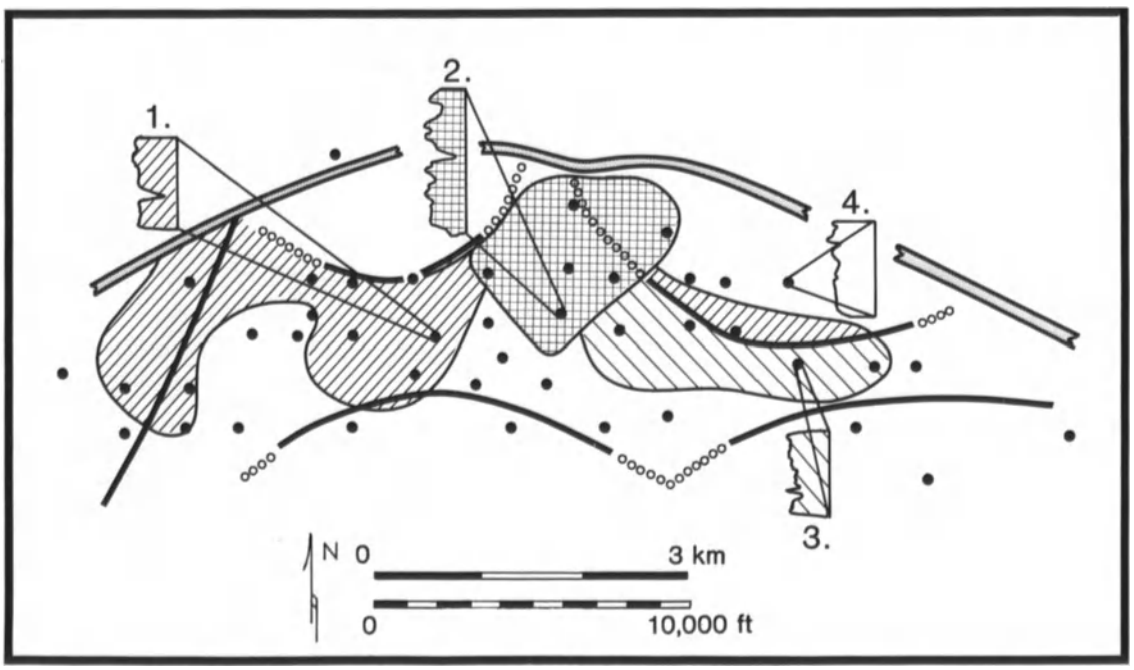

Figure 6.13. Distribution of carbonate cementation patterns as deduced from neutron density logs across Lockhart Crossing field. Neutron density logs were classified as one of four types on the basis of their general character: (1) prominent carbonate tight zone near the lower/upper littoral zone contact; (2) channel-fill facies incised into the littoral sequence, which commonly shows carbonate cementation at the incision boundary; (3) prominent carbonate tight zone modified, possibly by calcite cement dissolution as in Fig. 6.5; and (4) no prominent carbonate tight zone observed. The concentration of the carbonate along the crest of the structure and adjacent to faults suggests that carbonate precipitation was partially controlled by loss of acidity due to carbon dioxide loss across fault zones, or else by mixture of locally-derived formation waters with waters introduced via the fault planes and the channel-fill facies.

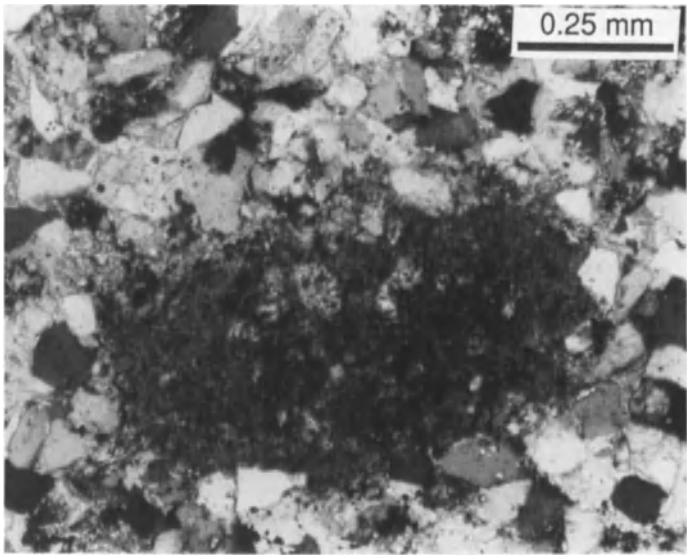

Figure 6.14. One potential source for carbonate cements consists of rip-up clasts and pellets of syndepositionally formed calcites and dolomites. This clast consists of calcite full of clay and framboidal pyrite (product of anaerobic bacteria). Because the diameter of the clast is so large, compared to the well-sorted host sandstone, it is probable that it formed in the local depositional environment. From 10,212 ft core depth, Callon Pet. No. 2 Inter. Paper Comp., Sec. 17, T6S R3E.

Intermediate Compactional Regime

With continued burial, precipitation of potassium feldspar overgrowths ceased, potassium feldspar dissolution began, quartz overgrowth precipitation began, and carbonate cementation accelerated. Most of the carbonate cement is calcite and ankerite. Interrelations between the two are complex, suggesting there were probably several periods of carbonate precipitation and later dissolution or recrystallization. Isotopes and petrology suggest that most of the calcite reached its final form at temperatures of 60°C (Johansen and Strickler, 1987). This would have been a depth of about 5,000 ft (1500 m), if it is assumed that geothermal gradients were relatively constant through the Tertiary, and subsurface waters were isotopically similar to modern waters at equivalent depths. It is useful to think of the origins and distribution of the carbonate cements in terms of (1) sources of cations and carbonate anions, (2) mechanisms for mobilizing the cations and anions in subsurface waters, and (3) mechanisms for precipitation of the carbonate.

Sources of carbonate cations and anions were abundant at Lockhart Crossing. These included the abundant detrital marine shells in the underlying marine mudstones and the

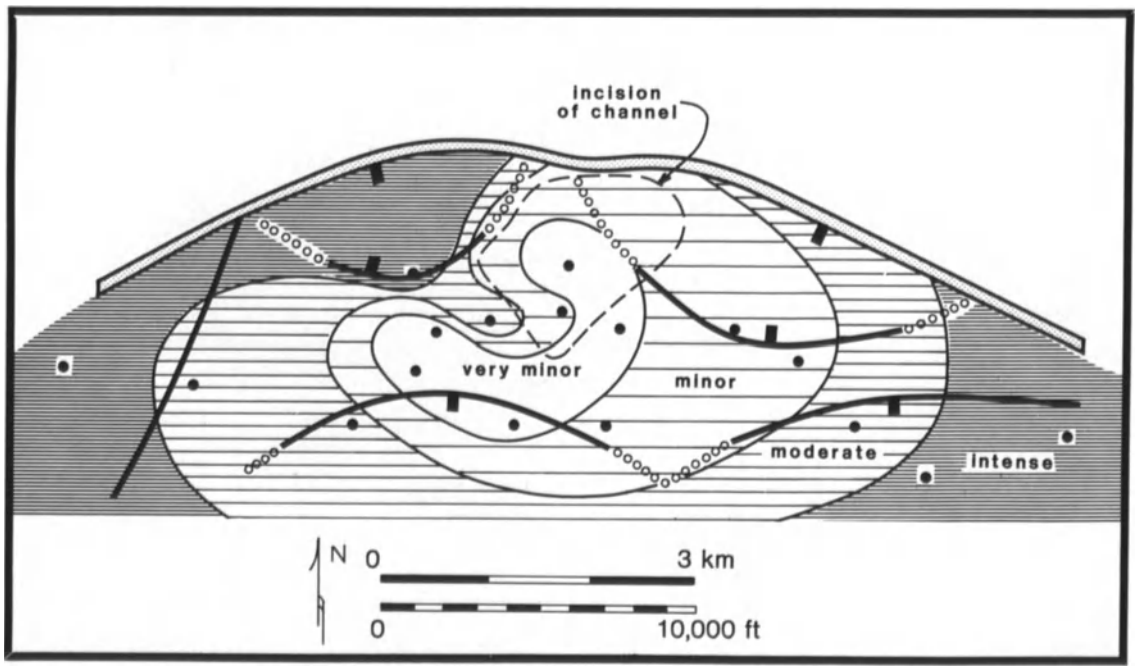

Figure 6.15. Distribution of early diagenetic, mostly concretionary pyrite in 17 cores from Lockhart Crossing field. Superimposed are traces of faults. These concretionary pyrites formed in anoxic, sulfate-rich waters by bacterial processes. This distribution could reflect either the relative abundance of dissolved iron or of dissolved sulfate in the early pore waters. Because iron is ubiquitous in most siliciclastic sediments, this distribution suggests that marine-derived, sulfate-rich waters dominated the margins of the field, while meteoric, sulfate-poor waters dominated the crest of the structure, near the incision of the channel-fill facies. Meteoric waters must have flushed the littoral sandstone soon after deposition through the channel incision and/or the channel-fill facies.

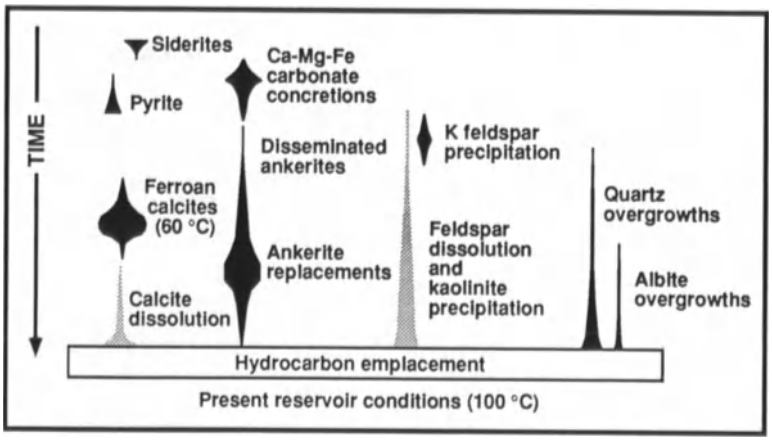

Figure 6.16. Relative timing of major chemical diagenetic events. Physical compaction has not been incorporated into this diagram. Relative timing and temperatures for carbonate diagenesis are from Johansen, Strickler, and Ferrell (unpublished data).

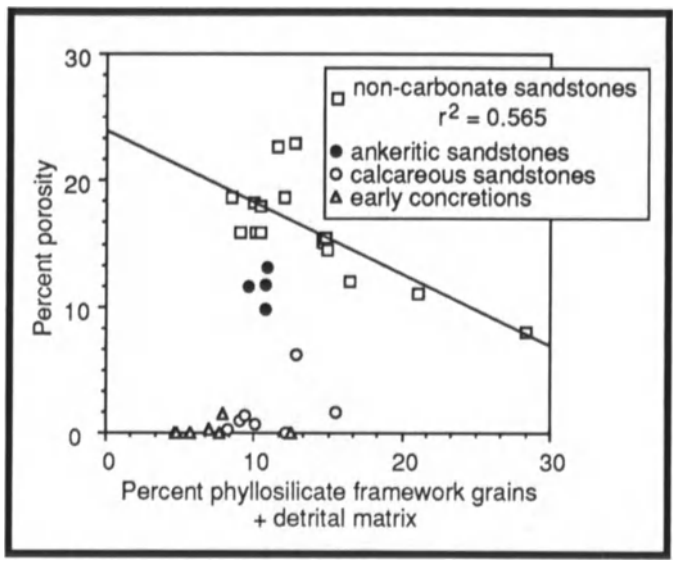

Figure 6.17. Porosity of non-carbonate-cemented sandstones is partially a function of the amount of glauconite, clay clasts, and detrital matrix in the sandstone. These components are strongly controlled by depositional facies. Results are based upon point counts of 35 thin sections with apparent mean grain diameters between 3.0 and 3.5 phi, all from the littoral facies. Data are tabulated in Johansen (1987).

lower portion of the littoral facies, and the early diagenetic siderites, ankerites, and calcites that were discussed above. Calcium may also have been contributed by feldspar dissolution.

The mechanisms for carbonate mobilization in the intermediate compactional regime are not fully known. It has been shown for several Gulf Coast Tertiary units that some shales lose carbonate during diagenesis (Hower et al., 1976; Loucks et al., 1981), and the presence of shell impressions, with little remaining shell material, in the marine shales surrounding the Lockhart Crossing reservoir suggests that similar processes acted here, too. Acids evidently are generated in many shale sequences in the intermediate compactional regime, and these acids dissolve and mobilize the carbonate, although it is not certain whether these acids are organic acids derived of organic matter (Surdam et al., 1984) or acids released by clay diagenetic reactions (Lundegard and Land, 1986) Whatever their origins, acids dissolved fossil detritus and early diagenetic carbonates within the shales and adjacent sandstones, and compaction expulsed these carbonate-rich waters into the sandstones.

Once in the sandstones, any of several poorly understood processes caused the carbonate to precipitate. Potential causes of precipitation include the loss of acidity due to degassing of dissolved CO_2, loss of acidity due to consumption of hydrogen ions by framework grain dissolution, or loss of acidity due to destruction of organic acid anions (Surdam, et al., 1984; Siebert et al., 1984; Lundegard and Land, 1986). *Where* in the sandstones a carbonate is precipitated is of great interest to the reservoir geologist, but few detailed studies have investigated this. The data presented here allow for a qualitative assessment of the current debate on the mechanisms of carbonate cementation and also present a model for use in understanding carbonate cementation in similar reservoirs.

The distribution of carbonate cement at Lockhart Crossing is most clearly understood in the context of the hydrology (Johansen, 1988). There were basically two hydrologic systems present in the field at the time of carbonate precipitation. One system was a relatively stagnant system that occupied the marine mudstone sequences. Although most shale compaction would have been completed by this time (Galloway, 1984), small amounts of fluid would continue to be expulsed, and this fluid would have been charged with organic acids and dissolved carbonates. This shale-water regime of acidity extended into the low-permeability, calcareous, offshore marine subunit of the lower littoral facies (Fig. 6.18). The second hydrologic regime was a dynamic system with regional groundwater flow; it consisted of sand-

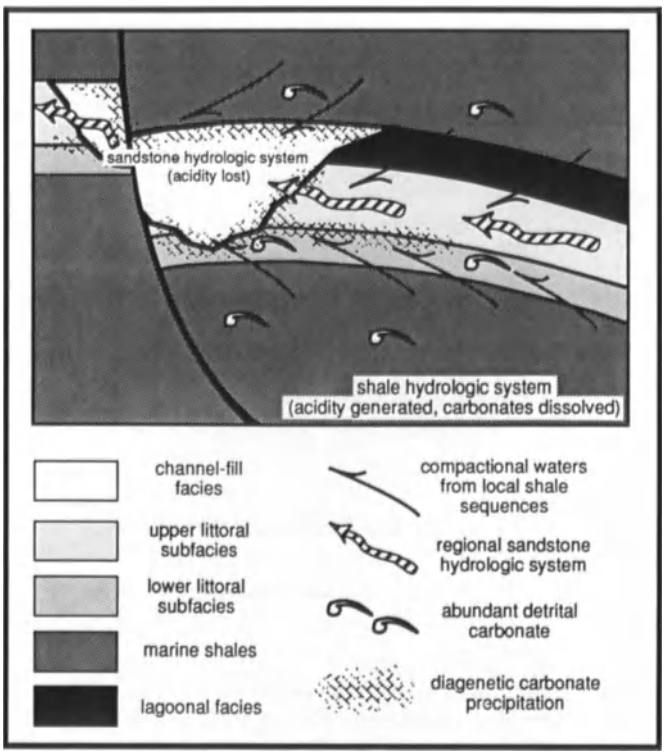

Figure 6.18. A model for the precipitation of carbonate cement in Lockhart Crossing field. Carbonate source is detrital carbonates in the marine shales and the lower littoral sequence. It is dissolved by acidic waters that are produced in the shale sequences during their diagenesis, and these waters gradually are expulsed (small arrows). The shale waters mix with less acidic waters in the sandstones that are part of regional groundwater flow systems (large arrows). These regional groundwater systems are less acidic, due to the loss of CO_2 from the regional groundwater system and also due to other acid-consuming processes in the sandstones. The carbonate is concentrated at facies boundaries that are major discontinuities in permeability. Note that carbonate cement is not plentiful near the contact with the upper sandstone boundary, possibly because the overlying brackish-water shales contained little original carbonate debris. However, when the channel-fill facies is immediately overlain by transgressive marine mudstones, carbonate stringers may be present.

stones with good permeabilites and lateral continuity. The shoreface sequence and the channel-fill sequence are relatively more permeable, and they were in hydrologic continuity with strata updip of the growth-fault zone whenever movement on the fault juxtaposed them against sandstones in the upthrown block. Waters in this regional sandstone system were less acidic than waters in the shale-dominated system, due to the acid-destroying mechanisms discussed above.

Carbonates precipitated at the boundary of these two hydrologic systems (Fig. 6.18). This boundary was not constant. At times, it was the boundary between the offshore marine and shoreface sequence, and at times, it moved to the boundary between the channel-fill and littoral sequence; the relative position at any time probably depended on the relative permeability of the units, the location of any pre-existing carbonate cemented zones, rates of regional groundwater flow, rates of CO_2 loss, rates of acid generation and carbonate dissolution in the mudstones, rates of acid destruction in the sandstone hydrologic regime, and rates of shale-water expulsion. The final distribution of carbonate reflects major hydrologic subunits of the reservoir sandstone (Fig. 6.18), and also proximity to the channel incision facies and the post-Wilcox fault, suggesting that both may have controlled the loss of CO_2 gas from the reservoir.

It is clear from the distribution of carbonate in the reservoir (Figs. 6.6, 6.13, and 6.17) that carbonate precipitation is not solely a function of proximity to a sand/shale contact, nor is it solely related to sandstone permeability or to proximity to faults. Little carbonate is present in the relatively permeable sandstones at the top of the littoral sandstone. This reflects the dearth of detrital calcium carbonate in the brackish-water lagoonal facies and the upper portions of the littoral facies. Carbonate precipitation is common at the contact between the upper and lower littoral subfacies, at an abrupt permeability change related to depositional facies. This in part reflects the abundance of detrital calcium carbonate in this portion of the stratigraphic section, and in part reflects the control of permeability on the hydrologic regime boundary. Once carbonate precipitation began, the resultant porosity loss would have accentuated the abruptness of this hydrologic boundary. The lateral distribution of the carbonate emphasizes the importance of the fault zones, although it is not clear whether this reflects the loss of CO_2 upsection along fault zones, or changes in the partial pressure of CO_2 as waters move across fault zones, or the abrupt mixing of waters from two different fault blocks.

Late Compactional Regime

Diagenetic alteration continued with increasingly deep burial. The non-carbonate-cemented sandstones have much better quartz overgrowths than the calcite-cemented intervals, suggesting that quartz overgrowths continued to develop after calcite precipitation ceased. Non-calcite-cemented sandstones also have less feldspar, documenting that feldspar dissolution continued. Incipient albite overgrowths are present in the sandstones, but they are volumetrically a very minor phase. Some diagenetic illites are present, and possibly some diagenetic chlorites, but they are minor compared to the abundant chlorite cements present in delta-front Wilcox sandstones of other Louisiana fields (LeMoine and Moslow, 1987). This may reflect either a lack of detrital clay and iron oxide cutins in the Lockhart

Table 6.1. Feldspar abundance and known lost feldspar, normalized to quartz, littoral depositional facies

Diagenetic Facies	Present ratio feldspar / feldspar + quartz	Present feldspar / quartz	Known missing feldspar / quartz	Known original feldspar / quartz	Oversized pores / quartz	Known % of feldspar lost
Silica cement n = 16	0.285 ± 0.037	0.403 ± 0.073	0.078 ± 0.035	0.481 ± 0.093	0.083 ± 0.057	16%
Concretions n = 7	0.278 ± 0.015	0.386 ± 0.029	0.020 ± 0.018	0.406 ± 0.031	None	5%
Calcite cement n = 7	0.305 ± 0.024	0.441 ± 0.052	0.030 ± 0.037	0.471 ± 0.072	0.007 ± 0.013	6%
Ankerite cement n = 4	0.287 ± 0.036	0.406 ± 0.072	0.133 ± 0.065	0.539 ± 0.030	0.042 ± 0.020	25%

Crossing sandstones at deposition, due to their abrasive removal by littoral processes, or that the abundance of carbonate in the Lockhart Crossing reservoir kept most of the iron and magnesium tied up as carbonate species.

Very late ankerites aggressively replace carbonates and feldspars in some places, and secondary porosity after calcite cement is present. The degree of calcite dissolution is difficult to quantify. The vertical distribution of ankerite, calcite, and porosity in the M. I. Stewart well at the littoral subfacies boundary (Fig. 6.6), coupled with carbonate replacement and dissolution textures observed with optical and scanning electron microscopes, suggests a three-fold history of events at that contact: (1) calcite and ankerite precipitated; (2) a late ankerite began to replace calcite; and (3) calcite incompletely dissolved, leaving a thin zone of anomolously high porosity. It is not known if calcite dissolution contributed to the anomolously high porosities at this contact in three adjacent wells (Fig. 6.13), and there is no strong evidence for volumetrically significant calcite cement dissolution elsewhere in the reservoir sandstone.

Generation of secondary porosity by the dissolution of feldspar occurred throughout the compactional history of sediment, but accelerated in the higher-temperature environments of later burial. The relative importance of feldspar dissolution for both the production of significant secondary porosity and as a source of dissolved cations for other cements is still debated (Milliken et al., 1989). Relevant statistics on the question, derived from detailed point counts of Lockhart Crossing sandstones, are presented in Table 6.1. Table 6.1 is based on 300 points per slide of 34 thin sections from littoral-sequence sandstones with apparent mean grain sizes of between 3.0 and 3.5 phi (data from Johansen, 1987). Monocrystalline feldspar grains and feldspar crystals larger than 30 μm within rock fragments were included in this tabulation. Generally speaking, the present ratios of feldspar to quartz for the different diagenetic phases are not statistically different at a 90% confidence level. Indeed, the early-formed carbonate concretions, which might have preserved feldspars from later dissolution, are as depleted in feldspar as the other sandstones. It can be texturally demonstrated that between 5% and 25% of the feldspar volume has dissolved. If all the oversized pores are assumed to have once contained feldspars, then a maximum estimate of 30% loss of original feldspar is obtained. If compaction processes destroyed oversized pores that formed after feldspar, as suggested by Milliken et al. (1989), then more feldspar may have been present. However, this is difficult to reconcile with the relatively constant feldspar/quartz ratios in all diagenetic facies, especially the early concretions.

Summary of Diagenetic Modification of the Reservoir Sandstone

Present porosities for non-carbonate cemented, littoral, very fine-grained sandstones are estimated by point counts to be about 16% (Fig. 6.19). Most porosity loss was due to compactional processes, and the number of labile fragments in the sandstone had a measurable effect on the final porosity (Fig. 6.17). Amazingly, the volume of visible secondary porosity in the littoral facies is equal to the volume of primary porosity lost to cementation (Fig. 6.19), although the mineral phases present are different. The littoral sandstones appear to have lost potassium, sodium, aluminum, and silicon; and appear to have gained calcium, iron, magnesium, carbonate, and sulfide. Strickler (1988) documented large volumes of kaolinite present in some sandstones of the channel-fill facies (Fig. 6.10); this may account for the missing alumino-silicate. Some of the missing silica might also be present in unrecognized quartz overgrowths. Potassium may have gone into detrital phyllite components of these sands, which probably lost potassium during weathering prior to deposition. Much of the apparent gain in iron and sulfide is due to abundant syndepositional and early diagenetic pyrite in the Lockhart

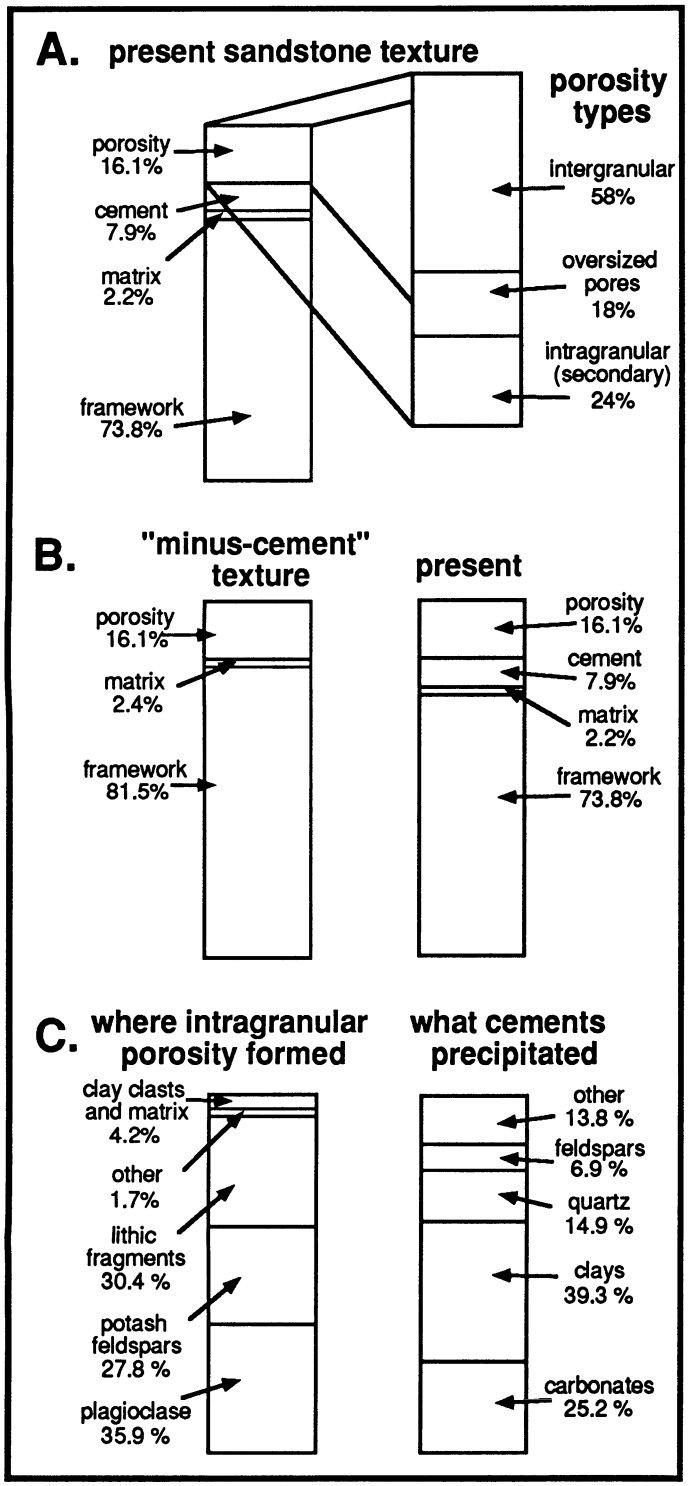

Figure 6.19. Present fabric of the littoral sandstones. All figures are based on detailed point counts of 16 littoral-facies sandstones that were not tight with carbonate cement and have apparent grain sizes between 3.0 and 3.5 phi (Johansen, 1987). A. The average F-M-C-P ratio (McBride, 1977) and the recognized porosity types. B. If the readily apparent effects of diagenesis are ignored (i.e., intragranular porosity and cements), then a "pre-diagenesis" fabric for the sandstones can be estimated. This "pre-diagenesis" fabric has a very low porosity compared to deposited sandstones because the effects of mechanical compaction are ignored. This method also ignores all grains that dissolved totally, leaving no trace. The "pre-diagenesis" porosity equals the "present" porosity, implying that the volume of porosity lost to the precipitation of cement equals the volume of dissolution porosity. C. A comparison of known secondary porosity to the cements. The "other" column in the intragranular porosity is porosity in shells, organic matter, and heavy minerals. The "other" column in the cements is mostly pyrite. Even ignoring the sand grains that dissolved totally, it appears that the sands have lost some alumino-silicate and gained carbonate and pyrite.

Crossing reservoir, and this reflects the relatively long periods of time during which these littoral/lower coastal plain sands interacted with lower coastal-plain surface waters. Gains in calcium, magnesium, iron, and carbonate also reflect the early addition of materials from lower coastal-plain surface waters, and probably the addition of some components from the shales.

Zones tight with carbonate cement are volumetrically minor in Lockhart Crossing field, but could interfere with secondary recovery. They are at facies boundaries, between sandstone units with markedly different permeabilities. Although ankerites and siderites are sparse throughout the sandstones and are concentrated into small (1 to 3 ft, or 1/3 to 1 m) zones, the volume of iron and magnesium in these carbonates is substantial; had it been spread through the reservoir as pore-lining chlorite, serious permeability losses would have resulted.

Emplacement of Oil

The emplacement of oil appears to be a late event, because no systematic differences in diagenesis between the oil and water zones were detected. The degree of feldspar dissolution and quartz overgrowths is visually the same above and below the oil/water contact. The oil/water contact approximates the facies boundary between the offshore marine and shoreface units in much of the field, and so is approximately at the zone of carbonate cementation. However, this reflects increased capillary forces in the lower sandstones of the littoral sequence (Self and others, 1986). The carbonate cement horizon is not directly related to the oil/water contact, because in some wells, carbonate is well above the oil/water contact, while in others, carbonate is well below the contact.

The origin of oil in the Wilcox of Louisiana is a subject of ongoing debate. Sassen (1988) argues from geochemical evidence that the oil could be derived from Lower Tertiary or uppermost Mesozoic source units, which are now in the zone of oil generation down-dip of Lockhart Crossing. This model requires that oil migration had a large component of lateral flow. Bissada and others (1987) argue that the oil

sources were deeper in the Mesozoic section, and oil migration was largely vertical. Any successful model will have to explain an apparently late timing for oil emplacement in Lockhart Crossing Field.

Conclusions

For the bulk of the reservoir sandstone, the final porosity and permeability were determined by the depositional system. The very fine-grained, matrix-enriched, shale-clast-bearing and glauconitic sandstones of the offshore marine subfacies have the poorest permeabilities because of their very fine grain size, matrix content, and the ductile deformation during compaction of clay clasts and glauconite (cf., Beard and Weyl, 1973; McBride, 1977). The upward-coarsening shoreface portion of the littoral sequence is generally homogeneous in its three-dimensional distribution of porosity and permeability. Compaction has reduced porosity; the amount of porosity that is clearly secondary after framework grains is about equal to the amount of porosity lost to diagenetic cements. The best porosities and permeabilities are in the medium-grained sandstones of the channel-fill facies. This facies does not have the three-dimensional homogeneity of the littoral sequences, which is a reflection of its depositional fabric. Diagenesis has accentuated this heterogeneity, because secondary porosity has preferentially increased porosity and permeability in the cleaner sandstones, and precipitation of kaolinite has occluded pore spaces and throats in the adjacent shale-clast conglomeratic sandstones.

The distribution of carbonate cements in this reservoir is a useful model for similar reservoirs that are compartmentalized by carbonates. Carbonates precipitated at depositional-unit boundaries in close proximity to a post-depositional fault and along the crest of the trapping roll-over structure. This might reflect three different, fundamental controls on the carbonate cement:

(1) Carbonate cements are generally localized near a source for carbonates, in this case the underlying marine shales and the off-shore marine sandstones; carbonates other than small amounts of siderite are generally not abundant when the adjacent shale unit is nonmarine.

(2) Most carbonate cements are localized at major hydrologic boundaries that separate highly permeable, laterally connected sandstone conduits from less permeable sandstones that are charged with porewaters expulsed from marine shales. The actual boundary probably fluctuates through time, but generally coincides with a facies boundary that juxtapositions low-permeability sandstones (at present typically $\leq$10 md) and more permeable sandstones (at present typically 20–100 md).

(3) Carbonate is best developed near the crest of the trapping structure near two features that might have served as escape conduits for CO_2 gas or as important conduits for regional hydrologic flow systems. One of these features is the highly permeable channel-fill facies, which would have served as the best conduit for up-dip migration of fluids through much of the reservoir's history. The second feature is a fault that post-dates syndepositional normal fault structures.

Acknowledgments

This work was completed while the author was employed by the Basin Research Institute at Louisiana State University. Access to core material, electric logs, base maps, and water analyses was provided by Amoco Production Company. Charles Smith provided supplementary logs and maps. The depositional systems interpretations were influenced by lively discussions with Tom Moslow, Phil Lowry, Bob Tye, and Rowdy Lemoine. Bill Wade provided education in electric-log analysis. Geochemical concepts were influenced by long discussion with Mike Strickler, Tim Jackson, Hans Machel, and Kitty Milliken.

References

Beard, D.C., and Weyl, P.K., 1973, Influence of texture on porosity and permeability of unconsolidated sand: Amer. Assoc. Pet. Geol. Bull., v. 57, p. 349–369.

Bethke, C.M., Harrison, W.J., Upson, C., and Altaner, S.P., 1987, Supercomputer analysis of sedimentary basins: Science, v. 239, p. 261–267.

Berner, R.A., 1980, Early Diagenesis: Princeton, NJ, Princeton Univ. Press, 241 p.

Bissada, K.K., Katz, B.J., Barnicle, S.C., and Schunk, D.J., 1987, Origins of hydrocarbons in Gulf of Mexico Basin: A reappraisal [abs.]: Amer. Assoc. Petrol. Geol. Bull., v. 72, p. 163.

Curtis, C.D., and Coleman, M.L., 1986, Controls on the precipitation of early diagenetic calcite, dolomite and siderite concretions in complex depositional sequences, *in* Gautier, D.L., ed., Roles of organic matter in sediment diagenesis: S.E.P.M. Spec. Publ. 38, p. 24–33.

Dury, G.H., 1971, Relict deep weathering and duricrusting in relation to the paleoenvironments of middle latitudes: Geograph. Jour., v. 137 p. 511–522.

Folk, R.L., 1974, Petrology of sedimentary rocks: Austin, Texas, Hemphill, 182 p.

Galloway, W.E., 1984, Hydrologic regimes of sandstone diagenesis, *in* McDonald, D.A., and Surdam, R.C., eds., Clastic diagenesis: Amer. Assoc. Petrol. Geol. Mem. 37, p. 3–13.

Galloway, W.E., and Kaiser, W.R., 1980, Catahoula Formation of the Texas coastal plain: Origin, geochemical evolution, and characteristics of uranium deposits: Tex. Bur. Econ. Geol. Rept. Invest. 100, 81 p.

Hanor, J.S., Bailey, J.E., Rogers, M.C., and Milner, L.R., 1986, Regional variations in physical and chemical properties of south Louisiana oil field brines: Trans. Gulf Coast Assoc. Geol. Soc., v. 36, p. 144–149.

Hovland, M., Talbot, M.R, Qvale, H., Olaussen, S., and Aasberg, L.,

1987, Methane-related carbonate cements in pockmarks of the North Sea: Jour. Sed. Petrol., v. 57, p. 881–892.

Hower, J., Eslinger, E.V., Hower, M.E., and Perry, E.A., 1976, Mechanism of burial metamorphism of argillaceous secliment: 1. Mineralogical and chemical evidence: Geol. Soc. Amer. Bull., 87, p. 725–737.

Johansen, S.J., 1987, Summaries of point coint data, microprobe data, and isotope data, Lockhart Crossing Reservoir, Livingston Parish, Louisiana: Basin Research Institute, Louisiana State University, unpublished open-file report.

Johansen, S.J., 1988, Facies and structural controls on carbonate cementation in a siliciclastic reservoir [abs.]: Amer. Assoc. Petr. Geol. Bull., v. 72, p. 201–202.

Johansen, S.J., and Strickler, M.E., 1987, Petrography of the Lockhart Crossing Field (upper Wilcox), Livingston Parish, Louisiana [abs.]: S.E.P.M. Annual Midyear Meeting Abstracts, v. 4, p. 39.

Judson, S., 1975, Evolution of Appalachian topography, *in* Melhorn, W.N. and Flemal, R.C. eds., Theories of landform development: London, George Allen and Unwin, p. 29–44.

Kantorowicz, J.D., Bryant, I.D., and Dawans, J.M., 1987, Controls on the geometry and distribution of carbonate cements in Jurassic sandstones: Bridport Sands, southern England and Viking Group, Troll Field, Norway: Geological Society (London) Special Publication 36, p. 103–118.

Kehle, R.O., 1971, Geothermal survey of North America: 1971 annual progress report; Research Committee: Tulsa, OK, Amer. Assoc. Pet. Geol., 31 p.

Kocurko, M.J., 1986, Interaction of organic matter and crystallization of high magnesium calcite, south Louisiana, *in* Gautier, D.L., ed. Roles of organic matter in sediment diagenesis: Soc. Econ. Paleon. Miner. Spec. Publ. 38, p. 13–21.

Lemoine, R.C., and Moslow, T.F., 1987, Effects of primary sedimentary processes on reservoir quality of "deep Wilcox" (Eocene) sandstones in Fordoche field, Louisiana [abs.]: Soc. Econ. Geophys. 57th Meeting (New Orleans) Abstracts Volume, p. 284–286.

Loucks, R.G., Richmann, D.L., and Milliken, K.L., 1981, Factors controlling reservoir quality in Tertiary sandstones and their significance to geopressured geothermal production: Austin, University of Texas, Bureau of Econ. Geol., Report of Investigation No. 111, 41 p.

Lowry, P., 1987, Stratigraphic framework and sedimentary facies of a clastic shelf margin: Wilcox Group (Paleocene–Eocene), central Louisiana [Ph.D. dissertation]: Baton Rouge, Lonisiana State University, 320 p.

Lundegard, P.D., and Land, L.S., 1986, Carbon dioxide and organic acids: Their role in porosity enhancement and cementation, Paleogene of the Texas Gulf coast, *in* Gautier, D.L., ed., Roles of organic matter in sediment diagenesis: Soc. Econ. Paleon. Miner. Spec. Publ. 38, p. 129–147.

McBride, E.F., 1977, Sandstones, *in* Jonas, E.C., and McBride, E.F., eds., Diagenesis of sandstone and shale; Application to exploration for hydrocarbons: Univ. Texas at Austin Cont. Education Prog. Publ. #1, p. 1–120.

Milliken, K.L., McBride, E.F., and Land, L.S., 1989, Numerical assessment of dissolution verus replacement in the subsurface destruction of detrital feldspars, Oligocene Frio Formation, south Texas: Jour. Sed. Petrol., v. 59, p. 740–757.

Morton, R.A., and Land, L.S. 1987, Regional variations in formation water chemistry, Frio Formation (Oligocene) Texas Gulf Coast: Amer. Assoc. Petro. Geol., v. 71, p. 191–206.

Moslow, T.F., 1984, Depositional models of shelf and shoreline sandstones: Amer. Assoc. Petrol. Geol. Cont. Ed. Course Notes #27,102 p.

Pryor, W.A., and Glass, H.D., 1961, Cretaceous-Tertiary clay mineralogy of the upper Mississippi embayment: Jour. Sed. Pet., v. 31 p. 38–51.

Sassen, R., 1988, Origin of crude oil in eastern Gulf Coast; Upper Jurassic, Upper Cretaceous, and Lower Tertiary source rocks [abs.]: Amer. Assoc. Petrol. Geol. Bull., v. 72, p. 243–244.

Self, G.A., Bread, S.Q., Rael, H.P., Stein, J.A., and Thayer, P.A., 1986, Lockhart Crossing Field: New Wilcox trend in southeastem Louisiana: Amer. Assoc. of Petrol. Geol. Bull., v. 70, p. 501–515.

Siebert, R.M., Moncure, G.K., and Lahann, R.W., 1984, A theory of framework grain dissolution in sandstones, *in* McDonald, D.A., and Surdam, R.C., eds., Clastic diagenesis: Amer. Assoc. Petrol. Geol. Mem. 37, p. 163–176.

Sigleo, W., and Reinhardt, J., 1988, Paleosols from some Cretaceous environments in the southeastern United States: Geol. Soc. Amer. Spec. Paper 216, p. 123–142.

Stenzel, H.B., 1940, The Yegua problem: Austin, University of Texas Publ. 3945, p. 847–910.

Strickler, M.E., 1988, Clay mineral diagenesis in the lower Eocene Wilcox, Lockhart Crossing Field, Livingston Parish, Louisiana [MS thesis]: Baton Rouge, Lousiana State University, 190 p.

Strickler, M.E., and Ferrell, R.E., Jr., 1990, Fe substitution for Al in glauconite with increasing diagenesis in the first Wilcox Ss (lower Eocene), Livingston Parish, Louisiana: Clay and Clay Minerals, v. 38, p. 69–76.

Strickler, M.E., and Ferrell, R.E., Jr., 1992, Provenance: The dominant factor in clay mineralogy of the upper Wilcox Formation: Proceedings IXth International Clay Conference (Strasbourg), August 28–September 2, 1989 (in press).

Surdam, R.C., Boese, S.W., and Crossey, L.J., 1984, The chemistry of secondary porosity; *in* McDonald, D.A., and Surdam, R.C., eds., Clastic diagenesis: Amer. Assoc. Petrol. Geol. Mem. 37, p. 127–149.

Todd, T.W., and Folk, R.L., 1957, Basal Claiborne of Texas, record of Appalachian tectonism during Eocene: Am. Assoc. Petrol. Geol. Bull, v. 41, p. 2545–2566.

Winker, C.D., 1982, Cenozoic shelf margins, northwestern Gulf of Mexico basin: Gulf Coast Assoc. Geol. Soc. Trans., v. 32, p. 427–448.

CHAPTER 7

Shelf Sandstones of the Deep Wilcox Trend, Central Texas Gulf Coast

Jeffrey A. May

Introduction

The late Paleocene–early Eocene Wilcox Group represents the first major, regional clastic wedge built over and beyond the Cretaceous carbonate shelf edges along the Texas Gulf Coast. The Wilcox produces hydrocarbons along a strip paralleling the coastline from the Mississippi–Alabama state line to the Mexico border. This sequence also yields fresh water, lignite, ceramic clay, and industrial sand, and is a potential geopressured geothermal reservoir.

In Texas, shales of the Midway Group underlie Wilcox sediments, and shales and marls of the Claiborne Group cap the succession (Fig. 7.1a). The Wilcox Group ranges to 1000 ft (300 m) thick along its outcrop (Fig. 7.1b), and thickens basinward to over 10,000 ft (3000 m) within a distance of 100 mi (160 km). In the deep downdip portions, the mode of deposition provides a source of controversy. Were these Wilcox sands laid down entirely by shallow-marine processes, or was deep-water sedimentation also involved?

To interpret depositional environments within the Deep Wilcox trend, an integrated regional Wilcox study took place. Work encompassed sedimentological and petrological analysis of cores from 15 wells (May and Stonecipher, 1990; Stonecipher and May, 1990), correlation of electric-log patterns to facies, paleontologic study for bathymetric assignments, and seismic-stratigraphic interpretation. This paper documents part of this work, describing two of the three most basinward and deepest Wilcox cores along the central Texas Gulf Coast, collected from the Amerada #1 Kovar and Sun #1 Urban wells (Fig. 7.1b). The third deep core, from the Amerada #1 Talley well, is shale dominated and not included. Sedimentary processes are inferred by defining the texture, composition, physical and biogenic sedimentary structures, and bedding contacts in the cores on a bed-by-bed basis. The final depositional model is based, in part, on recognizing "genetic" stratigraphic units, and how these units are interrelated and how they changed through time (Siemers and Tillman, 1981). Genetic stratigraphic units are defined by vertical similarity and by vertical changes in depositional processes.

Regional Setting

The Gulf of Mexico is a small ocean basin, approximately 900 mi (1500 km) in diameter, bordered by continental masses (Antoine and Ewing, 1962). Perhaps preceded by an earlier basin that closed during the late Paleozoic, the present Gulf originated when the North American plate began separating from the South American and African plates in the Late Triassic. As rifting continued through late Middle or early Late Jurassic time, thick evaporites developed during intermittent advances of the sea. Carbonate sedimentation occurred along the northern and western margins of the Gulf from Late Jurassic through Cretaceous time; a change to terrigenous progradation, producing a clastic wedge up to 9 mi (15 km) thick, characterized the Tertiary and Quaternary. To the east and south, on the Florida and Yucatan platforms, carbonate deposition has persisted to the present (Salvador and Buffler, 1986).

During Wilcox deposition (late Paleocene–early Eocene), much of the Gulf Coast was a broad, flat, low-lying coastal plain (Murray and Thomas, 1945; Albach, 1979). Drainage axes of the present Gulf Coast roughly coincide with the positions of the Wilcox fluvial systems

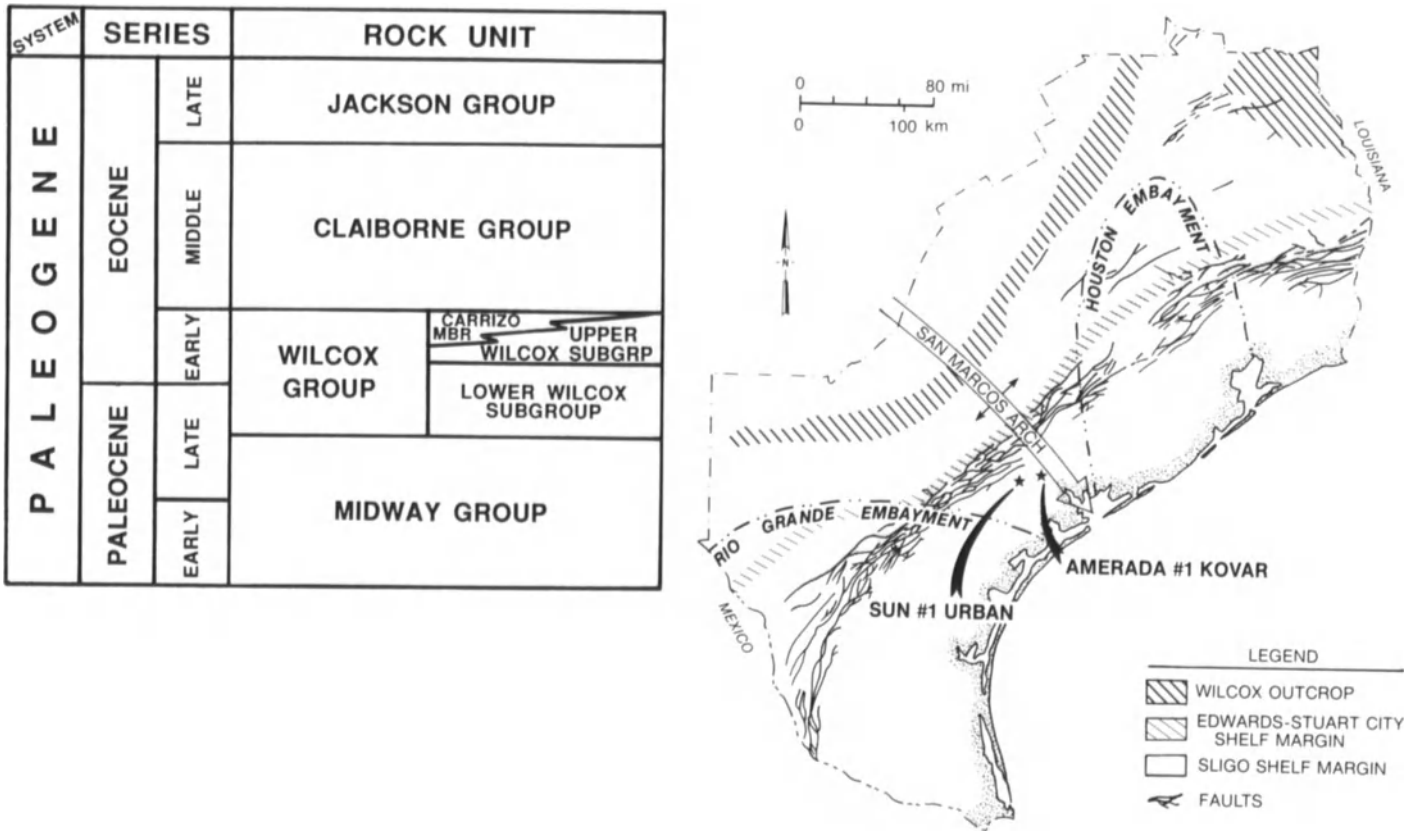

Figure 7.1. (A) Simplified stratigraphic chart for the Paleocene through early Eocene of the Texas Gulf Coast. (B) Map of the Texas Gulf Coast showing the location of the two upper Wilcox wells, Sun #1 Urban and Amerada #1 Kovar, described and interpreted for this study. Also shown are major structural features—the San Marcos Arch and regional Wilcox growth-fault trend—and the positions of the underlying Cretaceous reef tracts and the Wilcox outcrop in Texas. (Modified from Bebout et al., 1979.)

(Galloway, 1968; Tye et al., 1991). The southern Appalachian region provided detritus to the ancestral Apalachicola, Mississippi, and Sabine rivers of the northern Gulf Coast (Fig. 7.2; Murray, 1961; Mann and Thomas, 1968). The Ouachita Mountains supplanted the Appalachians as a supplier of Wilcox sediments westward, with the ancestral Brazos and Colorado rivers flowing into the upper and central Texas coast. The ancestral Rio Grande River of the lower Texas coast drained local volcanic and sedimentary sources (Fig. 7.2; Hardin, 1962; Harris, 1962; Loucks et al., 1979; Oliver, 1980). The southern Rocky Mountains were not a major source Gulf Coast sediments until late Paleogene (Mann and Thomas, 1968).

In Louisiana and Mississippi, a relatively straight northeast-trending coastline extended into the Mississippi Embayment during the late Paleocene through early Eocene (Albach, 1979). Concurrently, the large Holly Springs Delta system, fed by the ancestral Mississippi River, began filling this embayment (Galloway, 1968). The Texas coastline was much more irregular; significant deposition occurred during two major progradational phases, the lower and upper Wilcox (Fig. 7.1a; Hargis, 1985). Fluvial-dominated deltas, of a style and size similar to the Holocene Mississippi deltas, characterized the lower Wilcox "Rockdale System" along the upper Texas Gulf Coast (Fig. 7.3a). Longshore currents redistributed sand from this delta system into a strand plain to the southwest (Fisher and McGowen, 1967). In contrast, the upper Wilcox comprised numerous small, wave-dominated deltas (Fig. 7.3b; Fisher, 1969). Along the lower Texas Gulf Coast, these deltas rapidly prograded basinward, forming the shelf-edge "Rosita System" (Fig. 3b; Edwards, 1981).

Central Texas Gulf Coast: Wilcox Geology and Hydrocarbon Production

A major structural feature, the southeast-trending San Marcos Arch, bisects the central Texas Gulf Coast, separating the Houston Embayment to the northeast from the Rio Grande Embayment to the southwest (Fig. 7.1b). This structural high also separates the more oil-prone Wilcox

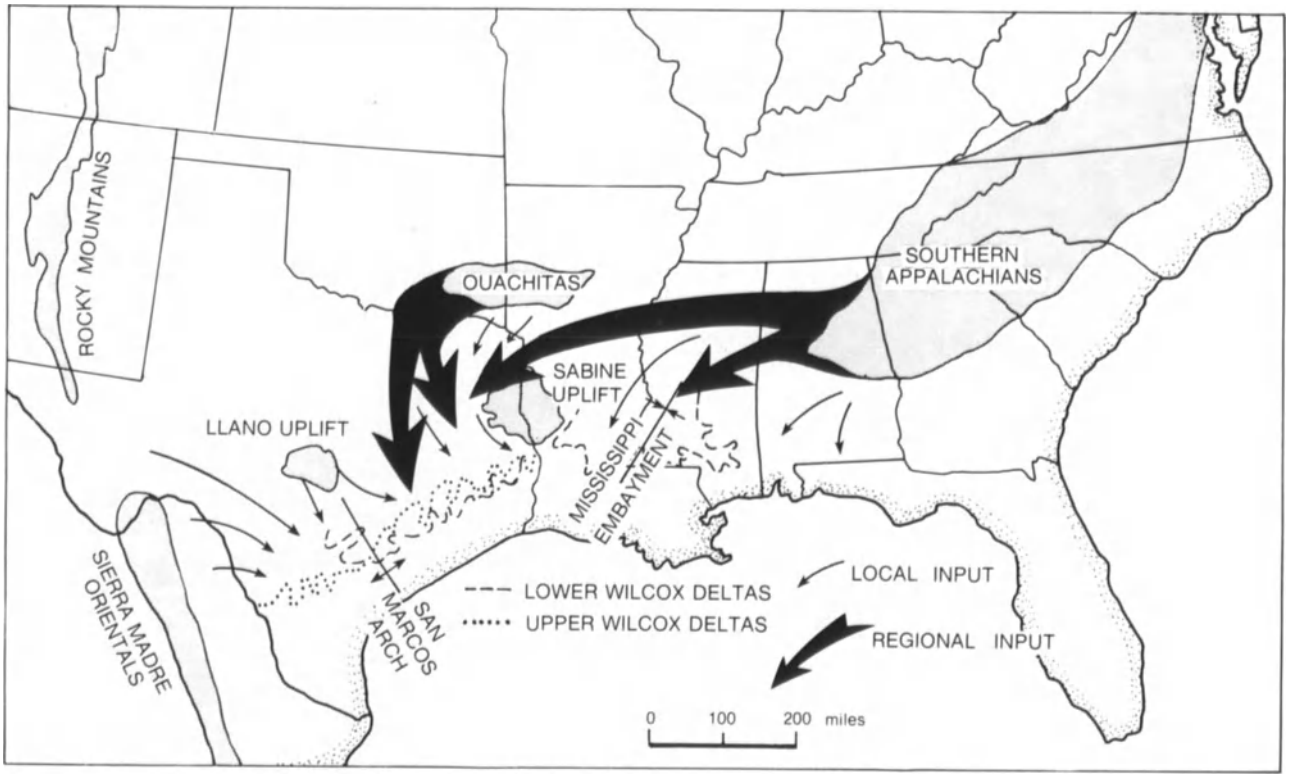

Figure 7.2. Interpretation of the regional and local source-area transport paths for the Wilcox Group of the Gulf Coast. Thickness of the source-area paths represents the relative importance of Wilcox sources (based on data from Hardin, 1962; Harris, 1962; Loucks et al., 1979; Murray, 1961; Mann and Thomas, 1968; Oliver, 1980).

province of the upper Texas region from more gas-prone Wilcox units of south Texas (Vlissides, 1964; Fisher et al., 1969).

Trending perpendicular to the San Marcos Arch and paralleling the coastline is a regional Paleogene growth-fault trend. This band of faults narrows through central Texas and expands into the Houston and Rio Grande embayments (Fig. 7.1b). The locations and stacking patterns of underlying carbonate shelf edges apparently controlled this growth-fault configuration. Along the central Texas Gulf Coast, the Late Cretaceous Edwards–Stuart City reef trend built up on top of the Early Cretaceous Sligo tract, whereas in the Houston and Rio Grande embayments, the younger Edwards–Stuart City system backstepped landward from the Sligo buildup (Fig. 7.1b). Where the Sligo formed a relatively stable and shallow platform in front of the younger carbonates, a syndepositional growth-fault zone migrated basinward during progradation of the Wilcox depocenters. In contrast, where the Cretaceous reef tracts were vertically stacked, Wilcox growth faults apparently bottomed out deeper than the Sligo shelf edge and maintained their position by continued expansion rather than stepping outward.

The dominant stratigraphic feature within the Wilcox of the central Texas Gulf Coast is a series of submarine canyons just east of the San Marcos Arch (Fig. 7.4). These include the lower Wilcox Lavaca and Smothers channels and middle Wilcox Yoakum channel (Hoyt, 1959; Vormelker, 1979; Chuber and Begeman, 1982; Galloway et al., 1989; Dingus and Galloway, 1990). The Yoakum Channel is 80 mi (130 km) long, up to 12 mi (20 km) wide, and deepens up to 3500 ft (1050 m) near the paleo-shelf edge (Galloway et al., 1989). The Lavaca Channel is much shorter and broader; it extends 12 mi (20 km) landward, is over 15 mi (25 km) wide, and about 1000 ft (300 m) deep (Chuber and Begeman, 1982). The canyon fills are dominated by mudstone and are capped by progradational shoreface and deltaic sequences.

Most of the hydrocarbon production from the central Texas Wilcox is due to trapping by growth faults, with or without anticlinal rollover. Five major Wilcox oil fields—those with reserves over 10 million barrels of oil (MMBO)—produce from the west flank of the San Marcos arch (Fig. 7.4). Falls City Field contains over 22 million barrels of recoverable oil in lower Wilcox sands; the Slick, Weigang, Cottonwood Creek South, and Helen Gohlke fields will ultimately produce over 67 MMBO total from upper Wilcox units (Galloway et al., 1983). Structural trapping is also important in major Wilcox gas fields. The Nord-

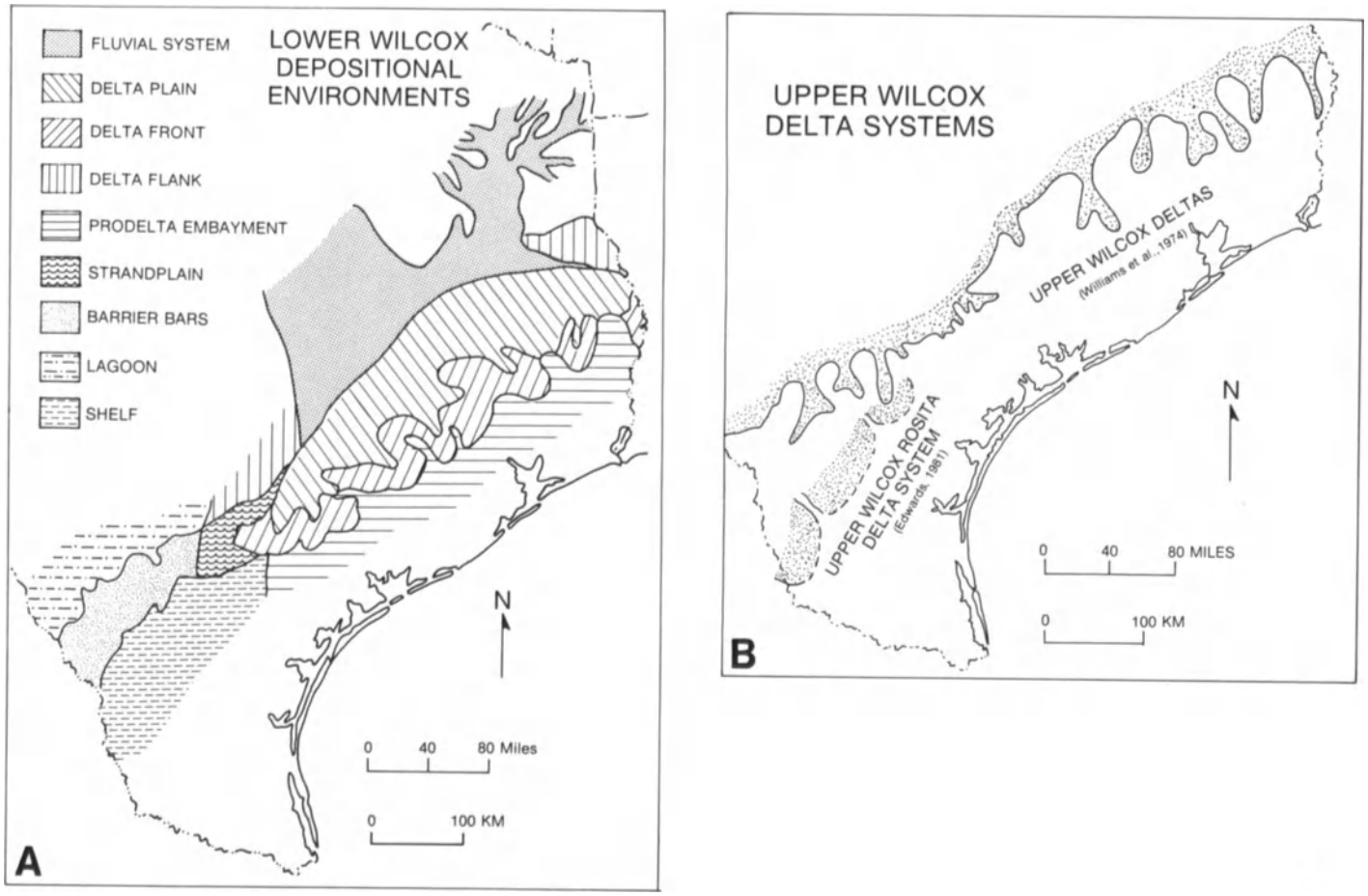

Figure 7.3. (A) Map of lower Wilcox depositional systems. (Modified from Fisher, 1969.) (B) Map of upper Wilcox depositional systems. (Williams et al., 1974; Edwards, 1981.)

heim, Provident City, and Columbus fields have each already yielded over 50 billion cubic feet of gas (BCFG) from the Wilcox, and the Sheridan Field has estimates of over 1 trillion cubic feet recoverable reserves (Fig. 7.4; Lofton, 1962; Billingsely, 1982; International Oil Scouts, 1982). Many smaller Wilcox oil and gas fields occur along this same trend (Fisher et al., 1969).

Lesser amounts of Wilcox production are associated with the subsurface submarine canyons of the central Texas area. Numerous reservoirs occur as stratigraphic traps beneath these largely shale-filled systems. Yoakum Field (Fig. 7.4) results from entrapment of gas against the Yoakum Channel margin (Hoyt, 1959; Chuber, 1986). Discovered in 1945, this field has yielded over 13 BCFG and 2 MMBO from middle Wilcox shelf sands truncated by the canyon (Chuber, 1986). More recent sub-unconformity discoveries are related to the Lavaca and Smothers canyons. Production below erosional bases of these systems occurs in the Valentine, Menking, South Hallettsville, and Kinkler fields (Fig. 7.4). Reservoir sandstones of these fields have been variously interpreted as older deltaic, barrier-bar, or turbidite-channel units; production in Kinkler Field also occurs from sandstones within the canyon fill (Berg, 1979; Chuber, 1979; Chuber and Begeman, 1982; Edwards, 1986). Kinkler Field has yielded over 8 BCFG and 100,000 barrels of condensate since its 1968 discovery (Chuber and Begeman, 1982). Valentine field, discovered in 1973, contains over 6 MMBO and almost 9 BCFG in place; approximately 1 MMBO and 6 BCFG are considered recoverable (Chuber, 1979). The smaller Menking Field is expected to yield over 300,000 barrels of oil (Chuber, 1979). The 1976 discovery well of South Hallettsville Field flowed at almost 24 MMCFG per day and produced over 2 BCFG within two years; more than 15 wells are now productive (Switek et al., 1979).

The Lavaca system also contains many newly discovered reservoirs within the updip part of the canyon fill. These occur as combination structural-stratigraphic traps (Chuber and Howell, 1989). The productive sandstones probably represent distributary channels of deltaic complexes that

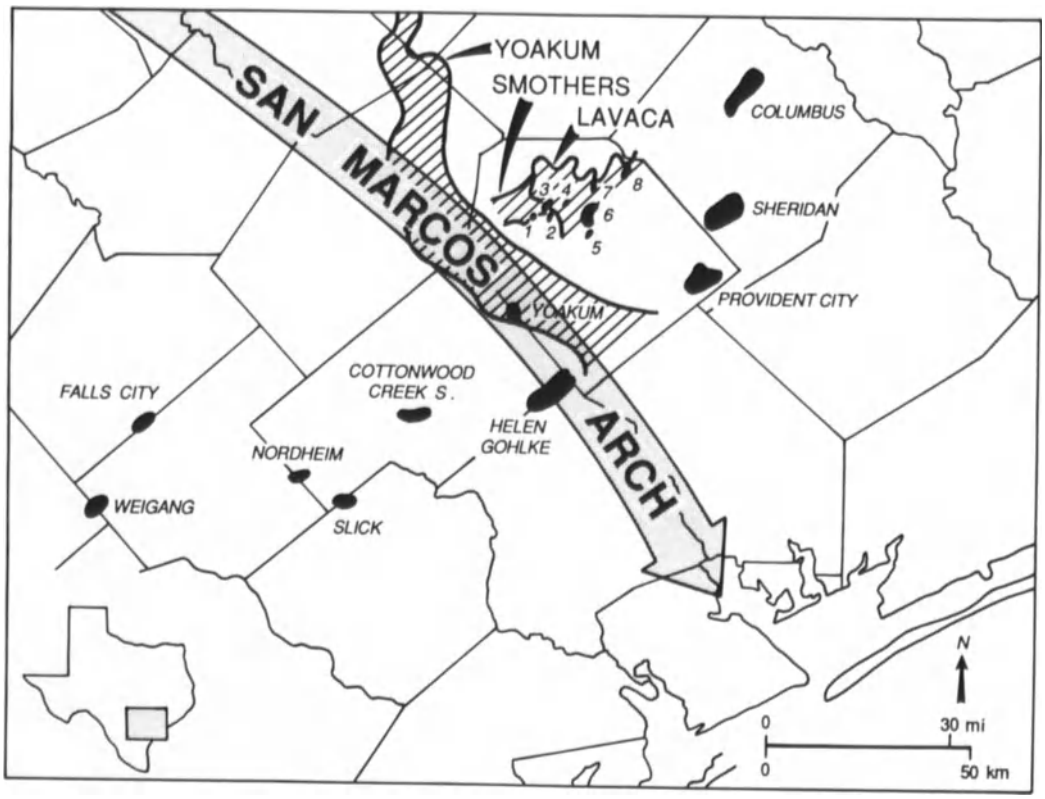

Figure 7.4. Major Wilcox oil and gas fields of the central Texas Gulf Coast. Outlined in bold lines are the Wilcox-aged submarine canyons: Lavaca, Smothers, and Yoakum channels. Smaller fields associated with the Lavaca and Smothers systems are numbered: 1. Menking; 2. Mule Springs; 3. Valentine; 4. Campbell Creek; 5. Good Hope; 6. South Halletsville, Halletsville East, and Halletsville Burns; 7. Charlie Daubert North; and 8. Kinkler.

prograded into and filled the canyon head (Allen and Howell, 1987; Chuber and Howell, 1989). These reservoirs encompass the Hallettsville East, Halletsville Burns, Good Hope, and Campbell Creek fields (Fig. 7.4). Two older fields, Mule Springs and Charlie Daubert North (Fig. 7.4), apparently produce from similar but separate distributary channels within Lavaca Canyon (Chuber and Howell, 1989). Altogether, these six fields have yielded almost 1 million barrels of oil or condensate and over 10 billion cubic feet of gas (Chuber and Howell, 1989). The most prolific well is the Howell #4 Golsch, the discovery well for Hallettsville East, which has produced over 3.8 billion cubic feet of gas and 150,000 barrels of condensate since late 1983 (Chuber and Howell, 1989).

Submarine-Fan Reservoirs?

Wilcox submarine canyons not only have provided for subunconformity and updip canyon-fill hydrocarbon plays, but have also offered the potential for associated downdip submarine-fan hydrocarbon reservoirs. A great amount of sand was presumably removed by canyon erosion and flushed basinward. Halbouty (1969) estimated that 75 cubic miles, or 250,000,000 acre-feet, of sediment has been redeposited downdip of the Yoakum Channel. This concept—submarine fans located basinward of the canyon mouths—spurred deep drilling in front of the Yoakum system. Two wells drilled at its mouth in Jackson County (Fig. 7.5) attempted to find sands eroded from the shelf and redeposited downdip. However, neither the Humble #1 Robinson, abandoned at 17,030 ft (5192 m), nor the Halbouty et al. #1-B Hollingsworth, drilled to 18,030 ft (5497 m), encountered Wilcox sands (Vormelker, 1979).

In contrast, thick intervals of thin Wilcox sandstones intercalated with mudstones are present in the three wells south of Yoakum Channel in Victoria County (Fig. 7.5). The Amerada #1 Talley was drilled to 23,855 ft (7273 m) in 1964. The intervals from 14,375 to 14,380 ft (4382.6–4384.1 m) and 14,575 to 14,580 ft (4443.6–4445.1 m) were acidized and fractured; the well initially flowed dry gas, then stopped flowing, and was abandoned after the casing collapsed (Vormelker, 1979). The Sun #1 Urban and Amerada #1 Kovar wells, drilled, respectively, in late 1964 to 17,467 ft (5325 m) and in 1965 to 15,803 ft (4818 m), were both dry and subsequently abandoned.

Various workers (e.g., Vormelker, 1979) have surmised that the sandstones in these deep Wilcox wells of Victoria County represent the distal portion of a submarine fan. Such an interpretation, though, requires the fan to be extremely areally restricted and to have formed at a sharp right-angle bend off the Yoakum Channel mouth (Fig. 7.5).

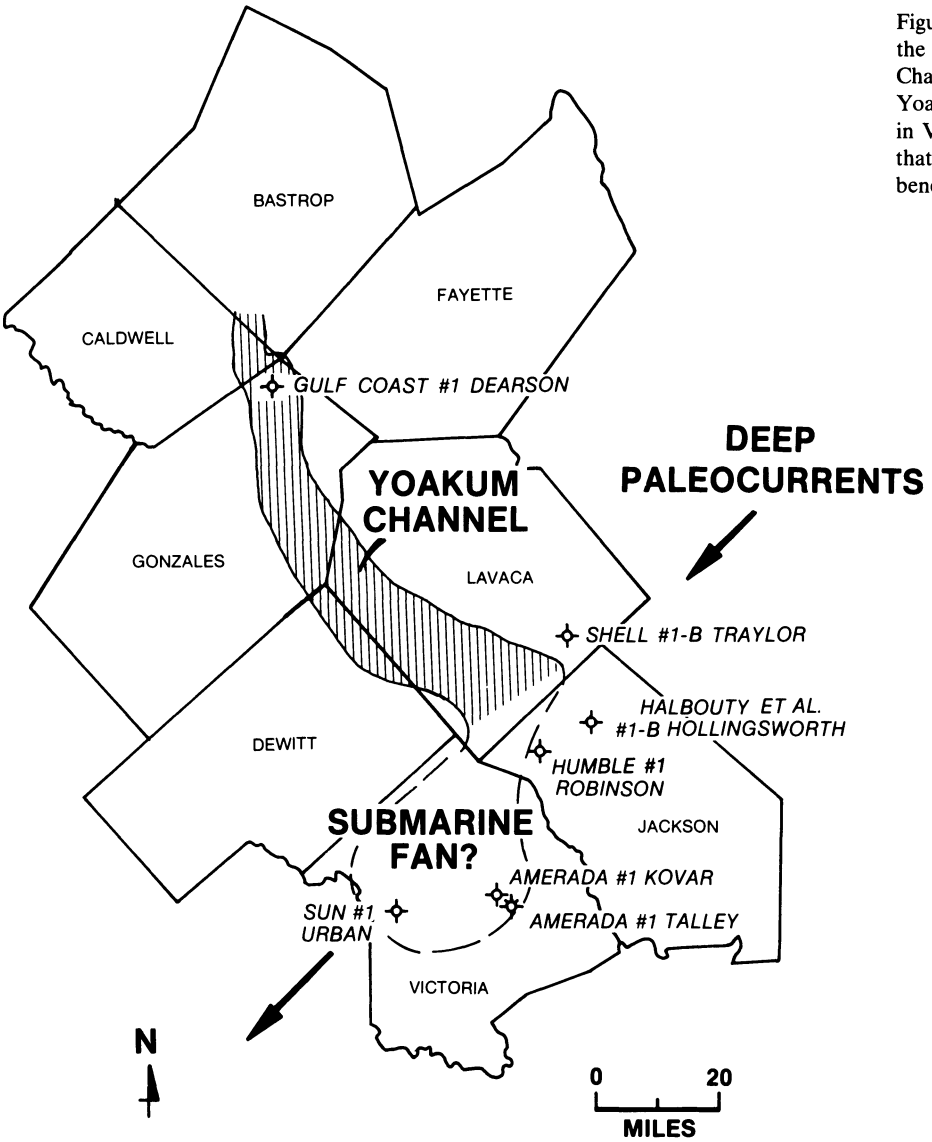

Figure 7.5. Location of deep, downdip Wilcox wells of the central Texas Gulf Coast in relation to Yoakum Channel. The absence of Wilcox sands at the mouth of Yoakum Channel, and their presence to the southwest in Victoria County, led Vormelker (1979) to propose that a downdip submarine fan took a sharp right-angle bend due to the influence of "deep paleocurrents."

Cores from two wells drilled into this supposed submarine fan are described and displayed below. However, sandstones in these cores apparently were *not* dominated by turbidity-current deposition. Instead, features suggest episodic sedimentation on a muddy continental shelf, in relatively shallow water but below fairweather wave base, during storm and possibly tidal events.

Core Descriptions

Interpretation of upper Wilcox shelf deposits is based on 590 ft (180 m) of relatively continuous core, collected from two portions of the Sun #1 Urban well (13,875–13,922 ft and 14,020–14,120 ft) and three intervals of the Amerada #1 Kovar well (14,511–14,906 ft, 14,981–15,023 ft, and 15,067–15,172 ft). Summary lithologic logs of the two #1 Urban cores and the uppermost #1 Kovar core are shown in Figures 7.6 and 7.7, and are correlated to the petrophysical logs in Figure 7.8. Photographs of selected core intervals and core pieces are also included as Figures 7.9 through 7.12.

Sun #1 E. R. Urban

Five lithofacies are identified in the upper Wilcox from the Sun #1 Urban well. Three of the rock types are fine grained: (1) interlaminated siltstone and mudstone, (2) bioturbated muddy siltstone, and (3) horizontally laminated and ripple cross-laminated siltstone. These three lithofacies are interbedded and somewhat gradational from

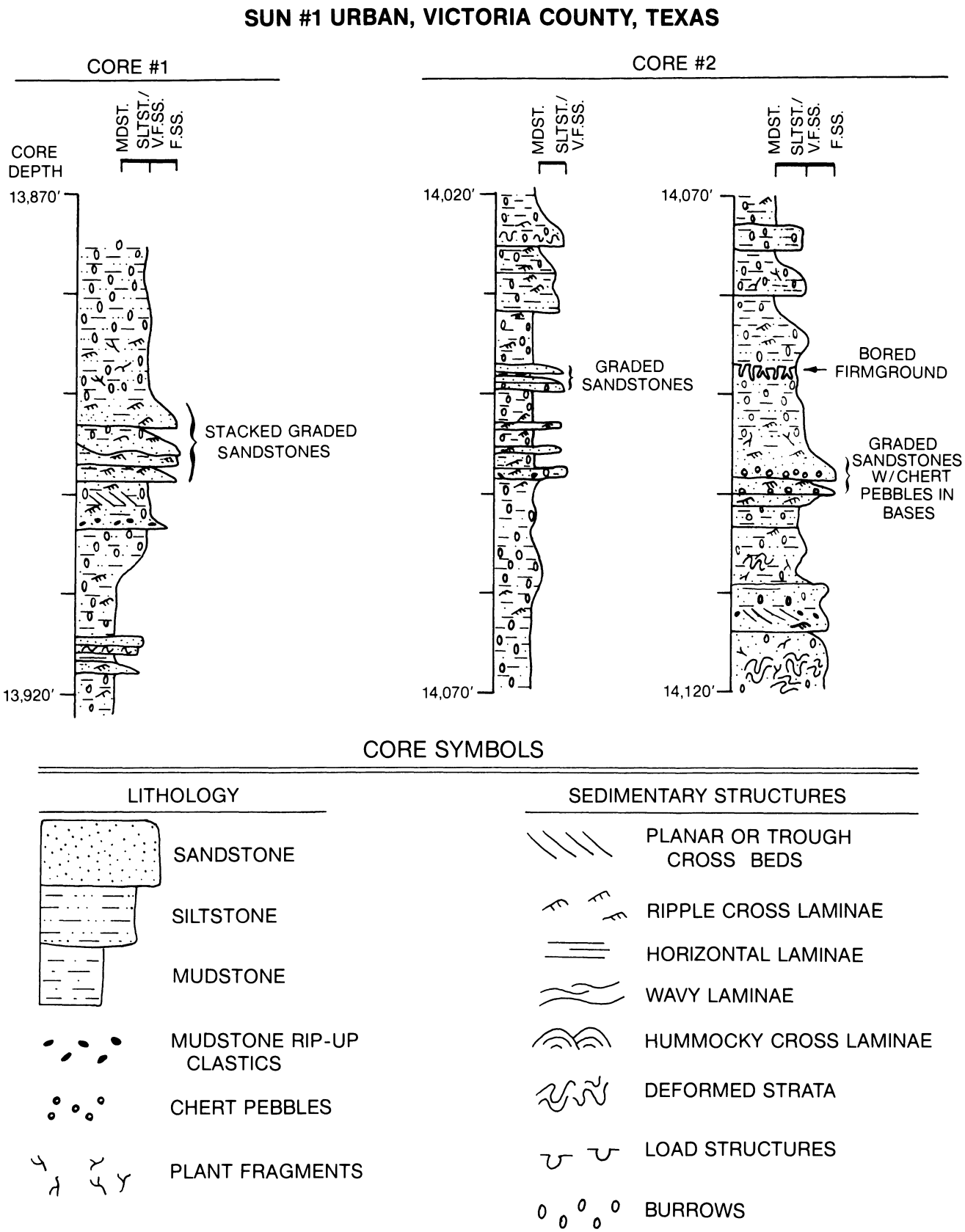

Figure 7.6. Columnar stratigraphic sections of the two cores from the Sun #1 Urban well. Also shown are core symbols used in this figure and Figure 7.7.

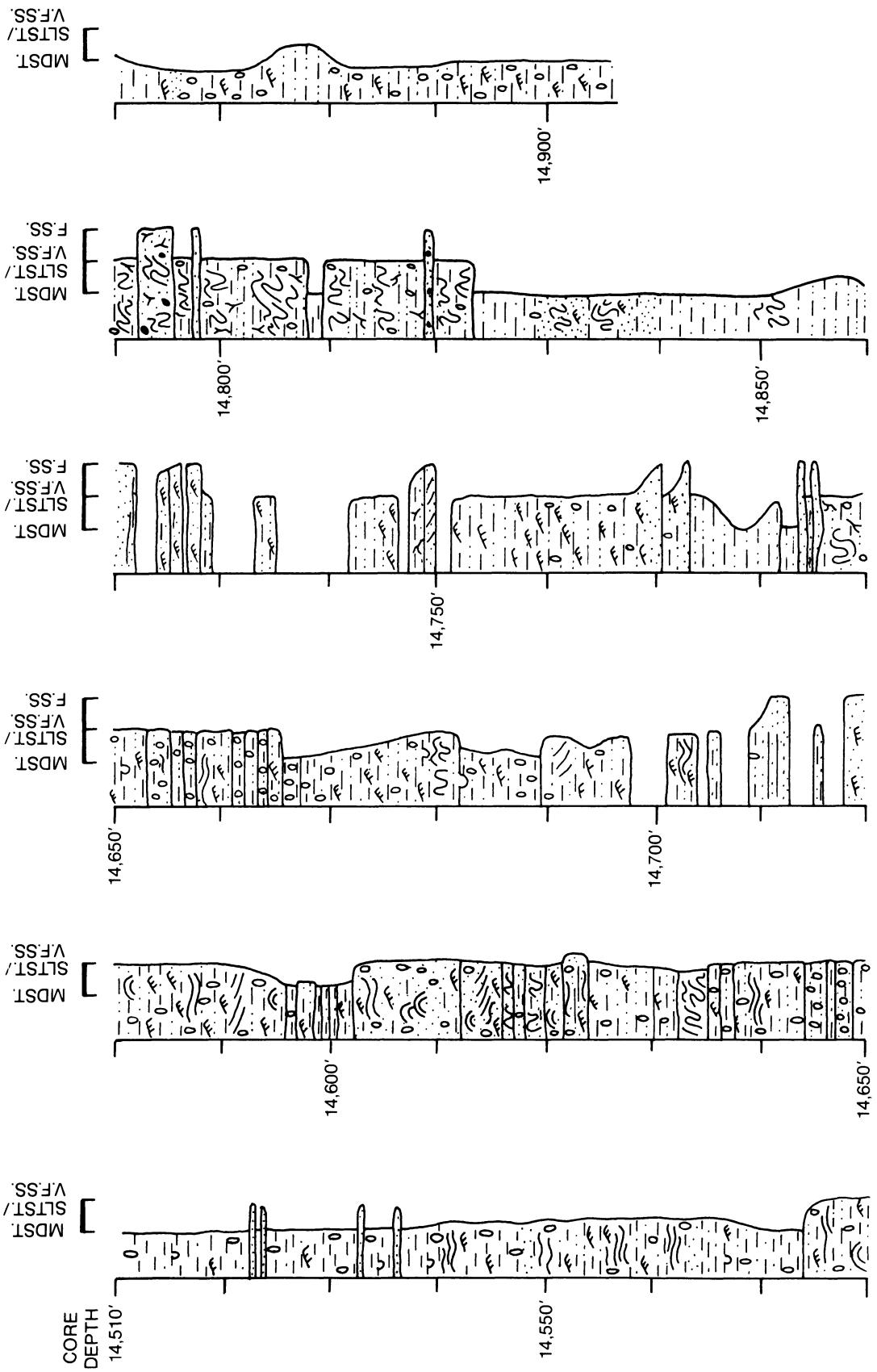

Figure 7.7. Columnar stratigraphic sections of the uppermost core from the Amerada #1 Kovar well. The two lower cores from this well (14,981–15,023 ft and 15,067–15,172 ft) are entirely shale and interlaminated mudstone and siltstone, and are not shown. Core symbols are the same as in Figure 7.6.

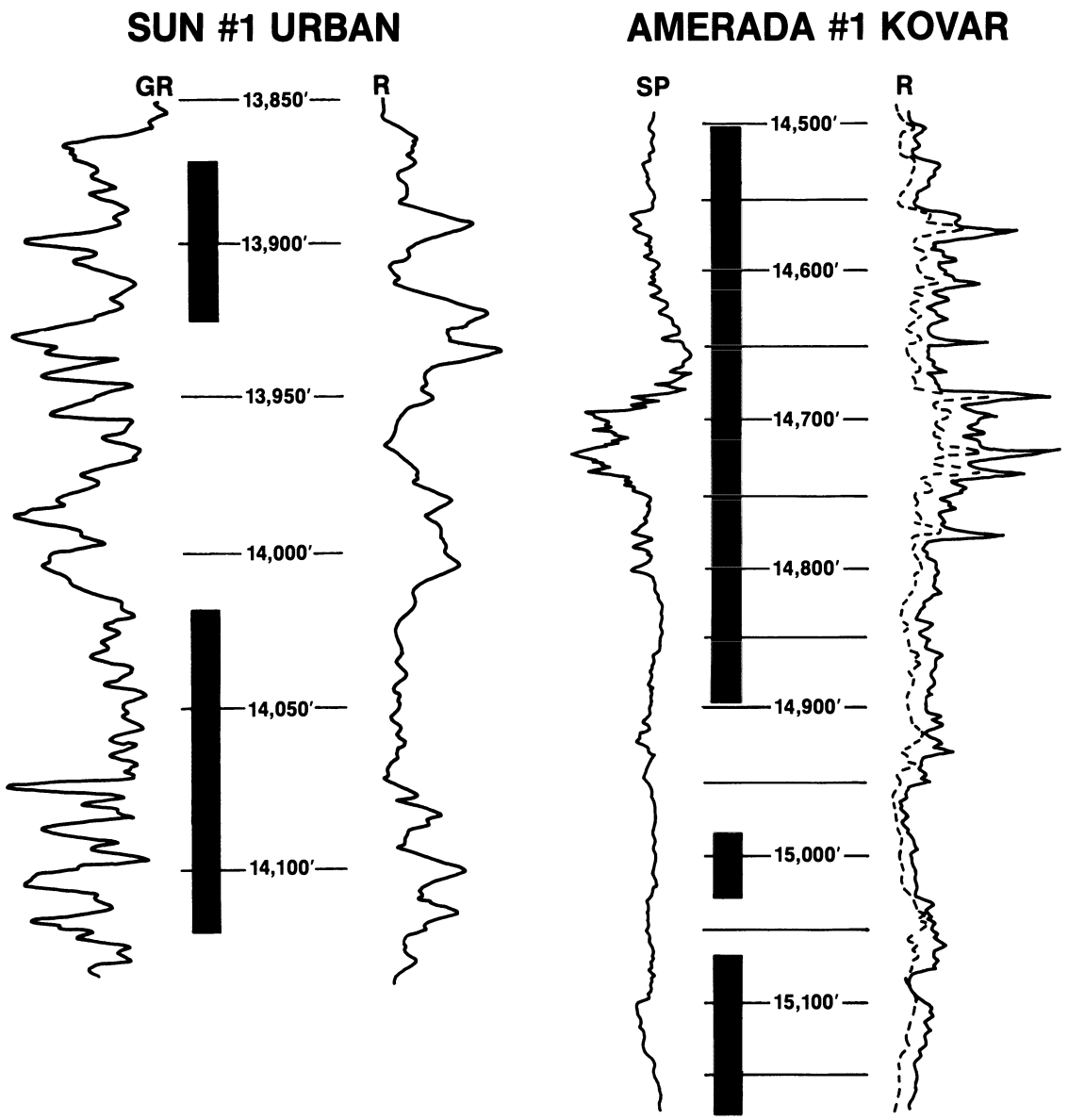

Figure 7.8. Subsurface induction-electrical logs for the Sun #1 Urban and Amerada #1 Kovar wells. Spontaneous-potential (SP), gamma-ray (GR), and resistivity (R) logs are shown. Cored intervals are shown in bold black bars along the depth scale; cores have been "slipped" to match log depths. Note the difference in vertical scales between the logs.

one to another; they dominate the cores (Fig. 7.6). Two coarse-grained lithofacies, (4) (trough, planar, and hummocky) cross-bedded sandstone and (5) normally graded sandstone, irregularly punctuate the fine-grained intervals. Lithofacies 4 and 5 typically are sharp based and fine upward into facies 1, 2, or 3.

Lithofacies 1: Interlaminated Siltstone and Mudstone

This lithofacies is predominant throughout the #1 Urban cores (Figs. 7.9 and 7.10a). Medium to dark gray, clayey mudstone alternates with light gray siltstone. The siltstone occurs as thin stringers and lenses that are horizontally laminated and ripple cross-laminated. Low-amplitude, starved ripples are common; flaser and wavy bedding also occur. Burrows typically disrupt bedding, mixing silt into the mudstone layers and leaving behind remnants of siltstone laminae. Loading of siltstone laminae onto the mudstone also caused deformation. The basal bed (14,114–14,118 ft) of interlaminated siltstone and mudstone is completely contorted (Figs. 7.6 and 7.9c), presumably due to synsedimentary slumping.

Common burrows include *Terebellina*, *Chondrites*, *Hel-*

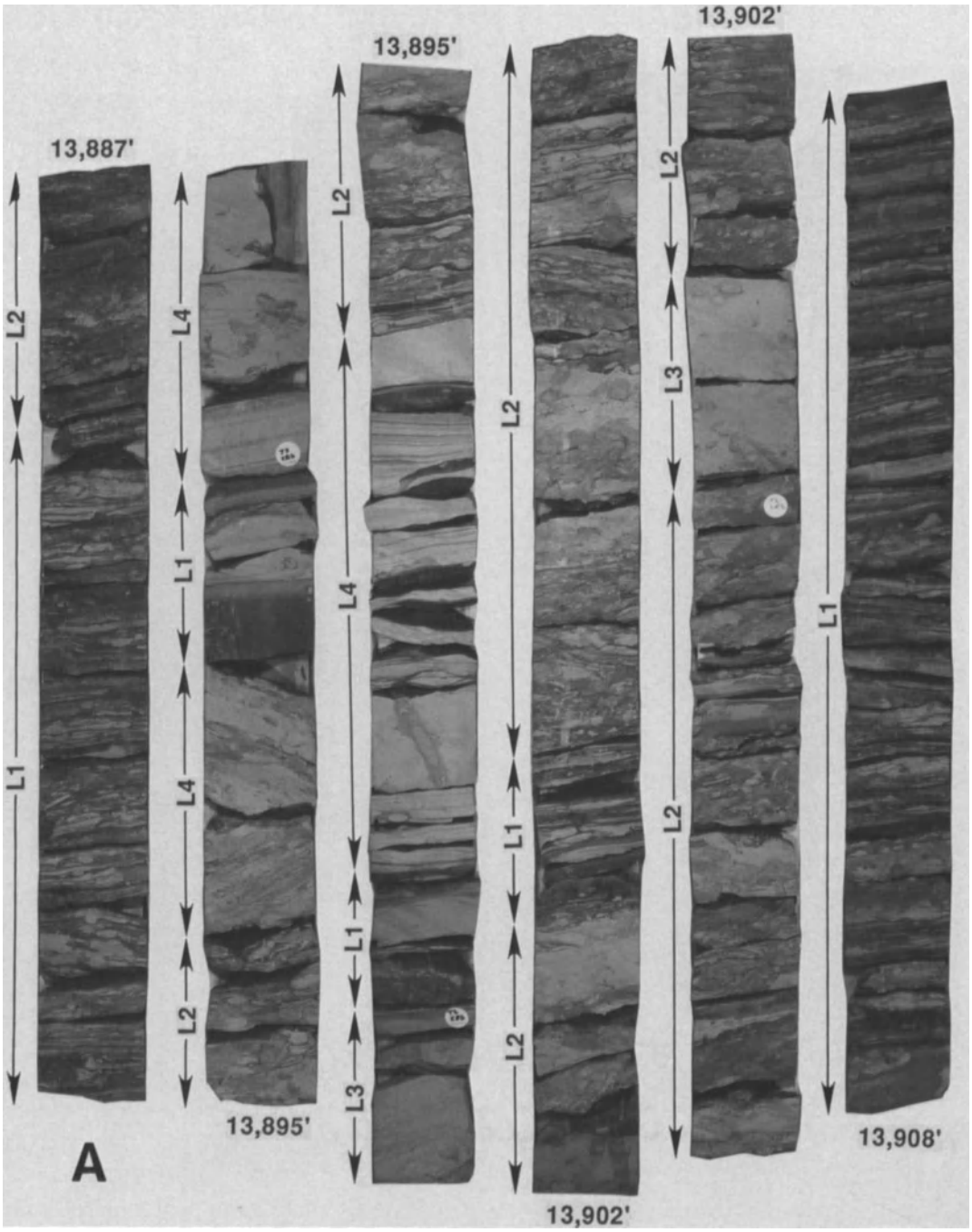

Figure 7.9. Three representative sections of relatively continuous core from the Sun #1 Urban well. Cores are 4 inches wide. Each vertical strip represents approximately 3 ft of core. Bottom is to lower right, top is to upper left. The distribution of lithofacies is shown to the left of each strip (L1. Interlaminated siltstone and mudstone; L2. Bioturbated muddy siltstone; L3. Laminated siltstone; L4. Cross-bedded sandstone; L5. Normally graded sandstone). (A) Core from 13,887 to 13,908 ft. Burrowing in the siltstones and sandstones is dominantly *Asterosoma*. (B) Core from 14,032 to 14,048.5 ft. Interlaminated siltstone and mudstone predominate. Note *Gyrolithes* (G) at 14,037.5 to 14,038 ft. (C) Core from 14,079 to 14,117 ft. Abundant *Terebellina* are present from 14,081 to 14,082 ft. The bioturbated muddy siltstone from 14,085 to 14,089.25 ft contains a bored horizon (B) at 14,086.75 ft.

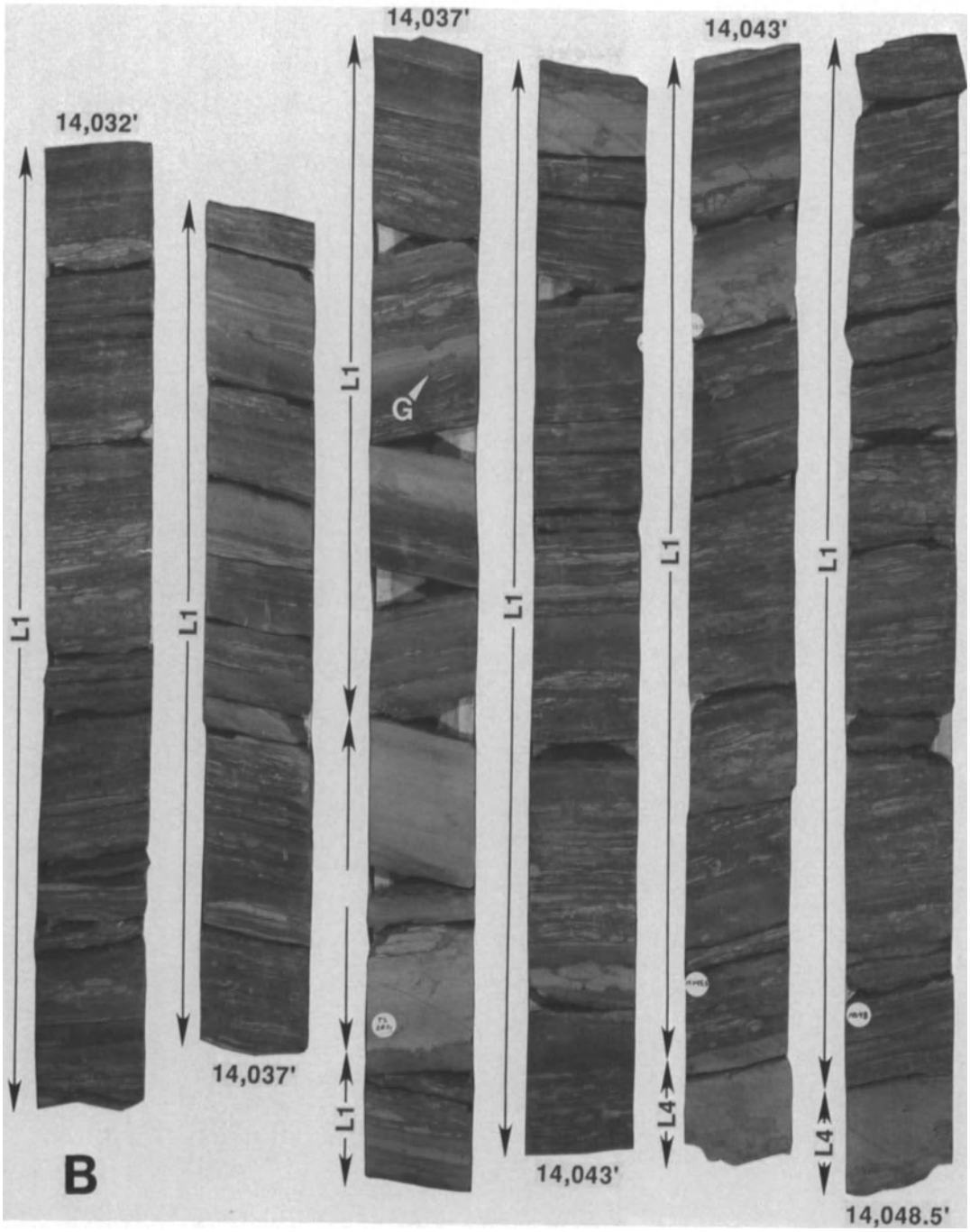

Figure 7.9. *Continued*

minthoida, and *Asterosoma*. Less abundant forms are *Diplocraterion*, *Teichichnus*, and *Gyrolithes*. Body fossils are absent; scattered plant fragments are rare.

Lithofacies 2: Bioturbated Muddy Siltstone

Pervasive bioturbation of interlaminated siltstone and mudstone produces medium to dark gray, muddy siltstone (Figs. 7.9 and 7.10b). Burrowing intensity and, hence, intermixing appear to increase as silt content increases. The least intermixed muddy siltstone has a "speckled" appearance, due to thin, dark, mudstone laminae that are deformed and wrapped around a profusion of minute, light-gray, silt-filled, horizontal burrows. Identifiable burrows include *Terebellina*, *Planolites*, *Chondrites*, and *Zoophycos*. A bored horizon characterized by a *Glossifungites* trace-fossil assemblage occurs in the "speckled" siltstone at 14,087 ft

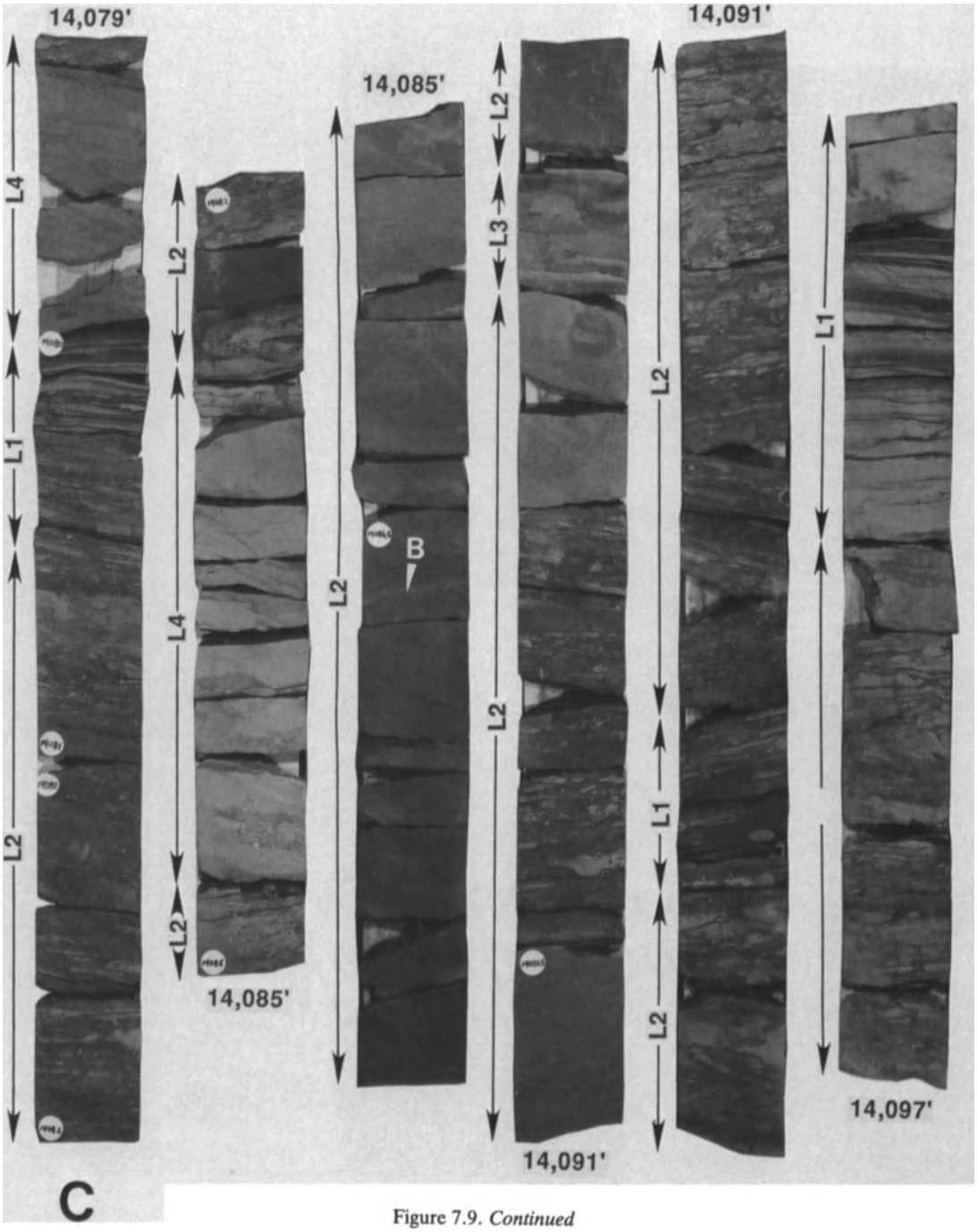

Figure 7.9. *Continued*

(Figs. 7.6 and 7.10c). This horizon also displays mineralization by corrensite, a regularly interstratified chlorite-montmorillonite mixed-layer clay (S.A. Stonecipher, personal communication, 1991).

Lithofacies 3: Laminated Siltstone

Light to medium gray, horizontally laminated and ripple cross-laminated siltstone occurs in very thin to thin beds (Fig. 7.9). Mudstone laminae commonly separate these beds. Some of the laminated siltstone beds cap graded sandstones (lithofacies 5); in such cases, the siltstones are also normally graded. These graded siltstones display a vertical bedding sequence that indicates waning flow during deposition. Horizontal laminae are overlain by ripple cross-laminae, and mud drapes increasingly punctuate the rippled siltstones upward (producing flaser to wavy bedding, e.g., at 14,095 ft on Fig. 7.9c). These normally graded siltstones

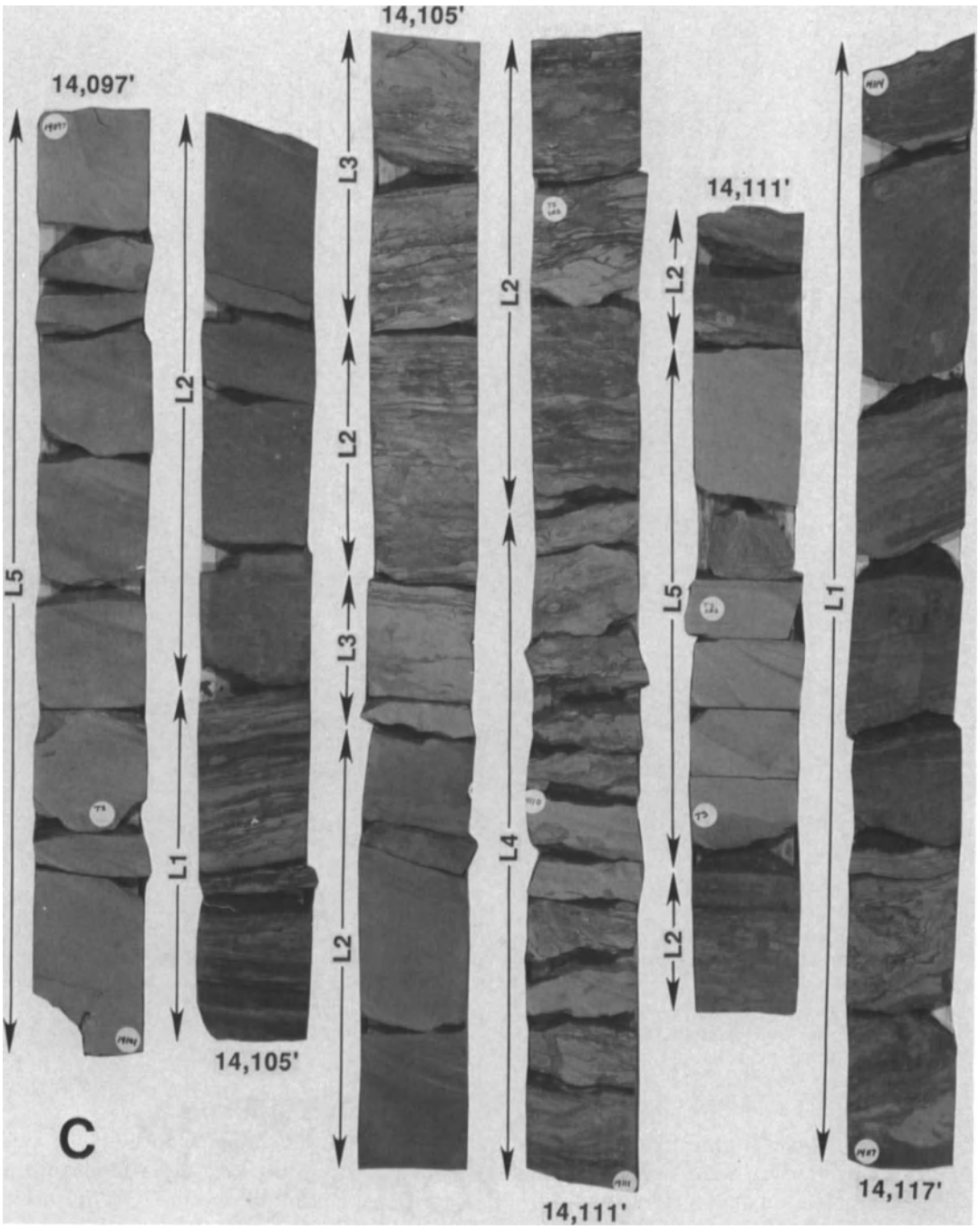

Figure 7.9. *Continued*

are often capped by burrowed siltstone. More rarely, laminated siltstone beds are inversely graded and demonstrate increasing depositional energy (from low- to high-flow-regime, tractive-bedform migration) with time; ripple cross-laminae change to horizontal laminae upward.

Burrows are rare to common in the laminated siltstones; traces include *Ophiomorpha* and *Asterosoma*. Organic plant fragments are often present.

Lithofacies 4: Cross-bedded Sandstone

Light gray, fine-grained to very fine-grained sandstone is variably trough, tabular, and hummocky cross-bedded (Figs. 7.9 and 7.10d). Cross-lamination is both high angle (greater than 10°) and low angle. Some wavy laminations highlighted by mud drapes also occur. Beds are typically less than 1 ft (30 cm) thick. Bases of these units are often subtly

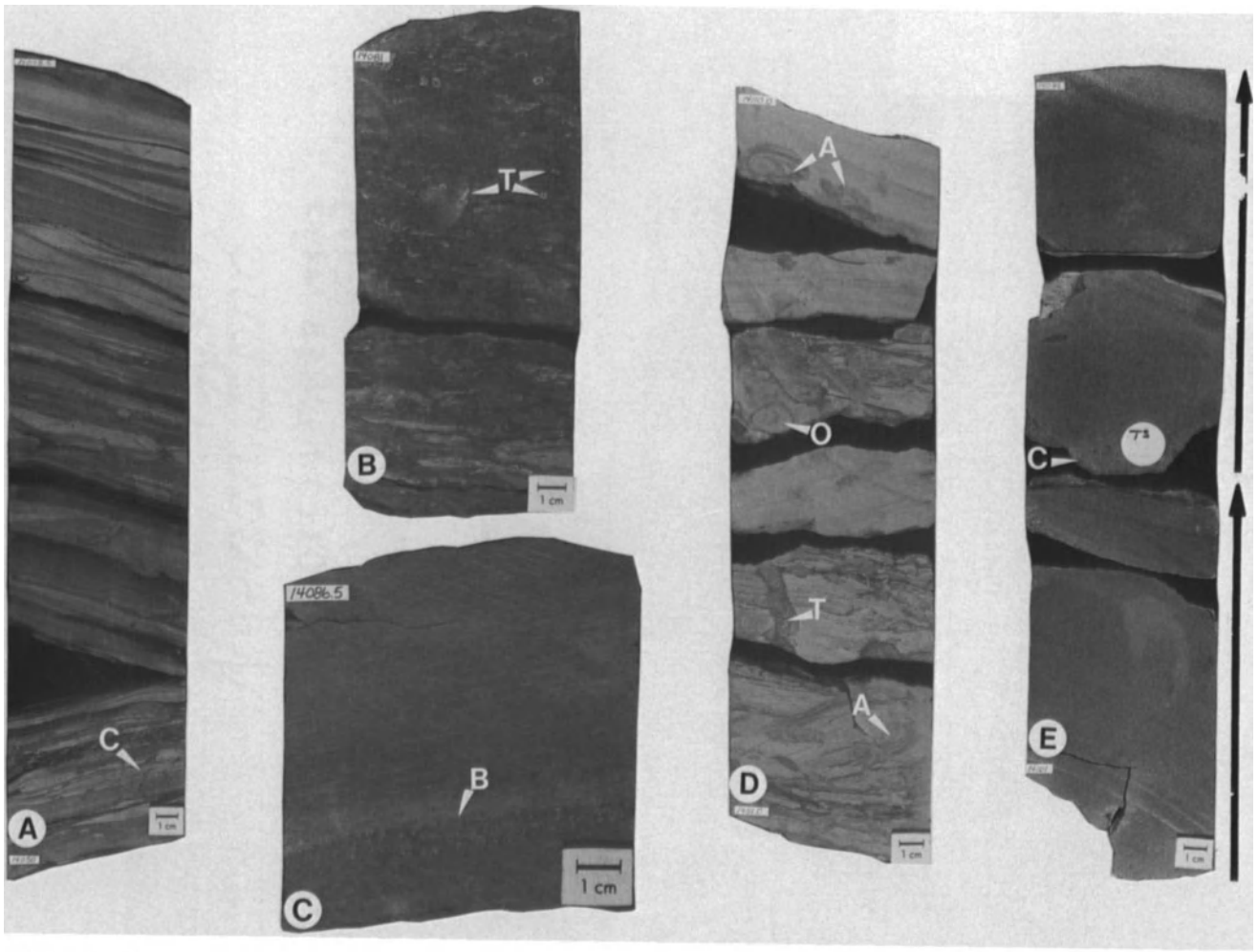

Figure 7.10. Core pieces from the Sun #1 Urban well. (A) Lithofacies 1, interlaminated siltstone and mudstone (14,048.5–14,050 ft). Burrows marked by "C" are *Chondrites*. (B) Lithofacies 2, bioturbated muddy siltstone (14,081–14,081.5 ft). The irregular and deformed white ellipses and circles are *Terebellina* (T). (C) A bored firmground or hardground at 14,086.75 ft, marked by "B," with a *Glossifungites* trace-fossil assemblage. (D) Lithofacies 4, cross-bedded sandstone (14,110–14,111 ft). High- and low-angle cross-laminae and horizontal laminae are disrupted by *Asterosoma* (A), *Ophiomorpha* (O), and *Teichichnus* (T). (E) Lithofacies 5, graded sandstone (14,099–14,101 ft). Two fining-upward beds are indicated by the two arrows. The lower structureless bed is faintly laminated, and then rippled, near its top, and capped by a shale drape, giving this bed the form of a turbidite T_{abc} sequence. The upper structureless bed contains chert granules (C) along its base.

scoured into underlying siltstones or mudstones. Internally, there is no "characteristic" vertical sequence, i.e., no evidence of smoothly waning or waxing current flow during deposition of these sandstones. Tops of beds are either burrowed or show a rapid change into a thin, rippled-and-draped siltstone cap or only a mudstone drape. Burrows vary from absent to common in the cross-bedded sandstones, dominated by *Ophiomorpha* and *Asterosoma*.

Figure 7.11. Five representative sections of relatively continuous core from the Amerada #1 Kovar well. Cores are 2 inches wide. Cores are jumbled, and many pieces are missing. Bottom is to lower right; top is to upper left. The distribution of lithofacies is shown to the left of each strip (same abbreviations as in Fig. 7.9, plus L6. Silty Shale). (A) Core from 14,517 to 14,538 ft. Silty shale dominates the upper two thirds of this interval. (B) Core from 14,578 to 14,599 ft. Interlaminated siltstone and mudstone grades up to horizontal-laminated and rippled siltstone. Probable herringbone cross-bedding (H) occurs at 14,587.9 ft. (C) Core from 14,623 to 14,641 ft. This interval of interlaminated siltstone and mudstone contains a slumped portion from 14,633.3 to 14,635 ft. (D) Core from 14,709 to 14,740 ft. These medium and thick beds of siltstone are characteristically horizontally laminated with rippled tops. Mud and mica line many of the laminae. (E) Core from 14,759 to 14,795 ft. This is an upward-coarsening sequence of ripple-laminated siltstone overlying interlaminated siltstone and mudstone, which grades upward from bioturbated muddy siltstone. Bedding in the portion below 14,784.5 ft is contorted.

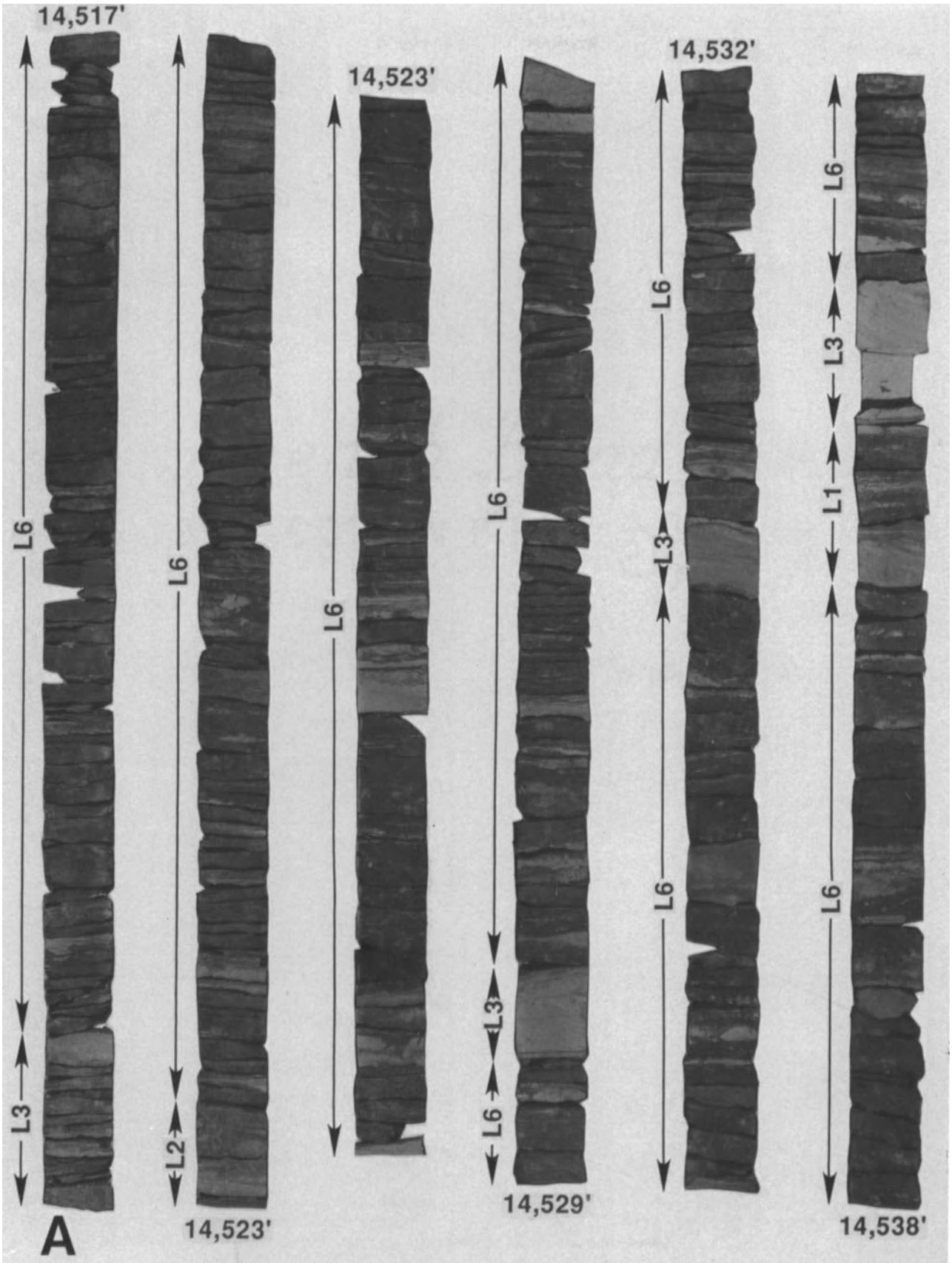

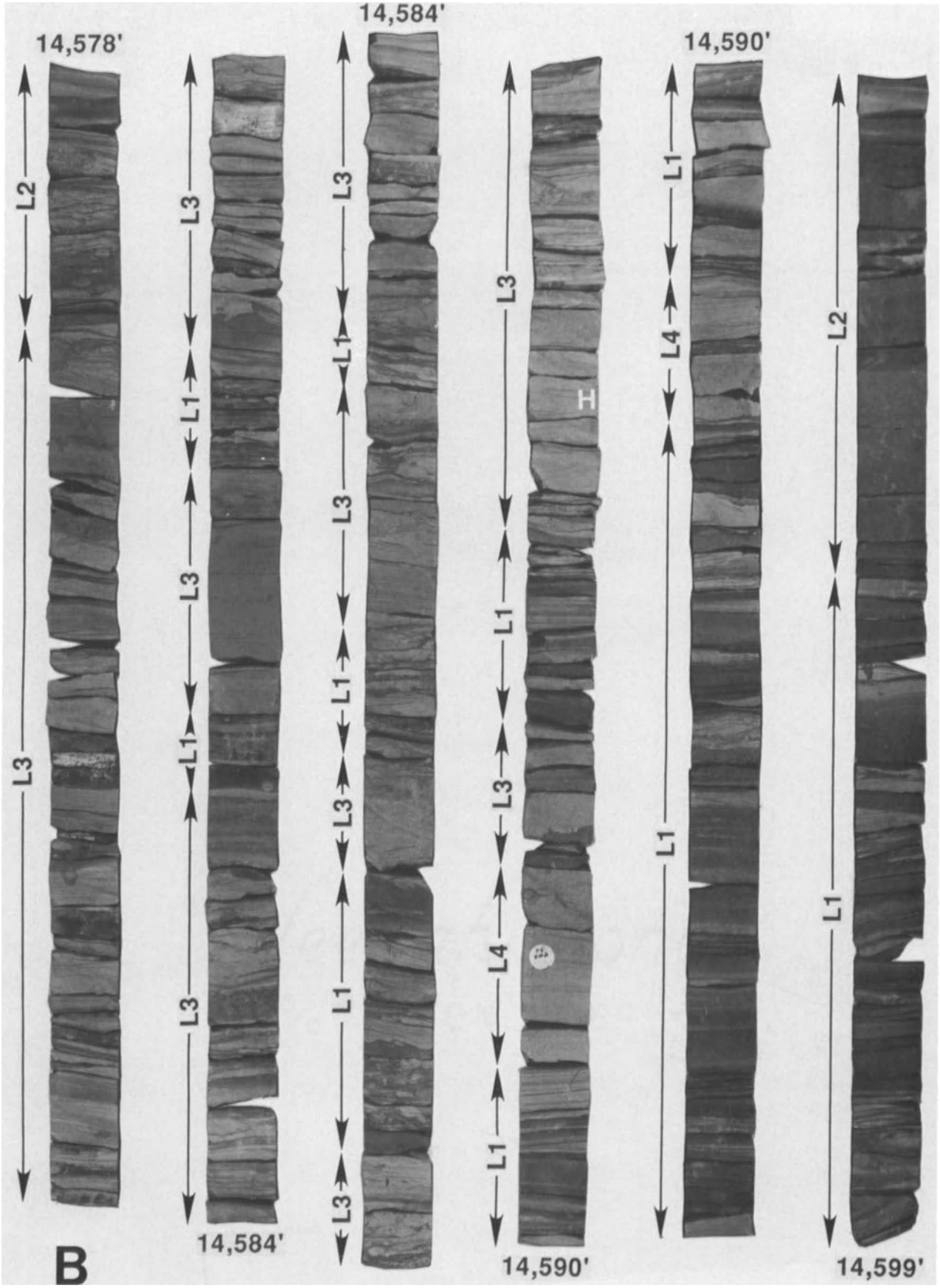

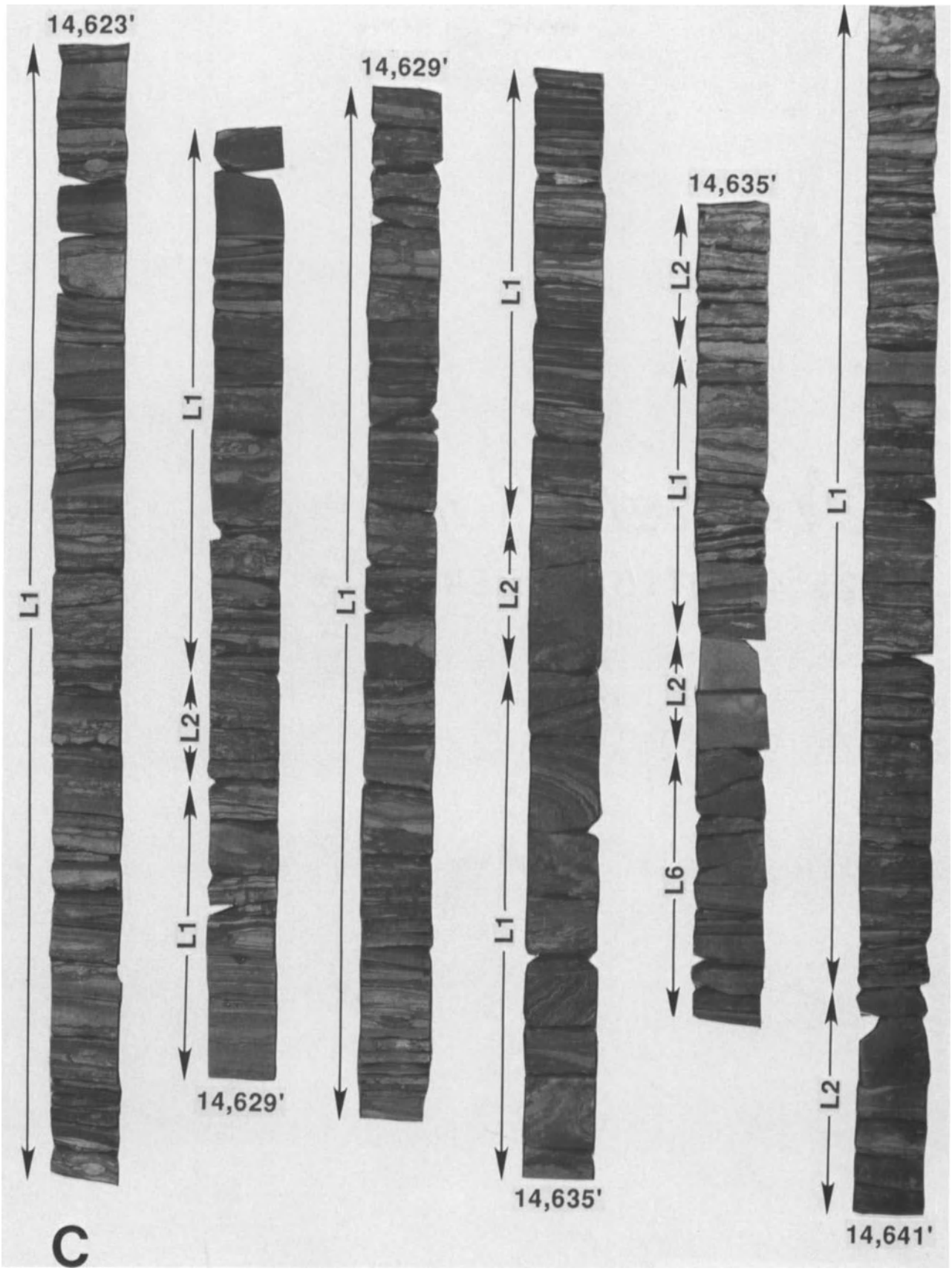

Figure 7.11. *Continued*

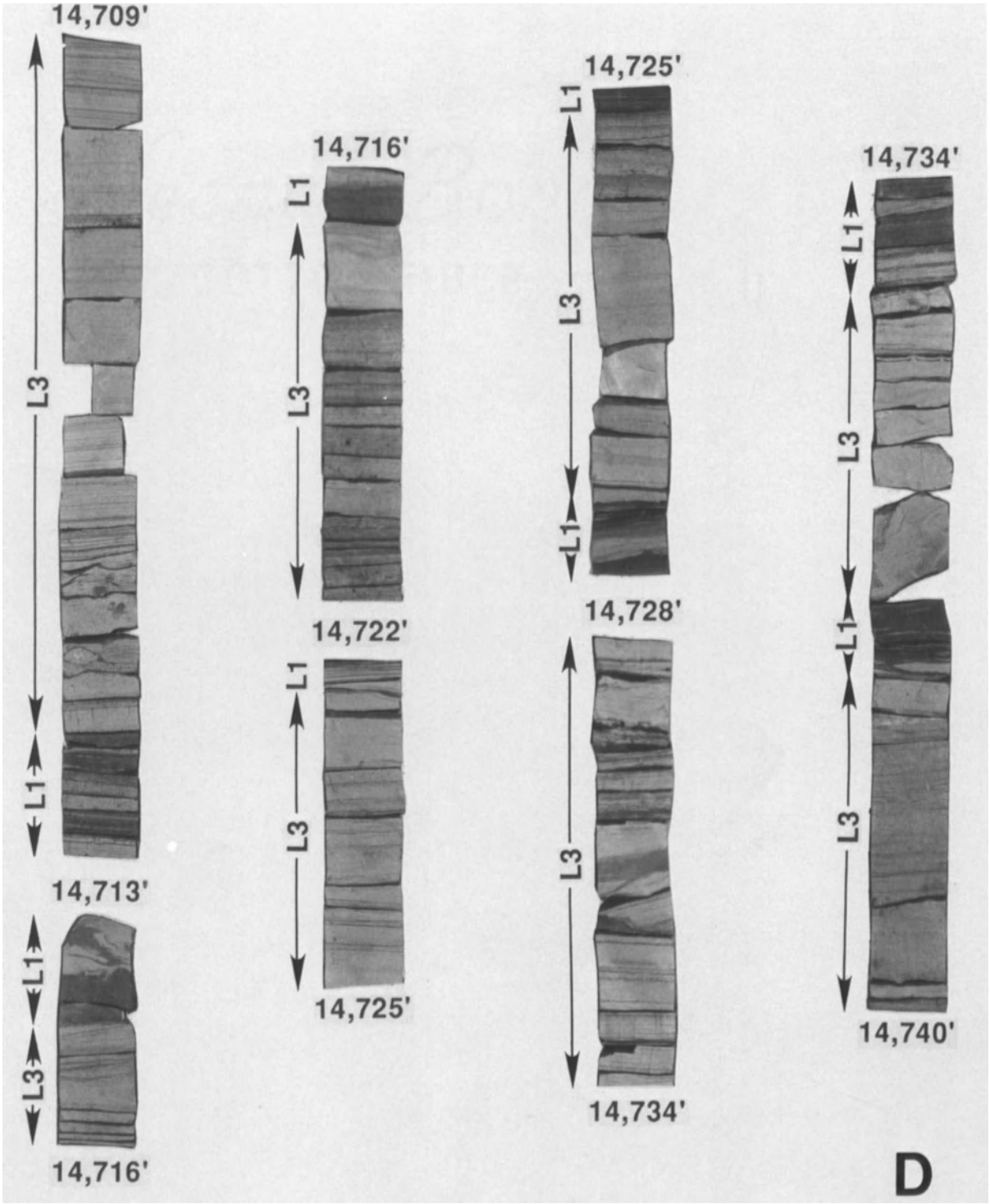

Figure 7.11. *Continued*

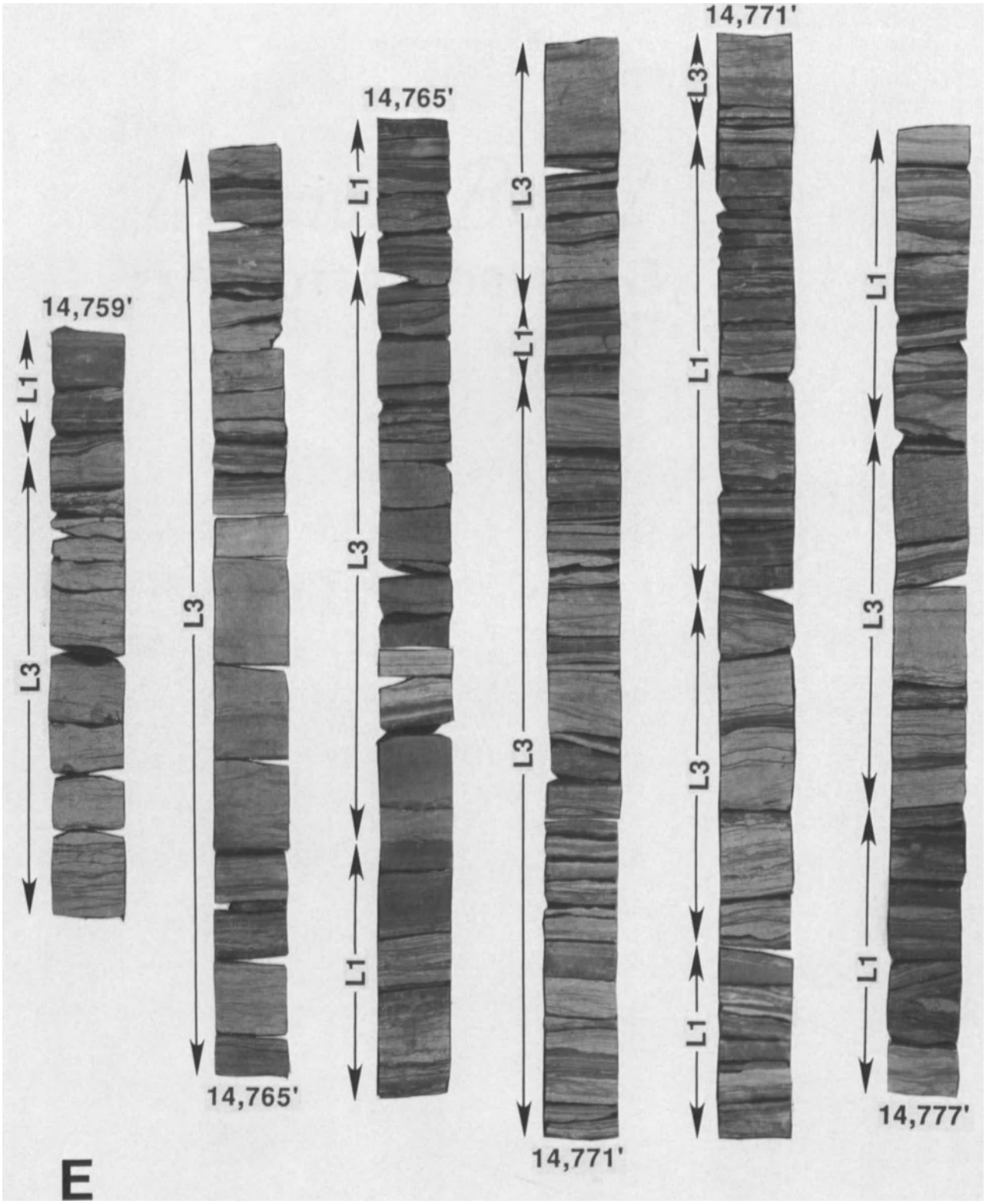

Figure 7.11. *Continued*

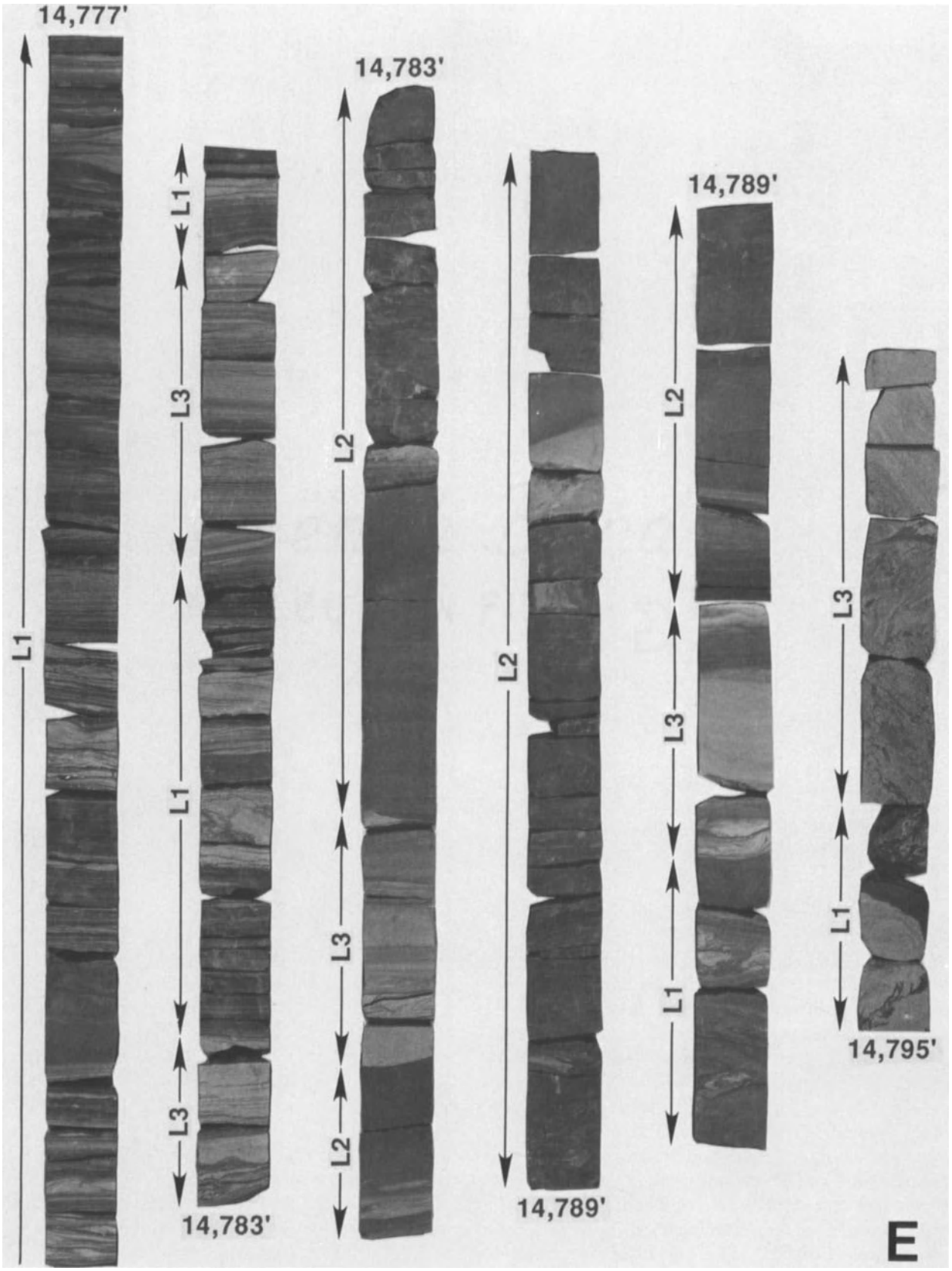

Figure 7.11. *Continued*

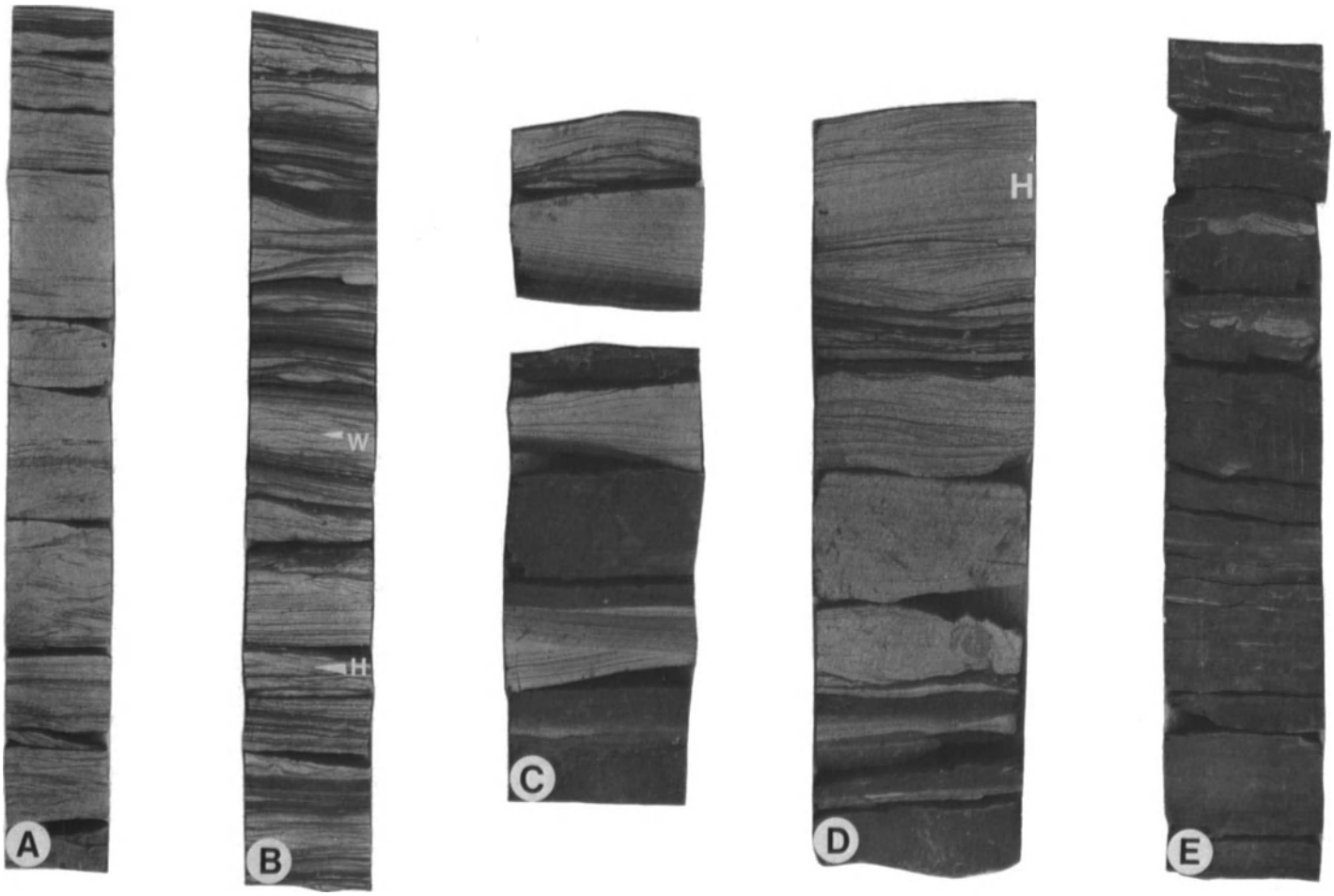

Figure 7.12. Core pieces from the Amerada #1 Kovar well. Cores are all 2 inches wide. (A) Lithofacies 3, laminated siltstone (14,762.7–14,764.7 ft). Thick siltstone bed of horizontal and wavy laminae alternating with ripple cross-laminae. (B) Lithofacies 1, interlaminated siltstone and mudstone (14,775.5–14,777 ft). Note wave ripples (W) and herringbone ripples (H). (C) Lithofacies 1, interlaminated siltstone and mudstone (14,592–14,592.5 ft, top piece, and 14,595.8–14,596.3 ft, bottom piece). Siltstone layers are hummocky cross-stratified. (D) Lithofacies 4, cross-bedded sandstone (14,593.2–14,593.8 ft). An *Asterosoma* burrow occurs in the basal low-angle cross-bedded sandstone. The upper hummocky cross-stratified portion (H) is capped by wave ripples. (E) Lithofacies 6, silty shale (14,849–14,850.4 ft).

Lithofacies 5: Normally Graded Sandstone

Light gray, fine-grained, normally graded sandstone is the least common lithofacies (Fig. 7.9). Basal bedding surfaces of these deposits are sharp and commonly erosional. Mudstone rip-up clasts or chert granules occur along the bases of some graded sandstone beds (Fig. 7.10e). Internally, the lower portions of these beds are either horizontally laminated or structureless and overlain by horizontal laminae. The horizontal-laminated portions grade upward to ripple cross-laminated, very fine-grained sandstone or siltstone, which may contain plant fragments. These vertical successions of sedimentary structures match those found in turbidites, and can be described as $T_{(a)bc}$ sequences (Bouma, 1962). Burrows are rare in this lithofacies.

Amerada #1 Allan Kovar

Four of the five lithofacies present in the Sun #1 Urban cores also occur in the Amerada #1 Kovar units; lithofacies 5 (normally graded sandstone) is absent. One additional lithofacies, a silty shale (lithofacies 6), exists in the #1 Kovar cores, as described below. Laminated siltstone (lithofacies 3) intervals are often much thicker in the uppermost #1 Kovar core than in the #1 Urban cores (up to 2.5 ft, 0.8 m). Horizontal to slightly wavy laminae variably dominate these thick siltstone beds, with ripples occurring only in the uppermost portions, or they alternate with ripple cross-laminae throughout (Figs. 7.11 and 7.12a). These siltstones commonly grade upward from low-angle cross-bedded or wavy-laminated sandstone beds, rather than from graded sandstones as in the #1 Urban units.

Hummocky cross-strata and symmetrical-ripple laminae (Fig. 7.12b) are more common in the #1 Kovar core versus the #1 Urban cores. These features are especially prevalent in the interlaminated siltstones and mudstones (lithofacies 1) (Figs. 7.7, 7.11, and 7.12c). Hummocky cross-laminae also occur in the laminated siltstones (Fig. 7.12d). Contorted bedding is more common in the #1 Kovar core. Thin, deformed beds of interlaminated siltstone and mudstone alternate with undeformed layers. Contorted bedding also affects a thick sequence of sandstone and bioturbated siltstone from 14,785 to 14,824 ft (Figs. 7.7 and 7.11e).

Lithofacies 6: Silty Shale

Dark gray, fissile, slightly silty shale contains rare light gray siltstone laminae and lenses. Small burrows are common. These traces include *Planolites*, *Terebellina*, and *Chondrites*; indistinct bioturbation also dominates some intervals. Burrowing increases adjacent to and within the siltstone laminae. In the #1 Kovar well, this lithofacies dominates the uppermost and lowermost portions of core 1 (Figs. 7.7 and 7.12e) and composes almost all of cores 2 and 3 (14,981–15,023 ft and 15,067.5–15,172 ft; Fig. 7.8b). These latter two cores are not illustrated.

Interpretation

Is the assemblage of six lithofacies described above part of a submarine-fan system? The abundant and diverse burrowing gives evidence that deposition took place under marine conditions. The presence of alternating coarse- and fine-grained lithologies points to sedimentation under fluctuating energy conditions, such as in a tidal setting or below fairweather wave base. Sedimentary structures and trace fossils indicate that deposition of these rocks probably occurred above storm wave base and not in a deep-marine setting.

Deposition by sediment-gravity flows below storm wave base dominates submarine fans. Such flows, which include turbidity currents, probably did produce some of the beds in the #1 Urban and #1 Kovar cores. The graded sandstones (lithofacies 5) display classic turbidite ($T_{abc(d)}$ and $T_{bc(d)}$) sequences (Bouma, 1962; Middleton and Hampton, 1976). However, turbidity currents arise not only in submarine-fan settings, but also in a variety of other environments, including lakes, delta fronts, and continental shelves. Furthermore, turbidity currents are *not* the primary mode of deposition interpreted in these upper Wilcox units. Instead tractive processes governed most of the sedimentation of sand and silt and produced environmentally significant structures, such as hummocky cross-bedding and symmetrical-ripple laminae.

Common tractive features in these cores are tabular and trough cross-bedding and current-ripple cross-laminae, all of which indicate the importance of migrating bed forms during deposition. Some of the current-rippled sequences, especially prevalent in the Amerada #1 Kovar core from 14,690 to 14,782 ft (Figs. 7.11d and 7.11e), appear to display herringbone cross-laminae. These structures suggest alternating, bidirectional flow directions during deposition. Somewhat less profuse than the tabular and trough cross-beds and ripple cross-laminae are hummocky cross-strata, wave ripples, and wave-current laminae. The hummocky beds are inferred from internal laminations, which gently cross-cut and diverge upward into domes. Hummocky cross-stratification is thought to form due to oscillatory or multidirectional storm waves acting below fairweather wave base (Duke, 1985). Symmetrical and sigmoid ripples, which also denote wave processes, cap many of the bedding sequences. Locally abundant are sandstone beds composed of horizontal laminae. In contrast to cleaner and thinner horizontal-laminated units formed by upper-flow-regime currents, these beds comprise stacked laminae of siltstone and fine-grained sandstone, each draped by mica and mud. Such intervals form due to oscillatory wave processes, and have been called wave-laminated beds (Tillman, 1985; Arnott and Southard, 1990).

Most diagnostic of shelf deposition are the hummocky cross-strata (Dott and Bourgeois, 1982; Duke, 1985). Although difficult to recognize in core, the domed, gently diverging laminae and low-angle truncations are becoming more widely accepted as indicating hummocky cross-stratification (Tillman, 1985; Walker, 1985c). The occurrence of tabular and trough cross-bedding, and beds formed during progressively increasing current flow, also limit the depth of deposition. The sustained currents and abundant migrating bed forms necessary to produce these features are rare in deep-marine (slope or basinal) positions. The conjunction of hummocky cross-strata and wave ripples, with the tabular and trough cross-bedded sandstones, probably indicates that intermittent, high-energy, geostrophic storm flows, modified by oscillatory wave-orbital currents, dominated coarse-grained sedimentation recorded in these cores (Swift, 1985; Arnott and Southard, 1990; Duke, 1990).

Other primary sedimentary structures lend support to a shelf interpretation for the upper Wilcox in this area of the central Texas Gulf Coast. The graded beds could have formed in numerous environments, but their relative scarcity and their preservation along with wave-formed features is typical of both modern and ancient shelf sands deposited below fairweather wave base (e.g., Swift, 1985; Tillman, 1985; Walker, 1985a,d). The exact mode of generation

of shelf turbidity currents, whether by delta outflow, shoreline-parallel geostrophic flow, or basin-directed storm-surge ebb, is still under debate (Swift, 1985; Walker, 1985a; Duke, 1990). Furthermore, the bored hardground or firmground at 14,087 ft in the lower #1 Urban core conforms to a shelf setting. Similar features have been described from both carbonate and siliciclastic shelves (e.g., Aigner, 1982; Swift, 1985). Finally, the rare herringbone ripple cross-laminae are typical of relatively shallow-water deposition, probably due either to tidal currents or switching storm currents (Swift, 1985; Tillman, 1985; Walker, 1985b).

Another characteristic of the #1 Urban and #1 Kovar cores consistent with a shelf setting is the episodic style of deposition. Active pulses of sedimentation waned and gave way to periods of quiescence. Shales and mudstones with thin siltstone laminae are predominant. Sandstone and siltstone beds typically are separated by mudstones. Most of the coarse-grained units display internal bedding sequences formed by decreasing flow. Cross-beds progress upward to horizontal laminae then ripples, and finally ripple-and-drape (flaser and wavy bedding).

These discrete changes and breaks in depositional energies, combined with the variety of physical sedimentary structures, indicate sedimentation in relatively shallow water, below fairweather wave base but above storm wave base. The preponderance of thin-bedded and laminated heterolithic strata is typical of muddy or deeper (distal) shelf settings (Aigner, 1985; Pedersen, 1985; Swift, 1985; Nittrouer et al., 1986; Snedden et al., 1988; Leithold, 1989). Similar beds occur in outer shelf deposits in the Wilcox of Louisiana (Lowry et al., 1986). In such environments, wave-orbital currents do not readily entrain coarse-grained sediments, and the bedding is thin, lacks lateral continuity, and is clay rich. Only large storms can create sufficient bottom currents to sustain large-scale bedform migration, producing fine-grained tabular and trough cross-bedded sandstones. Combined storm flow leads to hummocky cross-stratification.

In addition, the trace-fossil assemblage independently corroborates the environmental interpretation based on physical sedimentary structures and sequences. The most common burrows in these rocks are *Ophiomorpha*, *Asterosoma*, *Terebellina*, *Chondrites*, and *Helminthoida*. The first two forms are typical of sandy, high-energy environments. *Ophiomorpha* occurs from the shoreline/tidal-flat zone to deep-sea settings; *Asterosoma*, in contrast, has not been reported beyond the shelf/slope break (Chamberlain 1978). The other traces predominate in fine-grained sediments from low-energy settings. *Chondrites* and *Helminthoida* are both common throughout the nearshore to deep-marine range. *Terebellina*, however, has been observed only from the nearshore through outer shelf (Chamberlain, 1978). Because this trace-fossil assemblage encompasses both deposit and suspension feeders, conditions were not dominated by either high-energy waves (very shallow marine) or passive pelagic conditions (deep marine away from sediment input). This high-diversity association most likely was produced within a neritic (continental shelf) setting.

Conclusions

The deepest and most basinward Wilcox units encountered in wells along the central Texas Gulf Coast were not formed in a submarine fan, in contrast to suppositions by previous workers. Based on examination of physical and biogenic sedimentary structures and vertical bedding sequences, the upper Wilcox cores from the Sun #1 Urban and Amerada #1 Kovar wells, Victoria County, instead represent deposition upon a middle to outer, storm-dominated, continental shelf. Any sand bodies formed in this environment would have been thin and discontinuous; their potential as hydrocarbon reservoirs is minimal. If any submarine fan does exist in association with the Wilcox-aged Yoakum submarine canyon, it probably is located farther downdip or deeper than the present limits of drilling, and therefore, the full potential of the Wilcox remains to be discovered.

Acknowledgments

Marathon Oil Company is gratefully acknowledged for permission to publish these results. Convenient access to core material was provided by the Bureau of Economic Geology, University of Texas, Austin. D. Arteaga interpreted provenance data from various literature sources to produce Figure 2. The technical aid of J. McCain, M. Riddle, S. Hartline, J. Barcewski, and J. Cooper is sincerely appreciated.

References

Aigner, T., 1982, Event-stratification in nummulite accumulations and in shell beds from the Eocene of Egypt, *in* Einsele, G., and Seilacher, A., eds., Cyclic and event stratification: New York, Springer-Verlag, p. 248–262.

Aigner, T., 1985, Storm depositional systems; Lecture notes in earth sciences, Volume 3: Berlin, Springer-Verlag, 174 p.

Albach, D.C., 1979, The depositional history of the uppermost Wilcox (lower Eocene) of the west-central Beauregard Parish, Louisiana [M.S. thesis]: Baton Rouge, Louisiana State University, 98 p.

Allen, J., and Howell, J., Sr., 1987, Using "poor man's 3-D" to identify

distributary channel sands in the Wilcox Formation, Lavaca County, Texas: Leading Edge, v. 6, no. 10, p. 8–15.

Antoine, J., and Ewing, J., 1962, Seismic refraction measurements of the margins of the Gulf of Mexico: Jour. Geophys. Res., v. 68, p. 1975–1996.

Arnott, R.W., and Southard, J.B., 1990, Exploratory flow-duct experiments on combined-flow bed configurations and some implications for interpreting storm-event stratification: Jour. Sed. Pet., v. 60, p. 211–219.

Bebout, D.G., Weise, B.R., Gregory, A.R., and Edwards, M.B., 1979, Wilcox sandstone reservoirs in the deep subsurface along the Texas Gulf Coast, their potential for production of geopressured geothermal energy: Austin, University of Texas, Bureau of Economic Geology, Report Prepared for the U.S. Dept. of Energy, Division of Geothermal Energy, 219 p.

Berg, R.R., 1979, Characteristics of lower Wilcox reservoirs, Valentine and South Hallettsville fields, Lavaca County, Texas: Gulf Coast Assoc. Geol. Socs. Trans., v. 29, p. 11–13.

Billingsely, L.T., 1982, Geometry and mechanisms of folding related to growth faulting in Nordheim Field area (Wilcox), DeWitt County, Texas: Gulf Coast Assoc. Geol. Socs. Trans., v. 32, p. 263–274.

Bouma, A.H., 1962, Sedimentology of some flysch deposits: Amsterdam, Elsevier, 168 p.

Chamberlain, C.K., 1978, Recognition of trace fossils in cores, *in* Basan, P.B., ed., Trace fossil concepts: Short Course No. 5, Soc. Econ. Paleontologists Mineralogists, p. 119–166.

Chuber, S., 1979, Exploration methods of discovery and development of lower Wilcox reservoirs in Valentine and Menking fields, Lavaca County, Texas: Gulf Coast Assoc. Geol. Socs. Trans., v. 29, p. 42–51.

Chuber, S., 1986, Computer-aided geologic study of Yoakum Field, Dewitt and Lavaca counties, Texas, *in* Stapp, W.L., and others, eds., Contributions to the geology of south Texas: South Texas Geological Society, p. 232–251.

Chuber, S., and Begeman, R.L., 1982, Productive lower Wilcox stratigraphic traps from an entrenched valley in Kinkler Field, Lavaca County, Texas: Gulf Coast Assoc. Geol. Socs. Trans., v. 32, p. 255–262.

Chuber, S., and Howell, H.H., 1989, Productive lower Wilcox (Eocene) distributary channel sands of the Hallettsville Embayment, Lavaca County, Texas, *in* Chuber, S., and others, eds., Lower Wilcox core workshop: Hallettsville Field, Lavaca County: Short Course No. 3, Texas Geol. Soc., unpaginated.

Dingus, W.F., and Galloway, W.E., 1990, Morphology, paleogeographic setting, and origin of the middle Wilcox Yoakum Canyon, Texas coastal plain: Amer. Assoc. Pet. Geol. Bull., v. 74, p. 1055–1076.

Dott, R.H., Jr., and Bourgeois, J., 1982, Hummocky stratification: Significance of its variable bedding sequences: Geol. Soc. Amer. Bull., v. 93, p. 663–680.

Duke, W.L., 1985, Hummocky cross-stratification, tropical hurricanes, and intense winter storms: Sedimentology, v. 32, p. 167–194.

Duke, W.L., 1990, Geostrophic circulation or shallow marine turbidity currents? The dilemma of paleoflow patterns in storm-influenced prograding shoreline systems: Jour. Sed. Pet., v. 60, p. 870–883.

Edwards, M.B., 1981, Upper Wilcox Rosita delta system of south Texas: Growth-faulted shelf-edge deltas: Amer. Assoc. Pet. Geol. Bull., v. 65, p. 54–73.

Edwards, M.B., 1986, A reappraisal of depositional environment (barrier bar or submarine fan) for lower Wilcox reservoirs of Valentine Field, Lavaca County, Texas Gulf Coast, *in* Stapp, W.L., and others, eds., Contributions to the geology of south Texas: South Texas Geological Society, p. 252–259.

Fisher, W.L., 1969, Facies characterization of Gulf Coast basin delta systems, with some Holocene analogues: Gulf Coast Assoc. Geol. Socs. Trans., v. 19, p. 239–261.

Fisher, W.L., and McGowen, J.H., 1967, Depositional systems in the Wilcox Group of Texas and their relationship to occurrence of oil and gas: Gulf Coast Assoc. Geol. Socs. Trans., v. 17, p. 105–125.

Fisher, W.L., Brown, L.F., Jr., Scott, A.J., and McGowen, J.H., 1969, Delta systems in the exploration for oil and gas: A research colloquium: Austin, University of Texas, Bureau of Economic Geology, 212 p.

Galloway, W.E., 1968, Depositional systems of the lower Wilcox Group, north-central Gulf Basin: Gulf Coast Assoc. Geol. Socs. Trans., v. 18, p. 275–289.

Galloway, W.E., Ewing, T.E., Garrett, C.M., Tyler, N., and Bebout, D.G., 1983, Atlas of major Texas oil reservoirs: Austin, University of Texas, Bureau of Economic Geology, 139 p.

Galloway, W.E., Dingus, W.F., and Paige, R.E., 1989, Seismic and depositional facies of Paleocene-Eocene Wilcox Group submarine canyon fills, N.W. Gulf Coast, U.S.A., *in* Chuber, S., and others, eds., Lower Wilcox core workshop: Hallettsville Field, Lavaca County, Texas: Short Course No. 3, South Texas Geol. Soc., unpaginated.

Halbouty, M.T., 1969, Hidden trends and subtle traps in Gulf Coast: Amer. Assoc. Pet. Geol. Bull., v. 53, p. 3–29.

Hargis, R.N., 1985, Proposed lithostratigraphic classification of the Wilcox Group of south Texas: Gulf Coast Assoc. Geol. Soc. Trans., v. 35, p. 107–116.

Hardin, G.C., 1962, Notes on Cenozoic sedimentation in the Gulf Coast geosyncline, U.S.A., *in* Rainwater, E.H., and Zingula, R.P., eds., Geology of the Gulf Coast and central Texas and guidebook of excursions: Houston, TX, Houston Geological Society, p. 1–15.

Harris, J.R., 1962, Petrology of the Eocene Sabinetown-Carrizo contact, Bastrop County, Texas: Jour. Sed. Pet., v. 32, p. 263–283.

Hoyt, W.V., 1959, Erosional channel in the middle Wilcox near Yoakum, Lavaca County, Texas: Gulf Coast Assoc. Geol. Socs. Trans., v. 9, p. 41–50.

International Oil Scouts, 1982, International oil and gas development. Part II—Production: Austin, TX, Internat'l Oil Scouts Assoc., v. 51–52, 794 p.

Leithold, E.L., 1989, Depositional processes on an ancient and modern muddy shelf, northern California: Sedimentology, v. 36, p. 179–202.

Lofton, C.I., 1962, Sheridan Field, Colorado County, Texas, *in* Denham, R.L., ed., Typical oil and gas fields of southeast Texas: Houston, TX, Houston Geological Society, p. 192–197.

Loucks, R.G., Dodge, M.M., and Galloway, W.E., 1979, Sandstone consolidation analysis to delineate areas of high-quality reservoirs suitable for production of geopressured geothermal energy along the Texas Gulf Coast: Austin, University of Texas, Bureau of Economic Geology, Report Prepared for U.S. Department of Energy, Division of Geothermal Energy, 98 p.

Lowry, P., Lemoine, R.C., and Moslow, T.F., 1986, Sedimentary facies of the uppermost Wilcox shelf-margin trend: South-central Louisiana, *in* Moslow, T.F., and Rhodes, E.G., eds., Modern and ancient clastics: Core Workshop No. 9, Soc. Econ. Paleontologists and Mineralogists, p. 363–412.

Mann, C.J., and Thomas, W.A., 1968, The ancient Mississippi River: Gulf Coast Assoc. Geol. Socs. Trans., v. 18, p. 187–204.

May, J.A., and Stonecipher, S.A., 1990, Depositional environments of the Wilcox Group, Texas Gulf Coast: Stratigraphic and early diagenetic signatures: Gulf Coast Assoc. Geol. Socs. Trans., v. 40, p. 551–574.

Middleton, G.V., and Hampton, M.A., 1976, Subaqueous sediment transport and deposition by sediment gravity flows, *in* Stanley, D.J., and Swift, D.J.P., eds., Marine sediment transport and environmental management: New York, John Wiley and Sons, p. 197–218.

Murray, G.E., 1961, Geology of the Atlantic and Gulf Coastal province of North America: New York, Harper and Bros., 692 p.

Murray, G.E., and Thomas, E.P., 1945, Midway-Wilcox surface stratigraphy of Sabine uplift, Louisiana and Texas: Amer. Assoc. Pet. Geol.

Bull., v. 29, p. 45–70.
Nittrouer, C.A., DeMaster, D.J., Kuehl, S.A., and McKee, B.A., 1986, Association of sand with mud deposits accumulating on continental shelves, *in* Knight, R.J., and McLean, J.R., eds., Shelf sands and sandstones: Can. Soc. Pet. Geol. Memoir 11, p. 17–25.
Oliver, R.D., 1980, Depositional environments of the upper Wilcox Group (Eocene) in Shelby County and portions of Panola and Harrison Counties, Texas [M.S. thesis]: Nacogdoches, TX, Stephen F. Austin State University, 98 p.
Pedersen, G.K., 1985, Thin, fine-grained storm layers in a muddy shelf sequence: An example from the lower Jurassic in the Stenlille 1 well, Denmark: Jour. Geol. Soc. (London), v. 142, p. 357–374.
Salvador, A., and Buffler, R.T., 1986, The Gulf of Mexico Basin, *in* Bally, A.W., Hoffman, P.F., Skinner, B.J., and Hanshaw, B.B., eds., The geology of North America: Boulder, CO, Geological Society of America, p. 157–162.
Siemers, C.T., and Tillman, R.W., 1981, Recommendations for the proper handling of cores and sedimentological analysis of core sequences, *in* Siemers, C.T., Tillman, R.W., and Williamson, C.R., eds., Deep water clastic sediments: Core Workshop No. 2, Soc. Econ. Paleontologists Mineralogists, p. 20–44.
Snedden, J.W., Nummedal, D., and Amos, A.F., 1988, Storm- and fair-weather combined flow on the central Texas continental shelf: Jour. Sed. Pet., v. 58, p. 580–595.
Stonecipher, S.A., and May, J.A., 1990, Facies control on early diagenesis: Wilcox Group, Texas Gulf Coast, *in* Meshri, I.D., and Ortoleva, P.J., eds., Prediction of reservoir quality through chemical modeling: Amer. Assoc. Pet. Geol. Memoir 49, p. 25–44.
Swift, D.J.P., 1985, Response of the shelf floor to flow, *in* Tillman, R.W., Swift, D.J.P., and Walker, R.G., eds., Shelf Sands and Sandstones: Short Course Notes No. 13, Soc. Econ. Paleontologists Mineralogists, p. 135–241.
Switek, M.J., Rust, C.C., and Bennett, R.L., 1979, South Hallettsville, a gas field in the Lower Wilcox, Lavaca County: Amer. Assoc. Pet. Geol. Bull., v. 63, p. 536.
Tillman, R.W., 1985, A spectrum of shelf sands and sandstones, *in* Tillman, R.W., Swift, D.J.P., and Walker, R.G., eds., Shelf sands and sandstone reservoirs: Short Course Notes No. 13, Soc. Econ. Paleontologists Mineralogists, p. 1–46.
Tye, R.S., Moslow, T.F., Kimbrell, W.C., and Wheeler, C.W., 1991, Lithostratigraphy and Production characteristics of the Wilcox Group (Paleocene-Eocene) in Central Louisiana: Amer. Assoc. Pet. Geol. Bull., v. 75, p. 1675–1713.
Vlissides, S.D., 1964, Map of Texas showing oil and gas fields, pipelines, and areas of exposed basement rocks: U.S. Geol. Survey, Oil and Gas Investigations, Map OM-214.
Vormelker, R.S., 1979, Mid Wilcox channel: Deep exploration potential: So. Tx. Geol. Soc. Bull., v. 20, p. 10–40.
Walker, R.G., 1985a, Geologic evidence for storm transportation and deposition on ancient shelves, *in* Tillman, R.W., Swift, D.J.P., and Walker, R.G., eds., Shelf sands and sandstone reservoirs: Short Course Notes No. 13, Soc. Econ. Paleontologists Mineralogists, p. 243–302.
Walker, R.G., 1985b, Ancient examples of tidal sand bodies formed in open, shallow seas, *in* ibid., p. 303–341.
Walker, R.G., 1985c, Cardium Formation 4. Review of facies and depositional processes in the southern foothills and plains, Alberta, Canada, *in* ibid., p. 353–402.
Walker, R.G., 1985d, Comparison of shelf environments and deep basin turbidite systems, *in* ibid., p. 465–502.
Williams, C.E., Travis, L.R., and Hoover, E.M., 1974, Depositional environments interpreted from stratigraphic, seismic, and paleoenvironmental analyses: Upper Wilcox Katy Field, Texas: Gulf Coast Assoc. Geol. Socs. Trans., v. 24, p. 129–137.

CHAPTER 8

Facies, Reservoirs and Stratigraphic Framework of the Mossoró Member (Latest Cenomanian-Earliest Turonian) in Potiguar Basin, NE Brazil: An Example of a Tide and Wave Dominated Delta

Joel Carneiro De Castro

Introduction

The Potiguar Basin is located in northeastern Brazil and occupies an area of about 40,000 km^2, distributed both onshore and offshore (Fig. 8.1). It is one of the Brazilian marginal basins originated by Africa–South America rifting in the Early Cretaceous. In recent years, the onshore portion has undergone intense exploration, resulting in the discovery of several small oil fields that produce from Lower and middle Cretaceous rocks. The mid-Cretaceous is represented by the clastics of the Açu Formation, which comprises a lower fluvial unit and an upper, transitional unit known as the Mossoró member.

This study focuses on the paleogeography of the Mossoró member by making use of outcrop and subsurface data, including continuous cored sections from four oil fields. Detailed stratigraphic correlation within the Mossoró member has facilitated the characterization of facies geometries and system tracts, and the mapping of an important regressive event, the Mossoró Sandstone, which is a tongue of that member and represents the main reservoir in those fields. The designation "Mossoró Sandstone" is given by petroleum development geologists for the main reservoir of Mossoró member in four oil fields, based on detailed correlation; this statement is reinforced by facies characteristics and sequences. Since no significant diagenetic change is imprinted on the sandstones of the Açu Fm, the most important factor controlling the porosity development in the reservoirs is the original depositional environment and resulting facies. A tide- and wave-dominated deltaic model similar to the modern Açu River on the mesotidal northeastern Brazilian coast is proposed.

Structural and Stratigraphic Framework

The structural setting of the Potiguar Basin is dominated by a series of half grabens oriented northeast-southwest onshore and west-northwest/east-southeast in the offshore portion of the basin (Fig. 8.1). These grabens originated during the Africa–South America rifting of the Early Cretaceous. During this stage (Neocomian/Aptian), up to 4,000 m of fluvial, deltaic lacustrine and deep-water lacustrine sediments were deposited.

The Açu Fm (Albian/Cenomanian) is a coarse clastic unit that occurs as a blanket all over the basin. It unconformably overlies the older nonmarine section in the graben areas. In the wide platforms that flank the central grabens, and in the outcrop belt, it directly overlies a metamorphic basement (Fig. 8.1). The limestones of the Jandaíra Fm (Turonian/Santonian) crop out in most of the onshore portion of the basin.

The stratigraphic column of the Potiguar Basin is completed with Campanian/Maastrichtian and Cenozoic rocks that crop out in the littoral zone and fully develop offshore.

A dip-oriented stratigraphic section (Fig. 8.2) shows the blanket nature of the Açu and Jandaíra Fms, as well as the stratigraphic correlation between the Açu Fm clastics and its distal equivalents. In the onshore setting, the Açu Fm comprises two units: (1) a lower unit, 300–700 m thick, formed by coarse clastics of fluvial and fluvio-estuarine origin; and (2) an upper one, known as the Mossoró member, that is 50–100 m thick and dominated by transitional-marine fine clastics. The lower unit of coarse clastics of the Açu Fm grades offshore to fine clastics deposited in a shelf setting and to the limestones of the Ponta do Mel Fm, the latter forming a narrow and extensive platform during

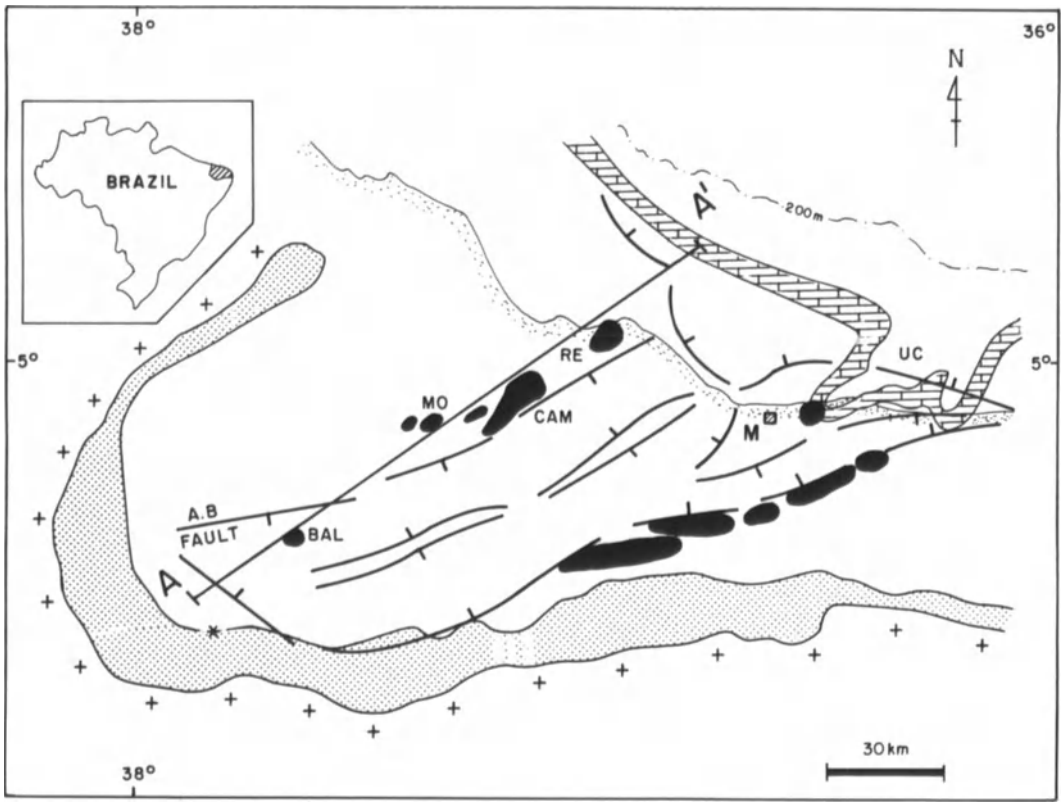

Figure 8.1. Main features of the Potiguar Basin in northeastern Brazil. Oil fields (shown in black) that have been studied are located along a major structural lineament, the Areia Branca fault (AB): Baixa do Algodão, Mossoró, Canto do Amaro, and Redonda (BAL, MO, CAM, RE). NE-SW oriented, onshore, and WNW-ESE, offshore grabens delimit the occurrence of Lower Cretaceous rocks. Basement is shown by crosses, Açu Fm outcrop by dots, and Ponta do Mel carbonate platform by a brick pattern; the asterisk localizes the Apodi outcrop. The town of Macau and Ubarana Canyon are indicated (M, UC).

Albian time (Figs. 8.1 and 8.2). Another important contemporaneous system is the deep-water complex of Latest Albian to Middle Cenomanian age that occurs at Ubarana canyon, an erosional reentrance clearly delineated in the Ponta do Mel carbonate platform (Fig. 8.1).

The upper unit of the Açu Fm, the Mossoró member, is regionally distributed and bounded by approximate time lines. The lower boundary (marker I) represents a major transgressive event that records the onset of a transitional marine environment following a period of extensive alluvial sedimentation (lower Açu unit) in the basin. The upper boundary marks the beginning of carbonate deposition that has resulted from a transgression over a nearly flat surface (Fig. 8.2). Thus, both contacts of the Mossoró member rise stratigraphically toward the margin of the basin to the south; that is, they become slightly younger in that direction.

The stratigraphic framework of the Mossoró member (latest Cenomanian to earliest Turonian) will be discussed in this chapter.

Facies Analysis

The Mossoró member encompasses four main depositional systems, ranging from dominantly fluvial in the outcrop belt to marine in the offshore portion of the basin. Between these two geographic extremes, four oil fields in the onshore portion of the Potiguar Basin produce from the following systems: (1) meandering fluvial, represented by the Baixa do Algodão field; (2) delta plain, represented by the Mossoró field; and (3) estuarine/tidal flat, represented by the Canto do Amaro and Redonda fields.

Thus, each depositional system is represented by one oil field, except for the offshore marine system, which does not have reservoir rocks. The estuarine/tidal-flat system is represented by the Canto do Amaro field (see also Bagnoli, this volume). In the following sections, the depositional systems (= facies association) will be characterized by analysis of the vertical sequences and geometric properties of their component facies.

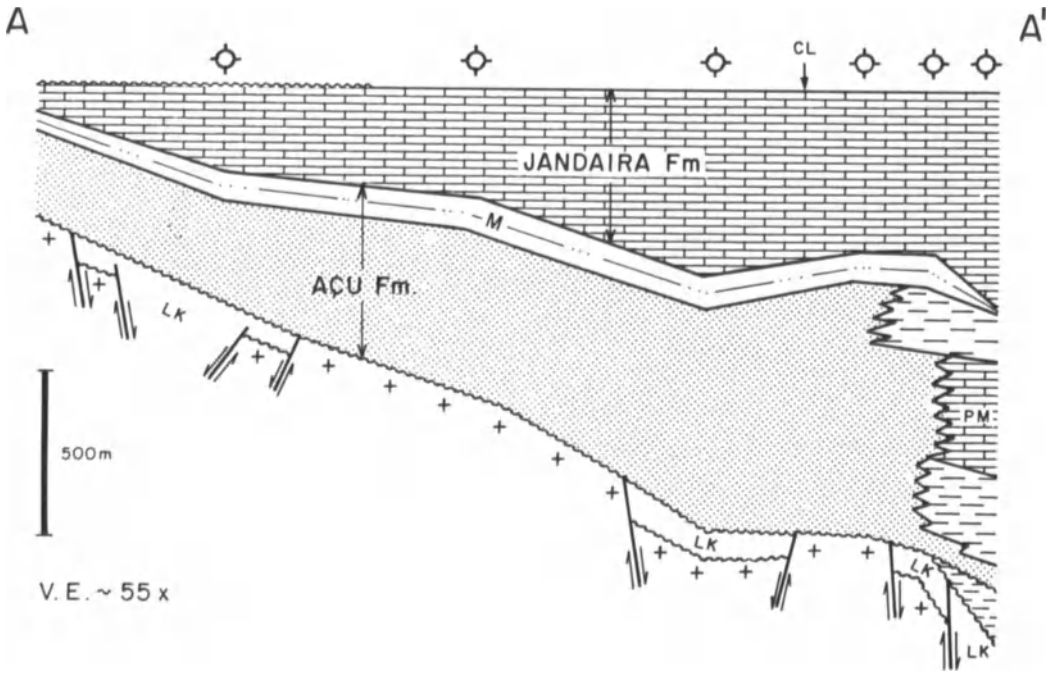

Figure 8.2. Dip-oriented stratigraphic cross section AA′ (Fig. 8.1), showing the blanket nature of Açu and Jandaíra Formations and the offshore facies changing of the coarse clastics of the Açu Fm to fine clastics and to carbonates (Ponta do Mel Fm = PM). (Datum = top of Jandaíra Fm; M = Mossoró member; LK = Lower Cretaceous; CL = coastline).

Outcrop Data

The 50-m-thick continuous exposure of the upper part of the Açu Fm near the town of Apodi (Fig. 8.1) has been studied by the author and colleagues in order to understand the facies and their geometries for a comparison with subsurface data. The section measured in this outcrop is nearly equivalent to the Mossoró member and represents its proximal deposits. Besides these dominantly fluvial sandstones, other facies—such as crevasse lobe sandstones/siltstones, estuarine sandstones, and tidal-flat shales/dolomitic marls/cemented sandstones—are also characterized. Thus, the outcrop data offer a unique opportunity to examine 3-D facies relations that can be tied to the regional framework of the Mossoró member.

At least four fluvial intervals (facies A1, Fig. 8.3F) are present. Each one is 4–5 m thick and formed by two units. The lower unit is thinner, has an erosional base, channel form, and a fining-upward trend formed by small sets of trough cross-bedded sandstones rich in shale clasts that grade into cross-laminated sandstones, which are overlain by thin shale beds. The upper sandy unit is thicker, and has a flat base and a convex shape that suggests bar deposits; internally, it has thick sets of tabular cross beds with tangential contacts.

Possible overbank deposits composed of brown shales and very fine sandstones with sigmoidal cross beds and geometry (facies A3, Fig. 8.3E) locally overlie fluvial sandstones. Crevasse lobe sandstones and siltstones (facies A2, Fig. 8.3C and D) have a sharp base and grade vertically and laterally from tabular cross-bedded and horizontally laminated fine sandstones, to partly bioturbated, ripple drift cross-laminated, very fine sandstones, and to siltstones.

Estuarine sandstones (Fig. 8.3A and B) are well documented by the occurrence of mud flasers intercalated with the topmost fluvial sandstone, suggesting an upper estuarine setting. The presence of bioturbated sandstones in the upper portion or overlying crevasse and overbank deposits is also indicative of brackish conditions.

The uppermost facies (C1, Fig. 8.3A) present in the outcrop that directly underlies the dolomitic limestones of the Jandaíra Fm is the tidal flat association of gray shales, cream dolomitic marls containing a poor fauna of arenaceous foraminifers, and cemented/fossiliferous sandstones with tidal-modified cross bedding.

Baixa do Algodão Oil Field: The Fluvial Meandering System

The Baixa do Algodão oil field is located on a dome-shaped structural high. It produces 147 m^3/day of 28° API oil from

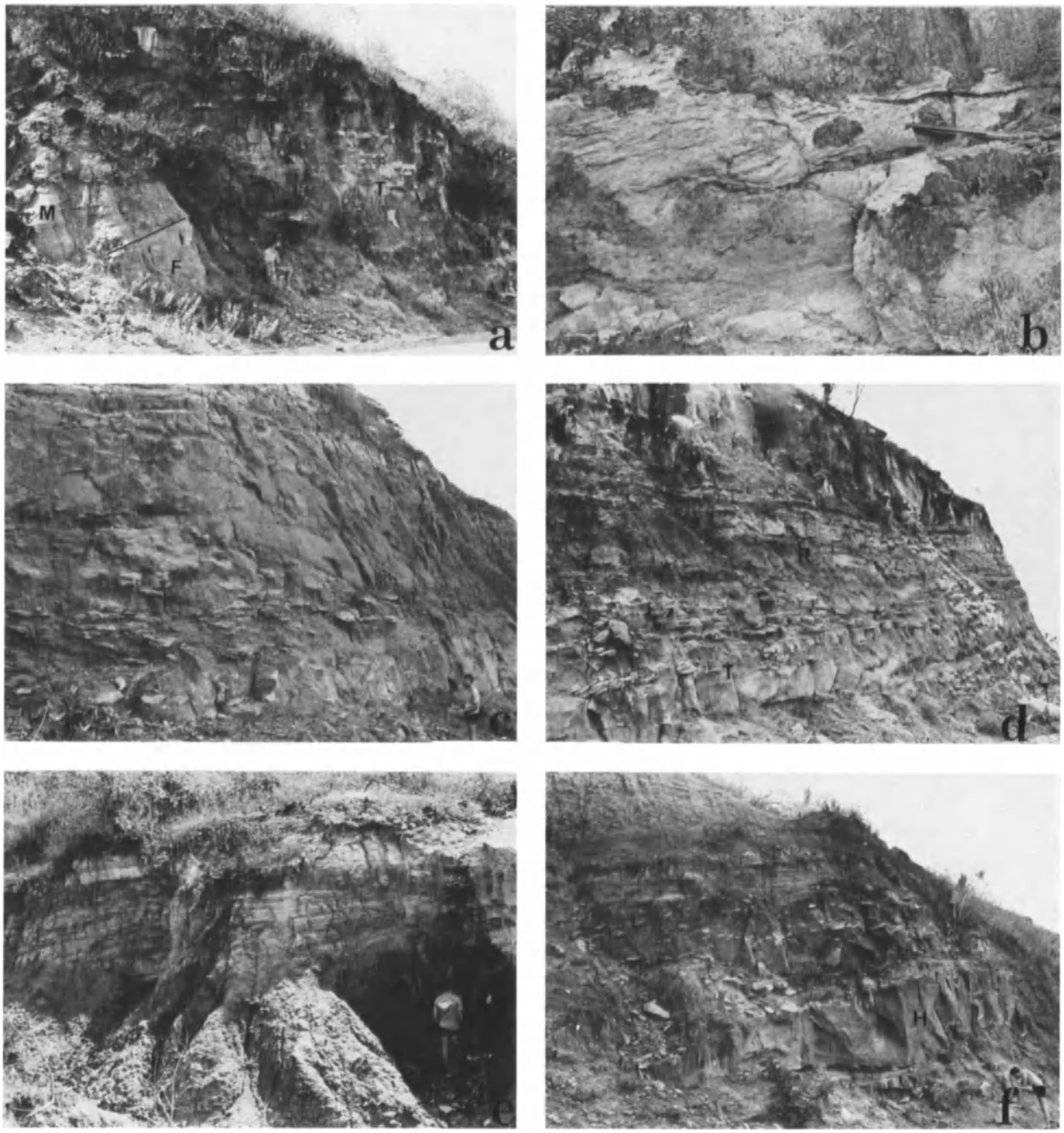

Figure 8.3. Apodi outcrop. (A) Lagoonal shale (M, facies C1) onlapping fluvial bar sandstone (F, facies A1); the shale unit wedges toward the top of the bar (T; see detail in B). (B) Detail of mud flasers at point T (previous photo). (C) Crevasse sandstones (facies A2) abruptly overlying fluvial sandstone. (D) Crevasse deposits: tabular and horizontally laminated sandstones (T) fining upward to bioturbated, ripple-drift cross-laminated sandstone and siltstone (R). (E) Sigmoidal cross-bedded, very fine sandstone overlying brown shales with mudcracks (facies A3 and F1). (F) Fluvial bar (see H in photo) overlying a channel sequence, facies A1 (see Fig. 8.15, for photograph position in the outcrop section).

16 wells. The main reservoir, known as the Mossoró Sandstone, is subdivided into three production zones, MO-I to MO-III. Two cored wells, 7-BAL-5-RN (Fig. 8.4) and 7-BAL-14-RN, adequately document the Mossoró member in this field.

Facies

Eight facies are recognized and described as follows. Facies A1 is represented by trough cross-bedded, medium- and coarse-grained sandstones, with erosional base and abun-

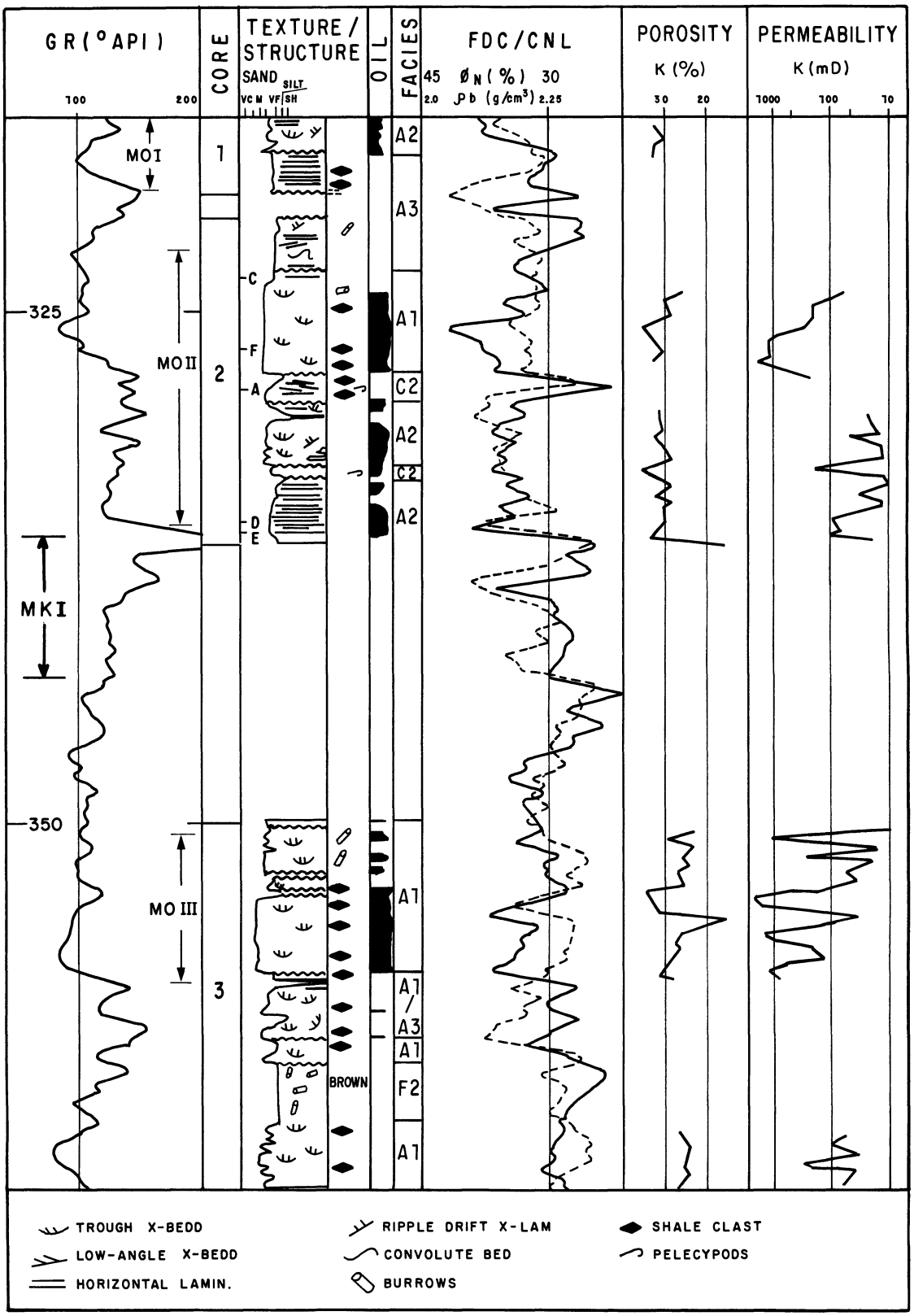

Figure 8.4. Sequential analysis of cores from well 7-BAL-5-RN (description by E. Bagnoli); MO-I, MO-II, MO-III are production zones, and MK-I is marker I. The position of core photographs (Fig. 8.5) is indicated at left of the texture column.

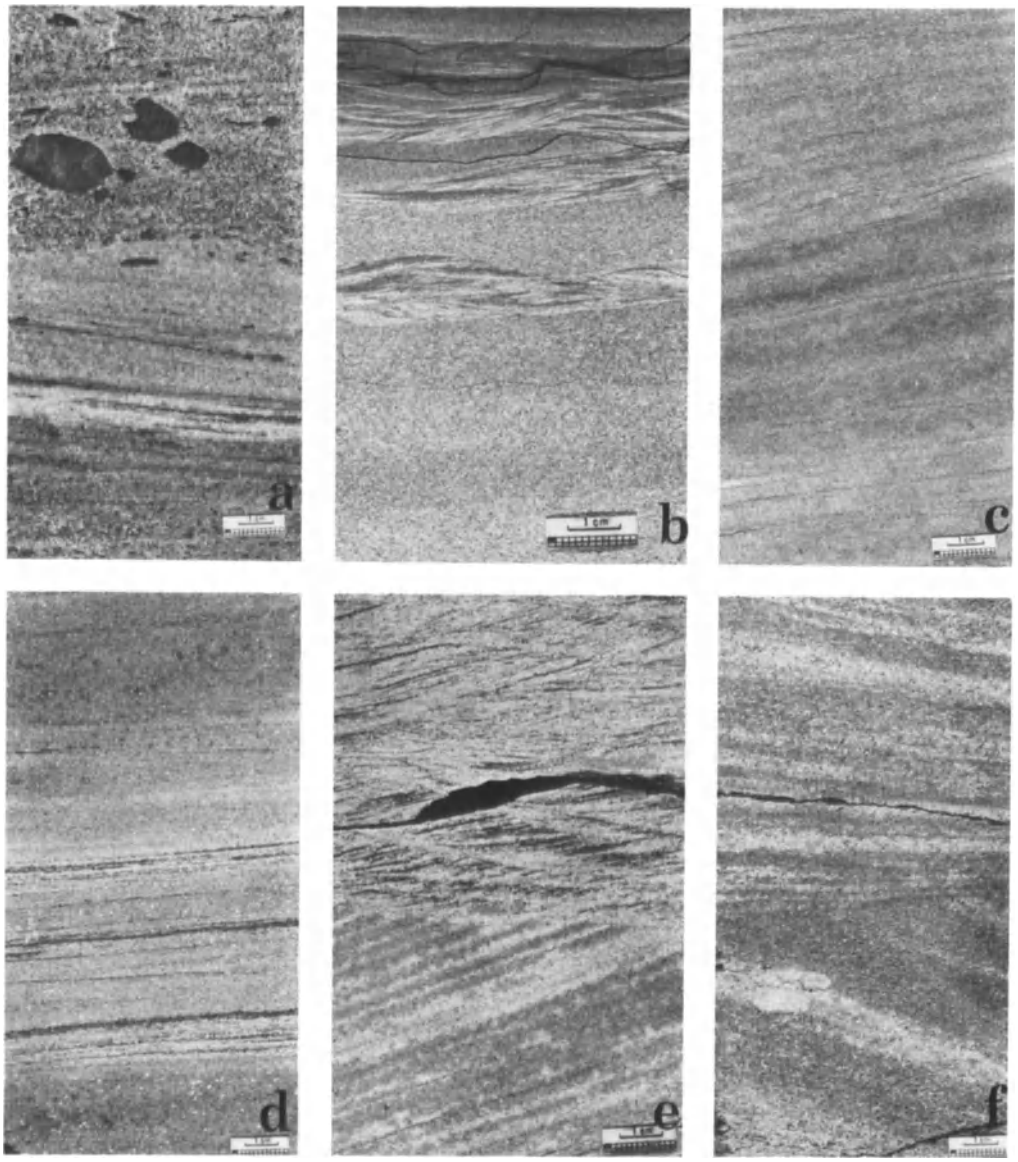

Figure 8.5. Core photographs of Baixa do Algodão field. (A) Low-angle, cross-bedded, cemented sandstone with shale clasts, facies C2. (B) Rhythmites with graded bedding (top) or massive to ripple-drift cross lamination, facies F3 (from BAL-14-RN). (C, D, E). Tangential tabular cross-bedded, horizontally laminated, and ripple-drift/cross-bedded sandstones of facies A2. (F) Cross-bedded sandstone with shale clasts in the foresets, facies A1.

dant shale clasts (Fig. 8.5F). It may be followed upward by a thin interval of tabular-tangential, cross-bedded, micaceous fine sandstone. This facies is interpreted as a point bar in a fluvial meandering system.

Facies A2 is formed by fining-upward sequences from bottom to top: tabular cross-bedded, medium to fine sandstone, which may be associated with ripple drift cross-lamination (Fig. 8.5E), followed by horizontally laminated or sigmoidal cross-bedded, fine sandstone (Fig. 8.5D and C), and by ripple drift cross-laminated, fine to very fine sandstone, bioturbated and silty toward the top. This facies is interpreted as crevasse lobe deposits with possible estuarine influence.

Facies A3 is represented by fining-upward sequences with massive or graded fine sandstone and ripple drift cross-laminated, micaceous, fine to very fine sandstone (Fig. 8.5C); it probably records overbank and flood-plain deposition.

The shaly facies are of three types: brown siltstone-shale (F1); gray-brown, massive to bioturbated siltstone to silty sandstone (F2) of flood-plain origin; and thin rhythmites of sandstone and shale (Fig. 8.5B), with graded bedding and

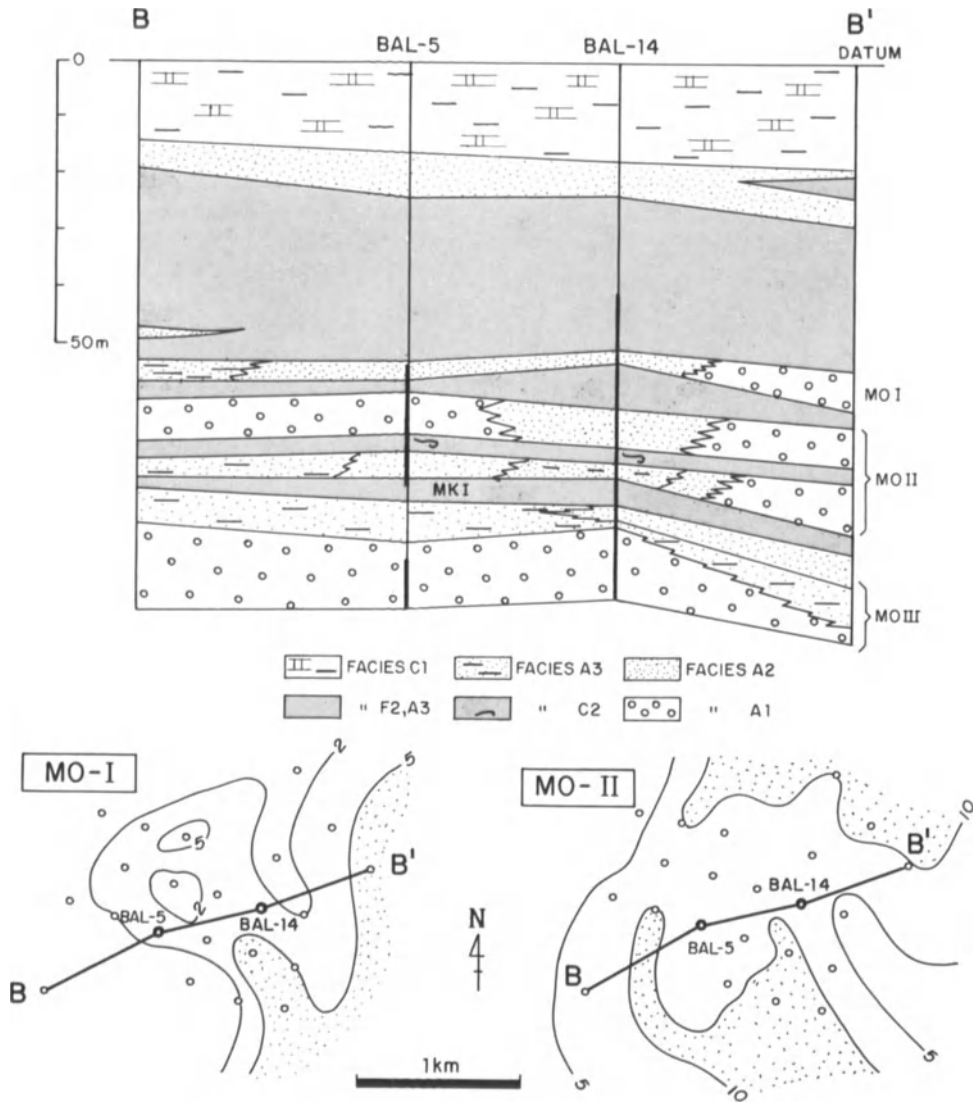

Figure 8.6. Baixa do Algodão oil field (top). Cross section BB′ in Mossoró member showing facies distribution (see text). MO-I, MO-II, MO-III and MK-I refer to Mossoró Sandstone zones I, II, III and to marker I; vertical bars indicate cored sections; base of Jandaíra Fm is datum. Isolithic map (bottom) of Mossoró Sandstone shows zones MO-I (left) and MO-II (right); contours in meters (maps prepared by M.A. Castelo Branco).

climbing ripples (F3) that grade to dark gray-brown shale and represent oxbow-lake deposition (E. Bagnoli, personal communication, 1991).

The last two facies (C1 and C2) are carbonate-rich sandstones that constitute transgressive events. Facies C1 is composed of fossiliferous/cemented sandstone, detrital dolomitic marl, and greenish-gray shale; it occurs toward the top of the unit and is interpreted as a tidal flat. Facies C2 is made up of cemented, intraclast-rich, low-angle, cross-bedded sandstone with occasional pelecypod and phosphatic debris, making up a possible storm deposit (Fig. 8.5A).

Facies relations and sandstone geometry

The geometric relations among lithofacies of the Baixa do Algodão oil field, as well as the Mossoró Sandstone geometry, are shown in Figure 8.6. Despite its tabular shape, the fluvial sand bodies (facies A1) show significant lateral facies change to marginal deposits of facies A3, with corresponding permeability variation from high (up to 3.5 d) to low (Figs. 8.4 and 8.6). Thus, the oil reservoirs are facies A1 and, to a lesser extent, facies A2 sandstones; the seal rocks are shales and very fine, micaceous sandstones (facies F2 and A3; Fig. 8.4).

Another interesting aspect of this unit is the presence of thin transgressive intervals composed of the intraclast-rich. cemented sandstone (facies C2) that interrupts the dominant alluvial sedimentation and also acts as a seal.

The isopach maps of the Mossoró Sandstone (Fig. 8.6, bottom) strongly support a meandering fluvial origin for the sand bodies. The isopach map of the MO-I producer zone map suggests a complete channel/crevasse/flood-plain setting.

Mossoró Field: The Delta Plain System

The Mossoró oil field, which was the first discovery in the onshore part of the basin, is located on a northeastward-dipping structural nose. The daily production averages 10 m^3 of a 27° API oil, from 15 wells. Its low performance is mainly due to the limited extent of the Mossoró Sandstone reservoir. Except for well 9-MO-13-RN, which continuously cored the Mossoró member, other wells were cored only for the Mossoró Sandstone.

Facies

Seven facies were mapped in the Mossoró member: three of them are porous sandstones, two are siltstones/shales, and two are cemented, fossiliferous sandstones. Figure 8.7 depicts part of the continuous core from 9-MO-13-RN, with the sequential facies analysis and calibration of logs and petrophysical data.

Facies A2 and A3 have already been discussed in the Baixa do Algodão oil field section. Two important aspects of the facies are the close association in facies A2 between tabular cross bedding and ripple-drift cross lamination, both dipping in the same direction (Fig. 8.8D); and the fining-upward sequence of facies A3, which is formed by massive bedding containing shale clasts, sigmoidal cross bedding and ripple-drift cross lamination (Fig. 8.8A, B, and C). Facies A2 is interpreted as crevasse lobe deposits or the upper part of a fluvial point bar, whereas facies A3 is interpreted as crevasse-overbank deposits.

Facies A4 is characteristic of the Mossoró Sandstone reservoir. It comprises a major fining-upward sequence, which is itself composed of smaller ones. The sequences start with trough and tabular cross-bedded, medium-fine sandstones containing shale clasts (Fig. 8.9C), overlying an erosional base. This lithofacies is followed by horizontally laminated, well-sorted fine sandstone, rich in micaceous laminae toward the top (Fig. 8.9B); and a ripple-drift, cross-laminated, very fine sandstone, that is siltier and burrowed on the top (Fig. 8.9A). The sequence ends with brown, massive to deformed siltstones (facies F1). The fining-upward trend (Fig. 8.7) is associated with reduced permeabilities and increased water saturation due to the shaliness of the ripple-drift/bioturbated uppermost interval. This facies is interpreted as a crevasse lobe sand body (Castro et al., 1982) from evidence suggesting a combination of unidirectional, bedload, and suspended-load deposition (Coleman, 1969); bioturbation may be indicative of a estuarine setting.

The finer-grained facies F1 and F2 have already been described.

The fossiliferous/dolomitic sandstones are of two types: (1) bioturbated, silty sandstone with plant remains (facies C3, Fig. 8.9D); and (2) horizontally laminated and bioturbated, in part by *Ophiomorpha*, very fine to fine sandstone (facies C4, Fig. 8.9E). These facies can be related to transgressive settings (beach, lagoon) set up after crevasse abandonment and submergence (Saxena, 1976).

Facies relations and reservoir geometry

Figure 8.10 displays the spatial distribution of the seven facies previously identified in the Mossoró member type section. The predominance of crevasse and overbank deposits (facies A2, A3, A4, F1, and F2), interrupted by intervals of cemented sandstones of transgressive origin (facies C3 and C4), is readily observed.

The main reservoir of the field, the Mossoró Sandstone, shows rapid facies changes from medium to fine, porous sandstones (facies A4) to very fine sandstones and siltstones with low porosity (facies A3/F1). This relation is demonstrated in the sandstone isolithic map (porosity cutoff of 28%), where the wells with best production are within the 5-m contour, whereas those wells with no production plot within the less-than-2-m contour area (Fig. 8.10). The general oval geometry and the dimensions of the sand body are comparable to those of modern crevasse-lobe deposits in deltaic settings (Donaldson et al., 1970). The absence of associated fluvial channel deposits suggests similarities to the modern Açu delta (discussed below) where at least 80% of the delta-plain area is dominated by crevasse lobes and subdeltas.

Canto do Amaro and Redonda Fields: Estuarine/Tidal-Flat System

The Canto do Amaro accumulation, like Mossoró, is an anticlinal nose dipping to the northeast. It is the best oil field in the onshore portion of Potiguar Basin, where it produces from several reservoirs in the Açu Fm, including the Mossoró member. The main reservoir in this unit is the Mossoró Sandstone, and indeed, it is situated at the same

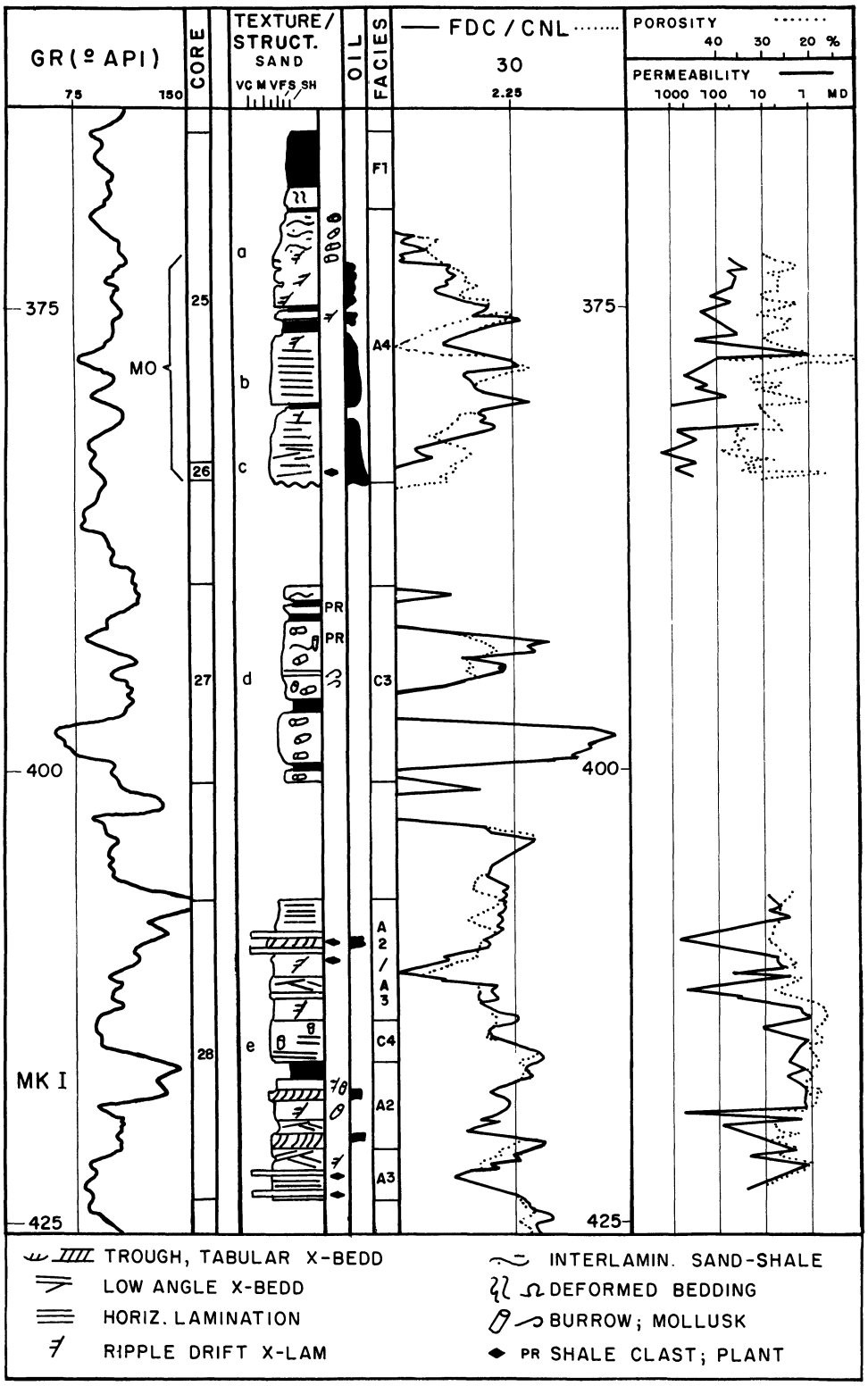

Figure 8.7. Sequential analysis of cores from 9-MO-13-RN well. Position of core photographs (Fig. 8.9) at left of Texture column. MO = Mossoró Sandstone; Mk I = marker I.

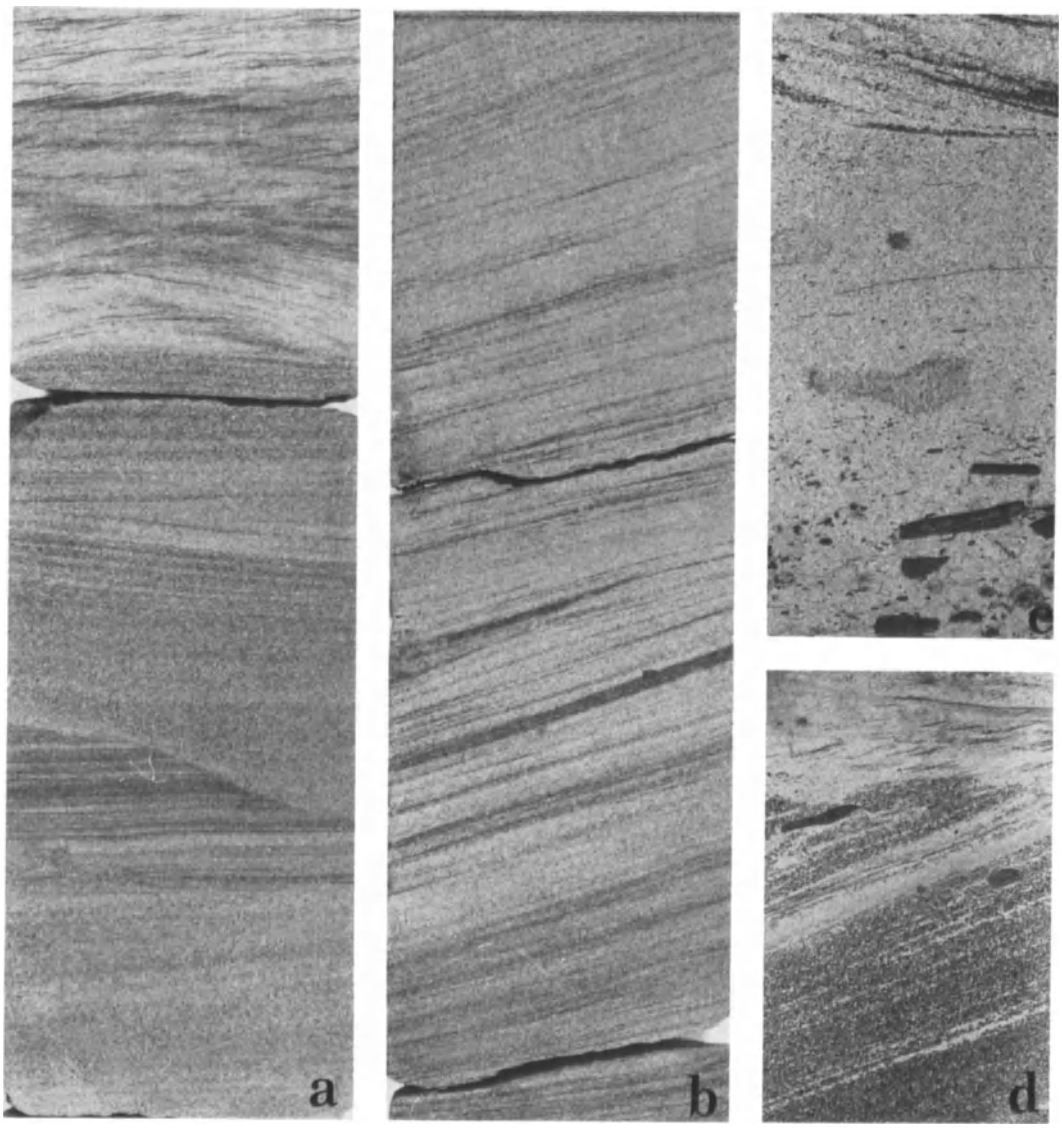

Figure 8.8. Core photographs of Mossoró field. (A, B, C) Crevasse/overbank sandstones and siltstones, facies A3. Fining-upward sequence of massive to sigmoidal cross-bedded sandstones, with shale clasts (C), tabular-tangential cross-bedded sandstone (B), and graded, low-angle (sigmoidal) cross-bedded to ripple-drift cross-laminated sandstone (A). (D) Tabular cross-bedded and ripple-drift cross-laminated sandstone, with shale clasts of facies A2 (Core widths, 10 cm).

stratigraphic level as the Mossoró Sandstone in the type section (Mossoró oil field). The oil production from this sandstone amounts to 400 m^3/day from 41 wells, with 28° API.

Facies

Seven wells were cored in the Mossoró Sandstone in the Canto do Amaro oil field; two of them, 7-CAM-7-RN and 7-CAM-63-RN (Fig. 8.11), have sampled thick sections of the Mossoró member.

It is possible to identify 8 facies in the Canto do Amaro oil field (see Bagnoli, this volume): two sandy reservoirs (facies A2, A5), four silty-shale seals (F2, F4, F5, F6), and two cemented sandstones/dolosparites (C3, C5). For comparison, these facies correspond respectively to E. Bagnoli's lithofacies 2, 1, 3, 6, 5, 8, 4, and 7(this volume). Two new sandy lithofacies, A6 and A7, are characteristic of the Redonda oil field, where the Mossoró member was extensively cored (Fig. 8.12): facies A6 can be recognized in Canto do Amaro (Fig. 8.11), which it has been included in E. Bagnoli's lithofacies 4 (this volume).

Facies A2, already described, is dominated by ripple-

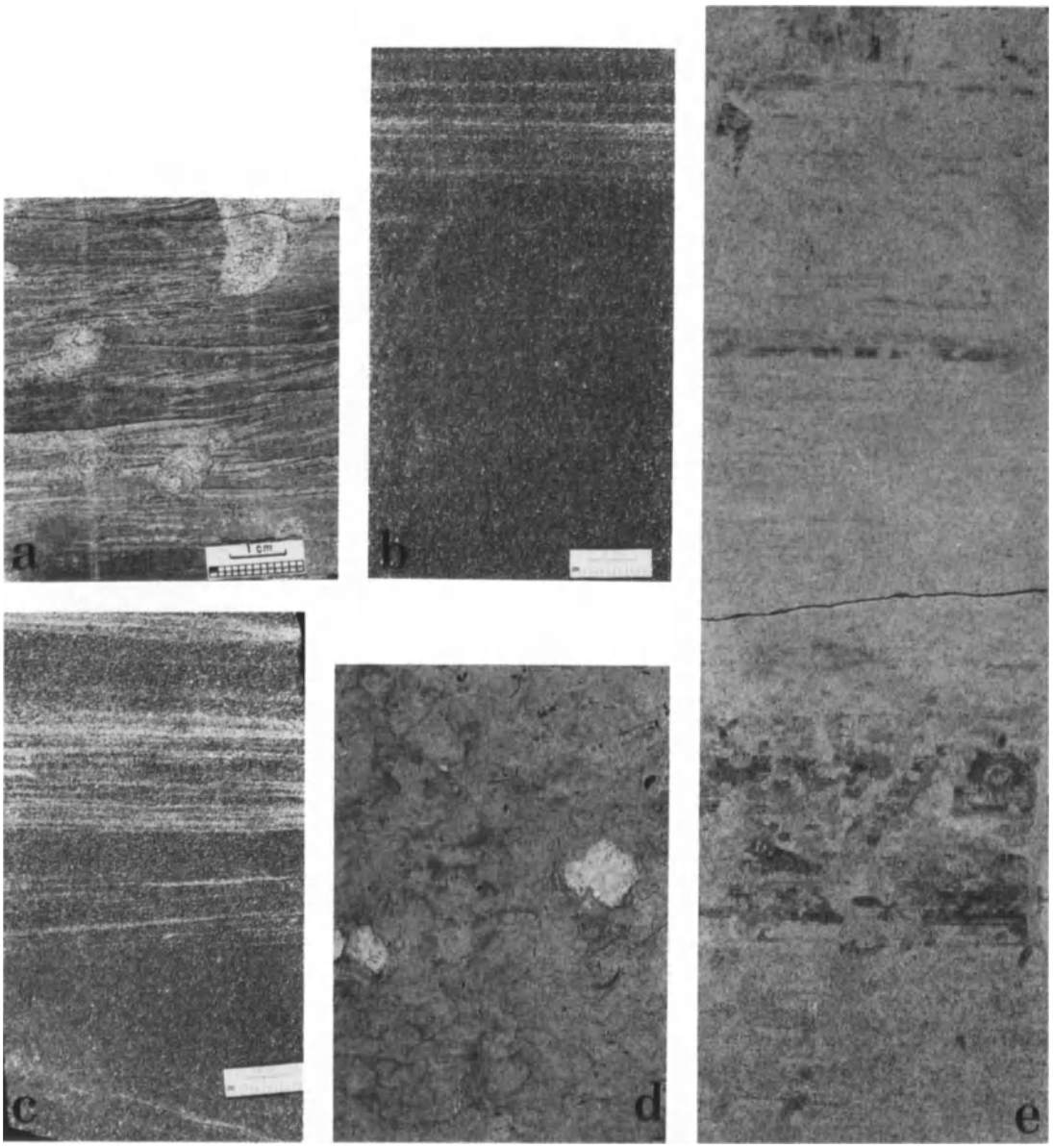

Figure 8.9. Core photographs of Mossoró field, well Mo-13 (see Fig. 8.7). (A, B, C) Fining-upward sequence of crevasse lobe deposits, facies A4, formed by low-angle, cross-bedded sandstone (C), horizontally laminated sandstone with micaceous laminae (B), and ripple-drift cross-laminated/bioturbated sandstone (A). (D) Bioturbated, very fine sandstone; black dots are plant remains, and white spots are recrystallized mollusk debris, facies C3. (E) Horizontally laminated and bioturbated sandstone, facies C4.

drift, cross-laminated, very fine sandstone (Fig. 8.13A), and subordinate horizontally laminated and cross-bedded fine sandstones.

Facies A5 represents a fining-upward sequence, which is itself composed of smaller ones. It begins at the base with shale-intraclast conglomerate, up to 0.2 m thick, resting on an erosional surface. This surface passes upward into trough and tabular cross-bedded, fine sandstone, containing shale clasts in the foresets (Fig. 8.13D), overlain by massive or horizontally laminated, fine to very fine sandstone to ripple drift, cross-laminated, micaceous, very fine sandstone (Fig. 8.13C) with thin shale interbeds. Shale drapes may occur within the sandstones, whereas bioturbation is present on the top of the sequence (Fig. 8.13B), preceding siltstones and shales of facies F2.

The A5 facies is representative of the Mossoró Sandstone in Canto do Amaro field: lithologically and compositionally (arkoses), it resembles facies A4.

At Redonda, the A5 facies exhibits more marine influences, as demonstrated by the presence of phosphatic

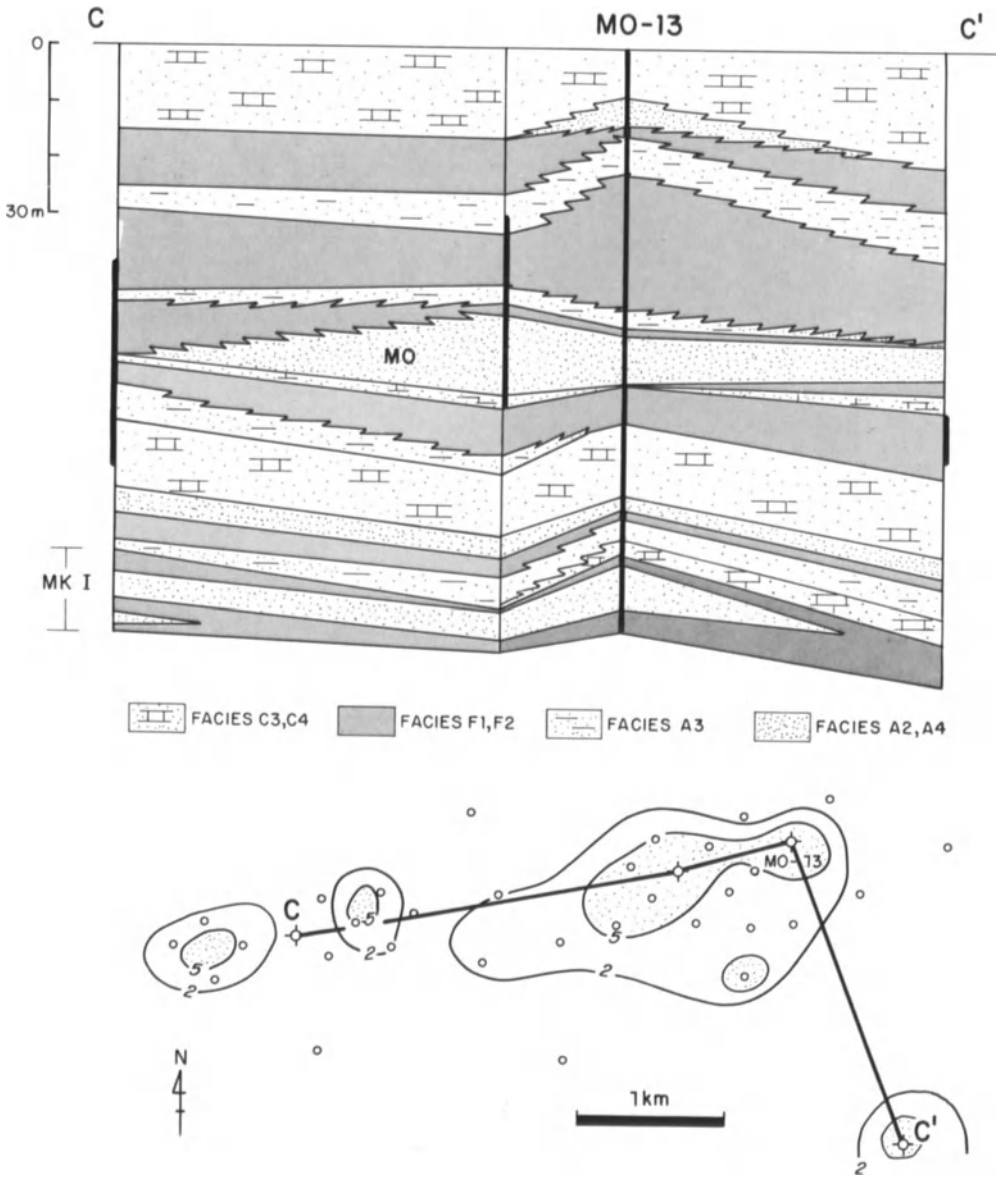

Figure 8.10. Mossoró oil field. Cross-section CC′ (top) of Mossoró member in the type section, showing vertical and lateral facies relations. (For facies code, see text. MO = Mossoró Sandstone. Vertical bars-cored intervals.) Mossoró Sandstone isopach map (bottom: porosity cutoff of 28%) exhibiting the oval geometry of crevasse lobe deposits.

and mollusk debris in the basal shale-intraclast conglomerate, and locally by *Ophiomorpha* burrows. An estuarine channel-mouth bar origin is proposed for facies A5.

The A6 facies is represented by cross-bedded, fine to medium sandstones, displaying an erosional base enriched in shale clasts, as well as flaser bedding and shale drapes in the foresets. It shows a distinct fining-upward trend due to increasing bioturbation toward the top (by *Ophiomorpha* and horizontal burrows); local herringbone cross-bedding may occur (Fig. 8.13E and F). Facies A6 forms the upper portion of coarsening-upward sequences (Fig. 8.11, 8.12) as it overlies fossiliferous, bioturbated silty sandstones (facies C3). At Redonda, the CU sequence is made more complete by the introduction of pelecypod-rich, hummocky-structured, very fine sandstones (facies A7, next) between facies A6 and C3. We suggest an estuarine channel-ebb tidal delta for the origin of such sequence.

The A7 facies, mainly developed in the Redonda oil field, consists of wavy-bedded sandstones and shales intercalated with fossiliferous, cemented very fine sandstones with truncated undulating laminations (microhummocky) and thin vertical burrows. The A7 facies also constitutes the upper portion of coarsening-upward sequences as it overlies bioturbated, silty sandstones, and siltstones/shales with *Chondrites* and horizontal burrows (facies C3 and F5, Fig. 8.12). Besides its presence in the coarsening-upward sequences, as previously described (facies F5-C3-A7-A6), the A7 facies also represents a lateral equivalent of the A6 facies in the Redonda oil field. We may assume an ebb-tidal delta/shallow-marine origin for the sequence.

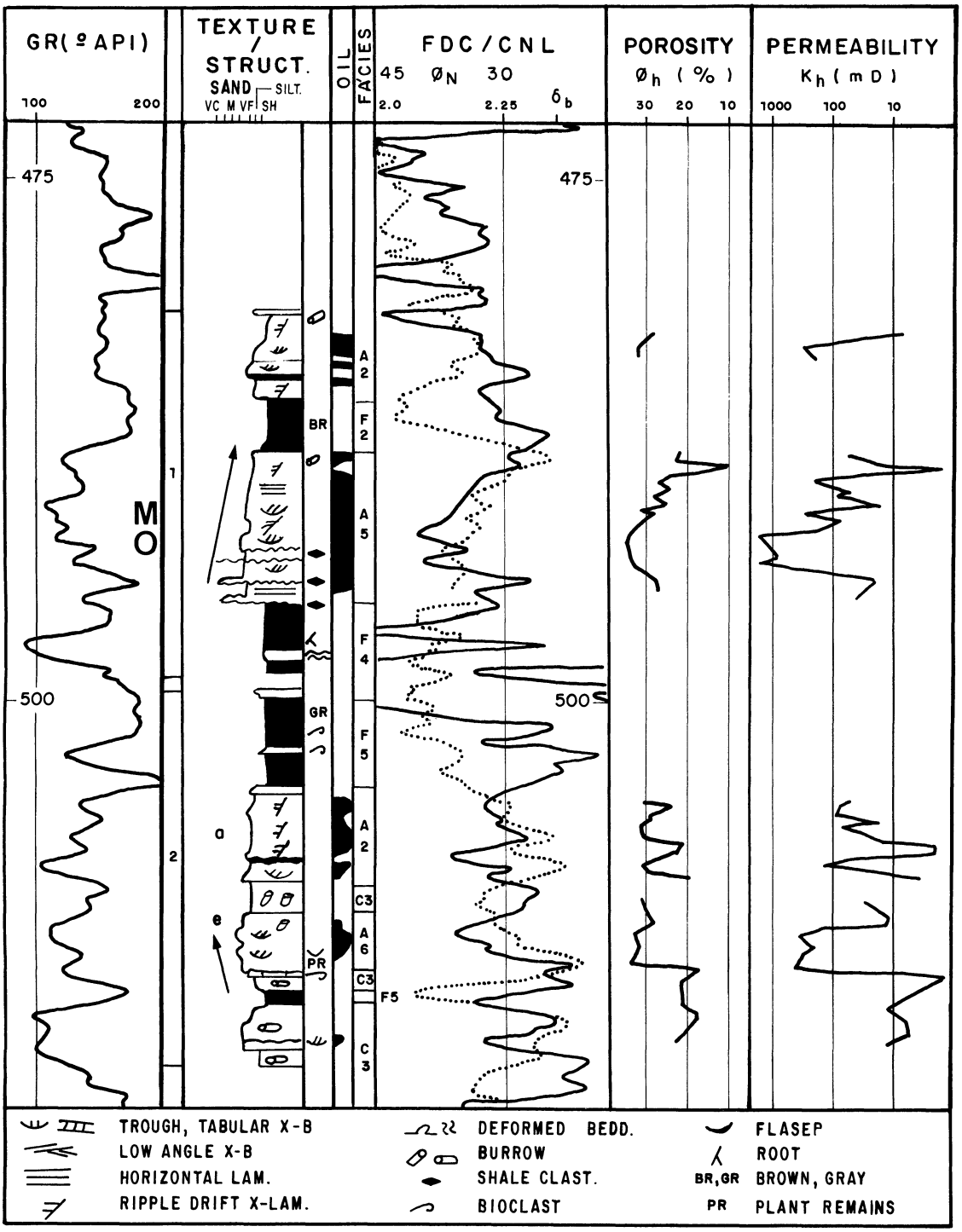

Figure 8.11. Sequential analysis of cores from 7-CAM-63-RN well. Notice FU trend of the Mossoró Sandstone and CU trend of the transgressive, wave- and tide-reworked sandstone/shale.

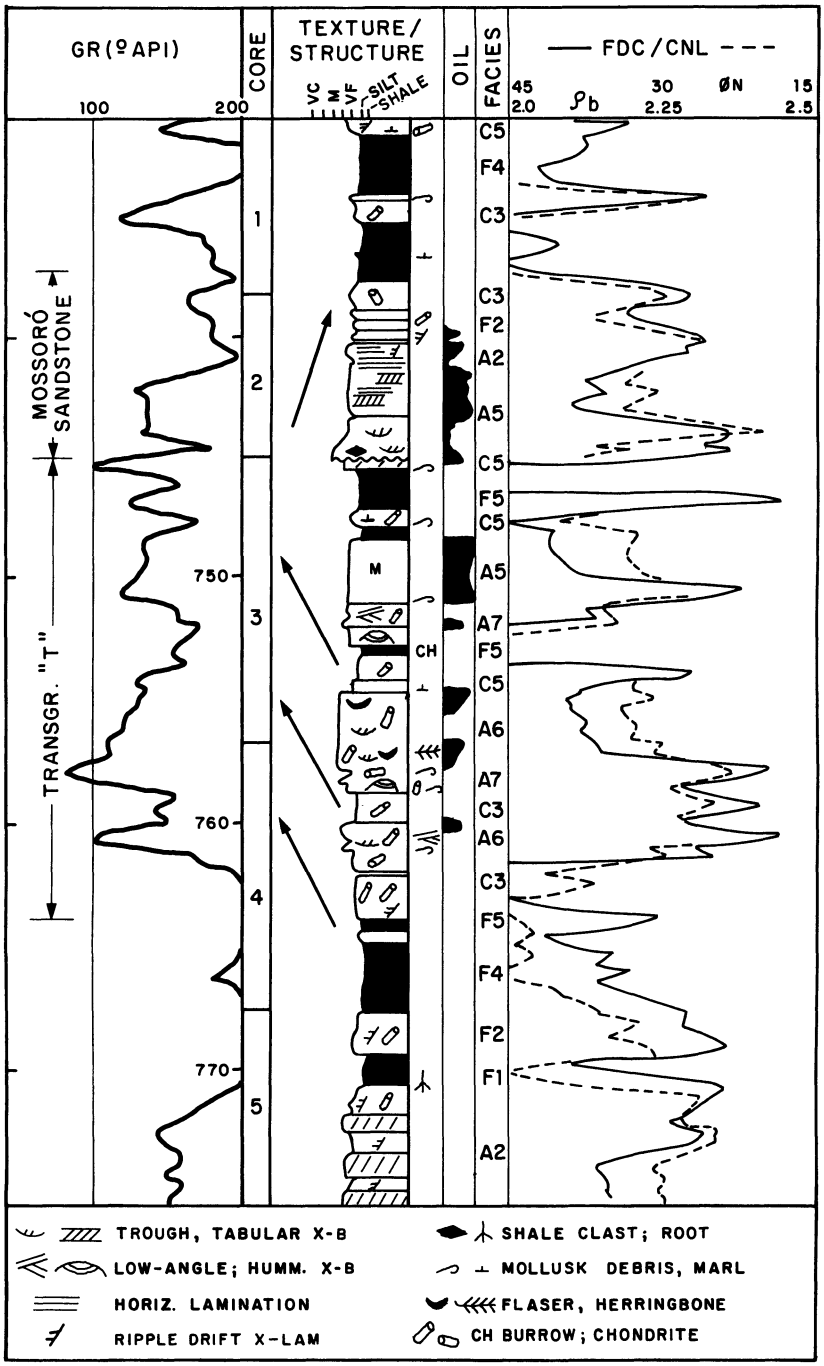

Figure 8.12. Sequential analysis of cores from RE-8-RN well, showing the FU sequence of the Mossoró Sandstone and CU sequences in the lower sandstones (which correspond to T, Fig. 8.15).

We should refer here to another wave-reworked facies, which is represented by fossiliferous, cross-bedded to horizontally laminated fine sandstones displaying *Ophiomorpha* burrows. The sandstones are locally cemented by dolomite and may grade above and below to bioturbated silty sandstones of facies C3; they can be related to facies C4 (originally defined at the Mossoró oil field), which was interpreted as beach deposits.

The shaly F4 facies consists of green-brown massive shales, sometimes with pedogenic calcite concretions and root-cast marks; it was deposited on an aggradational delta plain or supratidal flat.

Facies F5 is a pyritic, greenish-gray shale with plant remains intercalated with *Chondrites*-burrowed siltstone and with limestone layers (up to 5 cm) composed of pelecypod or gastropod coquinas and algal mat laminations. This facies corresponds to a tidal flat or a very shallow lagoonal setting.

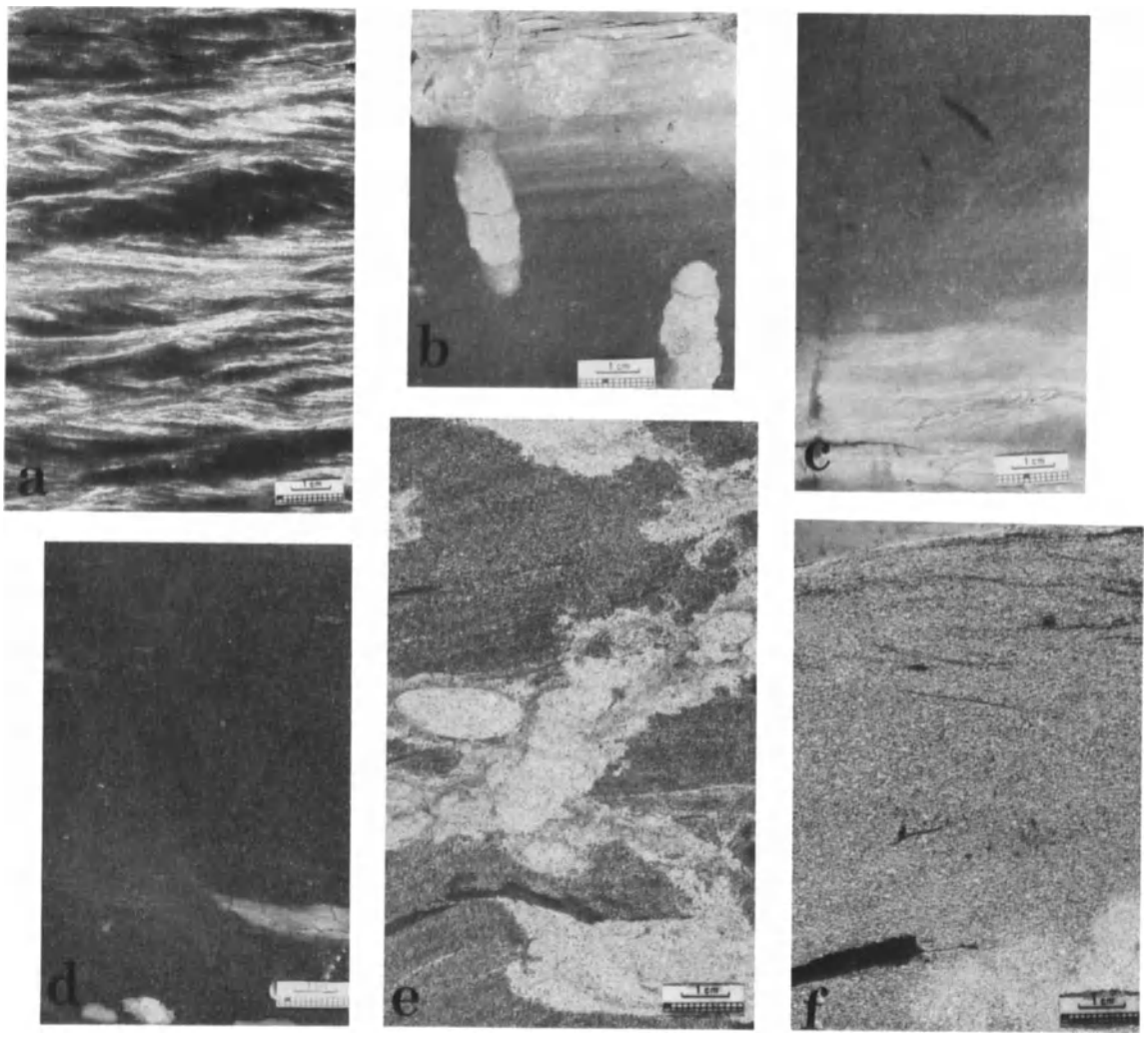

Figure 8.13. Core photographs of Canto do Amaro field. (A) Ripple-drift cross-laminated sandstone, facies A2. (B, C, D) Fining-upward sequence of facies A5. Cross-bedded sandstone with shale clasts (D), cross-bedded over ripple-drift cross-laminated sandstone (C), and horizontally laminated sandstone, argillaceous and bioturbated toward the top (D). (E, F) Cross-bedded sandstones of facies A6, with shale drapes and *Ophiomorpha* burrows (E), or shale clasts and 180° opposed cross lamination on top.

Commonly associated with facies F5, the C5 facies is a bioturbated sandy dolosparite with mollusk molds and vertebrate and plant debris.

The F6 facies occurs locally, represented by carbonaceous shales and coals deposited in an intertidal mangrove environment.

Facies relations and reservoir geometry

The stratigraphic distribution of the main facies groups is displayed schematically in Figure 8.14 by using the best cored wells of the Canto do Amaro field. There is a close relation between the physically structured, fining-upward sandstones (facies A2, A5) and the tidally reworked or bioturbated, fining-upward sandstones within coarsening-upward sequences (facies A6 and C3). The aggradational shaly units of tidal flat or supratidal/delta plain (facies F2, F4, and F5) make up the seals in the field, whereas the sandy carbonates (facies C5) are transgressive units.

The Mossoró Sandstone (Fig. 8.11) forms a distinctive tabular unit with a thick, lobate-shape accumulation of sand following a northeast-southwest trend that matches the structure of the field. It thins in all directions, except to the southeast.

Facies changes are observed in the Canto do Amaro

field, indicating: (1) marine influences toward the northeast; (2) development of a soil unit (facies F4) on top of marker T, in the southwestern margin (Fig. 8.14); (3) better developed Mossoró Sandstone (facies A5) toward the northeast; and (4) finer-grained material intercalated with the Mossoró Sandstone, probably representing an aggradational delta plain in the southwest (facies F2) and a shallow lagoon to the northeast (facies F5).

In the Redonda oil field, the vertical sequence of facies of the Mossoró member, as well as the facies and reservoir characteristics of the Mossoró Sandstone, are similar to the Canto do Amaro oil field, except for more marine influences due to the regional setting (Figs. 8.1, 8.12). The Mossoró Sandstone at Redonda is elongated in a northeast-southwest direction due to lateral and updip wedging out of the sandstone. As in the Ganto do Amaro, the sands are better developed in the downdip, northeast direction. Within the Mossoró Sandstone, we can observe a facies change from A5 to A6, indicating a more distal estuarine channel-mouth bar setting (see additional comments about geometry and origin in the Stratigraphic Framework discussion, below).

Shallow Marine System

A shallow marine association is present in the Mossoró member in two areas: (1) in the offshore wells where the unit is entirely marine, and (2) in some onshore wells near the littoral, Redonda-like area (only on top of the Mossoró member) (Fig. 8.15).

The marine association is represented by facies C6: dark gray shales and bioturbated, detrital/bioclastic/peloidal calcarenites grading to fossiliferous sandstones. The fauna includes micritic and arenaceous foraminifers, ostracods, and prismatic pelecypod debris. No reservoirs are present in this system.

Stratigraphic Framework of the Mossoró Member

In order to establish the regional stratigraphic framework for the Mossoró member, a detailed correlation of its lithofacies was prepared using electrical logs and core information. The overall transgressive nature of the Mossoró member and the Jandaíra Fm implies that the base of the Mossoró member (marker I) rises chronostratigraphically toward the continent, and on a smaller scale, the same is expected to occur with the base of the Jandaíra Fm (Figs. 8.15 and 8.16).

Despite the representation of only four lithofacies groups in Figures 8.15 and 8.16 (medium/coarse sandstones; very fine to fine sandstones; siltstones and shales; cemented sandstones to detrital limestones), the presence of four major systems in the framework of the Mossoró member is noteworthy. These depositional systems are described as follows:

- Meandering fluvial (Outcrop and Baixa do Algodão field): coarse-grained and fine to very fine-grained sandstones of facies A1 and A2/A3, respectively representing point bar and crevasse/overbank deposits. Finer-grained facies F1, F2, and F3 document overbank and flood-plain deposition, while the intraclast-rich, cemented sandstones of facies C2 are transgressive storm (?) events;
- Delta plain (Mossoró field): fine to very fine sandstones of facies A2, A3, and A4 associated with siltstones and shales of facies F1 and F2, representing crevasse lobes/subdeltas and overbank deposits. The transgressive elements are cemented/bioturbated sandstones and silty sandstones of facies C3 and C4;
- Estuarine/tidal flat (Canto do Amaro and Redonda fields): an association of fine to very fine-grained sandstones, in part tidally reworked (facies A5 and A6) with massive or *Chondrites*-burrowed siltstones and shales (facies F4 and F5), and transgressive detrital dolosparites (facies C3, C4, C5).
- Shallow marine (offshore area): shales and detrital/fossiliferous calcarenites of facies C6.

The facies changes among the four systems are clearly shown in Figure 8.15. The oil-bearing Mossoró Sandstone (M, in Figs. 8.15 and 8.16) is a good example, as it grades from fluvial (facies A1, A2), to delta-plain crevasse lobe (facies A4), to estuarine channel-mouth bar (facies A5, A6), and finally to a marine facies association. The transitional environments typically display the lenticular, isolated nature of sandstone reservoirs imposing the stratigraphic control on the Mossoró and Canto do Amaro/Redonda oil fields. The Mossoró Sandstone overlies a transgressive interval (T, Figs. 8.15 and 8.16) that can be traced from onshore up to the Baixa do Algodão field. These two major events, one transgressive (T) and one regressive (M) provide a better comprehension of the stratigraphic evolution of the Mossoró member, which is net transgressive (Fig. 8.15).

Figure 8.17 is helpful in understanding the depositional model for the Mossoró member and particularly the Mossoró Sandstone. First, the major depositional systems of the Mossoró member are displayed parallel to the Açu Fm isopachs, and therefore parallel to the Mossoró member isopachs (not shown, but their attenuation mimics the Açu Fm isopachs). Second, the depositional systems distribution for the Mossoró Sandstone is not different from the Mossoró member (Fig. 8.17).

The Mossoró Sandstone is the main reservoir in four oil fields analyzed herein, and the stratigraphic control is criti-

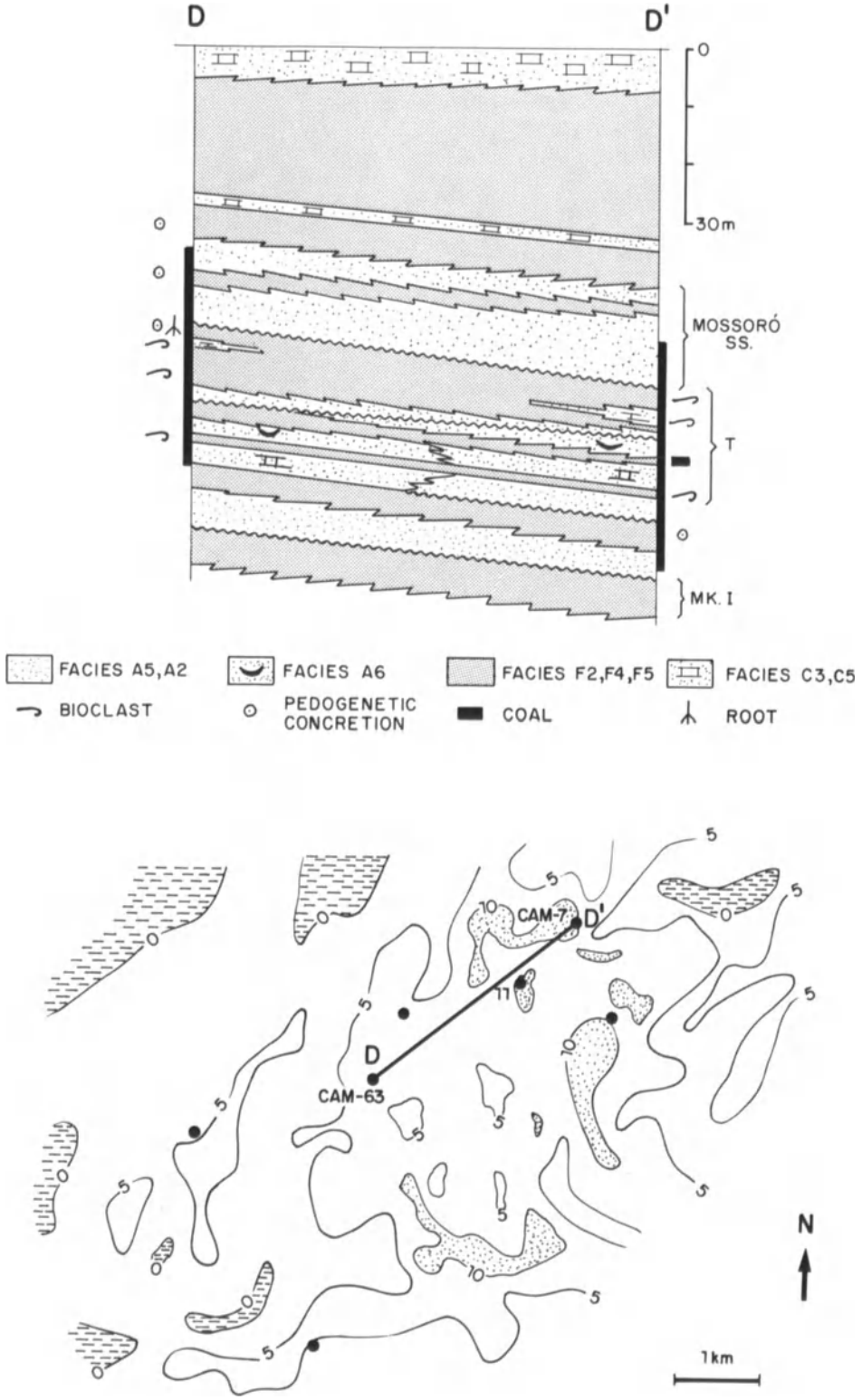

Figure 8.14. Canto do Amaro oil field. Cross-section DD′ (top) between 7-CAM-63 (left) and 7-CAM-7 (right), showing facies relations (vertical bars for cored sections; datum is base of Jandaíra Fm; see text for facies code). T is the transgressive interval of Fig. 8.15. Isolithic map (bottom) of the Mossoró Sandstone showing a NE = SW orientation that is coincident with the field structure, (only cored wells are indicated; map prepared by F. Nolla)

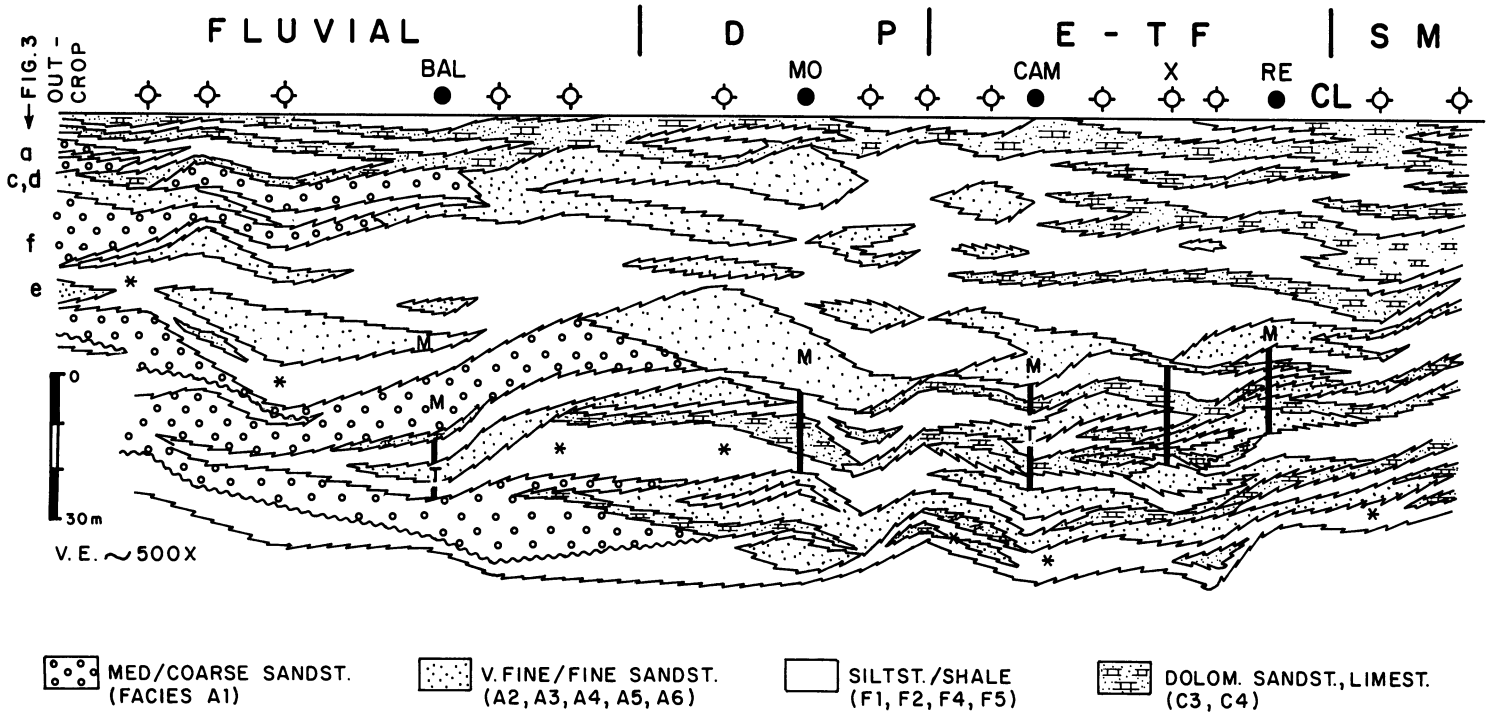

Figure 8.15. Dip-stratigraphic cross section EE′ (Fig. 8.17) showing lithologic correlation and the depositional systems of the Mossoró member. Notice the main reservoir, Mossoró Sandstone (M), as a probable regressive episode, overlying a transgressive interval (T). DP = delta plain; ETF = estuarine/tidal flat; SM = shallow marine; CL = coastline; X = crossing with section FF′ (Fig. 8.16). The marker I (*) rises chronostratigraphically; base of Jandaíra Fm is datum.

cal in three of them. Despite the similarities in composition and sequential organization of texture and structure between delta-plain and estuarine systems, the size, facies relations, and orientation of sand bodies are quite distinctive. Estuarine channel-mouth bar sandstones (facies A5) are bigger and elongated in a northeast-southwest direction perpendicular to a probable ancient coastline. They show an updip pinch-out and downdip disconfinement (notice channel and lobate geometries in the insets of Fig. 8.17); they also change laterally to tidal-reworked sandstones (facies A6).

Few ancient models for wave- and tide-dominated deltas are available in the literature. Campbell and Horne (1986) proposed a tidal inlet/shoreline model for the genesis of the Middle Triassic Halfway Fm in the Western Canada Basin. The area investigated is assumed to be lateral to a delta, so it would be a marginal deltaic setting supplied by longshore currents. Despite the convincing vertical sequence and geometric characterization of inlet and barrier facies, it is difficult to compare the single regressive sequence of the Halfway Fm with the complex Mossoró member framework.

Two recent contributions investigate the Upper Cretaceous from the Western Interior of North America (Rahmani, 1988) and the lower Eocene from the southern Pyrenees, Spain (Yang and Nio, 1989). Both papers describe major CU, regressive sequences, from marine to coastal, which contrast with the general transgressive setting of the Mossoró member. Some similarities can be observed, however, in the sequential organization and geometry of the coastal facies.

Rahmani's CU marine sequence (prodelta silt/shale, interbedded sand/shale, and delta-front parallel-laminated to low-angle cross-bedded sandstone) is scoured by a tidal-dominated estuarine channel (cross-bedded sandstone with tidal bundling and mud drapes) and overlain by tidal flats and carbonaceous marshes and swamps. He also recognizes a tripartite division of the narrow and elongated estuarine channel (fluvial sand in the upper estuary, mud in the middle estuary, tidal sand in the lower estuary) and makes appropriate comparisons with modern environments.

Yang and Nio (1989) describe the Roda Sandstone and compare it with the modern ebb-tide delta of the Eastern Scheldt estuary, southwest Netherlands. The authors identify transverse sand bars and estuarine channel sands with fining-upward sequential organization, and downdip ebb-tide deltas with coarsening-upward sequences. The estuarine channel FU sequence develops by lateral migration of the thalweg (large-scale, ebb-oriented cross bedding with tidal bundles in the foresets) and accretion of the inner

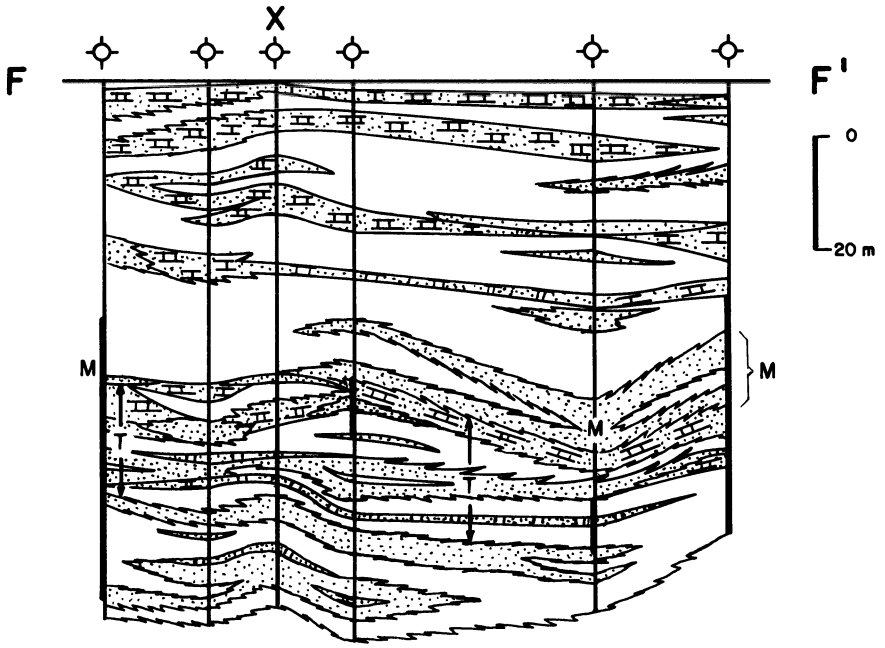

Figure 8.16. Strike-stratigraphic cross section FF' (Fig. 8.17) along the estuarine/tidal-flat system of the Mossoró member, showing lithologic correlation. The Mossoró Sandstone (M) developed to the east, overlying the transgressive interval (T). Base of Jandaíra Fm is datum; vertical bars are cored sections. Lithology symbols are the same as Fig. 8.15.

bend of the channel (small-scale cross beds and flaser bedding). Intense bioturbation at the top of the FU sequence will characterize the abandonment of the channel. The ebb-tide-delta CU sequence develops by progradation over marine deposits (bioturbated siltstones/marls) of ebb-tide lobes fed by ebb-tidal channels (low-angle cross-bedded sandstone capped by tabular cross-bedded sandstone without shale drapes). Both sequences are always capped by thin, laterally persistent, calcareous sandstone, which transgresses and interrupts the clastic sedimentation.

We can compare our CU sequences described in Redonda (facies F5-C3-A7-A6, Fig. 8.12) with Rahmani's prodelta/delta front/lower estuarine sand-channel sequence, and Yang and Nio's ebb-tide delta sequence; this comparison is reinforced if we consider the shallow-marine setting offshore (northward) of Redonda. The FU facies A5, typical of the Mossoró Sandstone from Canto do Amaro and Redonda, poses more difficulties. At Redonda, the A5 facies already displays lateral gradations to facies A6 and A7, indicating a possible lower estuarine channel setting. This statement is supported by the Mossoró Sandstone geometry in those oil fields: a northeast/southwest-elongated shape with narrowing updip and widening downdip (insets, Fig. 8.17). So, the comparison of facies A5 with Rahmani's (1988) and Yang and Nio's (1989) lower estuarine sandy channel seems quite convincing for Redonda. However, the absence of specific tidal features, mainly in the Canto do Amaro area (tidal bundles, shale drapes, and flasers)—other than the opposed paleocurrents reported in the dipmeter log by E. Bagnoli (this volume)—is intriguing. We could be dealing with channel-mouth bar features, possibly with tidal reworking. Perhaps an answer for such questions can be found in modern deltaic settings from mesotidal areas.

A Modern Analog: the Açu River Delta

The modern wave- and tide-dominated Açu River delta has been used as a modern analog for the mid-Cretaceous Açu Fm (Castro et al., 1982).

The Açu River flows along some 500 km in northeastern Brazil. The river is ephemeral due to the semiarid climate; its discharge is significant for only two to three months a year. Man-made modifications (dams, dikes, etc.) in the lower course affect the river discharge in the delta area during flood season.

The Açu River is building a delta with an area of 500 km^2 in the Macau region of the Potiguar Basin. Mesotidal conditions are indicated by the spring tidal amplitudes of 3.0 m. In addition, strong winds from the northeast originate western-directed longshore currents and coastal dunes associated with barriers (Fig. 8.18).

Like other wave- and tide-dominated river deltas, such as the Copper and the Burdekin (Galloway, 1975), three geomorphic areas are distinctive: delta plain, tidal lagoon, and shoreline (Fig. 8.18). The sandy-muddy delta plain is dominated by two distributaries (only the eastern one is presently active) and by crevasse lobes and subdeltas, similar to bay-head deltas (Donaldson et al., 1970). The muddy tidal lagoon has large supratidal areas (used by man as "salinas") cut by estuarine and tidal channels, and the

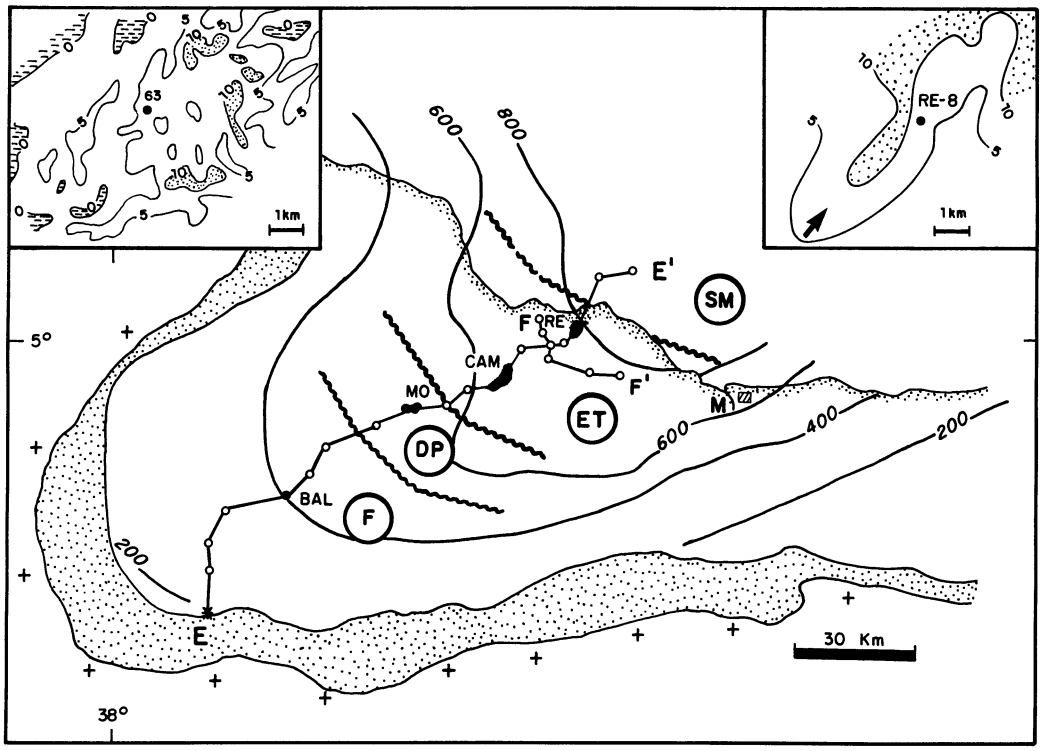

Figure 8.17. Depositional setting of Mossoró member, and Açu Fm isopachs. Notice the disconnected, lenticular geometries of Mossoró Sandstone in the Canto do Amaro (CAM) and Redonda (RE) oil fields (see sand isolith maps in the insets). F = fluvial; DP = delta plain; ET = estuarine/tidal flat, SM = shallow marine. Locations of cross sections EE′ and FF′ are indicated.

sandy shoreline has barrier islands and associated coastal dunes interrupted at estuary entrances by ebb tidal deltas (= estuarine mouth bars). So, four potential reservoirs develop in this model: fluvial channels and crevasse subdeltas (delta plain), estuarine channels, and ebb-tidal deltas/barrier islands (shoreline).

Despite the lack of radiocarbon data, the presence of fossil barrier trends and the observation of bay deposits underlying the actual delta plain (seen in artificial channel cuts) indicate a general coastline progradation for the area. The progradation probably began following the maximum marine invasion (some 5,000 years ago), when the entire delta area was a large embayment. Progradation resulted in a general "regressive" pattern associated with a period of stable or descending sea level and/or with a high sedimentation rate due to the river supply. The non-uniform migration of the shoreline is furnishing discontinuous, mud-encased barrier/ebb-tidal-delta sandy reservoirs, a situation comparable to that of the Mossoró member.

Conclusions

The Mossoró member was deposited in an extensive, low-energy coastal-plain setting formed by alluvial, deltaic, tidal-flat/estuarine and marine systems, under a general period of sea-level rise. The Mossoró Sandstone can be related to a minor regressive episode (under stable or even descending sea level) that was responsible for the deposition of reservoirs ranging from blanketing sheets to isolated sandstone bodies. Alternatively, the Mossoró oil field reservoir is interpreted as a delta-plain crevasse lobe, and the Canto do Amaro and Redonda oil fields as estuarine channel-mouth bars at different stages of shoreline progradation.

The Mossoró Sandstone depositional model is tentatively compared with the Holocene "regressive" episode (last 5,000 years) of the Açu River delta. However, it is difficult to understand how the entire Mossoró member, which basically represents a major transgressive period, developed.

Probably the central problem concerning the Mossoró Sandstone episode (M, Figs. 8.15 and 8.16) is understanding the nature and evolutionary pattern of sand accumulations at the estuarine settings. For example, how does the river supply (via channels and crevasse subdeltas) interact with tidal reworking in the upper estuary? Is the middle estuarine channel really muddy, and is the shelf the source for the lower estuary sands (Rahmani, 1988; Yang and Nio, 1989)?

Recent research in the Açu River delta (C. G. Silva,

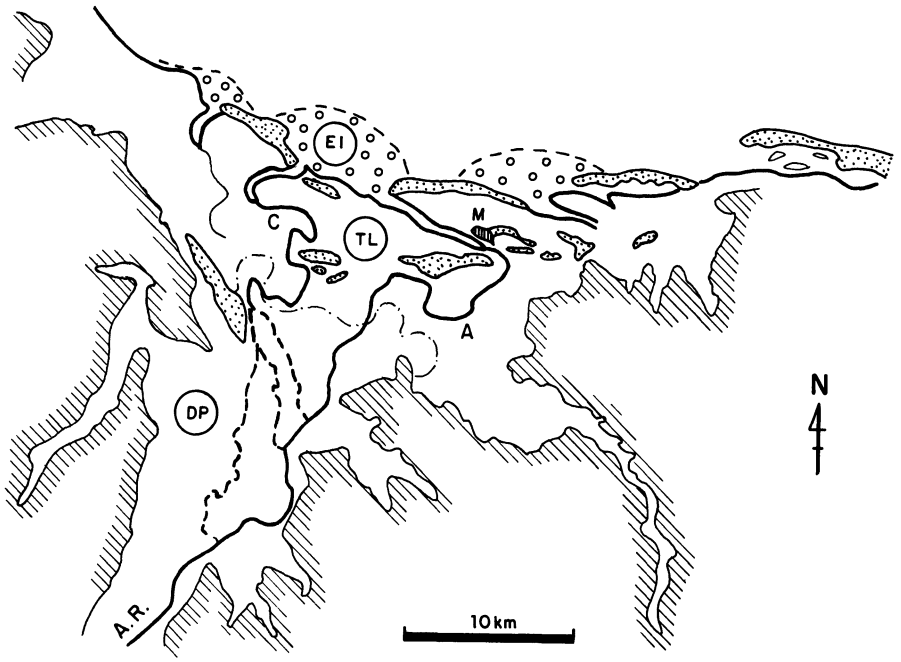

Figure 8.18. The modern tide- and wave-dominated Açu River delta. Notice the Açu River (AR) and its estuarine channel (A), as well as former fluvial courses (traces) and the estuarine channel of the Cavalas River (C). Fossil barriers occur in the muddy tidal lagoon (TL); modern barriers and ebb-tidal deltas (EI) characterize the sandy shoreline. DP = delta plain; M = Macau; and dashed areas are rocks older than Quaternary (original map by F. Fortes).

Ph.D. thesis, in preparation) has revealed the presence of tidally reworked sandy bars in the estuarine channel, which is itself encased in lagoonal muds. Coring in these bars reveals: (1) preservation of river suspension deposits intercalated with tidally wavy bedded sand/mud and bioturbated sands in the upper estuary, and predominance of thick sand/mud interbeds and sands with mud drapes in the middle and lower estuary. These results support the estuarine meander model proposed by Smith (1988). Also, the general evolutionary pattern of the tide- and wave-dominated deltaic system demonstrates the river's contribution to the estuary and to the shoreline; this must be favored when river flood periods coincide with spring low tides, for example.

The second question focuses on the evolutionary pattern of the Mossoró member. The major transgressive pattern presented by that unit was interrupted by minor regressive episodes such as the Mossoró Sandstone (Fig. 8.15); so, the Mossoró member and the succeeding Jandaíra Limestone (Late Cretaceous) can be correlated with an ascending sea level and/or diminishing sediment supply from source areas.

Acknowledgments

I thank Petróleo Brasileiro S.A., PETROBRÁS, for permission to publish this article. My colleagues E. Bagnoli and A. B. França reviewed the text, and F.S.E. de Deus helped with the correlation of Figure 8.15. I am also indebted to many colleagues at the Potiguar Basin Exploration District (DEBAR) and Risk Contract Superintendence (SUPEX) for valuable information on subsurface data.

References

Campbell, C.V., and Horne, J.C., 1986, Depositional facies of the Middle Triassic Halfway Formation, Western Canada Basin, *in* Moslow, T.F., and Rhodes, E.G., eds., Modern and ancient shelf clastics: Core Workshop n. 9, Soc. Econ. Paleont. Mineral., p. 413–459.

Castro, J.C., Barrocas, S.L.S., and Lima, H.P., 1982, A sedimentação da Formação Açu, Cretáceo Médio da Bacia Potiguar, e um análogo recente: o estuário do rio Açu na região de Macau, RN: Anais XXXII Cong. Bras. de Geologia, Salvador, Bahia, v. 5, p. 2417–2423.

Coleman, J.M., 1969, Brahmaputra River: Channel processes and sedimentation: Sediment. Geol., v. 3, p. 129–239.

Donaldson, A.C., Martin, R.H., and Kanes, W.H., 1970, Holocene Guadalupe delta of Texas Gulf Coast, *in* Morgan, J.P., ed., Deltaic sedimentation, modern and ancient: Soc. Econ. Paleont. Mineral. Spec. Publ. 15, p. 107–137.

Galloway, W.E., 1975, Process framework for describing the morphologic and stratigraphic evolution of deltaic depositional systems, *in* Broussard, M.L., ed., Deltas, models for exploration: Houston TX, Houston Geol. Soc. p. 87–98.

Rahmani, R.A., 1988, Estuarine tidal channel and nearshore sedimentation of a Late Cretaceous epicontinental sea, Drumheller, Alberta, Canada, *in* de Boer, P.L., van Gelder, A. and Nio, S.D., eds. Tide-influenced sedimentary environments and facies: Boston D. Reidel, p. 433–474.

Saxena, R.S., 1976, Modern Mississippi delta: Guidebook, Am. Assoc. Petrol. Geol.–Soc. Econ. Paleont. Mineral. Convention, New Orleans, LA, 125 p.

Smith, D.G., 1988, Modern point bar deposits analogous to the Athabasca oil sands, Alberta, Canada, *in* de Boer, P.L. van Gelder, A. and Nio, S.D. eds., Tide-influenced sedimentary environments and facies: Boston, D. Reidel, p. 417–432

Yang, C.S., and Nio, S.D., 1989, An ebb-tide delta depositional model—A comparison between the modern eastern Scheldt tidal basin (southwest Netherlands) and the Lower Eocene Roda Sandstone in the southern Pyrenees, Spain: Sed. Geology, v. 64, p. 175–196.

CHAPTER 9

The Mossoró Sandstone, Canto do Amaro Oil Field, Late Cretaceous of the Potiguar Basin, Brazil: An Example of a Tidal Inlet-Channel Reservoir

Eduardo Bagnoli

Introduction

The discovery of the Canto do Amaro oil field in November 1985 is a milestone in the exploratory history of the Potiguar Basin, which has turned out to be the most productive onshore oil field of Brazil and has opened new prospects in an area previously considered to be of minor importance. The Canto do Amaro oil field is located in the onshore part of the Potiguar Basin, Rio Grande do Norte State, in the extreme northeast corner of Brazil (Fig. 9.1). This field has nineteen producing zones, all of them in sandstones of the Upper Cretaceous Açu Fm. The Açu Fm in the Canto do Amaro area is about 650 m thick, and shows, from the base to the top, a transition from coarse sandstones deposited by braided rivers, through medium sandstones deposited by meandering rivers, to fine sandstones deposited in a marginal marine system. The fine sandstones grade upward into an argillaceous zone and then into the shallow-marine limestones of the Jandaíra Fm, making up a transgressive megasequence (Fig. 9.2).

The present work focuses exclusively on reservoir rocks of the transitional section of the Açu Fm, which is informally named the Mossoró Sandstone and is Late Cenomanian in age. These reservoir sandstones, found at a depth of about 500 m, have an average thickness of 7 m and cover an area of approximately 40 km^2, with 18 million m^3 (113 million barrels) of oil in place rated at 28° API (Fig. 9.3). The volume of recoverable oil is about 4.0 million m^3 (25 million barrels), of which 220,000 m^3 (1.4 million barrels) had already been produced up to June 1988. The 67 wells completed in this zone yield a daily average of 9 m^3 (56 barrels) of oil each using mechanical pumping.

The Canto do Amaro oil field is located on a northeast-dipping structural nose that reflects the presence of a high in the basement at a depth of 1120 m. The trap of the Mossoró Sandstone is structural/stratigraphic and was formed by the structure in combination with a lateral pinchout of the sandstones.

This work presents a sedimentological and reservoir analysis of the Mossoró Sandstone.

Macroscopic Characterization of the Lithofacies

About 188 m of core from 6 fairly representative wells (Fig. 9.3) were studied, resulting in the definition of eight lithofacies based on differences in texture, sedimentary structure, and fossil content. These lithofacies occur in three typical associations, as shown in Figure 9.4 and in the core descriptions of Figures 9.5, 9.6, and 9.7.

Lithofacies 1

This lithofacies is characterized by a basal conglomerate or conglomeratic sandstone containing a sandy matrix and millimetric to centimetric clay and carbonate intraclasts (Fig. 9.8A). This lag deposit grades upward into fine to medium sandstone with low-angle cross bedding, trough cross bedding, planar to plane-parallel cross bedding, and also herringbone cross bedding, the laminations of which are generally enhanced by the concentration of small argillaceous intraclasts (Fig. 9.8B), or are locally covered by clay drapes and rare mud couplets (Visser, 1980). This sec-

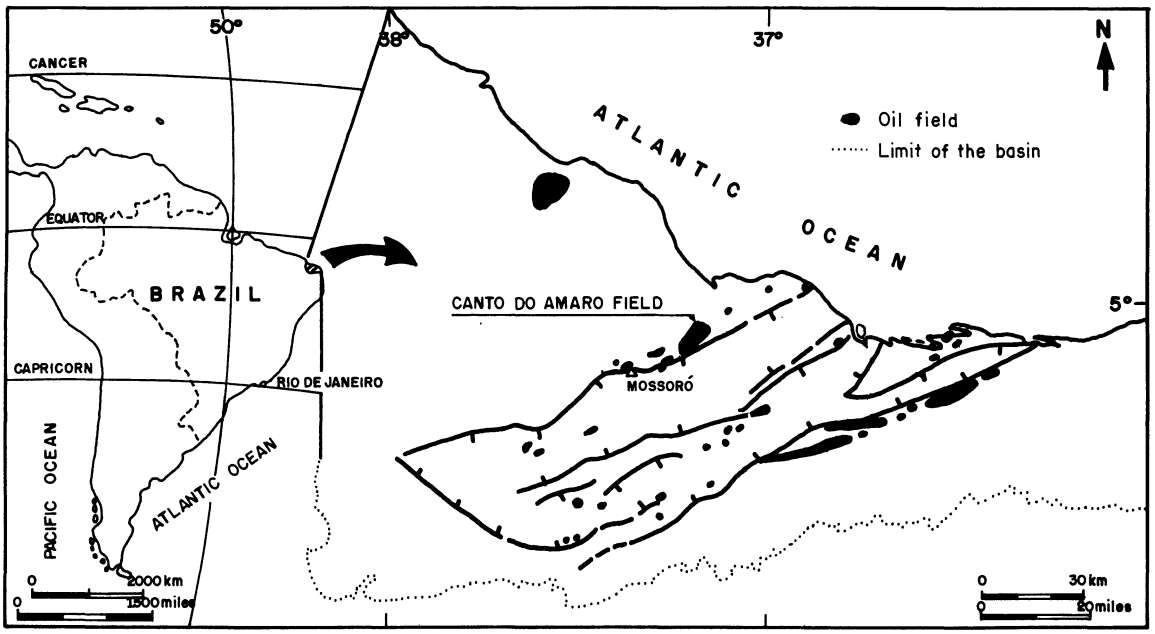

Figure 9.1. Location map of the Potiguar Basin and Canto do Amaro oil field.

tion in turn grades upward into fine to very fine massive sandstone with increasing bioturbation toward the top (Fig. 9.4, sequence A), or to the very fine sandstone with climbing ripples of lithofacies 2 (Fig. 9.4, sequence B). The thickness of lithofacies 1 varies from 2 to 8 m.

Lithofacies 2

This lithofacies is composed of very fine sandstones with climbing ripples, and ripple-drift cross lamination, which is commonly enhanced by the concentration of decanted clay that often forms flasers and drapes (Fig. 9.8C). It generally shows little bioturbation and grades upward into the siltstone of lithofacies 3 (Fig. 9.4, sequence B), or directly into the pelitic sediments of lithofacies 5 and 6. It normally overlies lithofacies 1 (Fig. 9.4, sequence B) and has thickness ranging from a few decimeters to 3 m.

Lithofacies 3

This lithofacies comprises argillaceous siltstone with climbing ripples (Fig. 9.8D). It is commonly bioturbated, showing horizontal to subvertical burrows with millimetric circular to elliptical sections, locally resembling root casts. Bioturbation increases upward and may totally mask the sedimentary structures. Lithofacies 3 is up to 3 m thick and overlies lithofacies 2 or, more frequently, forms thin layers interbedded with shales (Fig. 9.4, sequences A and B).

Lithofacies 4

Lithofacies 4 is made up of very fine, argillaceous sandstone, containing scattered plant and pelecypod remains (Fig. 9.8E). This lithofacies displays a mottled appearance due to intense bioturbation. The burrows are both horizontal and subvertical (mainly the former), and those of *Ophiomorpha* and *Chondrites* have been identified among others. Planar or low-angle cross-bedding(?) with clay drapes has been identified locally where bioturbation is less intense. Lithofacies 4 is up to 5 m thick and commonly shows a coarsening-upward pattern and a gradational contact with the underlying pelitic sediments of lithofacies 5 and 6 and the overlying carbonaceous sediments of lithofacies 8 (Fig. 9.4, sequence C).

Lithofacies 5

This lithofacies is characterized by the alternation of centimeter to decimeter-thick layers of shale and dolomitic carbonate. The shale layers have irregular plane-parallel laminations and are locally bioturbated and pyritic; they contain some plant remains, chiefly grasses(?), together with some pelecypod and oyster molds. The dolomitic carbonate beds consist of marls with irregular laminations (probably algal mats), bioclastic calcilutites, and coquinas composed of gastropods and, to a lesser extent, pelecypods (Fig. 9.8F). Root casts, mud cracks, and paleosoil development are relatively common, as is bioturbation by *Chon-*

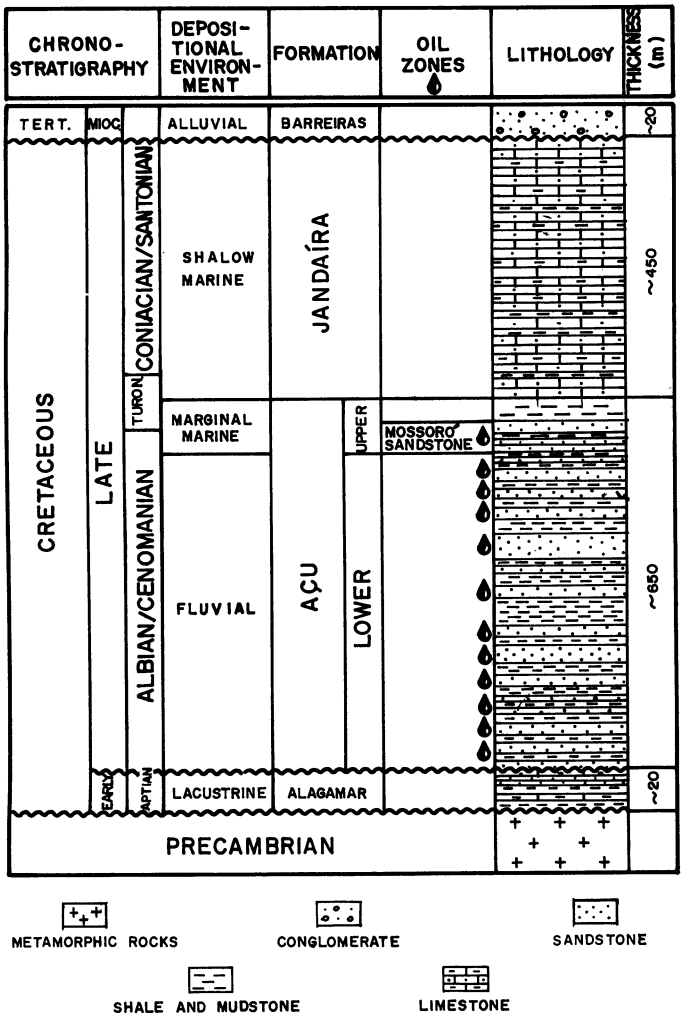

Figure 9.2. Stratigraphic column of the Potiguar Basin in the Canto do Amaro oil-field area.

drites, among others. Thin layers of very fine sandstone and silt, with climbing ripples and lenticular bedding, are locally intercalated with the shales and marls.

Lithofacies 6

Lithofacies 6 is composed of massive, homogeneous, locally highly pyritic mudstone (Fig. 9.9A). Bioturbation is evident only in the more silty portions. Thickness varies from 1 to 6 m.

Lithofacies 7

The same marls—with irregular laminations, bioclastic calcilutites, and coquinas—that form thin layers interbedded with shales in lithofacies 5 can locally attain a few meters of thickness (Fig. 9.9B), characterizing a distinct unit that has been named lithofacies 7 (Fig. 9.4, sequence B, and Fig. 9.5).

Lithofacies 8

The scattered carbonaceous organic matter, composed mainly of plant remains (Fig. 9.9C), that is found in lithofacies 4 may form peat layers up to 1 m thick, constituting lithofacies 8 (Fig. 9.4, sequence C, and Fig. 9.6).

Environmental Interpretation

The interpretation of the depositional environment of the Mossoró Sandstone and associated sealant rocks is based on the sedimentologic characteristics of the lithofacies and lithofacies associations, the fossil content, and on paleocurrent analysis (Fig. 9.10).

The vertical succession of sedimentary structures and the textural fining-upward pattern, commonly observed in lithofacies 1, are typical of inlet-channel deposits such as those described by Kumar and Sanders (1974), Moslow (1984), and Moslow and Tye (1985). The inlet floor deposit described by these authors is characterized in lithofacies 1 by the basal conglomerate, whereas the active inlet channel is represented by the crossbedded sandstone. The presence of clay drapes and mud couplets within the cross-bedded sandstone is indicative of the tidal influence on the deposition (Visser, 1980; Rahmani, 1988). These mud layers are formed by the decantation of mud caused by the deceleration of tidal currents in the periods preceding the changing of the tide (slack-water periods). Paleocurrent azimuth frequency plots using a dipmeter log analysis of lithofacies 1 cross bedding show a bipolar distribution (Fig. 9.7), which is in agreement with the inlet channel interpretation. The bipolar distribution of paleocurrents toward the northeast and southwest is shown clearly in the lower plot of Figure 9.7. The medium plot of this figure still shows the bimodal distribution of paleocurrents; however, the southwest component is more developed than the northeast one. In the upper plot, the most developed component points to the northeast. It is interesting to note that the northeast-southwest direction shown in Figure 9.7 matches the depocenter direction of the Mossoró Sandstone around the 7-CAM-30-RN well, where the dipmeter was logged (Fig. 9.3). This coincidence suggests that the depositional axis of this elongated sandstone body represents the paleo-inlet channel axis. Therefore, it is inferred that the paleoshoreline was oriented northwest-southeast, approximately parallel to the present shoreline (Fig. 9.1). If this is

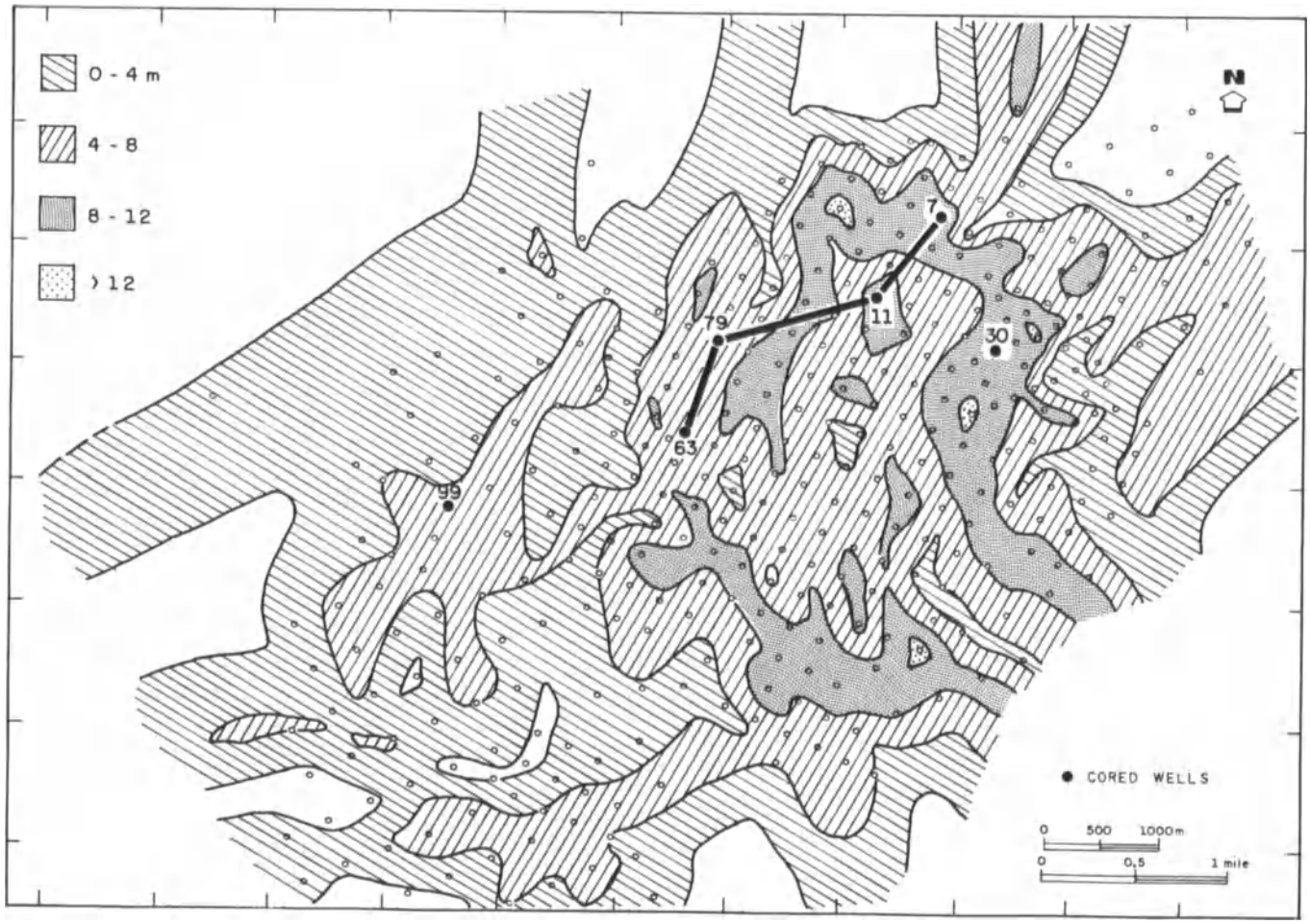

Figure 9.3. Map showing distribution and thickness of the Mossoró Sandstone and locations of cored wells (modified from Nolla and Souto, unpublished).

true, the southwest component of the paleo-current (Fig. 9.7) must represent the flood-tidal current, and the northeast component the ebb-tidal current (Figs. 9.1 and 9.11). Bipolar crossbedded sandstones in tidal inlet sequences were described by Hayes and Kana (1976), and Donselaar and Nio (1982). Barwis and Makurath (1978) and Donselaar and Nio (1982) also made interpretations of paleoshorelines based on paleocurrent distribution.

The current ripple cross-bedded sandstone of lithofacies 2 (Fig. 9.4, sequence B) represents the lower-energy deposition on top of laterally accreted channel-fill deposits during migration of the inlet channel. The presence of flasers and clay drapes in this sandstone is evidence of tidal influence on the deposition (Reineck and Singh, 1980).

The fining-upward sequence of the inlet fill ends with the bioturbated, locally rooted siltstone of lithofacies 3 (Fig. 9.4 sequence B). This deposit represents low-energy intertidal deposition, typical of inlet-channel abandonment. Commonly, lithofacies 3 occurs isolated within tidal-flat-lagoon sediments and probably represents small tidal creeks within the tidal flat (Fig. 9.4, sequences A and B, and Fig. 9.10).

The bioturbated argillaceous sandstone of lithofacies 4 is interpreted as a flood-tidal delta deposit (Fig. 9.4, sequence C). The mottled appearance caused by bioturbation, the coarsening-upward profile, and the high clay content, are typical of flood-tidal delta deposits as described by Israel et al. (1987). *Ophiomorpha* burrowing points to marine influence, whereas the great quantity of plant fragments indicates a continental component. The common capping of lithofacies 4. with the peat deposit of lithofacies 8 (Fig. 9.4, sequence C, and Fig. 9.6) denotes temporary subaerial exposure of the flood-tidal delta, providing conditions for plant colonization (Fig. 9.10). According to McCubbin (1982), flood-tidal deltas often become partially exposed, resulting in marsh growth. Palynological analysis of one sample of the peat deposit (lithofacies 8) has shown a large quantity, as well as great diversity, of pollens and spores,

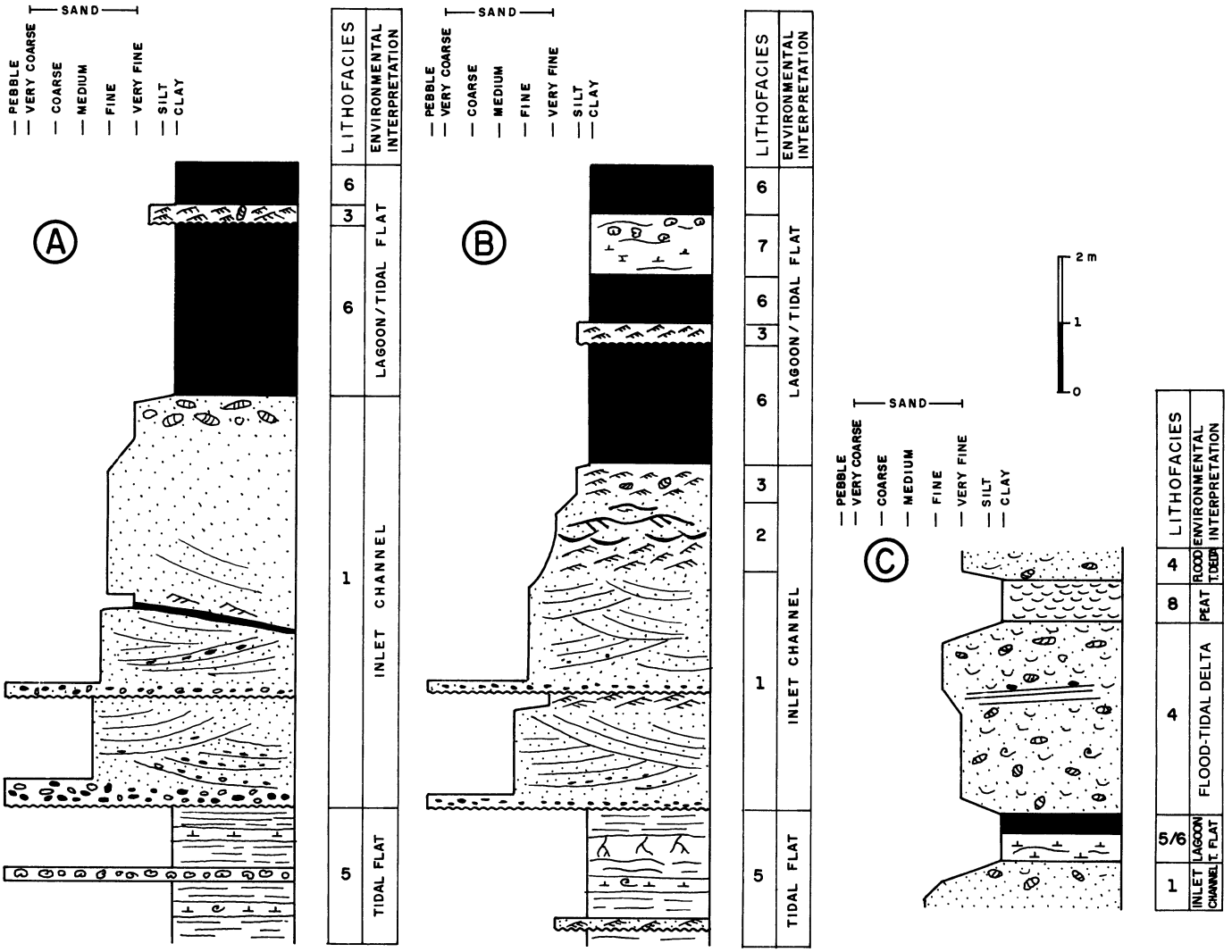

Figure 9.4. Three typical vertical successions of lithofacies and environmental interpretation of the Mossoró Sandstone. Succession (A) represents the typical inlet-channel sequence of the east-northeast part of the Canto do Amaro field, and succession (B) the typical inlet-channel sequence of the west-southwest part of the field. Succession (C) represents the typical flood-tidal delta sequence of the Canto do Amaro field (see text for description of lithofacies).

such as *Triorites africaensis*, *Araucariacites australis*, *Equisetosporites* sp., *Classopollis major*, and *Cicatricosisporites purbeckensis*. Cuticles and wooden fragments are also present, suggesting a continental environment containing both autochthonous and transported flora. Some marine influence is indicated by the presence of a few dinoflagellates. The sample contained no foraminifers.

Lithofacies 5 is interpreted as a tidal-flat deposit on the basis of the following evidence: (1) lithology (interlaminations of shale, algal mats, bioclastic calcilutite, and lag gastropod deposits); (2) presence of exposure features (root casts, mud cracks, and pedogenic features, with yellow color due to probable aluminum concentration); and (3) fossil content (oysters, gastropods, pelecypods, and grass remains). The lag deposits of mollusc shells, whose origin is probably related to periodic storm tides, are commonly found on tidal flats (Duc and Tye, 1987). Palynological analyses on samples of lithofacies 5 have shown a large quantity and great diversity of pollens and spores such as *Classopolis major*, *Ephedripites ambiguus*, *Tricolpites* sp., *Rizophora*, and *Cicatricosisporites purbeckensis*. These, plus the presence of chitinous microforaminifers, indicate a continental-marine transitional environment. The same samples contained no other, more marine foraminifers.

Lithofacies 6 is composed of homogeneous and massive lagoonal mudstones. Similar sediments have been described and interpreted as bay deposits by Israel et al. (1987). The absence of primary sedimentary structures and

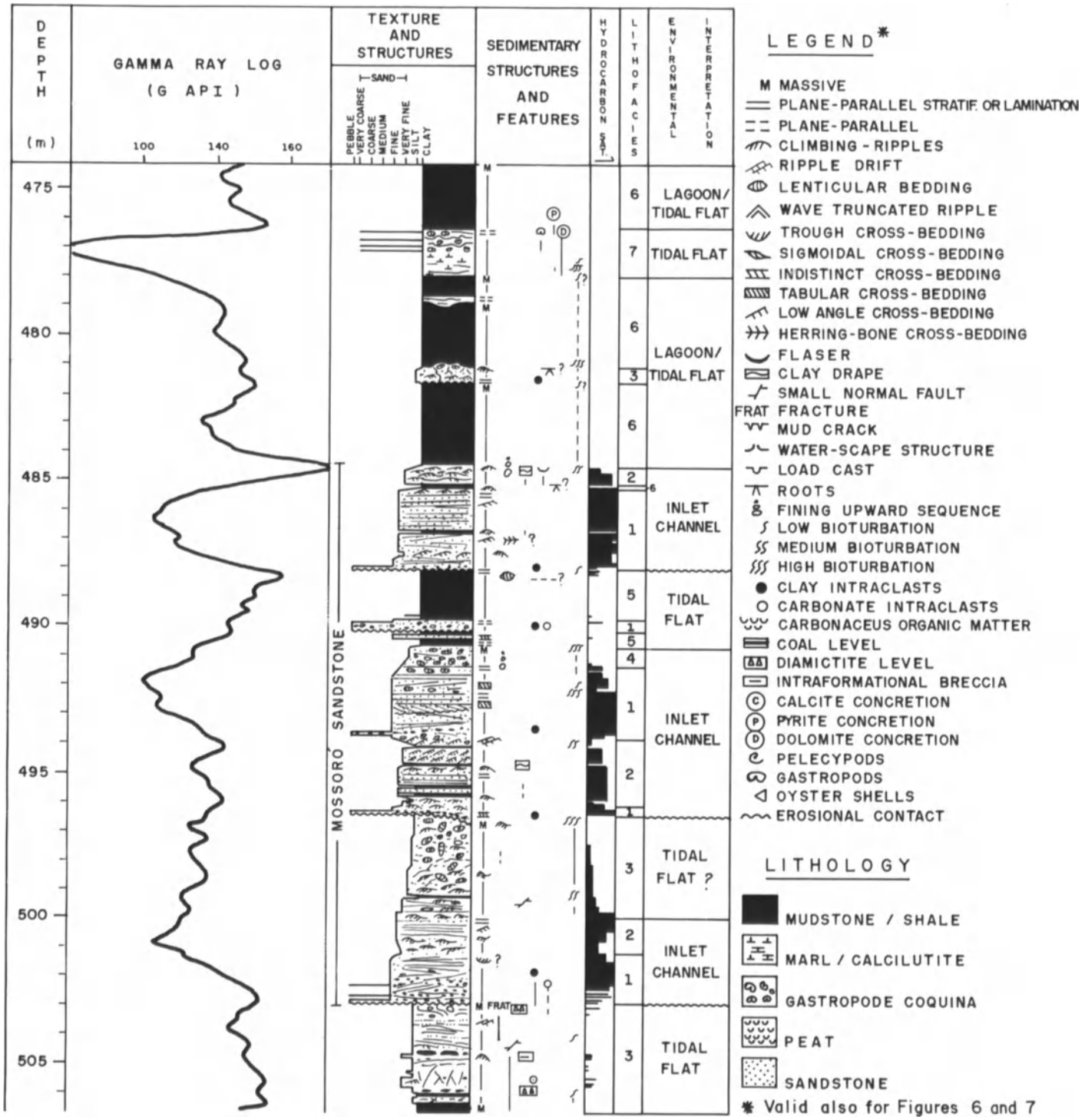

Figure 9.5. Core description of well 7-CAM-79-RN with electric-log correlation.

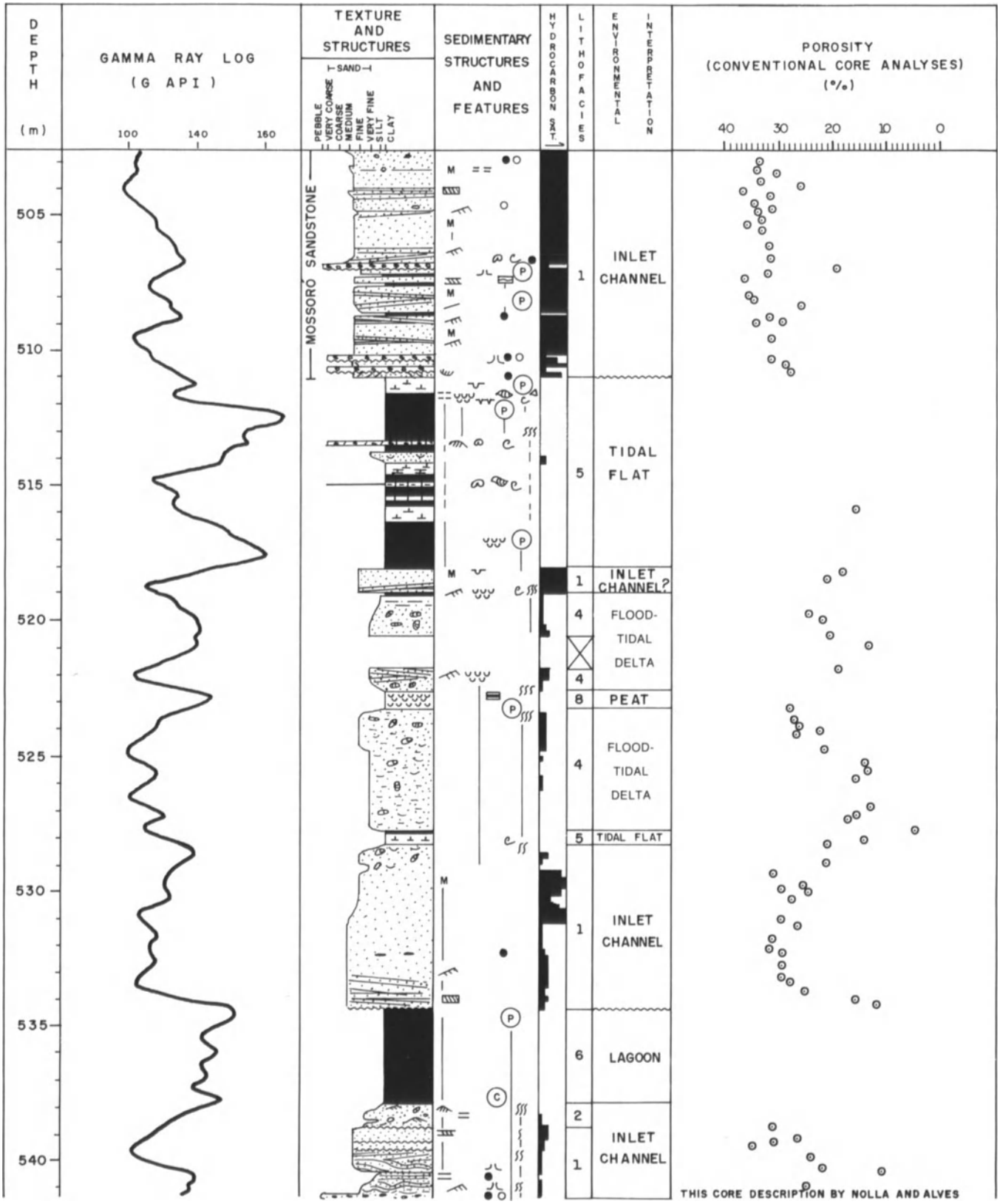

Figure 9.6. Core description of well 7-CAM-7-RN with electric-log correlation and petrophysical data.

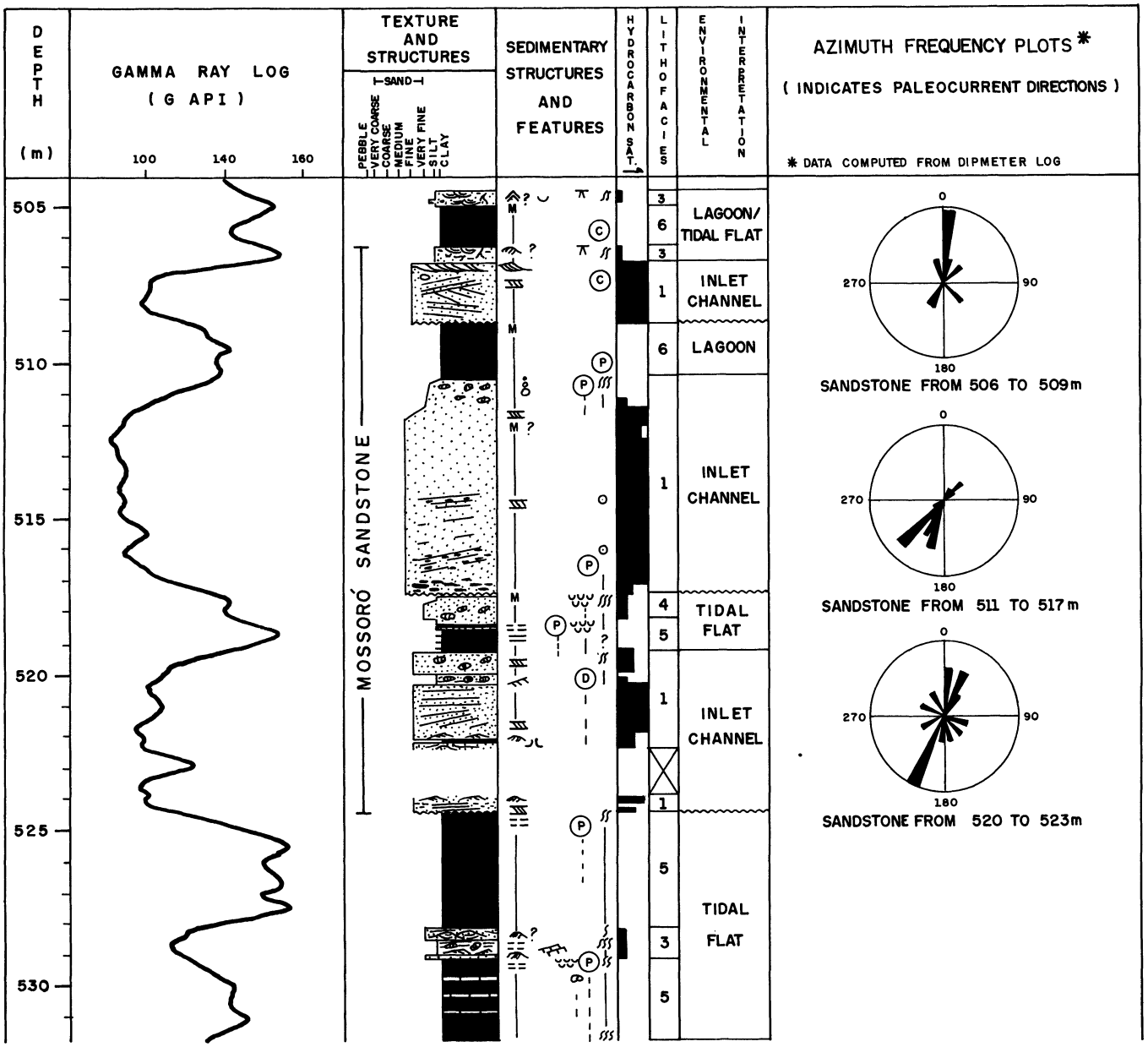

Figure 9.7. Core description of well 7-CAM-30-RN with electric-log correlation and azimuth frequency plots showing paleocurrent trends of the vertical stacked inlet channel sandstones.

fossils in these mudstones is quite intriguing. However, the presence of interbedded tidal-flat deposits strengthens the interpretation of lagoonal deposits (Fig. 9.10).

Lithofacies 7, comprising algal mats interbedded with gastropod coquinas and bioclastic calcilutites, represents an extensive tidal-flat deposit that is an important transgressive mark, easily identified in wireline logs throughout the Canto do Amaro field (see datum in Fig. 9.12).

The vertical successions of lithofacies A and B displayed in figure 9.4 are an attempt to show a variation that actually occurs in the Canto do Amaro field. The inlet channel deposits of sequence A are typical of the east-northeast area of the field, where sandstones are thicker, such as those observed on cores of the wells 7-CAM-7-RN, 7-CAM-11-RN, and 7-CAM-30-RN (Figs. 9.3, 9.6. and 9.7). On the other hand, the deposits of sequence B are typical of the west-southwest part of the field, represented by the cores of the wells 7-CAM-63-RN, 7-CAM-79-RN, and 7-CAM-99-RN (Figs. 9.3 and 9.5). A tentative explanation of such variation is given later.

The inlet-channel deposits in the Canto do Amaro field overlie back-barrier sediments (Figs. 9.10 and 9.12), sug-

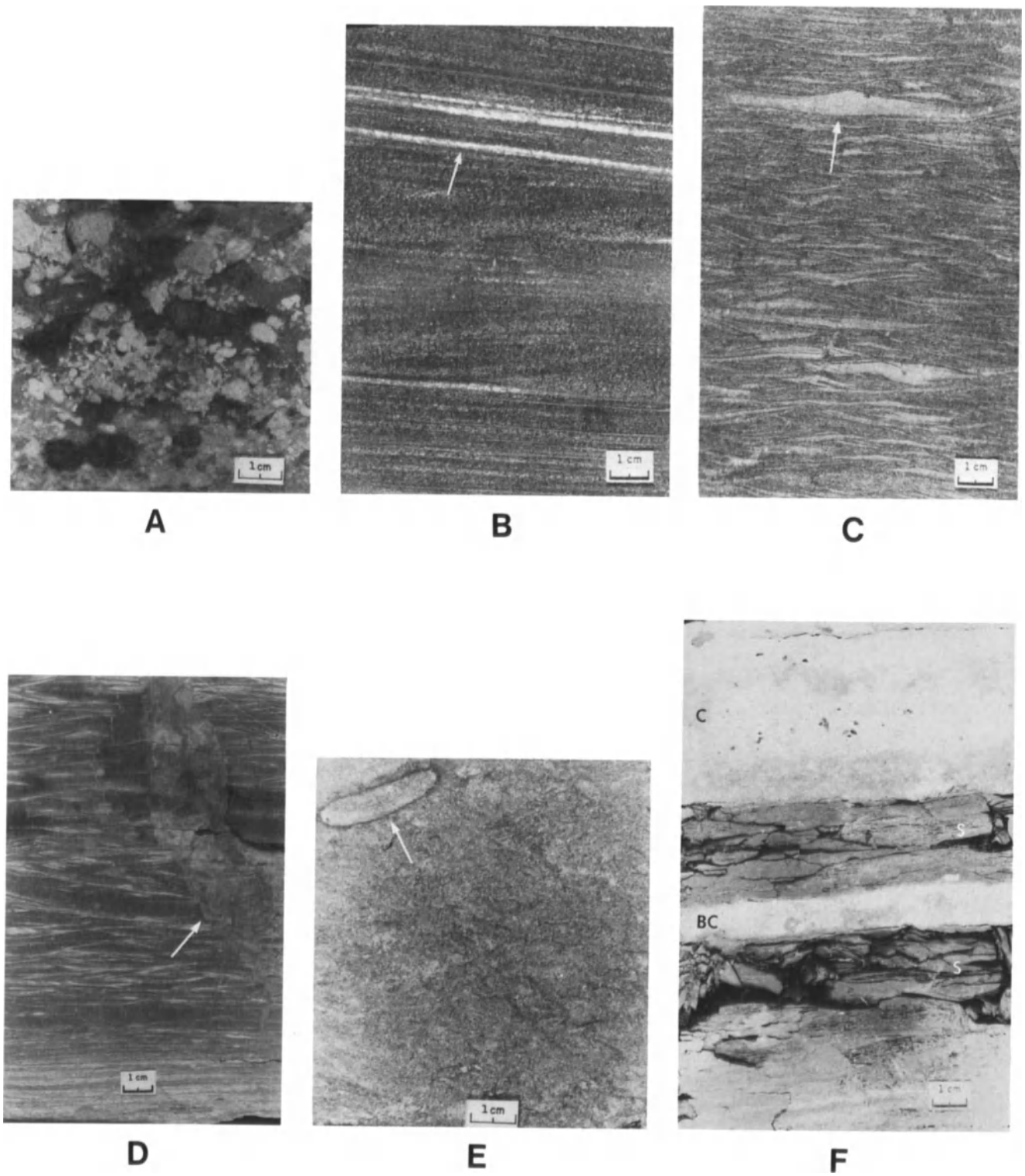

Figure 9.8. Photographs of the Mossoró Sandstone lithofacies. (A) Lithofacies 1: lag conglomerate composed of clay (gray) and carbonate (white) intraclasts with little sandy matrix. (B) Lithofacies 1: fine to medium sandstone with low-angle cross stratification enhanced by the concentration of tiny clay intraclasts (arrow). (C) Lithofacies 2: very fine sandstone with climbing ripples, flasers, and clay drapes (arrow). (D) Lithofacies 3: siltstone with climbing ripples and root cast (arrow). (E) Lithofacies 4: highly bioturbated argillaceous sandstone showing *Ophiomorpha* burrow (arrow). (F) Lithofacies 5: interbedded bioclastic calcilutite (BC) and gastropod coquina (C) with shale layers (S) showing plane-parallel lamination.

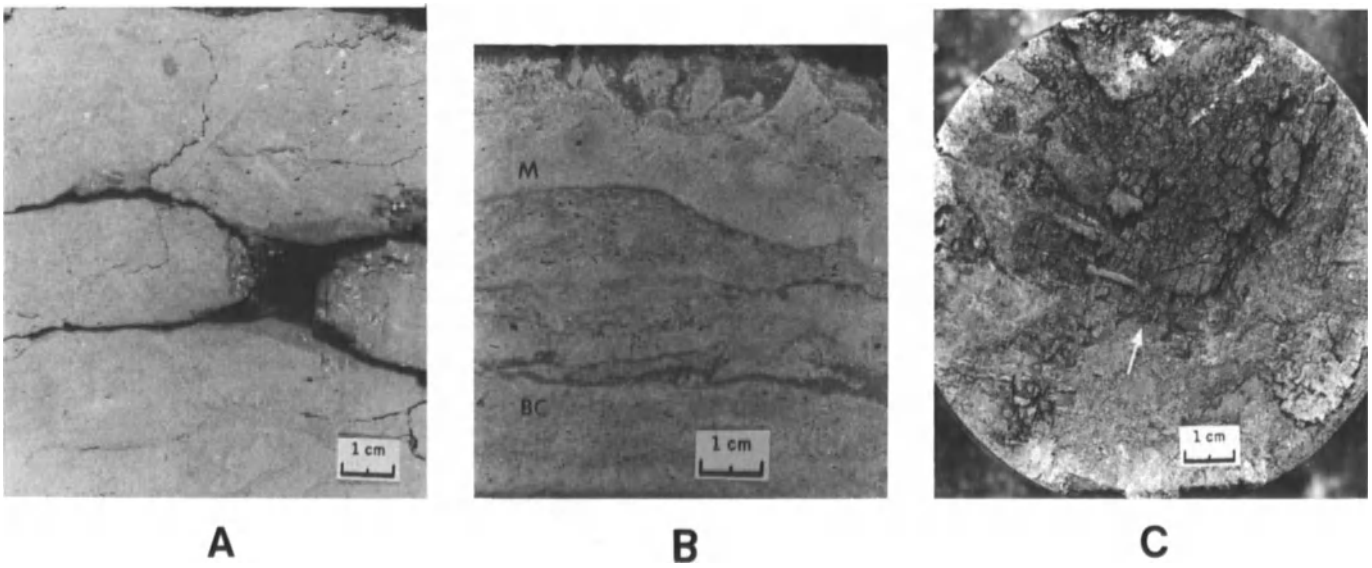

Figure 9.9. Photographs of the Mossoró Sandstone lithofacies. (A) Lithofacies 6: massive, homogeneous mudstone. (B) Lithofacies 7: marl (M) and bioclastic calcilutite (BC) with irregular lamination. (C) Lithofacies 8: wood remains in argillaceous matrix (arrow).

gesting that their origin is related to transgressive events. On the other hand, the inlet-channel deposits are always covered by regressive sequences represented by the same lagoon and tidal-flat sediments (Fig. 9.12). However, this interval is part of a large transgressive system that contains the entire Açu Fm. This transgressive event is characterized by the transition of the continental sediments of the Açu Fm to the shallow-marine limestones of the Jandaíra Fm (Fig. 9.2). By understanding the evolution of this major transgression, it is possible to explain the variation in thickness of the Mossoró Sandstone along the Canto do Amaro oil field. The major transgression led to the southwestward migration of the paleoshoreline, intercalated with phases of minor progradation and periods of stable sea level. These periods of stable sea level must have allowed the establishment of a barrier island/inlet-channel system, with the consequent development of thick sandstone bodies. Two such major periods can be proposed to explain the presence of localized thicker portions of the Mossoró Sandstone (positions I and II, Fig. 9.11). The stable period I (Fig. 9.11) represents a longer period of time than period II and must have led to the thicker sand deposition in the east-northeast part of the field. After the deposition of the less expressive sands of the stable period II (Fig. 9.11), the southwestward migration of the paleoshoreline continued, probably with increasing velocity, leading to the sandstone pinch-out in this direction.

Typical coarsening-upward barrier-island sequences, such as those described by Moslow (1984) and McCubbin (1982), among others, have not been found in the Canto do Amaro field. Two hypotheses can be proposed to explain the absence of barrier-island sediments in the Canto do Amaro oil field.

(1) According to Hobday and Horne (1977) and Moslow (1984), the uppermost foreshore and shoreface parts of the barrier island are reworked during a transgression. Looking at Figure 9.10, it is easy to imagine that the major transgression that took place during the Mossoró Sandstone deposition exposed the top of the barrier island to wave action, causing its total reworking.

(2) Barrier-island sediments do occur along the paleoshoreline, but have not yet been found because the drilling, for oil exploration purposes, is being restricted to a narrow zone normal to the paleoshoreline (see the alignment of the oil fields in the Canto do Amaro trend, Fig. 9.1).

The Geometry of the Mossoró Sandstone

The fining-upward pattern of the inlet-channel fill in the Canto do Amaro field shows a transition from the inlet floor lag to the active inlet channel, abandoned inlet channel, and clay plug (Fig. 9.4, sequences A and B). Moslow (1984) considers this sequence to be typical of tide-dominated inlets developed in mesotidal coasts. According to this author, in such an environment, the inlet channel migrates parallel to the shoreline in a back-and-forth movement, and if subsiding conditions and/or elevations of sea level are favorable, this kind of migration will tend to develop a series of interconnected stacked inlet-channel deposits with good lateral continuity (Fig. 9.10). Actually, this happens in the Mossoró Sandstone, which is made up of vertical

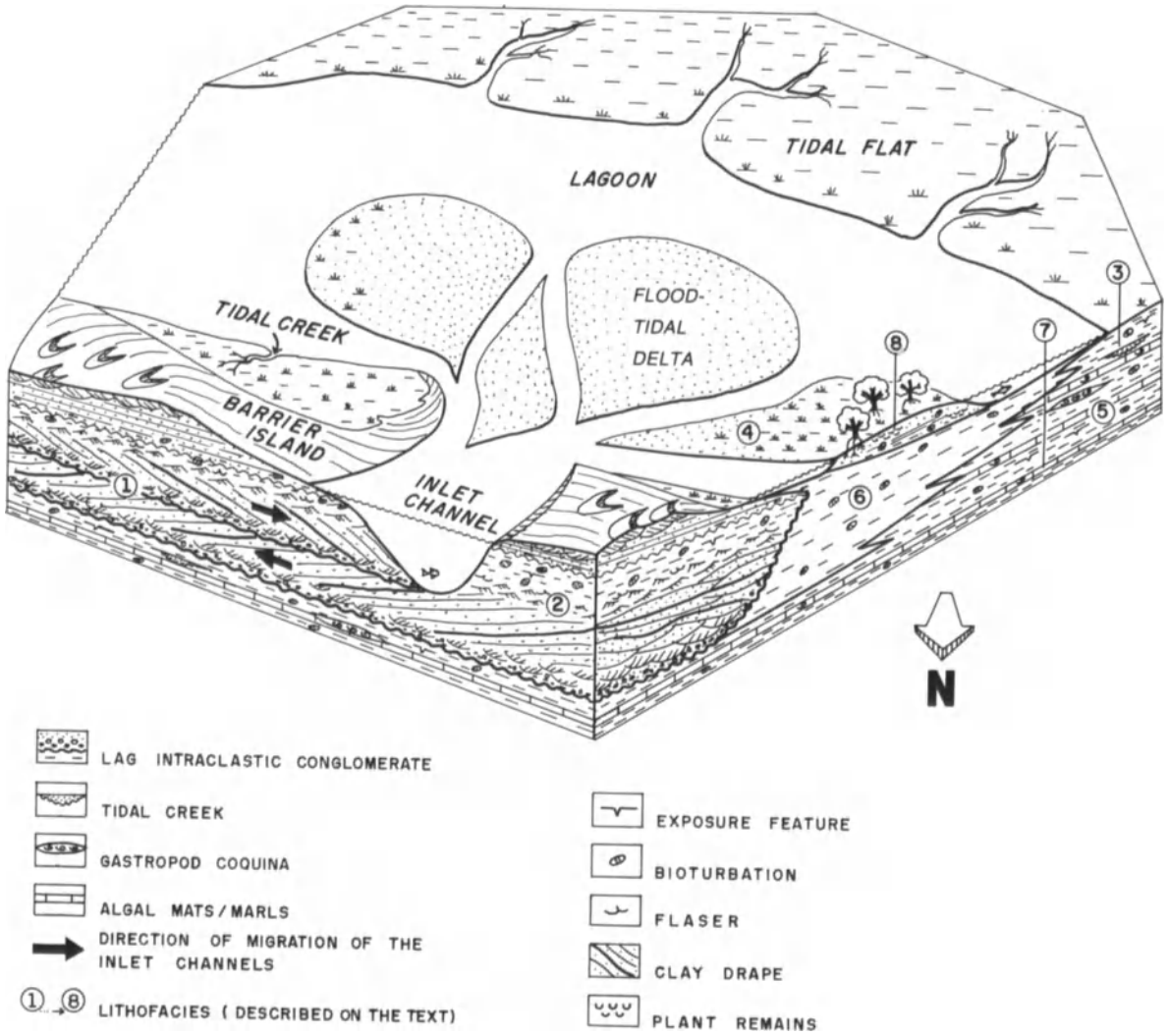

Figure 9.10. Idealized three-dimensional block diagram showing the depositional environment of the Mossoró Sandstone and associated sealant rocks (not to scale).

stacked inlet channels that behave as a single reservoir, where the pressure is constant throughout the field (Figs. 9.12 and 9.13). The vertical stacking of inlet sequences seems to be a common feature, as it has been observed by several authors (Horne and Ferm, 1976; Barwis and Makurath, 1978; Galloway and Hobday, 1983; Moslow, 1984).

The Mossoró Sandstone reservoirs are composed of tabular continuous sandstone bodies, similar to the blanket inlet-filling sands described by Kumar and Sanders (1974) and interpreted as the product of the inlet migration along the shore (Figs. 9.12 and 9.13).

Although the Mossoró Sandstone is not delimited in the Canto do Amaro field, some pinch-outs can be seen toward the northeast around well 7-CAM-12-RN (Fig. 9.13), as well as to the north-northwest and south-southwest (Fig. 9.3).

Reservoir Petrology

The main reservoirs of the Canto do Amaro field are the inlet-channel deposits chiefly represented by lithofacies 1 and, to a lesser extent, by lithofacies 2. Lithofacies 4, representative of flood-tidal delta deposits, may locally attain some reservoir characteristics.

The framework grain composition of the reservoirs was obtained by point counting 23 stained thin sections (Alizarin Red S), taken from blue-epoxy-impregnated core samples (Fig. 9.14). The sandstones of lithofacies 1 and 4 are

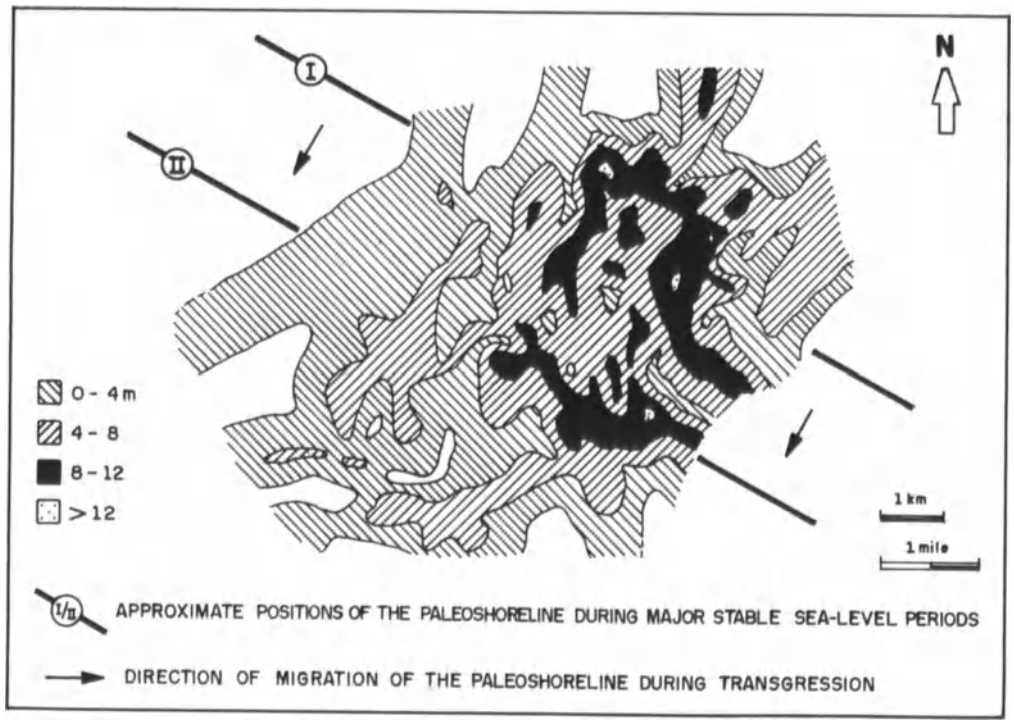

Figure 9.11. Isopach map of the Mossoró Sandstone showing the inferred positions of the advancing paleoshoreline.

arkoses, whereas the sandstones of lithofacies 2 are subarkoses. Quartz is the main framework grain, averaging 67 percent. Feldspar follows, with an average of 32.5 percent. The K-feldspar is much more common than plagioclase. Rock fragments are quite rare, averaging only 0.5 percent.

The whole-rock compositional data of lithofacies 1, 2, and 4 are summarized in Table 9.1. Because of the changing characteristics of lithofacies 1 across the field (Fig. 9.4), its data are presented in two distinct columns. The whole-rock composition is similar for the sandstones across the field (Table 9.1). However, the inlet-channel sandstones of the west-southwest part of the field (right-hand column) have less porosity and more clay matrix than the sandstones of the east-northeast part (left-hand column). This is in agreement with the proposed hypothesis that the tidal energy of the inlet channels decreases from the east-northeast to the west-southwest. Lithofacies 2 contains the highest amount of mica, which is compatible with the increased traction-plus-fallout depositional conditions of this lithofacies. Matrix clay and organic debris are found predominantly in lithofacies 4, and as a consequence, this is the least porous and permeable unit.

Cumulative granulometric curves of lithofacies 1, based on 7 samples from well 7-CAM-7-RN, are displayed in Figure 9.15. The curves are homogeneous and show that the sandstones of lithofacies 1 are moderately to well-sorted, ranging from medium to very fine grained.

Diagenesis and Reservoir Quality

The major diagenetic processes affecting the reservoir quality of the Mossoró Sandstone are mechanical and chemical compaction, precipitation of calcite with replacement of some detrital framework grains, leaching of calcite cement to create secondary porosity, and precipitation of subordinate authigenic cements. These processes appear to have operated similarly on lithofacies 1, 2, and 4.

Mechanical compaction is common throughout, and probably occurred during the first few hundred meters of burial, leading to primary porosity reduction. It consists of slippage and rotation of grains, and ductile deformation of micas, clay intraclasts, and organic debris (Fig. 9.16A), with the development of pseudomatrix (Dickinson, 1970). Chemical compaction, consisting of grain-to-grain pressure solution and feldspar overgrowth, has also contributed to reducing the porosity (Fig. 9.16A). The next diagenetic process to occur was precipitation of calcite within the remaining primary porosity, and the partial to total replacement of feldspar and quartz grains by calcite (Fig. 9.16B). Later, much of the calcite cement, including the replacement calcite, was leached, causing development of secondary porosity (Fig. 9.16C). Textural evidence (Schmidt and McDonald, 1979) supporting this interpretation includes elongated pores (Fig. 9.16C), inhomogeneity of packing (Fig. 9.16D), and the corroded margins of detrital grains

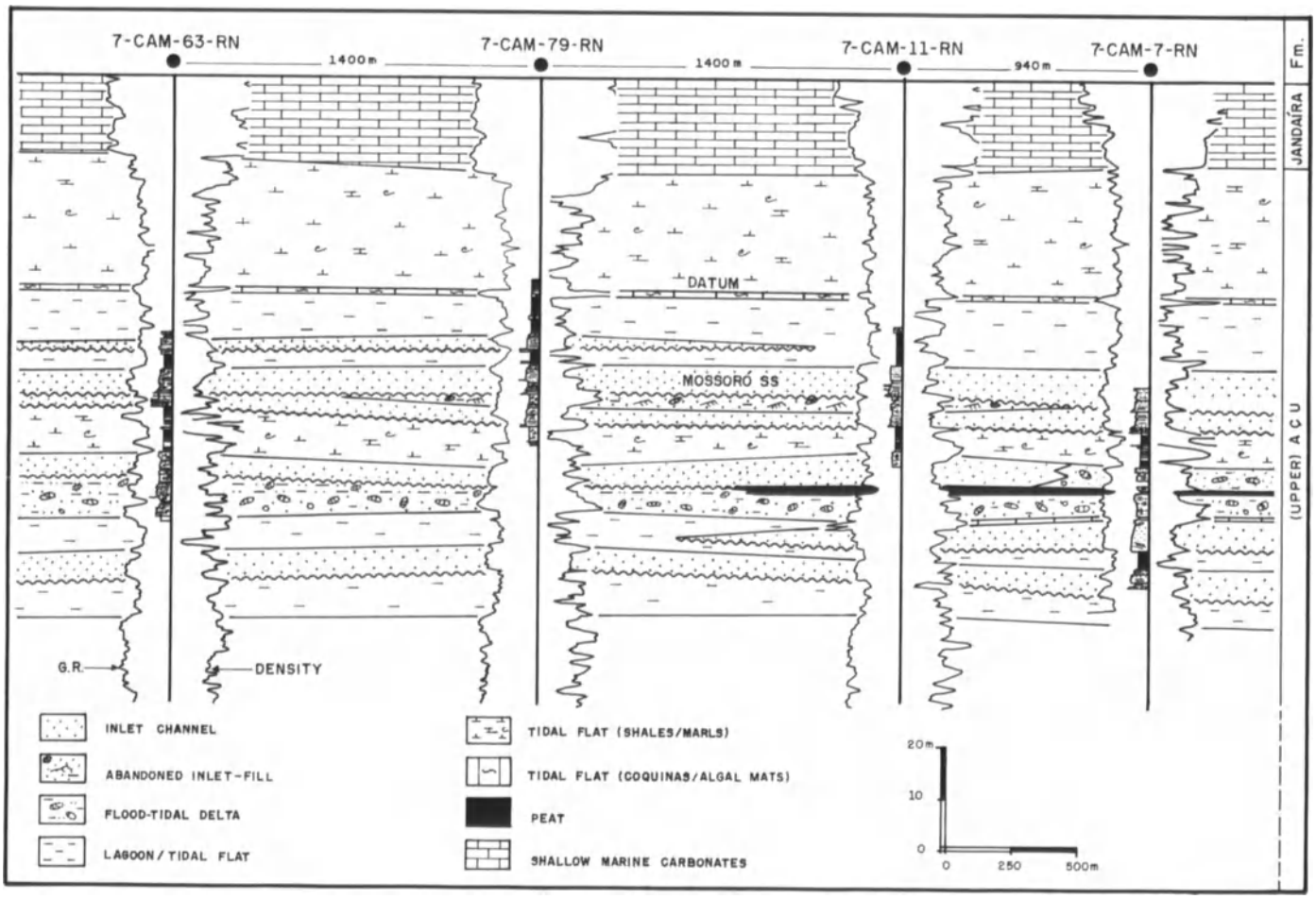

Figure 9.12. Stratigraphic section across the cored wells showing the transgressive sequence from the transitional sandstones of the Upper Açu Fm to the shallow-marine carbonates of the Jandaíra Fm (cross section location shown in Fig. 9.3).

(Fig. 9.16E). Concomitant with, or just after, the calcite dissolution, the precipitation of kaolinite (Curtis, 1983) as pore-filling cement took place (Fig. 9.16D and F). Clusters of small euhedral anatase crystals also formed as a pore lining after the calcite dissolution (Figs. 9.16E and F). The development of anatase (titanium oxide) likely relates to the alteration of framework heavy minerals, which commonly occur concentrated in laminae. Ixer and others (1979; Turner, 1980) suggest that titanium ions might be released into the interstitial groundwaters during the martitization of detrital titanomagnetite. The diagenetic sequence ended with the precipitation of minor amounts of illite-smectite, pyrite, and dolomite. Hydrocarbon migration followed this last stage of diagenesis.

Cements rarely form more than 15% of the whole-rock volume (Table 9.1) and do not seriously affect reservoir quality. Although diagenesis has significantly modified the amount and geometry of the pore spaces, it is the grain size, sorting, and quantity of primary clay matrix that control porosity and permeability in the reservoirs of the Mossoró Sandstone. Since these parameters are governed by the depositional environment, it appears that the reservoir quality of the Mossoró Sandstone is basically controlled by its depositional setting. Consequently, the coarser-grained sandstones of lithofacies 1, deposited by high-energy processes, are better reservoirs than the finer-grained sandstones of lithofacies 2, deposited by lower-energy processes.

Petrophysical Characterization of the Reservoirs

About 160 conventional core plugs were analyzed in order to determine average values of porosity and permeability and the variation of these two parameters throughout the Canto do Amaro field (Table 9.2). The sandstones of lithofacies 1 in the east-northeast part of the field have 29.9% average porosity and average permeability of 926 md,

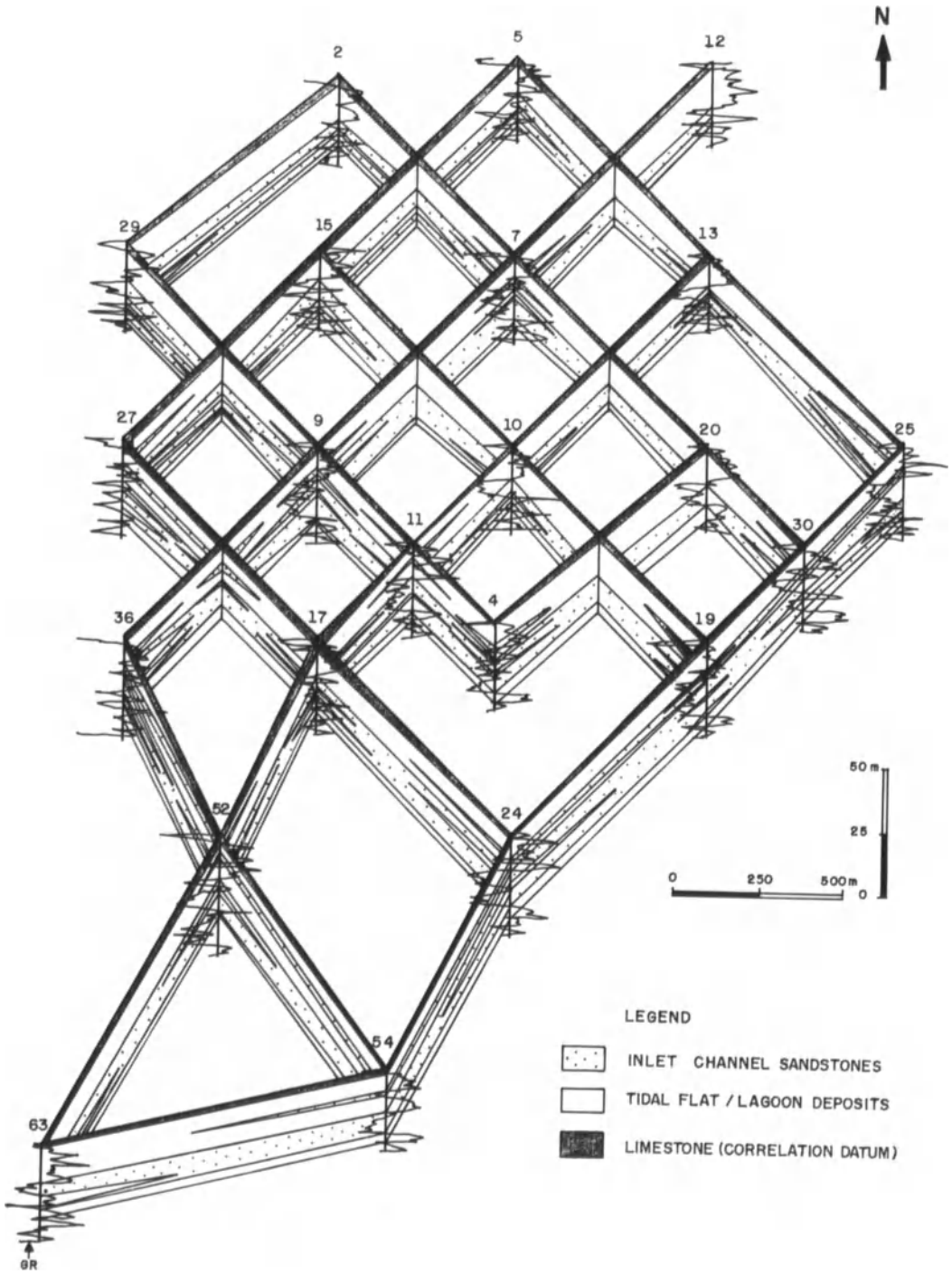

Figure 9.13. Fence diagram showing vertical and lateral distribution of the Mossoró inlet-channel reservoirs.

whereas in the west-southwest section, the same sandstones have 28.5% average porosity and 277 md average permeability. Although lithofacies 2 and 4 show good average porosity, they have low permeability (Table 9.2). This is probably due to the presence of lower-energy sedimentary structures and finer grain size in lithofacies 2, and the intense bioturbation in lithofacies 4.

Conclusions

The Mossoró Sandstone is a tidal deposit of Late Cretaceous age. The characteristics of the eight lithofacies described above have led to identification of several subenvironments, including inlet channel, tidal flat, lagoon, flood-tidal delta, and marsh. The vertical sequence of the

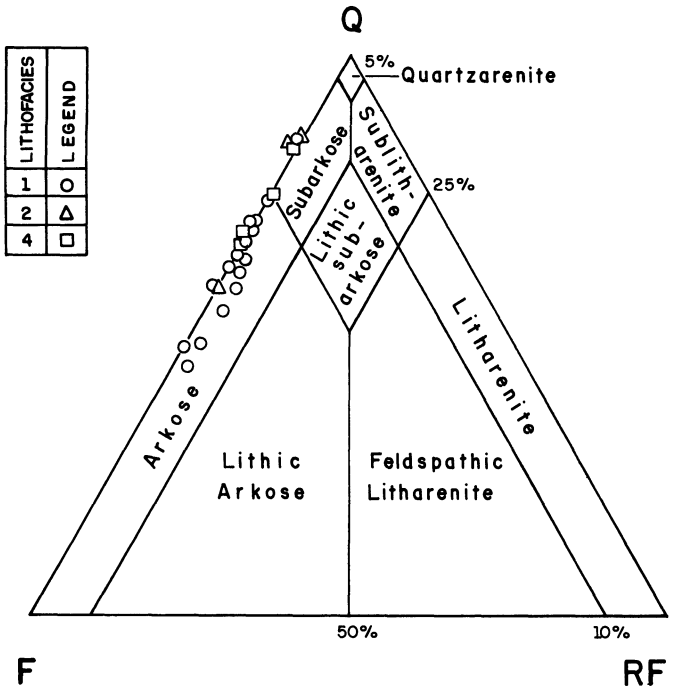

Figure 9.14. Petrographic classification of the Mossoró Reservoirs presented on McBride's (1963) diagram.

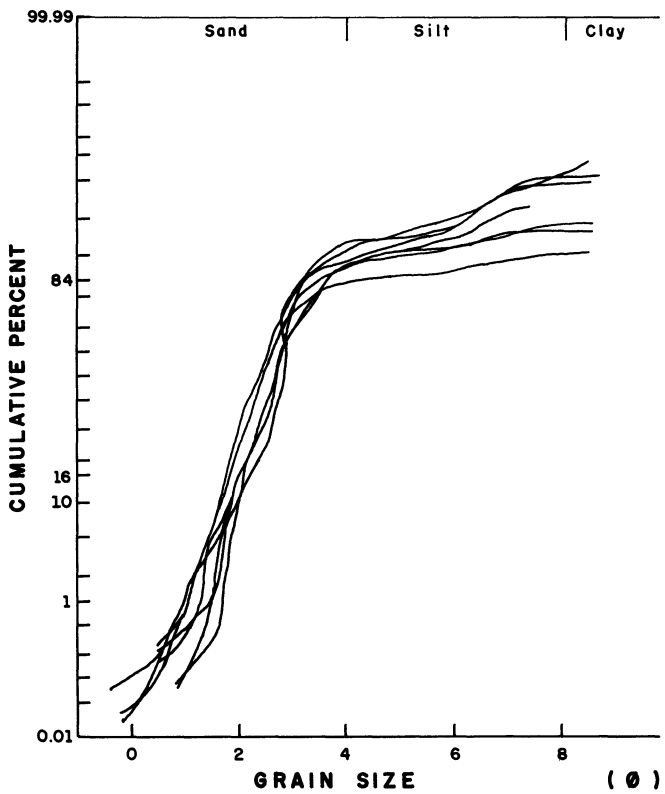

Figure 9.15. Cumulative granulometric curves of lithofacies 1, the main reservoir of the Mossoró Sandstone. Data from well 7-CAM-7-RN (depth range: 499.9 to 529.3 m; see Fig. 9.6).

Table 9.1. Whole-rock compositional data of the Mossoró Reservoirs.

	Lithofacies			
	1(14)[1] %	1(3)[1] %	2(3)[1] %	4(4)[1] %
	Inlet channel		Top of	Flood-tidal
Clastic constituents	[2]	[3]	inlet fill	delta
Quartz	36.3	28.6	36.0	38.7
Feldspar	17.9	20.3	11.3	14.2
Mica	1.1	3.2	5.3	2.7
Clay intraclasts	6.3	4.3	2.6	—
Rock fragments	0.5	0.2	—	—
Accessories[4]	tr	tr	tr	tr
Organic debris	—	tr	tr	0.5
Matrix clay	3.6	22.3	4.0	24.0
Authigenic constituents				
Clacite	4.1	4.8	1.6	2.7
Dolomite	—	1.0	tr	4.0
Kaolinite	3.2	2.3	1.3	0.7
Anatase	0.3	0.3	0.3	1.2
Pirite	0.2	0.3	tr	tr
Illite-smectite	0.1	0.2	—	1.0
Feldspar overgrowths	1.5	1.0	1.5	tr
Pores				
Micropores[5]	4.7	6.0	9.3	4.5
Macroporos[6]	18.3	8.6	7.3	4.7

[1] Numbers in parentheses = number of samples point counted.
[2] Represents inlet-channel reservoirs from the ENE part of the field.
[3] Represents inlet-channel reservoirs from the WSW part of the field.
[4] Includes zircon, tourmaline, garnet, and detrital opaque minerals.
[5] Includes all pores less than 0.062 mm in diameter.
[6] Includes all pores more than 0.062 mm in diameter.
tr = traces

lithofacies suggests that the deposition of the Mossoró Sandstone took place in a tide-dominated setting. The main reservoir sandstones comprise inlet-channel deposits is whose characteristics change across the field, suggesting decreasing depositional energy from east-northeast to west-southwest. An analysis of the paleocurrent direction provided by the dipmeter log suggests a northeast-southwest direction for the paleo-inlet channels. This direction is confirmed by the orientation of the thickest sandstone bodies apparent in the isopach map of the Mossoró Sandstone. This interpretation also implies a northwest-southeast orientation for the ancient shoreline.

The inlet-channel deposits of the Canto do Amaro oil field commonly display an erosive base with lag intraclastic conglomerate followed by sandstones with a fining-upward pattern. They form extensive tabular reservoirs composed of up to three vertical stacked inlet channels. Texturally, these sandstones are medium to very fine, moderately to well-sorted, and have an arkosic composition.

Diagenesis has acted homogeneously throughout the field, affecting all the porous lithofacies. The major di-

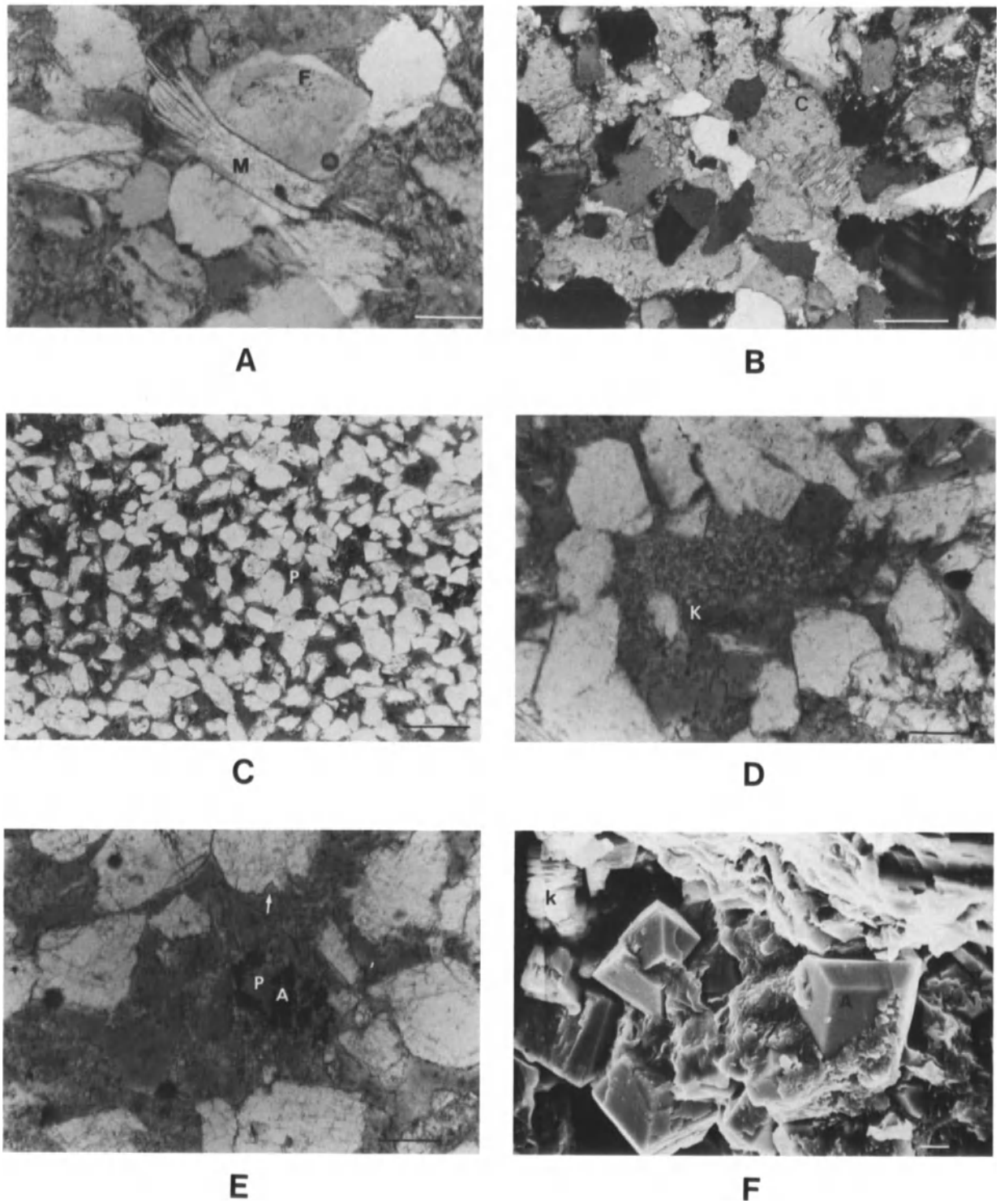

Figure 9.16. Thin-section and SEM photomicrographs of the Mossoró Reservoirs. (A) Muscovite (M) grain showing evidence of mechanical compaction, and feldspar grain (F) displaying overgrowth. Cross-polarized light. Scale bar = 100 μm. (B) Pore-filling poikilotopic calcite cement (C), also replacing feldspar grains (F). Cross-polarized light. Scale bar = 200 μm. (C) Fine-grained, well-sorted sandstone showing good porosity (gray). Elongated pores (P) and inhomogeneity of packing are also visible. Plane-polarized light. Scale bar = 500 μm. (D) Pore-filling authigenic kaolinite cement (K). Plane-polarized light. Scale bar = 100 μm. (E) Clusters of anatase cristals (A) lining pore spaces (P). Corroded margins of detrital grains also visible (arrow). Plane-polarized light. Scale bar = 100 μm. (F) SEM photomicrograph of kaolinite (K) and anatase (A) authigenic cements. Scale bar = 5 μm.

Table 9.2. Petrophysical data of the Mossoró Reservoirs

	Lithofacies			
	1[1]	1[2]	2	4
	Inlet Channel		Top of inlet fill	Food-tidal delta
Mean porosity (%)	29.9	28.5	28.9	21.8
Mean permeability (md)	926	277	64	28

[1]Represents inlet-channel reservoirs from the ENE part of the field.
[2]Represents inlet-channel reservoirs from the WSW part of the field.

agenetic processes, in order of occurrence, are mechanical and chemical compaction, precipitation of calcite cement, leaching of calcite cement and development of secondary porosity, and precipitation of kaolinite, anatase, and other subordinate authigenic cements. Although diagenesis has significantly modified the amount and geometry of the pore spaces, it is the depositional environment that controls the porosity and permeability. The coarser lithofacies deposited by high-energy processes are more porous and permeable than finer lithofacies deposited by lower-energy processes. The permeability and, to a lesser extent, the porosity, significantly decrease from the east-northeast to the west-southwest, supporting the hypothesis that the inlet channels lose energy in this direction.

It is hoped that the data presented in this paper improve the understanding of ancient inlet-channel deposits, and that this work aids in identifying similar reservoirs in the geologic record, diminishing the exploratory risk in such complex lithologic sequences.

Acknowledgments

The author is grateful to Petróleo Brasileiro S.A. (Petrobrás) for the opportunity to write this paper and permission to publish it, and to Thomas F. Moslow for providing many helpful ideas and the initial stimulus to prepare it. The author thanks Pedro I.S. de Assis for the dipmeter computing, Rodolfo Dino for the palynological analyses, Ricardo L.M. Azevedo for the foraminifer analyses, Frederico R. Nolla for preparing stratigraphic cross sections for the fence diagram, and Joel C. de Castro for many fruitful discussions. Almério B. França and Maurício O. de Lima helped with the thin-section descriptions and, together with Anibal C. Alves, Renato T. Bertani, David M. Hassett, and the editor's reviewers, provided critical reviews improving the manuscript. Finally, the author thanks Carlucio F. da Silva for preparing some illustrations and typing, and Ubiratan J. Fernandes for drawing the figures.

References

Barwis, J.H., and Makurath, J.H., 1978, Recognition of ancient tidal inlet sequences: An example from the Upper Silurian Keyser Limestone in Virginia: Sedimentology, v. 25, p. 61–82.

Curtis, C.D., 1983, Link between aluminum mobility and destruction of secondary porosity: Am. Assoc. Petrol. Geol. Bull., v. 67, p. 380–393.

Dickinson, W.R., 1970, Interpreting detrital modes of graywacke and arkose: J. Sediment. Petrol., v. 40, p. 695–707.

Donselaar, M.E., and Nio, S.D., 1982, An Eocene tidal inlet/washover type barrier island complex in the South Pyrenean marginal basin, Spain; Geol. Mijnb., v. 61, p. 343–353.

Duc, A.W., and Tye, R.S., 1987, Evolution and stratigraphy of a regressive barrier/backbarrier complex: Kiawah Island, South Carolina: Sedimentology, v. 34, p. 237–251.

Galloway, W.E., and Hobday, D.K., 1983, Terrigenous clastic depositional environments: New York, Springer-Verlag, 423 p.

Hayes, M.O., and Kana, T.W., 1976, Terrigenous clastic depositional environments—some modern examples: Columbia University of South Carolina, Coastal Research Division, Tech. Rept. II-CRD, p. I-131–II-184.

Hobday, D.K., and Horne, J.C., 1977, Tidally influenced barrier island and estuarine sedimentation in the Upper Carboniferous of southern West Virginia: Sedimentary Geology, v. 18, p. 97–122.

Horne, J.C., and Ferm, J.C., 1976, Carboniferous depositional environments in the Pochahontas Basin, eastern Kentucky and southern West Virginia: Columbia University of South Carolina, Field Course Guidebook.

Israel, A.M., Ethridge, F.G., and Estes, E.L., 1987, A sedimentologic description of a microtidal, flood-tidal delta, San Luis Pass, Texas: J. Sediment. Petrol., v. 57, p. 288–300.

Ixer, R.A., Turner, P., and Waugh, B., 1979, Authigenic iron and titanium oxides in Triassic red beds: St. Bees Sandstone, Cumbria, Northern England: Geol. J., v. 14, p. 179–192.

Kumar, N., and Sanders, J.E., 1974, Inlet sequence: A vertical succession of sedimentary structures and textures created by the lateral migration of tidal inlets; Sedimentology, v. 21, p. 491–532.

McBride, E.F., 1963, A classification of common sandstones: J. Sediment. Petrol., v. 33, p. 664–669.

McCubbin, D.G., 1982, Barrier-island and strand-plain facies, *in* Scholle, P.A., and Spearing, D., eds., Sandstone depositional environments: Am. Assoc. Petrol. Geol. Memoir 31, p. 247–279.

Moslow, T.F., 1984, Depositional models of shelf and shoreline sandstones: Am. Assoc. Petrol. Geol. Cont. Ed. Course Notes, Series 27, 102 p.

Moslow, T.F., and Tye, R.S., 1985, Recognition and characterization of Holocene tidal inlet sequences: Marine Geol., v. 63, p. 129–151.

Rahmani, R.A., 1988, Estuarine tidal channel and nearshore sedimentation of a Late Cretaceous epicontinental sea, Drumheller, Alberta, Canada, *in* de Boer, P.L., van Gelder, A., and Nio, S.D., eds., Tide-influenced sedimentary environments and facies: Boston D. Reidel, p. 433–471.

Reineck, H.-E., Sing, I.B., 1980, Depositional sedimentary environments; 2nd ed.: Berlin, Springer-Verlag, 549 p.

Schmidt, V., and McDonald, D.A., 1979, Texture and recognition of secondary porosity in sandstones, *in* Scholle, P.A., and Schluger, P.R., eds., Aspects of diagenesis: Soc. Econ. Paleont. Mineral. Spec. Publ. 26, p. 209–225.

Turner, P., 1980, Continental red beds: Amsterdam, Elsevier, 562 p.

Visser, M.J., 1980, Neap-spring cycles reflected in Holocene subtidal large-scale bedform deposits A preliminary note: Geology, v. 8, p. 543–546.

CHAPTER 10

Depositional History and Performance of a Permian Bell Canyon Sandstone Reservoir, Ford-Geraldine Field, West Texas

Robert W. Ruggiero

Introduction

Location

The Permian Basin of western Texas and southeastern New Mexico is a mature petroleum exploration province. The western portion of this basin complex is the Delaware Basin (Fig. 10.1). This subsurface study focuses on the uppermost Guadalupian sandstone, the Ramsey member, of the Bell Canyon Formation (Delaware Mountain Group) where it subcrops near the center of the Delaware Basin (Fig. 10.2).

Ramsey sandstones constitute important, shallow (2,000 to 3,000 ft deep; 610 m to 914 m) oil reservoirs in the Delaware Basin (Fig. 10.3). In the Ford-Geraldine field, these sandstones form a stratigraphic trap containing an estimated 93 million barrels of oil in place. The field reservoir is the terminal or most distal portion of a fan channel that became structurally high by eastward tilting during the Late Permian and again in the Late Cretaceous (Hills, 1984). The field was discovered in 1956 and had been waterflooded since 1969 before carbon-dioxide (CO_2) injection began in 1981. At the start of tertiary injection, a disappointing 22% of the oil in place had been produced, necessitating a more detailed geological description of the reservoir; hence, the impetus for this study.

This study provided a detailed geological description of a producing reservoir (the Ramsey member of the Bell Canyon Formation) in the Ford-Geraldine field early in the installation of a tertiary recovery program. The resulting geological model helped predict tertiary recovery performance and provides an analog for similar reservoirs in the Delaware Basin.

Previous Work

King (1942) provided the initial discussion of provenance and depositional processes of the Delaware sands in his study of the outcropping erosional channels in the Guadalupe Mountains of west Texas. Since King's early work, there have been many hypotheses to explain the depositional processes of the basinal facies (Fischer and Sarnthein, 1988). McDermott (1984) summarized and grouped the key literature by its focus. The works of Harms (1974), Williamson (1978, 1979), Harms and Williamson (1988), Bozanich (1978), and McDermott (1984) form the basis for this study.

Harms (1974) redescribed the outcropping, erosional channels recognized by King and questioned the applicability of previous deep-sea fan models that had been proposed for the Brushy Canyon Fm (e.g., Jacka and others, 1968). He compared the features of Jacka's model with his field observations, which differed dramatically (Harms and Williamson, 1988). To explain this disparity, he postulated the existence of density-driven currents (either hypersaline or cold). Depending on the density contrast between an incoming flow and the density-stratified basin waters, a current would either hug the channel bottom (hyperpycnal) or sheet out over more dense water layers (hypopycnal). Those that remained within the previously eroded channel would transport and deposit coarser sediment. Those that flowed atop more dense water layers fanned out over a wide area. The finer sediment that these hypopycnal flows transported settled from suspension, draping channel fill and margin evenly.

Williamson (1978, 1979) expanded Harms' concepts with a thorough outcrop and basin-wide subsurface study of the

Figure 10.1. Permian tectonic and paleogeographic features, west Texas and southwest New Mexico. Location of the study area near the center of the Delaware Basin. After Williamson (1978).

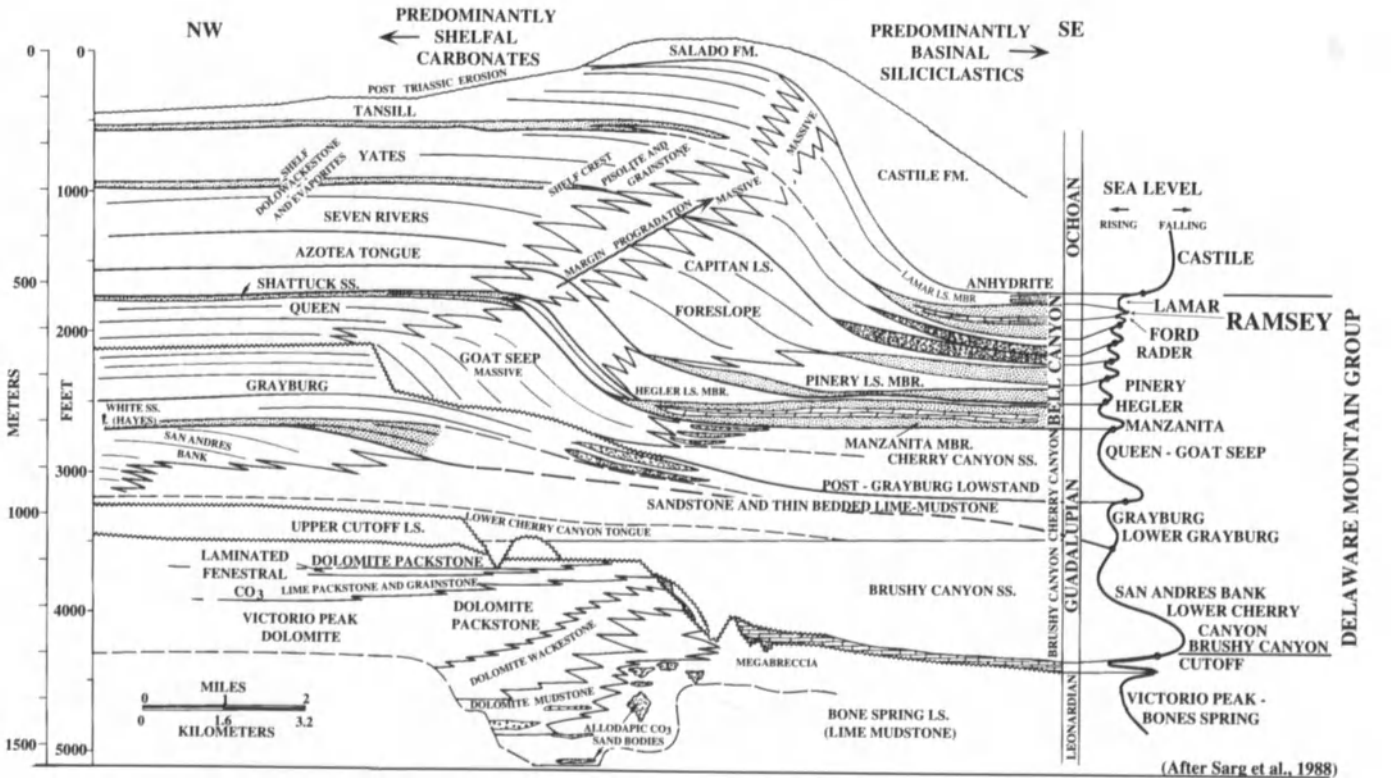

Figure 10.2. Stratigraphic relation of Permian rocks of the Delaware basin, northern shelf margin, Texas and New Mexico (after Sarg and others, 1988). The Upper Guadalupian Ramsey sands are the last marine sands deposited on a thick, siliciclastic submarine fan. The Ramsey is equivalent to prograding and aggrading shelf-margin carbonates.

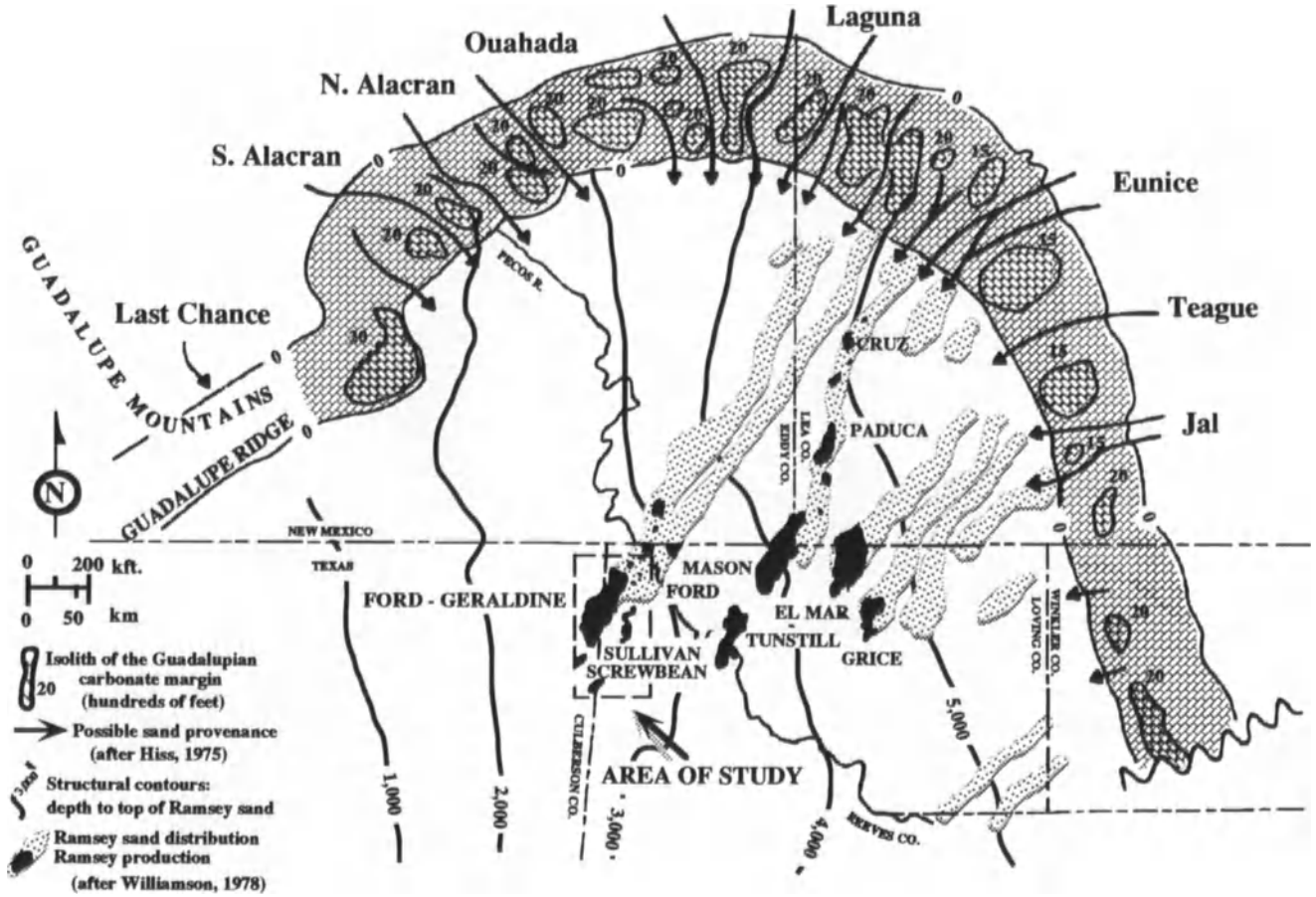

Figure 10.3. Possible transport paths for lagoonal siliciclastics to bypass the carbonate shelf margin. Dramatic thins in the carbonates appear to coincide with major linear sand trends of the Ramsey, suggesting sediment bypass in canyons. The area from Eunice canyon south to Jal canyon appears to have been the major axis. Significant Ramsey fields are shown in black. The fields are coincident with the eastward-tilted terminal lobes of submarine channel fill. (Carbonate margin after Hiss, 1975; Ramsey channels and structural contours after Williamson, 1978.)

Delaware sandstones, specifically the Bell Canyon Formation. He made isopach maps of the gross Ramsey interval in the Delaware Basin, which demonstrate the sub-parallel, multi-point source nature of the channels that trend basinward, perpendicular to the shelf margin (Fig. 10.3).

Bozanich (1978, 1979) studied Cherry Canyon and Bell Canyon subcrops in the eastern Delaware Basin. His depositional model for the eastern shelf is similar to Harms' (1974) and Williamson's (1978) for the northern shelf, except that channels as well defined or as thickly filled were not observed. He attributed these differences to the reduced supply of sediment from the eastern shelf, which was farther from its corresponding source. He believed that the Midland Basin, nearly filled by late Guadalupian time, acted as an extension of the shelf and supplied clastic sediment and dense, saline water to the Delaware Basin.

McDermott (1984) described the Cherry Canyon–Upper San Andres shelf margin/slope break where it crops out in Last Chance Canyon, southeastern New Mexico. He recognized submarine channels carved into interchannel slope siltstones. The channels were filled predominantly by sandstone (lagoonal siliciclastics). Multiple events of erosion, deposition, and slumping were observed. In addition, he recorded examples of channel-fill events that were mantled (and thus, separated) by horizontally stratified, bioturbated siltstone and sandstone. After the channels were abandoned, they were followed by progradation and aggradation of normal shelf deposits (principally carbonate).

From his field observations, McDermott concluded that hypersaline, bottom-hugging currents off the embanked shelf transported siliciclastic lagoonal sediments through breaches (channels) in the shelf shoal and interchannel slope. Like Harms (1974), Williamson (1978), and Bozanich (1978), McDermott believed the density flows to be long-lived (long enough to form and sustain migrating sand waves). Williamson (1978) and McDermott postulated that

the Ramsey channels were back filled and that the sandstone lobes are imbricated or lapping atop one another back toward the shelf.

McDermott proposed several causes for this imbrication: (1) a diminishing sediment supply due to a retreating sediment source, (2) a decreasing velocity for successive density flows, (3) a decreasing volume of dense saline water flowing through the channels because of channel constriction or abandonment, and (4) a decreasing density of successive flows.

Control

The Ramsey reservoir was examined through 506 gamma-ray/neutron or gamma-ray/sonic logs and 27 cores, primarily from the unitized Ford-Geraldine field (Fig. 10.4). Logs from cored wells were correlated to the core and served as cornerposts for the correlation grid. In addition, core porosity and permeability data from 181 wells were plotted against depth to examine reservoir segregation. These plots served as useful correlation tools as well. An example plot of these data mimics the gamma-ray curve and was used to correlate logs of differing vintage and quality (Fig. 10.5). Nineteen stratigraphic cross sections were constructed, of which six are included in Figure 10.4. Interval isopach and structure maps on each stratigraphic interval (Fig. 10.5) helped determine controlling factors on production.

Lithofacies

Three major rock types are present in the subsurface upper Bell Canyon Fm of the Ford-Geraldine field area. In order of increasing average grain size, they are: lutite (oranic-rich siltstone), laminated siltstone (laminite), and very fine-grained sandstone. This classification scheme is modeled after Bozanich (1978, 1979). The most notable feature of the lithotypes is that they are virtually clay-shale free (Williamson, 1978); lutite has the highest clay content.

These three lithotypes make up a depositional cycle, wherein lutite is the finest-grained, "lowest energy" end member; laminated siltstone is the intermediate member; and sandstone the coarsest-grained, "highest energy" end member. Lutite and laminite were deposited by processes that are distinct from sandstone deposition.

Lutite

The lutite facies is a fissile, dark, highly organic siltstone and the finest element of the basin fill. Watson (1974) reported 6% clay in the thickest lutite of the upper Bell

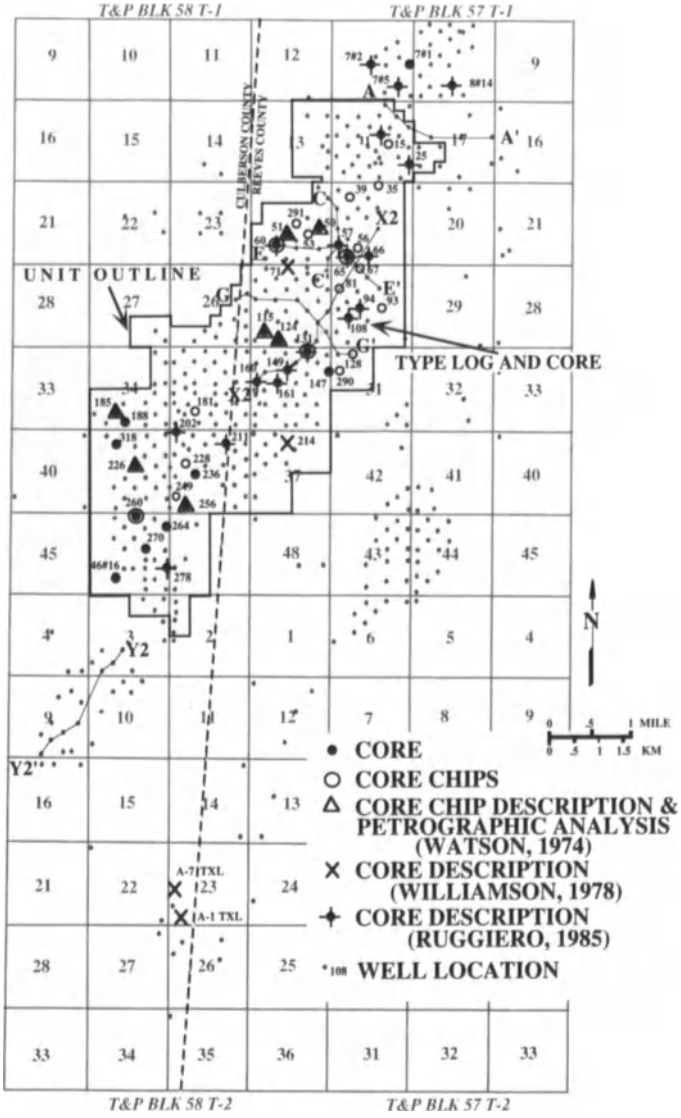

Figure 10.4. Location and type of control points. Type log and core indicated by arrow.

Canyon section (within the Ford laminated siltstone of Fig. 10.5). Most of the amorphous organic material is of marine planktonic origin (Payne, 1976) and was deposited by settling from suspension. The Ford lutite is approximately 2 ft (0.6 m) thick throughout the study area and makes up about 2% of the section from the base of the Ford siltstone to the top of the Trap siltstone.

The thicker lutites blanketed previously deposited sediment, thereby draping over the bottom topography; the thickness of each lutite is fairly constant. Laterally extensive throughout the basin, lutite is an excellent regional time marker, easily recognized in logs (Fig. 10.5) as an anomolously high gamma reading; where it is discontinuous, large channel scour may be indicated (Berg, 1979).

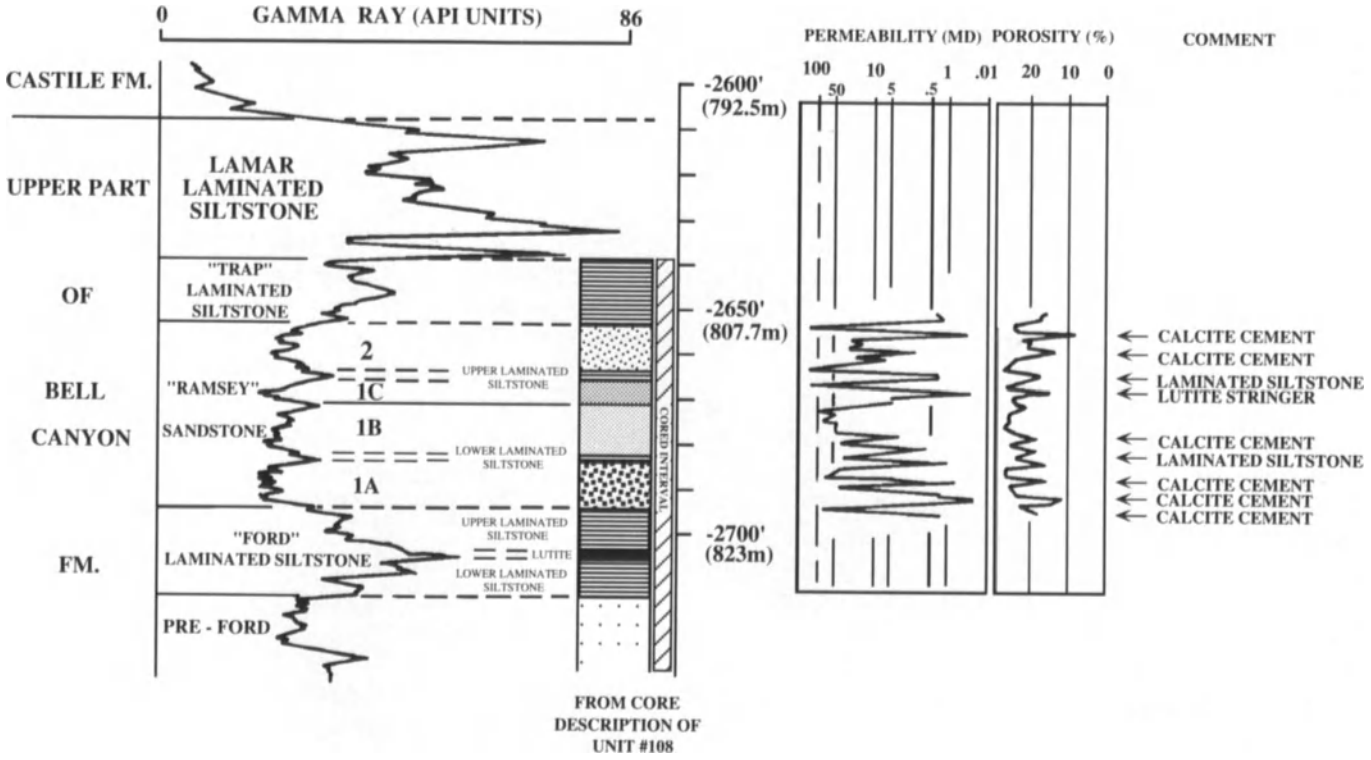

Figure 10.5. Type log and core (Ford-Geraldine Unit #108). The Ramsey is subdivided into six mapping and log correlation units based primarily on distinctive gamma ray log response. Porosity and permeability are adversely affected by pore-filling cement.

The organics within the lutites are sapropelic but were not buried deeply enough to generate the hydrocarbons in the reservoirs (Hills, 1984).

Depositional Processes—Interpretation. The presence of lutite is evidence of a period of reduced clastic deposition and a record of planktonic productivity in the more hospitable near-surface water layers. Lutite units are not interrupted or subdivided by major clastic hypo- or hyperpycnal flows, but rather have graded upper and lower contacts (where conformable) with laminated siltstone. As plankton died and settled to the deep ocean floor, the constituent organics were preserved in the anoxic, reducing conditions of the density-stratified, deep-water layers, thus accounting for the black color and organic richness of this lithotype (Williamson, 1978).

With a greater silt influx, resulting from more frequent hyperpycnal flows, organics (constantly raining down from suspension) became diluted by silt. The appearance of the resulting deposit approaches that of a laminated siltstone (laminite lithotype). Many of the lutite units in core have gradational contacts with laminite units. For example, below the base of the Ford lutite, organic-poor siltstone laminae become progressively fewer, and the organic laminae much thicker, creating an apparent upward-fining sequence into the lutite. The reverse sequence is true near the top of the lutite layer, which "grades" into laminite. The relations may be demonstrated on a typical log; the lutites within the Ford and Trap members are symmetrically bounded by laminite (Fig. 10.5). Moreover, sandstone was never observed in conformable contact with a major lutite. Therefore, lutite is interpreted to be the lowest-energy end member in an overall scheme of cyclic deposition where the base and top of each highest order cycle is lutite. Stratigraphic intervals to be discussed later that contain lutites are the Ford siltstone, Trap siltstone, and Lamar siltstone (Fig. 10.5).

Laminated Siltstone (Laminite)

Laminite is parallel-laminated siltstone with alternating laminae (0.2–2 mm thick) of amorphous organics and silt. As observed from the porosity/permeability data of 181 wells in the field, the porosity of laminite units is remarkably consistent: between 18 and 19%. The permeability is typically quite low, ranging from .01 to 4 millidarcies (md), but principally less than 2 md. Horizontal and vertical permeabilities are greatly reduced by the presence of pore-filling calcite cement. Permeability is least in the vertical

direction because of fine organic laminae that are stacked like a deck of cards. Laminite composes 50% of the section from the base of the Ford siltstone to the top of the Trap siltstone.

The "Ramsey" sandstones are encased in laminite that forms the seal of this stratigraphic trap and complicates production. Laminite sections may appear as monotonous, uninteresting, varve-like deposits, but an understanding of their geometry is the key to the architecture and depositional history of the fan.

Each light gray, coarse silt lamina can be coupled to one above it that is dark, organic-rich, and finer grained. In fact, each couplet apparently fines upward (Williamson, 1978) so that as silt size decreases, organic content increases.

In an interval of several feet of core, the couplets seem to have a higher order of sequence, often appearing as part of a general fining or coarsening trend. This apparent grading is not believed to be from one flow like the grading in a Bouma sequence, but rather a composite of individual "siltstone" events (hypopycnal flows) amid a constant background rain of organics. For example, the couplets in the upper Ford member just below the first Ramsey sand frequently thicken upward. Within each couplet, the light gray siltstone lamina is thicker, and the organic lamina thinner, than those in the preceding set. The overall effect is an upward-thickening and coarsening trend, which indicates a period of intensifying activity on the shelf that culminated in sand-laden density currents to the basin. After periods of episodic sand deposition gave way to more normal conditions, the sandstones (e.g., Ramsey) were followed by a reverse sequence of laminated siltstone characterized by upward-decreasing silt content (e.g., Trap), eventually "grading" into lutite (Fig. 10.5).

Interpretation. Like the lutite, laminite is deposited by settling from suspension. The important difference is that the silt fraction of the laminite most probably entered the basin by hyperpycnal density flows. Silt-laden currents of this nature are reported off the Gulf of Mexico shelf edge after the passage of "blue northers" (McGrail and Carnes, 1983). The cool, hypersaline density flows may have spilled through gaps in the shelf margin, met a point of equal density within the stratified basin, and sheeted out as inter-laminar flows. The transported silt settled from suspension, mantling bottom topography (Harms, 1968; Williamson, 1978) and sealing the "lid" on sandstone previously deposited in the submarine channels. Another difference is that the overall geometry of laminite is wedge-shaped, thinning toward the basin center (Fig. 10.27 and Meissner, 1972), whereas lutite is more blanket-like. For example, the Ford lutite maintains an average thickness of 2 ft (0.6 m) within and well outside the area of study.

Most probably, the organic laminae in laminite and lutite represent a constant basin-wide rain or "background" of organic material settling from suspension. The thickness of the silt fraction in each laminite couplet could indicate relative size of the driving force (i.e. ranging from a frontal passage to a tropical storm) that created the silt-laden density flows. The higher order coarsening and fining sequences of couplets could represent pulses of density flows from building or waning storms. Thus, laminite is a record of suspension sedimentation: the result of normal organic materials at "background" levels, punctuated by cyclic siltstone deposition from interlaminar flows.

The Ford siltstone, Trap siltstone, upper and lower laminated siltstone of the Ramsey member, and the Lamar siltstone are stratigraphic intervals deposited primarily by this process. These units (Fig. 10.5) will be discussed in more detail below.

Fine-grained Sandstone

The sandstone facies in the study area is a silty, very fine-grained, submature, moderately well-sorted arenite (Williamson, 1978; Payne, 1976). Porosity ranges between 20 and 24%, whereas permeability varies greatly (0.01 to 300 md), depending on the distribution of calcite and authigenic clay cements (Williamson, 1978). Unlike widespread lutite and laminite, sandstone is confined to channels that are well defined in outcrop and the subsurface.

Sandstone occurs as thin units (1–5 ft, or less than 1.6 m), reaching an aggregate maximum thickness of 65 ft (21 m) in the study area (Fig. 10.6). Each major correlative unit or package is composed of many smaller units and is laterally continuous along depositional strike, as denoted by porosity/permeability characteristics and log marker correlations (Fig. 10.5). Units pinch out against the channel margins and intra-channel erosional remnants downdip. Most sandstone appears massive, but on a wet, polished core face has thin, horizontal lamination (plane bed, upper flow regime) or parallel planar cross lamination (migrating dunes). This lithotype constitutes approximately 48% of a typical center-channel section.

Interpretation. The nature of the gravity flows that delivered sand and silt into the basin are widely described and discussed in previous literature. Two major schools of thought emerge: one calls for turbidity currents, and the other for hypersaline density currents. The principal ideas, as presented by their chief proponents, are addressed briefly herein.

Berg (1979) and others (Payne, 1973, 1976; Weinmeister, 1978) proposed meandering turbidity currents within leveed channels to account for apparent graded intervals in

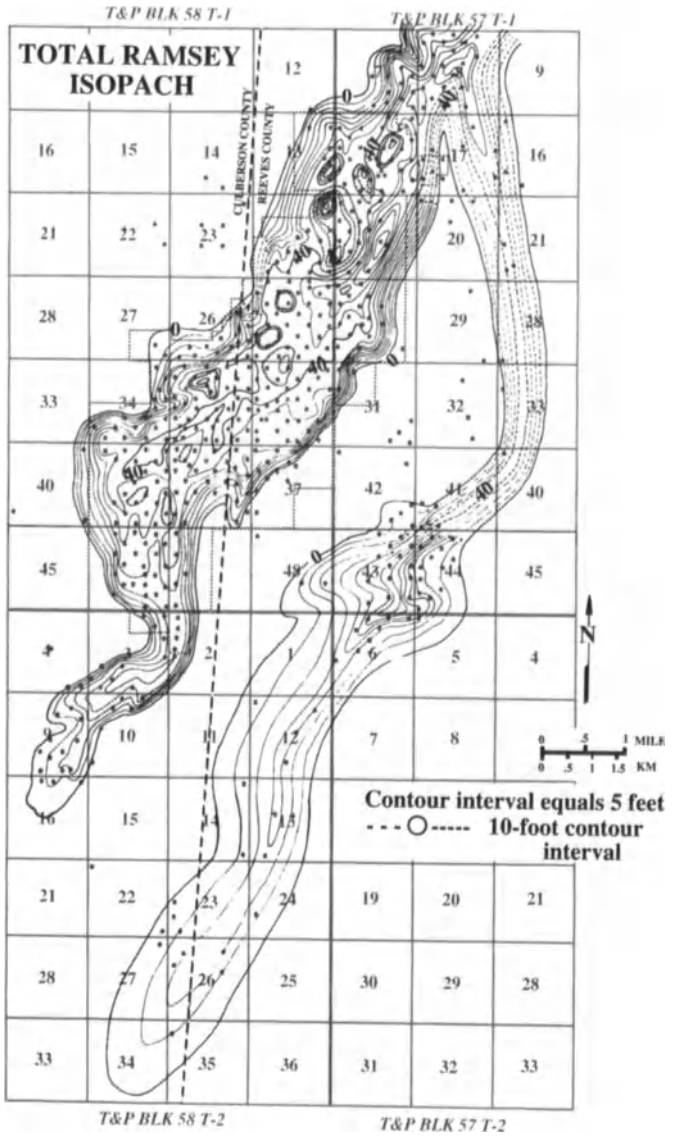

Figure 10.6. Isopach map of the total Ramsey interval as defined in Figure 5. Marked thinning of the sandstone within the channel indicates onlap onto erosional remnants that had topographic relief.

core and sinuous patterns on isopach maps. Leveed, meandering channels have been documented on recent fans composed of shale-rich sediment (Mississippi fan: Kastens and Shor, 1985; Bouma, et al., 1984; Amazon fan: Damuth and Flood, 1984). However, the apparent meanders in the sand-rich terminal lobes of the Delaware fan, like the Ford-Geraldine area, are shown in this study to be more likely caused by pinch-outs against erosional remnants within the primary channel (see Fig. 10.17) and to bottom topography at the time of sand lobe deposition, rather than to the dynamics of the depositing currents alone. Additionally, Ramsey channels in the Ford-Geraldine field do not have levees. The geometric relations of the lithofacies are discussed in a later section ("Results").

Moreover, many apparent inverse or normal graded intervals in core (based on the dispersal pattern of laminated siltstone rip-up clasts) are interpreted as increasing or decreasing flow strength, respectively. The rare, normally graded sequences in Ramsey cores, often described as "Bouma sequences" (Bouma, 1962) by other workers, may be the result of waning density currents and not necessarily turbidity flows. Because clay is required to maintain turbidity, and there is virtually no detrital clay in the Ramsey sandstones, turbidites are extremely rare in the section (Williamson, 1978).

Another point of general disagreement is the length of time during which sand was emplaced. At one end of the spectrum, Berg (1979) believes sand was deposited by turbidity flows as migrating point bars in a meandering channel; this process requires remarkably long-lived currents to explain the observed continuity of correlative sands across the width of the field. To account for this continuity, Berg's "point bars" would have to migrate laterally and down channel without interruption, and in such a manner that the lateral accretion process would yield sands of nearly identical log characteristics throughout the field. This proposed model of "submarine point bar" deposition is not consistent with other point bar facies tracts.

Williamson (1978) and McDermott (1984) discussed the hypothesis of long-lived hypersaline currents of fluctuating strength to explain alternating upper and lower flow-regime structures and dune migration down the axis of the channel. Their observations of primary structures on outcrop and core were corroborated by this study of cores from Ford-Geraldine Field.

Parallel planar cross lamination (suggesting dune migration) was present in cores within the "thalweg" of each Ramsey subunit (i.e. "1A," "1B," "1C," and "2"; cores Ramsey #8–14, FGU 66, 131, 149, and 160: Figs. 10.4 and 10.5). Although the basic observations coincide, the interpretations of density flow characteristics differ.

Herein, the Williamson (1978) model is modified to account for strong evidence of rapid deposition along the margins of the channel. Many observations of soft-sediment deformation, fluid-escape structures, and escape burrows indicate more rapidly emplaced sand. In one core from the edge of a channel, a large, laminite rip-up clast (2 cm across) at the base of an apparently normal-graded bed is interpreted to have been "frozen" in the process of disintegrating along lamination planes. At one end of the clast, laminae are undisturbed; at the other, massive, fine sand is present between flaring laminite couplets, indicating very rapid deposition of the enclosing sand.

These two opposing rates of deposition may be resolved by the following model. Assume that the bottom-hugging

currents (liquefied flows) had enough volume to fill the entire channel bottom in a sheet-like fashion from margin to margin, not confined within a narrow meander belt. When the flows encountered channel constrictions or obstructions, cross-sectional area was preserved; they thickened and became very erosive. This erosiveness is prevalent around the remnant high, which is demonstrated by isopach thins of the Ramsey sand (Fig. 10.6) in the northwest part of the field (cores FGU 57 and 60, Fig. 10.5). The channel deepens sharply to 65 ft (19.8 m) and narrows next to the topographic remnant. This narrow is analogous to a flume chute. As the flows left the constriction, they would have fanned out over the firm sandy substrate and refilled the channel from side to side. The velocity of the flows should have increased substantially in the throat of the constriction and dropped off fairly rapidly as the "head wave" flattened, increasing its surface area or footprint (see isopach Fig. 10.17 and 10.24).

By this or related processes, laterally extensive cross-bedded units with similar porosity and permeability can be explained. In addition, as the currents waned, their load was probably emplaced first along the channel edges where the flows were thinner and frictional forces weakened them sooner, and last along the axis or thalweg where they were thicker and had more momentum, much like a fluid lava flow. This "staged" emplacement can explain the higher frequency of cross-bedded units near thalweg axes and more quickly emplaced, horizontally stratified, or massive units on the channel margins.

Depositional Model

The depositional model presented here is derived from previous shelf and shelf-margin outcrop studies (i.e., McDermott, 1984) and the results of this subsurface study. The concepts of many previous workers are distilled from the literature and incorporated into this model (principally Harms 1974, Williamson 1978, and McDermott, 1984).

The Permian Basin was near the Permian paleo-equator (Habicht, 1979). The encircling shallow shelf and the nearly infilled Midland Basin had high rates of evaporation and were sources of hypersaline water. In this restricted basin, apparent sea-level rise and fall may have been due to a cycle of evaporative loss followed by episodic resupply of water from a more open marine source to the south (Silver and Todd, 1969).

During periods of relative highstand, siliciclastic sedi-

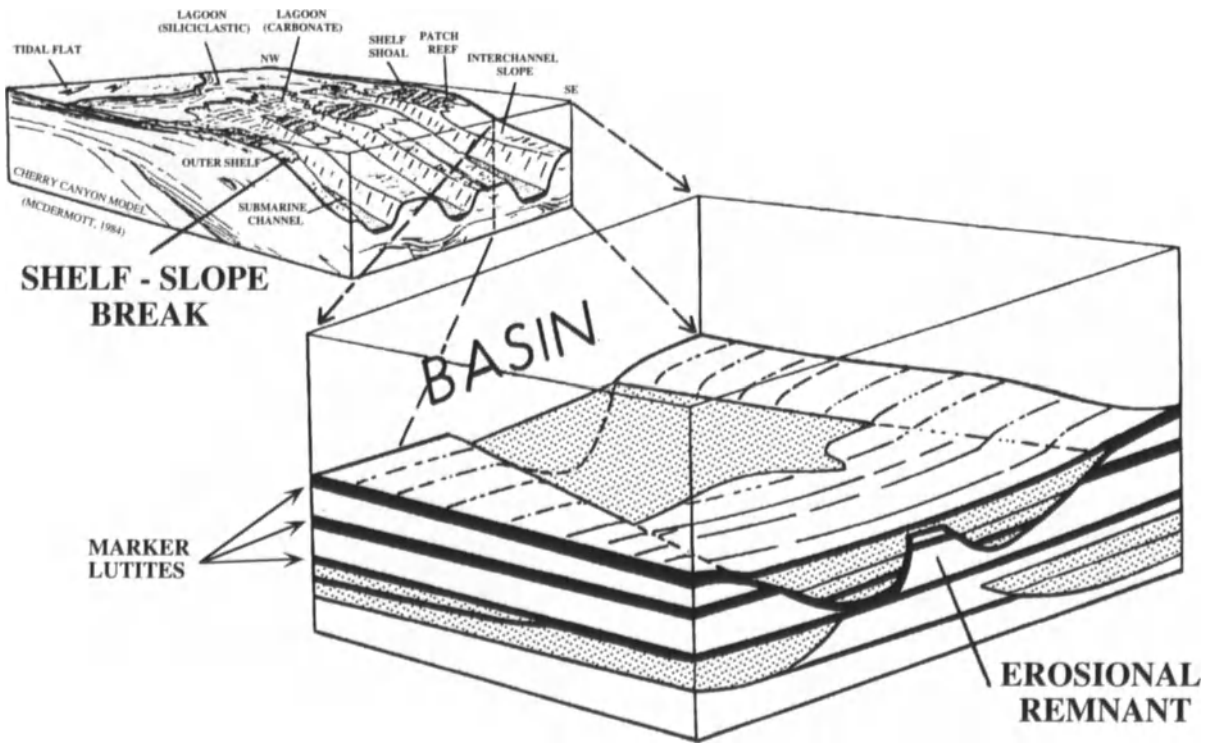

Figure 10.7. Perspective diagram of Ramsey depositional systems. The source for the basinal sands lies in the mixed carbonate and siliciclastic lagoon behind the shelf-slope break. A flexure of carbonate build-ups breached by submarine canyons characterizes the shelf margin. The basin channels are deeper, narrower, and more "V"-shaped nearer the shelf, and more shallow, broad, and "U"-shaped basinward. Erosional remnants with sharp topographic relief rise above the channel floor. (Shelf model from Cherry Canyon of Last Chance Canyon, McDermott, 1984)

ments were stored on the shelf well behind the shelf break; while at lowstand, siliciclastics prograded onto the shelf just behind the shelf margin, where they were swept basinward through breaches in the shelf margin by bottom-hugging, hypersaline density currents (McDermott, 1984) (Fig. 10.7). One model of fluctuating relative sea level (Pray, 1977) seems to fit with these interpretations. Pray believes that fluctuations of not more than 2 to 3 ft (0.6–0.9 m), were needed to effect this siliciclastic progradation onto the broad, shallow shelf.

Channels and Inferred Depositional History

Truncation of the regional lutite markers suggests that the channels that carried siliciclastics from the shelf were scoured by large flows prior to "Olds" or pre-Ford sandstone deposition (Berg, 1979; Weinmeister, 1978) (Fig. 10.8, Stage 1). The scour may have cut upsection as it flowed basinward (see Fig. 10.11). This observation coincides with the changes in channel characteristics from the shelf margin to the center of the basin. The channels that are more "V"-shaped, narrower (less than 1 mil; 1.6 km), and deeper (nearly 100 ft, 30 m, deep) proximally become more "U"-shaped, broader (2 mil, 3.2 km), and shallower (40 ft, 12 m) distally (Fig. 10.7; see also Fig. 10.12).

Incompletely scoured fan deposits within the channel (erosional remnants) became topographically high areas or "hills" on the channel bottom. The time equivalency of the erosional channel surface and tops of the topographic highs are established from an even draping of the surface by the lutite within the Ford siltstone (Fig. 10.8, Stage 2).

Bottom-hugging hypersaline density currents laden with fine-grained sand swept through the head of the channel

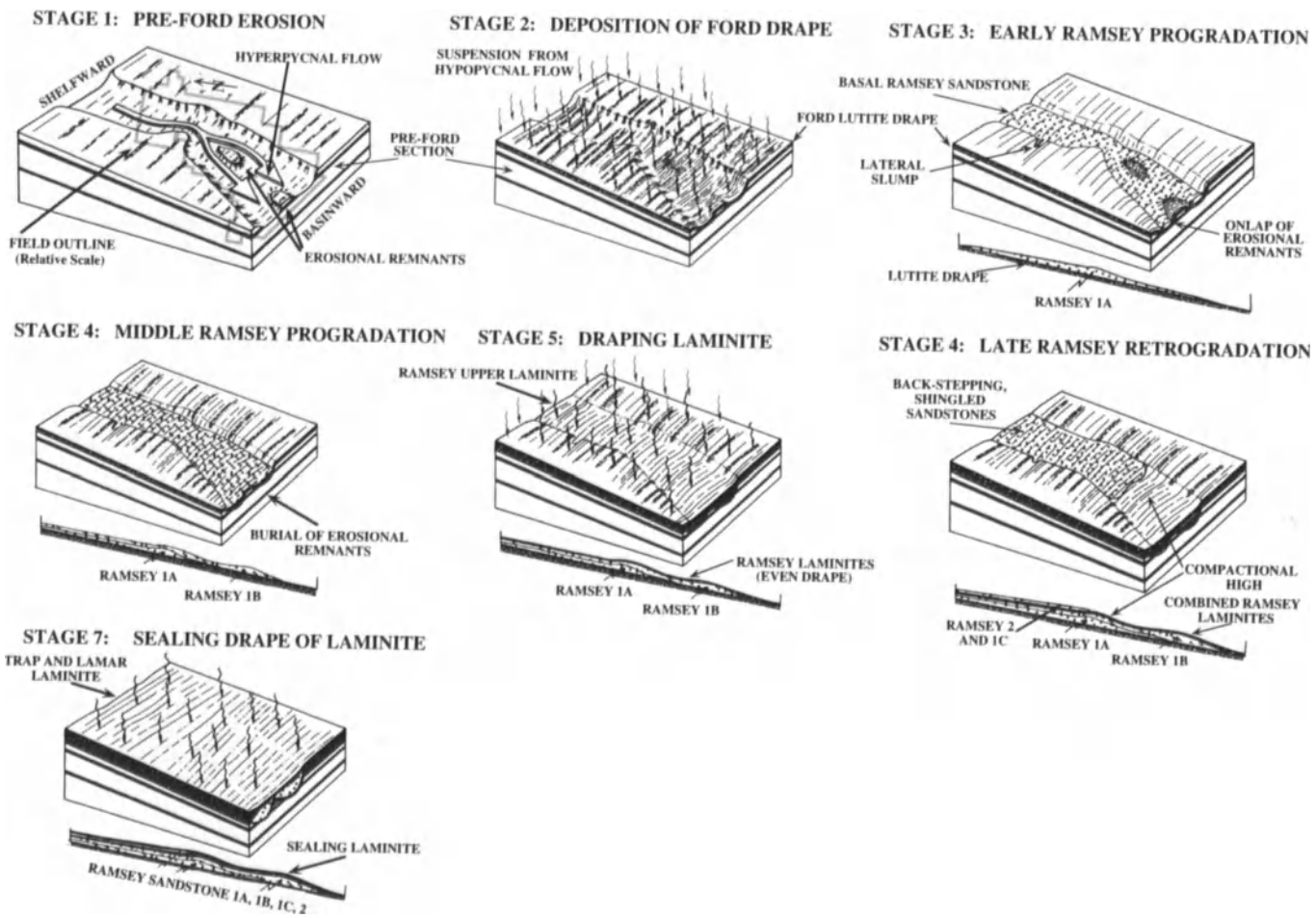

Figure 10.8. Stage 1: initial pre-Ford scour, as evidenced by truncation of lutite markers and resultant erosional remnants. Stage 2: deposition of Ford siltstone and lutite, which evenly drapes the channel. Stage 3: basal Ramsey (1A) sandstone progrades basinward and onlaps intra-channel highs. Stage 4: middle Ramsey (1B) sandstones prograde farther into the basin and are confined to the channel. Stage 5: laminite (e.g., upper Ramsey laminated siltstone) drapes channel fill. Stage 6: retrogradation or back-filling of the channel; Ramsey 2 sands encounter a compactional anticline along the channel axis from earlier sand deposition. Stage 7: Trap laminite drapes sandstones and creates numerous stratigraphic traps.

and flowed down the slope of the fan, confined within channel margins; there was little or no overbank flow. The path of these density flows was diverted around erosional remnants, which had a profound effect on the depositional history of the sandstone facies (Fig. 10.8, Stage 3). The first flows scoured into the Ford laminated siltstone; in some areas, as much as 10 ft (3 m) of it were removed and incorporated as rip-up clasts (see Fig. 10.18). Slumps along the channel margin occurred from undercutting. In the late progradational phase, sandstone nearly filled the channel and had covered most of the erosional remnants (Fig. 10.8, Stage 4).

Sand-laden flows from the shelf, which had been prograding basinward, ceased briefly during deposition of the Ramsey lower laminated siltstone (between Ramsey 1A and 1B deposition; similar to Fig. 10.8, Stage 5). Deposits classified as "progradational" persisted through deposition of Ramsey 1B.

Before the late onlap or retrogradational phase, sandstone-bearing currents were absent again during the more quiescent period of Ramsey upper laminated siltstone deposition (Fig. 10.8, Stage 5). The siltstone settled out of suspension from interlaminar flows, draping the channel-margin and channel-fill deposits evenly.

Sandstone deposition in the basin, and presumably, active sand transport on the shelf, resumed during Ramsey 2 time. Sand units continued to back-stack or onlap toward the shelf (Fig. 10.8, Stage 6) for several possible reasons: (1) a diminishing sediment supply due to a retreating sediment source, (2) a decreasing velocity for successive density flows, (3) a decreasing volume of dense saline water flowing through the channels because of channel constriction or abandonment, (4) a decreasing density of successive flows (McDermott, 1984), or (5) a decreasing slope gradient of the fan channnel. Although a combination of factors is probable, a decreasing channel gradient seems the most likely cause of the observed onlapping in Ford-Geraldine and similar Ramsey fields, like El Mar (Williamson, 1978, see Fig. 10.17).

Finally, after the last sands were transported basinward, the Trap and Lamar laminated siltstones were deposited (Fig. 10.8, Stage 7). Silt-laden interdensity flows cyclically interrupted the constant rain of organics. The silt and organics settled from suspension, evenly draping the sands within the channel and the previously deposited laminites at the channel margins and interchannel areas. The net effect was to seal the channel sandstones within laminite, creating the potential stratigraphic trap.

Results

Geometry of Channel Complex

An isopach of the gross Ramsey section indicates an elongate pod of sandstone that trends northeast-southwest, composing the Ford-Geraldine field. The eastern subparallel channel makes up the Sullivan and Screwbean field complex (Fig. 10.6). Strike cross section A-A' (Fig. 10.9)

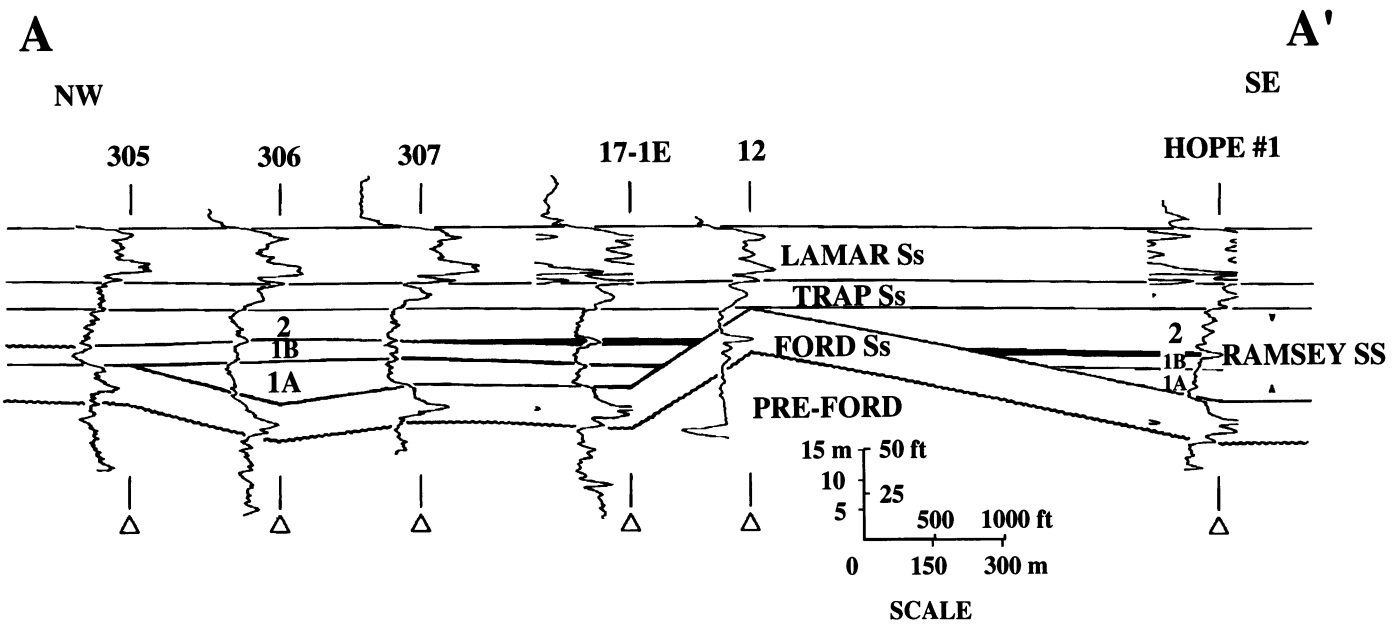

Figure 10.9. Strike section A-A' demonstrating channel geometry and bifurcation into Ford-Geraldine to the northwest and Sullivan-Screwbean to the southeast. The channels are narrow, deep, and more "V"-shaped.

demonstrates this bifurcation of the main channel. Both resultant channels are steep sided and nearly 60 ft (18 m) deep in this more proximal section. The sand units fill channel-bottom topography, are laterally extensive, and when deposited, nearly flat-topped.

Ford-Geraldine

Strike section G-G′ (Fig. 10.10) establishes the east-west channel geometry of the Ford-Geraldine. The channel widens to 2 mi (3.2 km) and becomes more shallow (40 ft or 12 m average depth) basinward. Progradational sandstone

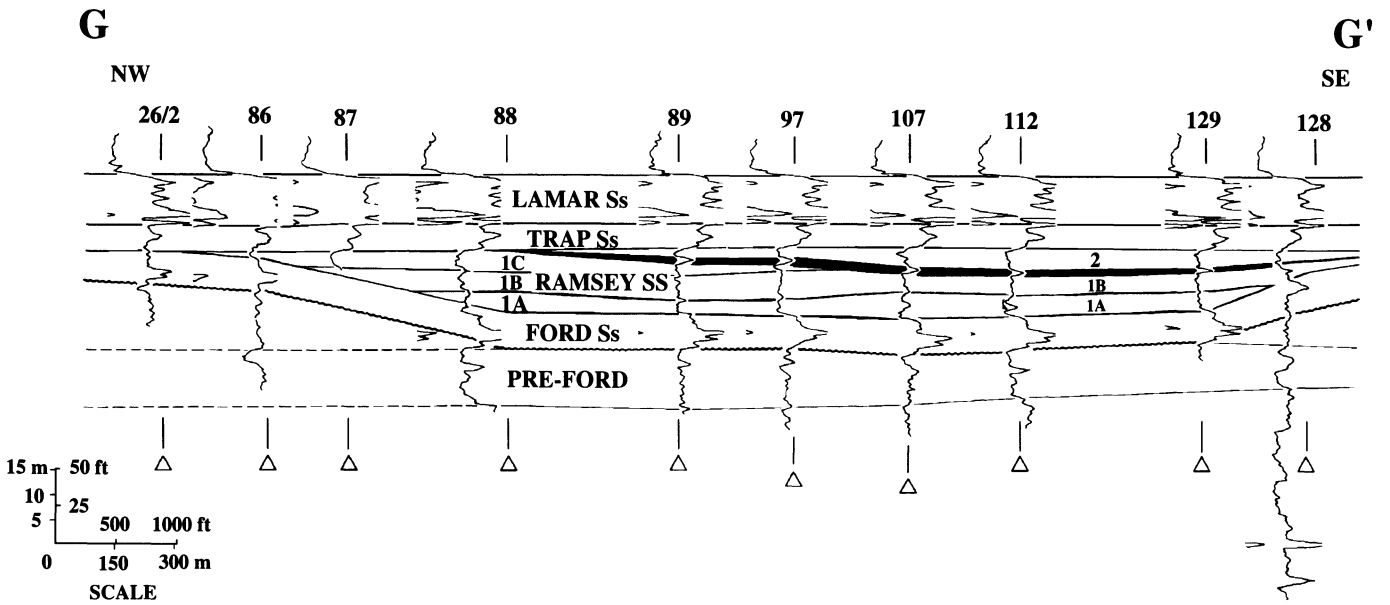

Figure 10.10. Strike section G-G′ demonstrating Ford-Geraldine channel geometry. The channel is shallow, broad, and more "U"-shaped. Lateral truncation of older sediment occurred before Ramsey upper laminite (solid black) was deposited.

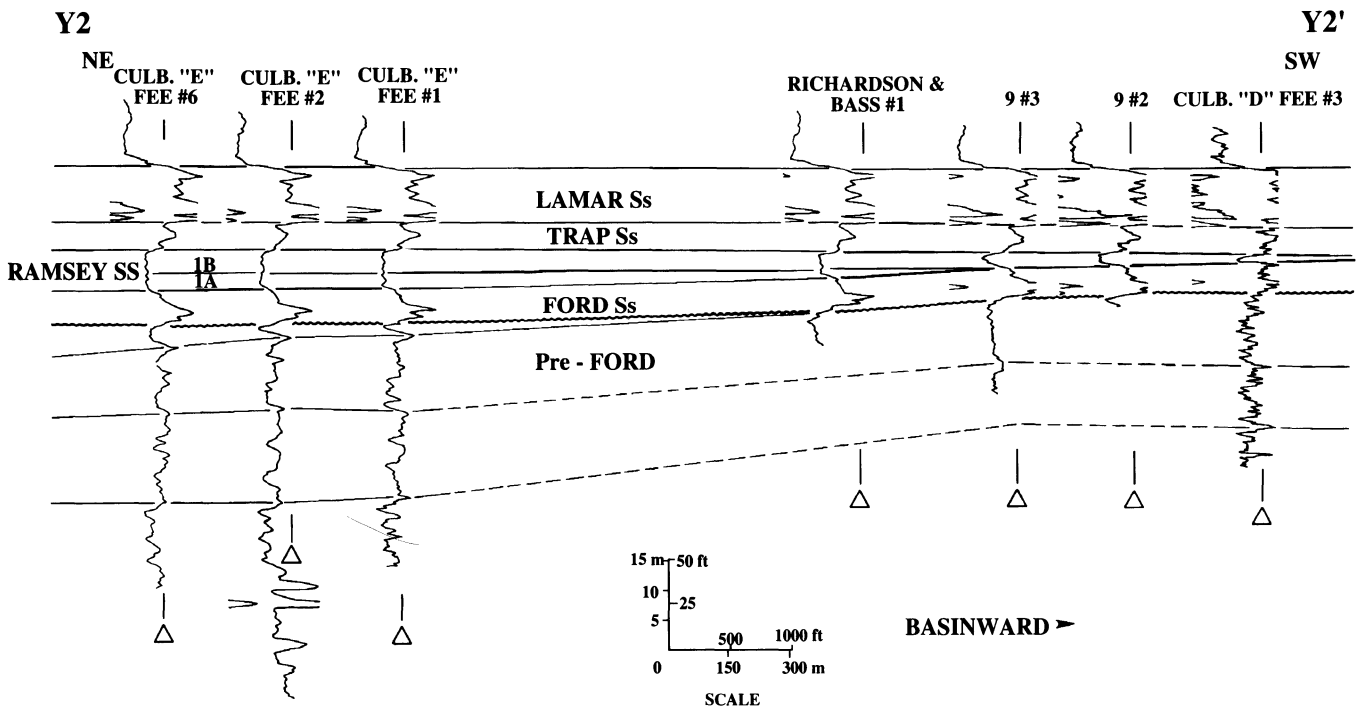

Figure 10.11. Dip section Y2-Y2′ demonstrating downlap of prograding sandstones. Ramsey 1B prograded the farthest basinward.

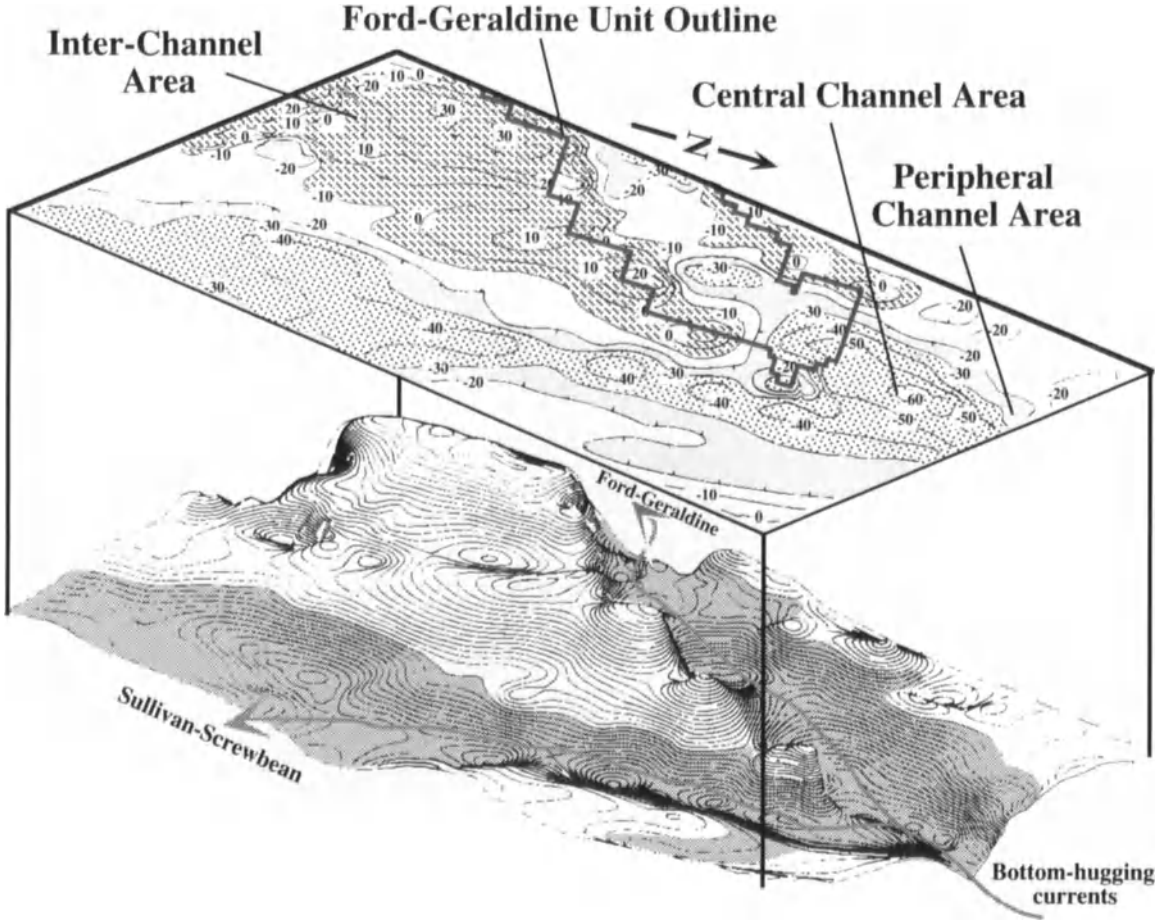

Figure 10.12. An isometric projection of the residual (regional dip subtracted out) structure on top of the Ford. This process creates a channel geometry. The aspect is down-channel where the bifurcation of the Ford-Geraldine and Sullivan-Screwbean channels occurs. Topographic highs control the path of bottom-hugging density currents.

units "1A" and "1B" fill the channel laterally from margin to margin by vertical accretion. One or more erosive events after "1C" and before upper laminite deposition are indicated.

Dip section Y2-Y2′ (Fig. 10.11) represents typical pinchout down depositional dip. In the Ford-Geraldine channel, the Ramsey 1B unit prograded farthest into the basin.

Figure 10.12 is an isometric projection of structure on top of the Ford siltstone (Fig. 10.13), with the eastward regional dip subtracted out. The projection is a representation of the channels, as depicted by Ford structure less the regional dip. Because the Ford siltstone evenly draped pre-existing topography of the fan surface, this type of restoration should indicate channel geometry most accurately. In the northern, or more proximal, portion of the study area the main channel is deeper (maximum of 65 ft or 20 m) and narrower (less than 1 m or 1.6 km wide). More basinward, past the largest erosional remnant, the Ford-Geraldine channel broadens to 2 mil (3.2 km) wide, becomes more shallow (40 ft or 12 m deep) and has more gently dipping channel margins.

Channel Fill and Isopach Analysis

The isopach of the gross total Ramsey interval (Fig. 10.6) shows a main channel that bifurcates into two linear, subparallel channels. This bifurcation occurs just north of the largest erosional remnant discussed below. The eastern or Sullivan-Screwbean channel was a "pressure relief" valve or splay for the bulk of the flows that encountered the remnant high in the Ford-Geraldine channel.

Paleotopographic Highs or Erosional Remnants

The thickest portion of the Ford-Geraldine channel fill (60–65 ft; 19.8 m) in Figure 10.6 follows an axis from T&P

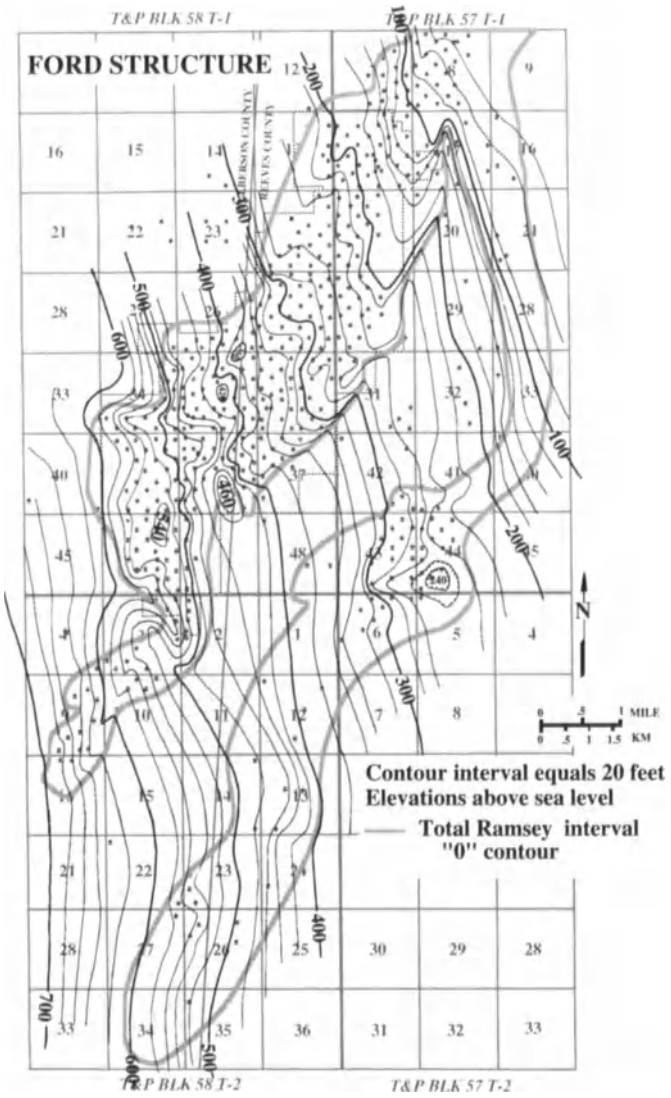

Figure 10.13. Structure on top of the Ford laminated siltstone. Structural closure is very rare.

Block 57 T-1 section 8, in the extreme north of the area, to Section 19, 3 mi (4.8 km) along depositional dip. West of this channel fill, along a similar axis, is a complex of erosional remnants or highs. These paleotopographic highs had an effect on the deposition of sandstone and production from the resultant reservoirs.

Cross section C-C′ (Fig. 10.14) connects the two remnant highs with greatest topographic relief, as determined by the thinning or absence of Ramsey sand over them. Well #38 has no sandstone in it, having the appearance of an interchannel well; however, its location is within the channel. Likewise, well #57 has a very thin sandstone interval in it and is flanked by wells with much more sandstone (cross section E-E′, Fig. 10.15). Well #57 is the southernmost location of this topographic high. Older sandstones pinch out against the topographic high, while succeeding ones lap over it, except at its highest point (unit well #38).

This topographic feature had a profound effect on the depositional history of the sands. An isopach of the average thickness of the total Ford interval (Fig. 10.16) reveals probable erosion of the Ford along the axis of the thickest "1A" sandstone. Because the Ford evenly drapes the original pre-Ford scour, the pattern of erosion reflects channel-bottom topography. The isopach of the 1A sandstone shows an area of nondeposition coincident with the location of the high (Fig. 10.17). Likewise, other erosional remnants can be seen as anomalous sandstone thins within the channel (e.g., T&P Block 58 T-1). The apparent sinuosity of this pattern of thicks juxtaposed to thins has been attributed by other workers (Berg, 1979) to deposition by sinuous turbidity currents. Isopachs of succeeding intervals suggest lateral filling by sheet-like flows that were constricted near topographic highs on the channel bottom, and elsewhere were allowed to fan out, scouring and filling the lows.

Ford and Ramsey 1A

The Ramsey "1A" sandstone interval represents the first flows scoured into the upper Ford laminite, removing as much as 10 ft (3 m) of it along the thalweg (Fig. 10.18). Other thin intervals of the laminite appear where the "1A" isopach takes large excursions northwestward. These areas quite possibly are slump locations along the channel margin where the margin was undercut by turbulent eddies. The slumped material was incorporated into the flows as rip-up clasts. The Ramsey 7 #5 (Fig. 10.4) is located at the edge of the channel near a possible slump site in T&P Blk 57, T-1, Section 7; core from the well indicates angular truncation of the Ford siltstone, which could have been caused by current or slump.

The "1A" interval prograded the farthest into the basin in the Sullivan-Screwbean channel and nearly as far as "1B" in the Ford-Geraldine channel. By far, the "1A" unit has the greatest volume of all the intervals. "1A" sandstone was not deposited over the largest erosional remnant in T&P Block 57-1 Section 19 (Fig. 10.17).

Lower Laminite

A short hiatus in sandstone deposition followed "1A" emplacement, during which silts rained down from interlaminar flows. The distribution of the lower laminated siltstone is shown in Figure 10.19. The very localized nature of this unit (which should otherwise be widespread) suggests that

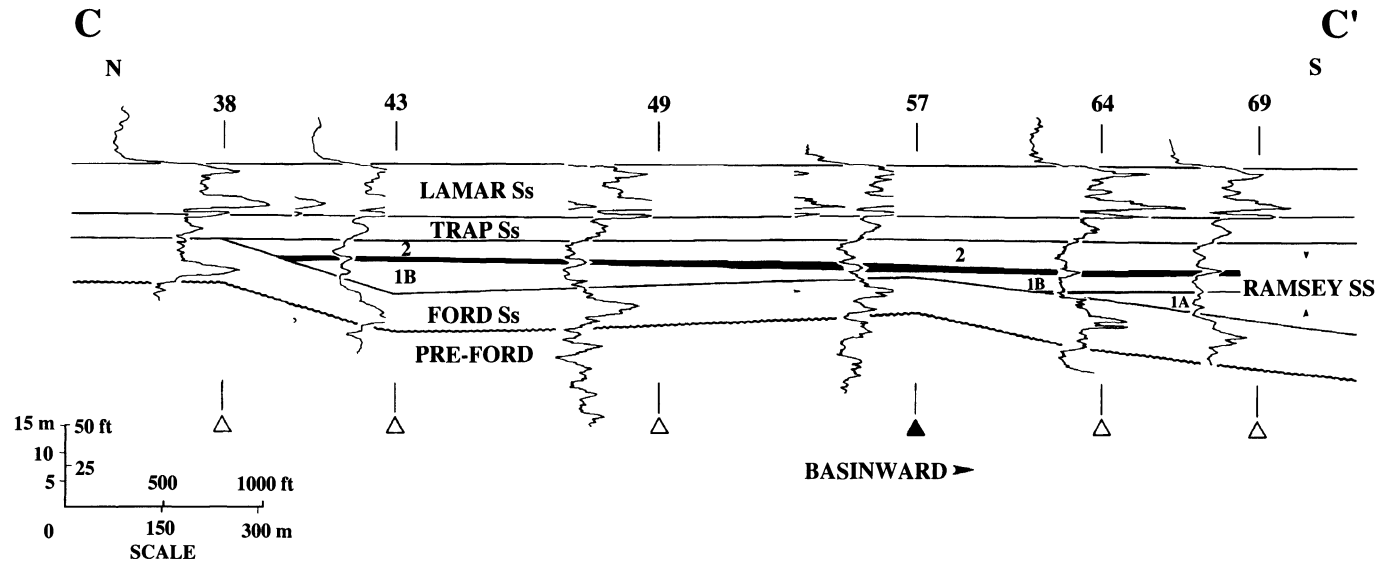

Figure 10.14. Strike cross section C-C′ along the crest of the highest erosional remnant. The sands onlapped the high but failed to bury the point of greatest relief, well #38. A darkened triangle below a well denotes a core control point.

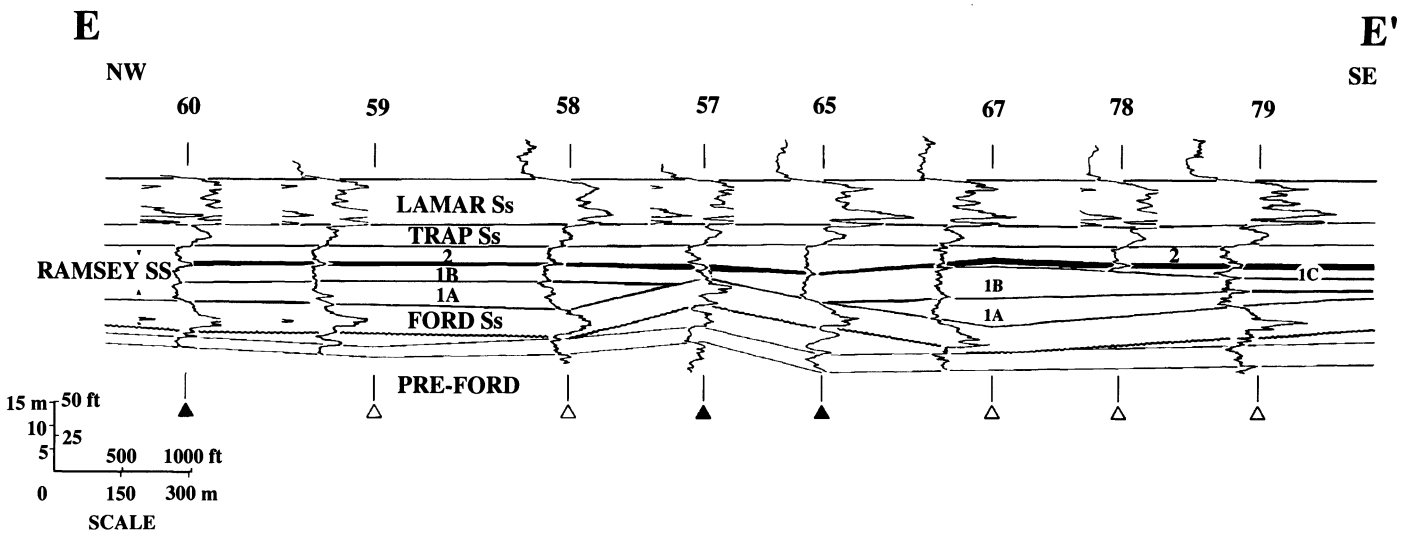

Figure 10.15. Strike cross-section E-E′ along the southern flank of the highest erosional remnant. The sands onlapped the flank of the high and buried it during Ramsey 1B deposition.

the successive "1B" flows were highly erosive. The lower laminite appears to be preserved where "1B" flows were diverted.

Ramsey 1B

The "1B" interval isopach (Fig. 10.20) suggests a "sinuous" thalweg and localized "point bar" areas of thicks (20 ft; 6.1 m). This superficial interpretation is overly simplistic. The pattern of 1B deposition, like that for all the other units, is created by a combination of deposition, non-deposition on highs, and erosion. For instance, the broad, thin area (15 ft thick; 4.6 m) in T&P Block 58 T-1 sections 25 and 36 of the 1B isopach is not the result of point bar deposition, but more likely the erosion of all of "1C" and a portion of "1B" prior to upper laminite deposition (see strike section G′-G′, Fig. 10.10).

The "1B" interval prograded the farthest into the basin in the Ford-Geraldine channel, but appears to be truncated by

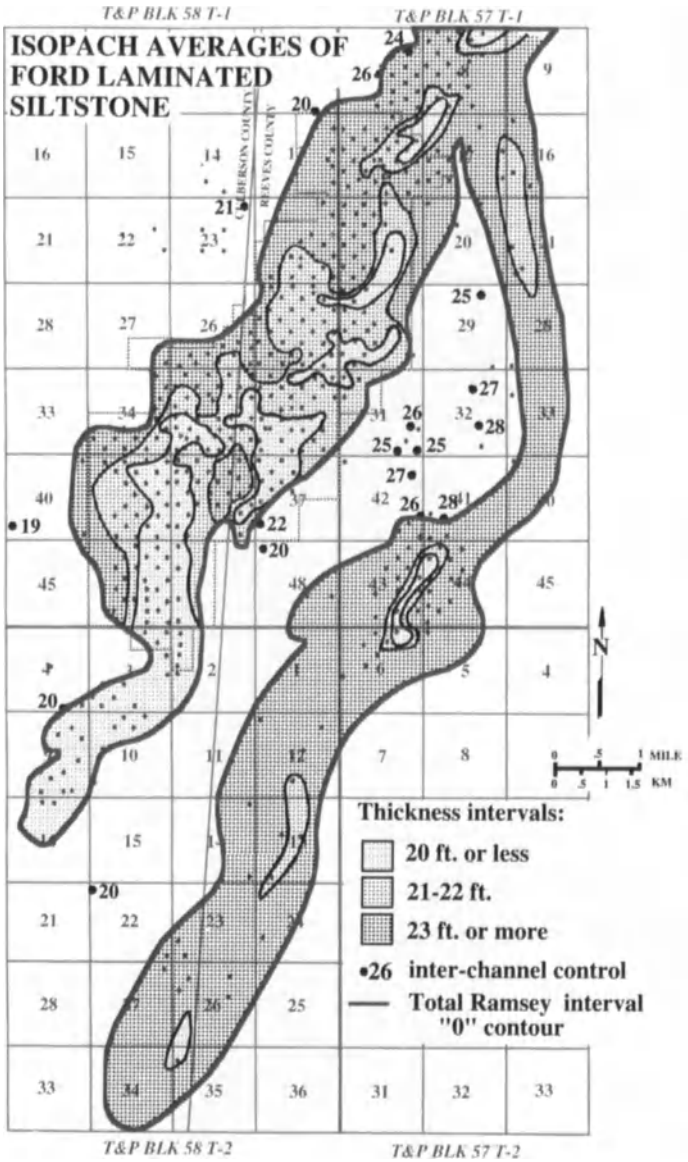

Figure 10.16. Averaged or smoothed isopach map of the Ford laminated siltstone. Thins correspond to the axis of the thickest Ramsey 1A interval. As evidenced by inter-channel control, the Ford gradually thins to the south.

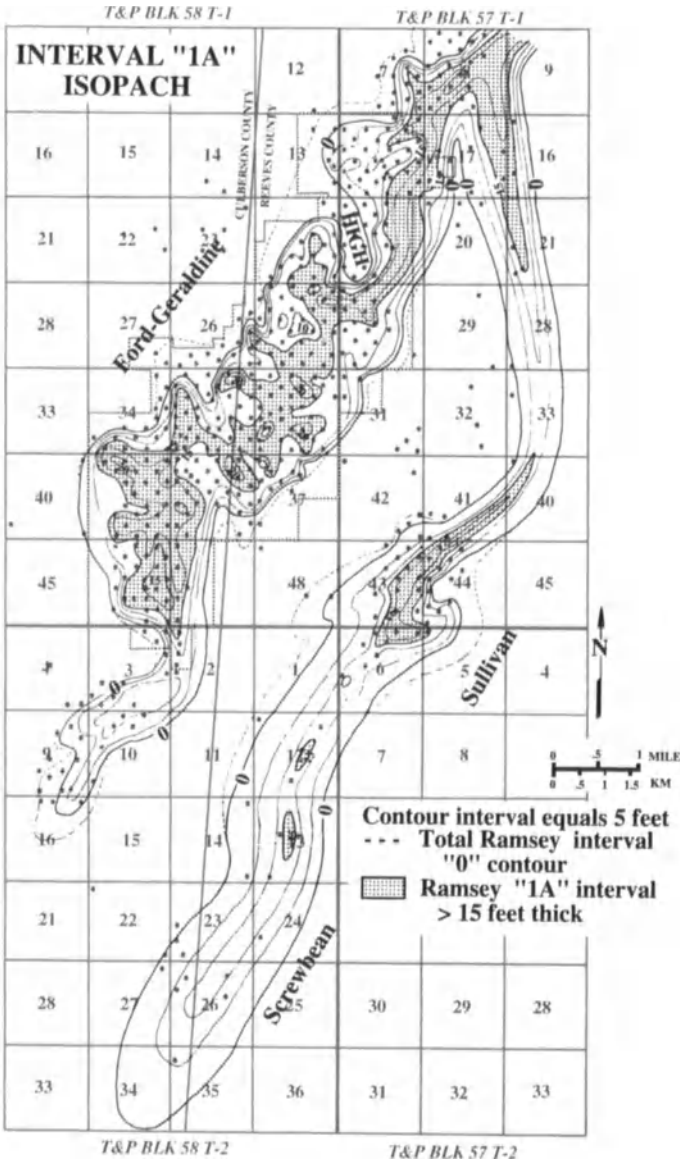

Figure 10.17. Isopach map of the Ramsey 1A interval. The thickest portion of the unit is shaded. The sinuous appearance of the shaded area is a result of sand-laden currents flowing around erosional remnants that had topographic relief.

erosion in the Sullivan-Screwbean channel. "1B" sandstone is deposited over the erosional remnant with the greatest relief in Ford-Geraldine.

Ramsey 1C

The "1C" interval (Fig. 10.21) differs from 1B in that it has a smaller areal extent. The pattern is dominated by erosion prior to upper laminite deposition; the upper laminite serves as a time marker of that erosional surface. Absent in the Sullivan-Screwbean channel, the "1C" interval appears to be the first imbricated sand package pinching out two-thirds of the way down the Ford-Geraldine channel.

Upper Laminite

The upper laminite evenly drapes the erosional surface that preceded it and has an average thickness of 2–3 ft (0.6–0.9

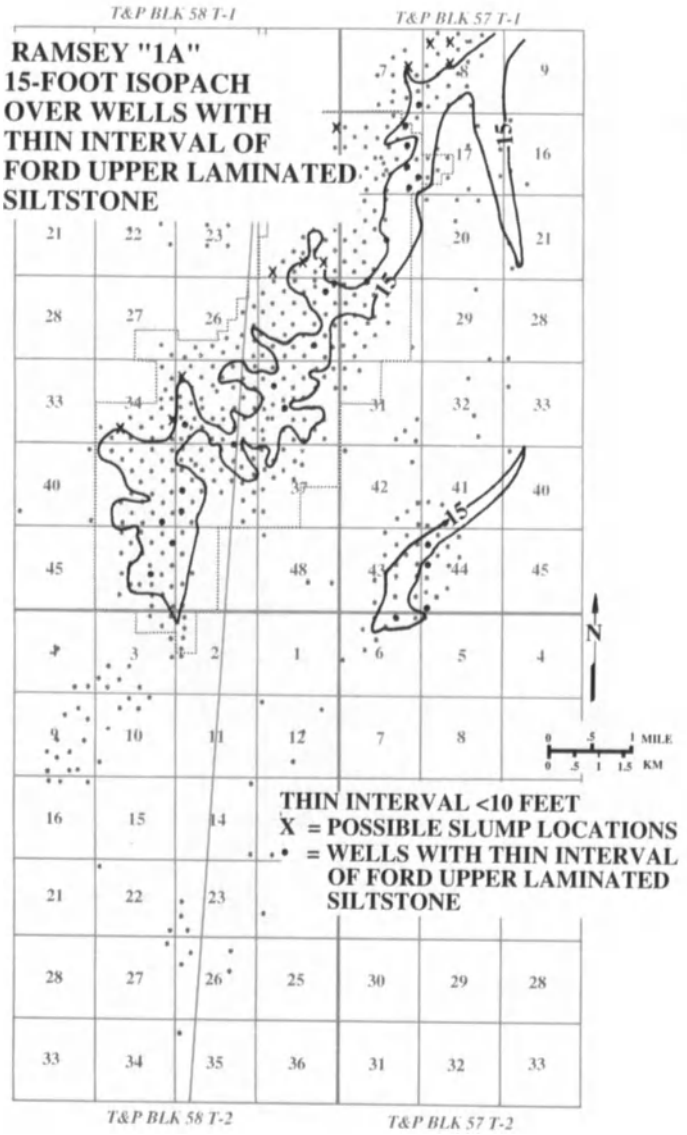

Figure 10.18. 15-foot isopach of the Ramsey 1A interval and anomalous thins in the underlying Ford laminated siltstone. The coincidence of the axis of 1A deposition and Ford thins is evidence of the erosive nature of the density currents. Erratic widening of the channel may be indicative of slumping of the channel margin.

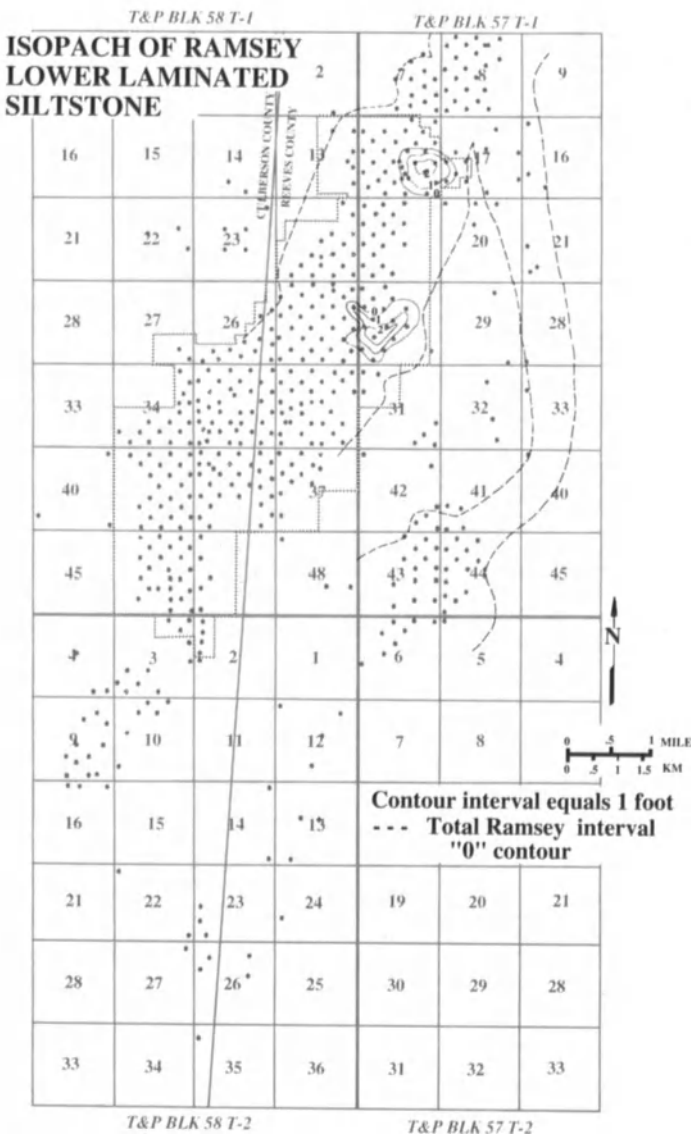

Figure 10.19. Isopach of the Ramsey lower laminated siltstone. Erosion by Ramsey 1B density flows may account for some of the limited extent of this interval.

m). This laminated siltstone unit is apparently truncated midway down the Ford-Geraldine field (Fig. 10.22) along a nearly north-south line. Adequate well control permitted excellent definition of this apparent thinning to the truncation line. The line also coincides with the pinch-out of the interval "2" sandstone.

An isopach of the Trap laminated siltstone which drapes interval "2" sands (see Fig. 10.27), reveals a thickening from its normal average of 15 ft (4.6 m) to an average of 18 ft (5.5 m) at the same apparent truncation line of the upper laminite and Ramsey 2 sandstone.

The Trap (15 ft, 4.6 m, average thickness) directly overlies the upper laminite (3 ft, 0.9 m, average thickness) at the Ramsey 2 truncation line, to result in a combined laminated siltstone interval of 18 ft (5.5 m). The Ramsey 2 sand does not "intervene" between the two laminite units down depositional dip of the truncation line, indicating a depositional pinchout of sandstone. Dip section X2-X2′ (Fig. 10.23) demonstrates the pinchout of the Ramsey 2 interval and the conformable contact of the two laminites. Strike section G-G′ (Fig. 10.10) shows this relation at the western pinchout of the interval "2" lobe. Where the two laminites are conformable, the Ramsey upper laminite cannot be discerned from the Trap laminite on well logs; however, a con-

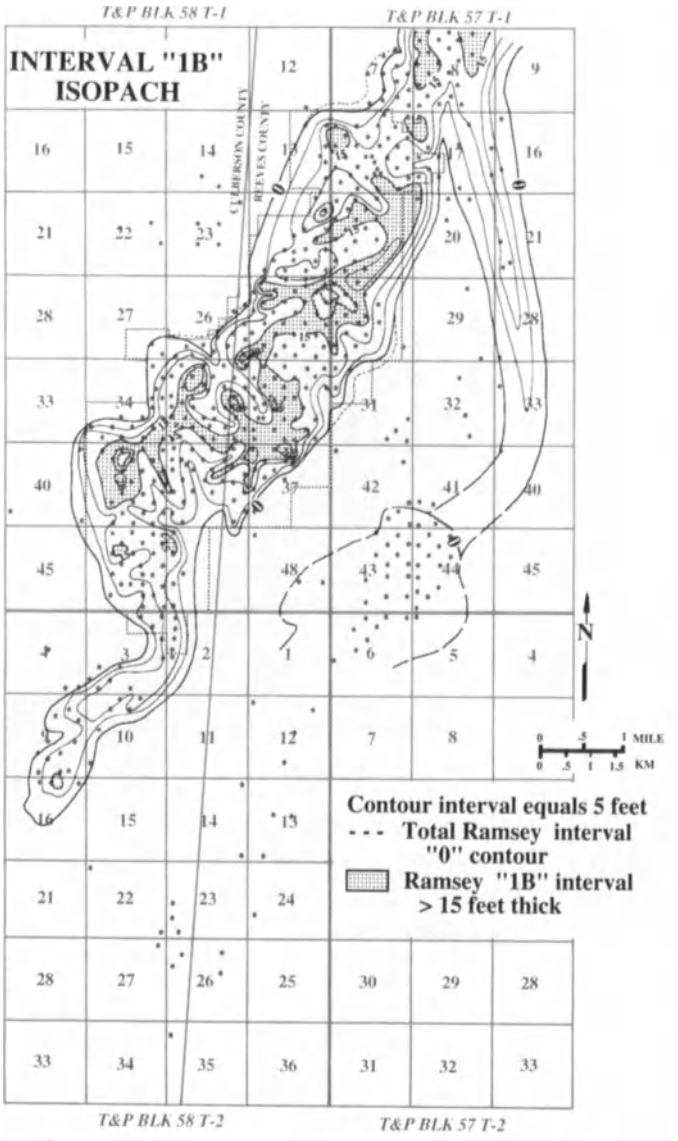

Figure 10.20. Isopach map of the Ramsey 1B sandstone. The sinuosity of the shaded portion of the map is probably a result of currents either having avoided topographic highs or having eroded deeply into previous deposits.

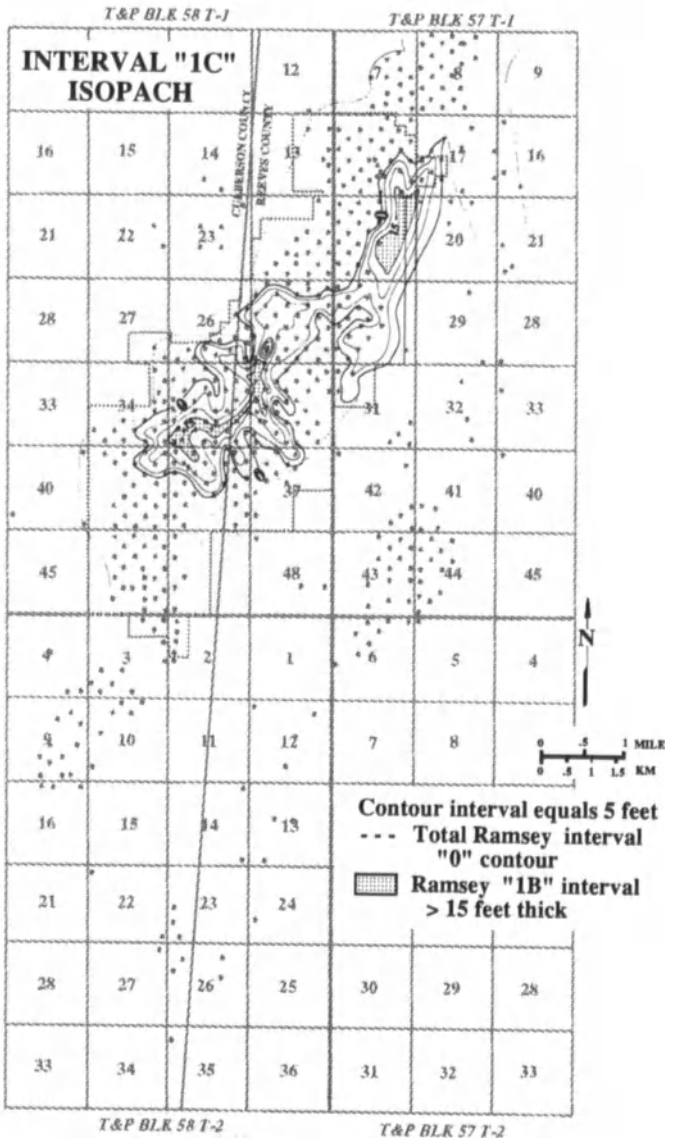

Figure 10.21. Isopach map of the Ramsey 1C sandstone. This interval has a limited distribution and may represent the first major imbricated or back-stepping episode.

tact determined by a zone of intense bioturbation (0.4 ft, 0.1 m, thick) can be marked in core (cores 202, 211, 161, and 7 #2; Fig. 10.4) approximately 3 ft (0.9 m) above the Ramsey-Trap contact. This top of the Ramsey upper laminite has similar, but less intense, burrowing where the Ramsey "2" sandstone unit overlies it. The degree of bioturbation is assumed to indicate the length of time the surface was at the sediment/water interface. Therefore, this zone is interpreted to be the surface of the fan just before and during interval "2" deposition.

As in the Ford-Geraldine channel, the upper laminite pinches out midway down the Sullivan-Screwbean channel (Fig. 10.22). Because of sparse well control in a narrow channel, the line is inferred. The upper laminite appears to be erosionally truncated by, or prior to, interval "2" deposition. The "1B" interval below the laminite is truncated at that line as well. Apparently, emplacement of the Ramsey 2 unit, primarily in this eastern channel, was a highly erosive event down channel, perhaps because of its chute-like geometry.

Ramsey 2

The "2" interval sandstone pinches out down-dip in the Ford-Geraldine and Sullivan-Screwbean channels (Fig.

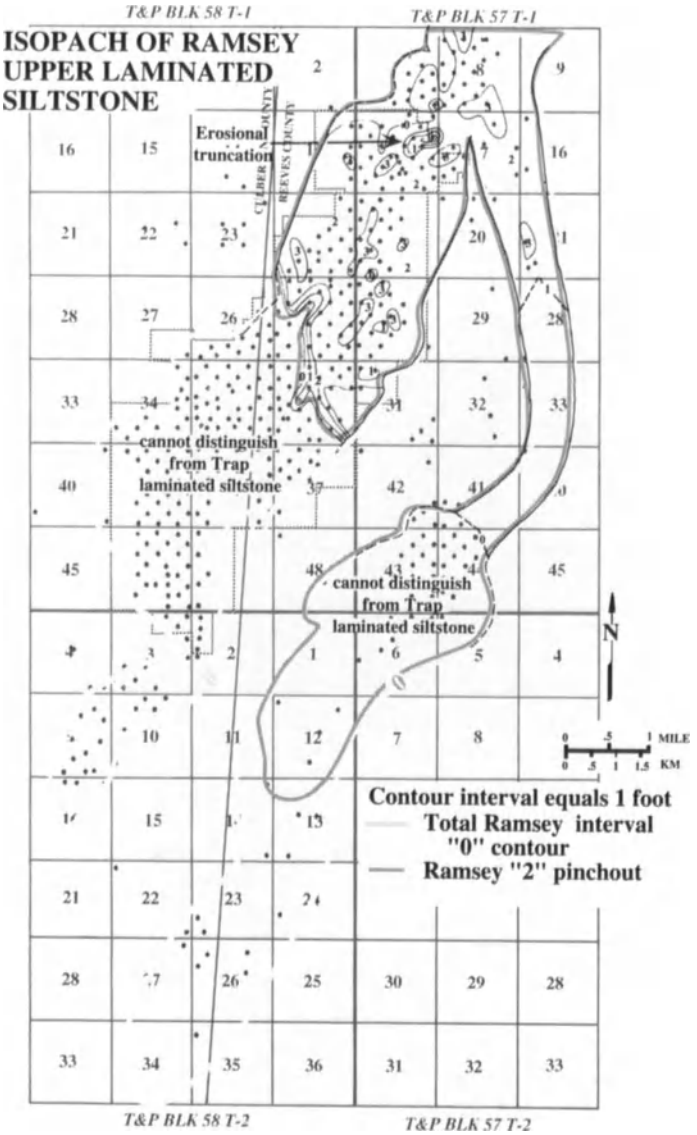

Figure 10.22. Isopach map of the Ramsey upper laminated siltstone. The zero isopach of this interval, shown in the middle of the field, represents the line at which the Ramsey 2 sand pinches out. Where sand is not present to separate the Ramsey upper laminated siltstone from the identical Trap laminated siltstone, the two siltstones are indistinguishable in log presentations.

10.24). The interval is thickest (25 ft; 7.6 m) at the head of the Sullivan-Screwbean and only 20 ft (6.1 m) in the Ford-Geraldine. In addition, the sandstone makes a more distant excursion basinward in the Sullivan-Screwbean. Apparently the eastern channel was the major locus of deposition for this interval.

Perhaps Ramsey 2 density flows met a more gentle channel gradient in the Ford-Geraldine because of the topographic expression of previous fill and found a steeper, more preferred gradient in the Sullivan-Screwbean. This hypothesis of channel switching is suggested by the zero ("0") isopach line of the "2" interval, as superimposed on a structure map of the pre-Trap surface (Fig. 10.25). The structure map represents a constructional or "compaction" anticline that plunges northeastward. The formation of a compaction anticline is summarized in Figure 10.26. The compaction anticline and its importance to the production history of the field are discussed later.

In the Ford-Geraldine, the zero ("O") isopach line of the Ramsey 2 unit closely mimics minor highs and lows on the pre-Trap surface, which must have existed at the time of deposition. The Ramsey 2 flows encountered a large, dam-like topographic high or ramp on the channel bottom, which was the expression of previously deposited and compacted sands. Minor crenulations or "gullies" in the north face of the ramp permitted more basinward excursions of sand. The net effect was that the ramp or compactional anticline dammed or ponded sand in the Ford-Geraldine channel. The bulk of later flows were diverted into the Sullivan-Screwbean channel.

The Ramsey 2 flows were not as erosive of laminite in the Ford-Geraldine as they may have been in the Sullivan-Screwbean channel. Areas of thinnest upper laminite (Fig. 10.22) are generally aligned along the axis of thickest Ramsey 2 sandstone, indicating local, minor erosion. For example, in T&P Block 57 T-1 section 18, the small area on the east line of the section, which encompasses thin or absent upper laminite, lies beneath the thalweg of the sandstones above. Natural communication of fluids between the Ramsey 2 and older reservoirs is limited to small areas like these.

Trap

The overall geometry of the Trap, like the Ford siltstone, is wedge-shaped, thinning basinward. The isopach averages of the Trap member (Fig. 10.27) indicate the depositional pinchout of Ramsey 2 sandstone in the Ford-Geraldine where the Trap laminite conformably overlies the Ramsey upper laminite, increasing from a 15-ft (4.6 m) average thickness to 18 ft (5.5 m) along the pinch-out. Inter-channel well control shows, on the average, an 18-ft-thick (5.5 m) laminite section. For example, the log of Ramsey 7 #2 (T&P Block 57 T-1, section 7, well #2; Fig. 10.4), which is just outside the western margin of the channel where Ramsey sand is absent, has 18 ft (5.5 m) of Trap laminated siltstone. Here, the Trap directly overlies the Ford laminated siltstone. The contact between the Ford and Trap in core is obvious and sharp, based on abrupt changes of color (organic content) and degree of bioturbation. Three feet (0.9 m) up-section from that contact is a zone of intense bioturbation, which correlates to the same interval at the

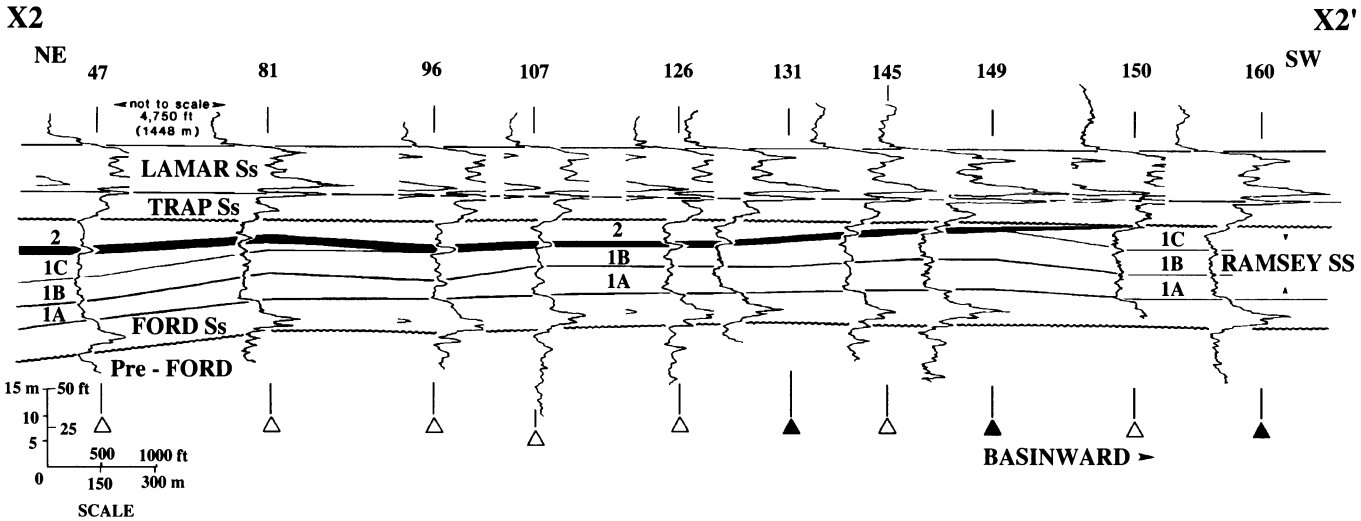

Figure 10.23. Dip cross section X2-X2′ demonstrates the pinchout of the Ramsey 2 sandstone and the conformable contact of the Ramsey upper laminated siltstone and the Trap laminated siltstone.

top of the Ramsey upper laminite in the channel. Therefore, the intra-channel thicknesses of laminated units are maintained outside the channel, indicating that laminite units evenly drape the channel-fill and inter-channel areas. The corollary to this conclusion is that there is no overbank deposition of finer fractions; otherwise, the thickness of laminated siltstone would be greater in interchannel areas.

Production History

The Ford-Geraldine field was discovered April 14, 1956, with the drilling of Chapman 1-18 (FGU 31) by Ford Chapman III. The well flowed 267 barrels of oil per day (BOPD) with a reservoir pressure of 1405 psi. The well site was located by linear extrapolation of net sandstone isopach maps and an apparent roll at the surface (Ford Chapman III, personal communication, 1982).

By late 1959, most of the field wells had been drilled (on a 20-acre spacing) and were producing. By mid-1958, just before production increased six-fold, the reservoir pressure must have decreased to near bubble point (1383 psi) because of a sharply rising gas/oil ratio and water production (Conoco, 1963). At this or lesser pressure, dissolved gases within the oil came out of solution, initially sustaining high rates of production. No attempt was made to maintain pressure early in the life of the field; the reservoir pressure dropped to between 300 and 500 psi by early 1968, reducing recovery efficiency. Cumulative primary production reached 13.2 million barrels of oil before unitization.

The field was unitized in November 1968, and secondary recovery (water injection) began in June 1969. After unitization, Conoco, having the largest interest in the 8,540 acre unit, became the operator. The reservoir pressure was brought back up to nearly 1400 psi for the waterflood. The field was divided into 5 stages (Fig. 10.28); Stage 5 was shut-in in March 1985. A pre-unitization engineering committee had determined that 110.4 million barrels of oil were originally in place in the field; this estimate was later revised to 93 million. By early 1975, the field attained a peak secondary recovery rate of 2,875 BOPD. By early 1981, that figure had dropped to 569 BOPD, or 6.79 million barrels cumulative production since unitization. Water cut had risen to 95% of production.

A continuous CO_2 flood was initiated in 1981 and was originally planned to be in two phases. Phase I began February 19, 1981; Phase II was to begin in 1986. Less CO_2 was injected than planned through December 1985, because regional pipelines were not completed; CO_2 supply to the project was a limiting factor. At that time, Phase 1 of the CO_2 flood was reduced to encompass the "Stage 2" area of the waterflood (Fig. 10.28), and a higher rate of injection (20 mmcf per day) was applied to the smaller area. In July 1987, the "Stage 1" area of the waterflood (Fig. 10.28) was activated with CO_2, and the north half of "Stage 3S" in April 1988. Expected production from the CO_2 flood (8.45 million barrels) and the results of primary, secondary, and tertiary (to December 1988) recovery are graphically summarized in Figure 10.29. Most of the preceding information is derived from a Conoco report (1979), an application for certification of the tertiary project (Conoco, 1981), and an update of data from Conoco in early 1989.

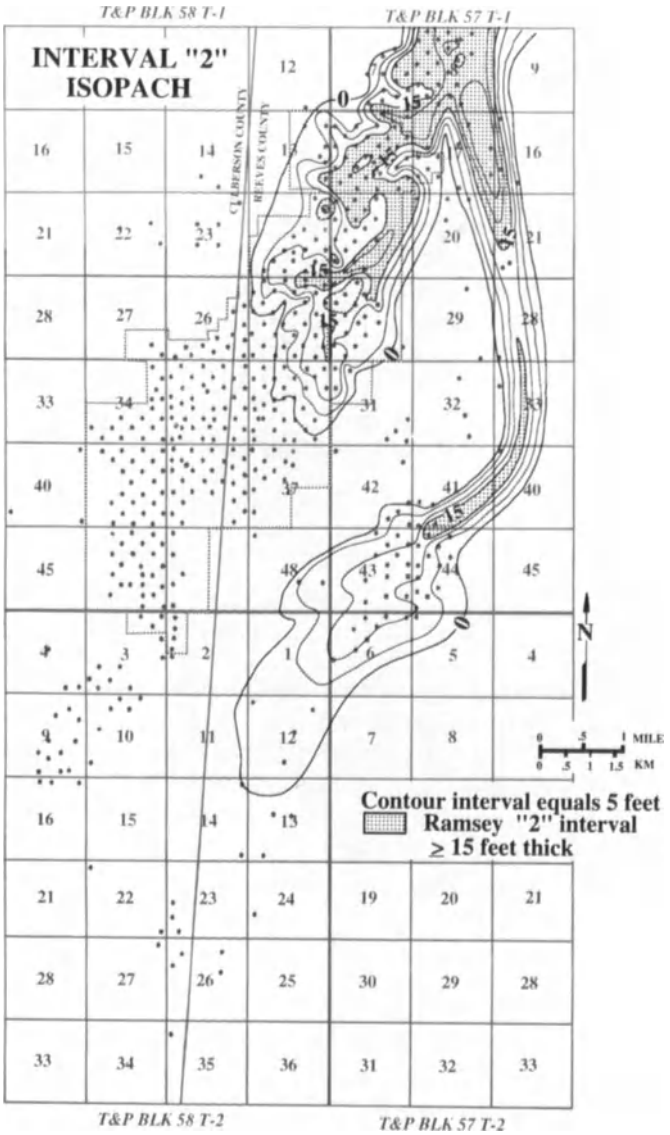

Figure 10.24. Isopach map of the Ramsey 2 sandstone demonstrating the pinchout mid-field. In the Sullivan-Screwbean channel, interval 2 was deposited more basinward than in Ford-Geraldine. The interval 2 sandstone probably encountered a compactional anticline composed of earlier progradational units that were naturally mounded, perhaps as deposits at the base of slope.

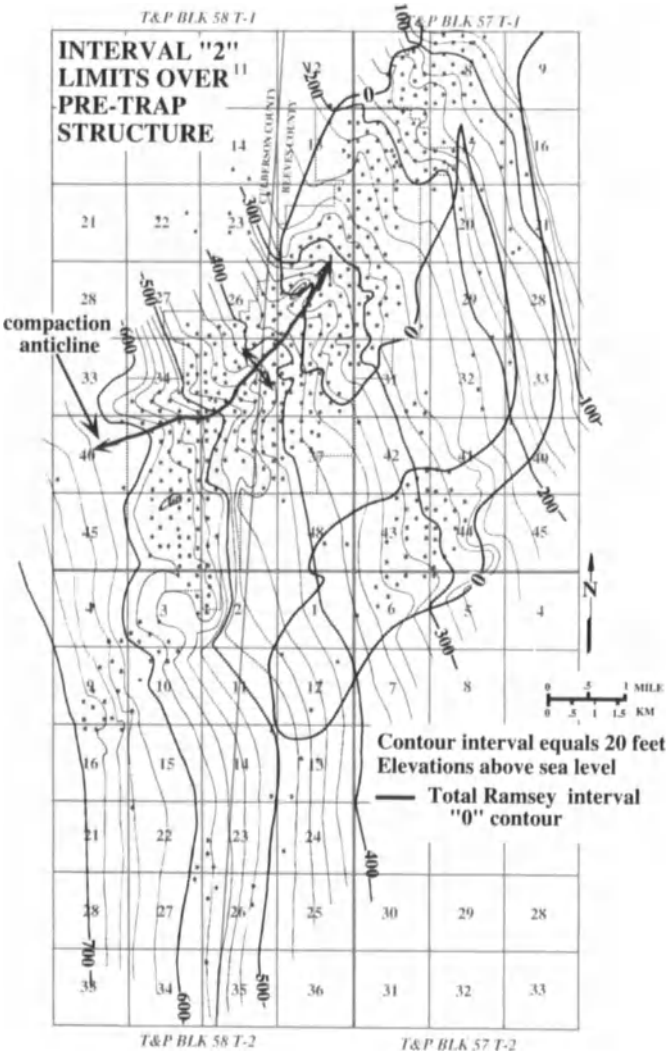

Figure 10.25. The zero isopach of the Ramsey 2 interval over pre-Trap structure. The compactional anticline is in the southern part of the field. Ramsey 2 density flows appear to have encountered a mound in the middle of the field and deposited onlapping sediment. The Sullivan-Screwbean channel served as a pressure-relief valve or splay for these blocked flows.

Primary Production

Figure 10.30 shows the results of primary production by pressure depletion (solution gas drive) superimposed on the structure map of the pre-Trap surface or top of the last sand. Production is divided into two areas separated by the largest erosional remnant. The NE-SW–trending area of maximum production falls along the crest of the compactional anticline; production figures decrease toward the flanks. Multiple oil-water contacts are encountered within the numerous subreservoirs at various elevations; there is no clear-cut, field-wide contact. Hydrocarbons are found from 160 ft (49 m) to more than 600 ft (183 m) above sea level. Like other Ramsey fields, the hydrocarbon column is larger than expected from capillary pressure calculations because of hydrodynamic banking (Berg 1975, Grauten 1965). Hydrodynamic banking is the extension of hydrocarbons down structural dip in a reservoir that has a dynamic water drive. Water at the tilted oil-water contact traps hydrocarbons farther down structural dip than would normally occur in a reservoir with a level oil-water contact.

The isolated area of primary production in the northern part of the field is the result of stratigraphic trapping against

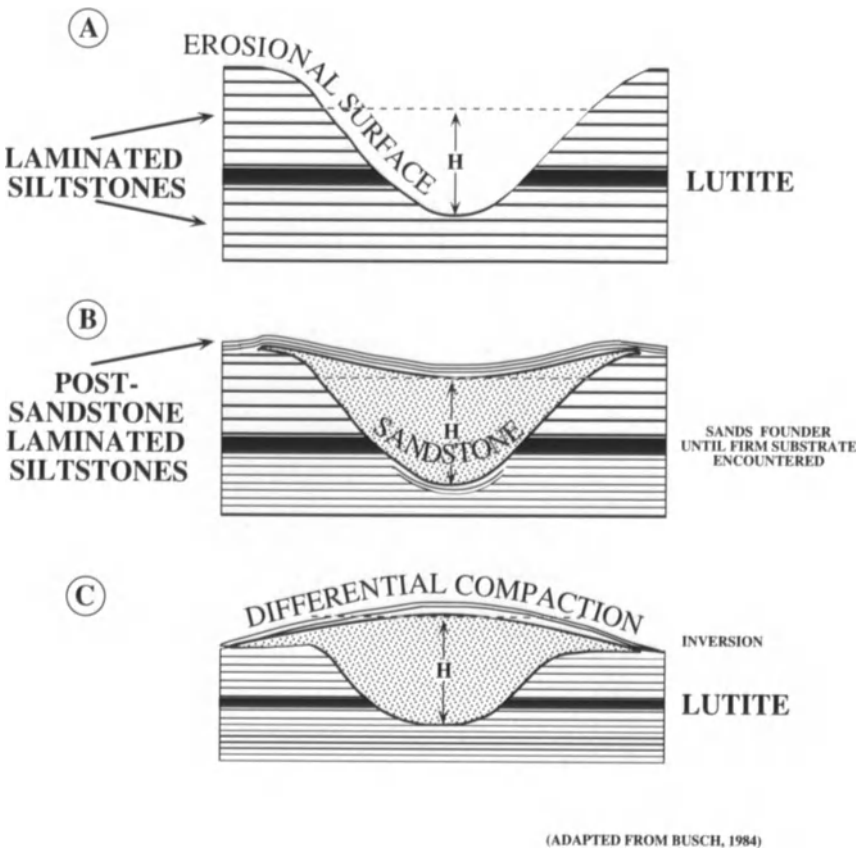

Figure 10.26. A possible mechanism for the formation of a compactional anticline (adapted from Busch, 1974).

the largest erosional remnant. In this region, hydrocarbons are trapped to the west by sandstone pinch-out into siltstone and to the south by pinch-outs against the erosional remnant (Fig. 10.6). To the east lies the main thickness of Ramsey sand, which is composed of more continuous units that wrap around the remnant and were possibly a path for hydrocarbons migrating toward the larger accumulation to the south. Apparently, this northern trap was filled to spill point. Hydrodynamic banking may have kept some of this accumulation from migrating up structural dip to the south.

As reservoir pressure dropped below bubble point, local gas caps developed, especially in up-dip areas like T&P Block 58 T-1, sections 39 and 46 (Conoco, 1963). The formation of gas caps further subdivided the already independent reservoirs, leaving pockets of oil in place.

Secondary Recovery

The Ford-Geraldine unit was created to more efficiently produce remaining reserves. A pressure-maintenance waterflood was chosen over an unpressured one for a more complete sweep of the reservoir. The field was computer modeled and then divided into five flood stages to be executed as in Figure 10.28. The results of the flood as of May 1978 are shown in Figure 10.31 superimposed over pre-Trap structure. Those wells indicated with a triangle or open circle were water injection wells, while those marked by a darkened circle or dot were problem wells that showed no increased oil production from water injection. The problem wells lie on the flanks of the compactional anticline, while those with increased or highest oil production lie more crestally or along the axis of the plunging nose. Areas of over 100,000 barrels production are on the most crestal portions of the structure at elevations from 400 to 600 ft (133 to 183 m) above sea level. Results of the flood were below expectations (Fig. 10.32).

The computer model (Conoco, 1969) applied to the reservoir did not account for permeability barriers parallel to bedding, which actually subdivide the reservoir. In addition, low injectivity to fresh and slightly saline water suggested the presence of fresh-water-sensitive authigenic clays. Continued injection of produced connate water (approximately 52,000 ppm chlorides) and Pecos River water probably damaged the formation and ultimately reduced production. By 1980, 8,400 barrels of water were being produced per day along with 569 barrels of oil, while 11,225 barrels of water were being injected daily. Over 64 million barrels of water were injected during the period from June 1969 to January 1981; 22 million barrels of water

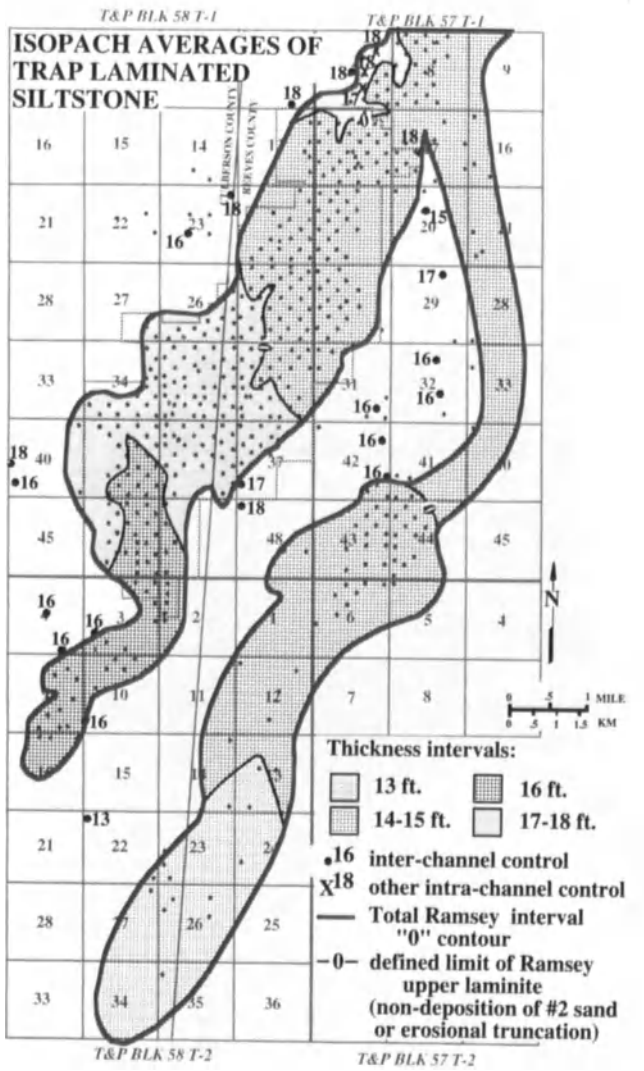

Figure 10.27. A smoothed or averaged isopach map of the Trap laminated siltstone. The Trap becomes three feet thicker basinward of a line coincident with the Ramsey 2 sandstone pinchout. The extra thickness is actually the upper laminated siltstone merging with the Trap where sand is not present to intervene.

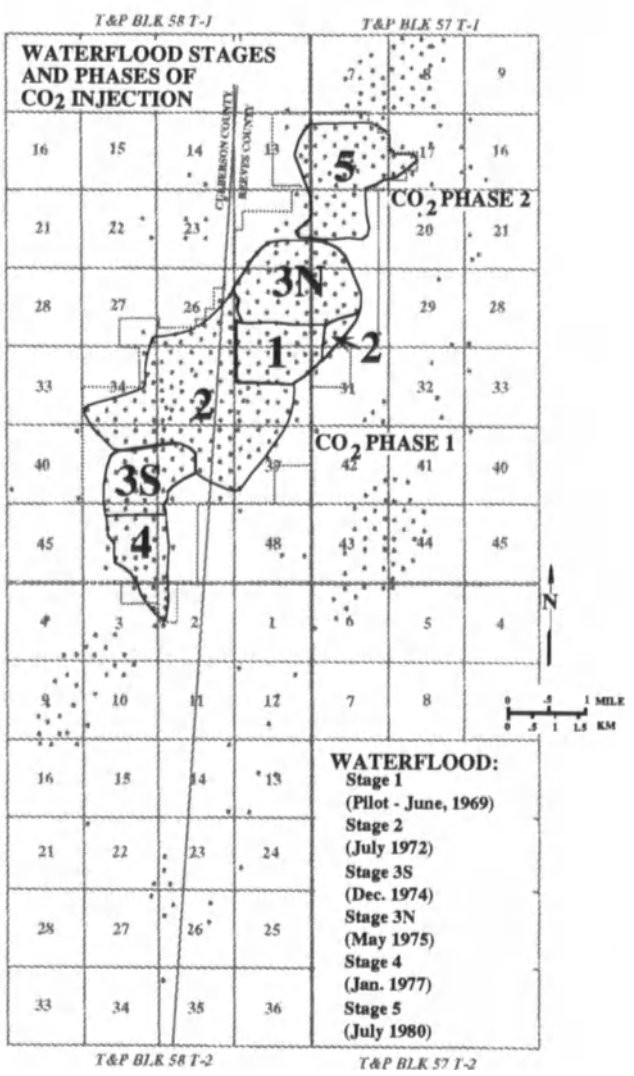

Figure 10.28. Five planned stages of the waterflood and the two phases of carbon dioxide injection.

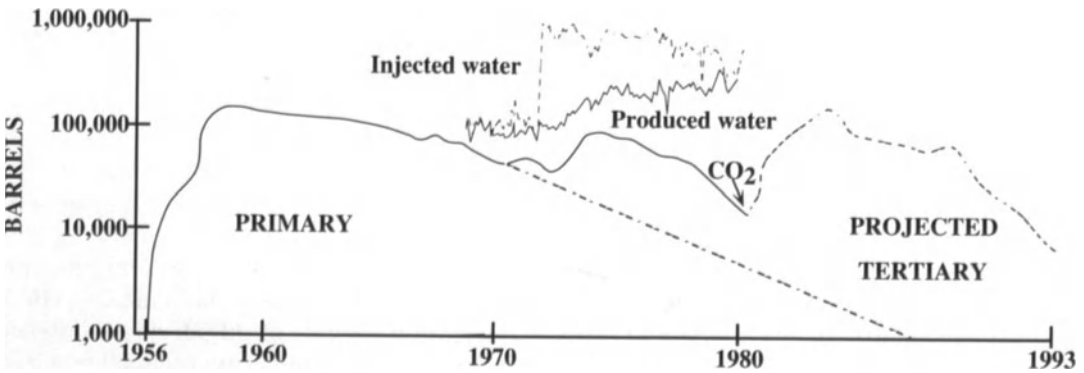

Figure 10.29. Production performance curves prior to commencing tertiary recovery (carbon dioxide injection) in 1981. Production from secondary recovery (waterflood) was declining rapidly.

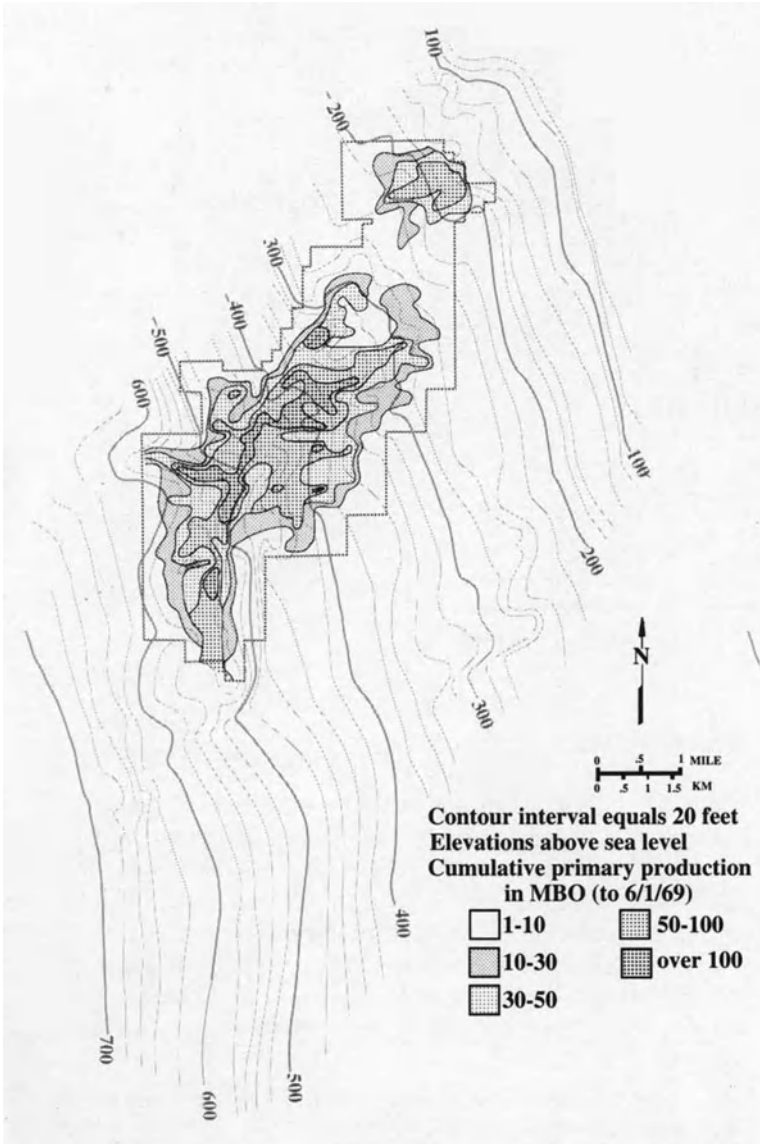

Figure 10.30. Total primary production and pre-Trap structure. The best primary production occurs along the crest of the compactional anticline in the southern half of the field. The northern pool is trapped against the largest topographic high.

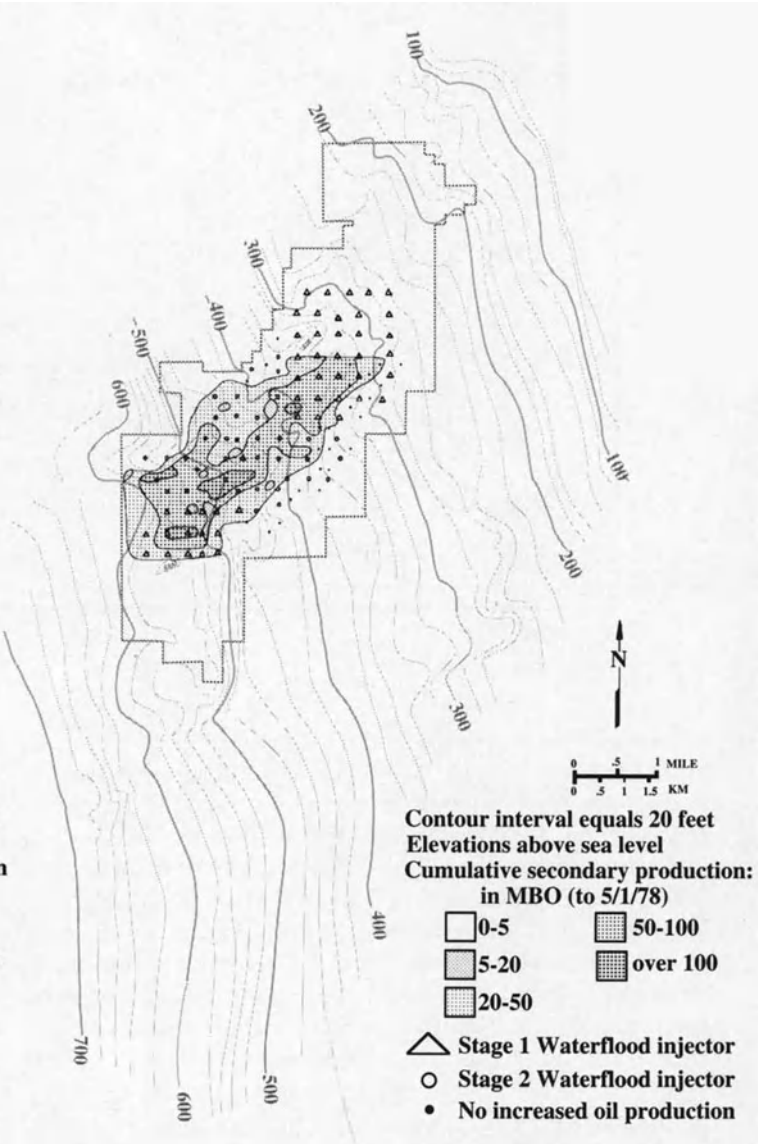

Figure 10.31. Total secondary production and pre-Trap structure. The best secondary production occurs along the crest of the compactional anticline in the southern half of the field along subtle structural features. "Problem" wells (black dots) with no increased oil production clearly are on the flanks of the compactional anticline.

and 6.8 million barrels of oil were produced in the same period. Production from the unit peaked in January 1975 at 2,875 BOPD.

Of the 6.8 million barrels (primary and secondary combined) produced since unitization, 3.5 million have been attributed to the waterflood; another 431,000 barrels are anticipated from the remainder of Stage V. The total falls short of the expected 6.8 million barrels for the flood alone (Fig. 10.32). After the waterflood, 21.5% of the original oil in place had been produced, leaving over 73 million barrels of oil behind.

Tertiary Recovery

A tertiary recovery project using continuous CO_2 injection was initiated in 1981 to increase production. Preliminary results (as of November 1981) of the project are superimposed on the pre-Trap structure map and pinch-out, or "O" isopach, of the Ramsey "2" unit (Fig. 10.33). The highest increase in barrels of oil per day occurs along the crest of the compaction anticline. Productive areas are apparently separated by the pinchout of the Ramsey "2" sand. This implies that the pinchout is trapping displaced oil.

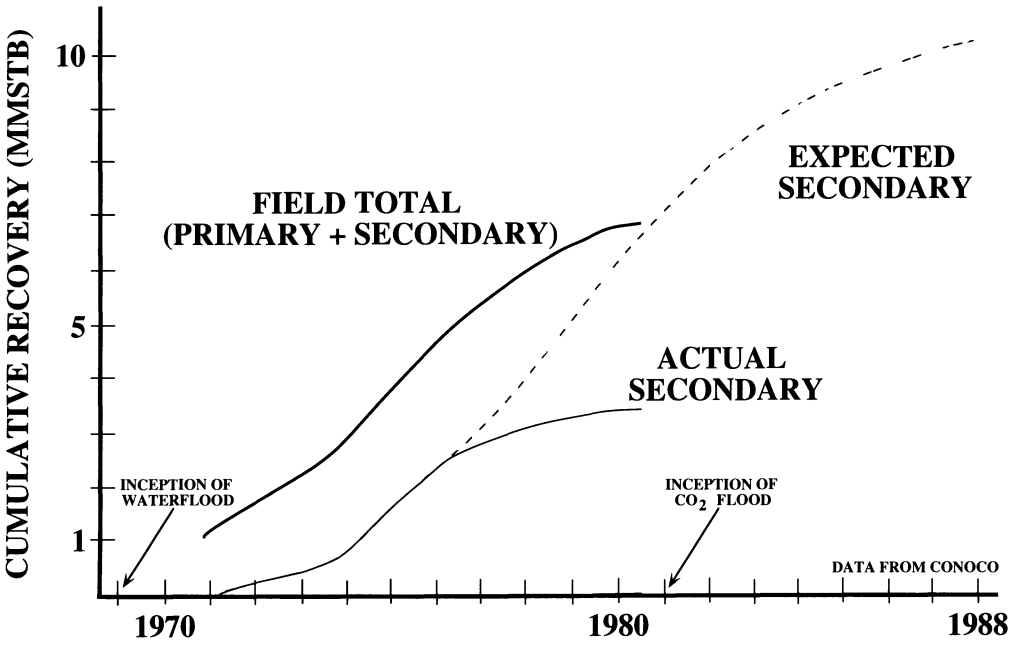

Figure 10.32. Secondary production performance. Results of the waterflood did not meet expectation.

A similar pattern developed during drawdown before the first CO_2 injection (Fig. 10.34). Water injection was discontinued; the reservoir pressure was 1400 psi. The reservoir was placed in a less dynamic state during this procedure, so that remaining pockets of production could be located.

Major difficulties with the project arose early. Carbon dioxide breakthrough (arrival of CO_2 at the production wells) was occurring too soon to sweep the reservoir efficiently. Figure 10.35 shows the percent breakthrough at each well. The highest CO_2 content was located within the crestal portion of the compaction anticline, which is to be expected. The CO_2 probably moved through the most permeable layers (which had already been depleted during primary production and swept by water during the secondary waterflood) and rose to the highest structural positions in the gas phase. CO_2 production was 30 percent of the injection rate at the end of 1988; four producers have been shut-in because of excessive CO_2 production. The results of the flood are summarized in the graph on Figure 10.36 and portrayed geographically in Figure 10.37.

The Ramsey is not a vertically homogeneous reservoir. Highly permeable units are laterally continuous, but are vertically separated from the rest of the reservoir by permeability barriers (either laminated siltstone or heavily calcite-cemented zones). The net effect is that they are like pipelines from the injection wells straight to the producing wells. The CO_2 may not sweep the less permeable oil-laden layers as planned. To remedy this situation, production rates have been reduced to retard CO_2 breakthrough and to maintain reservoir pressure above the minimum miscibility pressure of 900 psi.

Prediction and Expectations

The tertiary flood is expected to produce another 8.45 million barrels of oil, bringing the field total production to 31.7% of the original oil in place. The boundaries for the CO_2 flood stages should be derived from an understanding of the geometry or "plumbing" of the reservoir. Controlled by state regulation and influenced by competitive development, well-spotting should be sensitive to elements that affect production efficiency. These elements are discussed below:

(1) The Ramsey sandstone pinches out laterally and down depositional dip into densely calcite-cemented laminite (Fig. 10.6). This permeability barrier when combined with regional eastward dip, creates stratigraphic traps of all sizes along the western channel margin and at the channel terminus. The terminal portions of the fan-channel fill are the final, structurally highest traps and are prone to gas cap development. This distal facies covers a larger expanse than the proximal facies, but is often a lower quality reservoir. Usually, the thinner the sandstone, the more it is densely calcite cemented.

(2) The best production is along the axis of the northeast-plunging nose of the compaction anticline. The hydrocarbon column is extended by hydrodynamic banking. The eastern, northern, and western flanks are at higher water saturations. Attempts to sweep oil from these wet zones with CO_2 will probably be futile. Efforts should be concentrated on the area enclosed by the >35-ft (>10.7 m) total Ramsey isopach and south of the Ramsey "2" interval "0" isopach. Other pockets of potential production are along

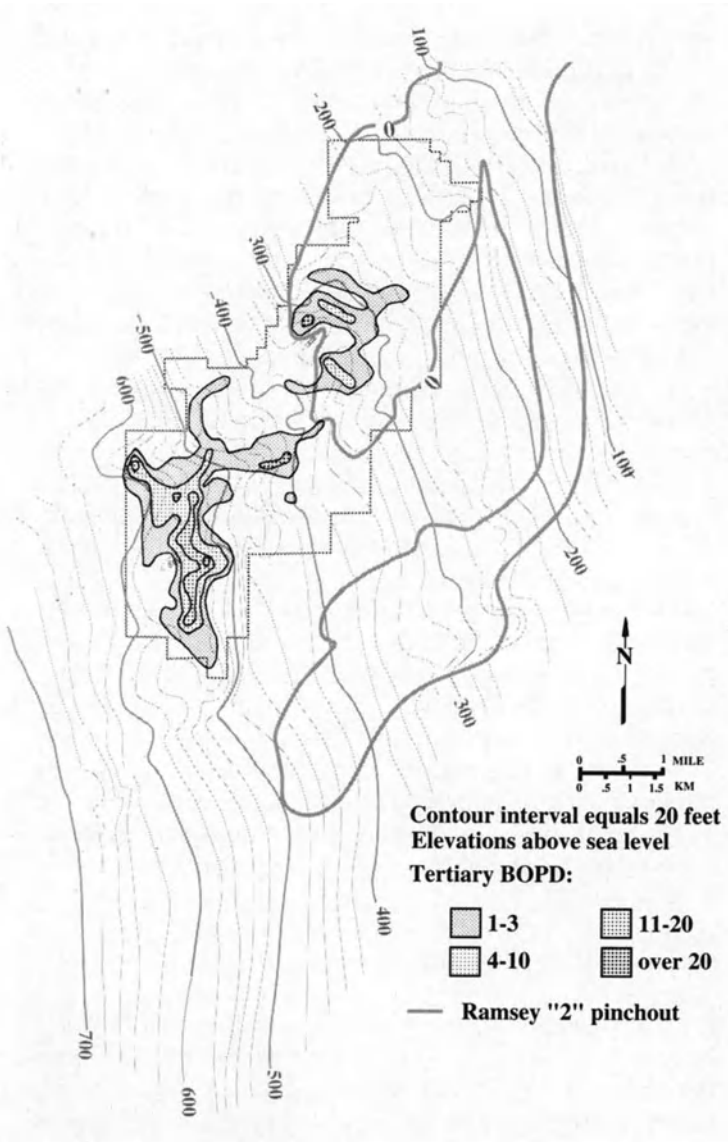

Figure 10.33. Early tertiary production performance. The best production occurred in the southern half of the field in the compactional anticline. A northern pool appears to be segregated by the pinchout of the interval 2 sandstone.

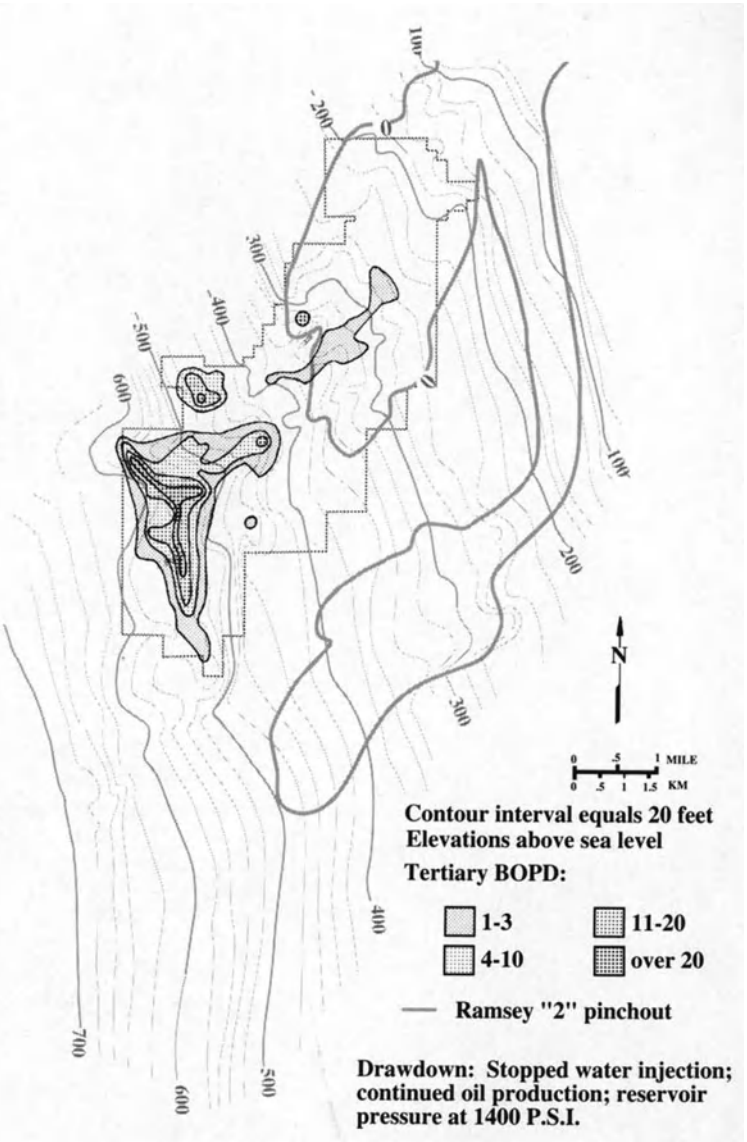

Figure 10.34. Production performance during drawdown. In a less dynamic state, pockets of highest production potential become evident. Again, the segregation of an area to the north of the main compactional anticline appears to be caused by a stratigraphic trap at the interval 2 sandstone pinchout.

the western and southern margins where small stratigraphic traps exist. Waterflood opportunities may exist within non-unitized portions of the channel south of the Ford-Geraldine field.

(3) The pinch-out of the Ramsey 2 interval at the conformable contact of Ramsey upper laminite and Trap laminite makes that sandstone an independent stratigraphic trap (Fig. 10.23). Ramsey production in this area is best along the main depositional axis south of the large erosional remnant. An injection program contained within the Ramsey 2 interval and designed to sweep the area south of the remnant (banking oil at the pinch-out) should prove successful. The results of a pilot CO_2 injection project in another Ramsey reservoir, Twofreds field, indicates an analogous "laminated shale and sand" permeability barrier within the field, which creates two reservoirs (Kumar et al., 1980). Apparently, an upper sandstone unit, like the Ramsey 2 interval in the Ford-Geraldine, pinches out midway in the field. Increased oil production (from 27 to 700 BPOD) was achieved in the upper sandstone. A conformable contact of two laminite units apparently forms the independent stratigraphic trap.

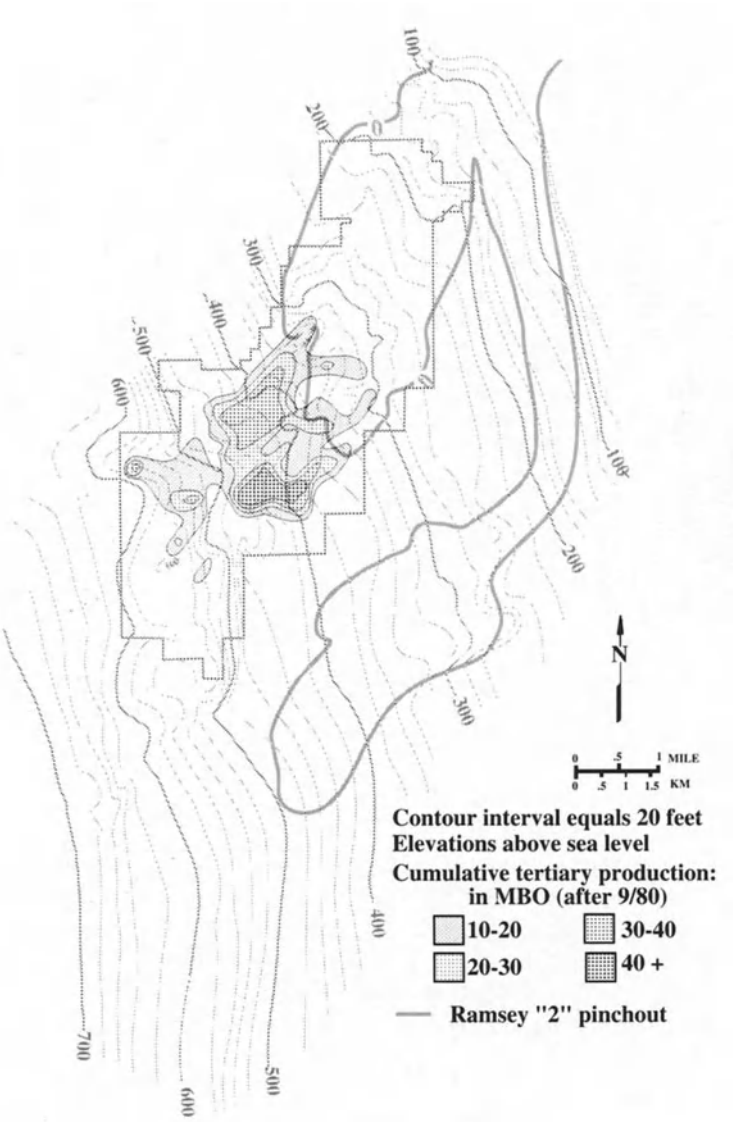

Figure 10.35 Percent injected carbon dioxide breakthrough. As carbon dioxide arrives at a producing well updip of an injection well, a strong increase in oil production should be evident. In an ideal case, the gas has thoroughly swept the reservoir and created a bank of oil ahead of it. Arrival of gas too early signals problems.

(4) Separate stratigraphic traps occur along the northern flank of the large, southeast-trending erosional remnant in the T&P Block 57 T-1 sections 18 and 19 (Fig. 10.6) where sandstone pinches out on the high. Primary production history (Fig. 10.30) substantiates trapping along the northern flank. This area should be treated differently from the other flood areas. Emphasis should be placed on the Ramsey 1A and 2 intervals. Erosional remnants like those in the Ford-Geraldine field are present in other Ramsey fields (e.g., E1 Mar field).

(5) Minor laminite intervals subdivide the Ramsey into smaller reservoirs. The Ramsey lower laminite is more locally distributed than the upper laminite, but acts just as effectively as a permeability barrier. Likewise, thin lutites at the tops of some units subdivide the sandstone section.

(6) Usually occurring within 2 ft (0.6 m) of a contact with laminated siltstone, densely calcite-cemented zones horizontally subdivide sandstone intervals into more complex production units. These calcite-cemented zones are correlative between wells, indicating lateral continuity. Locating exact points of CO_2 injection into the vertical sandstone section is critical to modeling the flow path of the gas.

(7) The type of depositional facies governs porosity/permeability trends. The tendency is for the main axis of each flow to have greater permeability than at the flow margin; this may be due to more abundant cross bedding in the channel axis. This factor may be important for setting different rates of CO_2 injection for wells along a row of injectors that crosses a channel axis.

(8) Porosity and permeability are chiefly reduced by diagenetic events like compaction and cement development. Pore-filling calcite and pore-lining chlorite and illite-smectite significantly reduce permeability. Local, dense cement growth can subcompartmentalize the reservoir. In addition, water-sensitive clays can swell to plug pore throats if too fresh an injection water is chosen. During acid injection (perhaps to dissolve calcite cement), iron-rich chlorite can be altered into a pore-plugging gel.

Summary of Conclusions

(1) The submarine fan channel, which funneled bottom-hugging hypersaline density currents 100 mi (161 km) from the shelf into the central depths of the Delaware basin, trends southwestard from breaches in the Guadalupian shelf margin. In the northern extremity of the study area, the channel bifurcates into the Ford-Geraldine and Sullivan-Screwbean channels. Cross-sectional area of the channel was conserved; the channel became deeper where narrower and more shallow where broader.

(2) Distribution of the Ramsey sandstone was confined to the channel that was eroded before Olds and again before Ford deposition; there was no overbank deposition. The path of the sheet-like density flows (liquefied flows; Lowe, 1975, 1976, 1979, 1982; Lowe and LoPiccolo, 1974) was diverted around paleotopographic highs or erosional remnants left from the scour phase. During each episode of deposition, sand was emplaced first at channel margins and then at the channel center. After partial filling of the scour, the channel fill became topographically positive (convex up) as a result of compaction and dewatering. Subsequent flows pinched out against the resultant compactional anticline. Back-stacking occurred until a steeper gradient was

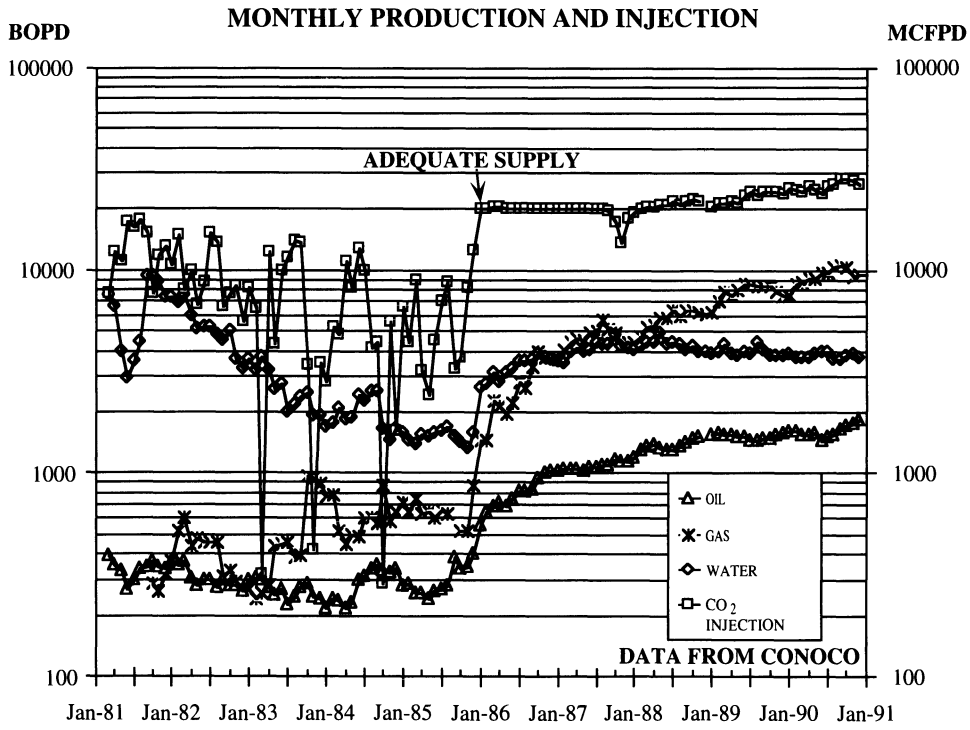

Figure 10.36 Tertiary production performance curves. With an adequate supply of carbon dioxide (on line by January 1986), field production is increasing but still quite below earlier projections.

found in the Sullivan-Screwbean channel, making it the most likely flow path. In this manner, the channels alternated depositional activity.

(3) Sandstone depositional patterns are a combination of erosion, non-deposition on highs, and deposition within the channel. Laminite and lutite are more laterally extensive and drape pre-existing topography evenly.

(4) The Ford-Geraldine field is a combination structural-stratigraphic-hydrodynamic trap with multiple oil/water contacts. Regional tilting to the east caused oil to migrate to the structurally higher "toes" of the fan channels. The main producing structure is a compactional or constructional anticline, with maximum production along the axial crest. A separate stratigraphic trap exists in the northern part of the field where sands pinch out against the largest erosional remnant. Fresher water is naturally introduced into the reservoir in the southern portion of the field, as indicated by a pre-flood chlorinity gradient. Hydrodynamic banking can explain the extended hydrocarbon column, the development of structurally deeper stratigraphic traps than those in the main producing area, and the water-wet limbs of the compaction anticline.

(5) Primary and secondary phases of production had similar recovery patterns. The first results of the CO_2 flood indicate the effect of the Ramsey "2" pinch-out midway down the field, and that the "2" sandstone should be dealt with separately from the rest of the flood.

(6) Incorporating a detailed geological model into development plans is essential to the success of any project. Clastic reservoirs should not be modeled as homogeneous sand. The gross reservoir is subdivided and complicated by abrupt porosity/permeability changes in the sandstone, intervening laminated siltstone, densely calcite-cemented zones, pinch-outs against erosional remnants, unconformities, hydrodynamic banking, multiple oil/water contacts, and subtle structural relief.

References

Berg, R.R., 1975, Capillary pressures in stratigraphic traps: AAPG Bulletin, v. 59, p. 939–956.

———, 1979, Reservoir sandstones of the Delaware Mountain Group, southeast New Mexico, *in* Sullivan, N.M., ed., Guadalupian Delaware Mountain Group of west Texas and southeast New Mexico, 1979, Symposium and Field Conference Guidebook: SEPM (Permian Basin Sec.) Pub. 79–18, p. 75–95.

Bouma, A.H., 1962, Sedimentology of some flysch deposits: Amsterdam, Elsevier, 168 p.

Bouma, A.H., Stelting, C.E., and Coleman, J.M., 1983/1984, Mississippi Fan: Internal structure and depositional processes: Geo-Marine Letters, v. 3, p. 147–153.

Bozanich, R.G., 1978, The Bell Canyon and Cherry Canyon Formations, southern Delware Basin [M.A. thesis]: Austin, University of Texas, 165 p.

———, 1979, The Bell Canyon and Cherry Canyon Formations, eastern Delaware Basin, Texas: Lithology, environments and mechanisms of deposition, *in* Sullivan, N.M., ed., Guadalupian Delaware Mountain Group of west Texas and southeast New Mexico, 1979, Symposium and

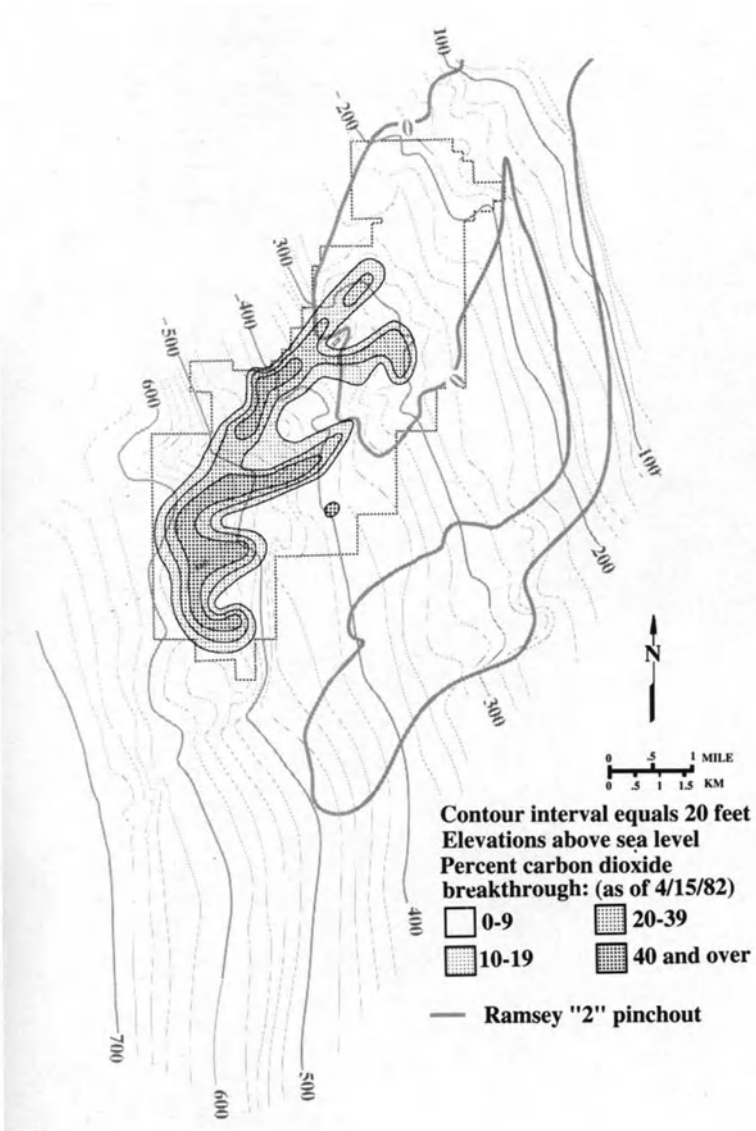

Figure 10.37. Map of cumulative tertiary production over pre-Trap structure. The best production appears to be on the southeast flank of the compaction anticline.

Field Conference Guidebook: SEPM (Permian Basin Sec.) Pub. 79-18, p. 121–141.

Busch, D.A., 1974, Stratigraphic traps in sandstones—exploration techniques: AAPG Memoir 21, 174 p.

Conoco, 1963, Ford-Geraldine field, secondary recovery and unitization study: Report to partners, 17 p.

———, 1969, Waterflood pattern and development plan, Ford-Geraldine (Delaware Sand) unit: Internal Report, 11 p.

———, 1979, Ford-Geraldine field, tertiary project: Geological study: Internal Report, 8 p.

———, 1981, Application for jurisdictional certification as a qualified tertiary oil recovery project, Ford-Geraldine unit: Presented to Railroad Commission of Texas, Oil and Gas Division, docket number 8-76377, 12 exhibits.

———, 1989, Ford Geraldine Unit CO_2 Flood: Internal documents.

Damuth, J.E., and Flood, R.D., 1983/1984, Morphology, sedimentation processes, and growth pattern of the Amazon deep-sea fan: Geo-Marine Letters, v. 3, p. 109–117.

Fischer, A.G., and Sarnthein, M., 1988, Airborne silts and dune-derived sands in the Permian of the Delaware Basin: Jour. Sed. Petrology, v. 58, p. 637–643.

Grauten, W.F., 1965, Fluid relationships in Delaware Mountain sandstone, in Young, A., and Galley, J.E., eds., Fluids in subsurface environments: AAPG Mem. 4, p. 294–307.

Habicht, J.K.A., 1979, Paleoclimate, paleomagnetism, and continental drift: AAPG Studies in Geology No. 9, 30 p.

Harms, J.C., 1968, Permian deep-water sedimentation by nonturbid currents, Guadalupe Mountains, Texas: Ged. Soc. Am. Spec. Paper 121, 127 p.

———, 1974, Brushy Canyon Formation, Texas: A deep-water density current deposit: Geol. Soc. Am. Bull., v. 85, p. 1763–1784.

Harms, J.C., and C.R., Williamson, 1988, Deep-water density current deposits of Delaware Mountain Group (Permian), Delaware Basin, Texas and New Mexico: AAPG Bulletin, v. 72, p. 299–317.

Hills, J.M., 1984, Sedimentation, tectonism and hydrocarbon generation in Delaware Basin, West Texas and southeastern New Mexico: AAPG Bulletin, v. 68, p. 250–267.

Hiss, W.L., 1975, Stratigraphy and groundwater hydrology of the Capitan aquifer, southeastern New Mexico and western Texas [Ph.D. dissertation]: Boulder, University of Colorado, 396 p.

Jacka, A.D., Beck, R.H., St. Germain, L.C., and Harrison, S.C., 1968, Permian deep-sea fans of the Delaware Mountain Group (Guadalupian), Delaware Basin: *in* Guadalupian facies, Apache Mountains area, west Texas: SEPM (Permian Basin Section) Pub. 68–11, p. 49–90.

Kastens, K.A., and Shor, A.N., 1985, Depositional processes of a meandering channel on Mississippi fan: AAPG Bulletin. v. 69. p 190–202.

King, P.B., 1942, Permian of west Texas and southeastem New Mexico: AAPG Bulletin, v. 26, p. 535–763.

Kumar, R.M., Watson, J.A., and Goodrich, J.H., 1980, CO_2 field injection project conducted by HNG Fossil Fuels Twofreds Field, west Texas: in Target reservoirs for CO_2 miscible flooding—final report: Dept. of Energy report MC 08341-17, v. 2, p. 120–136.

Lowe, D.R., 1975, Water-escape structurcs in coarse-grained sediments: Soc. Econ. Paleontologists and Mineralogists, v. 22, p. 157–204.

———, 1976, Subaqueous liquefied and fluidized sediment flows and their deposits: Sedimentology, v. 23, p. 253–308.

———, 1979, Sediment gravity flows: Their classification and some problems of application to natural flows and deposits: SEPM Special Pub. No. 27, p. 75–82.

———, 1982, Sediment gravity flows: II. Depositional models, with special reference to the deposits of high-density turbidity currents: Jour. Sed. Petrology, v. 52, p. 279–297.

———, and LoPiccolo, R.D., 1974, The characteristics and origins of dish and pillar structures: Jour. Sed. Petrology, v. 44, p. 484–501.

McDermott, R.W., 1984, Depositional processes and environments of the Permian sandstone tongue of the Cherry Canyon Formation and the upper San Andres Formation, Last Chance Canyon, southeastern New Mexico [M. A. thesis]: Austin, University of Texas, 179 p.

McGrail, D.W., and Carnes, N., 1983, Shelfedge dynarnics and the nepheloid layer in the northwestem Gulf of Mexico: SEPM Special Pub. No. 33, p. 251–264.

Meissner, F.F., 1972, Cyclic sedimentation in Middle Permian strata of the Permian basin, west Texas and New Mexico, *in* Cyclic sedimentation in the Permian basin, 2d ed.: West Texas Geol. Soc., p. 203–232.

Payne, M.W., 1973, Basinal sandstone facies of the Delaware Mountain Group, west Texas and southeast New Mexico [Ph.D. dissertation]: College Station, Texas A & M University, 150 p.

———, 1976, Basinal sandstone facies, Delaware basin, west Texas and southeast New Mexico: AAPG Bulletin, v. 60, p. 517–527.

Pray, L.C., 1977, The all wet constant sea level hypothesis of upper Guadalupian shelf and shelf edge strata, Guadalupe Mountains, New Mexico and Texas, *in* Upper Guadalupian facies: Permian reef complex; Guadalupe Mountains, New Mexico and west Texas: SEPM (Permian Basin Sec.) Pub. 77-16, p. 433.

Ruggiero, R.W., 1985, Depositional history and performance of a Bell Canyon sandstone reservoir, Ford-Geraldine field. west Texas [M.A. thesis]: Austin, University of Texas, 242 p.

Sarg, J.F., Rossen, C., Lehmann, P.J., and Pray, L.C., 1988, Geologic guide to the western escarpment, Guadalupe Mountains, Texas: SEPM (Permian Basin Sec.) Pub. 88-30, p. 60.

Silver, B.A., and Todd, R.G., 1969, Permian cyclic strata, northern Midland and Delaware Basins, west Texas and southeastern New Mexico: Am. Assoc. Pet. Geol. Bull., v. 53, p. 2223–2251.

Watson., W.G., 1974, Inhomogeneities of the Ramsey Member of the Bell Canyon Formation, Geraldine Ford Field, Culberson and Reeves Counties, Texas [M.A. thesis] University of Texas at Arlington, 122 p.

Weinmeister, M.P., 1978, Origin of upper Bell Canyon reservoir sandstones (Guadalupian), El Mar and Paduca fields, southeast New Mexico and west Texas [M.S. thesis]: College Station, Texas A & M University, 96 p.

Williamson, C.R., 1978, Depositional processes, diagenesis and reservoir properties of Permian deep sea sandstones, Bell Canyon Formation, Texas-New Mexico: Texas Petroleum Research Committee, Rept. No. UT 78-2, 261 p.

———, 1979, Deep sea sedimentation and stratigraphic traps, Bell Canyon Formation (Permian), Delaware basin, *in* Sullivan, N.M., ed., Guadalupian Delaware Mountain Group of west Texas and southeast New Mexico, 1979, Symposium and Field Conference Guidebook: SEPM (Permian Basin Soc.), Pub. 79-18, p. 39–74.

CHAPTER 11

Reservoir Character of Deep Marine Sandstones, Inglewood Field, Los Angeles Basin

June Gidman, Will J. Schweller, Chris W. Grant, and Alan A. Reed

Introduction

The Inglewood Field is located in the western Los Angeles Basin, southern California, about 8 mi (12.8 km) southwest of downtown Los Angeles (Fig. 11.1). It was discovered in 1924 by the Standard Oil Company of California, and was completed in the Pliocene Vickers zone. Subsequently, seven additional productive zones have been discovered and are producing in the field.

Oil accumulated in an anticlinal structure that lies along and is cut by the Newport-Inglewood fault (Fig. 11.2). This major strike-slip fault divides the field into eastern and western pools. Field estimates of original oil in place range from 800 to 1,000 million barrels. Production peaked in 1925 at 50,300 barrels per day and has diminished to the current rate of 7,750. Cumulative production is 325 million barrels, or 32.5% to 40.6% of the estimated oil in place.

The Vickers East Pool is the subject of this publication. Oil in the Vickers zone is heavy, with an API gravity of 18° and a viscosity of 65 centipoise at 100°F. The Vickers East Pool had an original oil-in-place estimate of 152 million barrels, and to date, 46.5 million (30.6%) have been recovered. Ultimate recovery is estimated to be 53.6 million barrels (35% of the oil in place). Current production is 1,500 barrels per day, with an oil/water ratio of 1:22. Water is being injected at a rate of 27,000 barrels per day.

A pilot waterflood was tested in the Vickers East Pool in 1954. The pool underwent widespread waterflooding in 1957, but no consistent fieldwide injection pattern was established. Peak production fell far short of expectations (4,000 barrels per day in 1964, compared with 8,000 predicted).

In 1985, a major waterflood realignment was initiated to improve the areal and vertical sweep efficiencies. The existing waterflood was poorly understood. Vertical sweep was poor in most injectors, and some had no water communication with the producers. Several thief zones caused water cycling and, ultimately, sand production and casing failure. Some reservoir zones would not accept water even at greater than fracture pressure, and the reliability of the porosity logs and the distribution of permeability were unknown.

A core study was planned to provide geological support to the waterflood realignment. Almost the entire Vickers zone was cored in the BC-403 well. Care was taken to ensure good core recovery. Over a period of 10 days, 1414 ft (431 m) of section were cored, with a recovery of 94%. Special wellsite-handling techniques were devised to maintain the integrity of the core without freezing it. This involved filling the annular space between the core barrel liner and the core with an isocyanate polyol resin (Gidman et al., 1987).

The core study focused on the BC-403 core and on six wells in its vicinity (Fig. 11.3). The core data were analyzed within the framework of the regional geology and our understanding of the field as a whole. The study was aimed at constructing a detailed picture of the depositional environment, describing the geometry of the Vickers zone sandstone bodies, and characterizing their vertical and horizontal continuity. It was also aimed at developing a quantitative correlation between measured permeability and porosity and log response.

Geologic Setting

The Inglewood Field is one of several major oil fields that occur along the northwest-trending Newport-Inglewood

Fault in the Los Angeles Basin (Fig. 11.1). The reservoir rocks in the basin are a thick series of deep-marine sandstones deposited during the period of rapid subsidence, which began in the late Miocene. Subsidence and deposition in the Inglewood portion of the Los Angeles Basin continued through the Pliocene. At the same time, some parts of the Miocene basin floor, such as the Palos Verdes area, began to rise and became bathymetric highs that helped to restrict the remaining parts of the basin. The combination of rapid subsidence of the basin floor and rising structural blocks around the basin perimeter allowed the accumulation of more than 19,000 ft (5800 m) of clastic sediments in the central trough of the Los Angeles Basin (Ingle, 1980).

The Inglewood Field occupies the crest of an elongate anticline on the northern part of the Newport-Inglewood Fault, a right-lateral strike-slip fault (Fig. 11.2). Production occurs on both sides of the fault, but the fault acts as a barrier to fluid flow in the field. Numerous secondary faults trend subparallel to the main fault and complicate the geometry of the reservoirs.

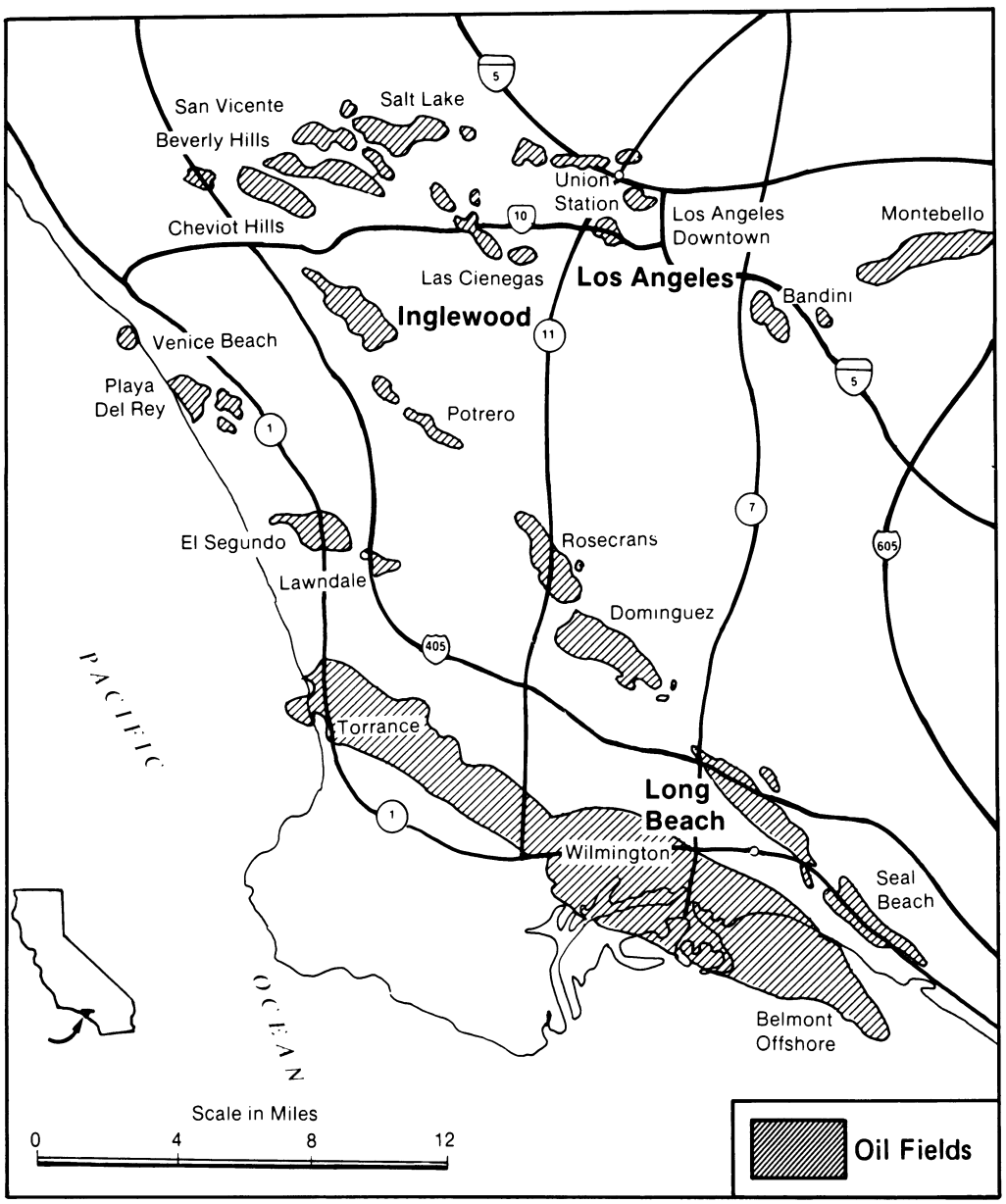

Figure 11.1. Location map showing Inglewood and other major oil fields in the Los Angeles Basin.

Paleontology

Thirty samples from the BC-403 core were analyzed for microfossils. All samples contain Pliocene foraminifers, as well as radiolaria, bivalve fragments, and woody debris. The cored interval contains benthic fauna typical of the Los Angeles Basin between 2.5 and 4 Ma, which correlates with the Middle Pico, Lower Pico, Upper Repetto, and Middle Repetto biostratigraphic subdivisions of the Pliocene (Fig. 11.4). A change in coiling ratio of a key planktic species between 1420 and 1430 ft (433 and 436 m) corresponds to an age of about 3 m.y. (see Ingle, 1967; Bandy et al., 1971; Bandy, 1972a–c).

Bathymetrically mixed Pliocene foraminifers were present in all samples and include species that indicate lower bathyal depths (>6500 ft or 2000 m). More than 90% of the specimens of each sample represent shallow-water species that had been displaced into the bathyal zone. Such displaced, mixed faunal assemblages are typical of turbidites. The analysis indicates that the basin floor remained at lower bathyal depths throughout the deposition of the interval.

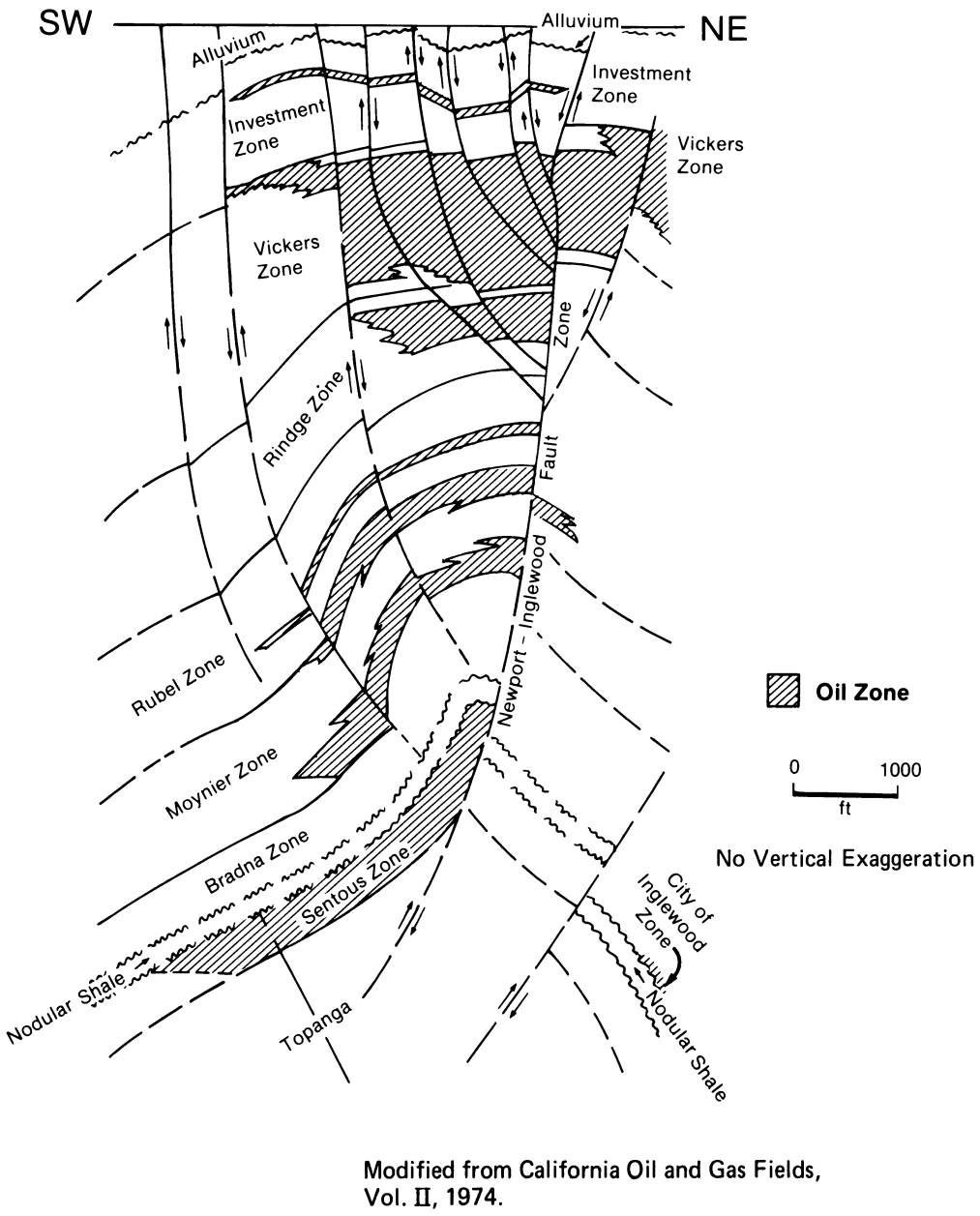

Figure 11.2. Cross section through the Inglewood Field showing major faults and stacked oil zones.

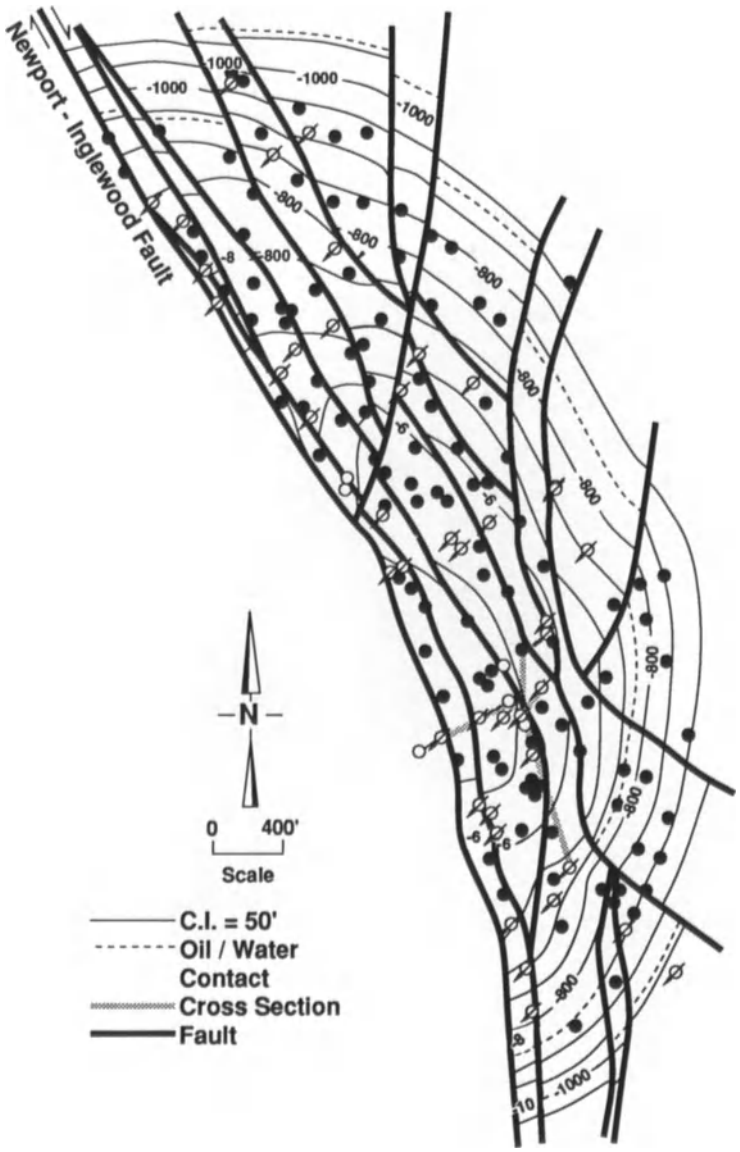

Figure 11.3. Map of the Inglewood Field showing structure on the top of the Alpha zone. Many of the wells are deviated into the field.

Lithology and Lithofacies

The Vickers zone is composed of thinly interbedded, poorly consolidated sandstones and mudstones. It is informally divided into a number of correlatable (sub)zones: Alpha through O. The core consists of several hundred alternating sandstone and mudstone beds. Individual beds range from less than 0.1 to more than 16 ft (0.03 to 4.9 m) thick. The lithology of a given core interval varies from almost entirely sandstone to predominantly mudstone.

Five lithofacies were defined on the basis of sandstone bed thickness, internal structures, and sandstone/mudstone ratio (Fig. 11.5). The lithofacies have descriptive names and are also assigned numbers, 1 through 5, for ease of representation on figures.

The lithofacies can be related to interpreted depositional environments. Figure 11.6 shows the vertical distribution of these lithofacies through the cored interval. The following section gives a description of each lithofacies and an interpretation of its depositional environment.

Massive Mudstone (Lithofacies 1)

The Massive Mudstone lithofacies consists of mudstone intervals at least 2 ft (0.6 m) thick that contain no sandstone beds (Fig. 11.7). The mudstone typically contains minor amounts of sandstone as small lenses or burrows, but the total sandstone content is less than 5%. The mudstones are olive gray, mottled and burrowed, silty, micaceous, and

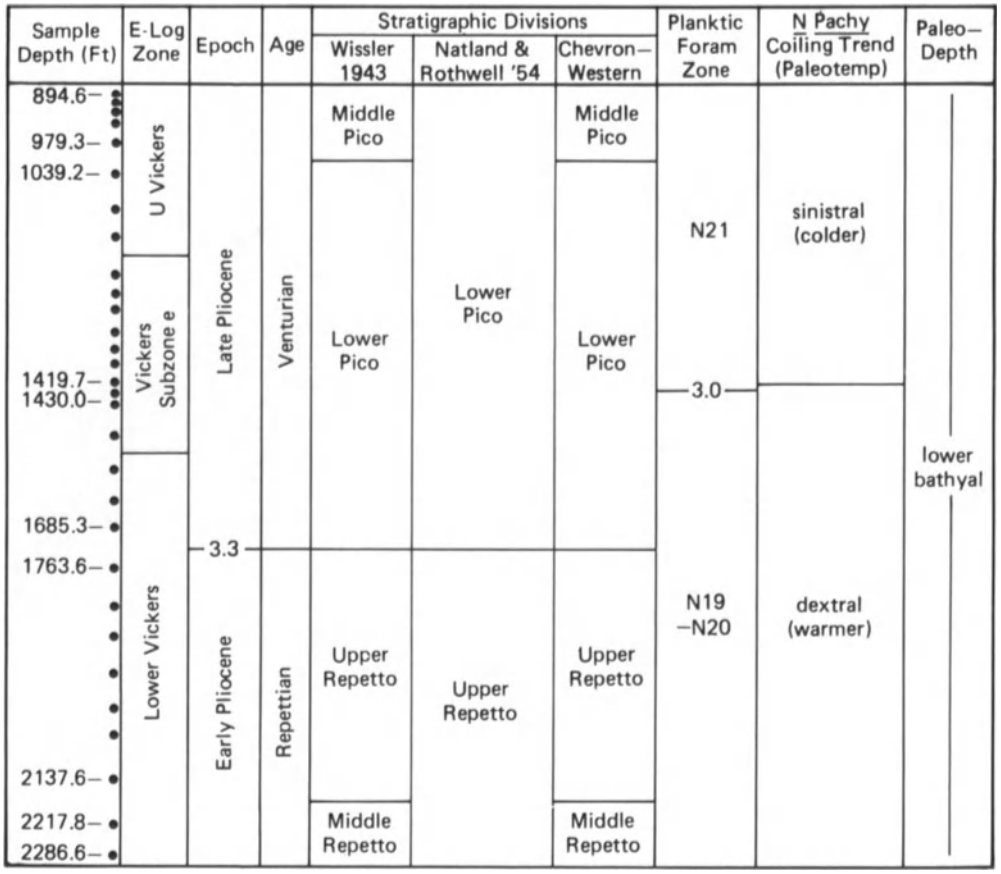

Figure 11.4. Correlation chart of biostratigraphic data from BC-403.

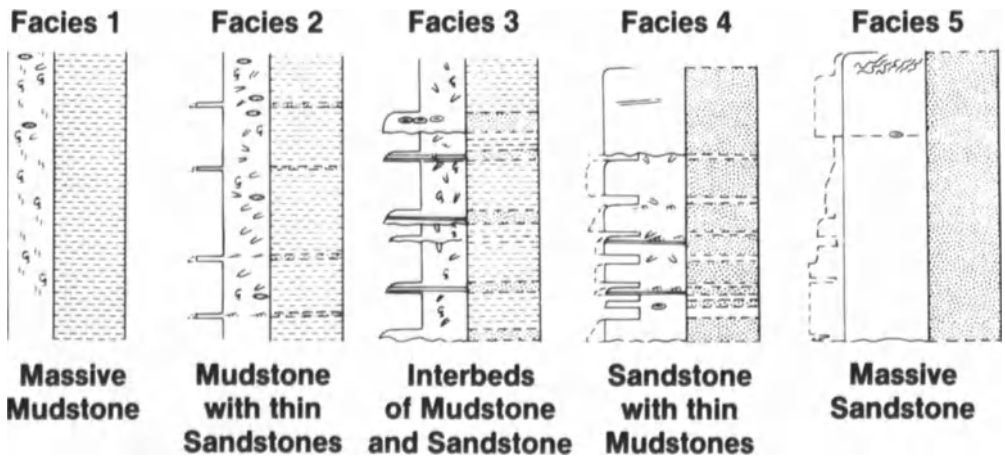

Figure 11.5. Lithofacies defined for the BC-403 core. Each facies shows a lithology column on the right (dots = sandstone; dashes = mudstone) and a grain-size profile and sedimentary structures on the left. The dashed lines in the grain-size column indicate the profile for the coarsest fraction of the sandstone.

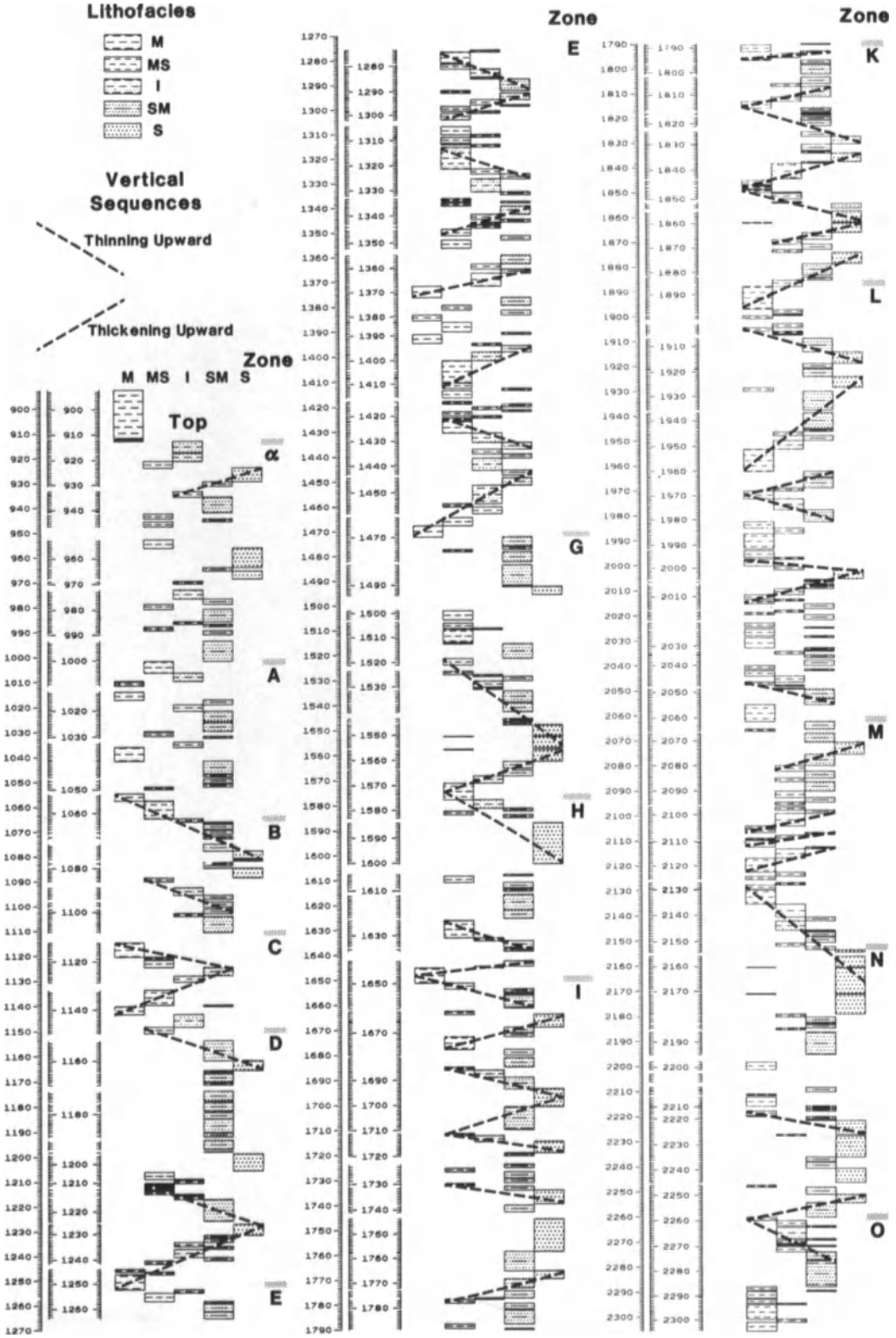

Figure 11.6. Vertical sequences of lithofacies in the BC-403 core. The cored interval starts at the top left and continues through to the bottom right. The core has been adjusted to log depth. The log-depth column is continuous, while the cored-depth column is broken.

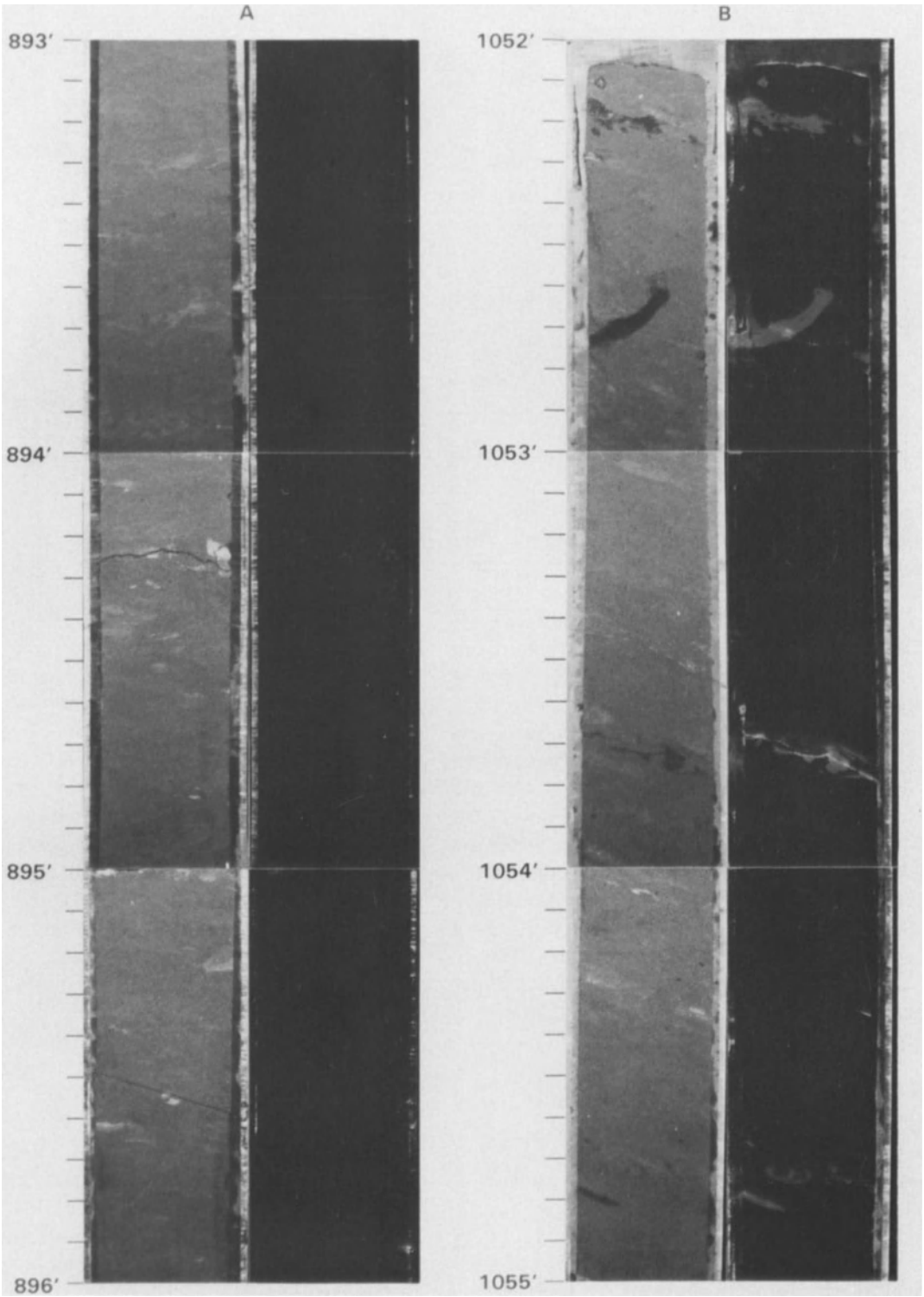

Figure 11.7. Examples of massive mudstone lithofacies. Left and right sides of photo pairs show the same core in plain and ultraviolet light, respectively. Note large, sand-filled burrows at 1052.2, 1052.7, 1053.7, and 1054.8 ft.

Table 11.1. Lithofacies statistics

Facies	Percent of Core	Depth of Core (ft)	Number of Intervals	Average Thickness (ft)	Maximum Thickness (ft)
1 Massive mudstone[1]	4.0	50.4	13	3.9	6.2
2 Mudstone with thin sandstones	24.2	304.7	102	3.0	10.9
3 Interbeds of mudstone and sandstone	17.3	217.2	96	2.3	8.1
4 Sandstone with thin mudstones	38.7	486.6	140	3.5	18.2
5 Massive sandstone	15.8	198.2	36	5.5	16.4
Total	100.0	1257.1	387	3.2	18.2

[1]Does not include one 20.6-ft bed of massive mudstone from above the top of the Vickers zone. All statistics include only Vickers zone cores.

slightly calcareous, and contain intact foraminifers. Bioturbation is generally intense and pervasive, with burrows up to 0.8 in. (2 cm) in diameter.

Massive Mudstone is the least common lithofacies. It occurs in 13 intervals that total 50.4 ft (15 m) of core from the Vickers zone, plus an interval 20.6 ft (6 m) thick that is above the Vickers zone (Table 11.1) at the top of the core. In the Vickers zone, Massive Mudstone beds are, on average, 3.9 ft (1 m) thick and account for 4% of the core. Most intervals occur in the Alpha through E zones, with the lowermost occurrence at the base of the H zone (Fig. 11.6).

The Massive Mudstone represents deep-marine, low-energy clastic deposition in a setting that was isolated from major sources of coarse clastic material. Possible modern analogs include continental slopes and the distal portions of basin floors away from active submarine fan lobes. The intense bioturbation is typical of deep-marine basins or slopes with slow sedimentation rates and adequate oxygen supply (Frey and Pemberton, 1984).

Mudstone with Thin Sandstones (Lithofacies 2)

The Mudstone with Thin Sandstones lithofacies consists of mudstone with thin layers and lenses of fine-grained sandstone that make up 0 to 10% of the lithofacies (Fig. 11.8). The mudstone is olive gray, mottled and burrowed, silty, micaceous, slightly calcareous, and contains whole foraminifer tests. The sandstone layers and lenses range up to 1.6 in. (4 cm) thick and are brown (oil stained), very fine- to fine-grained, laminated or ripple cross-bedded, and have sharp top and bottom contacts. Bioturbation is pervasive and includes large burrows that cut across bed boundaries.

Mudstone with Thin Sandstones is the second most common lithofacies in the core, amounting to 24.2% of the total interval. The 102 occurrences average 3 ft (0.9 m) thick and total 305 ft (93 m) of core (Table 11.1). It is most abundant, and constitutes the thickest intervals, in the E, L, and M zones (Fig. 11.6).

This lithofacies represents deep-marine clastic deposition under low- to moderate-energy conditions. The sandstones were deposited by intermittent higher-energy currents that winnowed and moved thin sand sheets across a predominantly muddy, biologically active sea floor. The sharp lower and upper contacts of the sandstones and the abundance of ripple bedding and laminations suggest that these deposits represent thin, fine-grained turbidites that may have been reworked by strong bottom currents after initial deposition.

The most likely depositional setting is on portions of a basin floor away from the feeder channels of deep-sea fan systems. In terms of models of deep-sea fans (Mutti and Ricci-Lucchi, 1972; Walker, 1978), this lithofacies would occupy most of the lower fan and portions of the channel levees and interchannel areas on the mid-fan and upper fan (Fig. 11.9).

Interbedded Mudstone and Sandstone (Lithofacies 3)

The Interbedded Mudstone and Sandstone consists of mudstone with interbeds of sandstone up to 6 in. (15 cm) thick that make up 10% to 50% of the lithofacies (Fig. 11.10). The mudstone is olive gray, mottled and bioturbated, silty, micaceous, slightly calcareous, and contains foraminifer tests, similar to mudstone in Lithofacies 2. Most upper contacts of the sandstones are bioturbated. Some thin sandstone beds have been almost completely bioturbated into chaotic sandy mudstone zones, as seen in Figure 11.10.

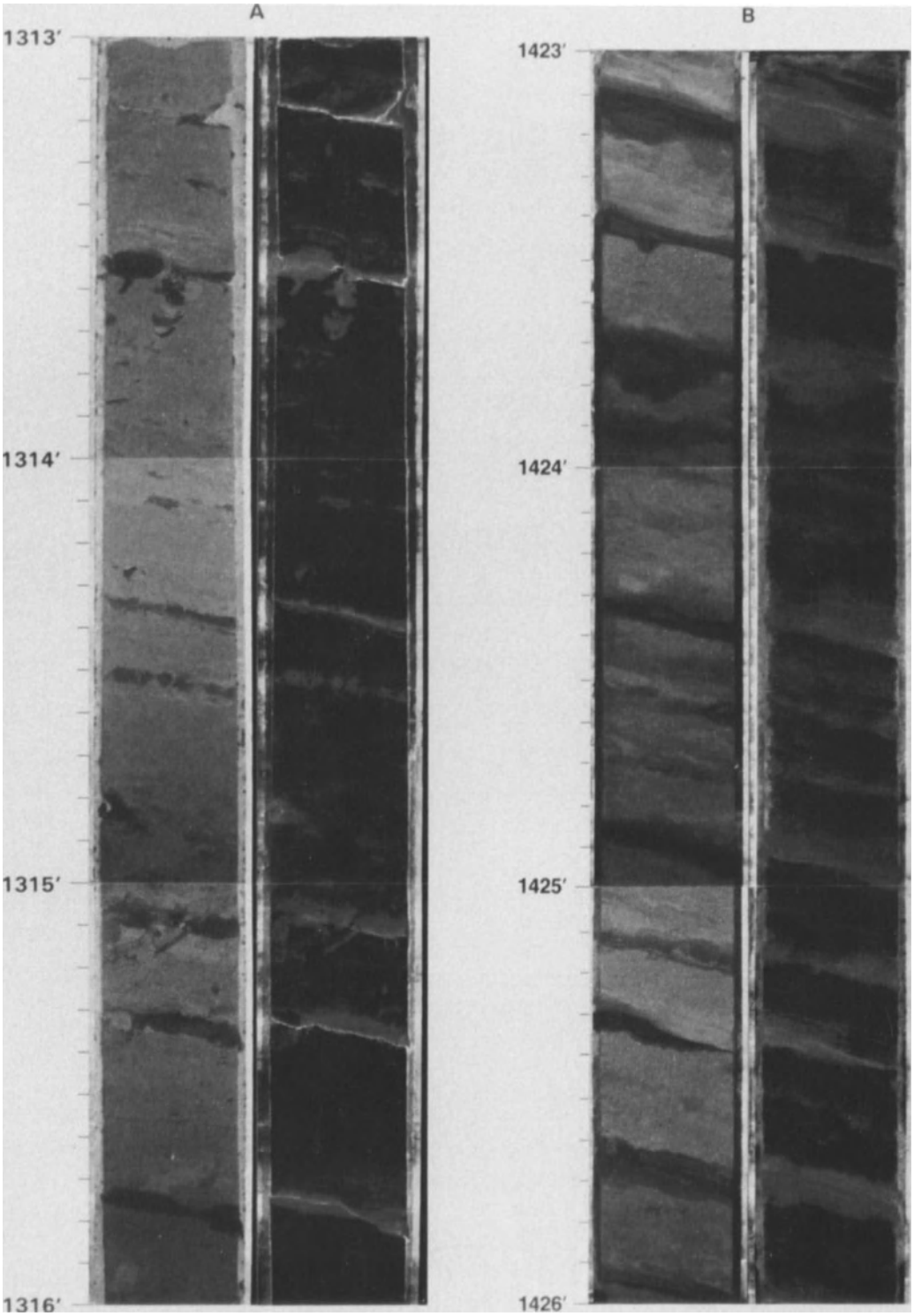

Figure 11.8. Examples of mudstone with thin sandstone lithofacies. Much of the core has been bioturbated. Some planar-laminated sandstone occurs at 1425.7 ft.

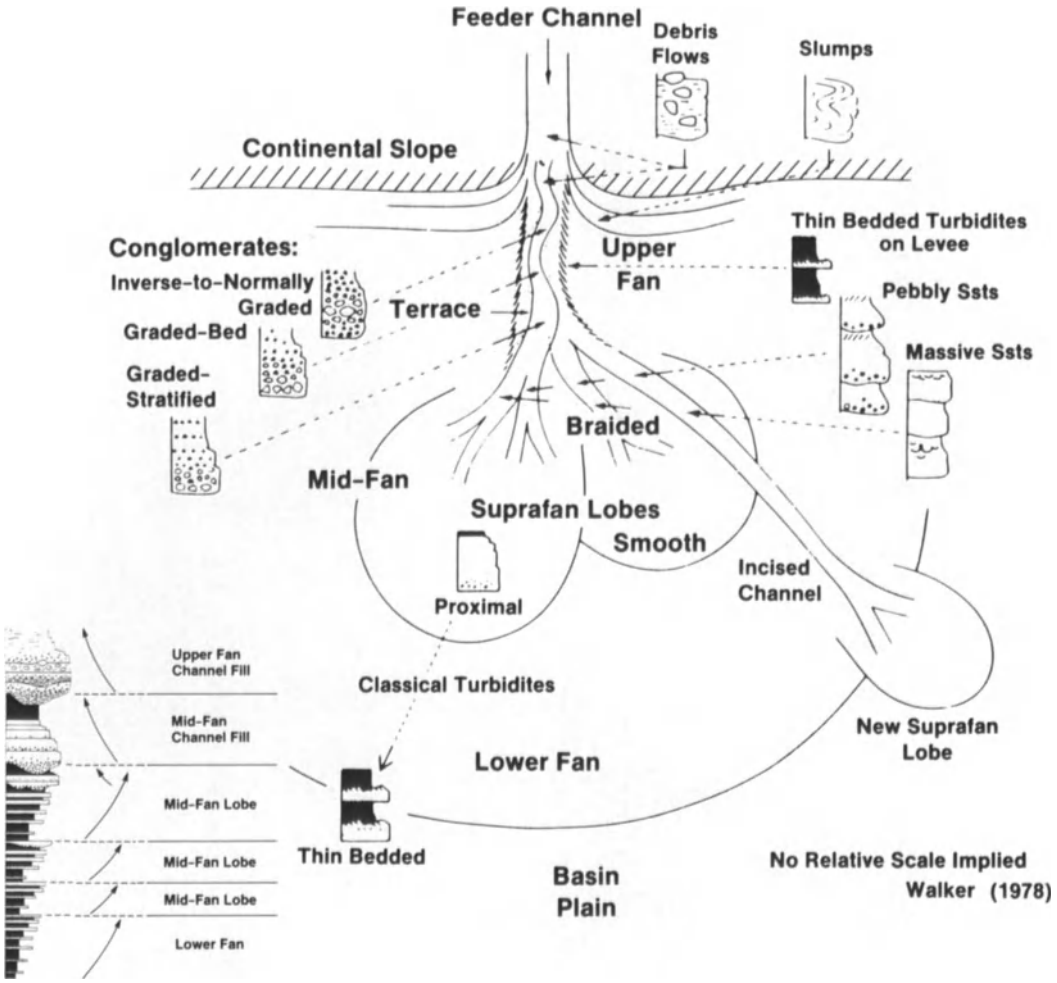

Figure 11.9. Deep-sea fan model showing the lateral distribution of lithofacies relative to fan subenvironments. Shown at the bottom left is the sequence that would theoretically form during fan progradation. (Modified after Walker, 1978; reprinted by permission.)

The sandstones are very fine to fine grained, moderately well sorted, and have planar, wavy, or ripple cross-laminations. Most sandstone beds have sharp bases and mottled tops that grade upward into bioturbated mudstone. Many of the thicker sandstones are normally graded and resemble thin turbidites with partial Bouma sequences (Bouma, 1962). These beds have a scoured lower contact overlain by a section of plane lamination that grades up into a finer-grained, better-sorted, wavy, cross-laminated interval.

The 96 occurrences amount to 17.3% of the total core (Table 11.1). Intervals are, on average, 2.3 ft (0.7 m) thick. The lithofacies is most common in the E, K, L, and M zones, and is only sparsely distributed elsewhere (Fig. 11.6).

The interbedded character of this lithofacies implies alternations between relatively long periods of low-energy mud deposition and shorter periods of moderate- to high-energy sand deposition. The cross-laminated and well-sorted sandstone beds indicate deposition by strong and continuous currents flowing across the basin floor, whereas the graded turbidites indicate deposition as part of a deep-sea fan system. The combined evidence suggests deposition in the middle to outer portions of a deep-sea fan but away from the locus of thickest sand deposition. In the deep-sea fan model of Walker (1978), these would be classified as lower fan or channel levee deposits (Fig. 11.9). The Interbedded Mudstone and Sandstone also could be interchannel deposits in the mid-fan, with some of the sands derived from channel overspill or flow-stripping of large channelized turbidites (Piper and Normark, 1983).

Sandstone with Thin Mudstone (Lithofacies 4)

The Sandstone with Thin Mudstones lithofacies consists of normally graded beds of sandstone, 0.5 to 3 ft (0.2 to 0.9 m) thick, separated by mudstones less than 0.5 ft (0.2 m) thick

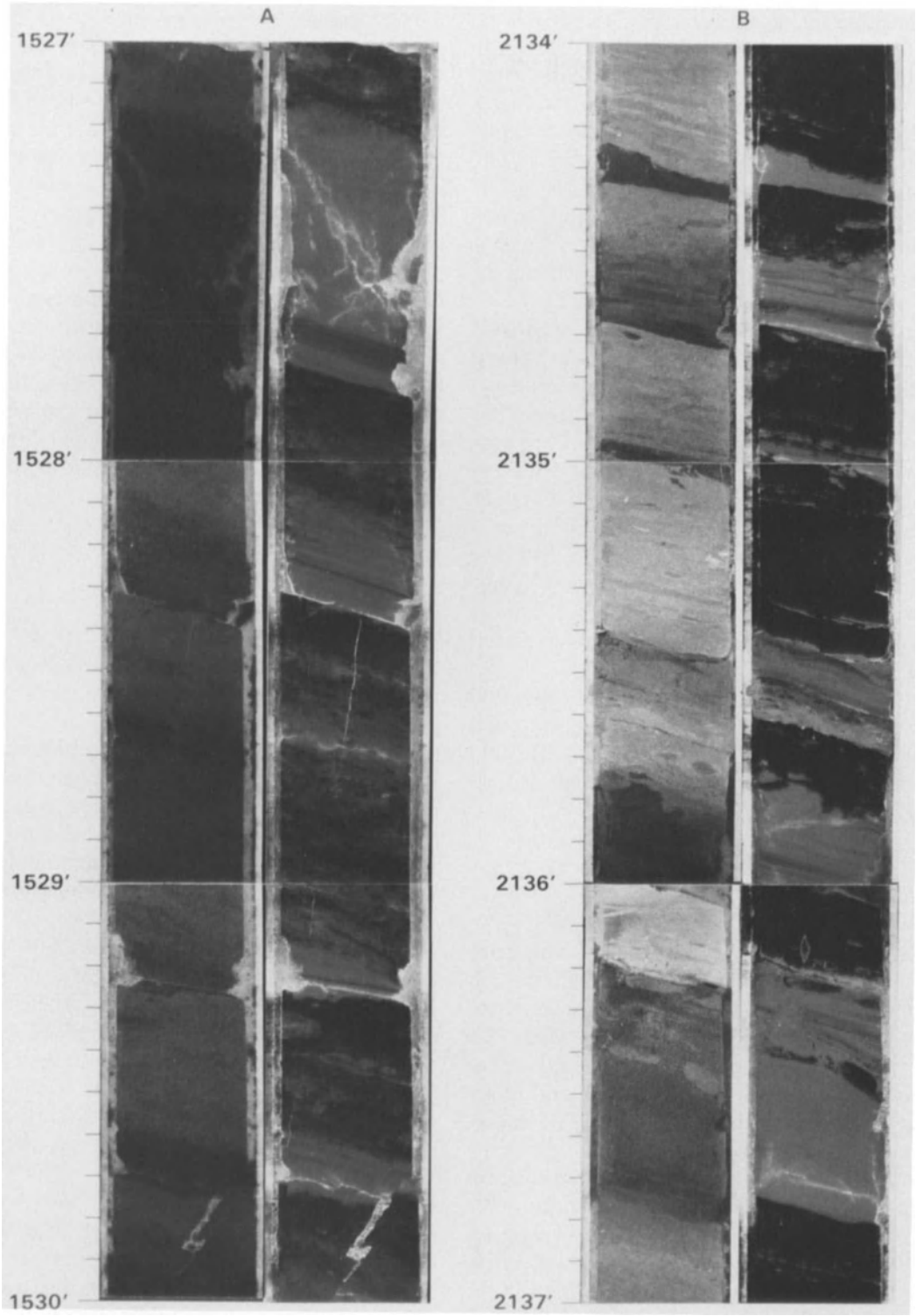

Figure 11.10. Examples of interbedded mudstone and sandstone lithofacies. Planar laminations can be seen at 1527.7, 1528.2, and 2136 ft. Ripple laminations occur at 2135.9 ft. Bioturbation is common. For example, the ultraviolet photographs show that much of the mudstone between 1528 and 1530 ft is mixed with a considerable amount of sandstone.

(Fig. 11.11). Sandstone makes up between 50 and 90% of this lithofacies. Individual sandstone beds have a sharp, scoured base and a gradational, usually bioturbated top. They contain a structureless lower section gradationally overlain by a thinner upper part that is commonly laminated or cross-bedded.

Most sandstone beds are poorly sorted in the lower part, becoming moderately well sorted toward the top. Sandstones thicker than 2 ft (0.6 m) commonly show normal grading of the coarse-grained fraction but little change in the modal grain size except near the top of the beds.

Upper contacts typically are bioturbated, commonly with large burrows. In contrast, most basal contacts are sharp and show evidence of scour into the underlying mudstone. The amount of scour is difficult to estimate and may be minor in most cases, since the mudstone interbeds are preserved. The thin mudstone beds are similar to mudstone in the Mudstone with Thin Sandstones lithofacies, but appear to be less pervasively bioturbated.

This is the most common lithofacies in BC-403, with 140 occurrences, which account for 38.7% of the total core. Although widely distributed throughout the core, it is most abundant and thickest in the Alpha through D zones and in zones I and K (Fig. 11.6).

Lithofacies 4 is a series of sandstone turbidites separated by thin mudstone interbeds. Within the deep-sea fan models of Walker (1978) and Mutti and Ricci-Lucchi (1972), this lithofacies would occur on the mid-fan depositional lobes (Fig. 11.9).

Massive Sandstone (Lithofacies 5)

The Massive Sandstone lithofacies consists of sandstone beds at least 3 ft (0.9 m) thick (Fig. 11.12). The sandstone is poorly to very poorly sorted, with maximum grain size up to 4 mm (granule) and a modal grain size of fine sand. The beds generally lack visible structures except in the upper portion of some beds, where sorting improves and cross-laminations and convolute laminations occur. The coarse fraction is typically normally graded.

Some of the thicker beds contain amalgamation surfaces defined by sharp changes in grain size. Bottom contacts are sharp and scoured into mudstone, whereas the tops are typically bioturbated and gradational into mudstone. These beds are similar to, but thicker than, the sandstones in the Sandstone with Thin Mudstones lithofacies.

This lithofacies accounts for 198.2 ft (60 m) or 15.8% of the total core. Beds are, on average, 5.5 ft (1.7 m) thick, with a maximum of over 16 ft (4.9 m). The occurrence and thickness of individual beds vary markedly down the cored section (Fig. 11.6). There are no Massive Sandstones in the E zone.

The Massive Sandstones appear to be amalgamated turbidites, similar to the turbidites in the Sandstone with Thin Mudstones lithofacies but lacking the thin mudstone interbeds. Most beds appear to have been formed by multiple flow events. The absence of mudstone at the amalgamation surfaces may be due to slightly more scour and erosion by successive turbidity currents than in the Sandstone with Thin Mudstones lithofacies. No pebbles or cobbles occur in the thick sandstone beds, nor as lags at their bases. The granular nature of the sandstones and the rare occurrences of mudstone clasts within the thick beds suggest a depositional setting in the proximal part of a suprafan lobe of a deep-sea fan (Fig. 11.9). Thick-bedded turbidites can occur as channel-fill deposits or as laterally extensive, nonchannelized deposits, presumably near the ends of channels. The extensive lateral continuity of this lithofacies, as seen on log cross sections (discussed later), argues for deposition beyond the channels.

Petrography

Seventy-three thin sections were prepared for petrographic analysis. The thin sections were made from core analysis plugs that were cut parallel to bedding. Half of each thin section was stained with sodium cobaltinitrite to aid in K-spar identification. Thirty-eight scanning electron microscope (SEM) samples were analyzed to determine clay fabrics and composition. Twenty-five x-ray diffraction analyses were made to quantify bulk mineralogic composition. There is little difference among the lithofacies in terms of composition.

The majority of the sandstones are arkosic arenites, according to the classification of Pettijohn et al. (1972). There are also lithic arenites and arkosic wackes. Feldspar and quartz are the dominant minerals (Table 11.2). Plagioclase (predominantly oligoclase) is commonly sericitized and is the dominant feldspar type, with lesser amounts of K-spar (orthoclase). Biotite is variably altered to amorphous green clay and is a common constituent of all the sandstones.

The arkosic arenites are typically very fine to fine grained and well to extremely well sorted. The lithic arenites are fine to medium grained and very poorly to moderately well sorted. The framework of the arkosic wackes is typically fine grained and well to extremely well sorted. Most grains in all samples are angular to subangular, and the coarsest grains are better rounded. Grain contacts are tangential to straight.

Thin-section porosity averages approximately 30% for the arenites and 14% for the wackes. Well-connected intergranular macropores are the predominant porosity type,

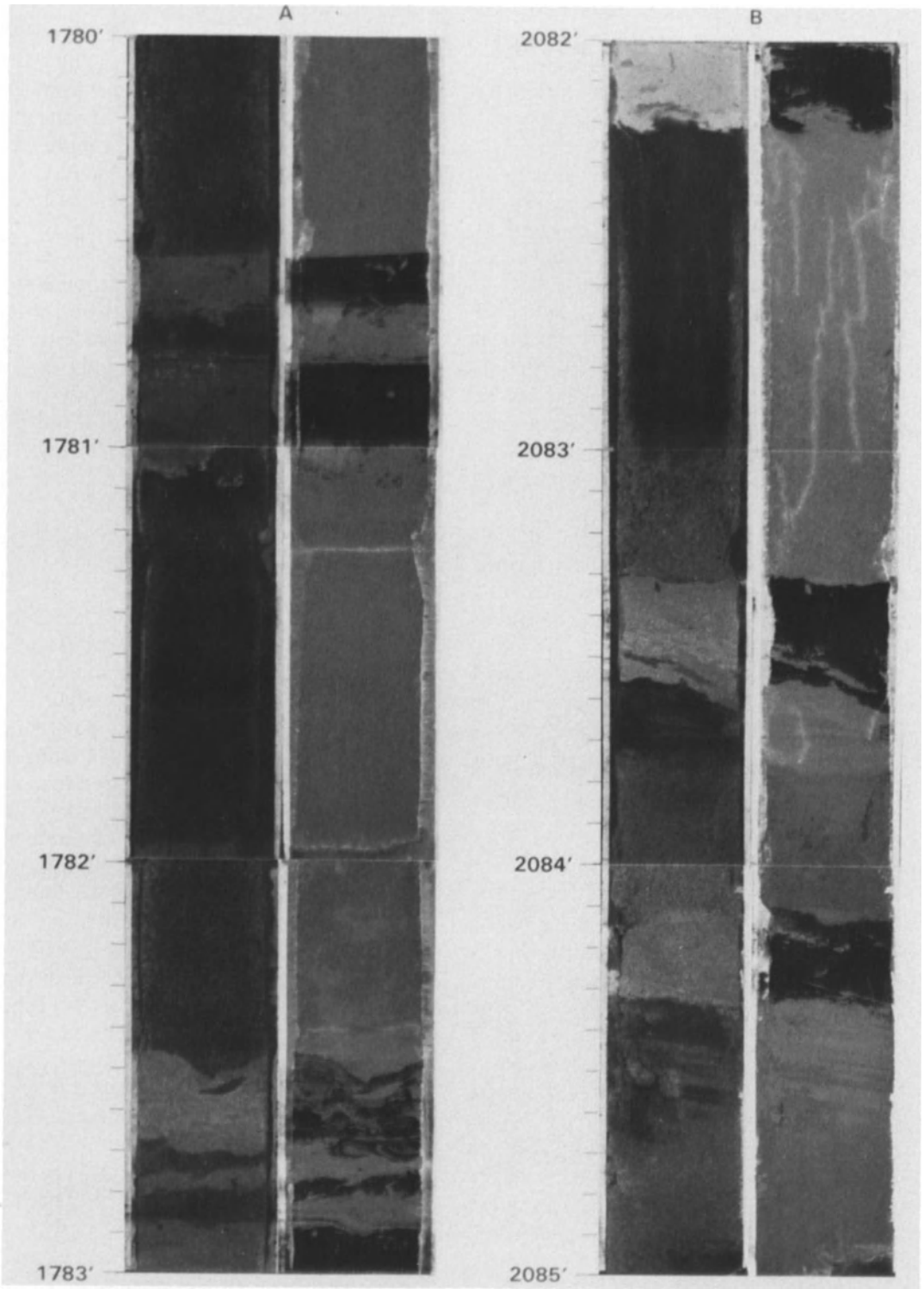

Figure 11.11. Examples of sandstone with thin mudstone lithofacies. Most sandstone beds are turbidites that show normal grading.

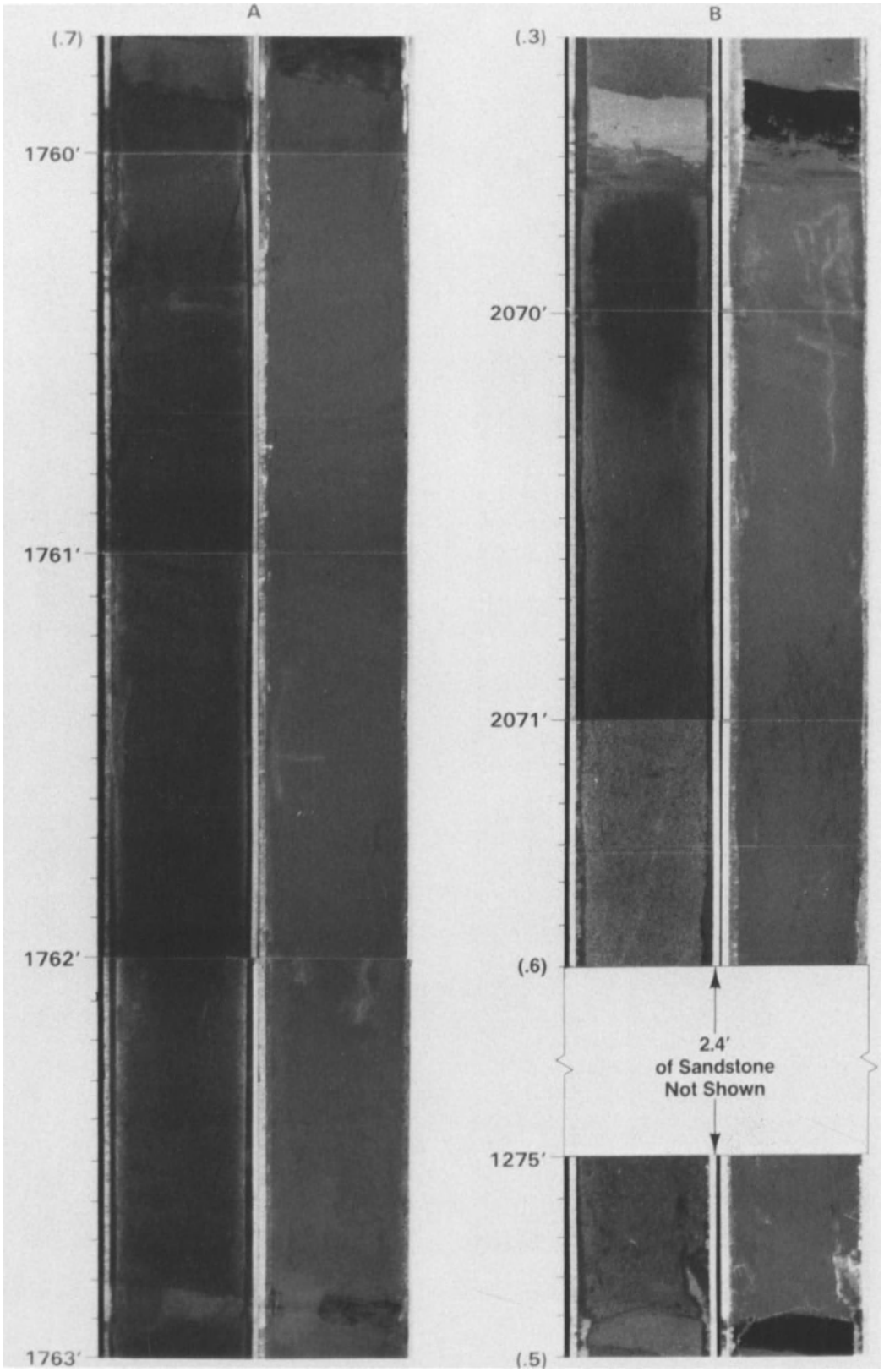

Figure 11.12. Examples of massive sandstone lithofacies. Sandstone beds are massive to graded with thin mudstone interbeds.

Table 11.2. Principal components of the BC-403 sandstones

Rock Class	Sample No.	Quartz	Feldspar	Lithics	Clay
Arkosic Arenites	53	Range: 10–43% Mean: 26.9%	Range: 13–28% Mean: 26.1%	Range: 0–20% Mean: 7.6%	Range: 0–9% Mean: 1.8%
Lithic Arenites	9	Range: 13–30% Mean: 20.6%	Range: 15–24% Mean: 18.7%	Range: 8–34% Mean: 23.8%	Range: 0–14% Mean: 3%
Arkosic Wackes	10	Range: 6–29% Mean: 19.1%	Range: 8–34% Mean: 23.6%	Range: 0–8% Mean: 3.5%	Range: 15–70% Mean: 31%
Lithic Wackes	1	11	17	28	25

with minor to moderate amounts of microporosity and intragranular macroporosity.

Detrital clay occurs in most samples in varying amounts and is composed primarily of biotite. The clay occurs as grain coats, patches on grains, and as pore fill. Microporosity is associated with the detrital clays. Where clay is abundant, there can be a significant difference between total and effective porosity.

Authigenic smectite occurs in most samples on detrital clays and silts and as patchy coats on framework grains. It is coarser and better developed in samples from the lower 300 ft of section, but is not abundant enough to occlude primary macropores. Authigenic zeolite (clinoptilolite-heulandite) occurs in several deep samples, intergrown with smectite on detrital grains. The increased abundance of smectite and zeolite with depth reduces the reservoir quality of the sandstones in the lower 300 ft of the core.

Cross Sections

Two stratigraphic and structural cross sections were constructed through the well BC-403: line 1 across dip, and line 2 along strike.

The structural cross sections were drawn with both horizontal and vertical scales of 1:600 and were photographically reduced for this publication (Fig. 11.13). Well paths are projected onto the section lines from the deviation surveys. Major faults are drawn as vertical, and correlations are made by reservoir zone.

Faults have removed about 30 ft (9 m) of the Alpha in the BC-354, and this entire zone in LW-402. In the BC-403, there is a fault in the H zone that has removed 15 ft (4.6 m) of section.

Zones G, E, D, and M show the most significant thickness variations. In the dip line, the M zone shows extreme thickness variation, probably resulting from fault-controlled sedimentation. The Newport-Inglewood fault was developed during middle Miocene time and is active to the present. It is quite possible that Pliocene movement along this fault affected deposition of the Vickers sandstones.

The dip and strike cross sections are approximately 510 and 1,225 ft long, respectively. The majority of the sandstone and mudstone beds, even those as thin as 1 or 2 ft, showed continuity across both stratigraphic section lines. The lithologies of the unrecovered intervals of the BC-403 were interpreted from the logs, and the net sand and gross interval thickness for each reservoir zone are given in Table 11.2.

Depositional Model and Vertical Sequences

Most simplified models predict that a deep-sea fan prograding across a basin floor will consist of coarsening- or thickening-upward depositional lobes overlain by fining-upward channel fills (Fig. 11.9). Using the five lithofacies defined for the BC-403 core, Figures 11.14A and B show lithofacies relation diagrams for idealized thickening- and thinning-upward sequences. By contrast, the BC-403 core shows numerous back-and-forth cycles of thickening and thinning, interspersed with a few intervals where the lithofacies appear random (Fig. 11.6). There are almost identical numbers of thickening- and thinning-upward lithofacies transitions (Fig. 11.14C).

The character of vertical sequences in the core indicates that a simple progradational-fan model does not explain this section of the Los Angeles Basin. Only a minor part of the core shows abrupt shifts of lithofacies that would correspond to abrupt channel abandonment (Fig. 11.15A). Instead, most of the core shows a gradual back-and-forth pattern, which suggests that the lobes were built by gradual lateral migration and vertical accretion of the lobe depocenter across the basin floor (Fig. 11.15B). There is no apparent evolution in the character of the vertical sequences from the bottom to the top of the cored interval, except that the uppermost 150 ft of the core show a more random pattern of lithofacies than most of the remainder.

The vertical gradations among lithofacies indicate that

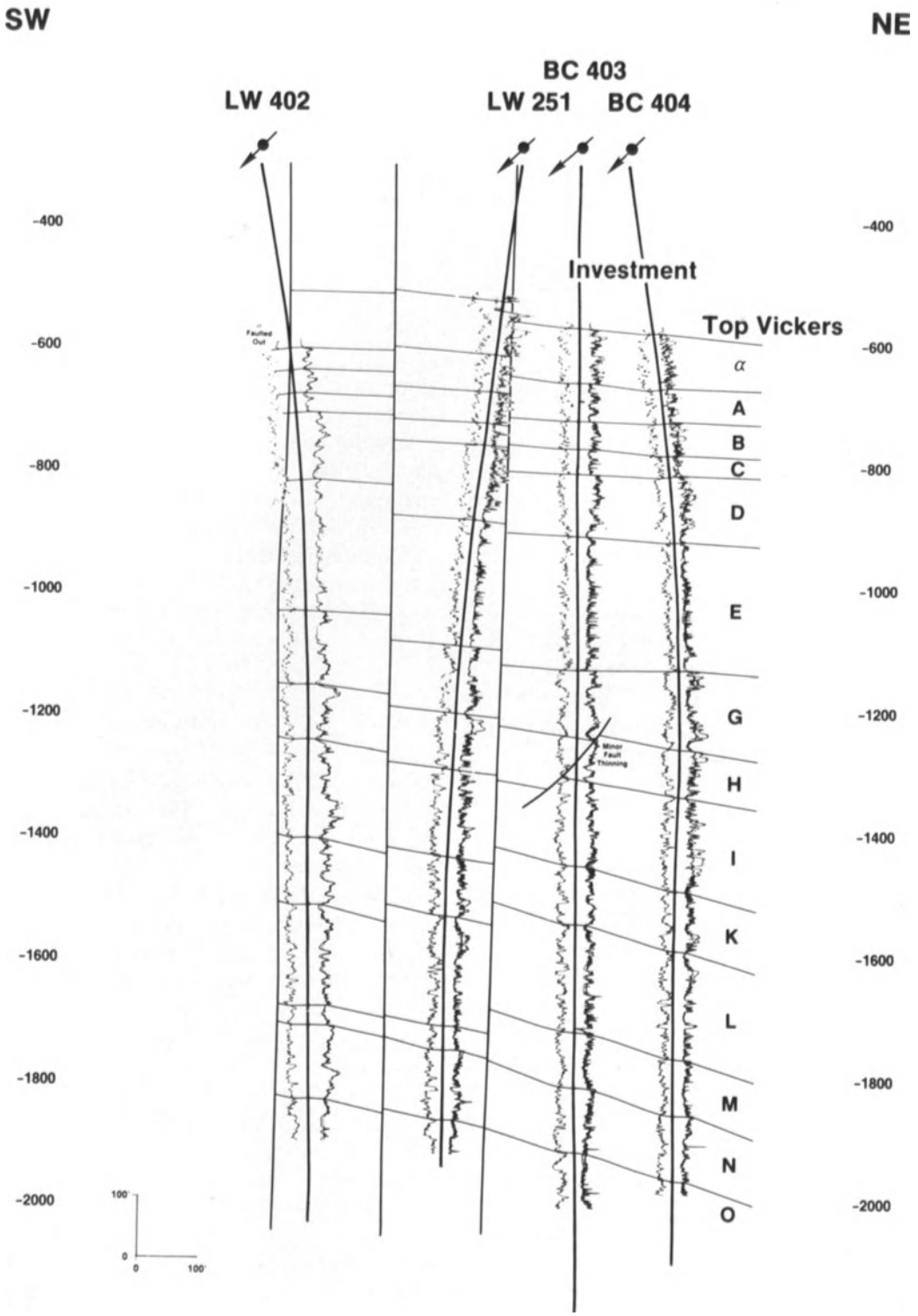

Figure 11.13. Structural cross sections. (A) SW-NE section is parallel to dip. Note the extreme thickness variation in the M zone. Major fault traces are shown as vertical. (B) NNW-SSE section parallel to strike. There are no major faults, but there are minor ones in wells BC-354 and BC-403.

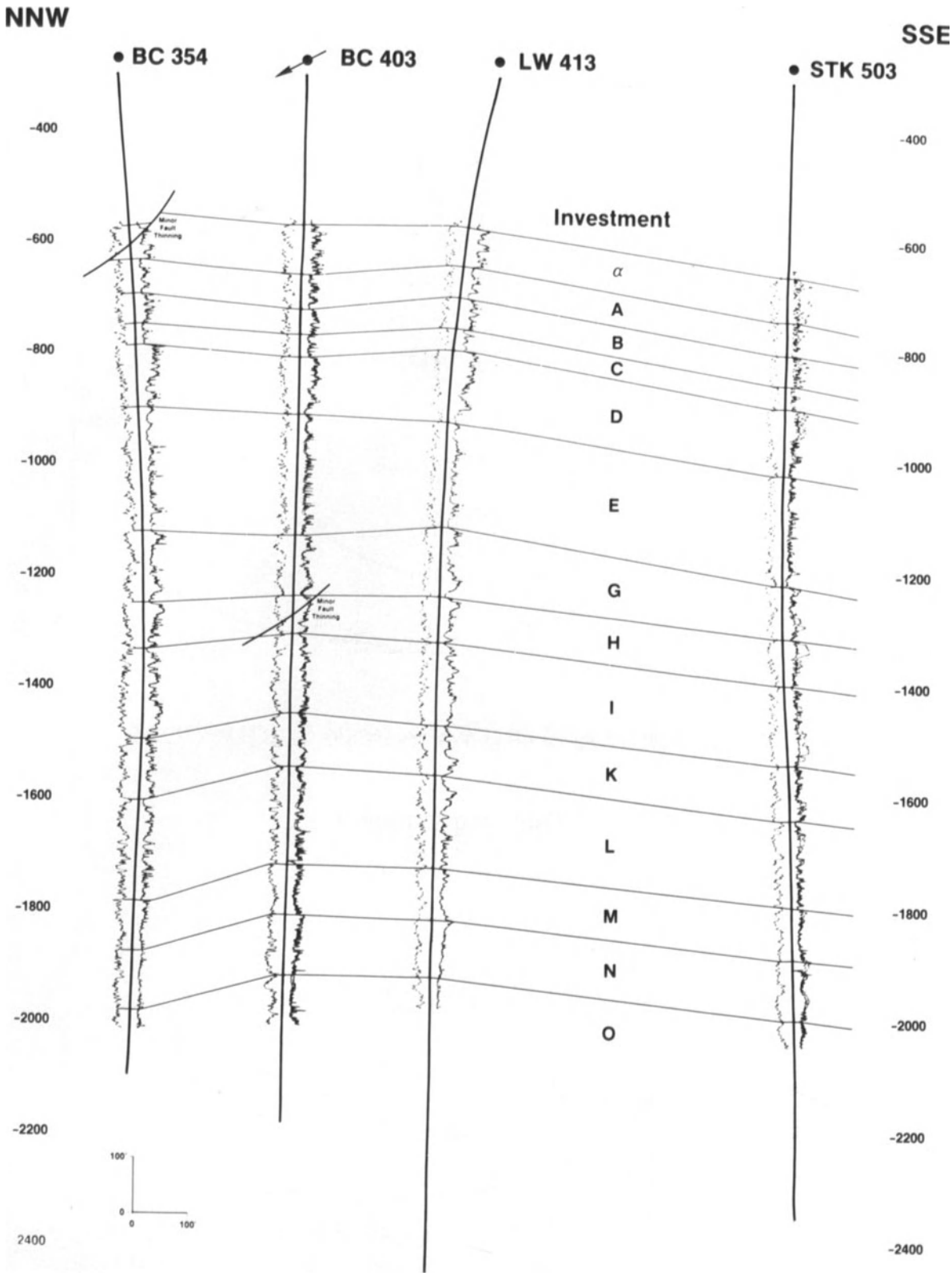

Figure 11.13. *Continued*

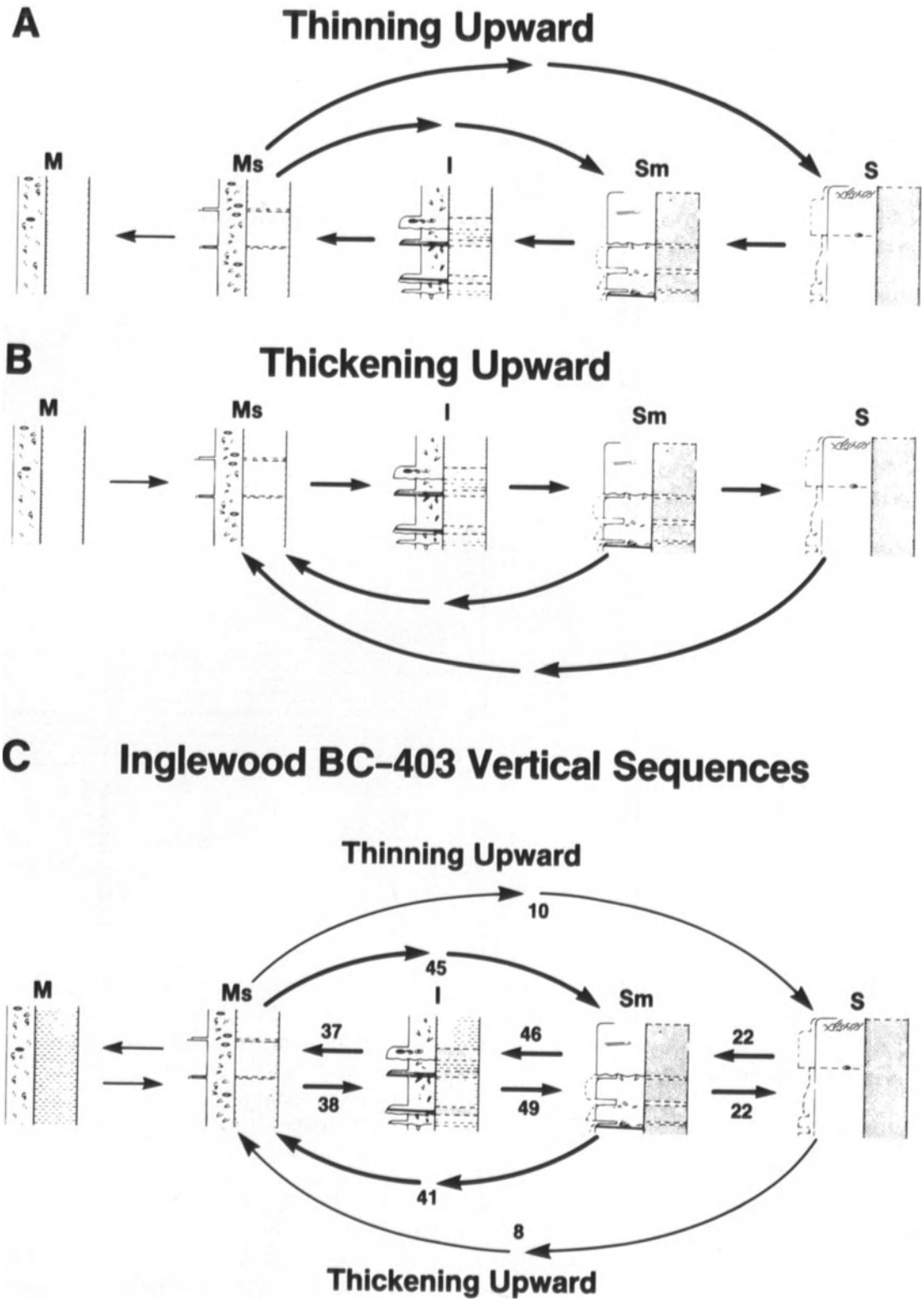

Figure 11.14. Facies diagrams with arrows showing number of upward transitions between pairs of lithofacies. (A) Idealized thinning-upward sequence from right to left. (B) Idealized thickening-upward sequence. (C) Actual vertical sequences from BC-403 have nearly equal numbers of thinning- and thickening-upward sequences.

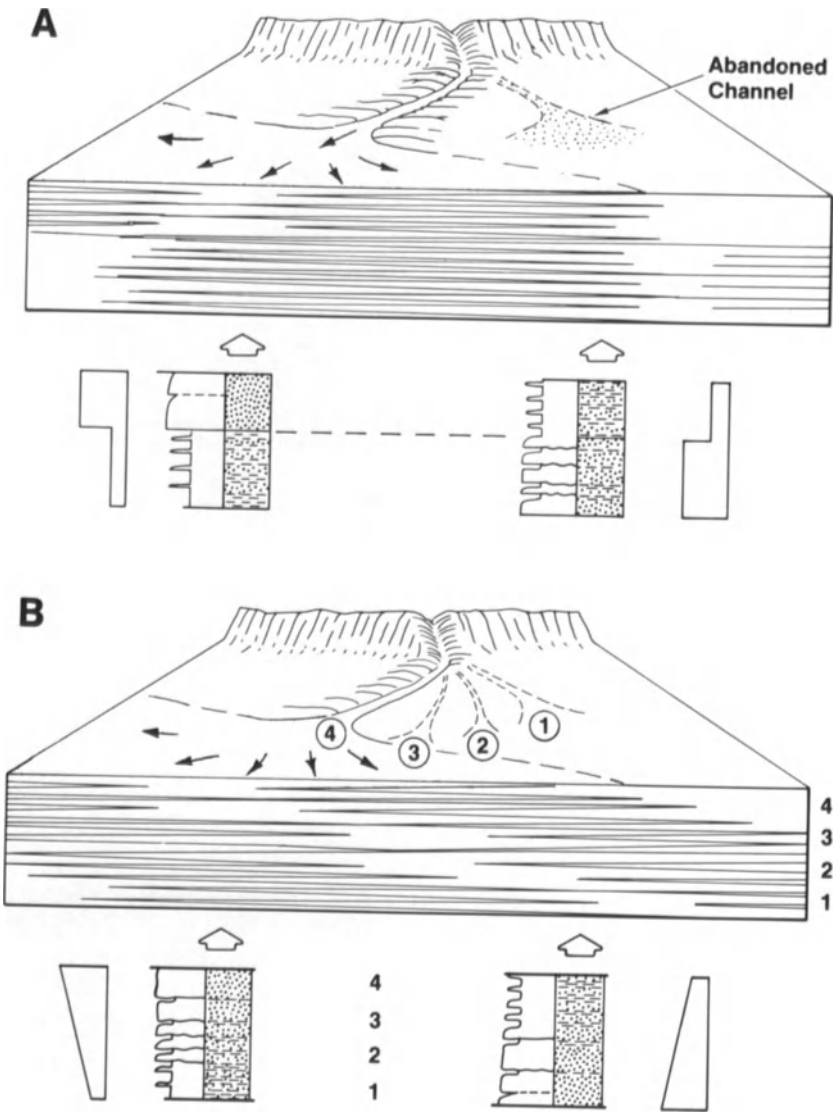

Figure 11.15. Depositional patterns for lobes on deep-sea fans. (A) Sudden shift of the depositional site, caused, for example, by channel abandonment, results in an abrupt change in the vertical sequences. (B) Gradual shifting of the channel produces progressive changes in the vertical sequences.

the BC-403 sediments were deposited in laterally adjacent subenvironments within a deep-sea fan system. Individual sandstones were deposited by turbidity currents that spread across a relatively flat basin floor. The Massive Sandstone and Sandstone with Thin Mudstones lithofacies probably represent the central portions of deep-sea-fan depositional lobes near the channel mouths, whereas the Interbedded Mudstone and Sandstone, the Mudstone with Thin Sandstones, and the Massive Mudstone lithofacies represent increasingly distal portions of the fan lobes (Fig. 11.16).

The poorly sorted and angular texture of the thicker sandstones suggests that clastic material was fed directly into the basin from fluvial sources without significant sorting or reworking in shallow-water, high-energy environments. The sandstones were deposited as thinner, finer-grained, and better-sorted beds as the turbidite currents spread over the suprafan lobes.

The high proportion of shallow-water benthic fauna in the mudstone beds indicates that the turbidity currents removed mud from the slopes and deposited it on the basin floor. Even with this addition of mud, the total proportion of sandstone in the cored interval is over 50% (Table 11.3). This percentage fits well with Conrey's (1967) regional maps, which show increasing sandstone percentage toward the northeast corner of the Los Angeles Basin in the early Pliocene. On the basis of the regional distribution of sandstone percentages and conglomerate grain size, Conrey (1967) suggested a dominant source of clastics entering the basin from the northeast corner. The Inglewood Field lies over 10 mi (16 km) from this coarse-grained corner of the basin, apparently far enough from the source area to allow accumulation of significant amounts of mudstone along with the sandstone.

The lateral continuity of lithofacies units on log-based

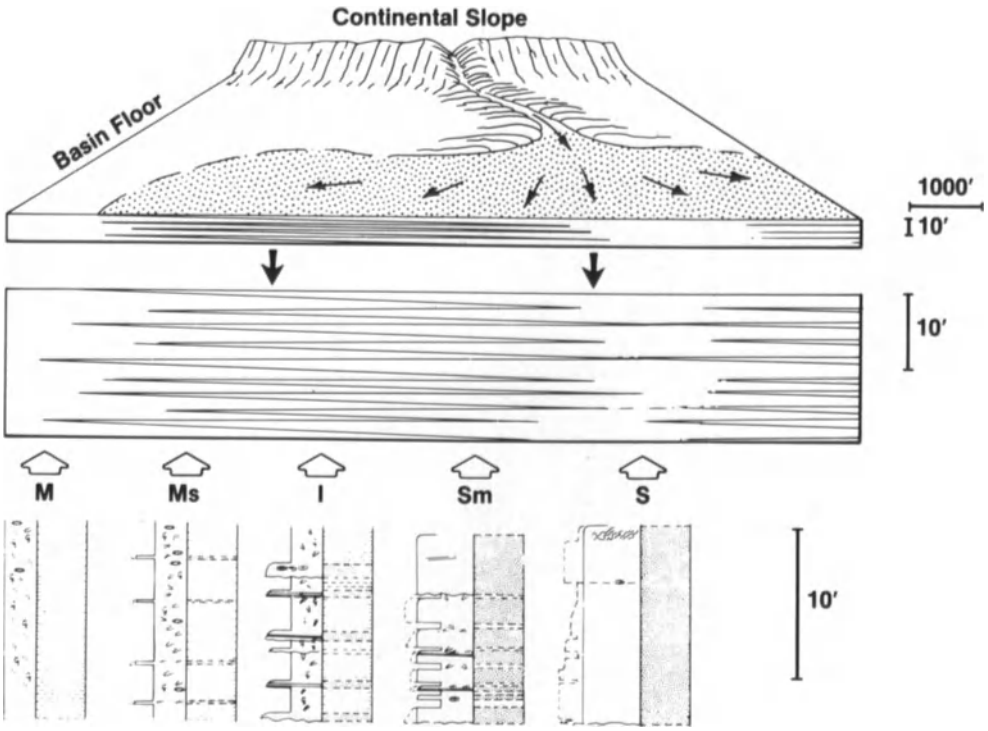

Figure 11.16. Position of the five BC-403 lithofacies on a depositional lobe. Note the vertical exaggeration of turbidite bed thickness compared with their lateral extent.

Table 11.3. Net and gross sand thicknesses by reservoir zone

Zone (Log Depth)	Net Sand (ft)	Gross Thickness (ft)	Net Sand/ gross Thickness (%)
α (911–1002′)	54.3	91	59.7
A (1002–1064′)	20.8	62	33.5
B (1064–1111′)	28.8	47	61.3
C (1111–1150′)	8.7	39	22.3
D (1150–1253′)	64.6	103	62.7
E (1253–1471′)	61.4	218	28.2
G (1471–1579′)	61.1	108	56.6
H (1579–1648′)	45.5	69	65.9
I (1648–1790′)	99.6	142	70.1
K (1790–1886′)	63.2	96	65.8
L (1886–2062′)	83.9	176	47.7
M (2062–2154′)	51.2	92	55.6
N (2154–2260′)	76.7	106	72.4
O (2260–2412′)	19.4	152	N/A[1]
Total	739.2	1501	49.2[2]

[1]Only top 47.1 ft of zone was cored.
[2]From top Vickers to base of cored interval.

cross sections suggests that no true channel deposits were cored in BC-403. The five lithofacies represent a range of deep-sea fan sediments deposited in the middle to outer portions of depositional lobes beyond the ends of suprafan channels. The style of middle and outer fan sedimentation is predominantly aggradational deposition without major episodes of erosion.

The cyclic character of the vertical sequences indicates that the fan did not prograde across the basin floor, but rather centers of sand deposition shifted laterally back and forth across it (Fig. 11.15). Such a pattern might be expected if the fan was large enough to nearly fill the floor of the topographically restricted Pliocene Los Angeles Basin. Regional studies suggest that deep-sea fans spread completely across the floor of the Los Angeles Basin in the early Pliocene (Conrey, 1967). Figure 11.17 shows a schematic model of the setting of the Inglewood Field during deposition of the sediments cored in BC-403.

The depositional model for the Inglewood Field predicts extensive lateral bed continuity of at least hundreds of feet, and probably of thousands of feet. The resulting reservoir geometry should support good lateral sweep efficiency in the sandstones, but since the mudstones are also laterally continuous, there will be poor vertical communication between sandstone beds.

Petrophysics

Porosity, permeability, and saturation (PKS) analysis was conducted on 719 plugs. Samples were taken at approximately 1-ft intervals in the sandstones. No mudstones were analyzed. One-inch by two-inch plugs were plunge-cut from the chilled bulk cores. Plugs were jacketed in lead sleeves

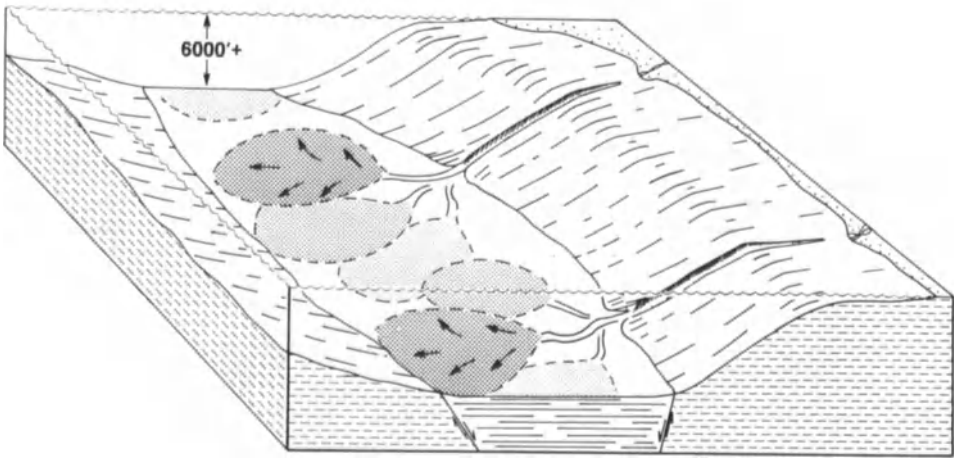

Figure 11.17. Model showing the depositional setting of the Inglewood Field.

with 200-mesh end screens. The jackets were seated at 400 psi, and analyses were made at present-day net effective stress based on the Repeat Formation Test (RFT) results. Stresses range from 516 to 1442 psi.

Porosity and Permeability

The helium porosity compares very favorably with the log measurement of bulk density, as shown in Figure 11.18, in which the two measurements are plotted at compatible scales (i.e., with a bulk density of 2.65, equivalent to 0% porosity).

The sandstones have an average porosity of 32.2% and a geometric mean permeability of 461 md. Analysis of variance was calculated to determine whether there is a significant difference among the lithofacies in terms of mean porosity and permeability. The results indicate that the mean porosities of lithofacies 2 and 3 are similar, but that they differ from lithofacies 4 and 5. There is not a significant difference among lithofacies in terms of geometric mean permeability. As lithofacies 2 and 3 are similar in both porosity and permeability, they have been grouped together and are referred to qualitatively as the thin-bedded sandstones.

Lithofacies 2 and 3 are significantly more porous than lithofacies 4 or 5, as shown by the porosity frequency distributions (Fig. 11.19A). The permeability frequency distributions of all lithofacies are similar, in agreement with results of the analysis of variance (Fig. 11.19B). The porosity/permeability cross plot has a large amount of scatter, as is typical for these plots (Fig. 11.20). A least-squares regression line can be calculated, but the correlation is meaningless because the fit is so poor.

Sieve Analysis

In order to analyze the scatter in the porosity/permeability cross plot, 34 of the actual PKS plugs were sieved. Wet/dry sieve analyses were made. Grain size and sorting were determined from the cumulative frequency curves and were measured in phi units where phi is -log mm. Sorting was calculated using the graphic standard deviation equation:

$$\text{Sorting} = \frac{\text{P84} - \text{P16}}{2}$$

where:

P16 = 16th percentile on cumulative frequency curve
P84 = 84th percentile on cumulative frequency curve.

This takes into account 68% of the grain-size distribution. The resultant values are expressed verbally as well-sorted, poorly sorted, etc. (Folk, 1974). Folk devised an alternative and slightly more complicated equation for calculating sorting that takes into account 90% of the distribution. A couple of samples were calculated using both equations, and the results were indistinguishable. The simpler method was therefore used for all samples.

The Wentworth (1922) scale is used to express size class based on the median grain size: the 50th percentile on the cumulative frequency curve.

Grain Size and Sorting

There is a strong correlation between median grain size and sorting (Fig. 11.21). The thin-bedded sandstones, lithofacies 2 and 3, are finer grained and better sorted than the thicker-bedded ones, lithofacies 4 and 5. The Massive

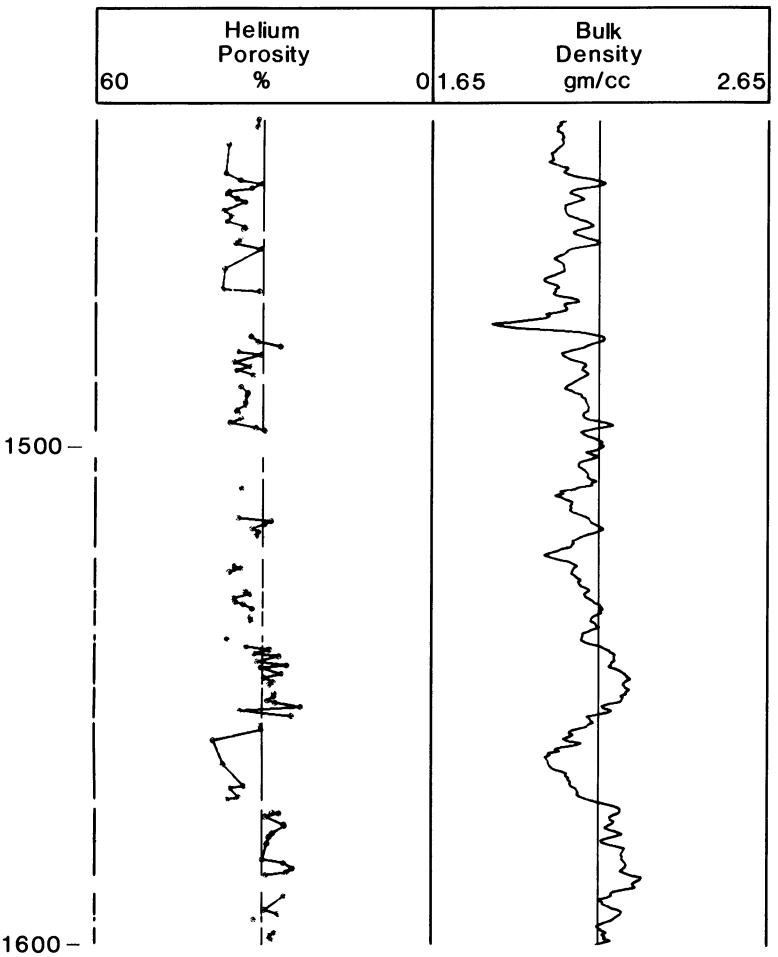

Figure 11.18. Depth plot of helium porosity and the bulk density log over a section of the cored interval. The two curves track each other if overlain.

Sandstones, lithofacies 5, are the coarsest grained and the poorest sorted.

Porosity, Sorting, and Grain Size

Porosity is influenced by sorting but is independent of grain size (Krumbein and Monk, 1942; Beard and Weyl, 1973). The porosity/sorting cross plot (Fig. 11.22A) shows that the highest porosity corresponds with the best sorting (lithofacies 2 and 3), and the lowest porosity with the poorest sorting (lithofacies 5).

Since the BC-403 sandstones also have a strong correlation between grain size and sorting, there is an equally strong correlation between grain size and porosity (Fig. 11.22B). The fine-grained, thin-bedded lithofacies (2 and 3) have the highest porosity. The sample with the highest porosity has a median grain size in the coarse silt range and is from the thinnest-bedded sandstone lithofacies (2).

Permeability, Sorting, and Grain Size

Permeability is influenced by both grain size and sorting (Krumbein and Monk, 1942), and because of this complexity, cross plots of permeability/sorting and permeability/median grain size show a complete lack of correlation (Fig. 11.23A and B). To better analyze the influences of grain size and sorting, porosity/permeability cross plots were made as described below.

Porosity, Permeability, Sorting, and Grain Size

Figure 11.24 is a porosity/permeability cross plot for the 34 sieved samples and has the same degree of scatter as the entire core analysis data set (Fig. 11.20). In Figure 11.25A, each data point in the cross plot is coded with its corresponding median grain size. Distinct boundaries can be drawn between the grain-size classes. For a given grain size,

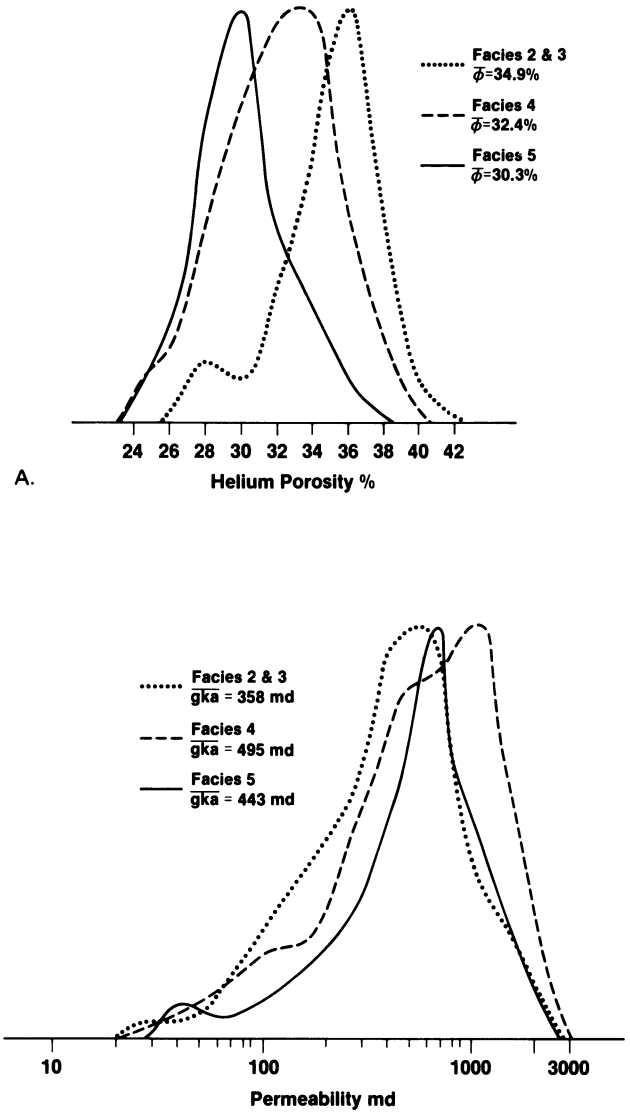

Figure 11.19. Frequency distributions of porosity and permeability data. (A) Porosity, $\bar{\phi}$ = mean porosity. (B) Permeability, $\overline{gka}$ = geometric mean permeability. (For facies numbers, refer to Figure 11.4.)

there is a reasonable correlation between porosity and permeability, and for a given porosity, the highest permeability samples are the coarser sandstones. However, it is also important to note that, for a given permeability, there can be quite a spread of grain size and porosity. For example, there are two sieved samples that have around 500 md permeability. One is a medium-grained sandstone with 27.1% porosity, and one is a coarse silt with 41.6% porosity.

Figure 11.25B is the porosity/permeability cross plot with data points coded according to sorting and with boundaries between the different sorting categories. These boundaries are not as distinct as those for grain size and are perpendicular to them. Of the two samples with around 500 md permeability, one is a moderately well-sorted coarse silt, and the other is a poorly sorted, medium-grained sandstone.

Permeability Prediction

Deriving porosity from logs is generally a fairly straightforward procedure. For example, for the BC-403 well, strong correlation exists between porosity and bulk density. Unfortunately, no log has been designed to measure permeability, and permeability data are essential for reservoir simulation. Most commonly, permeability values are obtained by first deriving porosity from logs, and then estimating permeability from a porosity/permeability correlation. Porosity/permeability correlations as poor as that seen with the BC-403 data (Fig. 11.20) are also quite common, and therefore, predicted permeability values are often flawed. Simple relations between porosity and permeability are the exception rather than the rule and might be found in rocks that have little variation in grain size, sorting, or cementation.

Alternative approaches were used for the BC-403 core. Multiple regression equations were derived to predict permeability from sieve data, combinations of sieve and log data, and finally from log data alone. We also predicted permeability from porosity in order to compare the results with the measured data and with data derived from multiple regression.

Porosities derived from the density log were entered into the porosity/permeability correlation equation to determine a predicted permeability. For the purpose of this publication, these values will be referred to as the transform permeabilities, to distinguish them from permeabilities calculated by other means. Since the porosity/permeability cross plot shows a lot of scatter and the correlation coefficient for the regression is low, it is expected and will be shown that permeability calculated by this method is meaningless.

A multiple regression procedure was used to develop a model for predicting permeability from the electric logs. The goal of regression is to account for changes in a dependent variable, in this case, permeability. If a single independent variable—porosity—fails to account for most of the change, it is reasonable to hypothesize that the dependent variable is influenced by two or more independent variables.

Prediction of permeability from logs is fraught with a number of difficulties. Rock integrity may be altered during coring or plugging. Clay fabric can be destroyed if, for example, the rock has been allowed to dry. If the rock is extremely variable, properties of a plug may not be equivalent

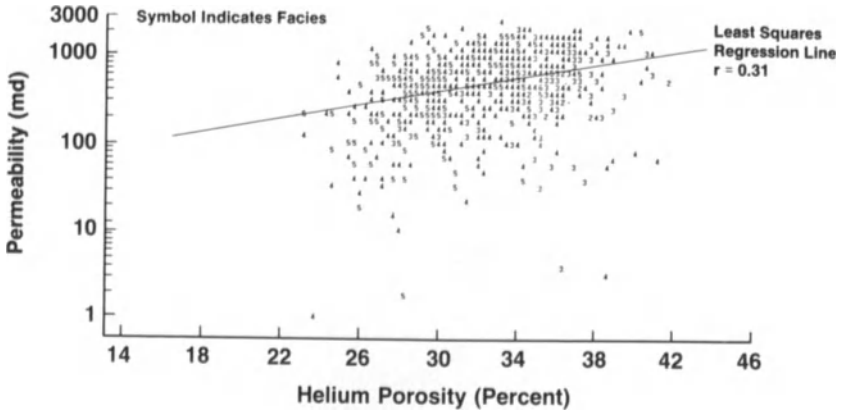

Figure 11.20. Porosity/permeability cross plot showing the least-squares regression line and the very low correlation coefficient (r). Numbers represent the facies for each data point. The data show a great deal of scatter.

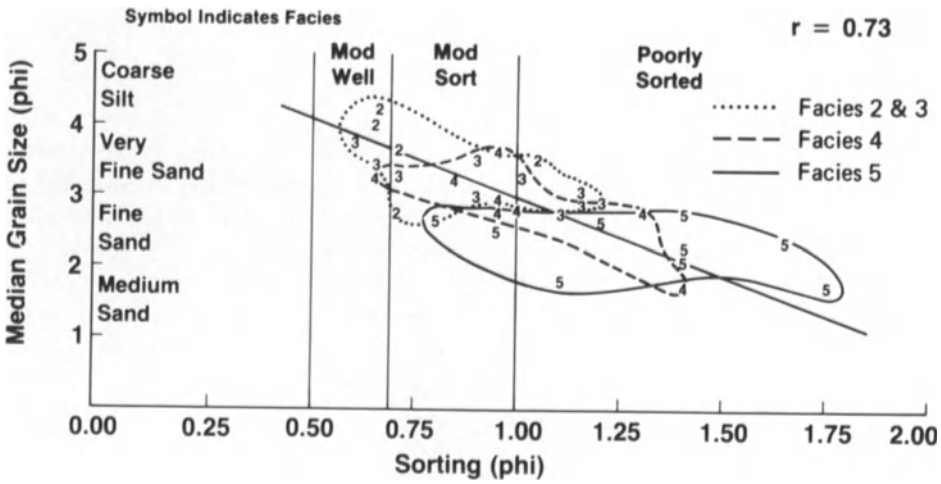

Figure 11.21. Cross plot showing a good correlation between grain size and sorting for the sieved samples. The massive sandstones (facies 5) are the coarsest and poorest sorted.

to average properties of the interval sampled for evaluation. Plug depths may not be accurately reported. Log data may be poor, and they average a greater volume of rock than core plugs. Core-to-log and log-to-log adjustments may not be precise. Furthermore, regression analyses estimate means and reduce the spread of distributions.

In this study, care was taken to ensure that the rock, plugs, adjustments, core analyses, and logs were quality controlled. Details of well-site core handling are given in Gidman et al. (1987). Plug depths were specified to 0.1 ft, and were chosen on the basis of core descriptions. Core-to-log adjustments (247) were made using the core descriptions at a scale of 1:24, and the electromagnetic propagation time (TPL) log trace at the same scale. Log values used in the regressions were hand-picked and quality controlled.

A specific type of multiple regression analysis was used: stepwise regression using the SAS computer software. In the stepwise procedure, the independent variables are brought into the equation one at a time. A threshold significance level is set for the variables being added to the equation. This level is based on the significance of an F-test analysis of covariance. The significance level was set at 0.15.

The independent variables are added by forward selection, provided that they meet the threshold significance level. After a variable is added, the stepwise procedure looks at all independent variables in the model and will reject those that, in the newly formed equation, do not meet the 0.15 significance level for retention. After this check, and necessary deletions, another variable can be added to the model. The process ends when the variables outside the model have an F-statistic significant entry level less than 0.15, or when the variable to be added to the model is the one just deleted from it.

The permeability data are log-normally distributed, and were transformed to a normal distribution by taking their logarithm to the base 10. Stepwise analyses were made with the logarithm of permeability as the dependent variable,

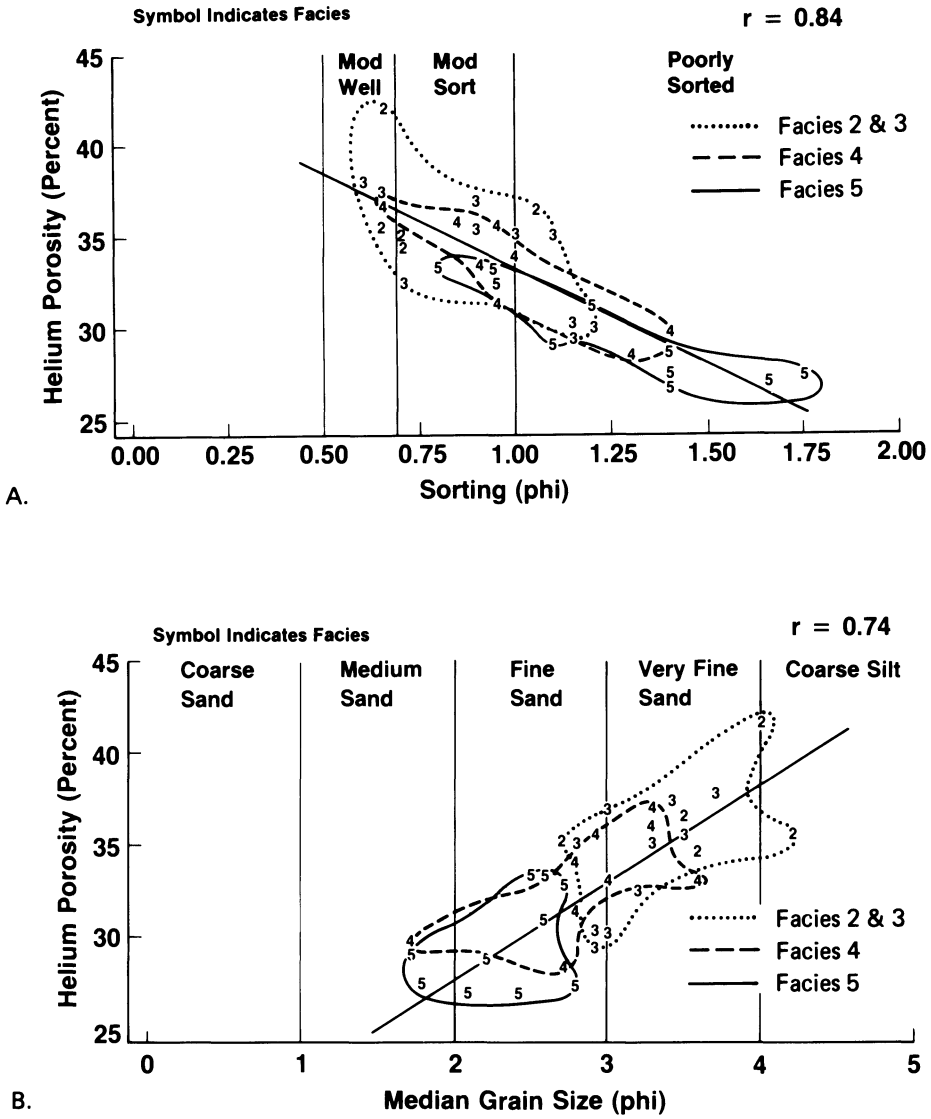

Figure 11.22. Cross plots showing (A) good correlation between helium porosity and sorting, and (B) good correlation between helium porosity and grain size.

and sieve data, combinations of sieve and log data, and log data as the independent variables.

Sieve Data

Variations in grain size and sorting account for the poor correlation between porosity and permeability, and contribute to the spread on the porosity/permeability cross plots.

All of the sieve data variables were considered in the stepwise regression. The results show that permeability can be predicted by an equation that takes into account grain size and sorting, in that the independent variables are the fine (P84), coarse (P5), and median (P50) grain sizes (Table 11.4).

Sieve and Log Data

A correlation matrix was derived to determine those logs that individually show the most significant correlation coefficients against the logarithm of permeability. Based on this, values of the microlaterolog (MSFL), electromagnetic propagation time (TPL), bulk density (RHOB), and gamma ray (GR) were hand-picked for each of the 34 sieved samples. The data were hand-picked to ensure appropriate log values; for example, to avoid spikes in the data. Step-

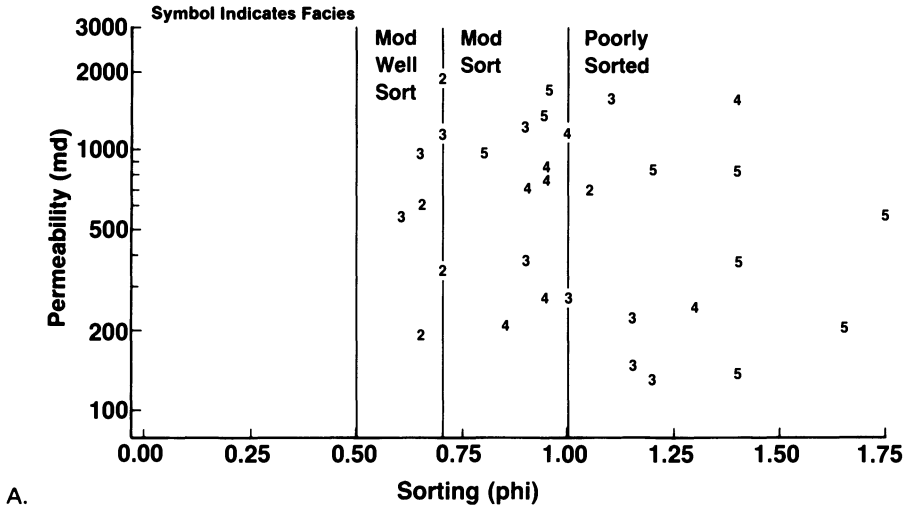

A.

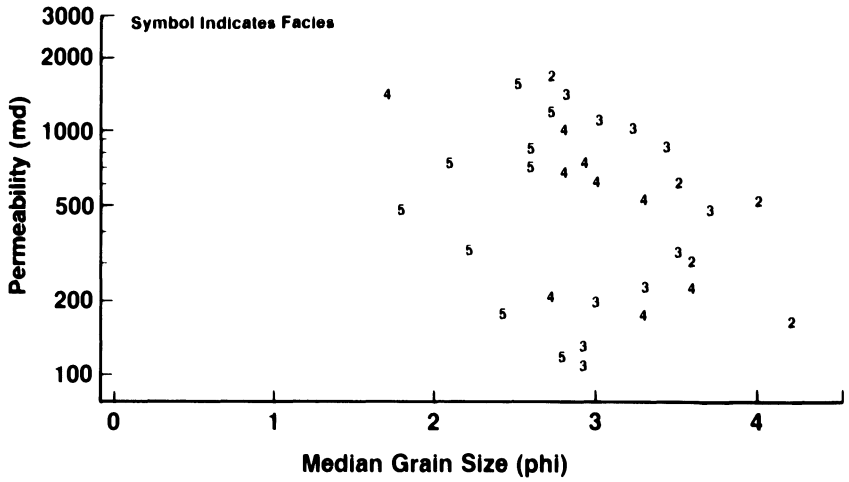

B.

Figure 11.23. Cross plots showing (A) no correlation between permeability and sorting, and (B) no correlation between permeability and grain size.

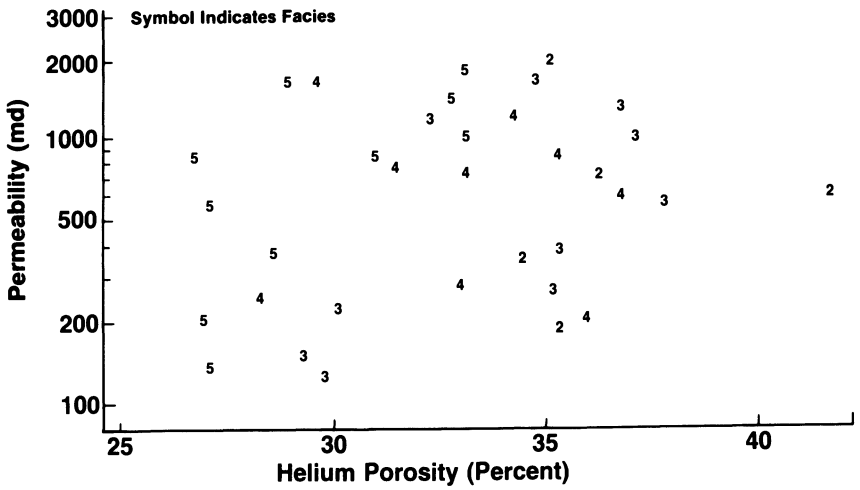

Figure 11.24. Porosity/permeability cross plot of the 34 sieved samples. Sieved samples were chosen to represent the degree of scatter shown by the whole core analysis data set (Fig. 11.19).

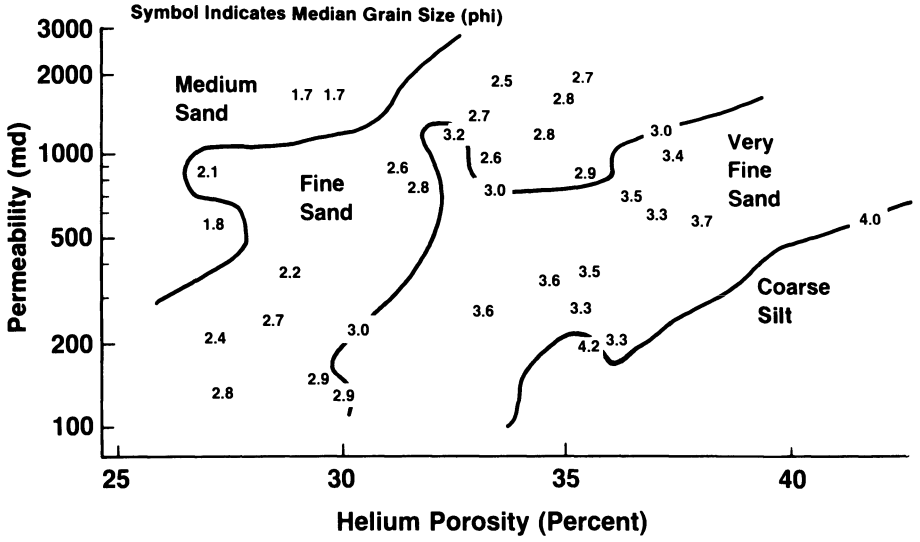

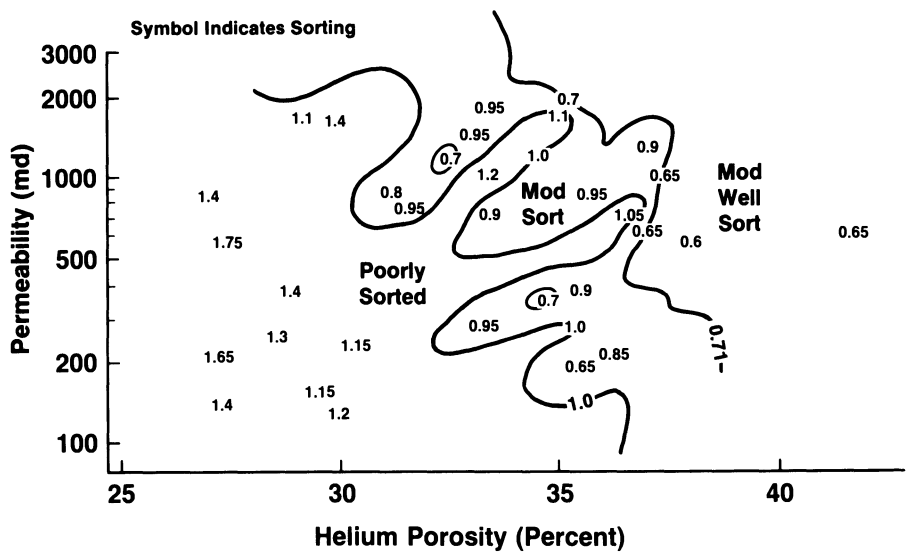

Figure 11.25. Porosity/permeability cross plots of the sieved samples. (A) Boundaries can be drawn between grain-size classes showing that for a given porosity the permeability increases with grain size. (B) Boundaries can be drawn between sorting classes. These are not as distinct as, and are perpendicular to, those shown in (A).

wise regression analyses were made for the sieve/log combinations shown in Table 11.3.

The MSFL and MSFL/GR, in combination with the sieve data, did not improve on the correlation that was based on sieve data alone.

The best correlation is derived from an equation that takes into account the coarse (P5) and fine (P84) sandstone fractions and RHOB. The equation is essentially predicting permeability from sorting (represented by P84 and P5) and porosity (represented by RHOB).

Log Data

The MSFL and TPL logs are recorded with a sample increment of 2 in. (5 cm), whereas the GR and RHOB record values every half foot (0.2 m). The MSFL and TPL were interpolated, so that all of the logs had values at every half foot.

The equation derived from the stepwise regression using these logs is given in Table 11.3. The equation was used to calculate permeability through the entire cored interval, the

Table 11.4. Data summary for stepwise regressions

Independent Variables	Dependent Variable: Logarithm of Permeability Variables in Model	Correlation Coefficient	Regression Equation
Sieve data only	P84 P5 P50	0.85	−1.336(P84) + 0.189(P5) + 0.365(P50) + 6.774
Sieve data + MSFL	P84 P5 P50	0.85	−1.336(P84) + 0.189(P5) + 0.365(P50) + 6.774
Sieve data + MSFL + GR	P84 P5 P50	0.85	−1.336(P84) + 0.189(P5) + 0.365(P50) + 6.774
Sieve data + TPL	P84 P5 TPL P50	0.86	−1.435(P84) + 0.153(P5) + 0.058(TPL) + 0.384(P50) + 6.407
Sieve data + TPL + GR	P84 P5 TPL P50	0.86	−1.435(P84) + 0.153(P5) + 0.058(TPL) + 0.384(P50) + 6.407
Sieve data + RHOB	P84 P5 RHOB	0.90	−0.948(P84) + 0.201(P5) − 2.188(RHOB) + 10.908
Sieve data + RHOB + GR	P84 P5 RHOB	0.90	−0.948(P84) + 0.201(P5) − 2.188(RHOB) + 10.908
Sieve data + all logs	P84 P5 RHOB	0.90	−0.948(P84) + 0.201(P5) − 2.188(RHOB) + 10.908
Logs only (MSFL, RHOB, TPL, GR)	RHOB MSFL GR	0.73	−4.040(RHOB) + 0.065(MSFL) − 0.018(GR) + 12.283

Key: P5, Fifth percentile on sieve analysis cumulative frequency curve (coarse fraction); P50, median grain size; P84, eighty-fourth percentile on sieve analysis cumulative frequency curve (fine fraction); MSFL, microlaterolog; TPL, electromagnetic propagation time; RHOB, bulk density; GR, gamma ray.

result being a permeability log with values at every half foot. The equation was derived from PKS samples, which are sandstones; therefore, the calculated permeability is appropriate only for sandstones. From matching the core descriptions with logs, it is apparent that the easiest and most reliable way to distinguish sandstones from mudstones is based on the MSFL. MSFL readings of 2 ohms or more correspond to sandstones. Depths that have an MSFL value of less than 2 ohms can be eliminated in order to derive a permeability log for sandstones only.

Figure 11.26A shows a cross plot of calculated versus measured permeability. Only PKS samples that fall on the foot or the half foot are represented, since these depths match with a permeability calculated from the logs. The data fall around the x = y line, confirming the ability of the log equation to predict permeability.

Comparison of Permeability Prediction Results

Two means of predicting permeability have been described. The simple porosity/permeability regression predicts what is referred to here as the transform permeability. In addition, the log data have been used in the multiple regression equation to determine what is referred to here as the calculated permeability.

The calculated permeability, plotted against measured values, shows a good distribution of data around the x = y line (Fig. 11.26A). To make a similar comparison, measured porosity data were used in the porosity/permeability regression equation to derive transform permeabilities. These were then plotted against the measured values (Fig. 11.26B). The plot shows a narrow distribution of transform permeability values scattered about 500 md. In other words, regardless of porosity, the transform predicts essentially one permeability: 500 md!

A typical section of the depth plot of measured, calculated, and transform permeabilities is shown in Figure 11.27. The calculated permeability matches well with the measured data, whereas the transform permeability throughout the entire cored interval is 500 md. The multiple regression equation is clearly superior to the porosity/permeability transform as a means of calculating permeability from the BC-403 data.

Conclusions

(1) The thinly interbedded, poorly consolidated sandstones and mudstones that compose the Vickers reservoir zone of Inglewood Field were deposited as part of a deep-sea fan system. Individual beds were deposited by turbidity currents that spread across a relatively flat basin floor. Water depth was estimated from microfossil analysis to be in excess of 6500 ft (2000 m).

(2) Based primarily on the texture and lateral continuity of the beds, the reservoir section is interpreted to have been deposited in the middle to outer portions of depositional lobes, beyond the ends of suprafan channels.

(3) The cyclically alternating thickening- and thinning-upward sequences suggest that fan lobes were built by gradual lateral migration of the lobe depocenter across a relatively small area of the basin floor.

(4) Based on the depositional model, the extensive lateral bed continuity, and negating the influence of any faulting, lateral sweep efficiency should be good, and vertical communication between sandstone beds should be poor.

(5) The sandstones are arkosic arenites, lithic arenites, and arkosic wackes. Well-connected macropores predominate; however, detrital clay reduces reservoir quality

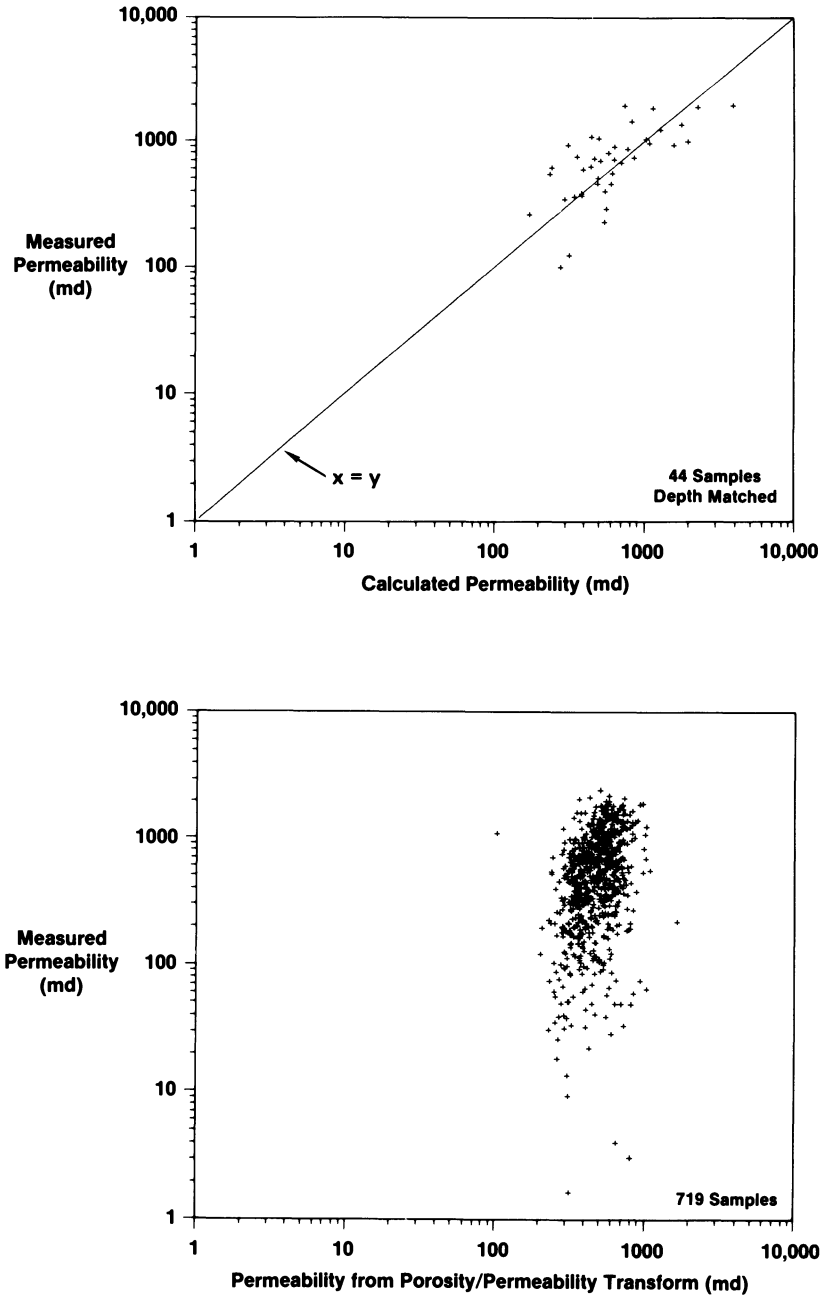

Figure 11.26. Cross plots showing (A) a good correlation between permeability measured from plugs and that calculated from the multiple regression analysis, and (B) poor correlation between permeability measured from plugs and that calculated from the porosity/permeability transform.

(geometric mean permeability of all sandstones sampled is 461 md).

(6) A strong correlation is observed between median grain size and sorting. The thin-bedded sandstones are finer grained and better sorted than the thicker-bedded ones. The massive sandstones are the coarsest grained and the poorest sorted.

(7) Porosity depends on sorting and, indirectly, on grain size, because of the strong correlation between grain size and sorting. Permeability depends on interrelated variables, including porosity, grain size, and sorting. There is no statistically significant linear relation between porosity and permeability as a result of the complex relations between the variables that influence permeability.

(8) A log-derived, multiple linear regression equation was developed to calculate the air permeability of sandstones throughout the reservoir section.

(9) The multiple regression equation is clearly superior to

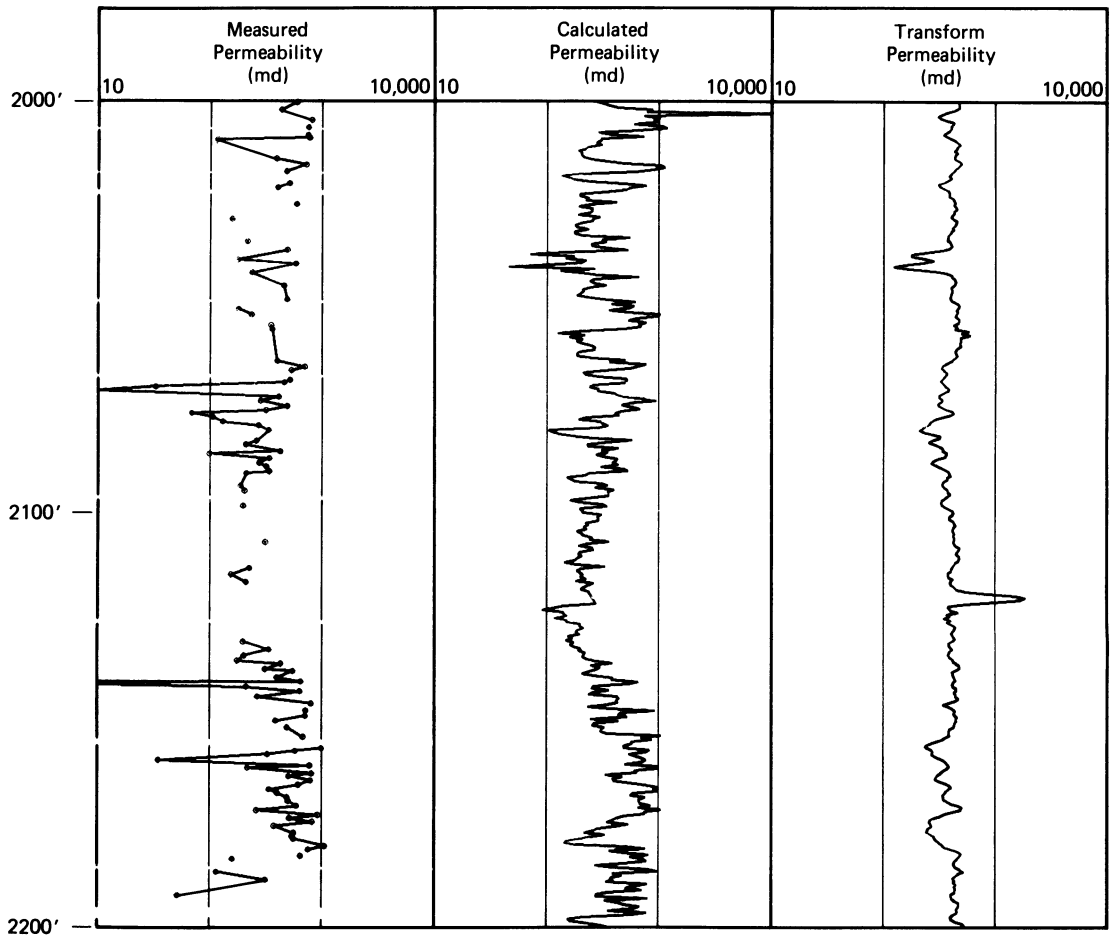

Figure 11.27. Depth plot of permeability over a typical section of the cored interval. Permeability calculated from the multiple regression tracks the measured data. Permeability from the porosity/permeability transform shows little variation, with all values at about 500 md.

the porosity/permeability transform as a means of calculating permeability in the BC-403 well.

Acknowledgments

We thank Chevron U.S.A. and Chevron Oil Field Research Company for permission to publish this paper. We also thank Ken Finger for the biostratigraphic analyses, Joyce Bube and Geology Drafting for work on the figures, and Julie Law for word processing.

References

Bandy, O.L., 1972a, Late Paleogene–Neogene planktonic biostratigraphy and some geologic implications, California, *in* Stinemeyer, E.H., ed., Proceedings of the Pacific Coast Miocene biostratigraphic symposium: Pacific Section, Society of Economic Paleontologists and Mineralogists, p. 37–51.

Bandy, O.L., 1972b, Origin and development of *Globorotalia* (*Turborotalia*) *pachyderma* (Ehrenberg): Micropaleontology, v. 18, no. 3, p. 294–318.

Bandy, O.L., 1972c, Neogene planktonic foraminiferal zones, California, and some geologic implications: Palaeogeography, Palaeoclimatology, Palaeoecology, v. 12, p. 131–150.

Bandy, O.L., Casey, R.E., and Wright, R.C., 1971, Late Neogene planktonic zonation, magnetic reversals, and radiometric dates, Antarctic to the tropics, *in* Reid, J.L., ed., Antarctic oceanology I: Washington, D.C., American Geophysical Union, p. 1–26.

Beard, D.C., and Weyl, P.K., 1973, Influence of texture on porosity and permeability of unconsolidated sand: Am. Assoc. Petrol. Geol. Bull., v. 57, p. 349–369.

Bouma, A.H., 1962, Sedimentology of some flysch deposits: A graphic approach to lithofacies interpretation: Amsterdam, Elsevier, 168 p.

Conrey, B.L., 1967, Early Pliocene sedimentary history of the Los Angeles Basin, California: California Division of Mines and Geology Special Report 93, 63 p.

Folk, R.L., 1974: Petrology of sedimentary rocks: Austin, TX, Hemphill, 182 p.

Frey, R.W., and Pemberton, S.G., 1984, Trace fossils facies models, *in* Walker, R.G., ed., Facies models, 2nd ed.: Geological Association of Canada Reprint Series 1, p. 189–207.

Gidman, J., Worthington, A.E., and Newman, G.H., 1987, Well-site handling of poorly consolidated core, Inglewood Field, Los Angeles: SEG Ann. Conv. Expanded Abstracts, p. 278–280.

Ingle, J.C., Jr., 1967, Foraminiferal biofacies variation and the Miocene-Pliocene boundary in southern California: Bulletins of American Paleontology, v. 52, p. 326–394.

Ingle, J.C., Jr., 1980, Cenozoic paleobathymetry and depositional history of selected sequences within the Southern California continental borderland; Cushman Foundation Spec. Publ. 19, p. 163–195.

Krumbein, W.C., and Monk, G.D., 1942, Permeability as a function of the size parameters of unconsolidated sand: Pet. Tech., AIME Pub. 1492, v. 5, no. 4, p. 153–163.

Mutti, E., and Ricci-Lucchi, F., 1972, Le turbiditi dell'Appennino settentrionale: Introduzione all'analisi di lithofacies; Soc. Geol. Ital. Mem. 11, p. 161–199. (Translation by T.H. Nilsen, 1978, *in* International Geology Review, v. 20, p. 125–166.)

Pettijohn, F.J., Potter, P.E., and Siever, R., 1972, Sand and sandstone: New York, Springer-Verlag, 158 p.

Piper, D.J.W., and Normark, W.R., 1983, Turbidite depositional patterns and flow characteristics, Navy submarine fan, California Borderlands: Sedimentology, v. 30. p. 681–694.

Walker, R.G., 1978, Deep water sandstone lithofacies and ancient submarine fans; Models for exploration for stratigraphic traps: Am. Assoc. Petrol. Geol. Bull., v. 62, p. 932–966.

Wentworth, C.K., 1922, A scale of size and class terms for clastic sediments: J. Geol., v. 30, p. 377–392.

CHAPTER 12

Scales of Geologic Heterogeneity of a Deep-Water Sand Giant Oil Field, Long Beach Unit, Wilmington Field, California

Roger M. Slatt, Sandra Phillips, Jeremy M. Boak, Martin B. Lagoe

Introduction

Deep-water sands form economically important hydrocarbon reservoirs in many parts of the world. Although they have been studied extensively from a traditional, somewhat qualitative perspective, quantitative reservoir characteristics are poorly understood, and often are not described in a format suitable for reservoir engineering applications. Like other types of sands, heterogeneities of deep-water sand reservoirs can be described at four scales (terminology after Krause et al., 1987): **microscale** (grains and pores), **mesoscale** (near well bore), **macroscale** (interwell), and **megascale** (field-size).

In this paper, the Long Beach Unit, which constitutes the southeastern part of the giant Wilmington Oil Field, Los Angeles basin, California (Figs. 12.1 and 12.2) is described in terms of these four scales of heterogeneity. The data set centers around detailed analysis of six long cores totalling over 5000 ft (1500 m) (Fig. 12.2), coupled with detailed well-log cross sections and isopachs.

The objective of the study was to evaluate the degree to which quantitative assessment can be made of geologic and reservoir parameters at each of the four scales, and the level of confidence that should be placed upon such assessments. In any producing oil or gas field, this knowledge can lead to improved reservoir management.

Regional Geology, Stratigraphy, and Structural History

The Wilmington Field is located in the southwestern part of the Los Angeles Basin, on the eastern end of a faulted asymmetric anticlinal crest (Figs. 12.2 and 12.3). The field is approximately 11 mi (18 km) long and 3 mi (4.9 km) wide, and encompasses 13,500 acres (Mayuga, 1970). The Wilmington Field was discovered in 1936, and development in the Long Beach Unit began in 1965.

Total original oil in place for the Long Beach Unit has been estimated at 3.8 billion barrels, of which 645 million barrels had been produced as of June, 1987 (Berman and Clarke, 1987). Production in the unit, as well as the entire Wilmington Field, comes from Mio-Pliocene sands, which are generally considered to have been deposited in a deep-water setting as a succession of sediment gravity-flow deposits (Slatt et al., 1988).

Los Angeles Basin

The middle Miocene to Recent Los Angeles basin consists of both the present-day northwesterly trending coastal lowland and the older depositional basin, which extended from the San Gabriel and San Bernardino Mountains to the Pacific Ocean, and from Santa Monica Bay to the Peninsular Ranges (Yerkes et al., 1965; Henry, 1987). It lies at the northern end of the northwest-trending Peninsular Ranges physiographic province, where it abuts the east-west-trending Transverse Ranges province. The structural complexity of the basin results in part from the interaction of the predominant tectonic trends of these two provinces. The interaction is in turn guided by the complicated history of plate motions along the western edge of North America.

The depositional basin resembled basins along the tectonically complex present-day California borderland, just offshore of the portion of California that lies west of the San Andreas Fault, on the Pacific Plate. The borderlands are

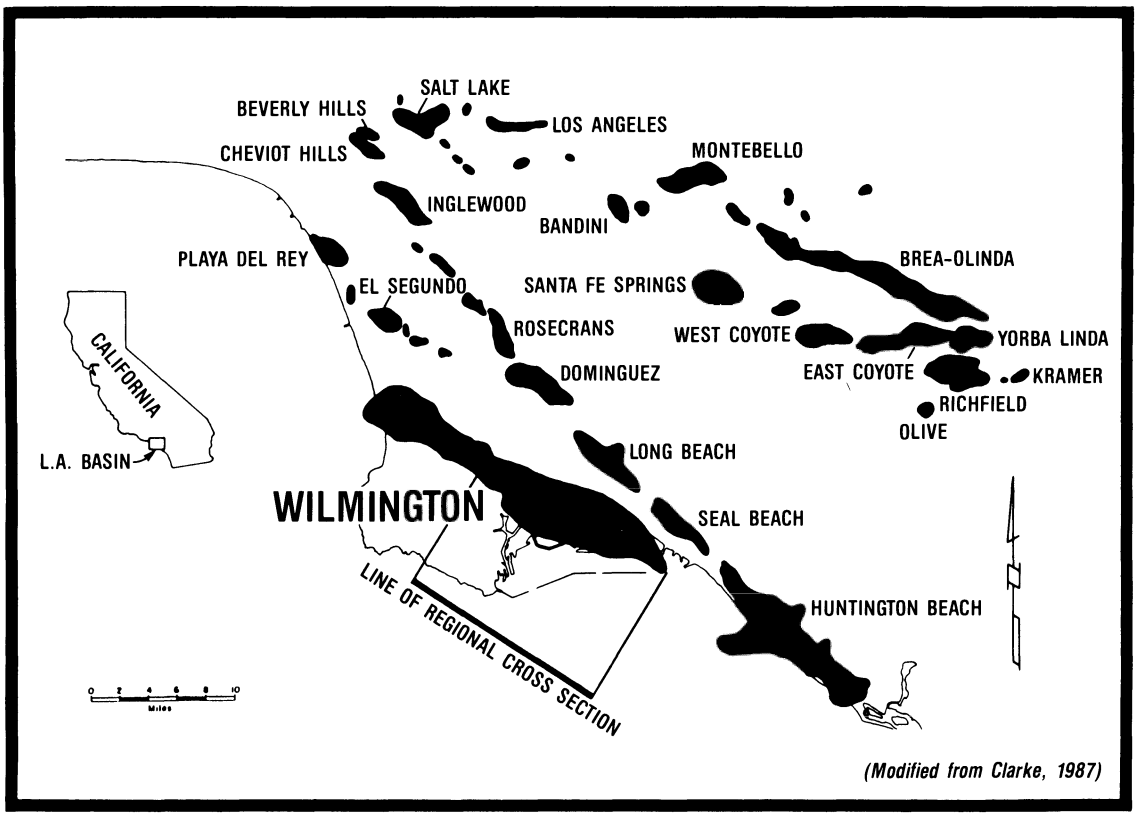

Figure 12.1. Los Angeles Basin oil fields. (After Clarke, 1987. Reprinted by permission.) Line of cross section in Figure 12.3 is shown.

characterized by small, deep basins separated by sills produced commonly by deformation along a series of transcurrent fault zones paralleling the plate margin. These basins step progressively outward and downward to the oceanic crust. During its maximum extent in the middle and upper Miocene, the Los Angeles basin was approximately 45 mi (74 km) wide and 65 mi (105 km) long (Henry, 1987), and was probably continuous with the contemporaneous Ventura Basin to the northwest (Yerkes et al., 1965).

At the time of deposition of the upper Miocene and lower Pliocene sands discussed in this paper, the basin was characterized by a narrow shelf to the northeast (Fig. 12.4) (Henry, 1987). Sediments that make up the Long Beach Unit were deposited 20 to 30 mi (33 to 49 km) seaward of the shelf, in a broad, northwest-trending deep basin. Whether or not the submarine slope was steep is questionable. The producing intervals in the Santa Fe Springs field (Fig. 12.4) (~10 mi from the shelf edge) are interpreted by Morrissey and Hickey (1988) to have been deposited in mid-fan channels of a submarine fan system. If these channels are related to fans in the Wilmington area, then the slope would probably have been steep. It is not possible to demonstrate connection between these two fan systems due to the lack of drilling data in the center of the basin. Alternatively, Lyons and Suchecki (1989) have suggested that Miocene deposition in the vicinity of the Puente Hills (Fig. 12.4) occurred in a submarine-ramp setting. If these deposits are related to Wilmington Field sediments, then a shallow-gradient slope may have prevailed, at least during Miocene deposition in the Long Beach Unit.

The western edge of the basin is not well defined. The eastern shelf edge appears to have been located farther to the southwest in Pliocene time than in the latest Miocene, and a marine shelf may have existed in the vicinity of the Palos Verdes Hills (Fig. 12.4) (Henry, 1987). As discussed in this paper, all of the rocks were deposited within the deep marine part of the basin, and remained deeply submerged throughout the Miocene and Pliocene. This is at variance with subaerial erosion proposed by Truex (1974).

Wilmington Structure

Mayuga (1970), Truex (1974), and Clarke (1987) discussed the structural evolution of the Wilmington Field. Truex (1974) suggested that the Wilmington structure was related to the Newport-Inglewood fault zone to the northwest and

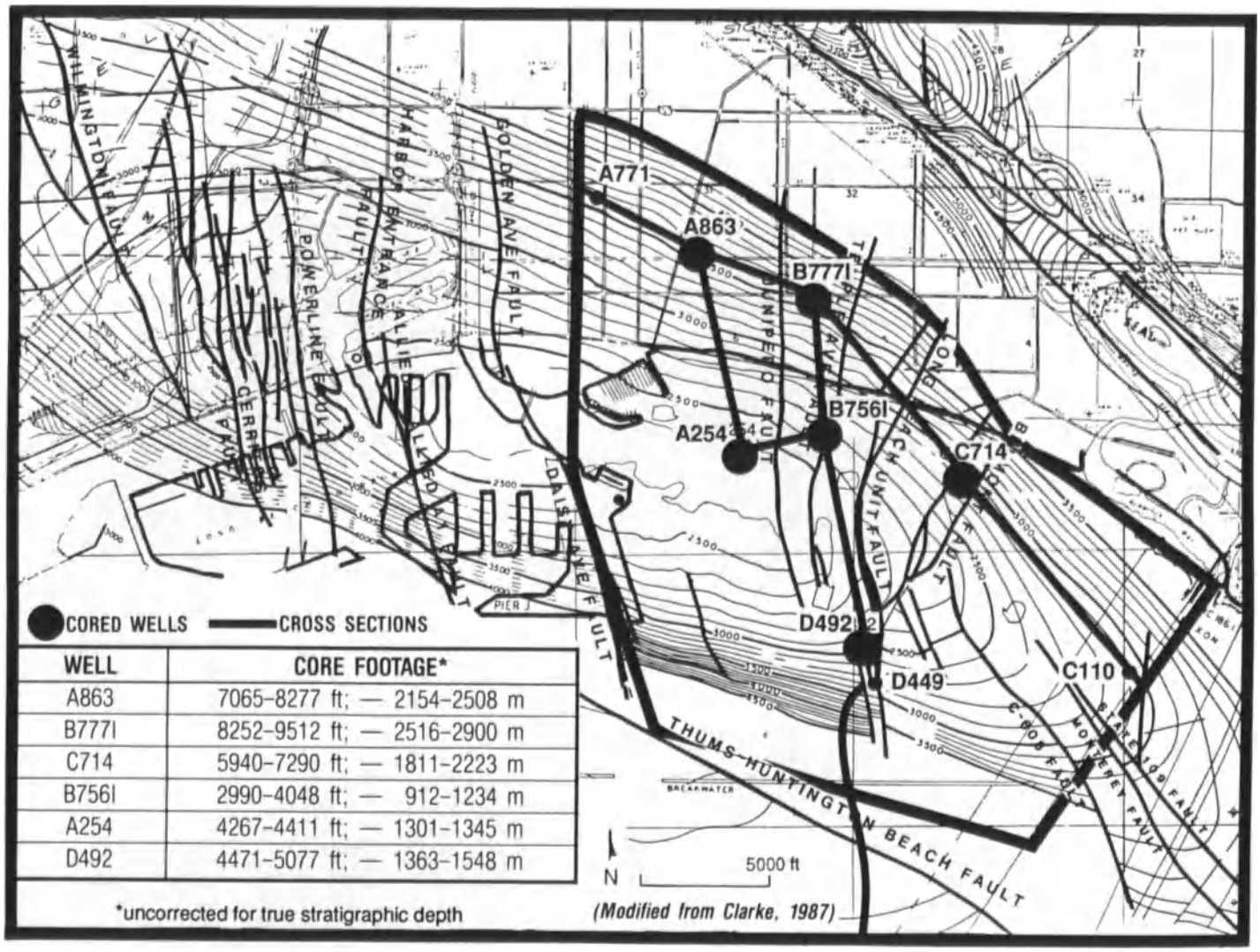

Figure 12.2 Structure and major faults of the Wilmington Oil Field (modified from Clarke, 1987 Reprinted by permission.). Long Beach Unit is outlined in heaviest line. Shoreline is shown by thick line. Location of cored wells and footages (inset table) are shown along with regional (Figs. 15 and 20) and detailed (Fig. 12.16) cross sections and outline for grid for detailed isopachs (Fig. 12.17).

the THUMS–Huntington Beach fault to the southwest. Clarke (1987) suggests that the entire 22-mi-long (36 km) Torrance-Wilmington structural trend results from wrench folding involving these faults and also the Palos Verdes fault, which occurs to the southwest. The Newport-Inglewood fault zone is a major zone of deformation that also separates two distinctly different basement types in the Los Angeles Basin (Yerkes et al., 1965). The fault is active at present, as indicated by the prominent line of hills (and oil fields) that marks its trace. The Palos Verdes fault is a reverse fault (Yerkes et al., 1965) and remains active today (Clarke, 1987).

The numerous normal faults that commonly form en echelon sets cutting the Torrance-Wilmington structure, are interpreted as cross faults in this wrench system (Clarke, 1987) (Figs. 12.2 and 12.3). The largest of these is the Long Beach fault, with offset of approximately 400 ft (133 m) (Clarke, 1987). Folding and faulting are interpreted to have occurred at various intervals in the history of the area (Truex, 1974). The episode of folding responsible for the current Wilmington structure occurred during early Pliocene time (Truex, 1974).

The Wilmington structure was planed off by a mid-Pliocene unconformity, and sediments above this level have not been folded (Fig. 12.3). The only fault that crosses this unconformity is the Long Beach Unit fault (Truex, 1974; Clarke, 1987a). Seaward tilting is the only evidence of the regionally extensive Pleistocene Pasadenan orogeny (Yerkes et al., 1965; Henry, 1987). Thus, the Wilmington Field structure is masked, unlike structures in the group of

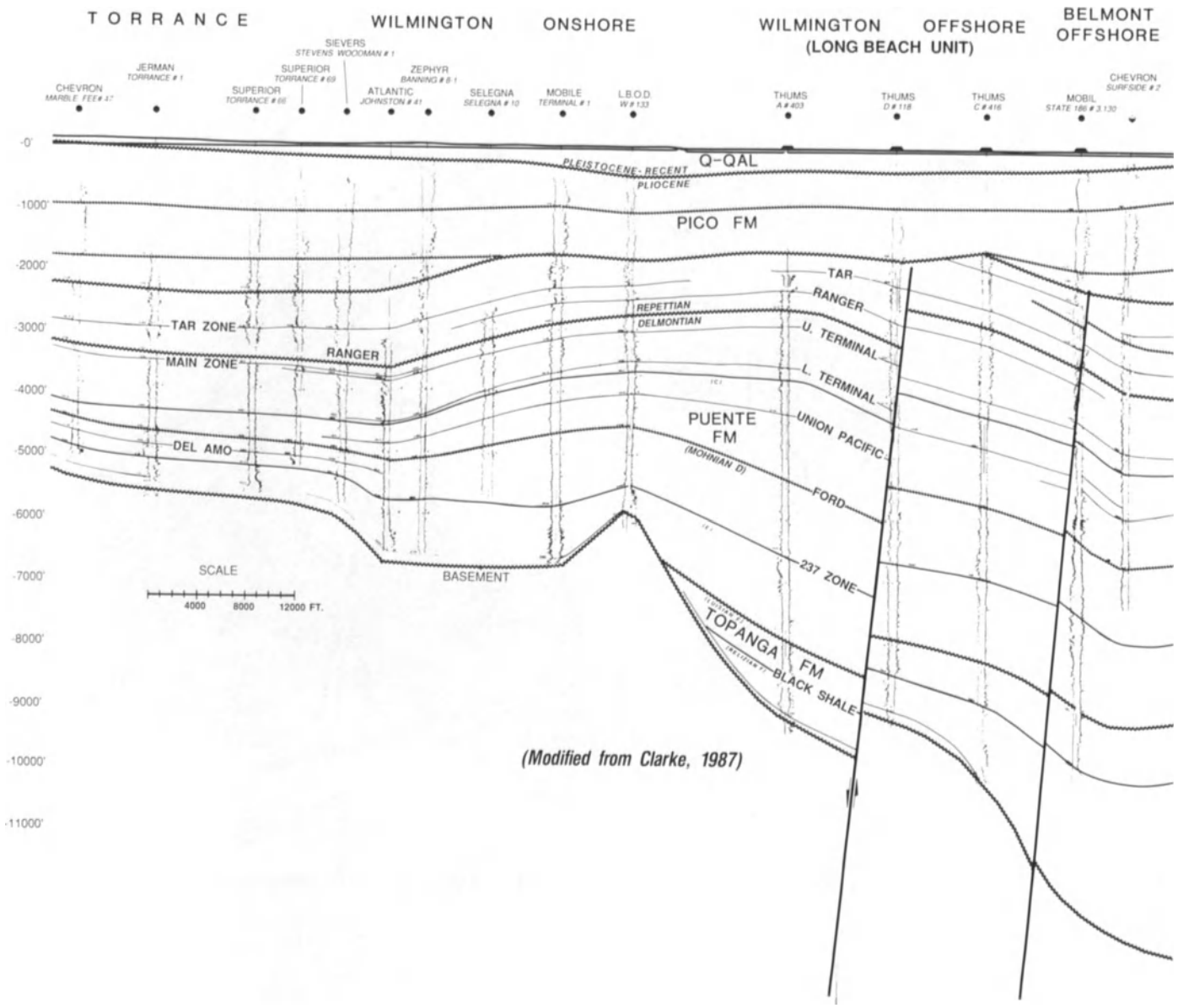

Figure 12.3 Regional stratigraphic cross section of the Wilmington Oil Field and adjacent areas. (Modified from Clarke, 1987. Reprinted by permission.) Major unconformities are illustrated by wavy lines. Locations of the cross section is shown in Figure 12.1.

oil fields above the Newport-Inglewood fault zone, indicating that recent deformation along the zone is areally restricted.

Stratigraphic/Geologic History

Various aspects of the general geology of Wilmington Field and the Long Beach Unit have been published by Mayuga (1970), Clarke (1987), Henderson (1987), and Slatt et al., (1988). The basement in the Wilmington field consists of the Catalina schist (Yerkes et al., 1965) (Fig. 12.3). The oldest sediments deposited upon the Catalina schist are middle Miocene conglomerates/breccias. These are followed by phosphatic shales, sandstones, cherts, limestones, and bentonites, which are correlative with the Altamira Shale member of the Monterey Fm (Truex, 1974; Randall, et al., 1983) and which have been considered to be comparable to some parts of the Topanga Formation (Henry, 1987). During late Miocene time, submarine-fan systems developed at bathyal depths, and in the area of the Wilmington Field, progressively sandier turbidites of the Puente Formation were deposited throughout Mohnian and Delmontian time (Fig. 12.3). Turbidite sedimenta-

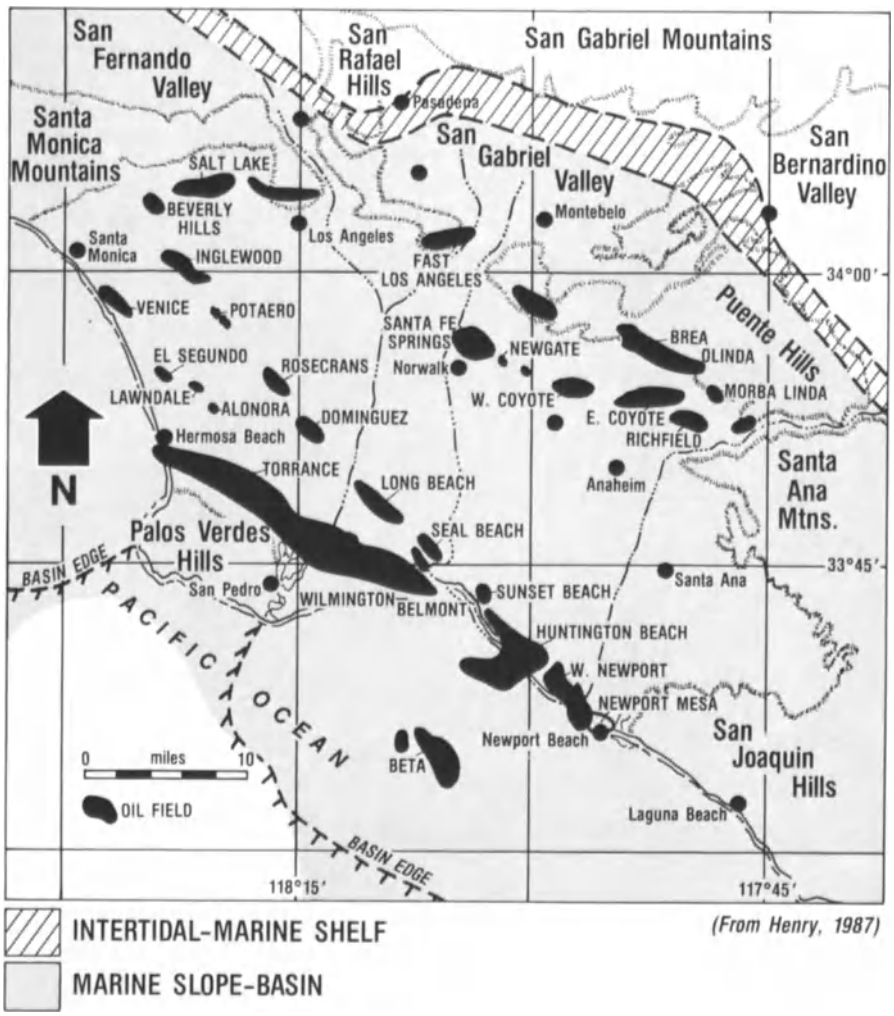

Figure 12.4 Regional paleogeography in the Los Angeles Basin during upper Miocene time. (After Henry, 1987. Reprinted by permission.)

tion continued in the early Pliocene with deposition of the lower Pico Formation (formerly the Repetto Formation). Reservoir sands of the upper part of the Long Beach Unit were deposited at this time. Similar turbiditic sands from higher in this formation form the reservoirs of the Inglewood Field (Schweller et al., 1988).

In part of the Los Angeles basin, the base of the Repettian section of early Pliocene age overlies a Pliocene unconformity (Fig. 12.3). In the Long Beach Unit, evidence for this unconformity is ambiguous, as discussed in a later section; however, a mid-Pliocene unconformity truncates the Wilmington anticline (Fig. 12.3).

Unitized Formations and Subzones

Subdivision of stratigraphic units within the Wilmington Field has been largely controlled by operational considerations. There are seven unitized zones in the Long Beach Unit, termed, in ascending order, the 237, Ford, Union Pacific, Lower Terminal, Upper Terminal, Ranger (Lower and Upper), and Tar (Figs. 12.3 and 12.5); each is named in some way from the wells that discovered the productive sands. This paper focuses on the Ranger unitized zone, which is the most hydrocarbon-productive interval in the Long Beach Unit.

Operational considerations have necessitated formal subdivision of these unitized zones. The relation between Los Angeles basin formation names, California foraminiferal stages, Wilmington Field unitized formation (= Zone) names, and field subzone markers is summarized in Figure 12.5, with the ages of the formations shown at the left. The Miocene/Pliocene boundary in the Los Angeles basin was formerly thought to occur at the Repettian/Delmontian stage boundary, but is now interpreted to be above that boundary. Subzone boundaries are generally picked at the top of prominent producing sands, however, some subzone boundaries have been picked at the base of producing sands. The nine original subzones of the Ranger Zone are termed the F1, F0, F, H, X, G, G4, G5, and G6 (Fig. 12.5).

Epoch (Stage)	Formation	Zone	Subzones
Pleistocene	San Pedro		
Upper Pliocene	Upper Pico		JF, KF
Lower Pliocene (Repettian)	Lower Pico (Repetto)		
		Tar	So, S, T, U, DU
		Upper Ranger	F1, F0, F, H, X
		Lower Ranger	G, G4, G5, G6
Miocene/ Pliocene (Mohnian/ Delmontian)	Puente	Upper Terminal	HX1,HX0,HX,HXb, HXc,J,Y,Y4,K,Z,W A
		Lower Terminal	AA, AB, AC, AD, ADI
		Union Pacific	AE, AF, AI, AK1, AK,AL1, AM
		Ford	AO, AOI, AR, AR1 AU, AU2, AV, AX, AY,AY1, AZ
		237	BA, BB, BC
Middle Miocene	Monterey		
?	Catalina Schist		

Figure 12.5 Stratigraphic intervals, zones, and subzones in Long Beach Unit.

Other subzones have since been added to account for: (1) previously insignificant sand that has been found to thicken into a major reservoir, (2) sands miscorrelated across faults, and (3) occurrences where multiple oil-water contacts indicate separation of the reservoir sands. At this time, more than 70 subzone markers have been picked.

Biostratigraphy

Benthic and planktic foraminifera distributions have been examined in detail from cores from wells A863 (31 samples), C714 (24 samples), B756I (25 samples), and B777I (21 samples) and in less detail from cores from the other two wells (Fig. 12.2). The succession of foraminiferal faunas is similar in all the wells (Fig. 12.6). Three major biostratigraphic units are recognized in the Ranger Zone. The lowermost unit occurs in the Puente Formation and is characterized by an assemblage that is diagnostic of the Delmontian Stage (Kleinpell, 1938, 1980) (Fig. 12.6). In the Los Angeles Basin, this stage is correlated to the upper *Nitzchia reinholdi* and lower *Thalassiosira oestrupil* zones, yielding a numerical age of ca. 4–6 Ma by calibration to the paleomagnetic time scale (Barron, 1986). The benthic foraminiferal fauna from this interval is indicative of upper middle bathyal (1500–4500 ft, 155–465 m) water depths (all paleobathymetries are estimated using the biofacies model of Ingle, 1980). This Delmontian fauna is similar to late Miocene benthic foraminiferal assemblages in the San Joaquin basin that appear to represent deposition under low oxygen conditions (Lagoe, 1987).

Overlying the Delmontian fauna is a relatively thin "foram-poor interval" containing few foraminifera but common siliceous microfossils (primarily radiolaria and sponge spicules in the >150-μm size fraction) (Fig. 12.6). This foraminiferal fauna is not recognized to be diagnostic of either the Delmontian or Repettian Stage. It is included in the Puente Formation because it may correlate to the "diatomite" at the top of the Puente Formation, which was formerly exposed in the downtown Los Angeles area (Soper and Grant, 1932).

The uppermost unit is in the basal Pico Formation and contains a diverse fauna typical of the Repettian Stage (Natland, 1952) (Fig. 12.6). This fauna reflects lower middle bathyal water depths (4500–6000 ft, 1400–1860 m) during deposition of the basal Pico Formation.

To summarize, the major paleoenvironmental trend was an increase in water depth from the Delmontian into the Repettian, from upper middle bathyal to lower middle bathyal. In addition, the Delmontian fauna appear to represent lower oxygen conditions in comparison with the high diversity Repettian faunas.

The "foram-poor interval" is enigmatic. It is present in all of the wells studied (Fig. 12.7), and is on the order of 50–100 ft (16–33 m) thick. The interval represents a bottom-water event in the Los Angeles Basin, during which there was increased carbonate dissolution. Keller and Barron (1983) identify several Neogene hiatuses in the deep sea that involve carbonate dissolution. Their hiatus NH7 (encompassing the period 4.7 to 5.2 Ma) may correlate to the "foram-poor interval" within the Ranger Zone. This carbonate dissolution would be linked to climatic cooling and the introduction of cold, carbonate-corrosive bottom water into the Los Angeles basin.

Samples from the "foram-poor interval" and adjacent strata from the B756I well were analyzed for siliceous

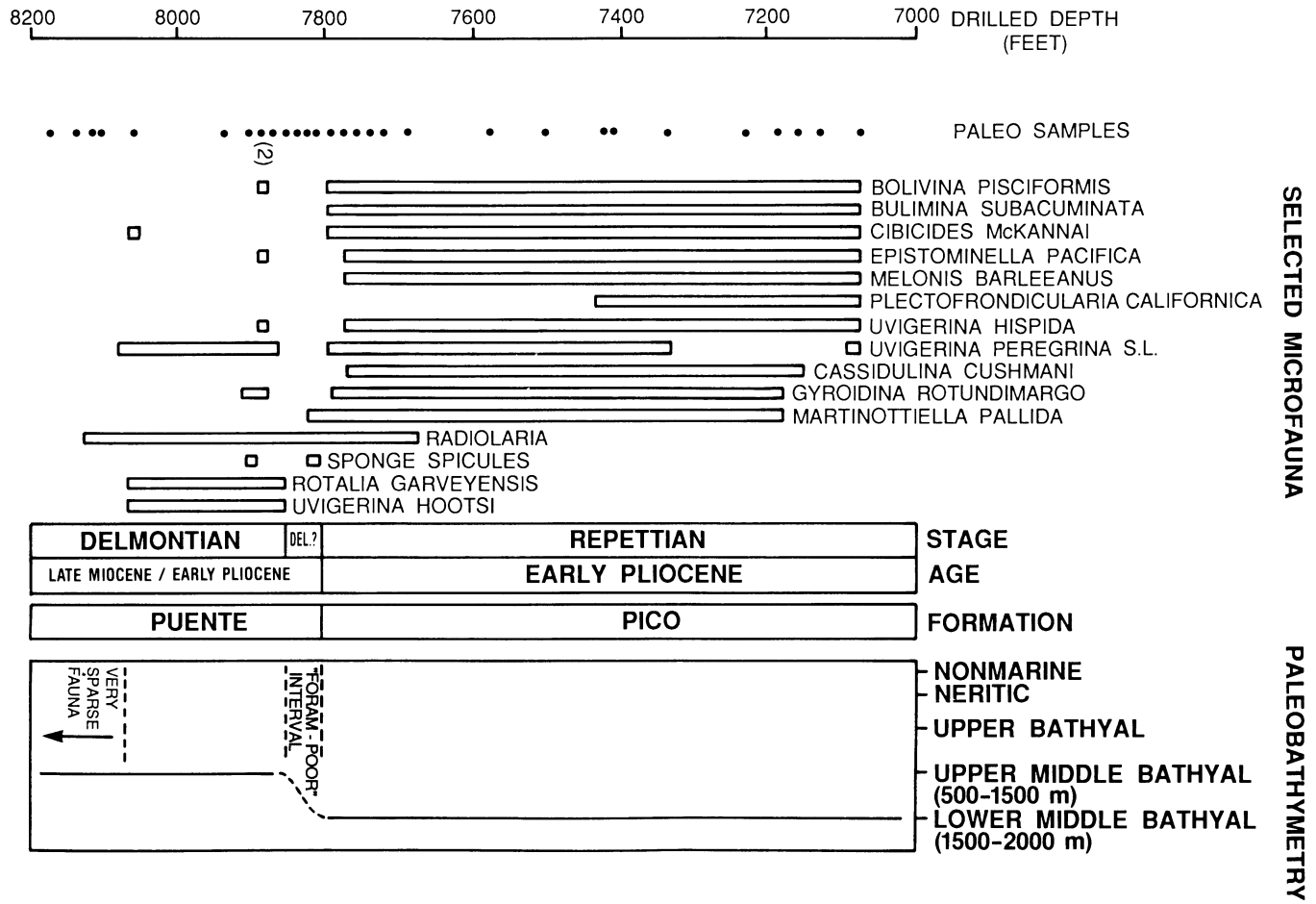

Figure 12.6 Biostratigraphy and paleoenvironments of the cored interval in Well A863. (Modified from Slatt et al. 1988.)

microfossils in order to better constrain the possible correlation with hiatus NH7. Results (S.A. Kling, personal communication, 1988) indicate that the "foram-poor interval" contains Pliocene radiolaria and fragmentary diatoms. A sample from just below the "foram-poor interval" (3691.5 ft in the B756I well) contains a diatom flora diagnostic of the lowermost *T. oestrupii* zone of Barron (1986), just above the Miocene/Pliocene boundary. An age of about 5 Ma is indicated by these data, supporting a correlation of the "foram-poor interval" with hiatus NH7.

Microscale and Mesoscale Heterogeneities

Microscale and **mesoscale** heterogeneities are the easiest to quantify, because they can be measured directly from cores and indirectly from wireline logs. **Microscale** heterogeneities include grain size, sorting, porosity, and permeability (Krause, et al., 1987). **Mesoscale** heterogeneities include lithology, lamination and bedding style, sedimentary structures, facies, stratification sequences, and flow units. These characteristics are treated together in this section in order to illustrate a progression of

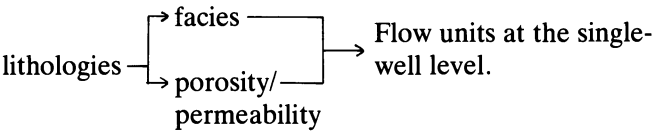

Lithologies

Based on detailed core description, three major lithologies were found to make up the Ranger Zone: massive sand, graded sand, and shale. Several less common lithologies are also present. Individual lithologies are described below and are discussed in more detail by Slatt et al., (1988). Although the cores were unslabbed because they are unconsolidated sand, the core surface was scraped with a knife so that sedimentary textures and structures could be examined.

Massive Sand is fine to medium grained, moderately to

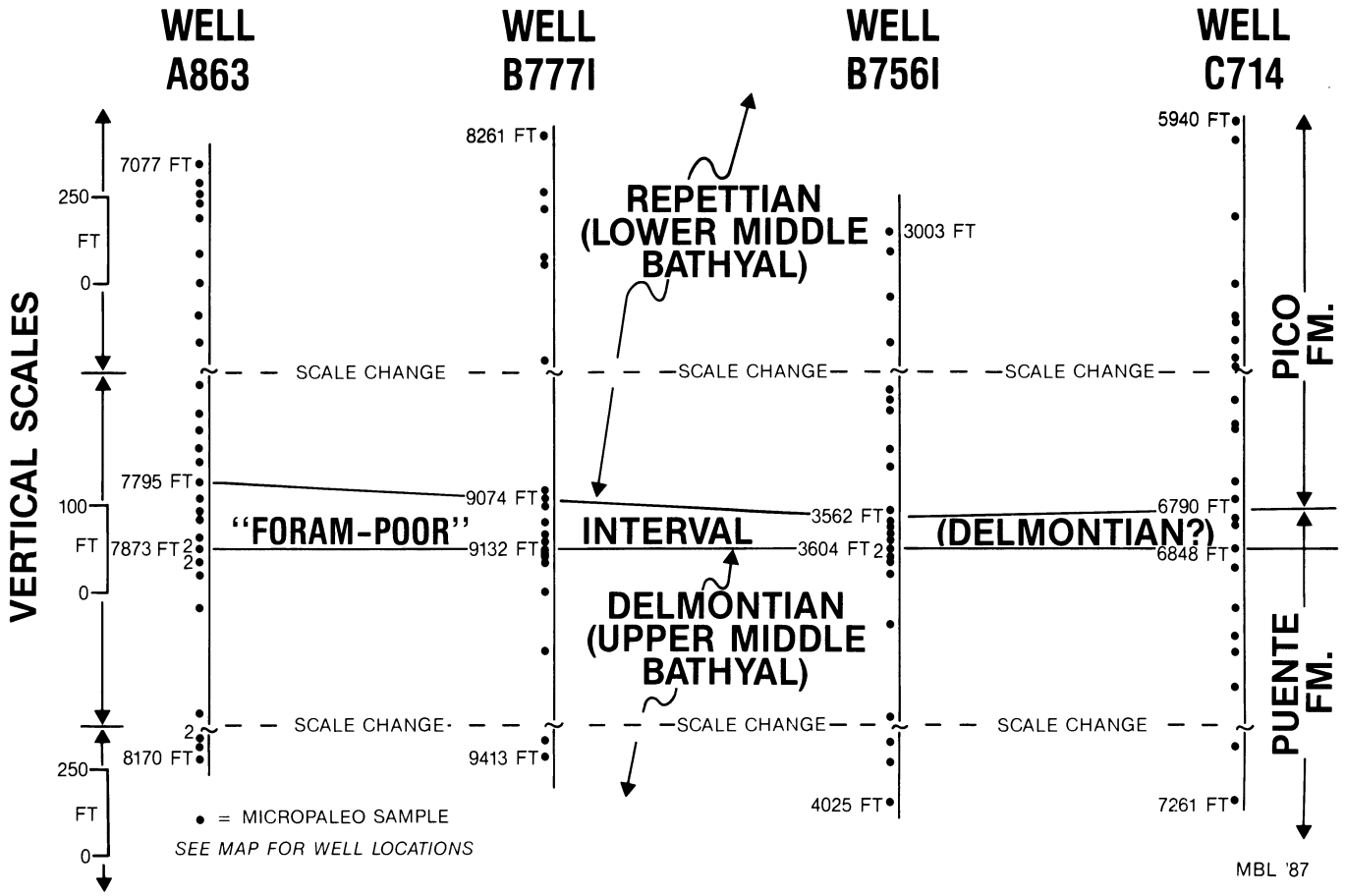

Figure 12.7 Regional biostratigraphy and paleoenvironments. Well locations are shown in Fig. 12.2.

poorly sorted, and shows very little vertical variation in grain size. The sand is unconsolidated except for occasional zones that are cemented with calcite. Individual beds range in thickness from 0.1 to 10+ ft (0.03 to 3+ m) and are normally separated by shale beds. Sand beds may be amalgamated and exhibit erosive bases; however, these features are difficult to recognize owing to the overall uniform nature of the grain size. Fluid escape structures, mainly dish structures, are preserved in some beds. It is possible that sedimentary structures are more common, but cannot be seen because of the unconsolidated nature of the sand, and in many parts of the cores, to the presence of oil stain. This sand tends to be somewhat coarser grained in the upper Ranger zone than in the lower Ranger zone.

Graded Sand is mainly fine- to medium-grained, (although rounded pebbles and shale clasts up to 20 mm in diameter are present in some beds), moderately to poorly sorted, 0.1–20 ft (0.03–6.1 m) thick, and separated by shale beds. Normal grading is subtle but obvious in most beds, and some beds appear to be inversely graded. Amalgamated beds are common, although they are often difficult to recognize. Most beds consist mainly of thin Bouma A graded intervals (Ta), although many are capped by thin Bouma B and/or C intervals (Tab or Tabc), and a few beds lack the Bouma A interval (Tb or Tbc). The bases of beds are generally sharp or erosive. This facies occurs throughout the Ranger Zone where cored, but tends to be thicker and coarser grained in the upper Ranger.

Miscellaneous Sands that do not readily fit into the above categories were observed in core. These beds, which make up only a small percentage of the total beds, are: (1) massive, muddy sand beds, which tend to be <1 ft (<0.3 m) thick; (2) sand and shale that are interlaminated at a centimeter scale; (3) burrowed or convoluted, fine- to very fine-grained sand beds up to about 3 ft (0.9 m) thick, which may contain shale clasts and variable mud content; (4) cross-laminated fine sand beds up to 2 ft (0.6 m) thick; (5) aggregates of sand grains in a micaceous muddy matrix (probably fault gauge) forming beds <1 ft (<0.3 m) thick; (6) shale-clast conglomerates with individual clasts ranging up to 60 mm in diameter in a muddy sandy matrix, and (7) fine- to medium-grained sand beds with coal-clast/fragment ("coffee-ground") laminae.

Shale, as used here, denotes a major class of fine-grained

clastic rocks (Potter et al, 1980). The component rock types within this class that are present in Long Beach Unit cores are dark brown to greenish black siltstone, mudstone, and claystone (see classification of Potter et al., 1980, pg. 14, for definitions).

Siltstone beds, ranging up to 10 ft (3 m) thick, are typically burrowed, not well-indurated, and occasionally contain laminated or thinly bedded sands. Mudstone (silt-clay admixture) is the most common type of shale in the cores. Beds, up to tens of feet thick, are slightly to moderately fissile. Claystone is much less common in the cored wells. It is characteristically very well indurated and massive and forms beds up to approximately 15 ft (4.6 m) in thickness.

Carbonate mudstone, in beds up to 4 ft (1.2 m) thick, is occasionally interbedded with siltstone and mudstone beds. These beds are mainly well-indurated, finely crystalline, impure dolomitic mudstone, but rarely the carbonate beds are impure limestone.

Diatomite beds occur occasionally within shale sections. These beds are finely (millimeter scale) laminated; laminae are generally parallel, but occasionally are convoluted.

Lithofacies

Figure 12.8 illustrates the frequency distribution of sand bed thicknesses. Mean sand bed thickness equals 2.0 ft (0.67 m), and there is a population break at about this thickness. On the basis of bed thickness, in addition to style of interbedding, the above lithologies are grouped into three major lithofacies: Thick-Bedded Sand Facies, Thin-Bedded Sand Facies, and Shale Facies.

Thick-Bedded Sand Facies (Fig. 12.9) consists of individual sand beds, generally from 2 ft (0.67 m) to 15 ft (4.5 m) thick, which are either amalgamated or separated by thin mudstones. Average sand bed thickness is 3.8 ft (1.1 m). Most of these sands are normally graded, but massive sands also occur.

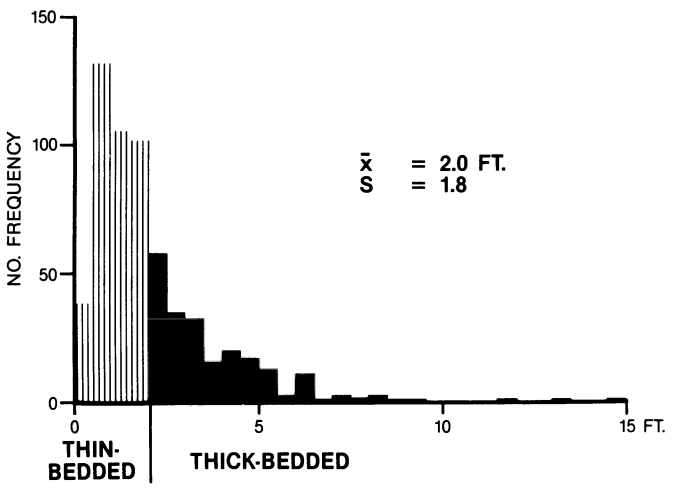

Figure 12.8 Frequency distribution of true stratigraphic thickness of Ranger Zone sands. Subdivision into *Thick-Bedded* and *Thin-Bedded Sand* is at 2 ft (0.67 m).

Thin-Bedded Sand Facies (Fig. 12.10) consists of individual sand beds up to 2 ft (0.67 m) thick that are arranged in stratigraphic intervals interbedded with mudstone. Average sand bed thickness is 1.1 ft (0.33 m). Interbedded shale beds are of equivalent thickness. Most of the sand beds are normally graded, but a few are massive sands.

Shale Facies consists mainly of mudstone. Beds range from 0.1 to 50 ft (0.03–15.2 m) thick. Thinner beds separate individual sands of the Thin-Bedded or Thick-Bedded lithofacies, whereas thick shales (tens of feet) separate major sand intervals. Analyses of 45 shale-bed samples from cores C714 and B756I (Fig. 12.2) for Total Organic Carbon (TOC) yielded a mean of 3.69 wt.% and a range of 1.46 to 6.50 wt.%.

Figure 12.11 displays a 200 ft-thick (67 m) section of core and its associated gamma-ray log and core-plug porosity and permeability profiles. This section illustrates the typical vertical characteristics of the Thick-Bedded and Thin-Bedded Sand Facies.

Grain-Size

Visual estimates have demonstrated that the Thick-Bedded Sand Facies and Thin-Bedded Sand Facies consist mainly of beds of fine- to medium-grained, moderately to poorly sorted sand (although some finer- and coarser-grained beds are present). Grain-size analyses were also completed on 85 sand samples from wells B-756I and B-777I. Samples were taken from each major subzone (Fig. 12.5) at approximately 50-ft (17 m) intervals. Standard sieve and pipette techniques (Folk, 1974) were used at 0.5-phi intervals to 6 phi, then whole phi intervals to 9 phi. Mean grain-size and sorting values for the Thick-Bedded Sand and Thin-Bedded Sand are summarized in Table 12.1. For each well, phi mean size is finer for Thin-Bedded than for Thick-Bedded Sand, and sorting is equal. The same relationship is apparent from the summary data; mean size of Thick-Bedded Sand is 2.6 phi (fine sand size class) and that of Thin-Bedded Sand is 2.9 phi (fine sand size class). A statistical t-test indicates these differences are significant at the 95% confidence level. Sorting of both facies is 1.6 phi (poorly sorted).

Porosity and Permeability

Porosity and permeability measurements were made on 1223 core plugs from the six cored wells. Frequency dis-

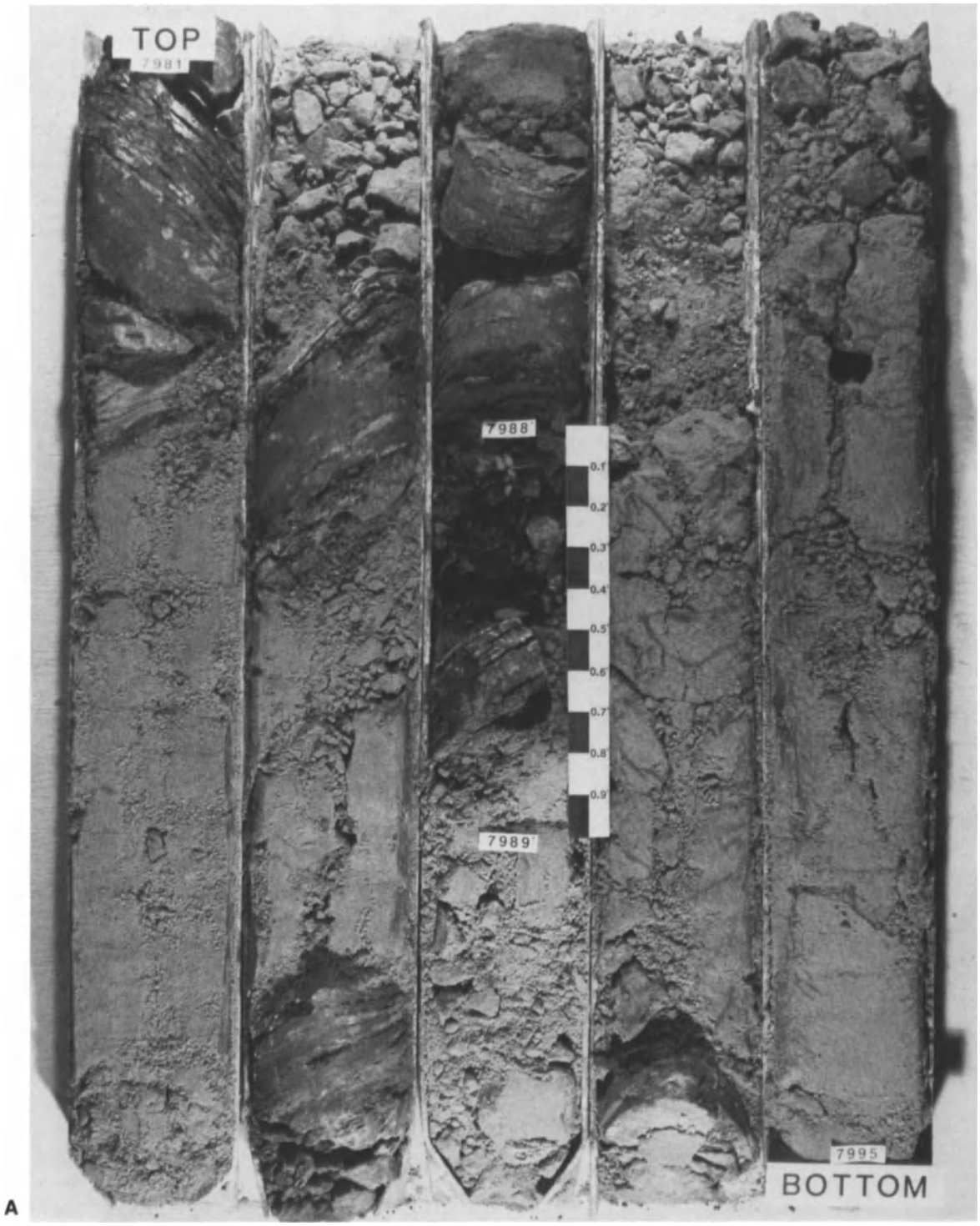

Figure 12.9 Examples of Thick-Bedded Facies in Well A863 (Fig. 12.2). The interval 7981 to 8006 ft (2433–2441 m) consists of a graded sand (7981.8–7984.8 ft; 2433.5–2434.4 m), thin massive sands (7985.2–7988.5 ft; 2434.5–2435.5 m), a graded sand (7988.8–7996.9 ft; 2435.6–2438.1 m), and a massive sand (7997.3–8005.7 ft; 2438.2–2440.8 m), each separated by shales (darker beds). All footages are as measured in the deviated well.

Figure 12.9 *Continued*

tributions of stressed (approximately 900 psi) and unstressed measurements are compared in Figure 12.12. Application of overburden stress has diminished average porosity by about 4%, and permeability by more than half. Mean-stressed porosity equals 28%, and the frequency distribution of values is approximately normal (Fig. 12.12). Mean (geometric) stressed permeability equals 422 md, and the distribution is negatively skewed (Fig. 12.12). In theory, porosities and permeabilities measured at overburden stress will approximate reservoir conditions. How-

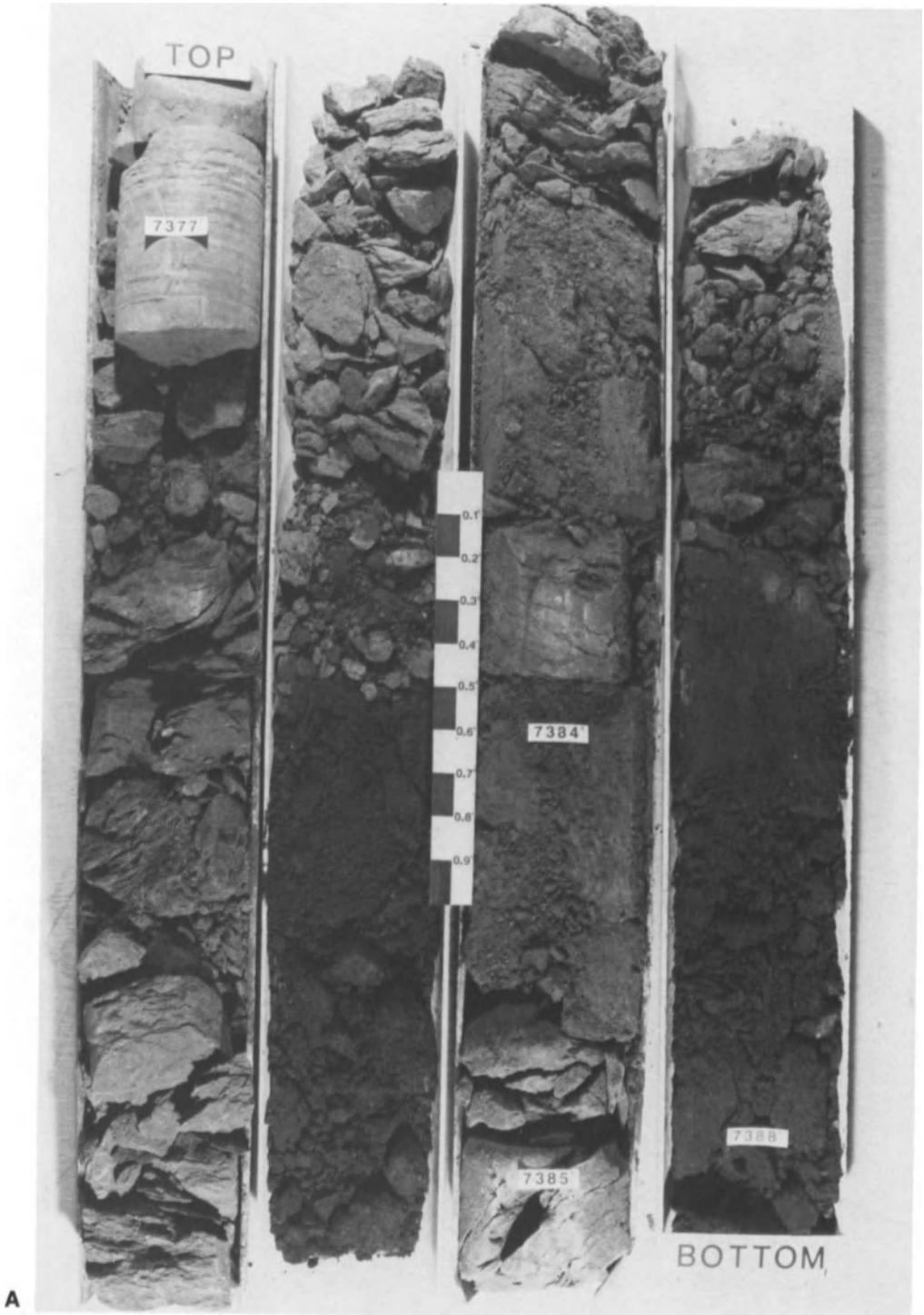

Figure 12.10 Example of Thin-Bedded Facies in Well A863. The interval 7377 to 7399 ft (2249–2256 m) is a series of thin, normally graded and massive-appearing sands separated by shale beds. The well-lithified bed at 7377 ft (2249 m) is a carbonate mudstone. The sands are moderately to heavily stained with oil. All footages are as measured in deviated wells.

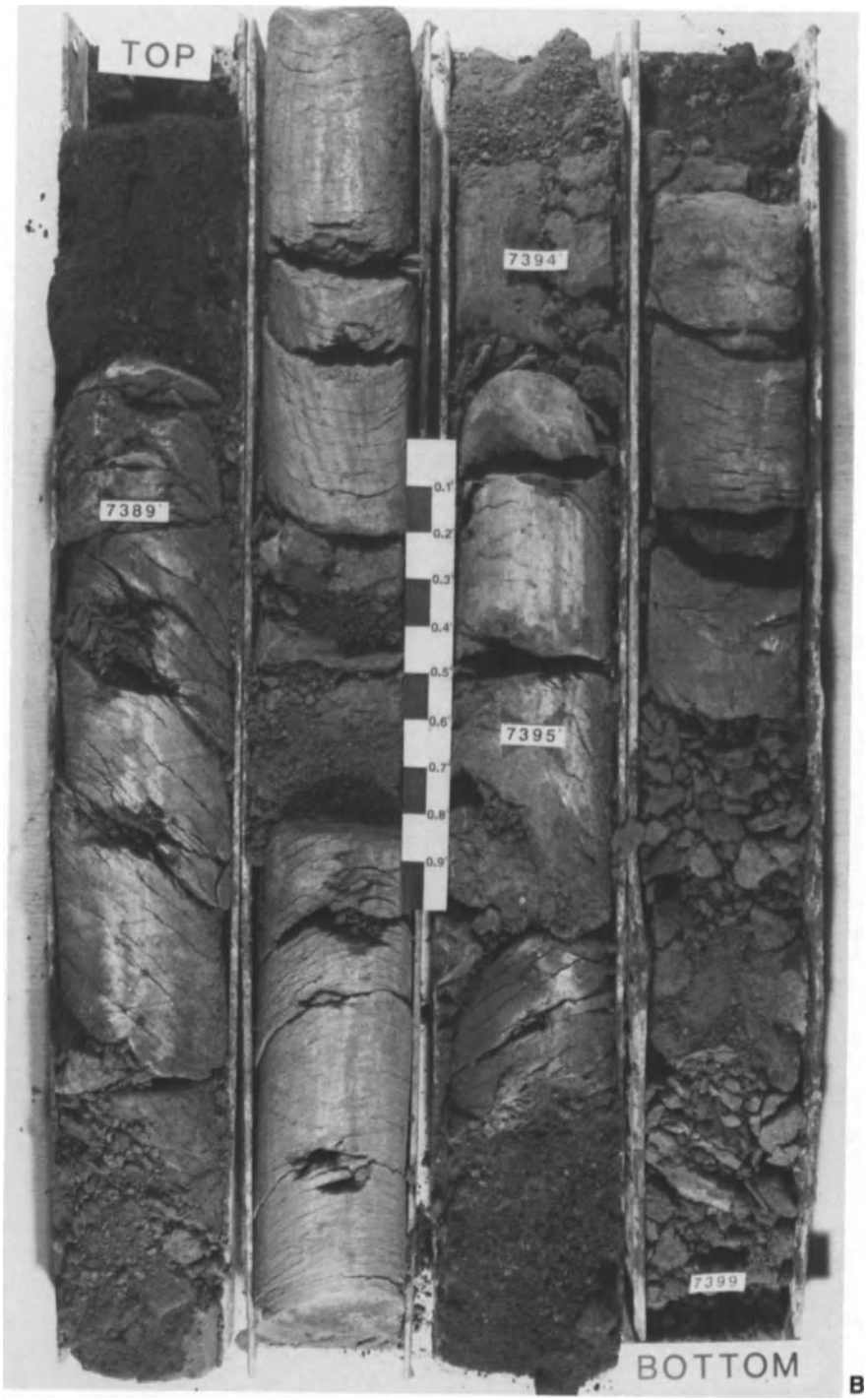

Figure 12.10 *Continued*

ever, in the case of the Long Beach Unit, these values do not represent reservoir conditions because of the unconsolidated nature of the sands that were plugged and because some sand grains are fractured, as discussed below. The extent of error between measured and in situ porosities and permeabilities resulting from these factors is not known. No comparison between core and log porosities was attempted.

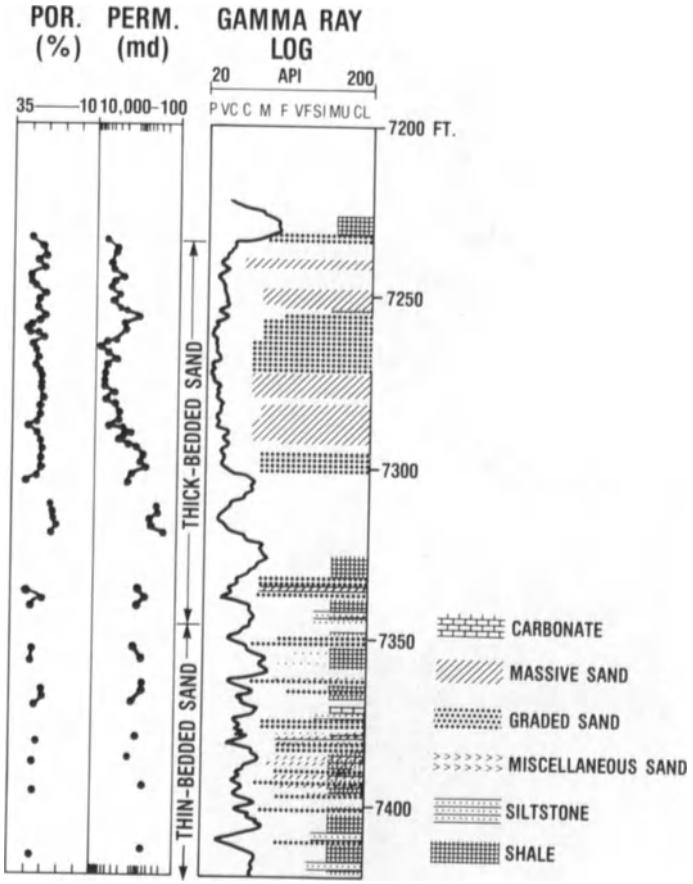

Figure 12.11 Portion of Well A863 illustrating core lithologies and facies, gamma-ray log, and core-plug porosity and permeability data. For grain-size scale, P = pebble, VC = very coarse sand; C = coarse sand, M = medium sand, F = fine sand, VF = very fine sand, S = silt, Mu = mud, and Cl = clay. Facies types are labelled. Blank areas are footages without core. All footages are as measured in deviated well.

Grain Size, Facies, and Reservoir Quality

Reservoir quality, particularly permeability, appears to be controlled, in large part, by grain size and sedimentary facies. For example, individual permeability values for the Thick-Bedded Sand Facies illustrated in Fig. 12.11 are considerably higher than values for the Thin-Bedded Sand Facies.

This relation is illustrated more comprehensively in Fig. 12.13, in which stressed porosity and permeability measurements are grouped according to facies. Geometric-mean permeability of Thick-Bedded Sand averages 457 md, whereas that of Thin-Bedded Sand averages 288 md. This difference is statistically significant at the 95% confidence level. By contrast, there is no significant variation between porosity of Thick-Bedded Sand and Thin-Bedded Sand; both average 28% (Fig. 12.13).

This relation between facies and reservoir quality is largely a manifestation of grain size variations that result from primary depositional processes. Slatt et al. (1988) presented evidence for deposition of Ranger Zone sands by a variety of mass-gravity flow processes. Potter and Scheidegger (1966), Sadler (1982) and Middleton and Neal (1989) have shown that turbidite bed thickness is directly proportional to grain size. This is because both more sand and coarser sand can be carried in suspension in a flow of greater turbulence than in a less turbulent flow, so that the lower the energy or turbulence of the flow, the thinner and finer grained will be the resultant sand bed. Thus, Thin-Bedded Sand lithofacies would tend to be finer grained than Thick-Bedded Sand lithofacies.

Table 12.1. Long beach unit statistical summary of grain-size distribution by well

	Thick-bedded sand				Thin-bedded sand			
Well	Grain Size		Sort	n	Grain Size		Sort	n
	ϕ	(mm)			ϕ	(mm)		
B756	2.7	(0.150)	1.5	15	3.0	(0.125)	1.5	20
B777	2.6	(0.165)	1.6	25	2.8	(0.140)	1.6	25
Both wells	2.6	(0.165)	1.6	40	2.9	(0.130)	1.6	45

The greater permeability of Thick-Bedded Sand than Thin-Bedded Sand is apparently the result of slightly coarser grain size. This equates to a smaller number of grain contacts and larger pore sizes per unit volume of sand, and resultant greater pore connectivity (Table 12.1). Equivalent porosity between both facies is apparently a result of equal sorting of the beds that make up both facies (Table 12.1). Because sorting is equivalent, the relative volumes of pores and grains per unit volume of each sand will not vary with grain size.

Moreover, the relation between reservoir quality and grain size also is recognized at the scale of individual sand beds. For example, Figure 12.11 illustrates this relationship for a graded sand between 7257 ft (2212 m) and 7276 ft (2218 m) depth. The upward gradation from medium/coarse-grained sand to fine-grained sand corresponds with an upward decrease in permeability.

As previously mentioned, some sand grains show evidence of grain crushing. In thin section, the broken pieces of grains have not moved, and thus retain the original form of the coarser original sand grain. Thus, these grains apparently have remained intact during and after coring, but undoubtedly would become separated during the sieving process. The effect of this phenomenon on grain-size distribution is to artificially reduce average grain size to an unknown degree and to worsen sorting. We make the assumption that the effect of fractured grains on grain-size analysis will be internally consistent between samples, so that results can be compared (Table 12.1). Nevertheless, these grain-size data should be interpreted with caution.

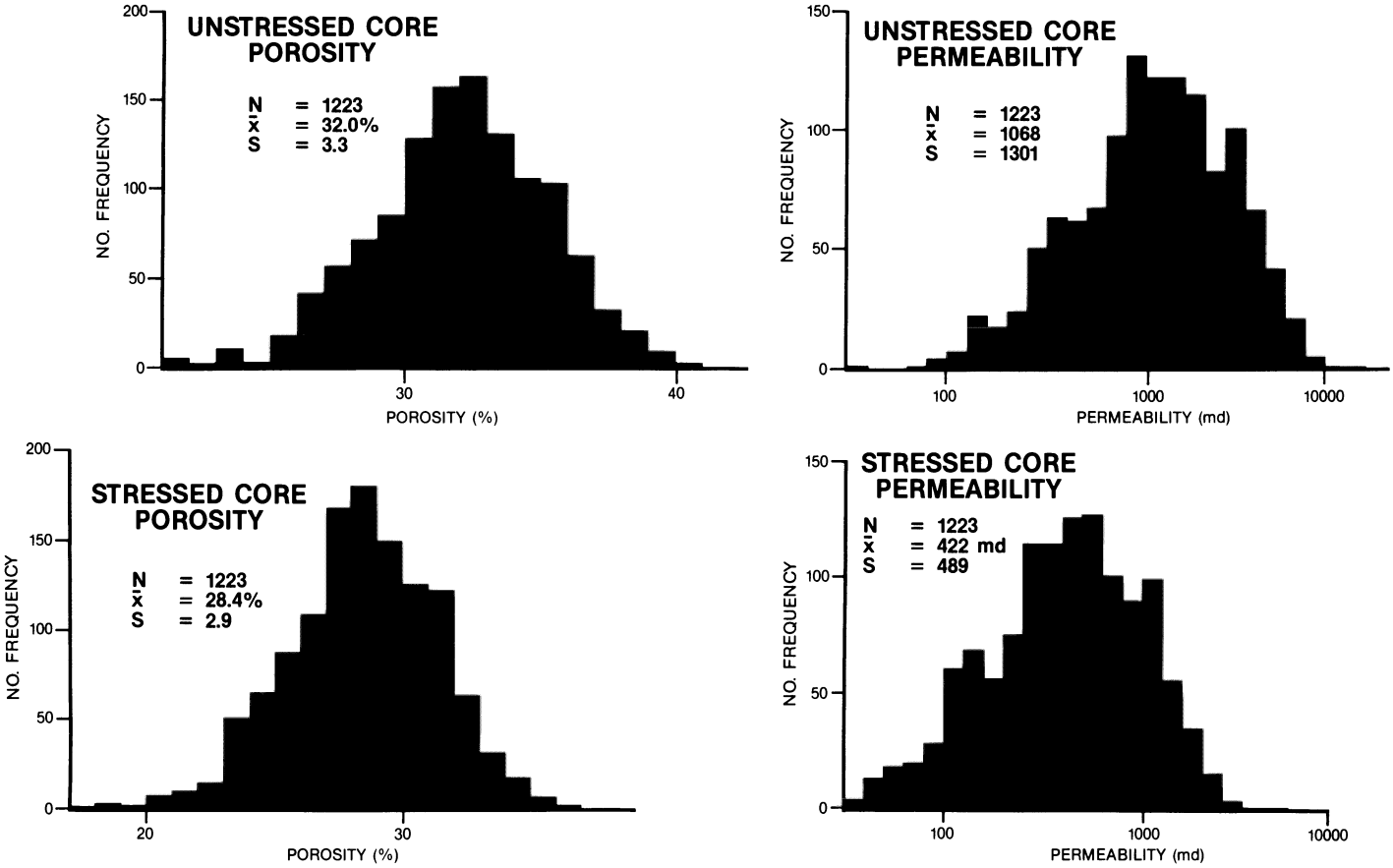

Figure 12.12 Frequency distributions of stressed (approximately 900 psi) and unstressed core plug porosity and permeability measurements.

Flow Units

A flow unit is a volume of rock subdivided according to geologic and petrophysical properties that influence the flow of fluids through it (Ebanks, 1987). Conversion of lithologies and lithofacies into flow units provides a means of "scaling-up" a reservoir description for simplifying inherent geologic complexities without losing significant aspects of the description. Based on the previous discussion, the three major lithofacies in the Long Beach Unit are equivalent to flow units, since each facies has distinctive porosity, permeability, grain size, and bedding characteristics.

A Thick-Bedded Sand flow unit is defined as consisting of groups of individual beds >2 ft (0.67 m) thick of poorly sorted, fine- to medium-grained sand, with an average of 28% porosity and 457 md permeability. The Thin-Bedded Sand flow unit consists of groups of individual beds <2 ft (0.67 m) thick of poorly sorted, fine- to medium-grained sand (slightly finer grained than the Thick-Bedded Sand), with an average of 28% porosity and 288 md permeability, which are interbedded with shale beds of equivalent thickness. Based on these characteristics, Thick-Bedded Sand is of better reservoir quality than Thin-Bedded Sand.

Shale is the third flow unit. Porosity and permeability values were not measured on this unit; however, they are low, and unless faulted, this flow unit will act as a permeability barrier to vertical migration of reservoir fluids. In effect, the shales probably isolate individual sand beds.

This correspondence between facies and flow units is not necessarily what is observed in other reservoirs. Many times, flow units subdivide facies (for example, see Hearn et al., 1984 and Slatt and Hopkins, 1988). In the case of the Long Beach Unit, undoubtedly a finer division of flow units is possible, but the three units defined here provide a practical means of subdividing the reservoir.

Figure 12.14 is an example of "scaling-up" of the reservoir description from beds to facies and flow units for well A863. The generally good correlation between lithofacies and reservoir properties is a result of a first-order sedimentologic control on these properties at the **microscale** and **mesoscale**, thus providing a sound basis for defining flow units at these scales. Comparison of average permeability values for flow units with permeability measurements for individual beds (Fig. 12.14) shows that flow unit values are within the same order of magnitude and probably provide appropriate numeric values for reservoir de-

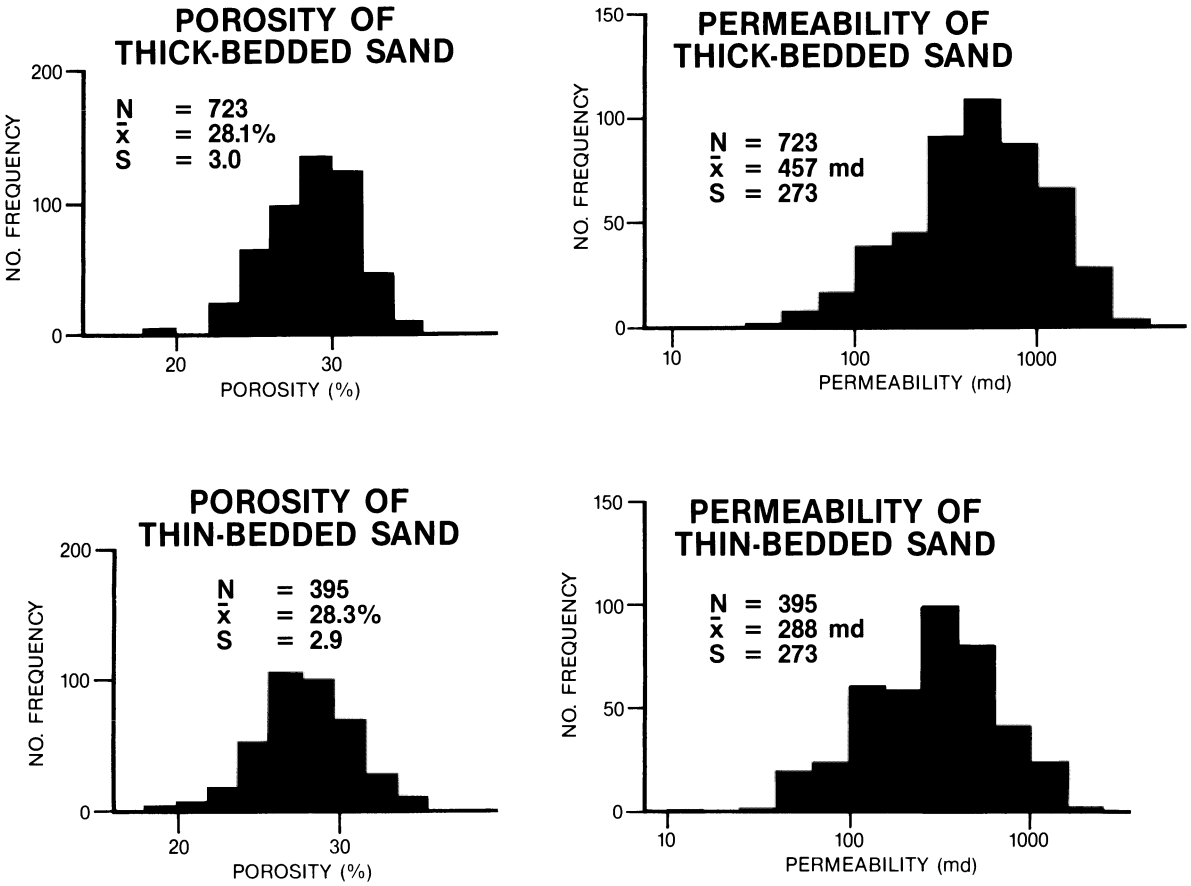

Figure 12.13 Frequency distributions of stressed porosity and permeability measurements for *Thick-Bedded Sand and Thin-Bedded Sand.*

scription purposes. However, the style of individual bedding, which can be important to fluid flow behavior, is lost by scaling-up to flow units.

Macroscale Heterogeneities

Macroscale, or interwell, heterogeneities include lateral bed continuity, stratification, interval geometries and thicknesses, facies distribution, and lateral variations in reservoir properties. Electric logs are the principal log type in the Long Beach Unit; gamma ray logs were usually run only on cored wells. Sensitivity of the SP to bedding style is not very good (Slatt et al., 1988); consequently, a reliable method has not yet been developed to consistently distinguish facies or flow units in uncored wells. Between-well correlation of beds in uncored wells was accomplished by correlating the numerous distinctive, continuous shales that occur within the Ranger Zone.

Two typical cross sections of the upper Ranger interval are shown in Figures 12.15 and 12.16. Figure 12.15 is a regional cross section covering the entire length of the Long Beach Unit (Fig. 12.2). Thick shales, which correspond to subzone picks (Fig. 12.5) can be correlated across the Unit. Figure 12.16 is a more detailed cross section of the upper Ranger interval over a lateral distance of about 1 mi (1.6 km). Thin shales, which are subzone picks, can be traced laterally across the length of the section. This continuity of shales, even those as thin as 2 ft (0.67 m), suggests that the reservoir is, in fact, composed of a series of laterally extensive, but vertically isolated sands.

To evaluate variations in thickness trends of individual sands, a correlation loop of cross sections was established with 18 infill wells within the loop. Figure 12.17 shows thickness trends of three subzones, FO-F, FJ-FK, and H1M-H1LA (Fig. 12.16). The FO-F interval thickens substantially toward the southeast, while FJ-FK thickens toward the north-northwest (Fig. 12.17). Interval H1M-H1LA is thinner than the others and thins subtly toward the south within the area of the correlation loop (Fig. 12.17). These three examples demonstrate that thickness trends are not the same among the various sands.

To illustrate lateral variations in some reservoir properties, the average value of permeability, the ratio of feet of

Table 12.2. Properties of subzones from two cored wells

Subzone	Average permeability	No. of permeability measurements	Interval thickness	Thick-Bedded Sand / Thin-Bedded Sand (ft)	Medium- to Coarse-grained Sand / Very Fine- to Fine-grained Sand (ft)
FO-F					
A863	1592	11	25 (7.5)	1.0	12.8
B777I	984	19	61 (18)	3.1	12.8
FJ-FK					
863	1066	35	71 (21)	21.5	8.3
B777I	870	14	73 (22)	5.4	1.6
H1M-H1LA					
A863	162	8	23 (6.9)	1.8	0.8
B777I	310	12	28 (8.4)	20.2	3.8

Thick-Bedded Sand to Thin-Bedded Sand and the ratio of feet of medium- to coarse-grained sand beds (grain size was determined by visual estimation) to feet of very fine- to fine-grained sand beds were calculated for the subzones FO-F, FJ-FK, and H1M-H1LA (Table 12.2) from core data in wells A-863 and B777I. These wells are spaced about a mile apart and are located at both ends of the cross section in Figure 12.16. Over this distance, permeability varies by less than an order of magnitude. Subzones H1M-H1LA and FJ-FK follow the permeability relation established at the **mesoscale** reservoir level; that is, higher permeabilities occur within the more thickly bedded and coarser-grained sand. This relation is not consistent for subzone FO-F, where lower average permeability is associated with relatively more Thick-Bedded Sand in core B777I.

These comparisons demonstrate the greater degree of uncertainty associated with predicting lateral variability in reservoir properties at the **macroscale**, or interwell scale, than at the **mesoscale**, or single well scale. At least some of this uncertainty is associated more with non-uniform sampling procedures than with natural variability. For example, the number of core-plug porosity and permeability measurements in Long Beach cores varies from 1 per 2 ft (0.67 m) of interval thickness to 1 per 5 ft (1.5 m) (Table 12.2, Interval Thickness divided by Number of Permeability Measurements), and plugs were not equally spaced throughout each interval. Nevertheless, average values of the properties measured are within an order of magnitude of variability between the two wells.

Megascale Heterogeneities

Megascale, or field-wide, heterogeneities include variations within the overall depositional system and its gross geometry and regional facies trend. Commonly cited depositional models are typically generalized and qualitative, and they rarely consider the complexities and uncertainties of internal lithofacies architecture. Further, comparison of many modern and ancient fans worldwide has shown that their overall shapes and sizes are quite variable (Fig. 12.18), and their form is dependent on size and geometry of the depositional basin, source drainage area, tectonic setting, etc. Thus, it is difficult to accurately describe three-dimensional **megascale** characteristics of a field unless the data grid (wells, seismic, etc.) completely encompasses the entire depositional system. In many fields, the size of the depositional system is indeed larger than the size of the field, so insufficient data from outside the boundaries of the field may preclude the possibility of accurately describing these **megascale** heterogeneities.

This is the case in the Long Beach Unit. The apparent size of the turbidite system(s) that composes the Ranger Zone is larger than the area of Long Beach Unit, so that depositional geometries have not been accurately ascertained. Evidence to suggest that deposition occurred, at least in part, as a series of basinal submarine fan lobes or sheets, as has been interpreted for similar deposits in the nearby Inglewood Field (Fig. 12.1) (Schweller et al., 1988) includes (1) biostratigraphic data (Figs. 12.6 and 12.7); (2) lateral continuity of shales (Figs. 12.15 and 12.16); (3) the apparent presence of a shelf edge >20 mi (33 km) landward of Long Beach Unit (Fig. 12.4), and (4) apparent complementary thickening of successive sand packages in certain intervals (Figs. 12.15, 12.16, and 12.17).

In order to demonstrate different perspectives for defining three-dimensional **megascale** heterogeneities when the depositional system extends beyond the limits of the field data, we have interpreted the Ranger Zone sediments using three different approaches: (1) utilizing depositional sequence stratigraphy concepts (Vail, 1987), (2) applying a classical progradational submarine fan model (Walker, 1978) and (3) interpreting an evolutionary scheme for a turbidite depositional system (Mutti, 1985; Mutti and Normark, 1987).

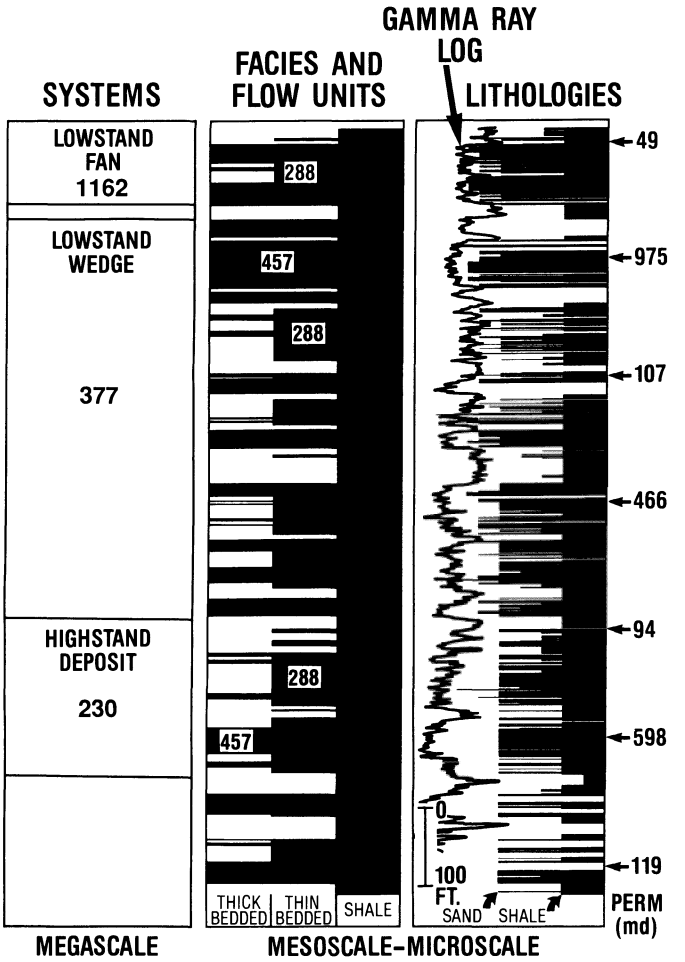

Figure 12.14 Comparison of lithologies, facies, and flow units, and gamma ray log for the cored interval of Well A863. Permeability measurements for individual sand beds are shown, as are average permeability values for selected *Thick-Bedded* and *Thin-Bedded Sand* flow units.

Sequence Stratigraphic Model

The sequence-stratigraphic approach is based on the delineation of time-rock stratigraphic units composed of genetically related strata bounded by unconformities and their correlative conformities (**depositional sequences**; Mitchum et al., 1977). The basic premise of sequence stratigraphy is that depositional sequences record the response of sediments to changes in rates of accommodation (space available for sedimentation; Baum and Vail, 1988; Posamentier et al., 1988), which result from fluctuations in eustatic sea level and subsidence. Climate and sediment supply are subordinate controls on the creation of accomodation space (Vail and Todd, 1981; Vail and others, 1982, 1984; Vail, 1987). Thus, sequence formation and architecture can be related to different components of a sea-level cycle.

The conventional sequence-stratigraphic model, which shows the relationship between relative changes of sea level and depositional stratal patterns for a deep-water basin having a distinct shelf-slope break, is shown in Figure 12.19. A depositional sequence representing a complete sea-level cycle consists of lowstand, transgressive, and highstand systems tracts. Sequence boundaries (unconformities and correlative downdip conformities) formed by relative drops in sea level occur at the base of lowstand and top of highstand systems tracts. The lowstand fan deposits form during falling sea level, when streams are actively eroding the exposed shelf and the supply of coarse clastics is abundant. At sea-level minima and during the ensuing rise, the lowstand wedge forms basinward of the shelf edge, but progressively onlapping in a landward direction. The transgressive surface occurs at the top of the lowstand wedge deposits formed by initial flooding of the shelf. The maximum flooding surface is developed during the maximum rate of sea-level rise and is associated with an interval of relative sediment starvation called the condensed section. The condensed section marks the boundary between the transgressive and highstand systems tracts. It is important to note that the terms lowstand, transgressive, and highstand refer to the strata deposited during a given phase of a sea-level cycle, and do not imply any particular clastic facies character.

Lyons and Suchecki (1989) have suggested that Miocene sequence development and systems tract geometries in the northeast Los Angeles basin developed from a complex interplay of eustatic sea-level and tectonic changes, with eustatic changes exhibiting first-order control. The following stratigraphic sequence analysis for the Ranger Zone lends credence to this interpretation. Our analysis is based on (1) facies variations from core, (2) facies distribution and stratal patterns from well-log cross sections and isopach maps, and (3) biostratigraphic and geochemical signatures in the Long Beach Unit, which suggest that systems tracts belonging to parts of three separate sequences can be interpreted in the Ranger Zone. These sequences are designated "lower Ranger," "upper Ranger A," and "upper Ranger B" (Fig. 12.20; note that Figs. 12.15 and 12.20 are of the same stratigraphic section, with the latter being re-datumed and correlated within a sequence-stratigraphic framework).

Two factors of scale must be considered with regard to the Ranger Zone sequence stratigraphy. The first concerns overall location of the Long Beach area within the shelf-to-basin profile. Owing to the paleogeographic setting of the Long Beach area during late Miocene and early Pliocene deposition of the Ranger Zone (Fig. 12.4), only the portions of the sequence systems tracts seaward of the shelf edge are seen on the data presented herein (Fig. 12.19). Secondly, because the Ranger Zone stratigraphic interval represents 2 to, at most, 4 m.y. of geologic time, only a small stratigraphic interval that contains parts of three

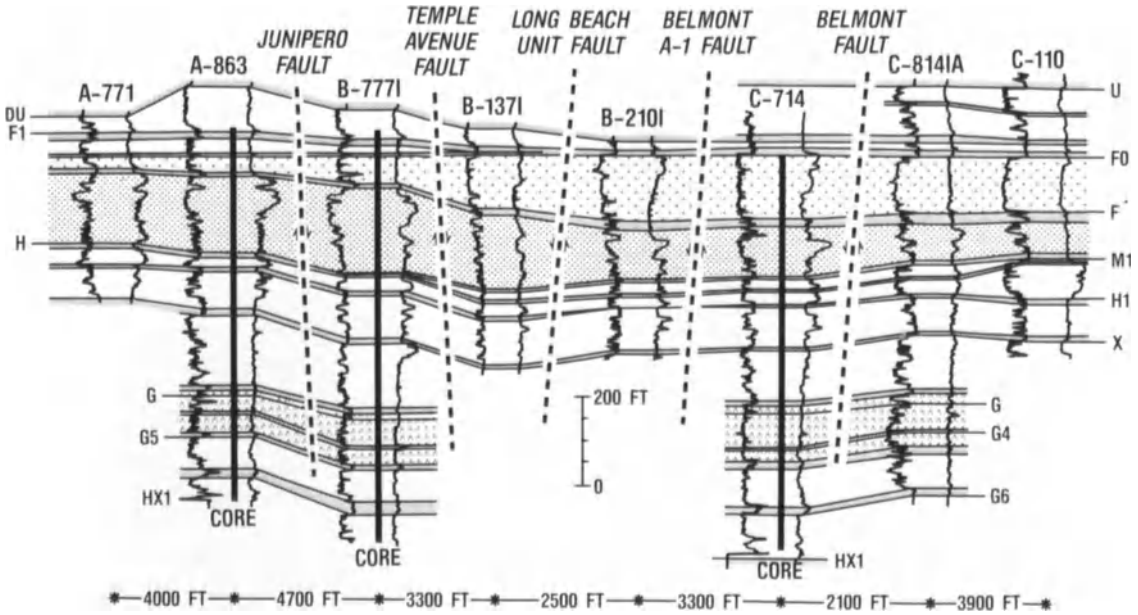

Figure 12.15 Northwest-southeast regional cross section of Ranger Zone (see Fig. 12.2 for location). Major subzone picks (tops of beds) (Fig. 12.5) are also shown. Well depths are corrected for true stratigraphic thickness.

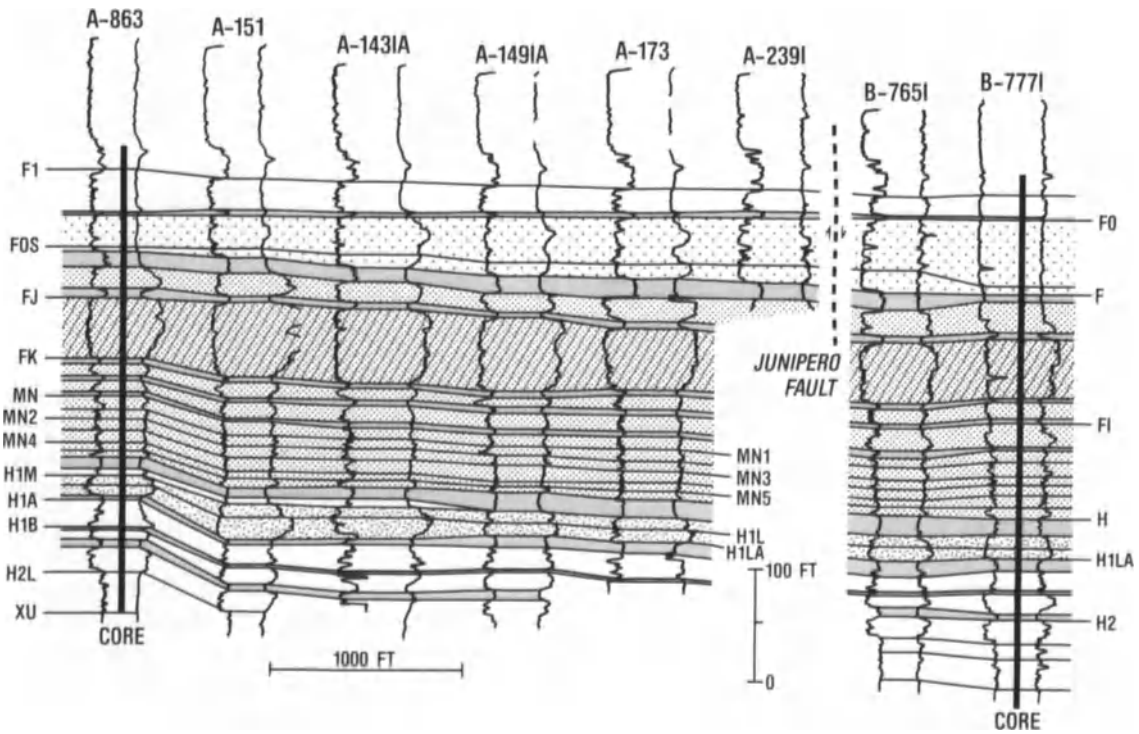

Figure 12.16 Northwest-southeast detailed stratigraphic cross section showing correlation of various sand and shale intervals and subzone horizon picks (Fig. 12.5) in the upper part of the Ranger Zone. Location of the cross section is illustrated in Fig. 12.2. Well depths are corrected for true stratigraphic thickness.

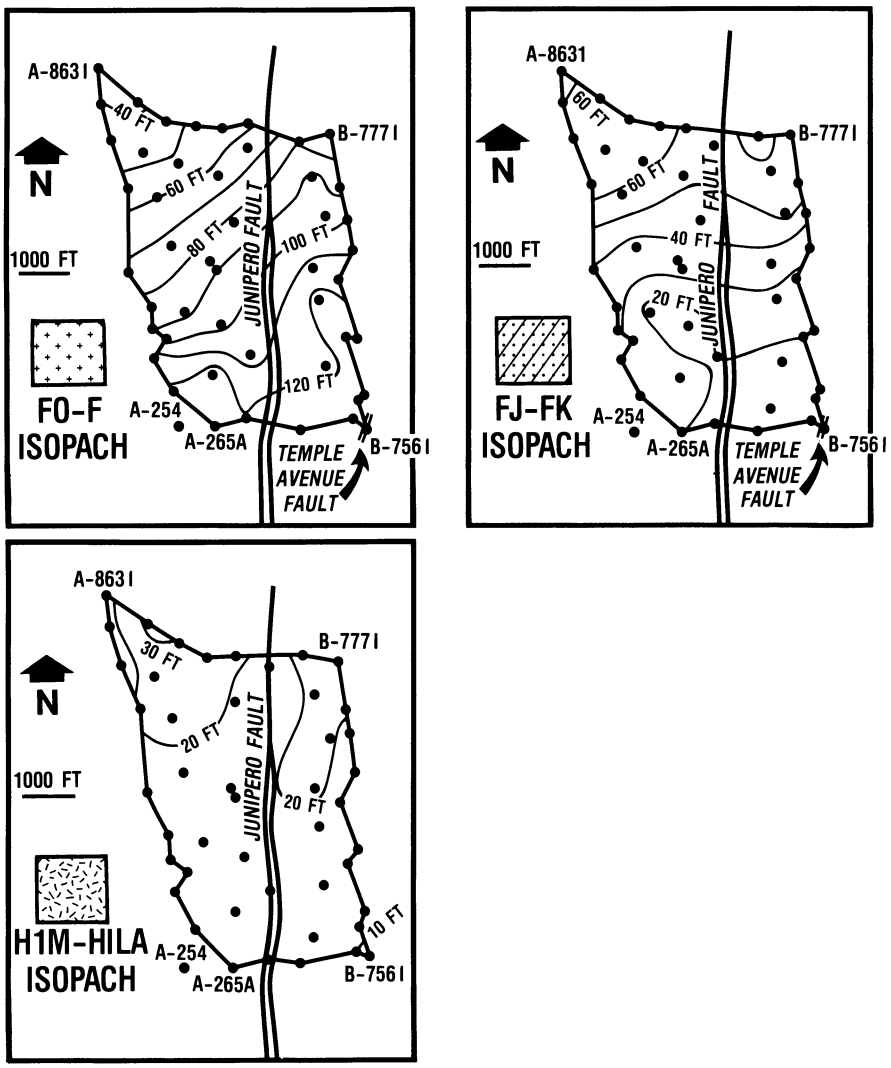

Figure 12.17 Isopachs of three stratigraphic intervals shown in Figure 12.16. Contour interval is 10 ft (3.3 m). Isopach intervals reflect true stratigraphic thicknesses.

sequences—not three complete sequences—is being analyzed.

Lower Ranger Sequence

The Puente Formation strata of the lower Ranger Zone are interpreted as the late lowstand wedge and distal highstand deposits that make up the upper part of a sequence of Delmontian age. Two key observations support this interpretation: (1) the section just above the G6 marker (Figs. 12.15 and 12.21) is an exceptionally organic-rich shale unit characteristic of a condensed section, and (2) significant changes in lithologic characteristics occur across the shale interval just above the G6 marker.

Condensed sections typically consist of organic-rich hemipelagic and pelagic sediments that were deposited during the period of maximum rate of relative sea-level rise (Loutit et al., 1988). They are often easily differentiated on a gamma ray log as "hot" intervals (Meyer and Nederlof, 1984; Loutit et al., 1988), such as the shale above the G6 sand (Fig. 12.21). The total organic carbon content of samples of this shale is anomalously high—exceeding 6%—further supporting interpretation of this shale interval as a condensed section.

Comparison of the lithologic and bedding characteristics of the sands below and above the G6 marker (Fig. 12.21) suggests a change in depositional style across this interval. Below the marker, sands are thick bedded, commonly massive, amalgamated units with a blocky to coarsening/thickening-upward-appearing log character (Figs. 12.15 and 12.21) that can be correlated over long distances. These characteristics are compatible with deposition in a prograding lowstand wedge system.

In contrast, sand beds overlying the marker (Fig. 12.21) are thinner bedded, and in the lower part of this interval,

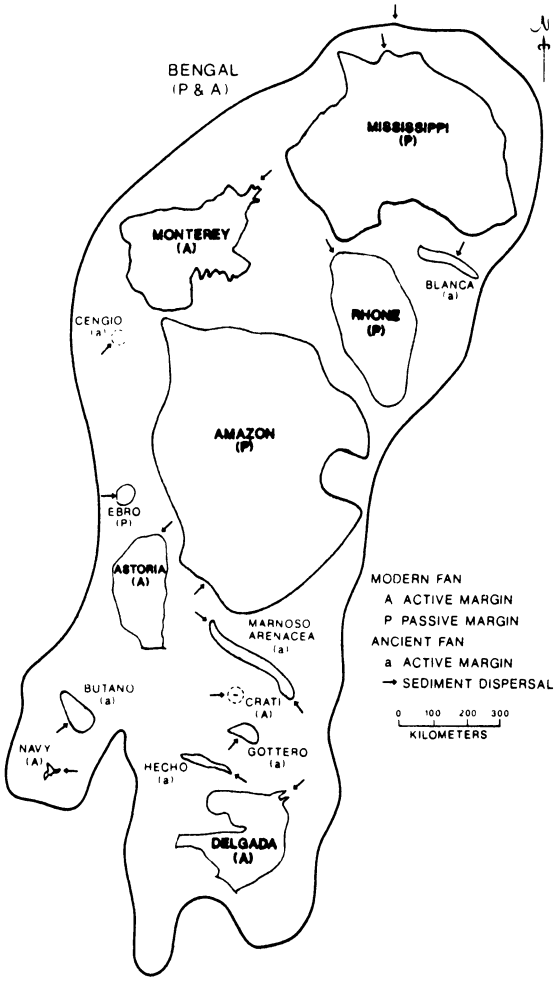

Figure 12.18 Outlines of selected modern and ancient submarine fans and turbidite systems showing variability in size and shape (Barnes and Normark, 1985).

they tend to contain a higher percentage of graded beds, convoluted bedding, and burrowed zones (termed "miscellaneous sands" in Fig. 12.21). Thus, deposition in a part of the basin that received sediments more episodically and/or was more distal to the source area at that time is implied. This trend may result from a decrease in the frequency and volume of sediment gravity flows in response to the landward shift of accommodation space during highstand deposition. Basinal turbidite deposition during highstand phases may have occurred dominantly as a result of major flood or storm events, and oversteepening and slumping of slopes at the depositional shelf edge during maximum progradation of the highstand deposits. An isopach map of the highstand systems tract (Fig. 12.22) shows a slight southwesterly thinning, suggesting a northeasterly source area and onlap direction.

A sequence boundary (downdip correlative conformity to an updip unconformity) is placed at the "foram-poor interval" referred to previously (Figs. 12.6, 12.7 and 12.20). The "foram-poor interval" also appears to correlate with the Delmontian/Repettian stage boundary in the Los Angeles Basin. This stage boundary, which is marked regionally by an unconformity, was formerly considered the Miocene/Pliocene boundary. It is commonly referred to in earlier literature as the Miocene/Pliocene or basal Pliocene unconformity. Yerkes et al., (1965) referred to erosional unconformities at the base of the Pliocene in the Inglewood and Huntington Beach oil fields, and in outcrop, near Newport Bay, in the Santa Ana Mountains, in the Coyote Hills, and in the Anaheim nose area. In the Long Beach area, a submarine unconformity has been inferred by Clarke (1987) and Henderson (1987).

Although we have found no evidence in the core or on log cross sections for an erosional unconformity at this interval, the documented increase in water depth from the Delmontian into the Repettian (Figs. 12.6 and 12.7) may record the interaction between eustatic fluctuations and late Miocene tectonic tilting that gave rise to uplift along the basin margin and water deepening toward the basin center, as has been suggested for this area by Lyons and Suchecki (1989). In addition, formation of the "foram-poor interval" at this time (correlating to the NH7 hiatus at 5 Ma) suggests an episode of tectonically and/or climatically induced changing oceanic circulation.

Changes in sand grain size, bed thickness, and stratal patterns also suggest that the lower and upper Ranger intervals belong to different depositional sequences. In general, Delmontian lower Ranger sands are relatively finer grained and tend to thin upward, whereas the overlying Repettian sands of the upper Ranger tend to be relatively coarser grained and thicken upward (compare the gross log characters on Fig. 12.20 below and above the sequence boundary).

Upper Ranger A Sequence

The upper Ranger A Sequence across the Long Beach Unit is composed of a series of sand packages, some of which tend to exhibit well-log characteristics of upward coarsening and upward bed thickening. (Fig. 12.20). These deposits are interpreted to make up a lowstand wedge prograding complex (Fig. 12.19), of the upper Ranger A sequence. An isopach map of the lowstand wedge (Fig. 12.23) indicates thinning to the south, which suggests a northerly source. Thinning is most pronounced north of the crest of the Wilmington structure (compare Figs. 12.2 and 12.23), so the thickness pattern could also have been influenced by structural growth if it was contemporaneous with sedimentation.

Overlying these lowstand wedge deposits is a laterally persistent shale (Fig. 12.20) unit that records either a shift

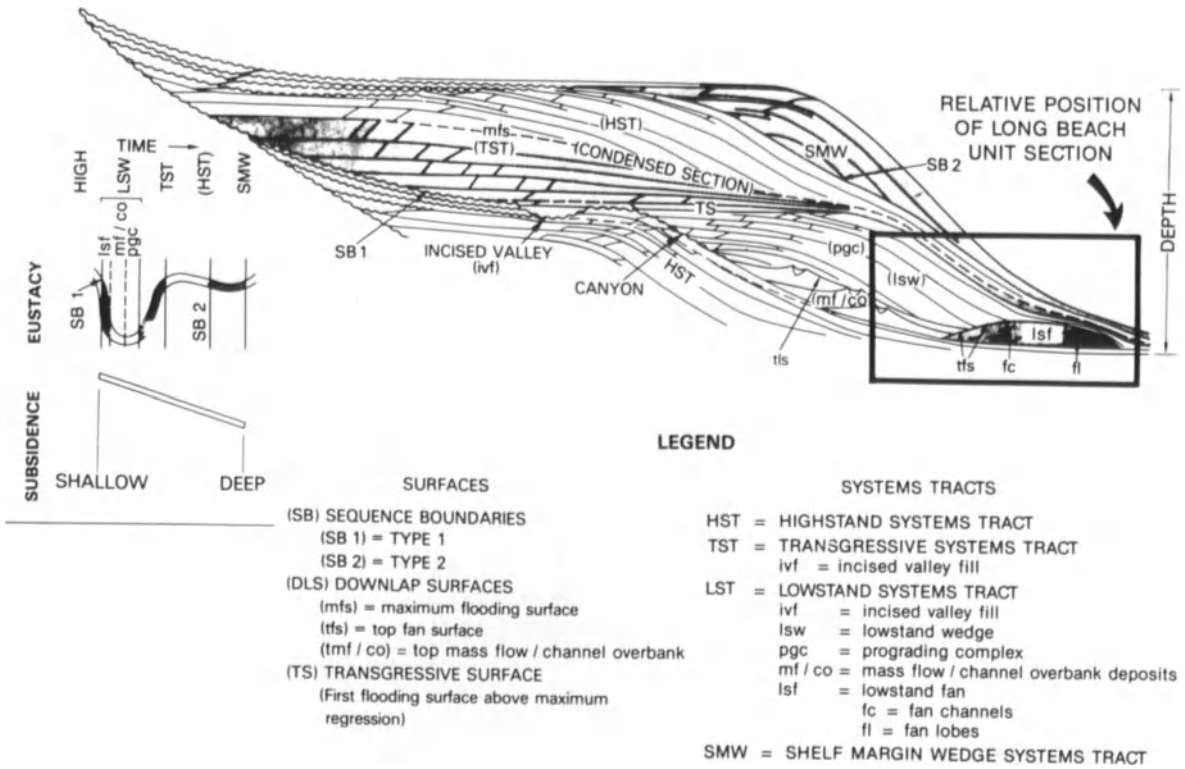

Figure 12.19 Idealized depositional sequence model showing the relative position of the Long Beach Unit within the shelf-to-basin profile. (Modified from Vail, 1987; Reprinted by permission.).

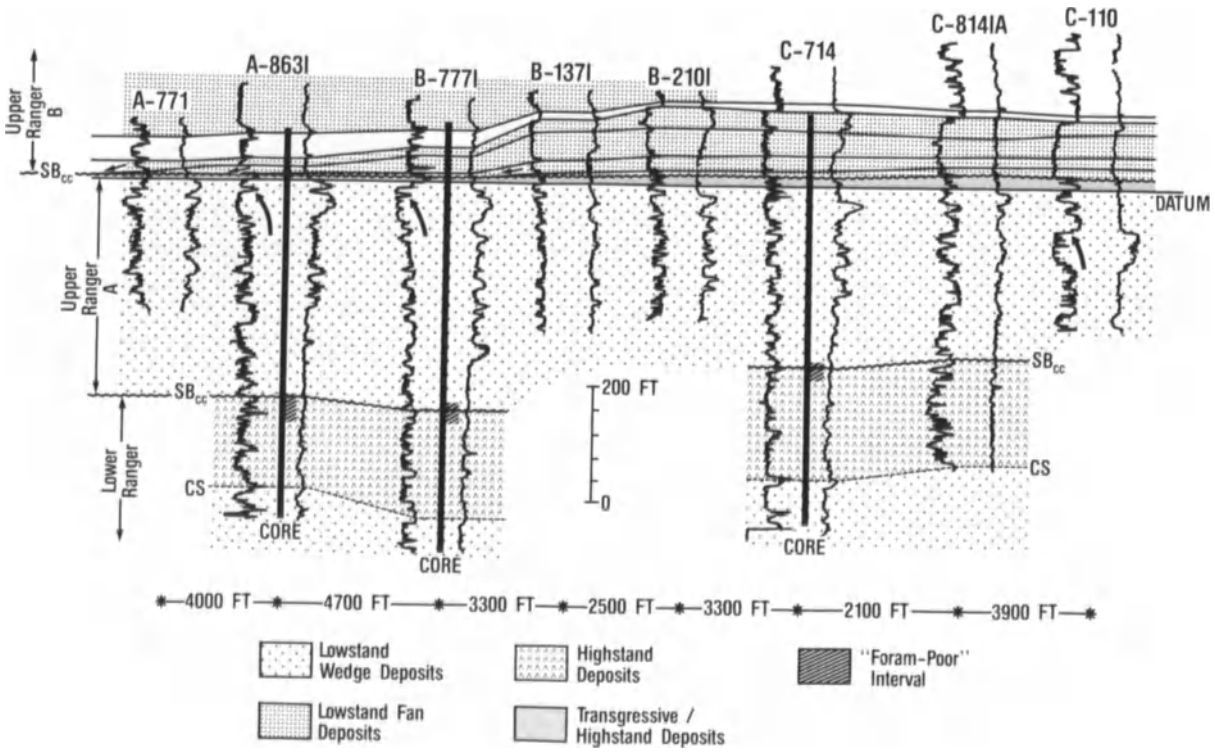

Figure 12.20 Northwest-southeast regional cross section showing lower Ranger, upper Ranger A and upper Ranger B sequences and depositional systems tracts. Abbreviations used are: CS = condensed section, SB_{cc} = sequence boundary (correlative conformity). Note northward downlap of stratal surfaces within lowstand fan deposits onto the upper Ranger B sequence boundary. Cross-section location is shown in Figure 12.2, and the cross section correlated by unit subzones is shown in Figure 12.15. Well depths are corrected for true stratigraphic thickness.

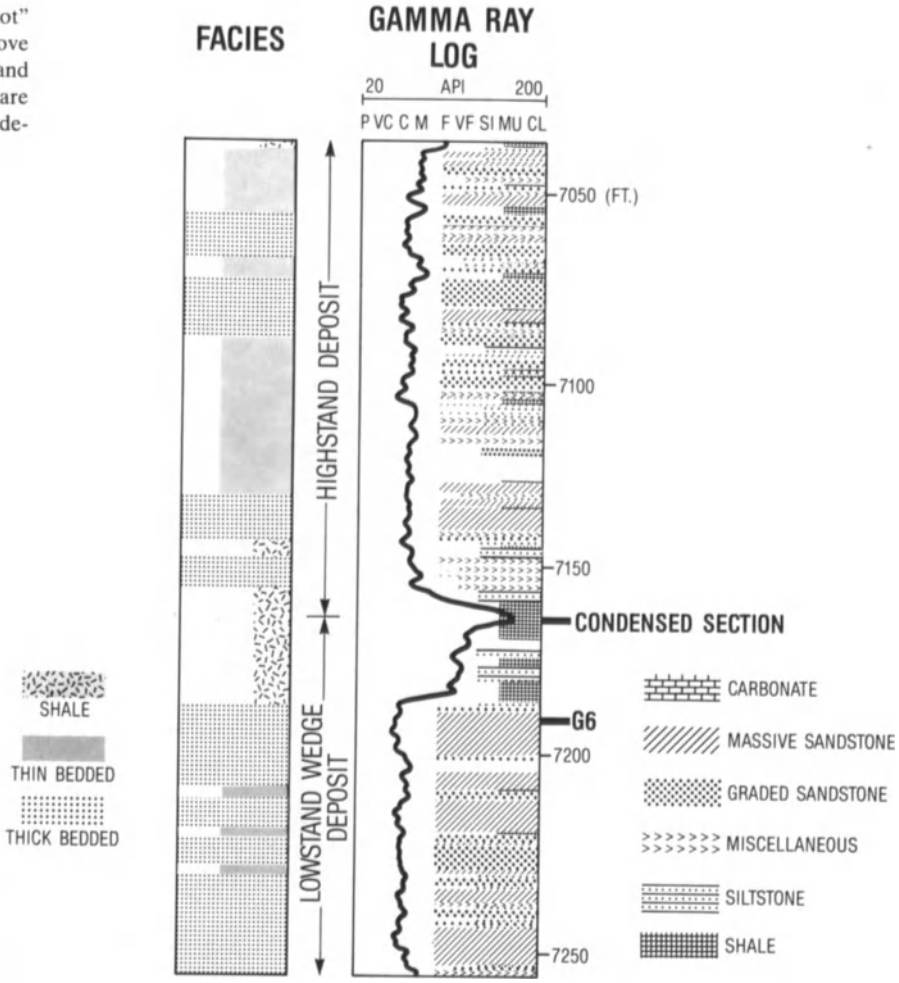

Figure 12.21 Portion of Well C714 illustrating "hot" gamma-ray log response of condensed-section shale above G6 subzone boundary, cored depositional facies, and sequence-systems tract interpretations. Blank areas are footages without core. All footages are as measured in deviated well. Refer to Figure 11 for descriptive terms.

in the locus of deposition or in the balance between sediment supply and accommodation potential (shift in systems tracts). Comparison of log characteristics of sands above and below this shale indicates a change in depositional style that suggests the two sand packages belong to separate depositional systems. Consequently, the shale unit itself is interpreted to include the basinal facies of the transgressive and highstand systems of the upper Ranger A sequence (Fig. 12.20). The correlative conformity of a sequence boundary separating the upper Ranger A and B sequences is interpreted to occur at the base of the overlying sand package (Fig. 12.20), which is interpreted to represent renewed lowstand deposition during the succeeding cycle.

Upper Ranger B Sequence

Basal sands of the upper Ranger B sequence (Fig. 12.20) have a distinctly blocky log character and consist of amalgamated, thickly bedded, very coarse- to fine-grained, poorly sorted sands. Several pebbly sand and pebble beds (pebbles up to 20 mm in diameter) occur exclusively within this interval. Beds also exhibit abrupt basal contacts and a stacked, aggradational character on well logs (Fig. 12.20). Sand packages show a lateral complementary thickening on well-log cross sections, suggesting that depositional topography localized sand deposition in low areas.

Using the shale just below the sequence boundary as a datum on regional cross sections, a downlap pattern is observed by correlating stratal surfaces within the sand packages (Fig. 12.20). This is the same type of stratal pattern that characterizes lowstand fan deposits on seismic data (McGovney and Radovich 1985; Mitchum, 1985). Both the coarse-grained, aggradational sedimentary character and stratal patterns of the upper Ranger B sands suggest that they were deposited as part of a lowstand fan, although they could represent the coarser-grained part of a lowstand wedge system (Fig. 12.19). A drop in relative sea level along the basin margin may have shifted the site for sediment accommodation more basinward at this time.

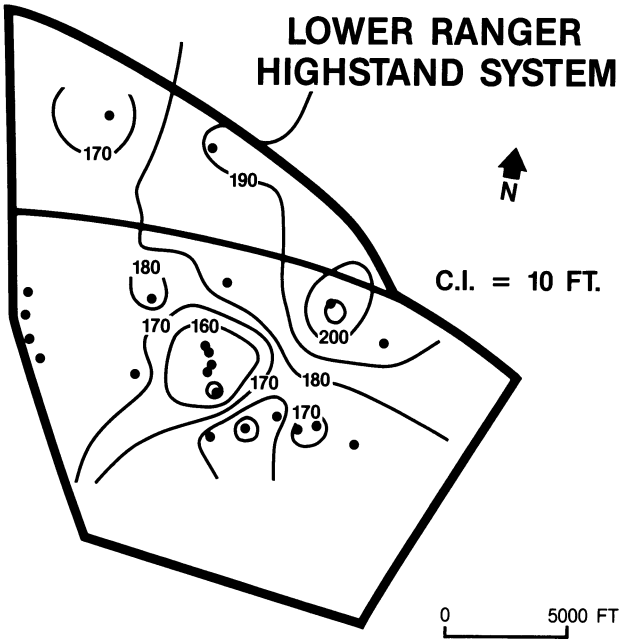

Figure 12.22 Regional isopach of Lower Ranger highstand systems tract. Contour interval = 10 ft (3.3 m).

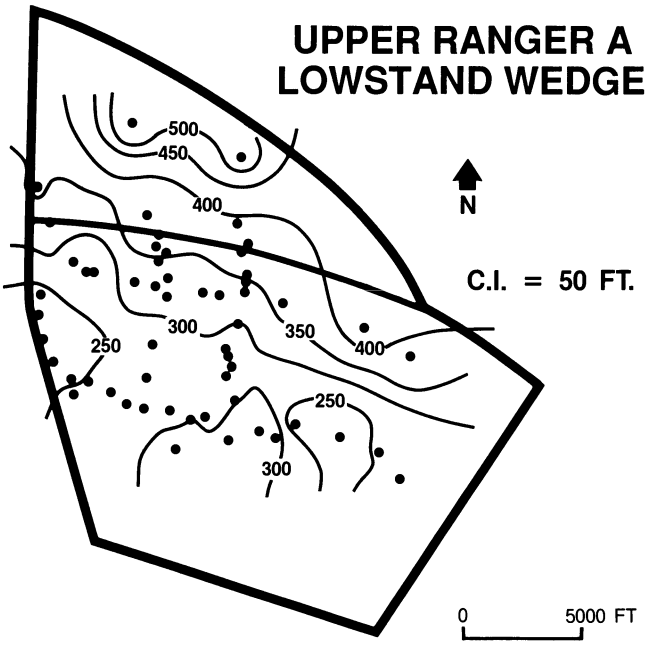

Figure 12.23 Regional isopach of upper Ranger A lowstand wedge systems tract. Contour interval = 50 ft (10.5 m).

Progradational Submarine Fan Model

Certain characteristics of the Ranger Zone sediments suggest that they can also be interpreted within the context of a progradational submarine fan model.

Walker (1978) published a depositional model (Fig. 12.24) that is today a standard reference. According to this model, fan progradation during one continuous depositional cycle will produce a distinctive vertical sequence that becomes coarser grained and thicker bedded upward. This vertical sequence represents successive deposition of more "proximal" facies, from lower fan to mid-fan suprafan lobes, to upper fan channel fill (the same channel system that fed the lower and mid-fan) at any one location. Facies also are suggested to vary systematically in the lateral and down-fan directions (Fig. 12.24).

In the gross sense, the interval from about the middle of the lower Ranger (at the Condensed Section in Figure 12.20) to the top of the upper Ranger B comprises a coarsening- and thickening-upward sequence of beds that can be interpreted as a single progradational depositional cycle. As previously mentioned, lower Ranger sands (Fig. 12.20) are generally finer grained and thinner bedded than overlying upper Ranger A sands, and upper Ranger B sands are the coarsest grained sands within the vertical succession. The thickening-upward character of the sands is also evident in Figure 12.16. However, interpreting the succession as a single continuous progradational interval is based mainly on the physical characteristics of the vertical sequence, and ignores much of the biostratigraphic, geochemical, and stratigraphic information applied to the sequence-stratigraphic interpretation. According to the progradational fan interpretation, the lower part of the Lower Ranger interval (Lowstand Wedge of Figure 12.20) is the upper part of an older progradational cycle, probably a mid-fan suprafan lobe.

Turbidite Systems Model

In an attempt to relate turbidite sediments and depositional sequences, Mutti (1985) introduced the concept of three main types of turbidite systems, called Type I, Type II, and Type III (Fig. 12.25). These systems differ from each other in terms of where sand is deposited and by the volume of sand available in the source area. A Type I system (Fig. 12.25) results when a large volume of sediment is deposited as elongate, thick-bedded sandstone lobes basinward of and physically detached from their channelized feeder system. A Type II system (Fig. 12.25) forms when lesser volumes of sediment are deposited in the lower reaches of channels and in the regions beyond the channel mouths. In the downflow direction, sands tend to become thinner bedded. A Type III system (Fig. 12.25) develops when sediment source is minimal; thus, it is characterized by small, sand-filled slope channels that are enclosed by mud (channel-levee complexes).

According to Mutti (1985), these three types of turbidite

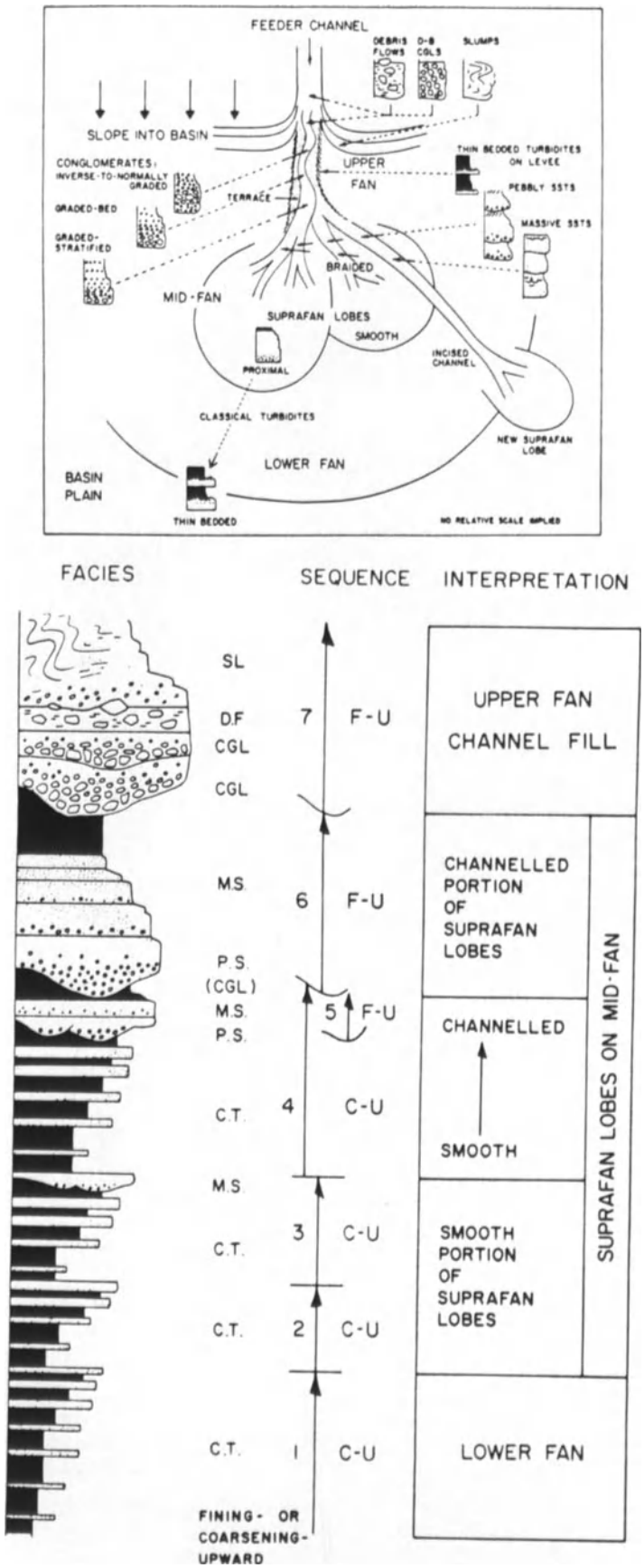

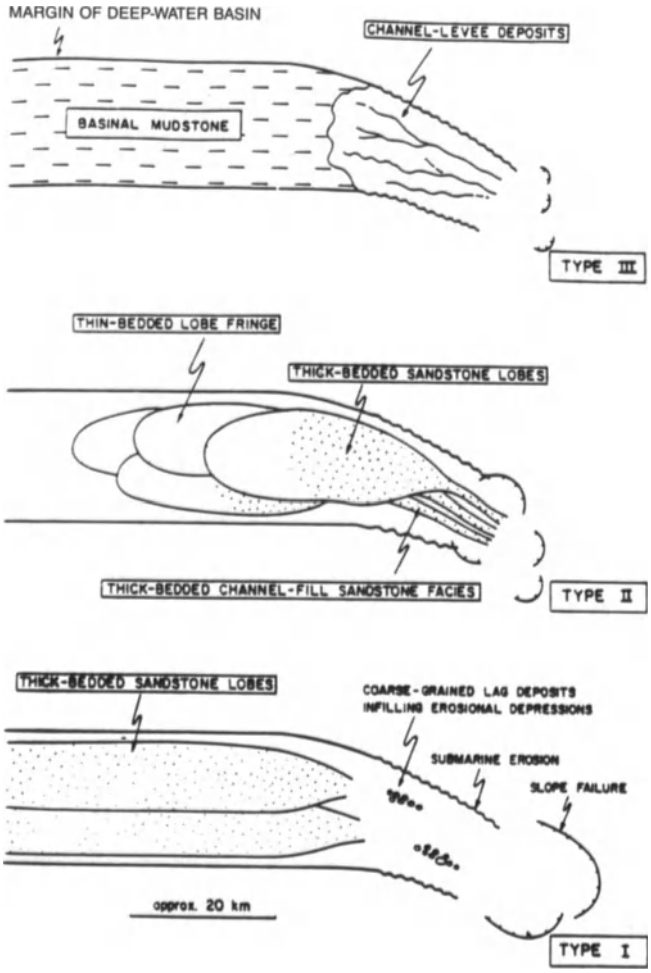

Figure 12.25 Plan view of main types of turbidite depositional systems. (Mutti, 1985; Reprinted with permission of Kluwer Academic Publishers.)

systems form an evolutionary sequence from Type I through Type III (Fig. 12.26), with a progressive rise in relative sea level and a reduction in sediment supply. The entire sequence is capped by basinal mudstone. The upper surface of the mudstone is a sequence boundary formed during the sea-level fall marking the onset of the next cycle of sedimentation.

The Ranger Zone sands can also be interpreted within the context of Mutti's (1985) model. Using the subdivision and terminology of Figure 12.20, the previously interpreted relatively thick-bedded lower Ranger lowstand wedge is a Mutti Type II system. The overlying, thinner-bedded interval of the lower Ranger to the top of the "foram-poor" interval is a Type II/III system. The upper boundary of the

Figure 12.24 Progradational submarine fan depositional model of Walker (1978; Reprinted by permission). No vertical or horizontal scale is intended.

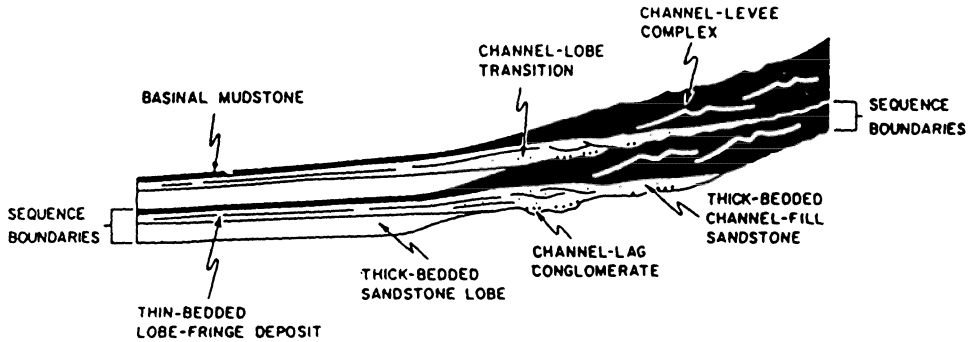

Figure 12.26 Diagrammatic cross section showing the various stages of cyclic turbidite deposition in the Eocene Hecho Group, Spain. (Mutti, 1985; Reprinted with permission of Kluwer Academic Publishers.). No vertical or horizontal scale is intended.

"foram-poor" interval is a sequence boundary. The upper Ranger A of Figure 12.20 is interpreted to form another sequence composed of Type II and III systems, and the coarser upper Ranger B is a Type I or coarse-grained Type II deposit, both separated by a sequence boundary.

Comparison of Models and Implications For Megascale Heterogeneities

The previous discussion is not intended to imply direct analogy between component parts of the three depositional

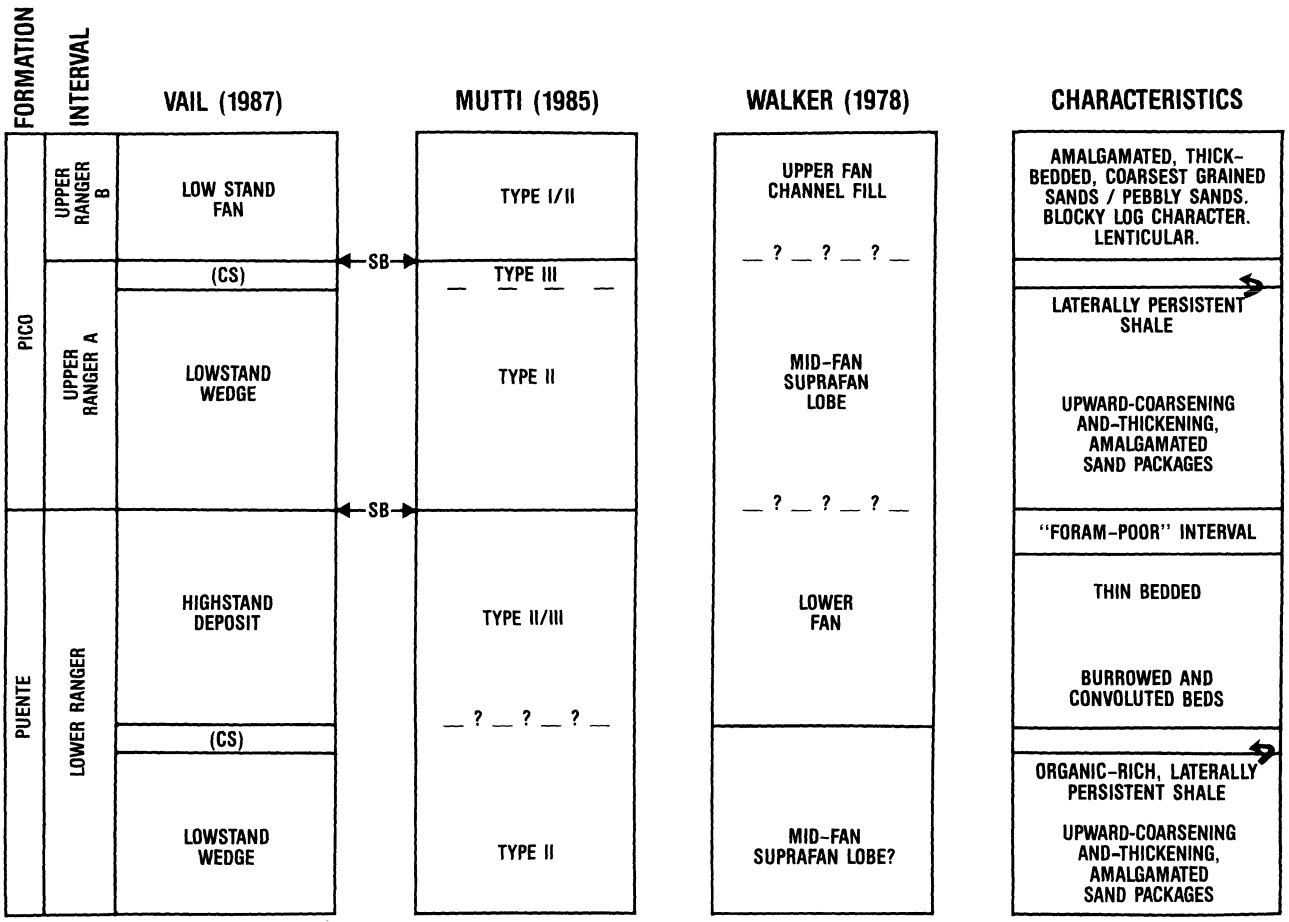

Figure 12.27 Main stratigraphic intervals and characteristics of the Ranger Zone in the Long Beach Unit, and three possible interpretations according to common models or approaches.

schemes. The important point is that, based on large-scale two-dimensional characteristics, Ranger Zone sands can be interpreted within the context of all three depositional schemes (Fig. 12.27), yet each scheme implies a different origin and three-dimensional geometry.

This latter point is significant because it bears on the interpretation of the regional geometry of the depositional system beyond the confines of the Long Beach Unit data grid. The sequence-stratigraphic model implies that "lowstand fan" deposits are fan shaped, and "lowstand wedge" deposits are wedge shaped, as inferred from the isopach of Figure 12.23. The "highstand deposit" is suggested to be more tabular in shape, again as implied by the isopach in Figure 12.22.

Application of the progradational submarine fan model of Figure 12.24 implies that the Ranger Zone sands make up a large, fan-shaped depositional lobe capped by an elongate, approximately north-south-trending main feeder channel.

The turbidite system model of Figures 12.25 and 12.26 is derived mainly from examination of the Eocene Hecho Group, Spain, which was deposited in a small, elongate, active-margin basin (Mutti, 1985) Thus, the overall shape of these systems will be elongate. Strict application of this model to the Long Beach Unit would imply an elongate depositional system.

The above comparison illustrates a potential problem that is encountered when attempting to interpret a depositional model for a succession of strata based on two-dimensional cross-section interpretation and/or when the size of the depositional system is larger than the grid size of the field data.

The effects of describing reservoir properties at the **megascale** for a single well are illustrated in Figure 12.28, using permeability as an example. At the **microscale–mesoscale**, there is about an order of magnitude variation in permeability measurements of individual beds. By scaling up to flow units, this heterogeneity is diminished, and the reservoir takes on a somewhat less complex character, as previously discussed. At the **megascale**, permeability is averaged over such a broad stratigraphic interval that it bears little resemblance to natural geologic heterogeneity. In addition, the style of interbedding is entirely lost at this scale, even though bedding style will significantly impact the fluid flow behavior of a reservoir.

The effects of describing interwell reservoir properties at the **megascale** were evaluated using the three reservoir parameters in Table 12.2 for the three cored wells along the cross section shown in Figure 12.20. These cored wells are almost 3 mi (1.8 km) apart. Consistent trends (Table 12.3) among (1) average permeability, (2) the ratio of Thick-Bedded Sand to Thin-Bedded Sand, and (3) the ratio of feet of medium- to coarse-grained sand beds to very fine- to

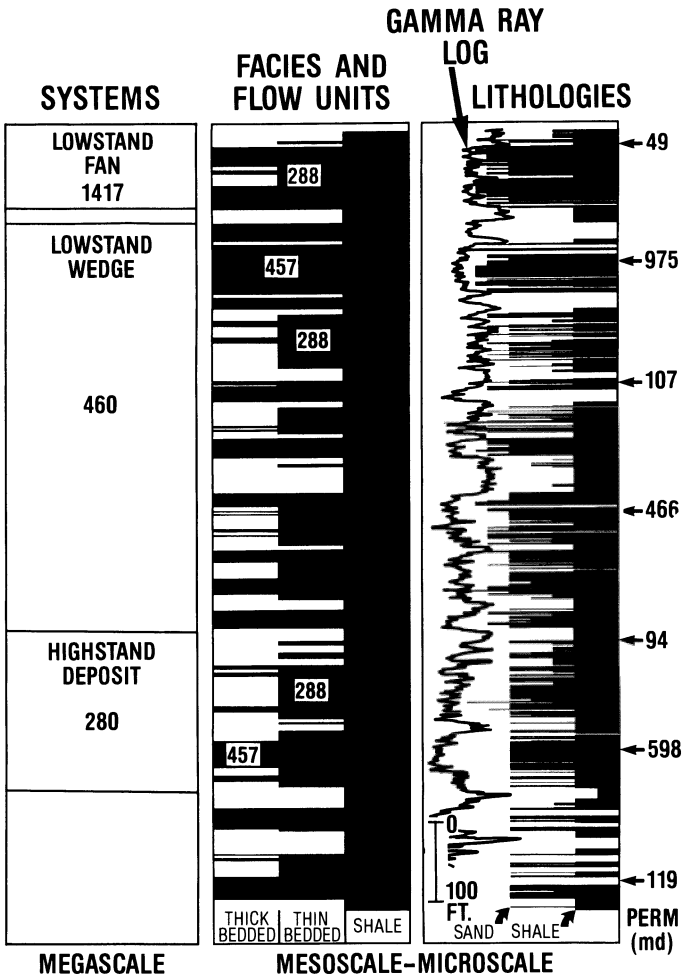

Figure 12.28 Comparison of permeability values at the scale of single lithologies, facies, flow units, and depositional systems (using the sequence stratigraphic terminology discussed in the text). Average permeability values at the megascale are taken from four cored wells, so are different from average permeability values in Table 3, taken from three cored wells.

fine-grained sand beds established at the single-well scale are not apparent at the **megascale** owing to the gross averaging technique that must be applied to these thick stratigraphic intervals. In addition, cores did not completely penetrate the entire upper Ranger B interval (Fig. 12.20), so average values may not be representative of that interval.

It is interesting to note that the overall average values (Table 12.3 and Fig. 12.28) of reservoir properties for the three stratigraphic intervals indicate that (1) the lower Ranger highstand deposit (using the sequence strtigraphic terminology of Figs. 12.19 and 12.20) is the finest grained, thinnest bedded, and least permeable of the three intervals; (2) the upper Ranger A lowstand wedge has intermediate values; and (3) the upper Ranger B lowstand fan exhibits the greatest permeability, is mostly composed of Thick-Bedded Sand, and is the coarsest-grained interval. These

Table 12.3 Properties of Depositional systems from three cored wells

Subzone	Average permeability	No. of permeability measurements	Interval thickness	Thick-Bedded Sand / Thin-Bedded Sand (ft)	Medium- to Coarse-grained Sand / Very Fine- to Fine-grained Sand (ft)
Upper Ranger B Lowstand Fan					
*A863	1127	36	>103 (>31)**	2.1	4.9
B777	1213	25	>74 (>23)**	2.8	7.5
C714	762	95	>230 (>70)**	10.6	9.6
$\bar{X}$	919		>136 (>41)**	6.3	7.9
Upper Ranger A Lowstand Wedge					
*A863	372	136	452 (138)	2.1	1.3
B777	400	101	495 (151)	2.5	2.2
C714	276	110	388 (118)	3.6	2.2
$\bar{X}$	350		445 (136)	2.7	1.9
Lower Ranger Highstand Deposit					
*A863	230	37	178 (54)	1.4	<.1
B777	295	79	218 (66)	3.3	<.1
C714	158	83	252 (77)	2.6	<.1
$\bar{X}$	226		216 (66)	2.5	<.1

*See Figure 20 for well locations.
**Cores did not penetrate this entire stratigraphic interval, so average values may not be representative of that interval.

characteristics are consistent with the interpretation of these intervals within a sequence-stratigraphic framework, as well as within the context of the coarsening- and thickening-upward progradational turbidite model, and illustrate that even at this **megascale**, the primary depositional control on reservoir properties is maintained.

Conclusions

The Ranger Zone sands in the Long Beach Unit can be described at four scales of heterogeneity, but the accuracy of description diminishes with increasing scale. At the **microscale** and **mesoscale**, the sands are composed of three major lithologies—massive sand, graded sand, and shale—which can be grouped into three lithofacies—Thin-Bedded Sand, Thick-Bedded Sand, and Shale. At these scales, permeability and porosity are related to sedimentary characteristics that reflect primary depositional processes. In particular, average permeability varies with sand facies, owing to mean grain-size variations, but porosity does not vary in the same manner because grain sorting in the facies is equivalent.

Lithofacies control on reservoir characteristics provides a sound basis for subdividing the Ranger Zone into flow units at the **mesoscale**. A Thick-Bedded Sand flow unit is defined as consisting of groups of individual beds >2 ft (0.67 m) thick of poorly sorted, fine- to medium-grained sand, with an average of 28% porosity and 457 md permeability. A Thin-Bedded Sand flow unit consists of groups of individual beds <2 ft (0.67 m) thick of poorly sorted, fine- to medium-grained (slightly finer-grained than the Thick-Bedded Sand) sand, with an average of 28% porosity and 288 md permeability; these thin-bedded sands are interbedded with shale beds of equivalent thickness. The Thick-Bedded Sand flow unit is of better reservoir quality than the Thin-Bedded Sand flow unit. Shale, the third flow unit, provides permeability barriers to vertical fluid flow. Recognition of flow units provides a convenient means of "scaling up" the reservoir description by combining various properties that will control the flow of fluids through the reservoir.

At the **macroscale**, individual sand and shale beds are laterally persistent across the reservoir; thus, shale beds probably form effective permeability barriers between individual sand beds. Individual sandy intervals do not show consistent thickness trends, owing to a combination of temporal variations in sediment transport directions and shifting loci of deposition into topographic lows. Within any one stratigraphic interval, reservoir properties such as permeability will vary laterally. Sometimes these variations are systematic and predictable, reflecting sedimentologic and reservoir property relations established at the **mesoscale**. However, between-well lateral relationships are not always predictable, owing to natural geologic variability that may not be detected due to uneven sampling. Lateral variability is generally within an order of magnitude.

At the **megascale**, three alternative interpretations of depositional sequences and systems are presented to illustrate that a unique interpretation is not possible at this scale when the overall size of a depositional system is larger than that of the field size data grid. In the case of the Long Beach Unit, two-dimensional cross sections can be interpreted according to the integrated sequence stratigraphy concepts of Vail (1987), the progradational submarine fan model of Walker (1978), and the active margin turbidite systems model of Mutti (1985). Each of these models involves different formative processes and eustatic-tectonic controls, as well as a different gross three-dimensional geometry. At the **megascale**, reservoir properties are averaged to such an extent over a large stratigraphic interval that there is very little interwell predictability of reservoir properties. Nevertheless, the primary depositional control on gross reservoir properties is maintained at this scale.

Acknowledgments

We thank the following individuals for assistance with this study. Gary Goodrich and Sandy A. Zucker gave consistently solid support by providing log plots, cross sections, and a system for computerized core-description data storage and output. James Bishop assisted in preparation of the core for description and in core photography, J.B. Johnson and H.R. Warner provided logistical support, John Parker and Karben Black graciously prepared superb core layout facilities and assisted with logistics of handling the large volume of core, Douglas W. Jordan completed grain-size analyses, Joseph T. Senftle completed organic content analyses, C.L. Vavra evaluated fractured sand grains in thin section, Susan Epperson developed a computer data base from raw core description data, and Carolyn Sockwell and Kristy Bianchi patiently and expertly typed several manuscript drafts. Manuscript drafts were reviewed by W.J. Ebanks, G.C. Gaynor, D.W. Jordan, J.H. McGowen, H.R. Warner, R.K. Suchecki, R.S. Tye, and J.B. Johnson. We thank ARCO Oil and Gas Company for permission to publish this paper. This manuscript and supporting data are the sole proprietary work product of ARCO Oil and Gas Company, a Division of Atlantic Richfield Company, and the authors. No other parties necessarily concur with or endorse any of the data, analysis, or conclusions presented in this manuscript.

References

Barnes, N.E., and Normark, W.R., 1985, Diagnostic parameters for comparing modern submarine fans and ancient turbidite systems, *in* Bouma, A.H., Normark, W.R., and Barnes, N.E., eds., Submarine fans and related turbidite systems: New York, Springer-Verlag, p. 13–14 and wall charts.

Barron, J.A., 1986, Updated diatom biostratigraphy for the Monterey Formation of California: Pac. Sec. Soc. Econ. Paleont. Mineral., Book 45, p. 105–120.

Baum, G.R., and Vail, P.R., 1988, Sequence stratigraphic concepts applied to Paleogene outcrops, Gulf and Atlantic Basins, *in* Wilgus, C.K., et al., eds., Sea level changes: An integrated approach: Soc. Econ. Paleo. and Miner. Spec. Publ. 42, p. 309–328.

Berman, B., and Clarke, D.C., 1987, THUMS Oil Operations, *in* Clarke, D., and Henderson, C., eds., Oil producing areas in Long Beach: Pac. Sec. Amer. Assoc. Petrol. Geol. Geologic Field Guide to the Long Beach area, p. 99–128.

Clarke, D.D., 1987, The structure of the Wilmington Oil Field, in Clarke, D., and Henderson, C., eds., Oil producing areas in Long Beach: Pac. Sec. Amer. Assoc. Petrol. Geol. Geologic Field Guide to the Long Beach area, p. 43–56.

Ebanks, W.J., Jr., 1987, Flow unit concept—Integrated approach to reservoir description for engineering projects, [abs.]: Amer. Assoc. Petrol. Geol. Bull., v. 71, p. 551–552.

Hearn, C.L., Ebanks, W.J., Jr., Tye, R.S., and Ranganathan, V., 1984, Geological factors influencing reservoir performance of the Hartzog Draw Field, Wyoming, *in* Proceedings 1983 Annual Technical Conference and Exhibit: Society of Petroleum Engineers, p. 1335–1344.

Henderson, C.P., 1987, The stratigraphy of the Wilmington Oil Field, *in* Clarke, D., and Henderson, C., eds., Oil Producing areas in Long Beach: Pac. Sec. Amer. Assoc. Petrol. Geol. Geologic Field Guide to the Long Beach area, p. 57–68.

Henry, M.J., 1987, Los Angeles Basin—An Overview, *in* Clarke, D., and Henderson, C., eds., Oil Producing areas in Long Beach: Pac. Sec. Amer. Assoc. Petrol. Geol. Geologic Field Guide to the Long Beach area, p. 1–30.

Ingle, J.C., Jr., 1980, Cenozoic paleobathymetry and depositional history of selected sequences within the southern California continental borderland: Cushman Foundation Spec. Publ. 19, p. 163–195.

Keller, G., and Barron, J.A., 1983, Paleo-oceanographic implications of Miocene deep sea hiatuses: Geol. Soc. Amer. Bull., v. 94, p. 590–613.

Krause, F.F., Collins, H.N., Nelson, D.A., Machemer, S.D., and French, P.R., 1987, Multiscale anatomy of a reservoir: Geological characterization of Pembina-Cardium Pool, West-central Alberta, Canada: Tulsa, Ok Amer. Assoc. Petrol. Geol. Bull., v. 71, p. 1233–1260.

Lagoe, M.B., 1987: The stratigraphic record of sea-level and climatic fluctuations in an active margin basin; the Stevens Sandstone, Coles Levee area, California: Palaios, v. 2, p. 48–68.

Loutit, T.S., Hardenbol, J., Vail, P.R., and Baum, G.R., 1988, Condensed sections: The key to age dating and correlation of continental margin sequences, *in* Wilgus, C.K., et al., eds., Sea level changes: An integrated approach: Soc. Econ. Paleot. Mineral. Spec. Publ. 42, p. 183–216.

Lyons, K.T., and Suchecki, R.K., 1989, Sequence stratigraphy of submarine-ramp deposits: Miocene Puente Formation, Los Angeles Basin [abs]: 64th Ann. Pac. Sect. Mtg., Palm Springs, Amer. Assoc. Petrol. Geol. Bull., v. 73, p. 544.

Mayuga, M.N., 1970, Geology and development of California's Giant Wilmington Oil Field: Amer. Assoc. Petrol. Geol. Mem. 14, p. 158–184.

McGovney, J.E., and Radovich, B.J., 1985, Seismic stratigraphy and facies of the Frigg fan complex, *in* Berg, O.R., and Woolverton, D.G., eds., Seismic Stratigraphy II: An integrated approach to hydrocarbon exploration: Amer Assoc. Petrol. Geol. Mem. 39, p. 139–156.

Meyer, B.L., and Nederlof, M.H., 1984, Identification of source rocks on wireline logs by density/resistivity and sonic transit time/resistivity crossplots: Amer. Assoc. Petrol. Geol. Bull. v. 68, p. 121–129.

Middleton, G.W., and Neal, W.J., 1989, Experiments on the thickness of beds deposited by turbidity currents: Jour. Sed. Petrol., v. 59, p. 297–307.

Mitchum, R.M., Jr., Vail, P.R., and Thompson, S. III, 1977, Seismic stratigraphy and global changes of sea level, Part 2: The depositional sequence as a basic unit for stratigraphic analysis, *in* Payton, C.E., ed., Seismic stratigraphy—Applications to hydrocarbon exploration: Amer. Assoc. Petrol. Geol. Mem. 26, p. 53–62.

Mitchum, R.M., Jr., 1985, Seismic stratigraphic expression of submarine fans, *in* Berg, O.R., and Woolverton, D.G., eds., Seismic Stratigraphy II: An Integrated Approach to Hydrocarbon Exploration: Amer. Assoc. Petrol. Geol. Mem. 39, p. 117–138.

Morissey, A.M., and Hickey, P.J., 1988, Application of reservoir description in Santa Fe Springs Field, Meyer Zone Waterflood, Los Angeles County, California [abs]: Ann. Mtg., Houston, Amer. Assoc. Petrol. Geol., v. 2, p. 255.

Mutti, E., 1985, Turbidite systems and their relations to depositional sequences, *in* Zuffa, G.G., ed., Provenance of Arenites: NATO-ASI Series, Reidel Publishing Co., Dordrecht, p. 65–93.

Mutti, E., and Normark, W.R., 1987, Comparing examples of modern and ancient turbidite systems–Problems and concepts, *in* Leggett, J.K., and Zuffa, G.G., eds., Marine clastic sedimentology: Graham and Trotman, London, p. 1–37.

Natland, M.L., 1952, Pleistocene and Pliocene stratigraphy of Southern California, [Ph.D. thesis]: University of California of Los Angeles, 165 p.

Posamentier, H.W., Jervey, M.T., and Vail, P.R., 1988, Eustatic controls on clastic deposition; I—Conceptual framework, *in*, Wilgus, C. K., et al., eds., Sea level changes: An integrated approach: Soc. Econ. Paleot. Mineral. Spec. Publ. 42, p. 109–124.

Potter, P.E., and Scheidegger, A.E., 1966, Bed thickness and grain size: Graded Beds, Sedimentology, v. 7, p. 233–240.

Potter, P.E., Maynard, J.B., and Pryor, W.A., 1980, Sedimentology of shale: New York, Springer-Verlag, 303 p.

Randall, et al., 1983,

Sadler, P.M., 1982, Bed-thickness and grain size of turbidites: Sedimentology, v. 29, p. 37–51.

Schweller, W.J., Gidman, J., Grant, C.W., and Reed, A.A., 1988, Lithofacies, depositional environments and reservoir quality of Pliocene deep-sea fan sediments, Inglewood Field, Los Angeles Basin, California, *in* Lomando, A.J., and Harris, P.M., eds., Giant oil and gas fields: Soc. Econ. Paleont. Mineral. Core Workshop #12, v. 1, p. 1–30.

Slatt, R.M., and Hopkins, G.D., 1988, Scales of geological reservoir description for engineering applications: North Sea oilfield example, *in* Form. Eval. and Res. Geol. Proceedings of the 1988 Ann. Tech. Conf. and Exhib. of the Society of Petroleum Engineers, p. 295–302.

Slatt, R.M., Boak, J.M., Goodrich, G.T., Lagoe, M.B., Vavra, C.L., Bishop, J.M., and Zucker, S.M., 1988, Depositional facies, paleoenvironments, reservoir quality, and well log characteristics of Mio-Pliocene deep water sands, Long Beach Unit, Wilmington Field, California, *in* Lomando, A.J., and Harris, P.M., eds., Giant oil and gas fields: Soc. Econ. Paleon. Mineral. Core Workshop #12, v. 1, p. 31–88.

Soper, E.K., and Grant, U.S. IV, 1932, Geology and paleontology of a portion of Los Angeles, California: Geol. Soc. Amer. Bull., v. 43, p. 1041–1067.

Truex, J.N., 1974, Structural evolution of Wilmington California anticline: Amer. Assoc. Petrol. Geol. Bull., v. 58, p. 2398–2410.

Vail, P.R., 1987, Seismic stratigraphy interpretation procedure, *in* Bally, A.W., Atlas of seismic stratigraphy: Amer. Assoc. Petrol. Geol. Studies in Geology No. 27, p. 1–10.

Vail, P.R., and Todd, R.G., 1981, Northern North Sea Jurassic unconformities, chronostratigraphy and sea-level changes from seismic stratigraphy: Proceedings Petroleum Geology, Continental Shelf Northwest Europe, p. 216–235.

Vail, P.R., Hardenbol, J., and Todd, R.G., 1982, Jurassic unconformities, chronostratigraphy, and sea-level changes from seismic stratigraphy and biostratigraphy, *in* Proceedings of the joint meeting of the China Geophysical Society and the Society of Exploration Geophysicists to discuss geophysical exploration for petroleum, Beijing, China, Sept. 7–11: 1981.

Vail, P.R., Hardenbol, J., and Todd, R.G., 1984, Jurassic unconformities, chronostratigraphy and sea-level changes from seismic stratigraphy and biostratigraphy, *in* Ventress, W.P.S., Bebout, D.G., Perkins, B.F., and Moore, C.H., eds., The Jurassic of the Gulf Rim: Soc. Econ. Paleon. and Mineral. Proceedings, v. 1, p. 347–364.

Walker, R.G., 1978, Deep-water sandstone facies and ancient submarine fans: Models for exploration for stratigraphic traps: Am. Assoc. Pet. Geol., Bull., v. 62, p. 932–966.

Yerkes, R.F., McCulloh, T.H., Schoellhamer, J.E., and Vedder, J.G., 1965, Geology of the Los Angeles Basin—An Introduction: U.S. Geol. Survey Prof. Paper 420-A, 57 p.

Index

Abandoned inlet channel
  Capers Inlet, 90
  Price Inlet, 90, 91
Abandoned-inlet channel (Ab) sedimentary facies, Price Inlet, 91
Abandoned tidal creek, Price Inlet, 90, 91
Abandonment, 95–96
Abrupt channel abandonment, 245
Abundance peaks, relation with systems tracts and well-log profiles, 24
Abyssal Plain, 102
Accretion, 10
Acids, Lockhart Crossing Reservoir, 129–130
Active-channel (AC) facies, Core Banks inlet-fill sequence, 87
Active inlet channel
  Capers Inlet, 90
  Captain Sam's Inlet, 85
  in representative examples of tidal-inlet fills, 88
  Johnson Creek (N.C.), 86
  Price Inlet, 90, 91
Active-inlet channel (Ac) sedimentary facies, Price Inlet, 91
Active tidal creek, Price Inlet, 90, 91
Açu Formation (Fm), 161–162
  crevasse lobes and subdeltas, 168
  dip-oriented stratigraphic cross section, blanket nature and offshore facies shown, 163
  isopachs, 180
  and major depositional systems of Mossoro member, 176
  transgressive system containing, 192
Açu River, 161
Açu River delta, 179–180
  fossil barriers, modern barriers and ebb-tidal deltas, 181
Africa-South America rifting of the Early Cretaceous, 161
Alberta (Canada), 13, 14, 16
  Cardium Pembina Field, 19
  Triassic Halfway Formation (Fm), 86–87
Alberta Basin, 13
Alberta foreland basin, 11
Albian/Cenomanian stage, 161
Albian to Cenomanian Logan Canyon Formation (Fm), 15
Albite overgrowths, carbonate diagenesis, 129
Algal mat laminations, 174
Algal mats, 184, 190, 192
Algal mats/marls, Mossoró Sandstone, 193
Alice Springs, 39, 45, 46
Alice Springs Orogeny, 44–45
Allied at Fault, 265
Alpine foreland basins, flysch-to-molasse sequence, 10
Altamira Shale member, 266
Alumino-silicate, 118
Amadeus Basin, 2, 40
  basin fill, 40–44
  basin morphology and evolution, 39–40
  clastic petroleum reservoirs, 39–72
  hydrocarbon potential, 45–46
  hydrocarbon resources, 45
  map showing location and main morphologic features, 40
  simplified sequence-stratigraphic chart and onlap curves for Late Proterozoic to Devonian sequences, 41
  structural history, 44
  thrust faulting, 44–45
Amoco No. 3 J.A. Thom, Section 41, T6S, R3E, 124
Amoco Production Company, 117
Amplitude, 21
Amplitude anomalies, 32, 33, 35, 36
Analogs
  ancient, introduction to, 113–115
  modern, 75
Anatase (titanium oxide)
  development in Mossoró Sandstone, 195, 198, 199
  Mossoró Sandstone lithofacies content, 197
Ancient analogs, introduction to, 113–115
Angle of facies migration, 4, 5, 7
Angle of progradation, 5
Angles of translation, 5
Anhydrite, 53, 55, 62, 71
Anhydrite cement, 71
Ankerite, 53, 125, 128, 131, 132
  carbonate diagenesis, 129
  percent found in littoral facies, 123
Ankerite cement, feldspar content, 131
Ankerite rhombs, 126
Antalya Basin, 102
Anticline, 44
  compactional, 209, 218, 220–221, 223–227
  doubly-plunging, 122
  elongate, 232
  Mereenie, 66
  roll-over, 118, 121, 137
  Wilmington, 267
Antithetic growth faults, 118
Apalachicola River, 136
Apodi outcrop, 162, 164
Appalachian Mountains, 118, 136
Aragonite, 124–125
Aralka Formation (Fm), 41
Araucariacites australis, 186, 190
Areia Branca fault, 162

Arenaceous foraminifers, 163
Arenig, 43, 58
Arenite, Permian Bell Canyon Sandstone Reservoir, 208
Areyonga Formation (Fm), 41, 42, 55
Arkose, Mossoró Reservoirs, 197
Arkosic arenites, 258
  Deep Marine Sandstone, 242, 245
Arkosic wackes, 258
  Deep Marine Sandstone, 242, 245
Arumbera Sandstone, 40, 42, 43, 45–55
  basinal setting, age and stratigraphy, 46
  depositional setting, 50–51
  diagenesis, 54–55
  facies analysis, 47–50
  gamma-ray and sonic logs in Dingo #2 well, 52
  isopach map, 46
  regional distribution, 46–47
  reservoir characterization, texture and mineralogy, 51–53
  reservoir quality, 53–54, 56
  two-way time to the base, 44
  vs. Pacoota Sandstone, 73
Arumbera Sandstone 1, 41
Arumbera Sandstone 2, 41
Arunta Block, 40
Arunta Complex, 40, 41
Asterosoma, 143–145, 147–148, 155, 157
Aswan, 103
Aswan High Dam, 101, 104, 107
Australian Bureau of Mineral Resources, 58
Australian craton, 2, 39
Australian early Datsonian, 58
Australian late Payntonian, 58
Authigenic clays, 65, 67
Authigenic minerals, 53
Authigenic smectite, Deep Marine Sandstone, 245
Authigenic zeolite (clinoptilolite-heulandite), Deep Marine Sandstone, 245
Autocyclicity, 4
Autocyclic switching, rate of, 4
Autocyclic switching of depositional fairways, 1
Autocyclic switching of sediment input points, 4
Average wave heights vs. mean tidal range for mid-Atlantic and SE coastline of U.S., 78
Ayres Rock, arkoses, 46
Azimuth frequency plots, 7-CAM-30-RN well, 190

Backbarrier (Bb), Johnson Creek (N.C.), 86
Backbarrier (Bb) silts, Core Banks inlet-fill sequence, 87
Backbarrier tidal-creek facies, 88
Baixa do Algodão Field (BAL), 162, 163–164, 176
  core photographs, 166
  facies distribution, 167
Banquereau Bank, 12, 13
Banquereau Formation (Fm), 19
Banquereau Plateau, 12
Barataria Bay (La.), tidal inlets along the barrier-island shoreline, location map, 93
Barataria Bight, 91
  active tidal inlets along the shoreline, 92
Barataria Pass, 92
Bar bypassing, 82–83, 87
  definition, 80
Bar deposits, 163
Barremian to Aptian Upper Missisauga Formation (Fm), 17
Barrier island, 5, 77, 89–90, 121
Barrier island facies, 88
Barrier-island reservoir facies, 77
Barrier-island reworking, 89
Barrier-island sediments, 192–193
Barrier-island shoreline, 78
  tide-dominated, percentage of Holocene as inlet fill, 90
  wave-dominated, percentage of Holocene as inlet fill, 90
Bartonian, 15
Basal bed, 143
Basal Pliocene unconformity, 283
Base-level change, 4
Base-level fall, 8
Basin-floor fan, 25, 28
  seismic section showing gas field that was developed, 25
  seismic, well-log, and lithologic characteristics, 26
Basin-floor fan systems tract, 23–24, 33–35
  seismic facies and their seismic, well-log, and lithologic characteristics, 26
  seismic section with trap developed along an updip pinch- out, 34, 35
Basin margin, 40
Basin Research Institute, 117
Basin subsidence, 90
Bathymetric highs, 232
Bathymetry, 101, 105
  generalized bathymetric map of the eastern Mediterranean, 102
BCFG (billion cubic feet of gas), 138
Beach deposits, 174
Beach ridge, Captain Sam's Inlet, 85
Bedform migration, 157
Bell Canyon Formation (Fm), 201–203
  lithofacies, 204
  location and type of control points, 204
  type log and core, 205
Belmont A-1 fault, 281
Belmont Fault, 265, 281
Benthic fauna, 233, 249
Benthic foraminiferal fauna, 268
Bentonites, 266
Bioclast
  7-CAM-63-RN well, 173
  Canto do Amaro oil field, 177
Bioclastic calcilutite, 184, 190
  Mossoró Sandstone, 191, 192
Biostratigraphic criteria, for identification of systems tracts, 23
Biotite, Deep Marine Sandstone, 242
Bioturbation
  7-CAM-79-RN well, 188
  Canto do Amaro Field, 172, 175
  Deep Marine Sandstone, 238, 241, 242
  Mossoró field, 171
  Mossoró member, 168
  Mossoró Sandstone, 184–186, 193, 197
  Permian Bell Canyon Sandstone Reservoir, Trap, 218–219
Bipolar crossbedded sandstones in tidal inlet sequences, 186
Bitter Springs Formation (Fm), 41, 42, 44, 45, 55
  formation and relation to depositional sequences with Arumbera Sandstone, 47
  massive salt core formed from the Gillen Member, 57
  salt highs' location, 46
Bivalve fragments, 233
Bloods Range Beds, 41
"Blue northers," 206
Bluesky Formation (Fm), 14
Bluesky Sandstone, 14
Bogue Banks (N.C.), preserved inlet fills, 91
Bolivina pisciformis, 269
Bouge Banks (N.C.), percentage of Holocene as inlet fill, 90
Bouma A graded intervals (T_a), 270
Bouma B intervals (T_{ab}), 270
Bouma C intervals (T_{abc}), 270
Bouma sequences, 206, 207, 240
Brachiopod fragments, inarticulate, 64
Brachiopods, 58
Brackish transgression, 15
Brazos River, 136
Brewer CGL, 41

British Columbia, Triassic Halfway Formation (Fm), 86–87
Browns Bank, 12
Brushy Canyon Formation (Fm), deep-sea fan model applicability, 201
Bulimina subacuminata, 269
Bulk density (RHOB), 255, 257–258
Burdekin delta, 179
Burial-induced silicification, 64
Burrows
  7-BAL-5-RN well, 165
  7-CAM-63-RN well, 173
  9-MO-13-RN well, 169
  RE-8-RN well, 174

C-608 Fault, 265
Cadomin Formation (Fm), 14
Calcarenites, 176
  detrital/fossiliferous, 176
Calcareous cement, 65, 69, 73
Calcareous fossils, 119, 124–125
Calcareous member (MBR), 15
Calcilutites, 185
Calcite, 68, 124–125, 128
  carbonate diagenesis, 129
  Ford-Geraldine Field, 226
  parasequence set 12, 72
  percent found in littoral facies, 123
  Permian Bell Canyon Reservoir, 206
  precipitation in Mossoró Sandstone, 195, 199
  source for carbonate cements, 128
Calcite cement, 66, 71, 131
  Bell Canyon Formation (Fm), 205
  feldspar content, 131
  leaching in Mossoró Sandstone, 199
  leaching to create secondary porosity in Mossoro Sandstone, 195, 199
  parasequence set 12, 70
  Permian Bell Canyon Sandstone Reservoir, 224
  pore-filling poikilotopic, Mossoró Reservoirs, 198
Calcite concretion, 7-CAM-79-RN well, 188
Calcium, 131, 132
Calculated permeability, 258, 259, 260
Callon Petroleum Company, 117
  M.I. Stewart No. 1, 123
Cambrian Period (sandstone), 16
Cambrian Period sedimentation, 43
Campanian-Maastrichtian (sandstone), 16
Campanian/Maastrichtian, 161
Campbell Creek Field, 139
Canada, relative highstand systems tracts, 17
Canto do Amaro Field (CAM), 114, 162, 179
  absence of barrier-island sediments, 192–193
  algal mats, 192
  core photographs, 175
  depositional setting, 180
  discovery, 183
  estuarine/tidal-flat system, 168–170
  facies, 170, 171
  facies relations and reservoir geometry, 175–176
  facies relations shown in cross-sections, 177
  flood-tidal delta sequence, 187
  inlet-channel sequence, 187
  location map, 184
  permeability, 197
  porosity, 197
  shallow marine system, 176
  stratigraphic column of the Potiguar Basin, 185
Canyon head, 138–139
Cape Hatteras, 82
Cape Lookout
  cuspate foreland, tidal inlets along the barrier islands, 79, 80
  historical analysis, 81, 82
Capers Inlet (S.C.), 80–81
  bar-bypass mechanism of inlet channel abandonment, 82
  geometries and facies relationships of tide-dominated inlet sand bodies, 88
  linear dimensions of tidal inlet-fill sequences, 84
  strike-oriented vibracore transects across the abandoned inlet channels, 90
  tidal-inlet migration, 88, 89, 90
Capers Island (S.C.), 88, 91
  cross section locations, 88
  inlet fill %, 90
  percentage of Holocene as inlet fill, 90
Cape Sebastian Sandstone, 16
Captain Sam's Inlet (S.C.), 85, 95
  geometries and facies relations, 83
  linear dimensions of tidal inlet-fill sequences, 84
  oblique aerial photograph, 84
  photograph of cored wave-dominated inlet-fill sequence, 85
  sedimentary facies, 85
  strike-oriented cross section for wave-dominated, 85
Carbonaceous organic matter, 7-CAM-79-RN well, 188
Carbonate, 40, 42, 132
  deposition of, 45
  stromatolitic, 48–49
Carbonate allochems, 124
Carbonate cementation patterns, distribution across Lockhart Crossing Field, 127
Carbonate cements, 123, 132
  distribution in Lockhart Crossing Reservoir, 133
  Lockhart Crossing distribution, 129, 130
  Lockhart Crossing Reservoir, 117
  trends through the littoral facies interval, 123
Carbonate diagenesis, relative timing and temperatures, 129
Carbonate dissolution, 268
Carbonate intraclasts, 191
  7-CAM-79-RN well, 188
Carbonate mudstone, Wilmington Field, 271
Carbonate sedimentation, Deep Wilcox trend, 135
Carbon dioxide injection, phases, Ford-Geraldine Field, 222–227
Carboniferous Period, 45
Cardium Formation (Fm), 13
Cardium oil fields, 13
Cardium Pembina Field, 19
Carmichael sub-basin, 40, 44, 45, 46
  depositional setting, 51
  facies analysis, 47, 48, 50
  idealized north-south cross sections, 47
Carmichael SST, 41
Carrizo member (MBR), 136
Cassidulina cushmani, 269
Castile Formation (Fm), 202
Catalina Schist, 266, 268
Cation-poor clays, 124
Cavalas River, 181
Cedar Inlet (N.C.), linear dimensions of tidal inlet-fill sequences, 84
Cemented sandstones/dolosparites, 170
Cenozoic Era, 161
Central Ridge, 46–47, 61–62, 64, 66–67
  basin mechanics and, 40, 42–43, 55
  depositional setting of the Arumbera Sandstone, 50–51
  parasequence set 10, 69
  parasequence set 12, 71
  parasequence set 13, 72
Cerritos Fault, 265
Chalks, 15
Chandler Formation (Fm), 41, 45
Chandler Limestone, 45–46

Channel facies, 23, 27, 28, 32, 35
slope-fan systems tract, 35
Channel-fill facies, 119–122, 126, 130–131, 133
composition, 125
distribution and thickness superimposed upon a structure contour map of the Wilcox Formation top, 125
and pyrite distribution in 17 cores of Lockhart Crossing Field, 128
stacking of, 127
Channel-fill plug, 87, 91
Channel levee facies, 27, 28
Capers Inlet, 90
seismic, well-log, and lithologic characteristics, 26
Channel scour, 86
Chaotic facies, 23, 27–28, 32
seismic, well-log, and lithologic characteristics, 26
Charlie Daubert North Field, 139
Cherry Canyon, 202, 203
Cherry Canyon-Upper San Andres shelf margin/slope break, 203
Chert, 53, 65, 68, 266
Chert granules, 155
Chert-pebble conglomerates, 16–17
Chlorite, 53–54, 62, 65, 67, 132
Ford-Geraldine Field, 226
late compactional regime, Lockhart Crossing Reservoir, 130
parasequence set 8, 68
Chondrites, 143–145, 148, 156–157, 172, 176
Mossoró Sandstone, 184–185
RE-8-RN well, 174
Cibicides McKannai, 269
Cicatricosisporites purbeckensis, 186, 190–192
Clacite, Mossoró Sandstone lithofacies content, 197
Claiborne Group rock unit, 118, 135, 136
Classopollis major, 186, 190
Clastic petroleum reservoirs, Late Proterozoic and Early Paleozoic Amadeus Basin, Central Australia, 39–72
Clastic reservoir units, 2
stages of basin development when deposits likely, 45
Clastics, 161
fine-grained, 66
Clastic wedges, 10–11
built over and beyond Cretaceous carbonate shelf edges, 135
Clasts, 120
Clay, Deep Marine Sandstone, 245
Clay clasts, 129
Clay drapes, 185, 186, 191
7-CAM-79-RN well, 188
Mossoró Sandstone, 193
Clay intraclasts, 191
7-CAM-79-RN well, 188
Mossoró Sandstone lithofacies content, 197
Clay rip-up clasts, 120
Claystone, Wilmington Field, 271
Cleland SST, 41
Cliffhouse Sandstone, 94
Climbing bedforms, 4
Climbing-ripples, 62
7-CAM-79-RN well, 188
Clinoforms, 4, 9
disrupted by rotational faults, 19
northward-prograding, 11
Upper Mannville, 14
Coal, Canto do Amaro oil field, 177
Coal level, 7-CAM-79-RN well, 188
Coarsening-upward parasequences, 50
Coarsening-upward sequences, 29, 30, 36
Canto do Amaro oil field, 172
Coastalplain sequences, 118
Cohasset A-52, 14
Coiling ratio, 233
Color (shale), 7-CAM-63-RN well, 173
Colorado River, 136
Columbus Field, 137–138, 139
Compactional regime, 123
Concretions, feldspar content, 131
Condensed section, 280, 282, 284, 285
Configuration, 21
Conoco reports, Ford-Geraldine Field production, 219
Conodonts, 58
correlation of Pacoota Sandstone Units from Palm Valley Field to Mereenie Field, 59, 60
parasequence set 13, 72
Contemporaneous fluvial-deltaic facies, 25–26
Continental margins
and Nile Fan, 106
stable progradational, vs. contemporaneous fluvial-deltaic facies, 25–26
unstable progradational, 23
Continental Shelf, 102
Continental Slope, 102
Continuity, 21
Contorted bedding, 156
Convolute bed, 7-BAL-5-RN well, 165
Copper delta, 179
Copper mineralization, 49
Coquinas, 184, 185
Core Banks (N.C.), 91
inlet fill %, 90
percentage of Holocene as inlet fill, 90
Core Banks (N.C.) inlet-fill sequence, wave-dominated, core photograph, 87
Core descriptions, 140–156
Core symbols, 141
Correlative downdip conformities, 280
Corrensite, 146
Cottonwood Creek South Field, 137, 139
Cretaceous (Period) reef tracts, 136, 137
Cretaceous Western Interior Seaway, 94
Crevasse deposits, Apodi outcrop, 164
Crevasse lobe deposits, 166, 168, 169
Crevasse lobe sand body, 168
Crevasse lobe sandstones/siltstones, 163
Crevasse lobes/subdeltas, 176
Crevasse/overbank deposits, 168, 169, 176
Crevasse/overbank sandstones and siltstones, Mossoró Field, 170
Crevasse sandstones, Apodi outcrop, 164
Cross faults, 265
Cruziana, 69
Cruziana ichnofauna, parasequence set 13, 72
Cruziana trace fossil, 66
Current-ripple cross-laminae, 156
Cyprus basin, 105–106

Daisy Avenue Fault, 265
Damietta distributary, 104, 109
Damietta Fan, 101
Darwin, 39
D. Brouweri, 24
D. Brouweri "A", 24
Dean Quartzite, 42
Deception Formation (Fm), 41
Dedolomitization, 62
Degree of preservation, 4
Deep Marine Sandstone, 231–260
cross sections, 245
depositional model and vertical sequences, 245–250
depth plot of permeability over a typical section of the cored interval, 260
frequency distributions of porosity and permeability data, 253
geologic setting, 231–232
grain size and sorting, 251–252
grain size/sorting crossplot for sieved samples, 254
helium porosity depth plot and bulk density log, 252
helium porosity/sorting crossplots, 255
lithofacies, porosity, 252
lithofacies, statistics, 238
lithology and lithofacies, 234–242
paleontology, 233–234
permeability, 251–260

permeability prediction, 253–260
permeability, sorting, and grain size, 252
petrography, 242–245
petrophysics, 250–253
porosity, 251–260
porosity/permeability crossplot showing least-squares regression line and correlation coefficient, 254
porosity, permeability, sorting, and grain size, 252–253, 255–259
porosity, sorting, and grain size, 252
sand thicknesses, net and gross, by reservoir zone, 250
sieve analysis, 251, 255–257
Deep-sea fan model (Walker), 240
Deep-sea fan system, 104, 238, 250, 258
depositional patterns, 249
Deep-water epicontinental basins, 114
Deep-Water Sand Giant Oil Field, geologic heterogeneity scales, 263–291; *see also* Wilmington Field
Deep Wilcox trend
Central Texas Gulf Coast: Wilcox geology and hydrocarbon production, 136–139
core descriptions, 140–156
interpretation, 156
lower Wilcox depositional systems, 138
regional setting, 135–136
shelf sandstones, 135–157
submarine-fan reservoirs, 139–140
upper Wilcox depositional systems, 138
Wilcox deposition, 135
Deep Wilcox wells, 114
Deformed bedding
7-CAM-63-RN well, 173
9-MO-13-RN well, 169
Delaware Basin, 114, 201, 203
Delaware Fan, meanders in sand-rich terminal lobes, 207
Delmontian fauna, 268
Delmontian/Repettian boundary, 283
Delmontian time, 266, 268, 270, 281
Deltaic distributary, coarser facies, 8
Delta plain, 162
Deltas, fluvial-dominated, 136
Density-driven currents, 201
Depocenters
Ordovician Period, 43–44
Wilcox, 137
Deposition, 3, 5, 6
reduced rate of, 106
Depositional base level, change of, 3
Depositional facies, 2, 5
Depositional facies sequences, 4
Depositional lobe, gradual migration across the basin floor, 115
Depositional sequences, 21, 280
Ranger Zone, 283
Depositional systems tracts, 9, 162
Depositional units, trends through the littoral facies interval, 123
Depth of water (D), 3
Detrital clay, 71
Detrital matrix, 126, 129
Detrital opaque minerals, Mossoró Sandstone lithofacies content, 197
Detrital quartz grains, 65
Devonian Catskill Delta, 51
Devonian Period, Amadeus basin final depositional episode, 44
Dewees Island (S.C.)
abandoned tidal inlet-channnel, 89
inlet fill %, 90
percentage of Holocene (epoch) as inlet fill, 90
Diagenesis, 68, 72, 73
burial, 73
carbonate, 129
of sandstone, 61–62
Diamictite level, 7-CAM-79-RN well, 188
Diapirism, 105, 106, 111
Diapirs, 101, 103
elongated, in the Nile Fan, 104
piercing of, 105
Diastems, 3
Diatomite, 268
Wilmington Field, 271
Dingo Field, 45, 51–52, 55, 66
distribution and isopachs of parasequence sets, 63
parasequence 8, 66
porosity logs for the reservoir interval, 53
seismic section (P80-11) showing well locations and reservoir interval, 57
structure contour map of top of the first gas pay, 57
Dingo structure, 55
Dinoflagellates, 190
Diplocraterion, 69, 145
parasequence set 12, 72
Dish structures, 270
Distal Continental Margin, 102
Doboy Inlet (S.C.), linear dimensions of tidal inlet-fill sequences, 84
Doboy Sound Inlet (Ga.), geometries and facies relationships of tide-dominated inlet sand bodies, 88
Dolomite, 53–55, 65, 69, 71, 73, 124–125
ferroan, 125
Mossoró Sandstone lithofacies content, 197
precipitation in Mossoró Sandstone, 196
source for carbonate cements, 128
Dolomite cements, 62–64, 69
parasequence set 8, 68
parasequence set 13, 71
Dolomite concretion, 7-CAM-79-RN well, 188
Dolosparites, 175
transgressive detrital, 176
Domes, 44
Downdip trend, 114
Downlap, 23
Downwarps, 44
Drainage axes, 135–136
Drapes, 183, 184
Drillstem test (DST #4), 68
D. Surculus, 24
Dunes
in representative examples of tidal-inlet fills, 88
Price Inlet, 90, 91

Early Cambrian period evaporites, 45
Early Cenozoic era, 104
Early Cretaceous (period) Sligo tract, 137
Early Mesozoic era, 111
Early Ordovician period, 43
Early Paleozoic era section, 42
Early Pleistocene epoch, 103–104
Early Pliocene epoch, 106
Early Pliocene (epoch) marine transgression, 103
Early Tertiary period, 45
Earthquakes
and downslope sediment flow off the Nile Delta, 111
and turbiditic flows, 106
East African plateau, 101
Eastern Fan Province, 102
Eastern Scheldt estuary, 178
Eastern Shoal, 12
Ebb-tidal deltas, morphology and sediment distribution patterns, 80
Edwards-Stuart City system, 137
Egyptian plateau, 103
Electromagnetic propagation time (TPL) log, 255, 257–258
Electromagnetic propagation time (TPL) log trace, 254
Ellery Creek, 66, 69, 72
Ellery Creek S., 61
El Mar Field, 203, 210
Elmworth gas field, 17
Embayment, 77–79, 95, 180
Emerald Bank, 12

En echelon anticlinal trends, 44
England, 15
  interbedded estuarine and shelf deposits, 15
Eocene Hampshire Basin, 15, 16
Eocene Hecho Group (Spain), various stages of cyclic turbidite deposition, diagrammatic cross section, 288
Eocene Series, 136
Eolian sand, 103
Eonile, 103
Epistominella pacifica, 269
Equisetosporites species, 186, 190
Eratosthenes Abyssal Plain, 102, 106
Eratosthenes Seamount, 101, 102, 106
Erosion, 3, 5, 6, 120
  severe coastal, 104
Erosional contact, 7-CAM-79-RN well, 188
Erosional sequence boundaries (ESB), 9, 19
Estuarine channel-mouth bar sandstones, 178
Estuarine sandstones, 8, 163
Estuarine/tidal flat, 162
Ethiopian plateau, 101
Eunice canyon, 203
Eustatic change, 5
Eustatic fall, 4
Eustatic sea-level change (fluctuations), 3, 4, 11
  Amadeus basin, 40
  and relative sea-level fluctuations, 22
Evaporites, 40, 42
  deposition of, 45
Exposure feature, Mossoró Sandstone, 193

Facies association, 162
Facies migration, 1
Fair-weather wave base, 6
Falls City Field, 137, 139
False anomalies, 35
False bright spots, 36
Faulted contact, 104
Faulted escarpments, 76, 101
Faulted terrain, 103
Faulting, 101, 105–106, 111, 264–265
  northwest-trending, in Nile Fan, 104
  seismic activity as trigger for turbiditic flows, 106
Fault zones, Lockhart Crossing Reservoir, 130
Fauna, Delmontian and Repettian stages, 268
Feldspars, 53, 62, 64, 73
  abundance and known lost, normalized to quartz, littoral depositional facies, 131
  Canto do Amaro Field, 194
  carbonate diagenesis, 129
  Deep Marine Sandstone, 242, 245
  dissolution, and quartz overgrowths, 132
  kaolinized, 73
  late compactional regime at Lockhart Crossing Reservoir, 130
  Lockhart Crossing Reservoir, 131
  Mossoró Sandstone lithofacies content, 197
  Pacoota Sandstone, 66
  parasequence set 8, 66–67, 68
  parasequence set 13, 71
  Tempe Vale #1 well, 72
Feldspar overgrowths, Mossoró Sandstone lithofacies content, 197
Feldspar/quartz ratios, 131
Feldspathic litharenite, Mossoró Reservoirs, 197
Feldspathic phyllarenites, 118
Feldspathic phyllarenite sandstone, 119–120
Ferroan calcites, carbonate diagenesis, 129
Ferruginous cements, 62, 67
Festoon cross bedding, 49
Fine-fraction x-ray diffraction (XRD) analyses, 65
Fining-upward cycles, 66
Fining-upward sequences, 29–30, 31, 166
  7-CAM-79-RN well, 188
  Canto do Amaro field, 175
  crevasse lobe deposits, 171
  Mossoró Field, 171
  Mossoró Field sandstones, 170
  Mossoró member (MBR), 168
Flaser bedding, 143, 146, 157, 172, 178–179
Flasers, 184, 186, 191
  7-CAM-63-RN well, 173
  7-CAM-79-RN well, 188
  Mossoró Sandstone, 193
  RE-8-RN well, herringbone, 174
Flood-plain deposits, 166, 176
Flood-tidal deltas, 186
  morphology and sediment distribution patterns, 80
Flora, 186, 190
Florence Rise, 102
Florida platform, 135
Flow units, 1
Fluid content, 21
Fluid escape structures, 270
Fluid production and injection histories, 115
Flume chute, 208
Fluvial bar overlying a channel sequence, Apodi outcrop, 164
Fluvial channel coarser facies, 8
Fluvial dominated deltas, 31–32
Fluvial facies, 58
Flysch phase, 10
Flysch-to-molasse sequence of Alpine foreland basins, 10
Folding, 265
Foraminiferal faunas, Wilmington Field, 268
Foraminifers, 176
  marine, 192
  Pliocene epoch, 233
Foram-poor interval, 268–270, 283–284, 287–288
Forced regression, 7
Ford-Geraldine channel, 213–215, 217–218, 226
  Ramsey 2 sandstone interval, 220
Ford-Geraldine Field, 204, 215
  carbon dioxide injection phases, 222–227
  channel geometry, 211–213
  cores studied, 207
  depositional history and performance, 201–228
  geometry of channel complex, 210–212
  laminated siltstone unit, 216
  lithofacies, 204
  permeability, 226
  porosity, 226
  production history, 219–226
  production performance curves, 222
  tertiary production, cumulative, 228
  total primary production and pre-Trap structure, 223
  total secondary production and pre-Trap structure, 223, 224
  transport paths for lagoonal siliciclastics to bypass the carbonate shelf margin, 203
  Unit #108, type log and core, 205
  waterflood stages, 222–225
Ford siltstone, 204–206, 209–210, 212–214, 216, 218
  isopach map, 216
  isopach map (Ramsey 1A interval), 215
  laminated, 210
  structure on top, 213
Foreland basins, 10–11
  basin subsidence, 10–11
  unconformity-bounded sequence development, 10
Foreshore
  Capers Inlet, 90
  Captain Sam's Inlet, 85
  in representative examples of tidal-inlet fills, 88
  Price Inlet, 91
Fossiliferous/dolomitic sandstones, 168
Frequency, 21

Frio barrier/strandplain system, 76
Frio Formation (Texas), 94
Frio interval (Texas), 123
F-test analysis of covariance, 254

Gamma ray (GR) log evaluation, 255, 257–258, 285
Garnet, Mossoró Sandstone lithofacies content, 197
Gas fields
  Mereenie Field, 45
  Palm Valley Field, 45
  production per systems tract, relative amounts, 34
  slope-fan systems tract, 35
  within a slope-fan systems tract, 35
Gastropod, 184
  7-CAM-79-RN well, 188
Gastropod coquina, 174, 192
  7-CAM-79-RN well, 188
  Mossoró Sandstone, 191, 193
Genetic hierarchy, 1
Genetic stratigraphic units, 135
Geomorphologic provinces of the Nile Fan, 101–111
Geomorphology, 76
Georges Bank, 12
Georgia
  channel-fill facies, 121
  tidal inlets, 77–79
Georgia Bight, 83
Georgia embayment, 77–79, 88
Geothermal reservoir, geopressured, 135
Geraldine Field, 114
Gething Formation (Fm), 11, 14
Giles CK DOL, 41
Gillen Member (MBR), 41, 44, 45, 55
  evaporites, 42
  massive salt core formed from, Bitter Springs Fm, 57
Glaciers, slope-fan systems tracts development, 25
Glaucogenesis, 69
Glauconite, 120, 126, 129, 133
  Amadeus basin, 58–60, 64
  in parasequence set 7, 66
  parasequence sets 10 and 11, 69
Glauconite and conodonts, correlation of Pacoota Sandstone Units from Palm Valley Field to Mereenie Field, 59, 60
Glauconitic sandstone, 119, 121
Glossifungites, 145–146, 148
Gog Sandstone, 16
Golden Avenue Fault, 265
Good Hope Field, 139
Goyder Formation (Fm), 41, 59, 60, 61
Grabens, 101, 107, 161
  offshore, 162
Graded Sand, 270
Grain crushing, 276
Grand Isle, 21
Gravitites, 109
Growth faulting, 24–25, 32, 76
  contemporaneous, 120–121, 126, 127
Gulf Coastal Plain basin, 123
Gulf Coast Tertiary oil fields, 117
Gulf Coast Tertiary units, 129
Gyroidina rotundimargo, 269
Gyrolithes, 144, 145

Half grabens, 161
Halfway Formation (Fm), 94
Hallettsville Burns Field, 139
Hallettsville East Field, 139
Halokinesis, 104, 105, 106
Harbor Entrance Fault, 265
Hardground, well-cemented submarine, 4
Heavitree Crite, 41
Heavitree Quartzite, 40–42
Heavy minerals, 69
Helen Gohlke Field, 137, 139
Helium porosity, Deep Marine Sandstones, 251, 252, 255, 257
Helminthoida, 143–145, 157
Hematite, 53
Hemipelagic facies, 27, 28–29, 32
  seismic, well-log, and lithologic characteristics, 26
Hemipelagic mud, 109
Hermannsburg SST, 41
Herodotus, 101, 104
Herodotus Abyssal Plain, 102, 106, 107, 109
Herringbone cross-bedding, 62, 148, 150
  7-CAM-79-RN well, 188
  Canto do Amaro Field, 172
Herringbone cross-lamination, 66, 156
Herringbone cross-stratification, 69
Herringbone ripple cross-laminae, 157
Hiatus NH7, 268–269, 283
High-amplitude facies, 23
  seismic, well-log, and lithologic characteristics, 26
High-amplitude reflections, 29
High-resolution seismic profile line, preservation of a tidal-inlet fill, 93
Highstand systems tracts, 9, 23–24, 31–32, 36
  block diagram illustration of one as developed in offshore Louisiana, 32
  Lower Ranger, 283, 286
  maximum flooding surfaces, 23
  reservoir sands, 61
  seismic facies and their seismic, well-log, and lithologic characteristics, 26
  seismic section, 31
  well-logs, 32
  Wilmington Field, 280, 284
Holly Springs Delta system, 136
Holocene barrier reworking, 90
Holocene barrier transgression, 90
Holocene epoch, 77, 104
Holocene Mississippi deltas, 136
Holocene Parasequence, 75
Holocene "regressive" episode, 180
Holocene shoreline sediments, 91, 96
Holocene tidal-inlet fill, estimated percentages, and active-tidal inlets for wave- and tide-dominated barrier island shorelines, 90
Holocene transgression, 13, 83
Horizontal lamination
  7-BAL-5-RN well, 165
  7-CAM-63-RN well, 173
  9-MO-13-RN well, 169
  RE-8-RN well, 174
Horn Valley Siltstone, 41, 43, 45–46, 61
Horsts, 107
  WNW-trending, 109
"Hot" gamma-ray character, Tempe Vale #1, 70
Houston Embayment, 136, 137
Hudson paleovalley, 8
Hugh River Shale, 41, 45–46
Hummocky cross-bedding, 156
  parasequence set 13, 72
Hummocky cross-stratification, 66, 155, 156, 157
Huntington Beach Field, unconformities, 283
Hurricanes, and bar bypassing, 82
Hydrocarbon
  Amadeus basin potential, 45–46
  Amadeus basin resources, 45
  Arumbera Sandstone potential, 55
  emplacement, and carbonate diagenesis, 129
  in transgressive and highstand systems tracts, 36
  occurrences within the Larapinta Group, 42
  Ramsey fields, 220
  reservoir facies in Western Canada, 87
Hydrocarbon anomalies, 35, 36
Hydrodynamic banking, 220, 224, 227
Hydrographic regime, 81–83, 88, 90
Hydrologic regime, 81, 83, 129, 130
Hydrology, 117
Hyperpycnal flows, 201, 205, 206
Hypersaline density currents, 206
Hypopycnal flows, 201, 205, 206

Idirriki sub-basin, 40, 46, 51
Illite, 53–55, 65–66, 68, 126
  authigenic, 64
  fibrous, 62, 65–67
  fibrous, in Arumbera Sandstone reservoir interval, 55
  late compactional regime, Lockhart Crossing Reservoir, 130
  parasequence set 8, 68
  parasequence set 12, 72
Illite-smectite, 66
  Ford-Geraldine Field, 226
  Mossoró Sandstone lithofacies content, 197
  precipitation in Mossoró Sandstone, 196
Imbrication, Permian Bell Canyon Sandstone Reservoir, 203–204
Impedance contrasts, 33, 35, 36
Inactive inlet channel, in representative examples of tidal-inlet fills, 88
Incised valley, 23
Inglewood Field, 115, 231–260
  cross section showing major faults and stacked oil zones, 233
  deposition, 279
  depositional model, 250, 251
  location map, 232
  map showing structure on the top of the Alpha zone, 234
  reservoirs formed by turbiditic sands higher in Pico Formation, 267
  unconformities, 283
Inlet-channel abandonment, 186
Inlet-fill facies, 75–76
Inlet-fill sand bodies, hypothetical sediment isopach maps for one depositional episode on tide- and wave-dominated shorelines, 96
Inlet-fill sequence, Johnson Creek (N.C.), 86
Inlet-floor (IF) facies
  Core Banks inlet-fill sequence, 87
  Johnson Creek (N.C.), 86
Inlet migration, 95–96
Inlet throat stability, 87
Inner-shelf slope, 90, 91
Interbedded mudstone and sandstone, Deep Marine Sandstone, 235, 238–240, 249
Interlamination, sand-shale, 9-MO-13-RN well, 169
Interlaminations of shale, 190
Interlocking grain boundaries, 64
Interval velocity, 21
Interwell heterogeneities. *see* Macroscale heterogeneities
Intraclasts, 183
Intracratonic sedimentation, 2
Intraformational breccia, 7-CAM-79-RN well, 188
Iron, 132
Iron oxides, 53, 65
Iskenderun Basin, 102
Isochron thickness, 32, 33
Isocyanate polyol resin, 231

Jackson County, 139
Jackson Group rock unit, 136
Jal canyon, 203
James Ranges, 66
Jandaira Formation (Fm), 161, 183
  base, 167
  dip-oriented stratigraphic cross section, blanket nature and offshore facies shown, 163
  facies relations of Canto do Amaro oil field, 177
  lithologic correlation, 179
  stratigraphic framework, 176
  stratigraphic section across the cored wells, 195
  transition of continental sediments of Açu Formation, 192
Jandaira Limestone (Late Cretaceous period), 181
Jay CK, 41
Johnson Creek (N.C.)
  inlet-fill sequence, 86, 87
  linear dimensions of tidal inlet-fill sequences, 84
  oblique aerial photograph of abandoned floor-tidal delta, 86
  strike-oriented cross section, 86
  vs. Triassic Halfway Formation bioclastic channel fills, 86–87
Johnson Creek Inlet (N.C.), geometries and facies relations, 83
Julie Formation (Fm), 41, 42, 47
  deposition of platform carbonates and sea-level, 51
  facies analysis, 48, 49
Junipero Fault, 265, 281, 282

Kaolinite, 53, 68, 118, 125
  carbonate diagenesis, 129
  Lockhart Crossing Reservoir, channel-fill facies, 131, 133
  Mossoró Sandstone lithofacies content, 197
  parasequence set 8, 68
  precipitation in Mossoró Sandstone, 195, 198, 199
Kaolinite cement, Mossoró Reservoirs, 198
Kaolinized feldspar, parasequence set 8, 68
Kiawah Island (S.C.), 85, 95
  inlet fill %, 90
  percentage of Holocene as inlet fill, 90
Kinkler Field, 138, 139
K-spar (orthoclase), Deep Marine Sandstone, 242

Lag conglomerate, 191
Lag gastropod deposits, 190
Lag intraclastic conglomerate, Mossoró Sandstone, 193
Lagoonal deposits, 192
Lagoonal facies, 119–121, 127, 130
Lagoonal sediments, 88
Lagoonal shale onlapping fluvial bar sandstone, Apodi outcrop, 164
LaHave Bank, 12
Lamar siltstone, 205, 206, 210, 214
Laminations, 143, 156
Laminite facies
  Bell Canyon Formation, 204, 205–206
  Permian Bell Canyon Sandstone Reservoir, 207, 212–213, 215–217, 221
Laramide orogen, 118
Larapinta Group, 55
  hydrocarbon occurrences, 42
Last Chance Canyon, 203
Late Cambrian Goyder Formation, 43
Late Cenomanian, 183
Late Cretaceous period, 201
Late Cretaceous Edwards-Stuart City reef trend, 137
Late Devonian molasse deposition, 64
Late Devonian period, sedimentation, 40
Late Jurassic period, 135
Late Mesozoic era, 45
Late Miocene (epoch) erosional surfaces, 104
Late Miocene (epoch) evaporite sequence, 104
Late Permian period, 201
Late Pleistocene epoch, 104
Late Pleistocene-Holocene (epoch) sediments, 110
Late Pleistocene (epoch) marine regression, 108
Late Proterozoic eon, 44, 55
  sedimentation, 40
Late Proterozoic eon and Early Paleozoic era Amadeus Basin, clastic petroleum reservoirs, 39–72; *see also* Amadeus basin
Late Proterozoic (eon) evaporites, 44, 45
Late Quaternary (period) sediments, 101
Laterally extensive sheet sand, 7
Latest Albian period, 162
Late Tertiary (period) sediments, 101

Lavaca Canyon, 138, 139
Lavaca Channel, 137
Lavaca system, 139
Lenticular bedding, 7-CAM-79-RN well, 188
Levant, 103, 105, 107
Levant Basin, 101, 105–106, 111
Levant Platform, 101
Levee deposits, slope-fan systems tract, 35
Levee reflections, 27, 28
Limestones, 266
Limonite, 62, 118, 124, 125
Litharenite, Mossoró Reservoirs, 197
Lithic arenites, 258
  Deep Marine Sandstone, 242, 245
Lithic arkoses, 118
  Mossoró Reservoirs, 197
Lithics, Deep Marine Sandstone, 245
Lithic subarkose, Mossoró Reservoirs, 197
Lithic wackes, Deep Marine Sandstone, 245
Lithofacies
  Canto do Amaro Field, 170
  Deep Marine Sandstone, 234–242
  Mossoró member, 164–169
  Mossoró Sandstone, 183–185, 193, 194, 199
  Mossoró Sandstone photographs, 191
  Sun #1 Urban well, 140, 143–155
Littoral facies, 119–121, 124, 127–131
  fabric of sandstones in Lockhart Crossing Reservoir, 132
  porosity, 132
Livingston Field, 121
Llano uplift, 137
Llara SST, 41
Load cast, 7-CAM-79-RN well, 188
Lockhart Crossing Reservoir, 113, 117, 121, 133
  acids, 129–130
  carbonate cement distribution, 130
  clay diagenesis, 117
  compactional regime, 123
  depositional and structural controls on the diagenesis of, 117–133
  depositional systems, 118–121
  depth, 124
  dip-oriented cross-section, 119
  distribution and thickness of the channel--fill facies superimposed upon a structure contour map, 125
  distribution of carbonate cementation patterns, 127
  early compactional regime, 126–128
  emplacement of oil, 132–133
  fault zones, 130
  feldspar, 131
  general geology, 117–123
  hydrologic and diagenetic history, 123–133
  hydrologic regime, 129, 130
  hydrologic regimes and the present reservoir setting, 123–124
  intermediate compactional regime, 128–129
  late compactional regime, 130–131
  location and approximate position of continental margin during Wilcox deposition, 118
  meteoric regime, 123
  paleohydrologic regime, 126
  porosity, 131
  porosity and permeability, 133
  porosity and permeability distribution-general statement, 122–123
  Provenance, 118
  pyrite distribution in 17 cores, 128
  salinity and alkalinity, 124
  sandstone from the base of the littoral facies, 124
  sandstone from the top of the littoral facies, 124
  sediment modification in the depositional environment and meteoric regime, 124–126
  strike cross section, 122
  structure, 121
  structure contour map of the top of the Wilcox Formation, 120
  summary of diagenetic modification of the reservoir sandstone, 131–132
  thermobaric regime, 123–124
Logan Canyon Formation (Fm), 14, 15
  transgression, 17
Long Beach Unit, geologic heterogeneity scales description, 263–291; *see also* Wilmington Field
Long Beach Unit Fault, 265, 281
Long Island, 77
Los Angeles Basin, 115, 231–232, 283
  regional paleogeography during upper Miocene epoch, 267
Louisiana, 77
  Lockhart Crossing Reservoir (Wilcox), depositional and structural controls on the diagenesis, 117
Louisiana Gulf Coast, offshore index map, 22
Loves CK member (MBR), 41
Low-angle cross-bedding
  7-BAL-5-RN well, 165
  7-CAM-63-RN well, 173
  7-CAM-79-RN well, 188
  9-MO-13-RN well, 168, 169
  Mossoró Field, 170
Low angle, hummocky cross-bedding, RE-8-RN well, 174
Lower Eocene epoch, 178
Lower Eocene rocks, 113
Lower Inindia Beds, 41
Lower Mannville, 11, 13, 14
Lower non-marine regressive path, 6
Lower non-marine transgressive path, 6
Lower Pacoota Sandstone, 61
Lower Pico Formation (Fm), 268
Lower (L.) Shannon, 41
Lower Tertiary period, 118
Lower Tertiary source units, 132
Lower Wilcox subgroup rock unit, 136
Low-resistivity clayshales, 118
Lowstand, Pleistocene sea-level, 6
Low-stand barriers, 13
Lowstand basin-floor fan systems tracts, 21, 24–25
  block diagram of one as developed in offshore Louisiana, 25
  development of, 24
Low-stand deltas, 13
Lowstand prograding wedge systems tract, 23, 29–30, 35, 36
  amplitude anomaly, 33
  block diagram illustration of one as developed in offshore Louisiana, 29
  Ranger Zone, 286
  reservoir sands, 61
  seismic facies and their seismic, well-log, and lithologic characteristics, 26
  seismic section of, 30
Lowstand slope-fan systems tract, 21–23, 25–29
  block diagram illustration of one as developed in offshore Louisiana, 27
  facies and isochron thickness map, 33
  seismic facies and their seismic, well-log, and lithologic characteristics, 26
Lowstand systems tracts, 9, 10, 24, 280, 284
  parasequence sets 10 and 11, 69
  reservoir sands, 61
Lutetian, 15
Lutite facies, 209, 226
  Bell Canyon Formation, 204–205, 206
  Permian Bell Canyon Sandstone Reservoir, 209–210, 221

Macau (town), 162, 181
MacDonnell Range, 40, 72
Macroscale heterogeneities, 263, 278–279, 290
Magnesium, 132
Major domes, 44
Major external variables, 3–4

Maloneys Creek, 72
Mannville clastic wedge, 11, 13
Mannville Group, 14
Marine dominated deltas, 29, 31
Marine regressive path, 6
Marine reservoir facies, 8
Marine shales, Mannville Group, 14–15
Marine shelf, transgressive path, 6
Marl/calcilutite, 7-CAM-79-RN well, 188
Marsh
  Capers Inlet, 90
  in representative examples of tidal-inlet fills, 88
  Price Inlet, 90, 91
Martinottiella pallida, 269
Massive mudstone lithofacies, Deep Marine Sandstone, 234–238
Massive sandstone, Deep Marine Sandstone, 235, 238, 242, 244, 249, 251–252
Mass wasting, 32
Matrix clay, Mossoró Sandstone lithofacies content, 197
Meandering fluvial, 162
Mean tidal range vs. average wave heights for mid-Atlantic and SE coastline of U.S., 78
Mechanical compaction, Mossoró Sandstone, 195
Mediterranean Basin, sedimentation during glacial ages, 108
Mediterranean geostrophic current, 101, 105, 108, 109
Mediterranean Ridge, 101, 102, 105, 106, 107
  seismic reflection profile, 103
Megaripples, 62, 66
Megascale heterogeneities, 263, 279–280, 289–291
  Wilmington Field, 288–290
Melonis barleeanus, 269
Menefee Formation (Fm), 94
Menking Field, 138, 139
Mereenie Field, 45, 57–58, 61–62, 64, 66
  computer reservoir simulation of the field, 66
  correlation of Pacoota Sandstone Units to Palm Valley Field, 59, 60
  distribution and isopachs of parasequence sets, 63
  P1-310 sand, 72
  P2-110 sand, 70
  parasequence set 4 and 5, 64
  parasequence set 8, 66
  parasequence set 12, 71
  porosity, 69
Mereenie SST, 41
Mesoscale, heterogeneities, 263–278, 279, 289, 290
Mesotidal coastline, 79
Mesozoic era, 104
Mesozoic source units, 132
Messinian, 103
Messinian evaporites, 104
  Nile Fan, 107
Messinian unconformity surface, 105
Metamorphic rock fragments, 53, 62
Meteoric regime, 123
Meteoric waters, 123
Mexico, Gulf of, 76, 77
  hydrographic setting, 92
Mica
  Canto do Amaro field, 194
  Mossoró Sandstone lithofacies content, 197
Microforaminifers, chitinous, 192
Microfossils, in marine shales, 15
Microhummocky, Redonda oil field, 172
Microlaterolog (MSFL), 255, 257–258
Microquartz crystals, 54
Microscale, heterogeneities, 263–278, 289, 290
Microstylolites, 68
Microstylolitization, 68
Middle Bank, 12
Middle Cenomanian Age, 162
Middle Mannville, 11, 13, 14
Middle Miocene (epoch), 105
Middle Miocene conglomerates/breccias, 266
Middle Ordovician period, depositional pattern changes, 43
Middle Pleistocene epoch, 104
Middle Pliocene (epoch) marine regression, 103
Middle Triassic Halfway Formation (Fm), 178
Midland Basin, 203, 208
Mid-Paleozoic sedimentary rocks, 44
Mid-Tertiary period, 111
Midway Group, 135
Midway Group rock unit, 136
Milk River Formation (Fm), 94
Miocene epoch, 103, 232, 245, 264
Miocene/Pliocene boundary, 283
Mio-Pliocene (epochs), 263
Misane Bank, 12
Missionary Plain Trough, 40, 42–46, 55, 62
  depositional setting, 51
  facies analysis, 47
  idealized north-south cross sections, 47
  parasequence set 10, 69
Mississauga Formation (Fm), 17
Mississippi Delta, switching of active lobes, 4
Mississippi Embayment, 118, 136, 137
Mississippi River, 136
M. I. Stewart well, 131
MMBO (10 million barrels of oil), 137, 138
MMCFG (10 million cubic feet of gas), 138
Modern analogs, 75
Mohnian, 266
Molasse, 44
Molasse phase, 10
Molluscs, 58
Mollusk debris, marl, RE-8-RN well, 174
Monocraterion, parasequence set 12, 72
Monocrystalline quartz, 65
Monterey Fault, 265
Monterey Formation (Fm), 266, 268
Mossoró Field (MO), 162, 168, 176
  core photographs, 170, 171
  facies relations shown in cross-section, 172
Mossoró member
  Canto do Amaro and Redonda fields: estuarine/tidal-flat system, 168–170
  depositional setting, 180
  facies, 164–167, 168, 170–175
  facies analysis, 162–176
  facies relations and reservoir geometry, 168
  facies relations and sandstone geometry, 167–168
  facies, reservoirs and stratigraphic framework, 161–181
  fluvial intervals, 163
  lithologic correlation, 178
  Mossoró field: the delta plain system, 168
  outcrop data, 163
  stratigraphic framework, 176–179
  strike-stratigraphic cross section along estuarine/tidal- flat system, 179
  structural and stratigraphic framework, 161–162
Mossoró Reservoirs
  petrographic classification, 197
  photomicrographs (thin-section and SEM), 198
  porosity, 198, 199
Mossoró Sandstone, 161, 164, 167, 180
  conclusions, 199
  cumulative granulometric curves of lithofacies 1, 197
  depositional environment and associated sealant rocks shown in block diagram, 193
  diagenesis, 199
  diagenesis and reservoir quality, 195–197
  distribution, thickness, and locations of cored wells, 186
  environmental interpretation, 185–193

facies, 168, 169
facies relations and reservoir geometry, 168, 175–176
geometry, 193–194
inlet-channel reservoir vertical and lateral distribution shown in fence diagram, 196
isolithic maps, 167, 168, 177
isopach maps, 167, 168, 172
isopach map showing advancing paleoshoreline, 194
lithofacies, 193, 194, 199
lithofacies and environmental interpretation, 187
lithofacies clastic constituents, authigenic constituents, micropores and macropores, 197
lithofacies photographs, 192
lithologic correlation, 179
macroscopic characterization of the lithofacies, 183–185
permeability, 196, 199
petrophysical characterization of the reservoirs, 197–199
porosity, 168, 196, 199
reservoir petrology, 194
thickness variation, 192
tidal inlet-channel reservoir, 183–199
trap, 183
trends in cores, 173
vertical stacked inlet channels that behave as a single reservoir, 193–194
vertical stacking of inlet sequences, 194
Mount Currie Conglomerate, 46
Mt. Harris Basalt, 41
Mud-chip breccias, 48, 49
Mud clasts, 62
Mud couplets, 94, 183, 185
Mud cracks, 184–185
7-CAM-79-RN well, 188
Mud drapes, 94, 95, 146, 147
Muddy Sandstone, 94
Mud flasers, Apodi outcrop, 164
Mud laminae, 94
Mudstone with thin sandstones, Deep Marine Sandstone, 235, 238, 239, 249
Mule Springs Field, 139
Muscovite, Mossoró Reservoirs, 198
Musgrave Block, 40
Musgrave Complex, 40
Mudstone, Wilmington Field, 271
Mudstone/shale, 7-CAM-79-RN well, 188

Namatjira Formation (Fm), 51
Namatjira lowstand systems tract (LST), 41
Nannofossils, 21
calcareous, 23
Neocomian/Aptian stage, 161
Neogene hiatuses, 268
Neonile, 104
Neritic microfaunas, 15, 17
Newport-Inglewood Fault, 231–232, 233, 245
Newport-Inglewood fault zone, 264–266
Nile Cone, 101–104
Nile Delta, 102
geomorphologic configuration, 104
Nile Escarpment, 76
Nile Fan, 76
bathymetric map of the eastern Mediterranean, 102
climatic oscillations and sedimentological variations, 108–109
cone configuration, 104
controls and sedimentation, 104
deposit formation, 101
distributaries, 104
facies distribution, 109–111
fluviatile system, 103
and geological setting, 101–107
geomorphology, 106–107, 111
lithofacies charts showing average sedimentation rate during past 60,000 years, 110
physiographic regions, 102
sea level and climate, 101–104
sedimentary distribution, 107–108
sedimentation rate, 101
sedimentologic and geomorphologic provinces of, 101–111
sedimentologic patterns, 107–111
sedimentology, 111
seismic profiles, 102
seismic profile showing contrasting structural patterns between eastern and western provinces, 105
seismic reflection profile, 103, 107
seismic reflection profile showing a collapse structure in the eastern fan province, 106
tectonics, 104–106
tectonophysical constraint, 104
Nile River, 104
1933 Drum Inlet, linear dimensions of tidal inlet-fill sequences, 84
Nitzchia reinholdi zone, 268
Nondeposition, 120
Nordheim Field, 137–138, 139
North Carolina, 77
active tidal inlet %, 96
historical evolution of the central North Carolina coast, 81
tidal inlets, 81, 82, 89
tidal inlets along barrier islands forming the Cape Lookout cuspate foreland, 79
North Swash Inlet (N.C.), linear dimensions of tidal inlet fill sequences, 84
Northwestern faulting trend, 105
North Zack Creek (N.C.), linear dimensions of tidal inlet-fill sequences, 84

Ocracoke Inlet, 82
stability, 81
Offshore bars, 6–7, 13
and transgressive systems tracts, 14
Offshore shelf sands, 61
Oil field
Mereenie Field, 45
production per systems tract, relative amounts, 34
within a slope-fan systems tract, 35
Oil-field reservoirs, subdivision based on rock character, 114
Oil migration, Lockhart Crossing Reservoir, 132–133
Old Drum Inlet (N.C.), geometries and facies relations, 83
Olympic Formation (Fm), 41
"O" Marker, 18
Onlap, 23
correlation of Pacoota Sandstone Units from Palm Valley Field to Mereenie Field, 59, 60
Onlap curves, 41
Ooraminna anticline, evaporite high amplitude, 44
Ooraminna sub-basin, 40, 45, 46
facies analysis, 47, 48, 49
idealized north-south cross sections, 47
Ophiomorpha, 94, 147, 148, 157, 168
Canto do Amaro field burrows, 175
Mossoró Sandstone, 184, 186, 191
parasequence set 12, 72
Redonda Field, 171–172
RE-8-RN well, 174
Orange Gas Field, 71
Ordovician Horn Valley Siltstone, 45
Ordovician Pacoota Sandstone, 45
Ordovician sediments, 43
Oregon, Cape Sebastian Sandstone, 16
Organic debris, Mossoró Sandstone lithofacies content, 197
Orogen, 10
Orogenic belt, 17
Ostracods, 176
Ostracod Zone, 15
Ouachita Mountains, 136
Ouachitas, 137

Outcrop Field, 176
Oval Syncline, 72
Overbank deposits, 163, 166, 176
Overbank facies, 23, 27–28, 32
  seismic, well-log, and lithologic characteristics, 26
Oversteepening, 24
Overturned crosslamination, 62
Overwash, Johnson Creek (N.C.), 86
Overwash (OW) sands, horizontally laminated Core Banks inlet-fill sequence, 87
Oxbow-lake deposition, 167
Oyster molds, Mossoró Sandstone, 184
Oyster shells, 7-CAM-79-RN well, 188

P1-310 sand, Mereenie Field, 72
P2-110 sand, Mereenie Field, 70
Pacoota Sandstone, 41, 43, 45–46, 55–72
  age and stratigraphy, 58
  comparison of stratigraphic subdivisions based on published Mereenie Field usage, 61
  distribution and isopachs of parasequence sets 3 to 13, 63
  east-to-west cross section from Tempe Vale #1 to Palm Valley #5, 71
  east-to-west gamma-ray and sonic-log cross section from Tempe Vale #1 to West Waterhouse #1, 70
  parasequence set 3, 62–64
  parasequence set 4, 64–65
  parasequence set 5, 64–65
  parasequence set 6, 64, 65–66
  parasequence set 7, 64, 66
  parasequence set 8, 62, 64, 66–69
  parasequence set 9, 66–69
  parasequence set 10, 69–71
  parasequence set 11, 69–71
  parasequence set 12, 71–72
  parasequence set 13, 71, 72
  permeability, 67–68
  porosity, 64, 65, 67–68, 70–73
  porosity distribution in the P units, 62
  reservoir characterization, 58–62
  sonic log-gamma ray log correlation of parasequence sets 8 to 9 eastward, 67
  subdivision of, 58
  vs. Arumbera Sandstone, 73
Pacoota Sandstone Units, correlated from Palm Valley Field to Mereenie Field, 59, 60
Paleobathymetries, 268
Paleocene Banquereau Formation (Fm), 17
Paleocene epoch, 136
Paleocurrent analysis, 185
  azimuth frequency plots, 185
  7-CAM-30-RN well, 190
Paleocurrents, deep, 140
Paleogene growth-fault trend, 137
Paleogene period, 136
Paleomagnetic time scale, 268
Paleonile, 103
Paleosoil development, 184–185
Paleotopography, 83, 85, 88
Paleovalleys, 120
Paleozoic era, 44
Palm Valley Field, 45, 58, 64, 68–70
  correlation of Pacoota Sandstone Units to Mereenie Field, 59, 60
  distribution and isopachs of parasequence sets, 63
  fracture porosity reservoir, 62
  parasequence set 8, 66
  parasequence set 12, 71
  parasequence set 13, 72
  silicification, 72
Palm Valley wells, 64
Palos Verdes area, 232
Palos Verdes fault, 265
Palynological analysis, 190
  Mossoró Sandstone, 186
Parasequences, 1
  definition, 8
  examples in marine sediments, 8
  relative highstand systems tracts, 17
  stacking patterns, 9
  transgressive systems tracts, 13, 15, 16
Parasequence sets, 1
  coarsening-upward, 18
  definition, 9
  Pacoota Sandstone, 58
  progradational, 17
  transgressive systems tracts, 13, 15, 16
  types of, 9
  Upper Mannville, 16
Parke SLT, 41
Pass Abel, 92
Passive pelagic conditions, 157
Pass Ronquille, 92
Pay zone, 33, 34
  basin floor fan, 25
Peat, 7-CAM-79-RN well, 188
Pedogenetic concretion, Canto do Amaro oil field, 177
Pedogenic (soil) clay rims, 53
Pelecypods, 174
  Baixa do Algodão oil field, 167
  7-BAL-5-RN well, 165
  7-CAM-79-RN well, 188
  Mossoró Sandstone, 184
  prismatic debris, 176
  Redonda oil field, 172
Permian Basin, 114, 208
Permian Bell Canyon Sandstone Reservoir
  channel fill and isopach analysis, 212
  channels and inferred depositional history (stages), 209–210
  control, 204
  depositional history and performance, 201–228
  depositional model, 208–209
  geometry of channel complex, 210–212
  isopach map of the total Ramsey interval, 207
  lower laminite, 213–214
  paleotopographic highs or erosional remnants, 212–213
  permeability, 206, 208
  porosity, 206, 208
  possible transport paths for lagoonal siliciclastics to bypass carbonate shelf margin, 203
  possible transport paths for lagoonal siliciclastics to bypass carbonate shelf margin, 203
  Ramsey depositional systems, perspective diagram, 208
  Ramsey 1A interval, 209, 210, 213, 215–216, 226
  Ramsey 1B deposition, 209, 210, 214–217
  Ramsey 1C interval, 209, 215, 217
  Ramsey 2 interval, 210, 217–219, 224–226
  Ramsey 2 sandstone, 222
  Ramsey 2 sandstone, isopach map, 220
  sandstone facies, 206–208
  stratigraphic relation of Permian rocks of the Delaware Basin, northern shelf margin, Texas and New Mexico, 202
  tectonic and paleogeographic features, 202
  type log and core (Ford-Geraldine Unit #108), 205
  upper laminite, 215–217
Permian paleo-equator, 208
Pertatataka Formation (Fm), 41, 42, 55
Petermann Ranges, 40, 41
Petermann Ranges Orogeny, 44–45, 50, 51
Petroleum exploration and development, seismic stratigraphy techniques applied, 21
Petroleum fields, distribution and isopachs of parasequence sets 3 to 13, 63
Phase, 21
Phosphatic pellets, parasequence set 12, 71

Phosphatic shales, 266
Phycodes
parasequence set 12, 72
parasequence set 13, 72
Phyllite components, detrital, 131
Pico Formation (Fm), 266–270, 288
Pilontary Inlet (N.C.), linear dimension of tidal inlet-fill sequences, 84
Pioneer Formation (Fm), 41
Pirite, Mossoró Sandstone lithofacies content, 197
Plagioclase
Canto do Amaro Field, 194
Deep Marine Sandstone, 242
Plagioclase feldspar, 65, 121
Plane-parallel stratification or lamination, 7-CAM-79-RN well, 188
Planktonic abundance curve, 24
Planktonic foraminifera, 21, 23
Planktonic microfossils, 23
Planolites, 145, 156
Plant remains, 184, 185
7-CAM-63-RN well, 173
in siltstones, 145, 147, 155
Mossoró Sandstone, 193
Plectofrondicularia californica, 269
Pleistocene clays, Core Banks inlet-fill sequence, 87
Pleistocene drainage systems, 83
Pleistocene epoch, 77, 105
Captain Sam's Inlet, 86
Johnson Creek (N.C.), 86
Price Inlet, 90, 91
Pleistocene foreland, 10
Pleistocene lowstand, 8, 12, 13
Pleistocene Pasadenan orogeny, 265
Pleistocene sea-level lowstand, 6
Pleistocene topography, 83
Pliocene epoch, 232, 245, 249
biostratigraphic subdivisions, 233
Los Angeles basin, 250
Nile sediments different from present patterns, 111
unconformity, 267
Wilmington Field, 264, 265
Pliocene foraminifers, 233
Pliocene-Pleistocene transition, 103
Plio-Pleistocene Gulf Coast of offshore Louisiana, 23–24
block diagram illustrating lowstand basin-floor fan systems tract, 25
block diagram illustrating lowstand prograding-wedge systems tract, 29
block diagram illustrating transgressive systems tract, 30
facies and isochron thickness map of part of a lowstand slope-fan systems tract, 33
lowstand slope-fan systems tract block diagram illustrated, 27
Plio-Pleistocene sedimentary sequence, 105, 107
Plio-Pleistocene sequence, 1, 107, 111
Plio-Pleistocene strata, offshore Louisiana, 21
Plio-Quaternary sedimentary prism, 104
Point bar, 207
deposits, 176
in a fluvial meandering system, 166
Pollens, 186, 190
Polycrystalline quartz, 53, 65
Polycrystalline quartz grains, 62
Ponta do Mel carbonate platform, 162
Ponta do Mel Formation (Fm), 161–162
Pores, Mossoró Sandstone lithofacies content, 197
Porosity, permeability, and saturation (PKS) analysis, 250
Portsmouth Banks (N.C.), percentage of Holocene as inlet fill, 90
Post-Arumbera Cleland Sandstone, 51
Post-Wilcox fault, 130
Potash feldspar, 121
Potassium, 131
Potassium feldspar, 65, 126
Canto do Amaro Field, 194
carbonate diagenesis, 129
overgrowths, 128
parasequence set 8, 68
parasequence set 12, 72
Potiguar Basin
location map, 184
main features and nearby oil fields, 162
Mossoró member facies, reservoir and stratigraphic framework, 161–181
Powerline Fault, 265
Pre-Holocene substrate, 81, 83
Pre-Messinian marls and limestones, 104
Preservation, 5
Preservation potential, 77
Preserved channel fills, 96
Price Inlet (S.C.), 80–81
bar-bypass mechanism of inlet channel abandonment, 82
cross section, 91
cross section locations, 88
geometries and facies relationships of tide-dominated inlet sand bodies, 88
inlet-channel migration and abandonment, 88
linear dimensions of tidal inlet-fill sequences, 84
photograph of core from tide-dominated inlet-fill sequence, 91
strike-oriented cross section, 87, 89
strike-oriented vibracore transects across the abandoned inlet channels, 90
Progradation
horizontal distance of, 5
of lowstand shorelines, 7–8
seaward, 7
Progradational clastic wedges, 113
Prograding wedge systems tract, 21, 23, 24
Proterozoic-Cambrian boundary, 46, 50, 51
Proterozoic salt, 42
Protonile, 103–104
Provident City Field, 137–138, 139
Puente Formation, 266, 268, 269, 270, 288
lower Ranger sequence, 282
Pyrenees (Spain), 178
Pyrite, 53, 65, 69, 125–126, 131–132
carbonate diagenesis, 129
distribution in 17 cores from Lockhart Crossing Field, 128
precipitation in Mossoró Sandstone, 196
Pyrite concretion, 7-CAM-79-RN well, 188
Pyritic shales, 120

Quandong Conglomerate, 46
Quartz, 53, 64, 65, 69
Canto do Amaro Field, 194
Deep Marine Sandstone, 242, 245
monocrystalline, 62
Mossoró Sandstone lithofacies content, 197
parasequence set 8, 68
parasequence set 9, 68
Quartzarenite, Mossoró Reservoirs, 197
Quartz cementation, 73
Quartz druse, 66
Quartz overgrowths, 65–66, 70–71
carbonate diagenesis, 129
cementation, 68
Lockhart Crossing Reservoir, 130
parasequence set 9, 68
parasequence set 13, 71
Quaternary period, 135
Quaternary period climatic and sea-level oscillations, 108
Quatre Bayou Pass, 92

Radioactivity, in marine shales, 14
Radiolaria, 233, 268, 269
Rahmanic CU marine sequence, 178
Rahmani's prodelta/delta front/lower estuarine sand-channel sequence, 179
Ramsey 1A interval, 209, 215, 226
isopach map, 215

Ramsey 1A sandstone interval, 209, 213, 216
Ramsey 2 sandstone, 209, 216, 225
Ramsey depositional systems, 208
Ramsey fields, hydrocarbons, 220
Ramsey lower laminated siltstone, isopach map, 216
Ramsey lower laminite, 226
Ramsey member (MBR), 201
  deposition process, 206
Ramsey reservoir
  control, 204
  type log and core, 205
Ramsey sandstone, 206
Ramsey-Trap contact, 217
Ramsey upper laminite, 209, 211–213, 216–219, 225–226
  isopach map, 218
Ranger Zone, 267–268, 270, 281–282
  lithologies, 269–271
  macroscale heterogeneities, 278
  NW-SE detailed stratigraphic cross section correlating sand and shale intervals and subzone horizon picks, 281
  northwest-southeast regional cross section, 281
  sequence stratigraphy, 280–281
  turbidite system, 279
Rapid deltaic progradation, 4
Ravinement surfaces, 3, 5
Redonda Field, 162, 170, 179
  depositional setting, 180
  estuarine/tidal-flat system, 168–170
  facies, 171–172
  facies equivalent to that of Canto do Amaro Field, 172
  facies relations and reservoir geometry, 176
Red Sea, northern, 106
Reflection geometries, 27
Reflections, high-amplitude, 29
Reflectors, 104–105
Regression, 5
  models of, 6
  with downcutting, 6
Regression analysis, 258–260
  data summary for stepwise regressions, 258
  stepwise, using SAS computer software, 254
Regression procedure, multiple, for model predicting permeability from electric logs, 253
Regressive depositional sequences, 16
Reklaw Formation (Fm), 118, 119
Reklaw/Wilcox contact, 121
Relative highstand systems tracts, 1, 9, 11, 16–17
Relative lowstand systems tracts, 1, 9, 11–13
Relative sea level, 5
Relative sea-level change, 5, 8
Repeat Formation Test (RFT) net effective stress, 251
Repettian, 268, 270
Repetto Formation (Fm), 267, 268
Resedimentation, 104
Reservoir facies, 1
Rhodes Basin, 102
Rhythmites, Baixa do Algodão Field, 166, 167
Rio Grande Embayment, 136, 137
Rio Grande River, 136
Ripple drift, 7-CAM-79-RN well, 188
Ripple drift cross-lamination
  7-BAL-5-RN well, 165
  7-CAM-63-RN well, 173
  Canto do Amaro Field, 175
  9-MO-13-RN well, 168, 169
  Mossoró Field, 170
  RE-8-RN well, 174
Ripple marks, 64, 66
Rip-up clasts, 64, 155
Rip-up clay clasts, 120
Rip-up shale clasts, 126
Rizophora, 190–192
Rock fragments, Mossoró Sandstone lithofacies content, 197
Rock units, 4
Rocky Mountains, 136, 137
Roda Sandstone, 94, 178
Rodingan unconformity, 65
Root
  7-CAM-63-RN well, 173
  7–CAM-79–RN well, 188
  Canto do Amaro oil field, 177
  RE-8-RN well, 174
Root casts, 184–185
Rosetta distributary, 104, 109
Rosetta Fan, 101
Rosita System, 136
Rotalia garveyensis, 269
Rotational faults, 17, 19

Sabine River, 136
Sabine Uplift, 137
Sable Island Bank, 12, 13
Salado Formation (Fm), 202
Salt marsh (M) sedimentary facies, Price Inlet, 91
Salt ridges, 76
  elongated, 101, 105
  Nile Fan, 107, 109
Salt tectonics, 44, 76
Salt walls, 104
San Andreas Fault, 263
Sand Island Inlet, linear dimensions of tidal inlet-fill sequences, 84
Sandstone and thin mudstone, Deep marine Sandstone, 235, 238, 240–243, 249
Sandstone facies, Bell Canyon Formation, 204
Sandstones, 266
  7-CAM-79-RN well, 188
  stacking up, 18
Sandy reservoirs, 170
San Joaquin basin, benthic foraminiferal assemblages, 268
San Marcos Arch, 136, 137, 139
San Pedro Formation (Fm), 268
Santa Fe Springs Field, 264
Sapropelic and oxygenated sedimentation, oceanographicconditions for deposition in the Mediterranean region, 108
Sapropel sequences, 109
Sausage Hill, 72
Scanning electron microscope (SEM) examinations, 65
Scolithids, 69
Scolithos, 64
  in parasequence set 7, 66
Scotian Shelf, 12, 13, 15, 17–19
Scour, 8
Scour and fill, 62, 64
Scour contacts, 88
Seabrook Island (S.C.), percentage of Holocene as inlet fill, 90
Sea-level rise, rate of, 90, 91
Seal facies, 35
Seaward tilting, 265
Sedimentary succession, idealized, for a single stage of rifting and thermal subsidence, 43
Sedimentation
  delta-front, 30
  hemipelagic, 23
  rates of, 3–4
  variations in, 5
Sedimentation rates, 11, 90
  distribution and thickness of systems tracts, 10
  Nile Fan, 101
  Nile Fan lithofacies charts, 110
  parasequences as result of variations, 16
  terrigenous, 23
Sediment gravity flows, 24, 26, 27, 30
Sedimentologic provinces of the Nile Fan, 101–111
Sediment supply, 81, 83, 88
Sediment supply factor, 8
Sediment supply-rate variations, 4

Sediment texture, trends through the littoral facies interval, 123
Seismic attribute analysis, 33
  definition, 21
Seismic criteria, for identification of systems tracts, 23–24
Seismic facies, 1–2, 21, 32, 33
  geometry developed along unstable progradational passive continental margins, 23
Seismic facies analysis, definition, 21
Seismic facies sequence, 8
Seismic profile, Nile Fan, 105
Seismic reflection profile, 103
  Nile Fan, 107
  Nile Fan, collapse structure in eastern fan province, 106
Seismic section, basin-floor fan with a gas field developed within, 25
Seismic stratigraphy, stages, 21
Semicontinuous to continuous facies, seismic, well-log, and lithologic characteristics, 26
Semicontinuous to discontinuous facies, seismic, well-log, and lithologic characteristics, 26
Sequence
  geometry developed along unstable progradational passive continental margins, 23
  types of, 8–9
Sequence analysis
  definition, 21
Sequence boundary, 24, 26–27, 280, 283, 285
Sequence stratigraphic analysis, 21–32
Sequence stratigraphy, 1, 3, 4, 8
  Amadeus basin Late Proterozoic to Devonian sequences, 41
1700's Drum Inlet (N.C.), linear dimensions of tidal inlet-fill sequences, 84
Seymour sub-basin, 40
Shackleford Banks (N.C.)
  inlet fill %, 90
  percentage of Holocene as inlet fill, 90
Shale, 66
  parasequence set 13, 72
  Wilmington Field, 270–271
Shale clast
  7-BAL-5-RN well, 165
  7-CAM-63-RN well, 173
  Canto do Amaro Field, 175
  9-MO-13-RN well, 169
  parasequence set 12, 71
  RE-8-RN well, 174
Shale drapes, 171, 172
Shale facies, Wilmington Field, 271
Shale-intraclast conglomerate, 171–172
Shallow marine reservoirs, examples, 11–17
Shannon and Jay Creek, 61
Sharp-based shoreline sandstone, 7
Sheet sand development, 7
Shelf bathymetry, 79
Shelf break, 11
Shelf margin reservoirs, growth-faulted, 2
Shelf margin wedge systems tract, 284
Shelf sand bodies, 13
Shelf sandstone bodies, 6–7
Shelly fossils, parasequence set 12, 72
Sheridan Field, 138, 139
Shoaling Cycles, correlation of Pacoota Sandstone Units from Palm Valley Field to Mereenie Field, 59, 60
Shoreface, Captain Sam's Inlet, 85
Shoreface regressive path, 6
Shoreface transgressive path, 6
Shoreline deposition, 13
Shoreline facies, 4
Shoreline-shelf reservoirs, 3–19
  geometries of, 6–8
Siderite, 125, 126, 132, 133
  carbonate diagenesis, 129
  percent found in littoral facies, 123
Siderite rhombs, 125
Sideritic shales, 120
Sierra Madre Orientals, 137
Sigmoidal cross-bedded sandstone overlying shales with mudcracks, Apodi outcrop, 164
Sigmoidal cross-bedding, 7-CAM-79-RN well, 188
Sigmoid ripples, 156
Silica, 53, 55, 62, 65, 73
  channel-fill facies, Gulf Coast of Louisiana, 131
  overgrowths, 66
Silica cement, 62, 67
  feldspar content, 131
Siliciclastic sandstones, 123
Siliciclastic shelf, 118
Siliciclastic submarine fan, 202
Silicification, 70–73
Siltstone, 66, 143–157
  parasequence set 13, 72
  Wilmington Field, 271
Silty shale, 148, 155, 156
Silty-shale seals, 170
Skolithos, 62
  correlation of Pacoota Sandstone Units from Palm Valley Field to Mereenie Field, 59, 60
  parasequence set 8, 66
  parasequence sets 10 and 11, 69
  parasequence set 12, 72
  parasequence set 13, 72
Slick Field, 137, 139
Sligo buildup, 137
Slope-fan systems tract, 21, 23–24, 29, 32
  gas fields, 35
  hemipelagic facies, 28
  oil and gas field, 35
  overbank and chaotic facies, 28
Slump folds, 48
Slump scars, 23, 29, 30
Small normal fault, 7-CAM-79-RN well, 188
Smectite, 126
  Deep Marine Sandstone, 245
Smothers Canyon, 138
Smothers Channel, 137
Smothers system, 139
Sorting, using graphic standard deviation equation, 251
South Carolina
  active tidal inlet %, 96
  tidal inlets, 77–79, 81, 89
Southern Appalachians, 137
South Hallettsville Field, 138, 139
South Swash Inlet (N.C.), linear dimensions of tidal inlet-fill sequences, 84
South Zack Creek (N.C.), linear dimensions of tidal inlet-fill sequences, 84
Spirit River, 14
Spirit River Formation (Fm), 11
  eustatic effects, 17
  gamma-ray log cross-section, 16
  gamma-ray logs of parasequences, 17
Spit platform
  Captain Sam's Inlet, 85
  Johnson Creek (N.C.), 86
Spit-platform (SP) facies, Core Banks inlet-fill sequence, 87
Spit-platform sediments, 95
Sponge spicules, 268, 269
Spores, 186, 190
Stacked reservoir facies, 76
Stacking patterns, of parasequences, 9
Stairway sandstone, 41, 61
Starved basin depositional regime, 106
State 109 Fault, 265
Stokes SLT, 41
Stono Inlet, 80–81, 95
Storm breaching, 92
Strabo, 104
Strike-slip fault, 231, 233
  right-lateral, 232
Structural-stratigraphic traps, 138
Structural trapping, gas fields, 137
Stylolites, 62
Stylolitization, 64
Subarkose, Mossoró Reservoirs, 197
Sub-basins, 39
Sublitharenite, Mossoró Reservoirs, 197

Submarine fans, 139–140, 156
Wilmington Field, 264, 266, 283
Wilmington Field progradational model, 286, 287, 289, 291
Submarine point bar deposition, 207
Subsidence (Sub), 3, 5
distribution and thickness of systems tracts, 10
tectonic, 4
Suburban fan, 157
Sullivan-Screwbean channel, 213–215, 217–218, 226–227
Ramsey 2 sandstone interval, 220
Sullivan-Screwbean field complex, channel geometry, 210–212
Suspensites, 109
Swash bars, 83, 87
Swash Inlet (N.C.), geometries and facies relations, 83
Swash platform (ebb-delta), in representative examples of tidal-inlet fills, 88
Swash platform/Upper shoreface VF-F sand, Capers Inlet, 90
Symmetrical-ripple laminae, 156
Syndepositional faulting, 120
Syndepositional growth faulting, 118
Syndepositional rip-up clasts, 124–125
Synsedimentary slumping, 143
Synthetic growth faults, 118
Systems-tract methodology, 58–59
Systems tracts, 21
basin-floor fan, 25, 26, 33–35
biostratigraphic criteria for identification of, 23
definition, 21
geometry developed along unstable progradational passive continental margins, 23
highstand, 26, 31–32, 36, 280, 284
highstand, Lower Ranger, 283, 286
lowstand, 280, 284
lowstand prograding wedge, 26, 29–30, 35, 36
lowstand slope-fan, 25–29, 33
lowstand wedge, Ranger Zone, 286
major types, 9
mapping, 32
production in gas and oil fields, relative amounts illustrated in a histogram, 34
relation with well-log profiles and abundance peaks, 24
relative highstand, 11, 16–17
relative lowstand, 11–13
seismic criteria for identification of, 23–24
shelf margin wedge, 284
slope-fan, 28, 29, 32, 35
transgressive, 10–11, 13–16, 26, 30–31, 35–36
transgressive, Wilmington Field, 280, 284
variations in proportions of, 9–10
well-log criteria for identification of, 23–24

Tabular cross-bedding, 156, 157
7-CAM-79-RN well, 188
Tabular-tangential cross-bedded sandstone, Mossoró Field, 170
Tectonics, 105
Nile Fan, 104–106
Tectonic stress, 62
Tectonic tilting, 283
Tectonic uplift, 4
Teichichnus, 145, 148
Tempe Formation (Fm), 41, 45–46
Temple Avenue fault, 281, 282
Terebellina, 143–145, 148, 156, 157
Tertiary Banquereau Formation (Fm), 19
Tertiary period, 128, 135
Tethyan passive continental margin, 106
Texas Gulf Coast, 76
shelf sandstones of the Deep Wilcox Trend, 135–157
stratigraphic chart for the Paleocene through early Eocene, 136
Thalassiosira oestrupil zone, 268
Thalweg, 178–179, 213, 218
Ramsey subunit of Ford-Geraldine Field, 207
sinuous, 214
successive filling of, 87
Thermobaric regime, 123–124
Thick-bedded sand facies
frequency distribution of true stratigraphic thickness, 271
permeability values, 276
Wilmington Field, 271, 272–275
Thickness of sediment deposited (Sed), 3
Thickness-to-width ratios, 96
Thief zones, 231
Thin-bedded sand facies
frequency distribution of true stratigraphic thickness, 271
Thin-section petrographic analysis, 65
Threshold significance level, 254
Thrust faults, 44
Thrust sheets, 39, 44
THUMS-Huntington Beach fault, 264–265
Tidal basin reservoirs, preservation style, 90–91
Tidal bundles, 94, 95
Tidal creek, Mossoró Sandstone, 193
Tidal-flat deposit, 190
Tidal-flat shales/dolomitic marls/cemented sandstones, 163
Tidal-inlet fill geometries
representative examples showing the geometries and facies relations, 83
wave-dominated, 83–87
Tidal-inlet fill preservation, 93
Tidal inlet-fill sequences, 95
Tidal inlet-fill sequences (N.C. and S.C.), linear dimensions, 84
Tidal-inlet migration, Johnson Creek, 87
Tidal inlet reservoirs, 77–97
ancient analogs, 94–95
controls on tidal inlet stratigraphy, 81–83
ebb-tidal delta deposits, 95
ebb-tidal deltas, 88
flood-tidal deltas, 88, 95
inlet morphology and processes, 79–81
physical and depositional setting, 77–79
porosity of deposits, 96
preservation potential: example from the Louisiana Continental Shelf, 91–94
sandstone distribution and reservoir potential, 95
subsurface variability and facies relations, 88–90
summary and conclusions, 95–97
tidal-inlet fill geometries, 83–88
tide-dominated, 89
wave-dominated, 88, 89, 92
Tidal inlets, 77
active and relict, wave-dominated, along barrier islands forming the Cape Lookout cuspate foreland, 79
basement-controlled, 89
ebb-tidal deltas, 82, 83
flood-tidal delta, Johnson Creek, 86
formation and distribution, 83
high wave energy relation, 80
mechanism of wave-dominated inlet channel closure from longshore sediment transport, 81
thickness-to-width ratios, 85
tide-dominated, 79, 82
tide-dominated inlet geomorphology and associated depositional environments, 80
wave-dominated inlet geomorphology and associated depositional environments, 80
width-to-thickness ratios, 85
Tidal inlet sequences
composite strike- and dip-oriented channel geometries for wave- and tide-dominated inlets, 92
tide-dominated, 87–88

Tidal-inlet stratigraphy, 77
Tidally reworked sandy bars, coring, 181
Tidal prism, 77, 85
Tidal range, 77
Tide-dominated inlet sequences, potential reservoir quality and gamma-log signatures, 97
Time-lag effect, 11
  clastic wedges, 10–11
Titanomagnetite, martitization in Mossoró Sandstone, 195
Todd River Dolomite, 41, 47–49, 51
T. oestrupii zone, 269
Topanga Formation, 266
Toplap, 23
Torrance-Wilmington structural trend, 265
Total Organic Carbon (TOC), analyses of shale-bed samples, Wilmington Field, 271
Tourmaline, 65, 68
  Mossoró Sandstone lithofacies content, 197
Township 73, 17
Transcurrent fault zones, 264
Transform permeability, 258, 259–260
Transgression, 5, 11
  models of, 6
  with downcutting, 6
Transgressive barriers, 7
Transgressively reworked deltas, 13
Transgressive megasequence, 183
Transgressive systems tracts, 10–11, 13–16, 23–24, 35–36
  Arumbera Sandstone, 73
  base characteristics, 31
  block diagram illustration of one as developed in offshore Louisiana, 30
  maximum flooding surfaces, 23
  parasequence sets 10 and 11, 69
  reservoir sands, 61
  seismic facies and their seismic, well-log, and lithologic characteristics, 26
  seismic section, 31
  Wilmington Field, 280, 284
Transgressive tidal-current ridges, 13
Trap laminite, 225
Trap siltstone, 204–206, 209–210, 214, 216–219
  laminated, isopach map, 222
  laminite, 218
Tremadoc, 58
Tiassic Halfway Formation (Fm), 86–87
Trilobites, 58, 66
  parasequence set 11, 69
Triorites africaensis, 186, 190
Triple Avenue Fault, 265
Trough and planar cross-beds, 66
Trough cross-bedding, 64, 156, 157
  7-BAL-5-RN well, 165
  7-CAM-63-RN well, 173
  7-CAM-79-RN well, 188
Trough, tabular cross-bedding
  9-MO-13-RN well, 168, 169
  RE-8-RN well, 174
Truncation surfaces, 3
Turbid flows, 109
Turbidite bed thickness, 276
Turbidite deposition, various stages of cycle, Eocene Hecho Group (Spain), 288
Turbidites, 155, 233
  Deep Marine Sandstone, 238, 240, 242, 243
  identification in Nile Fan, 109
  Permian Bell Canyon Sandstone reservoir, 207
  sedimentation, Wilmington Field, 266–267
Turbidite sequences, 156
Turbidite systems
  Ranger Zone of Long Beach Unit, 279
  Wilmington Field, 283
  Wilmington Field model of three types, 286–289, 291
Turbidite T_{abc} sequence, 148
Tubiditic sediment flow, 105
Turbiditic sediments, 106
Turbiditic sequences, lithology shown in lithofacies charts of the Nile Fan, 110
Turbidity currents, 156–157, 206–207, 242, 249, 258
Turonian/Santonian stage, 161
$T_{(a)bc}$ sequences, 155
Twofreds Field, 225
Type 1 sequence boundary, 6

Ubarana Canyon (UC), 162
Unconformities, 3, 5–6, 280
  Messinian surface, 105
  Pliocene epoch, 267
  Ranger Zone, 283
  sub-Cretaceous, 11
Unconformity bounded seismic sequence, 8
Unconformity-bounded sequence, 4, 9
  major types of systems tracts, 9
Unimodal cross-strata, 62
Unitization, Ford-Geraldine Field, 219
Updip fining-upward sequences, 30
Updip parallel facies, 29
  seismic, well-log, and lithologic characteristics, 26
Updip pinchouts, 33, 34
Upper Açu Formation (Fm), stratigraphic section across the cored wells, 195
Upper Cretaceous, 178
Upper Cretaceous Açu Formation (Fm), 183
Upper-flow-regime currents, 156
Upper Goyder Formation (Fm), 41
Upper Guadalupian Ramsey sands, 202
Upper Inindia Beds, 41
Upper Mannville, 11, 14, 16
  gamma-ray log cross-section, 16
Upper Miocene, regional paleography in Los Angeles Basin, 267
Upper Missisauga Formation (Fm), 18
Upper non-marine regressive path, 6
Upper nonmarine transgressive path, 6
Upper Pacoota Sandstone, 61
Upper Pico Formation (Fm), 268
Upper Shannon, 41
Upper Wilcox subgroup rock unit, 136
U-shaped burrows, 62, 72
Uvigerina hispida, 269
Uvigerina hootsi, 269
Uvigerina peregrina S.L., 269

Valentine Field, 138, 139
Variables, major external, 3–4
Ventura Basin, 264
Vertical burrows, 72
Vibracore CR-10, 94
  close-up photographs of tidal-inlet fill deposits, 95
Vibracore hole locations, 92, 93
Vickers East Pool, production and recovery, 231
Vickers reservoir zone, 258
Vickers zone, 231
  lithology and lithofacies, 233, 234, 238
Victoria County, 139, 140
Viking Formation (Fm), 13

Wallaby structure, 55
Warendian stage, 58
Washover, Price Inlet, 90
Waterflood
  five planned stages, Ford-Geraldine Field, 222–225
  Vickers East Pool, 231
Waterhouse anticline, evaporite high amplitude, 44
Water-scape structure, 7-CAM-79-RN well, 188
Watsons Range, 62
Wave- and tide-dominated mixed-energy coasts, 90
Wave-current laminae, 156

Wave-dominated inlet sequences, potential reservoir quality and gamma-log signatures, 97
Wave-laminated beds, 156
Wave regime, 77
Wave ripples, 156
Wave truncated ripple, 7-CAM-79-RN well, 188
Wavy bedding, 143, 146, 157
Weigang Field, 137, 139
Well log, 9, 11
Well-log criteria, for identification of systems tracts, 23–24
Well-log profiles, relation with systems tracts and abundance peaks, 24
Wentworth scale, 251
West Cameron, 21
Western Fan Province, 102
Western Interior of North America, 178
Whalebone Inlet (N.C.), linear dimensions of tidal inlet-fill sequences, 84
White quartzites, correlation of Pacoota Sandstone Units from Palm Valley Field to Mereenie Field, 59, 60
Wilcox Formation (Fm), 131
  isopach map of the interval between the top, and the base of the second Wilcox sandstone, 126
Wilcox Group, 118, 135
  regional and local source-area transport paths, 137
Wilcox Group rock unit, 136
Wilcox growth faults, 137
Wilcox growth-fault trend, 136
Wilcox Lavaca Channel, 137
Wilcox outcrop in Texas, 136
Wilcox "Rockdale System," 136
Wilcox rocks, 113
Wilcox sandstones, 117
Wilcox Yoakum Channel, 137
Wilcox Yoakum Field, 138
Wilmington Fault, 265
Wilmington Field, 115
  biostratigraphy, 268–269
  depositional systems tracts and Ranger sequences, 284
  flow units, 277–278, 290
  frequency distributions of stressed and unstressed core plug porosity and permeability measurements, 277
  geologic heterogeneity scales, 263–291
  grain-size, 271
  grain size, facies, and reservoir quality, 276–277
  idealized depositional sequence model showing relative position of Long Beach Unit with shelf-to-basin profile, 284
  isopachs of three stratigraphic intervals, 282
  lithofacies, 271
  Long Beach Unit statistical summary of grain-size distribution, 276
  Los Angeles Basin oil fields, 264
  lowstand wedge deposits, 283–286
  macroscale heterogeneities, 278–279, 290
  megascale heterogeneities, 279–280, 289–291
  megascale heterogeneities, comparison of models and implications, 288–290
  mesoscale heterogeneities, 277, 279, 289, 290
  microscale and mesoscale heterogeneities, 269–278
  microscale heterogeneities, 277, 289, 290
  NW-SE detailed straigraphic cross section of various sand and shale intervals and subzone horizon picks, upper Ranger Zone, 281
  NW-SE regional cross section of Ranger Zone, 281
  outlines of selected modern and ancient submarine fans and turbidite systems, 283
  permeability, 271–278, 289, 290
  porosity, 271–278, 290
  production and recovery, 263
  progradational submarine fan model, 286, 287, 289, 291
  regional geology, 263–267
  regional paleogeography in Los Angeles Basin during upper Miocene time, 267
  regional stratigraphic cross section, 266
  reservoir quality, 277
  sequence stratigraphic model, 280–286, 289, 291
  shale facies, 290
  shale facies, flow unit, 277
  stratigraphic/geologic history, 266–267
  stratigraphic intervals, zones, and subzones in Long Beach Unit, 268
  stratigraphy, 263–267
  structural history, 263, 264–266
  structure and major faults, 265
  thick-bedded sand facies, 279, 280, 289, 290
  thick-bedded sand facies, flow unit, 277
  thick-bedded sand facies, frequency distributions of stressed porosity and permeability, 278
  thin-bedded sand facies, 279, 280, 289, 290
  thin-bedded sand facies, flow unit, 277
  thin-bedded sand facies, frequency distributions of stressed porosity and permeability, 278
  turbidite systems (3 types) model, 286–288, 289, 291
  unitized formations and subzones, 267–268
Woody debris, 233
Wrench faulting, 44–45
Wrench folding, 265
Wyandot chalk, 17
Wyandot Formation (Fm), 19
Wyoming foreland, foreland-basin sequence model, 11

XRD analysis, 68

Yang and Nio's ebb-tide delta sequence, 179
Yegua barrier/strandplain system, 76
Yoakum Channel, 137, 138, 139
  deep, downdip Wilcox wells, location of, 140
Yoakum Field, 138, 139
Ypresian, 15
Yucatan platform, 135

Zeolite, Deep Marine Sandstone, 245
Zero isopach, 220
Zero isopach line, 218
Zircon, Mossoró Sandstone lithofacies content, 197
Zones of erosion, 4–5
Zones of preservation, 4–5
Zoophycos, 145